Recent Advances in Hydride Chemistry

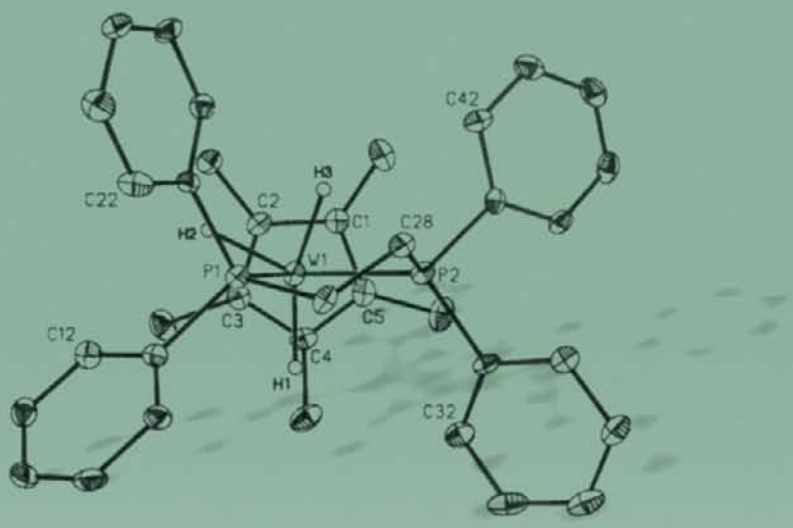

Edited by:
Maurizio Peruzzini
and
Rinaldo Poli

ELSEVIER

Recent Advances in Hydride Chemistry

This Page Intentionally Left Blank

Recent Advances in Hydride Chemistry

Edited by:

Maurizio Peruzzini
Instituto di Chimica
Composti Organometallici, CNR,
Florence, Italy

Rinaldo Poli
Laboratoire de Synthèse et d'Electrosynthèse
Organométalliques (LSEO),
Université de Bourgogne,
Dijon, France

2001

ELSEVIER
Amsterdam – London – New York – Oxford – Paris – Shannon – Tokyo

ELSEVIER SCIENCE B.V.
Sara Burgerhartstraat 25
P.O. Box 211, 1000 AE Amsterdam, The Netherlands

First edition 2001

Library of Congress Cataloging in Publication Data
A catalog record from the Library of Congress has been applied for.

ISBN:0-444-50733-7

Transferred to digital printing 2005

Printed and bound by Antony Rowe Ltd, Eastbourne

Dedicated to the memory
of Luigi Venanzi (1927 - 2000)

This Page Intentionally Left Blank

Preface

Metal hydrides play a central role in modern inorganic and organometallic chemistry and find a wide applicability in several key sectors of the chemical industry as highly selective and efficient catalysts for homogeneous processes and new materials for energy storage. Their involvement in metalloenzymes attending at important biochemical processes has also been established and represents an active area of research.

This ever intensifying research activity has generated a number of review articles over the years on an approximately constant frequency basis. We should also mention the publication of a previous monograph edited by A. Dedieu in 1990. Recent evolutions in this area, however, have been quite spectacular, especially the recognition of the hydrogen bonding capability of hydride ligands, the discovery of catalytic heterolytic hydrogenations, and important advances in the spectroscopic characterization techniques.

This state of affairs has convinced the European Commission to sponsor the organization of a Euroconference on hydride chemistry (EURO-Hydrides 2000), which was co-chaired by us and held in Dijon, France, in September 2000. The feedback from the conference has confirmed the high current interest in this area, especially from many young scientists, and has convinced us that it was appropriate to publish a new monograph updating the previous one and highlighting the many recent breakthroughs in this area. Many chapters have been written by the plenary lecturers of the EURO-Hydrides 2000 conference, but other leading scientists in this field have also been invited to contribute. The book has been conceived to collect the most important recent advances in all areas of hydride chemistry research, including chemical reactivity, instrumental investigation, theory, and applications in the areas of catalysis, biochemistry and materials science.

The first part of the book focuses on the chemistry and catalysis of transition metal hydrides. Knowledge on the heterolytic splitting of dihydrogen has made tremendous advances in the last few years. The heterolytic activation of H2, the reverse process of protonation of metal hydrides, the involvement of nonclassical hydrogen bonding along the reaction pathway relating H2 to H+ and H-, and catalytic applications are treated in detail in several chapters. Morris shows the preparation of dihydrogen complexes and the current knowledge on their acidity scale and ability to form nonclassical hydrogen bonds of types M(H2)...B and MH...HB. Norton et al. analyse the reverse process of hydride protonation, focusing on the kinetics of the proton transfer process. Jacobsen and Berke

define the concept of hydridicity and analyse the influence of the electronic structure and solvent on the hydride reactivity. In a chapter by Crabtree, Eisenstein and co-workers, a combined experimental and theoretical approach to the investigation of nonclassical hydrogen bonding and hydride reactivity is shown. Hidai and Nishibayashi review the specific application of heterolytic cleavage to the reduction of dinitrogen to ammonia. Poli reviews the current knowledge on the stability and reactivity of paramagnetic hydride complexes, with relevance to electrocatalytic applications. Esteruelas and López review their own work on the use of ruthenium and osmium hydrides to induce carbon-carbon and carbon-heteroatom coupling reactions, while Barbier-Baudry and Dormond survey the most recent developments in the area of the hydride chemistry of the lanthanides. In two more catalysis oriented chapters, Bianchini and Peruzzini review the catalytic uses of dihydrogen complexes, while Oro and Sola outline the dihydrogen activation by dinuclear compounds with application to catalysis. Other catalytic applications of the heterolytic H2 activation (ionic hydrogenation) are shown in the chapters by Norton et al. and by Jacobsen and Berke.

Another block of chapters illustrate the most recent advances in the application of instrumental techniques to the study of the properties and reactivity of hydride compounds. Duckett shows the advantages of using parahydrogen coupled with NMR spectroscopy to enhance the detection of small concentrations of species implicated as catalytic intermediates in hydrogenation processes. Aime et al. show the application of NMR with parahydrogen to the investigation of hydride clusters and their chemistry. Bakhmutov illustrates how the ionicity of the metal-hydrogen bond can be investigated by deuterium relaxation via 2H-NMR methods. Epstein et al., on the other hand, review the information that can be gathered on the thermodynamics and kinetics of nonclassical hydrogen bond formation and proton transfer by a combination of IR and NMR techniques. This "methodology" section is closed by a pedagogical chapter by Lledós et al., showing the powerful recent application of theoretical methods for the understanding of structure and dynamics of classical and nonclassical hydrides.

The final part of the book illustrates the relevance of metal-hydrogen bonds in biochemistry and materials science. A chapter by Henderson reviews the implication of hydrides in some enzymatic processes relevant to biochemistry. Ross shows the combined use of experiment and theory for the investigation of hydrogen in metals, while a closing chapter by Maeland shows the state of the art in the development of hydrogen storage materials for the application in automotive technology.

All chapters of this book have been evaluated by independent reviewers, to whom we are most grateful for the time they took to read the material and for their comments aimed at increasing the quality of this book.

In closing, we would like to mention that one of the pioneers of hydride chemistry research, Luigi Venanzi, passed away recently. Luigi had accepted to deliver the opening plenary lecture at EURO-Hydrides 2000 but his participation was prevented by the illness that eventually won the battle with him. In spite of being retired, he was continuing to produce original and elegant work on the chemistry of metal hydrides as "ligands" and a chapter written by him on this topic would have been extremely well suited for this monograph. Because of these considerations and because of our friendship and admiration of him as both a scholar and a gentleman, we find it most appropriate to dedicate this book to his memory.

Maurizio Peruzzini
Rinaldo Poli

Florence and Dijon, June 2001

This Page Intentionally Left Blank

Contents

Chapter 1

Non-classical Hydrogen Bonding along the Pathway to the Heterolytic Splitting of Dihydrogen

Robert H. Morris
Department of Chemistry, University of Toronto, 80 St George St., Toronto, Ont. M5S 3H6, Canada

CONTENTS

1.1 INTRODUCTION

Over the past 20 years several surprising intermediates have been discovered in the heterolytic cleavage of dihydrogen gas at a transition metal center [1-5]. In this process, dihydrogen reacts with a metal complex, designated as [M] in eq 1, and a base B to produce a proton and hydride. Three types of these intermediates that are formed along the pathway of this reaction are shown in eq 2-4. Dihydrogen can coordinate in a transition metal complex as an η^2-dihydrogen ligand and become more acidic (eq 2).

The η^2-H_2 designation [6] indicates the presence of the less common, 3 centre bonding at one metal coordination site, as in $W(\eta^2\text{-}H_2)(CO)_3(PCy_3)_2$, the first

dihydrogen complex to be identified by Kubas et al. in 1984 [7]. The more common form of bonding mode would be the dihydride form with two, two-center M-H bonds on two coordinate metal sites. The η^2-dihydrogen ligand in eq 3 is acting as a non-classical hydrogen-bond donor to an electronegative atom on the in-coming base B. A proton transfers to the base in eq 4, but then it remains associated with the hydride in the ion pair, $\{^-[M]H\cdots HB^+\}$, with a 1.7-2.0 Å contact, the hydride acting as non-classical hydrogen bond acceptor. The product of reaction 4 is written as an ion-pair because of the low dielectric constant of the solvents like THF and CH_2Cl_2 and aromatic hydrocarbons that are commonly employed to study η^2-dihydrogen complexes. We have referred to this short H···H interaction as a proton-hydride bond although others prefer the term dihydrogen bond. Calling it a dihydrogen bond can lead to confusion because the dihydrogen ligand has non-classical H-H bonding, itself, and can make non-classical hydrogen bonds to electronegative atoms; all of these interactions associated with dihydrogen are different. Perhaps the term hydridic-protonic bond is a good compromise. The $\{^-[M]H\cdots HB^+\}$ structure can then go on to form a new metal hydride and this is a common way to make hydrides from hydrogen gas (eq 1). Of course you can go the other way as well by adding an acid to a metal hydride (reverse of eq 4 then 3) to make a dihydrogen complex. These reactions are often reversible.

$$[M] + H_2 + B \rightleftharpoons {}^-[M]H + HB^+ \qquad (1)$$

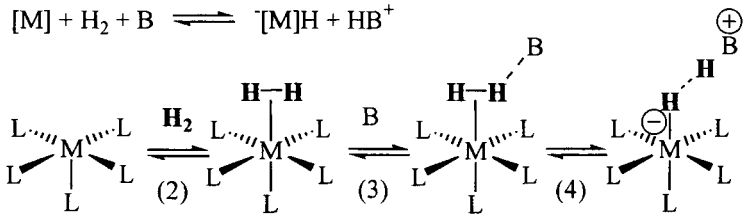

About 400 compounds containing the η^2-H_2 ligand have been made that are stable. Almost all of them are octahedral with the metal in the d^6 electron configuration, from Cr(0) to W(0) across the periodic table to Rh(III) and Ir(III). There are a few dihydrogen complexes known with metals in other oxidation states. These are relatively rare. There are seven coordinate rhenium compounds like $[Re(H_2)(H)_2(CO)(PMe_2Ph)_3]^+$ [8] and very unstable d^8 systems like $[Pt(\eta^2\text{-}H_2)(PR_3)_2H]^+$ [9]. Neutral and cationic complexes are known but not anionic ones. Presumably anionic dihydrogen complexes are unstable because the metal's $d\pi$ electron richness promotes the oxidative cleavage of the H-H bond by $d\pi(M) \rightarrow \sigma^*(H_2)$ donation.

The dihydrogen complex acids in eq 2-4 of our studies are all 6-coordinate. Their conjugate base forms, $[M]H^-$, are usually also 6 coordinate (note that cyclopentadienyl ligands are considered to occupy three coordination sites). We desig-

nate this conservation of coordination number as Δ=6/6. One interesting exception to this rule is the acid/base pair $RuH_2(\eta^2\text{-}H_2)_2(P^iPr_3)_2$/$[RuH_5(P^iPr_3)_2]^-$ with Δ=6/7 (see Table 1.3, Section 1.3) where the acid is a 6-coordinate bis-dihydrogen complex [10] while the base is a 7-coordinate pentagonal bipyramid [11]. When polyhydride η^2-dihydrogen complexes such as these are deprotonated, the base forms are too electron rich to retain H-H bonds.

An alternative pathway to eq 2-4 might be the classical dihydride route, eq 5-6. Here the oxidative addition of the dihydrogen ligand results in a seven-coordinate dihydride species. Reaction 6 has Δ=7/6 and might also result in the production of a hydridic-protonic bonded intermediate.

$$[M](\eta^2\text{-}H_2) \rightleftharpoons [M](H)_2 \quad (5)$$

$$[M](H)_2 + B \rightleftharpoons \{^-[M]H\cdots HB^+\} \quad (6)$$

1.1.1 Significance and objective of this research

Useful applied as well as fundamental knowledge is resulting from this work. The heterolytic splitting of dihydrogen on ruthenium catalysts is found in several useful processes for the hydrogenation of polar multiple bonds such as the CO bond in ketones, aldehydes and esters, the CN bond in nitriles and imines and the polar CC bond of some olefins [12-15]. Ruthenium-based homogeneous hydrogenation catalysts are found to be superior to the more expensive rhodium-based ones for this process [15]. Clearly a better understanding of the reactions of the hydride and dihydrogen intermediates will assist in the design of better catalysts. Hydride materials that are able to reversibly store dihydrogen according to eq 1 might have future uses when hydrogen gas becomes a common fuel. Note that half of the hydrogen is stored on the base in eq 1 while in conventional hydrogen storage materials such as MgH_2 or $TiFeH_{1,8+}$, the hydrogen content is limited by metal-hydrogen coordination. Metal hydrides are used in batteries as high energy materials; this might be another direction.

Our research endeavors to determine the strength of the acid produced in reaction (1), the structures of the intermediates on the way to the loss of the proton as in eq 2-4, and the implications for the mechanism of catalytic homogeneous hydrogenation of polar multiple bonds. We want to quantify the acidity of a wide range of metal hydrides in order to understand how the pK_a of the non-classical hydrogen-bond donor (the dihydrogen ligand of eq 3) and the basicity of the non-classical hydrogen-bond acceptor (the hydride ligand of eq 4) influence the strength of these new hydrogen bonds. We are learning about the influence of ion pairing. And we can construct new hydride materials via a self-assembly crystallization that is directed by these new bonds.

1.2 THE SYNTHESIS AND CHARACTERIZATION OF HYDRIDE AND DIHYDROGEN COMPLEXES WITH THE WIDEST RANGE POSSIBLE OF ACID-BASE REACTIVITY

1.2.1 Synthesis of anionic hydride complexes

A useful route to anionic hydrides of the type $[K(crown)][MH_x(PR_3)_y]$, M= W, Re, Ru, Os, Ir, x=3-6, y=2-3, R=Cy, Me, ^{i}Pr, Ph (Table 1.1) is the reaction of halide or hydridohalide precursors $MH_{(x-z-1)}X_z(PR_3)_y$, X= Cl or Br, in THF under H_2 with excess potassium hydride and one equivalent of a crown ether such as 18-crown-6 (Q), 1-aza-18-crown-6 (QNH), or 1,10-diaza-18-crown-6 (HNQNH) (eq 7) [11, 16-18].

$$MH_{(x-z-1)}X_z(PR_3)_y + (z+1)KH + crown \rightarrow [K(crown)][MH_x(PR_3)_y], + zKX \quad (7)$$

This route is particularly efficient because the halide precursors can be obtained in high yield from commercially available reagents and no valuable phosphine ligands are lost, a problem of other routes. The use of H_2(g) in eq 7 is thought to be necessary to stabilize intermediates, probably as dihydrogen complexes, and provide hydride ligands by heterolytic H_2 splitting reactions. Figure 1 illustrates the preparation of the complex $[K(QNH)][OsH_5(P^iPr_3)_2]$ by this method.

A second, better-known method [19] is the deprotonation of polyhydride complexes $MH_{(x+1)}(PR_3)_y$ with KH in the presence of crown or 2,2,2-crypt (eq 8).

$$MH_{(x+1)}(PR_3)_y + KH + crown\ or\ crypt \rightarrow [K(crown\ or\ crypt)][MH_x(PR_3)_y]+H_2 \quad (8)$$

Some of the white or yellow, water- and air-sensitive crystalline hydrido-metallates that have been prepared by our research group are listed in Table 1.1 along with the precursor complexes. Most of these complexes have also been structurally characterized by means of single crystal X-ray diffraction. The aza-crown complexes have short MH···HN contacts as will be discussed in Section 1.8.1.

1.2.2 Structures of anionic hydride complexes

The structures of 8 coordinate $[ReH_6(PR_3)_2]^-$ complexes have already been reported in the literature. We have crystal structures of beautiful 7-coordinate pentagonal-bipyramidal $[K(crown)]^+[MH_5(P^iPr_3)_2]^-$ M= Ru, Os [11] and 6 coordinate octahedral $[K(crown)]^+[IrH_4(P^iPr_3)_2]^-$ [17] with hydrides in refined positions. The potassium in the last structure sits on three of the hydrides of the cis-$[IrH_4(P^iPr_3)_2]^-$ anion. The structures of the aza-crown-containing complexes will be described in Section 1.8.2.

1.2.3 Synthesis of weakly acidic, neutral dihydrogen or polyhydride complexes

The protonation of anionic hydrides such as those in Table 1.1 produces neutral non-classical dihydrogen complexes such as $M(\eta^2\text{-}H_2)(H)_2(CO)(P^iPr_3)_2$,

M=Ru, Os, $Ru(H)_2(\eta^2\text{-}H_2)_2(P^iPr_3)_2$, $Ru(\eta^2\text{-}H_2)H_2(PPh_3)_3$ or conventional polyhydride complexes such as $Re(H)_7(PR_3)_2$, $Os(H)_6(P^iPr_3)_2$ and $Ir(H)_5(PR_3)_2$ (see Table 1.3, Section 1.3). The acid 1,3-benzenedimethanol in THF is particularly useful because the base form $[K(18\text{-crown-6})][C_6H_4(CH_2OH)(CH_2O)]$ precipitates from THF (eq 9).

$$[K(18\text{-crown-6})][RuH_5(P^iPr_3)_2] + C_6H_4(CH_2OH)_2 \rightarrow Ru(H)_2(\eta^2\text{-}H_2)_2(P^iPr_3)_2 + [K(18\text{-crown-6})][C_6H_4(CH_2OH)(CH_2O)] \quad (9)$$

In related reactions, protonation of $[K(18\text{-crown-6})][RuH_5(PCy_3)_2]$ yields the dihydrogen complex $RuH_2(\eta^2\text{-}H_2)_2(PCy_3)_2$ while protonation of $[K(18\text{-crown-6})][RuH_5(PPh_3)_2]$ yields the dimeric dihydrogen species, $(PPh_3)_2(H)Ru(\mu\text{-}H)_3Ru(\eta^2\text{-}H_2)(PPh_3)_2$.

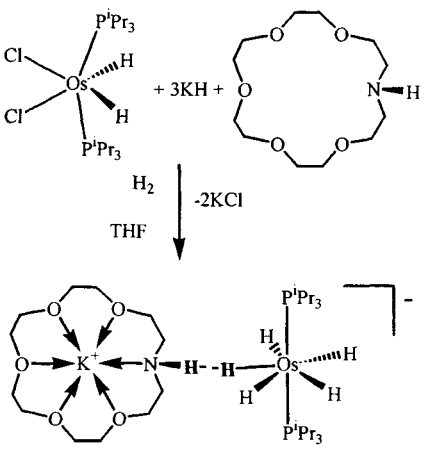

Figure 1. The preparation of $[K(QNH)][Os(H)_5(P^iPr_3)_2]$

New routes to several other transition metal hydride complexes were developed that involved other sources of hydride. The few steps now needed for their syntheses and the high yields in most cases makes their use as practical acids and bases more feasible. For example $ReH_3(PR_3)_4$, PR_3 = $PMePh_2$ and PMe_2Ph, were prepared in two steps: (1) rhenium powder/H_2O_2/HCl (2) $[N^nBu_4]BH_4$/phosphine. The complexes $OsH_2(PR_3)_4$ were obtained from OsO_4 efficiently by way of $K_2[OsO_2(OMe)_4]$ and its direct reaction with phosphine in ethanol. The complexes $Ir(H)_5(P^iPr_3)_2$ and $Ir(H)_3(PPh_3)_3$ were prepared by reaction of sodium alkoxides with the hydridohalo precursors $IrH(Cl)_2(P^iPr_3)_2$ and $IrH(Cl)_2(PPh_3)_3$, respectively, under H_2(g) in THF. It is likely that the heterolytic splitting of dihydrogen in intermediates containing dihydrogen ligands is important in these reactions.

Table 1.1. Selected precursor complexes and types of products produced via eq 7 or 8.[1]

Precursor $MH_{(x-z-1)}X_z(PR_3)_y$	$[K(crown)]^+$	$[MH_x(PR_3)_y]^-$	Ref
$Re(\eta^2\text{-}H_2)(Br)_2(NO)(P^iPr_3)_2$	$[K(Q)]^+$ or $[K(QNH)]^+$	$[ReH_3(NO)(P^iPr_3)_2]^-$	[16,20]
$ReH_7(PR_3)_2$, R=Me, ^{i}Pr, Cy, Ph	$[K(Q)]^+$ or $[K(HNQNH)]^+$	$[ReH_6(PR_3)_2]^-$	[18]
$ReH_7(PPh_2C_6H_4\text{-}4\text{-}F)_2$	$[K(Q)]^+$	$[ReH_6(PPh_2C_6H_4\text{-}4\text{-}F)_2]^-$	[21]
$RuCl_2(PPh_3)_3$	$[K(Q)]^+$ or $[K(QNH)]^+$	$[RuH_3(PPh_3)_3]^-$	[21]
$RuCl_3/2.5\ P^iPr_3$	$[K(Q)]^+$, $[K(QNH)]^+$ or $[K(HNQNH)]^+$	$[RuH_5(P^iPr_3)_2]^-$	[11]
$OsH_2Cl_2(P^iPr_3)_2$	$[K(Q)]^+$, $[K(QNH)]^+$ or $[K(HNQNH)]^+$	$[OsH_5(P^iPr_3)_2]^-$	[11]
$MHCl(CO)(P^iPr_3)_2$, M=Ru, Os	$[K(Q)]^+$ or $[K(QNH)]^+$	$[MH_3(CO)(P^iPr_3)_2]^-$	[16]
$IrHCl_2(PR_3)_2$, R=^{i}Pr, Cy	$[K(Q)]^+$, $[K(QNH)]^+$ or $[K(HNQNH)]^+$	$[IrH_4(PR_3)_2]^-$	[17, 22]

[1] $[K(Q)]^+$ = [K(18–crown–6)]$^+$, $[K(QNH)]^+$ = [K(aza–18–crown–6)]$^+$, $[K(HNQNH)]^+$ = [K(1,10–diaza–18–crown–6)]$^+$

Cationic hydride and dihydrogen complexes are usually prepared via the protonation of basic transition metal complexes and this area has been thoroughly reviewed [2, 5, 23]. One recent development is the synthesis of very acidic cationic dihydrogen complexes by displacement of a weakly coordinating anion such as triflate ($O_3SCF_3^-$). We have found that, when the triflate anion is coordinated on Ru(II) or Fe(II) trans to a strong field ligand such as CNH [24], η^5– $C_5R_5^-$ [25] or CO [26], it can be displaced by H_2(g) to produce dihydrogen complexes that are so acidic that they spontaneously eliminate the strong acid HO_3SCF_3 in the absence of excess acid. The acidity of these complexes must be ranked in a solvent like CH_2Cl_2 (Table 1.2, Section 1.3) because some can protonate THF. The Kubas group has reported the preparation of the very acidic complex $[Re(\eta^2\text{-}H_2)(CO)_4(PCy_3)]^+$ by displacing an Et_2O ligand with H_2 [27]. We have recently found that triflate trans to cyanide can also be replaced by dihydrogen (see Scheme 1, Section 1.4).

1.2.4 Structure determination of dihydrogen complexes

How do you find the distance between the hydrogens in these structures to determine if they are dihydrogen or hydride complexes? The definitive method is neutron diffraction from a large crystal. Our structures were determined by Tom Koetzle and co-workers at Brookhaven at the high neutron flux reactor. There are only a few places left in the world to do this now that the Brookhaven National Laboratory facility has been closed. Typically dihydrogen ligands have large ther-

mal ellipsoids indicating the smearing of hydrogen nuclear density even when the structure is done at 10 K. Of course hydrogen is a quantum mechanical particle with quantum dispersion so it is philosophical where the actual positions of the hydrogen are located. However an interpretation is that the H_2 ligand is undergoing a torsional libration about a line joining the metal and the H_2 centroid. It is necessary to correct crystallographic H-H distances for this motion in order to obtain correspondence with solid state ^{1}H NMR measurements.

The single crystal neutron diffraction structures and chemistry of the following of our complexes have been studied in collaboration with the group of Koetzle: $[M(\eta^2\text{-}H_2)H(dppe)_2]BPh_4$, M=Fe [28], Ru [29], $[Os(H\cdots H)(Cl)(dppe)_2]PF_6$ [30], $[Os(\eta^2\text{-}H_2)(H)(dppe)_2]PF_6$ (at 10, 50 and 100 K) [31] and $[Ru(H\cdots H)(C_5Me_5)(dppm)]BF_4$ [32]. The last three have H–H distances in the interesting range from 0.95–1.23 Å, that is on the borderline of dihydrogen and dihydride structures. The only other literature neutron structures with an H–H distance in this range are those of $Ir(\eta^2\text{-}H_2)(H)Cl(P^iPr_3)_2$ [33] and $[Cp^*Os(\eta^2\text{-}H_2)H_2(PPh_3)]^+$ [34]. There is minimal H-H orbital overlap beyond 1.2 Å so that these are considered dihydride structures, "compressed dihydrides" in the range 1.2 to 1.6 Å and then classical dihydrides.

We showed that the H–H distances from these and other structures correlate linearly with the coupling constant J(HD) measured from the ^{1}H NMR spectrum of the HD analogue in solution (eq 10) [30]. This equation is now an accepted method for determining the H–H distance of new dihydrogen complexes from the ^{1}H NMR spectrum of the HD complex in solution, such as the very long distance of 1.38 Å in fac-$[Re(H\cdots H)(dien)(PPh_3)(PF_3)]^+$ [35].

$$d(HH) = 1.42 - 0.0167\, J(HD) \qquad (10)$$

One complex that deviates from this relationship is $Ir(\eta^2\text{-}H_2)H(Cl)_2(P^iPr_3)_2$. The neutron structure in this case reveals the presence of non-classical hydrogen bonds between the η^2-dihydrogen ligand and adjacent hydride and chloride ligands including an $Ir(H_2)\cdots ClIr$ bond between neighboring molecules in the crystal [33]. This intermolecular interaction would not be of sufficient strength to compete with solvation forces in solution but might affect the solid state H-H distance enough to cause the deviation from the d(HH)/J(HD) correlation. This complex provides examples of non-classical hydrogen bonding where the protonic dihydrogen ligand is acting as a multiple hydrogen bond donor to hydride and chloride acceptors (also see Section 1.4).

We use X-ray diffraction from small crystals at low temperature with CCD detection to minimize absorption associated with the transition metal electrons. This gives reasonable hydrogen positions of hydride ligands in many cases and dihydrogen ligands in certain cases. The chemistry and X–ray structure determination of the following H_2 complexes have recently been studied in our group: $[Os(\eta^2\text{-}H_2)(CH_3CN)(dppe)_2](BF_4)_2$ [36], the most acidic dihydrogen complex

(see Table 1.2) to be structurally characterized and the first where the H_2 ligand is acting as a hydrogen bond donor to one BF_4^- anion (see Section 1.4); cis–[Ru(η^2-H_2)H(PMe_2Ph)$_4$]PF_6 [37], an alkyne hydrogenation catalyst and a complex with four distinct fluxional processes [Ru(η^2-H_2)H(*R,R'*-Me-DuPHOS)$_2$]PF_6 [38], the first structure of a chiral H_2 complex; [Ru(H···H)(Cl)(dppe)]PF_6 [39], a surprisingly acidic complex (Table 1.2) because of the H–H bond elongation; Ru(η^2-H_2)$_2$(H)$_2$(P^iPr_3)$_2$ [10], a rare structure of a bis–dihydrogen complex.

There are other physical methods for detecting the presence of a short H-H distance and studying the fascinating physical phenomena associated with dihydrogen and dihydride ligands. For example there are quantum mechanical tunnelling effects as detected by ^{1}H NMR, ^{2}D NMR and inelastic neutron scattering. We have analyzed the physics of spin–lattice relaxation (^{1}H NMR T_1) of rotating [30], librating and hopping dihydrogen ligands [40] and have provided experimental evidence for such motions in most known dihydrogen complexes [40]. Understanding the motion of the η^2-H_2 ligand allows a more accurate calculation of the H-H distance from the minimum T_1 of its ^{1}H resonance. Recently Facey et al. have shown that the H-D distance of an η^2-HD complex can be determined by a solid-state D NMR method [41].

1.3 ACIDITY SCALES FOR TRANSITION METAL HYDRIDES

1.3.1 Existing pK_a scales

There are only limited pK_a scales for transition metal hydride complexes compared to the extensive scales for organic and inorganic acids, despite the fact that hydrides often mediate organometallic reactions; these were reviewed in 1991 [42]. Most of these complexes contain carbonyl and/or phosphine ligands and are usually insoluble in water. The pK_a^{MeCN} for about 20 neutral hydrido-carbonyl compounds determined by NMR and IR measurements in acetonitrile (MeCN) was reported by Norton and co-workers, [43-45] and more recently 10 platinum-group hydrides [46] and the dihydrogen complex [Ru(Cp)($PMe_2CH_2CH_2PMe_2$)(H_2)]$^+$ [47] have been added to this scale. The high dielectric constant of MeCN (36) means that most ions are solvent separated and not ion-paired so that the pK_a^{MeCN} value is independent of the types of counter-ions used. However MeCN is not useful for many η^2–dihydrogen complexes because CH_3CN is a better ligand than η^2-H_2.

The high dielectric constant of dimethylsulfoxide (DMSO) at 46.6 makes it an excellent solvent for acid/base reactions of organic acids and pK_a^{DMSO} measurements have been made for over 1000 organic acids over a wide range: $0 < pK_a^{DMSO} < 35$ [48]. However DMSO is oxidizing and it is a medium strength ligand and can substitute H_2. This may explain why few pK_a^{DMSO} have been determined for hydrides.

We and others have found that CH_2Cl_2 is an excellent solvent for acidic dihydrogen and dihydride compounds. Methylene chloride has a low dielectric constant so that monocationic complexes will usually form 1:1 ion pairs below 0.01 M and higher aggregates above this concentration. Several pK_a^{aq} of metal hydride complexes in CH_2Cl_2 anchored to the pK_a^{aq} of phosphonium salts or other acids have been reported (e.g. see Table 1.2 from our work); they fall in the range from about –5 to 12 [23, 30, 49-52]. These are actually ion-pair pK values because they have not been corrected for the effects of ion-pairing.

However they illustrate the effect of charge of the complex on acidity. The replacement on Os(II) of the chloride in trans-$[Os(\eta^2\text{-}H_2)(Cl)(dppe)_2]PF_6$ by the acetonitrile in trans-$[Os(\eta^2\text{-}H_2)(NCMe)(dppe)_2](BF_4)_2$ results in a change of about 9 pK_a units. Methylene chloride is an excellent solvent for very acidic hydride complexes but it tends to react with nucleophilic hydrides.

Preliminary ion-pair pK values were reported for some dihydrogen complexes in THF, a solvent where 1:1 ion-pairing can also be expected. These values have now been roughly corrected for ion pairing (see 1.3.2).

Angelici and co-workers have ranked the acidity and the bond dissociation energies of about 50 cationic hydrides by protonating neutral metal complexes in CH_2ClCH_2Cl (DCE) with triflic acid ($HOSO_2CF_3$) and measuring the enthalpy of the reaction [53, 54]. These fall in the range of 10 to 40 kcal/mol. These results will be anion-dependent because of the low dielectric constant of this solvent.

Table 1.2. Approximate ion-pair $pK(HB^+)$ values for cationic dihydrogen acids in CH_2Cl_2.

Dihydrogen Complex	pK of $M(\eta^2\text{-}H_2)$	Reference acid HB^+	pK of HB^{+a}
trans-$[Os(\eta^2\text{-}H_2)(Cl)(dppe)_2]PF_6$	7 [30]	$[HPMePh_2]PF_6$	6.5
trans-$[Ru(\eta^2\text{-}H_2)(Cl)(dppe)_2]PF_6$	6 [39]	$[HPEtPh_2]PF_6$	5
$[Os(\eta^2\text{-}H_2)(Spy)(CO)(PPh_3)_2]\ BF_4$	~ -2 [55]	$[H_3O]BF_4$	~ -1
trans-$[Os(\eta^2\text{-}H_2)(NCMe)(dppe)_2](BF_4)_2$	~ -2 [36]	$[Et_2OH]BF_4$	~ -3
trans-$[Fe(\eta^2\text{-}H_2)(CNH)(dppe)_2]\ (OTf)_2$	~ -4 [56]	$[Et_2OH]BF_4$	~ -3
trans-$[Fe(\eta^2\text{-}H_2)(CO)(dppe)_2]\ (OTf)_2$	< -5 [56]	HOTf	~ -5

[a]Estimated from the aqueous pK_a

1.3.2 Construction of an acidity scale of phosphorus-containing compounds in THF that covers 35 pK_a units

Tetrahydrofuran is potentially an excellent solvent for measuring the widest possible range of transition metal hydride and dihydrogen acid strengths. The pK_a^{THF} values can range from approx. 0 for $H(THF)_x^+$ to greater than 50 for the deprotonation of THF. Streitwieser and co-workers [57, 58] and Antipin and co-workers [59, 60] have determined free ion pK_{fi}^{THF} that range from 11 to 40 (vs fluorene at 22) for neutral hydrocarbon acids AH in THF by use of dissociation constants, $K_d(\{M^+,A^-\} \rightarrow M^+ + A^-)$, for the ion pairs $\{M^+,A^-\}$ formed by the conjugate bases as in eq 11 [58].

$$pK_{fi}^{THF}(A_2H) = pK_{fi}^{THF}(A_1H) - pK - \log(K_d(\{M^+,A_2^-\})/K_d(\{M^+,A_1^-\})) \quad (11)$$

The 1:1 ion-pair dissociation constants are determined by use of conductivity measurements or are estimated theoretically, for example, by use of the Fuoss model of ion pairs (eq 12) [61].

$$K_d = 3000\, e^b/(4\pi N a^3) \quad (12)$$

where $b = -e^2/(a\varepsilon kT)$, $N = 6.02\times10^{23}$ mol^{-1}; a = inter-ion distance = $r^+ + r^-$ in Å; $e = 4.80\times10^{-10}$ esu; ε = dielectric constant; $k = 1.38\times10^{-16}$ erg/deg; T in K. We find that eq 12 reproduces literature values of K_d^{THF} within an order of magnitude when used with values of r^+ and r^- derived from appropriate crystal structures.

A difference from previous studies of metal hydride complexes is that we have created a continuous ladder of overlapping acid/base equilibria. This involved finding a series of phosphorus-containing compounds with pK_a that differ by less than 2 units, the limit of accurate determination of equilibrium constants K. We have determined the equilibrium constants, K, for cationic acid- neutral base reactions (eq 13) or neutral acid-anionic base reactions (eq 14) in THF or THF-d_8 by use of quantitative $^{31}P\{gated\ ^1H\}$ and ^1H NMR.

$$\{MH_2L_n^+,Y^-\} + B \rightleftharpoons MHL_n + \{HB^+,Y^-\} \quad (13)$$

where B= phosphine, amine, metal hydride, Y^- = BF_4^-, BPh_4^-, BAr'_4^-.

$$MHL_n + \{Q^+,A^-\} \rightleftharpoons \{Q^+,ML_n^-\} + AH \quad (14)$$

where A^- = organic or organometallic anion, Q^+ = $[K(18\text{-crown-6})]^+$ or $[K(2,2,2\text{-crypt})]^+$.

We define pK_α^{THF} according to eq 15. It is roughly corrected for ion-pair effects via the ΔpK_d term of eq 16 that makes use of the estimated inter-ion pair distances a for the two salts MA_1 and MA_2 from crystallographic studies and the Fuoss eq 12. The pK_α^{THF} should be approximately equal to absolute pK_a^{THF}, in part because of our choice of anchor for the scale, $[HPCy_3]BPh_4$, with $pK_\alpha^{THF} = pK_a^{aq} = 9.7$. This is shown for picric acid where the absolute pK_a^{THF} is 11.6 [62] while pK_α^{THF} is determined to be 10±2 (Table 1.3). The agreement will improve as actual K_d^{THF} values are determined by use of conductivity measurements.

$$pK_\alpha^{THF}(A_2H) = pK_\alpha^{THF}(A_1H) - pK + \Delta pK_d \quad (15)$$

$$\Delta pK_d = -33.5(1/a_{MA_1} - 1/a_{MA_2}) + 3\log(a_{MA_2}/a_{MA_1}) \quad (16)$$

Some $pK_\alpha^{THF}(HB^+)$ and $pK_\alpha^{THF}(HA)$ values that have been determined in our work are listed in Table 1.3. In some cases different counterions were used (spe-

cifically the anions BPh_4^- vs BAr'_4^-, Ar'= C_6H_3-3,5-$(CF_3)_2$ and cations $[K(Q)]^+$, Q = 18-crown-6 vs Z = 2,2,2-crypt, to show that pK_α^{THF} was corrected properly for ion-pairing effects). While equilibria between the phosphonium salts were fast, equilibria between complexes with several large ligands and high pK_α^{THF} such as $[Re(H)_4L_4]^+$ and $[Os(H)_3L_4]^+$ were very slow (12 h to 3 days). Steric effects are very important in such proton transfer reactions.

A novel feature of this work is the linking of cationic and neutral hydride scales. This was done by first finding a continuous set of overlapping equilibria starting from $HPCy_3^+$ with $pK_\alpha^{THF}(HB^+)$= 9.7 and ending with the least acidic cationic compound $ReH_2(PMe_3)_5^+$ with $pK_\alpha^{THF}(HB^+)$= 24±1. The error in the last value results from the fact that the errors in $pK_\alpha^{THF}(HB^+)$ that are determined as in eq 15 tend to accumulate as we move up the ladder to compounds less acidic than the anchor compound, $HPCy_3^+$.

Then the linking equilibrium between $\{ReH_2(PMe_3)_5^+,BPh_4^-\}$ and $ReH_7(PPh_2C_6H_4F)_2$ was discovered (eq 17). In order to calculate the $pK_\alpha^{THF}(ReH_7(PPh_2C_6H_4F)_2)$ from $pK_\alpha^{THF}(ReH_2(PMe_3)_5^+)$, three K_d values had to be estimated for the three salts in eq 17 by use of the Fuoss equation 12. This provides $pK_\alpha^{THF}(HA)$= 28±3 for $ReH_7(PPh_2C_6H_4F)_2$. Then a continuously linked set of neutral acids with pK_α^{THF} between 28 and 41±4 ($ReH_7(PCy_3)_2$) could be established by use of the equilibrium method represented by eq 14.

$$\{ReH_2(PMe_3)_5^+,BPh_4^-\} + \{K(18\text{-crown-6})^+,ReH_6(PPh_2C_6H_4F)_2^-\} \rightleftharpoons ReH(PMe_3)_5 + ReH_7(PPh_2C_6H_4F)_2 + \{K(18\text{-crown-6})^+,BPh_4^-\} \quad (17)$$

Other links between cationic and neutral compounds were discovered, of the type represented by eq 18:

$$B + HA \rightleftharpoons HB^+A^- \quad (18)$$

For example the reaction between $CH_2(CN)_2$ ($pK_\alpha^{THF}(HA)$ 24±2) and $ReH_3(PMe_2Ph)_4$ gives an equilibrium with $\{ReH_4(PMe_2Ph)_4^+,CH(CN)_2^-\}$, ($pK_\alpha^{THF}(BH^+)$ 20±1).

$$CH_2(CN)_2 + ReH_3(PMe_2Ph)_4 \rightleftharpoons \{ReH_4(PMe_2Ph)_4^+,CH(CN)_2^-\} \quad (19)$$

The reverse eq between $\{K(crypt)^+,CH(CN)_2^-\}$ and $\{ReH_4(PMe_2Ph)_4^+,BPh_4^-\}$ also established the $pK_\alpha^{THF}(HA)$ of $CH_2(CN)_2$ to be 24±2. The pK_a^{DMSO} ($CH_2(CN)_2$) of 11.1 has been reported. Picric acid ($pK_\alpha^{THF}(HA)$ 10±2) does not protonate PPh_3 ($pK_\alpha^{THF}(BH^+)$ ~ 3) while it does completely protonate $PEtPh_2$ ($pK_\alpha^{THF}(BH^+)$ = 5.3) to give $\{HPEtPh_2^+,OC_6H_2(NO_2)_3^-\}$. This is a useful result because pK_a^{DMSO}(picric) = 0.0±0.5 and pK_a^{THF}(picric) = 11.6 have already been reported. Therefore an equation that relates the DMSO and THF scales can be derived (see Section 1.3.2.1). $MoH(C_5H_5)(CO)_3$ ($pK_\alpha^{THF}(HA)$= 17±1) forms a

clean equilibrium by reacting with $OsH_2(PMePh_2)_4$ to give {$OsH_3(PMePh_2)_4$, $Mo(C_5H_5)(CO)_3$} ($pK_\alpha^{THF}(BH^+)$ = 12.4). The $MoH(C_5H_5)(CO)_3$ compound has a pK_a^{MeCN} = 13.9. This helps to relate the $pK_\alpha^{THF}(BH^+)$ scale with the pK_a^{MeCN} scale of hydridocarbonyl complexes determined by Norton and co-workers.

Table 1.3. Ladder of selected $pK_\alpha^{THF}(HB^+)$ values, mainly for phosphorus-containing acids[a]

Acid	Base	Δ	pK_α^{THF}
$IrH_5(P^iPr_3)_2$	$[cis\text{-}IrH_4(P^iPr_3)_2]^-$	7/6	≥43
$ReH_7(PCy_3)_2$	$[ReH_6(PCy_3)_2]^-$	9/8	41±4
Ph_2NH	$[Ph_2N]^-$	3/2	41±4
$RuH_2(\eta^2\text{-}H_2)_2(P^iPr_3)_2$	$[RuH_5(P^iPr_3)_2]^-$	6/7	39±4
$RuH_2(\eta^2\text{-}H_2)(CO)(P^iPr_3)_2$	$[RuH_3(CO)(P^iPr_3)_2]^-$	6/6	38±4
$Re(H)_4(NO)(P^iPr_3)_2$	$[ReH_3(NO)(P^iPr_3)_2]^-$	7/6	38±4
$HPPh_2$	$[PPh_2]^-$	3/2	38±4
$Os(\eta^2\text{-}H_2)(H)_2(CO)(P^iPr_3)_2$	$[OsH_3(CO)(P^iPr_3)_2]^-$	6/6	36±4
$RuH_2(\eta^2\text{-}H_2)(PPh_3)_3$	$[RuH_3(PPh_3)_3]^-$	6/6	36±4
$OsH_6(P^iPr_3)_2$	$[OsH_5(P^iPr_3)_2]^-$	8/7	35±4
$P(O)(OEt)_2PhNH$	$[P(O)(OEt)_2PhN]^-$	2/1	32±4
$Fe(C_5Me_5)(CO)_2H$	$[Fe(C_5Me_5)(CO)_2]^-$	6/5	31±4
$ReH_7(PPh_3)_2$	$[ReH_6(PPh_3)_2]^-$	9/8	30±3
$ReH_7(PPh_2C_6H_4F)_2$	$[ReH_6(PPh_2C_6H_4F)_2]^-$	9/8	28±3
$CH_2(CN)_2$	$[CH(CN)_2]^-$	4/3	24±2
$MoH(C_5H_5)(CO)_3$	$[Mo(C_5H_5)(CO)_3]^-$	7/6	17±1
$2,4,6\text{-}C_6H_2(NO_2)_3OH$	$[2,4,6\text{-}C_6H_2(NO_2)_3O]^-$	2/1	10±2
$[ReH_2(PMe_3)_5]^+$	$ReH(PMe_3)_5$	7/6	24.2
$[ReH_4(PMe_3)_4]^+$	$ReH_3(PMe_3)_4$	8/7	22.9
$[ReH_4(PMe_2Ph)_4]^+$	$ReH_3(PMe_2Ph)_4$	8/7	20.0
$[OsH_3(PEt_3)_4]^+$	$OsH_2(PEt_3)_4$	7/6	18.7
$[Ru(H)_2(C_5Me_5)(PMe_3)_2]^+$	$RuH(C_5Me_5)(PMe_3)_2$	7/6	16.5
$[ReH_4(PMePh_2)_4]^+$	$ReH_3(PMePh_2)_4$	8/7	15.8
$[HNEt_3]^+$	NEt_3	4/3	12.5
$[OsH_3(PMePh_2)_4]^+$	$cis\text{-}OsH_2(PMePh_2)_4$	7/6	12.4
$trans\text{-}[Fe(\eta^2\text{-}H_2)H(dppe)_2]^+$	$cis\text{-}FeH_2(dppe)_2$	6/6	12
$[Ru(H)_2(C_5Me_5)(PPh_3)_2]^+$	$RuH(C_5Me_5)(PPh_3)_2$	7/6	10.9
$[HP^tBu_3]^+$	P^tBu_3	4/3	10.6
$[HPCy_3]^+$	PCy_3	4/3	9.7
$[Ru(\eta^2\text{-}H_2)(C_5Me_5)(dppm)]^+$	$RuH(C_5Me_5)(dppm)$	6/6	9.2
$[Ru(H)_2(C_5Me_5)(dppm)]^+$	$RuH(C_5Me_5)(dppm)$	7/6	8.9
$[HP^nBu_3]^+$	P^nBu_3	4/3	8.9
$[HP^tBu_2Ph]^+$	P^tBu_2Ph	4/3	8.0
$[Ru(\eta^2\text{-}H_2)(C_5H_5)(dppm)]^+$	$RuH(C_5H_5)(dppm)$	6/6	7.2
$[HPMePh_2]^+$	$PMePh_2$	4/3	6.4
$[HPEtPh_2]^+$	$PEtPh_2$	4/3	5.3

[a]Abbreviations: $PPh_2CH_2PPh_2$ (dppm), $PPh_2CH_2CH_2PPh_2$ (dppe), Δ= change in coordination number

1.3.2.1 Equations linking other acidity scales

A significant observation is that, when pK_a^{DMSO} is plotted against pK_α^{THF} for four cationic acids (HB^+) and four neutral acids (HA) (examples shown in Figure 2), there are separate correlation lines (eq 20, 21).

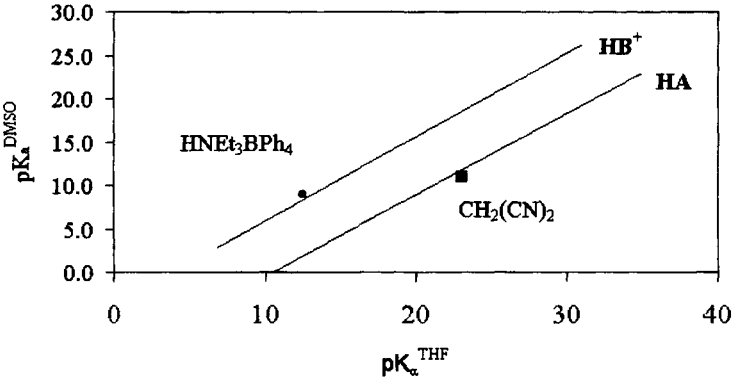

Figure 2. Correlation between scales of acids in dimethylsulfoxide versus tetrahydrofuran. Examples of acids are indicated.

$$pK_a^{DMSO} = 0.95\ pK_\alpha^{THF}(HB^+) - 3.0 \quad (20)$$

$$pK_a^{DMSO} = 0.85\ pK_\alpha^{THF}(HA) - 9.6 \quad (21)$$

These equations 20 and 21 can be used to convert the pK_a^{DMSO} of Bordwell and $pK_{fi}^{THF}(HA) \sim pK_a^{DMSO}$ of Streitweiser of over a thousand organic acids to the pK_α^{THF} scale, and therefore allow the prediction of many acid/base reactions between organic compounds and metal hydrides. Similarly there are separate pK_a^{MeCN}/ pK_α^{THF} correlations (eq 22, 23, Figure 3):

$$pK_a^{MeCN} = 1.13\ pK_\alpha^{THF}(HB^+) + 3.7 \quad (22)$$

$$pK_a^{MeCN} = 0.81\ pK_\alpha^{THF}(HA) + 1.0 \quad (23)$$

Eq 22 allows the approximate placement on our scale of 8 cationic nickel group hydrides $[MH(diphosphine)_2]^+$ where pK_a^{MeCN} were determined by DuBois and co-workers [46]. Eq 24 provides a link to relate the pK_a^{MeCN} of the twenty neutral carbonylhydride complexes studied by Norton and co-workers to the THF scale [42, 45].

There are also relatively poor correlations with the aqueous scale (eq 24, R^2 = 0.89) and Angelici's $-\Delta H_{HM}^{DCE}(HB^+OTf^-)$ scale (DCE= dichloroethane, eq 25, R^2 = 0.94):

$$pK_a^{aq} = 1.0\ pK_\alpha^{THF}(HB^+) - 0.7 \quad (24)$$

$$-\Delta H_{HM}^{DCE}(HB^+OTf^-) = 1.8\ pK_\alpha^{THF}(HB^+BPh_4^-) + 16.3 \quad (25)$$

Therefore the 50 cationic hydrides examined by Angelici can be placed, approximately on our scale via eq 25. Therefore it appears that a lot of acid-base data found in the literature can be unified by use of the pK_α^{THF} approach.

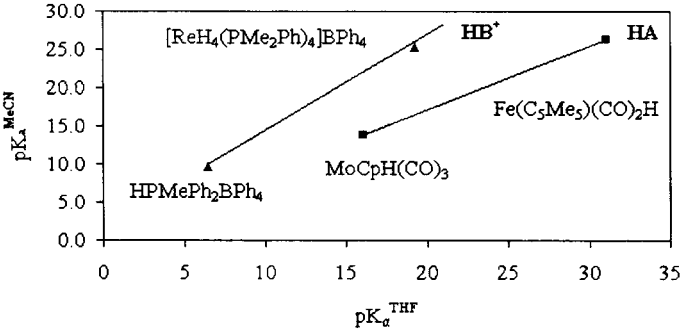

Figure 3. Correlations between scales of acids in acetonitrile versus tetrahydrofuran. Examples of acids are indicated.

1.3.2.2 The important effect of the dielectric constant of the solvent on acid/ base equilibria.

THF has a low dielectric constant compared to DMSO and CH_3CN and therefore disfavors the ionization of neutral acids HA compared to cationic acids HB^+. This explains why separate lines are found for $pK_\alpha^{THF}(HA)$ and $pK_\alpha^{THF}(HB^+)$ when plotted against pK_a^{DMSO} or pK_a^{MeCN}. Values of $pK_\alpha(HA)$ and $pK_\alpha(HB^+)$ determined in other low dielectric constant solvents like CH_2Cl_2 and DCE should also have two separate correlations of this type because of ion-pairing effects.

This effect explains the initially surprising result that $RuH(C_5H_5)(dppm)$ does not react with HBr (pK_a^{DMSO} 0.9) in THF [63]. Originally it was reported that $\{HOEt_2,BF_4\}$ does react with this hydride to give $\{Ru(\eta^2\text{-}H_2)(C_5H_5)(dppm),BF_4\}$ [50]. The present work shows that the dihydrogen complex has pK_α^{THF}= 7.4 while HBr has pK_α^{THF} approx. 12 on the basis of eq 21 and so the conjugate base form, $RuH(C_5H_5)(dppm)$, will not react. On the other hand this monohydride is expected to react with $\{HOEt_2,BF_4\}$, a stronger acid with a $pK_\alpha^{THF}(HB^+)$ of 0 or less.

1.3.2.3 Effect of the substituents and the metal on pK_a of hydride complexes

Replacing Me for Ph in the complexes $[Re(H)_4(PR_3)_4]^+$ causes a decrease in pK_α: PMe_3 (22.9) > PMe_2Ph (20.0) > $PMePh_2$ (15.8) (Table 1.3). A similar result

is observed for $[Os(H)_3(PR_3)_4]^+$: PMe_3 (16.9) > PMe_2Ph (14.9) > $PMePh_2$ (12.4). In addition $[Os(H)_3(PMe_3)_4]^+$ (16.9) is more acidic than $[Os(H)_3(PEt_3)_4]^+$ (18.7). Therefore we can take advantage of well-known substituent effects to prepare a series with a predictable range of acidities.

The cationic rhenium complexes are 4-6 units less acidic than the osmium ones with the same set of phosphine ligands (e.g. $[ReH_4(PMe_2Ph)_4]^+$ with 20.0 versus $[OsH_3(PMe_2Ph)_4]^+$ with 14.9, Table 1.3). This probably reflects the greater stabilization on going from 7-coordinate $Os^{IV}(d^4)$ to six-coordinate $Os^{II}(d^6)$ compared with going from 8-coordinate $Re^{V}(d^2)$ to 7-coordinate $Re^{III}(d^4)$.

A change of substituents on $ReH_7(PR_3)_2$ results in a surprisingly large change in the acidity of the complex. Changing from PPh_3 to PCy_3 results in a 11 pK unit change (Table 1.3). While the IR spectra of the neutral acids ReH_7L_2 are comparable, there are much lower ν(Re-H) modes for the PCy_3 complex (a strong mode at 1717 cm^{-1}) compared to those of the PPh_3 complex (1884, 1853 cm^{-1}). This indicates that the destabilization of rhenium-ligand bonding in the anions is a strong determinant of the acidity of the acid form. The replacement of two L=PPh_3 by two L=PMe_3 in $[Ru(C_5Me_5)L_2(H)_2]^+$ results in a ΔpK of 5.6 (Table 1.3), a much smaller change than that observed for ReH_7L_2. We note that, in general, the conjugate base hydride has lower M-H stretching wavenumbers than the acid form for the hydride complexes examined.

1.3.2.4 Effect of the metal and the substituents on pK_a of dihydrogen complexes.

We reported previously that the pK_a of bisditertiaryphosphine dihydrogen complexes increases in the aperiodic order Fe < Os < Ru. The pK_a order Os < Ru also applies to the neutral dihydrogen complexes $M(\eta^2\text{-}H_2)(H)_2(CO)(P^iPr_3)_2$ (Table 1.3). The Os complex has an elongated H-H distance of 1.14 Å while the Ru complex has a short H-H distance of 0.88 Å according to the minimum T_1 and J_{HD} data. The ruthenium dihydrogen complexes are thought to be less acidic than corresponding osmium ones because of the stronger (shorter) H-H bond [49]. This would also explain why the dihydrogen complex $Ru(\eta^2\text{-}H_2)_2(H)_2(P^iPr_3)_2$ is less acidic than the classical hexahydride $OsH_6(P^iPr_3)_2$ (Table 1.3). The usual rule is that the 5d metal hydride is less acidic than the 4d metal hydride. For example $Os(H)_2(CO)_4$ is less acidic than $Ru(H)_2(CO)_4$ in CH_3CN by 2.1 pK units [44].

Fairly predictable effects on the change of the ancillary ligands on the acidity of the dihydrogen have been reported previously. For example replacement of the less basic diphosphine dtfpe with the more basic dppe results in an increase in pK_α^{THF} [49]. Replacing a π-acid H_2 ligand with a π-acid CO ligand in the dihydrogen complexes $Ru(\eta^2\text{-}H_2)_2(H)_2(P^iPr_3)_2$ and $Ru(\eta^2\text{-}H_2)(CO)(H)_2(P^iPr_3)_2$ results in little change in the pK_α^{THF}.

The effect of charge on pK_a is very important. A change in the ligands from $Os^{II}(\eta^2\text{-}H_2)(CO)(H)_2(P^iPr_3)_2$ to $[Os^{II}(\eta^2\text{-}H_2)(NCMe)(dppe)_2]^{2+}$ results in a change

from pK_α^{THF}=36 (Table 1.3) to pK^{CH2Cl2}= -2 (Table 1.2), respectively. The J(HD) of the corresponding η^2-H_2 compounds are similar (16 vs 21 Hz, respectively) so that the NMR and H-H distance do not reflect the chemical activation of the H_2 ligand. The conjugate base compound $[Os(H)_3(CO)(P^iPr_3)_2]^-$ is very hydridic and so its hydrides serve as excellent hydrogen bond acceptors as will be shown in Section 1.8.1. The protonic dihydrogen ligand in the dicationic osmium complex serves as a hydrogen bond donor to BF_4^- as mentioned in section 1.4.

1.3.2.5 pK_a of dihydrogen gas

Dihydrogen is less acidic than the least acidic hydride of our scale and no direct equilibrium link has been found yet by us. However Buncel and Menon in 1977 determined the constant for the equilibrium set up by the reaction of H_2 with $Q[CH(C_6H_2\text{-}2,4\text{-}Me_2)_2]$ in THF [64]. The correlation between pK_α^{THF}(HA) and pK_a^{DMSO} (eq 21) allows an estimate of the pK_α^{THF} of H_2/Q^+H^- to be about 49 on the basis of work by Buncel and Menon. This means that pK_α^{THF} is greater than 51 for the acid/base pair $Ir(C_5Me_5)(H)_2(PMe_3)/Ir(C_5Me_5)(H)(Li)(PMe_3)$. This lithium salt deprotonates H_2(g) and DMSO but not toluene in THF [65].

The bond dissociation energy of H_2(g), BDE{H_2(g)/(2H·)}, is 103.25 kcal/mol and the redox potential $E_{1/2}\{(H\cdot+e^-)/H^-\}$ is -1.1 V vs $Fe(C_5H_5)_2^+/Fe(C_5H_5)_2$ in MeCN [66]. This allows the calculation of the $pK_a^{MeCN}\{H_2(g)/(H^-+H^+)\}$ to be 51 on the CH_3CN scale. Conversion equation 24 provides an extrapolated pK_α^{THF} value of 60. Therefore coordination of dihydrogen to a metal center can have a huge acidifying effect as noted by the pK_α^{THF} values of the dihydrogen complexes in the range from 7 to 39 (Table 1.3).

1.4 DIHYDROGEN COMPLEXES WHERE DIHYDROGEN ACTS AS A NON-CLASSICAL HYDROGEN BOND DONOR

Two single crystal neutron diffraction structures reported by other groups have short dihydrogen-(anionic ligand) contacts that can be interpreted as this type of non-classical hydrogen bond. The "cis-effect" between an η^2-H_2 ligand and hydride ligand with $H_2\cdots H$ 1.86(1) Å in $Fe(\eta^2\text{-}H_2)(H)_2(PEtPh_2)_3$ identified by Van Der Sluys et al. in 1990 [67] illustrates both the ability of η^2-H_2 to act as a H-bond donor and hydride, as an H-bond acceptor (Figure 4) [68]. There is non-classical $H_2\cdots H$ and $H_2\cdots Cl$ hydrogen bonding in the iridium complex $Ir(\eta^2\text{-}H_2)H(Cl)_2(P^iPr_3)_2$ [67] as was discussed above.

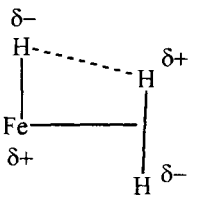

Figure 4. Dihydrogen acting as a hydrogen bond donor and hydride acting as a hydrogen bond acceptor in $Fe(\eta^2\text{-}H_2)(H)_2(PEtPh_2)_3$.

We have found evidence that dihydrogen can serve as an effective hydrogen bond donor in cationic and especially dicationic complexes. In this case the bonding is supported by ion-pairing. We have shown above that these complexes are strong acids. The dihydrogen ligand has protonic character because it loses electron density in its 3-center-2 electron $\sigma(H_2\text{-}M)$ bond. There is little or no $d\pi\text{–}\sigma^*$ backdonation to neutralize the positive charge in this case. Therefore, for example, the X-ray structure determination of the acidic complex $[Os(\eta^2\text{-}H_2)(CH_3CN)(dppe)_2](BF_4)_2$ [36] reveals that a fluorine of one of the two BF_4^- anions accepts a hydrogen bond from the H_2 with an H···F distance of about 2.4 Å which is less than the sum of the Van der Waals radii of hydrogen (1.2 Å) and fluorine (1.5 Å) (Figure 5).

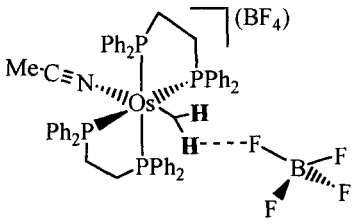

Figure 5. The protonic dihydrogen ligand in a 3-centre-two-electron bond to dicationic Os(II) acts as a hydrogen bond donor to one of the BF_4^- counter-anions.

This dihydrogen interaction with a counter-anion probably facilitates the mobility of the proton so that it can be shuttled by the hydrogen bond acceptor to other parts of the molecule. We, in a collaboration with Rigo's group, have preliminary evidence that the hydrogen bond formed between dihydrogen and a counter-anion can influence the relative stability of the tautomers in solution [69]. Triflate trans to cyanide in $Ru(dppe)_2(CN)(OSO_2CF_3)$ has a very long Ru-O bond of 2.4 Å (Scheme 1). This compound in CH_2Cl_2 at -10°C reacts with hydrogen and forms an $\eta^2\text{-}H_2$ compound that we believe to be $Ru(dppe)_2(\eta^2\text{-}H_2\cdots OSO_2CF_3)(CN)$ (Scheme 1). The ^1H chemical shift of the $\eta^2\text{-}H_2$ ligand is –7.3 ppm and the corresponding η^2-HD complex has J(HD) 32.5 Hz. At room temperature a rearrangement occurs to

the complex $Ru(dppe)_2(H)(CNH\cdots OSO_2CF_3)$ that has a classical CNH···O hydrogen bond. This compound is also the thermodynamic product of protonation of $Ru(dppe)_2H(CN)$ by $HOSO_2CF_3$. The NH···O hydrogen bond is probably stronger than the non-classical η^2-H_2···O one in the dihydrogen complex.

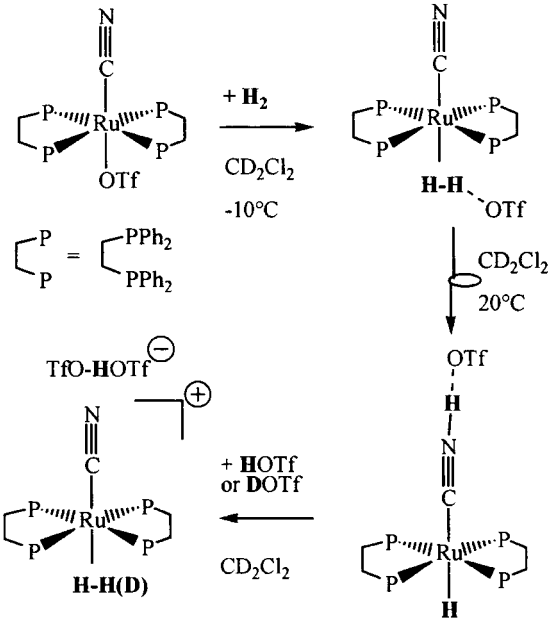

Scheme 1. Steps in the heterolytic cleavage of dihydrogen on Ru(II) starting with the complex trans-$Ru(OSO_2CF_3)(CN)(dppe)_2$.

The addition of one equivalent of triflic acid to $Ru(dppe)_2(H)(CNH\cdots OSO_2CF_3)$ gave a surprising outcome. Instead of the expected protonation of the Ru-H bond to produce $[Ru(dppe)_2(\eta^2\text{-}H_2)(CNH\cdots OSO_2CF_3)]^+$ ($CF_3SO_3^-$), addition occurs at the triflate anion to form a classical hydrogen bond in the counterion $[CF_3SO_3H\cdots OSO_2CF_3]^-$ of the new dihydrogen compound $[Ru(dppe)_2(\eta^2\text{-}H_2)(CN)]^+$ $[CF_3SO_3H\cdots OSO_2CF_3]^-$ (Scheme 1). The hydrogen bond to the CNH ligand is apparently weakened enough to cause the complex to tautomerize from the $Ru(dppe)_2(H)(CNH\cdots OSO_2CF_3)$ isomer to the $[Ru(dppe)_2(\eta^2\text{-}H_2)(CN)]^+$ $[CF_3SO_3H\cdots OSO_2CF_3]^-$ isomer. This dihydrogen complex has a chemical shift of –5.5 ppm, quite different from that (-7.3 ppm) of the complex where dihydrogen acts as a hydrogen bond donor but the η^2-HD complex $[Ru(dppe)_2(\eta^2\text{-}HD)(CN)]^+$ $[CF_3SO_3H\cdots OSO_2CF_3]^-$ has a similar J(HD) of 32.0 Hz. Therefore the non-classical H_2···O hydrogen bond appears to exert a large effect on the chemical shift but a small effect on the H-H distance.

We have demonstrated that both $[Fe](\eta^2\text{-}H_2)(CN)$ and [Fe](H)(CNH) isomers can form, depending on the ligands in the [Fe] fragment representing

$[Fe^{II}(diphosphine)_2][70]$. It seems logical that nature has also chosen low spin d^6 iron to activate dihydrogen in hydrogenase enzymes that contain $Fe(CO)_x(CN)_y(S\text{-}donor)_z$ sites [71, 72].

1.5 METAL HYDRIDE ACTING AS NON-CLASSICAL HYDROGEN BOND ACCEPTOR

In the heterolytic splitting of dihydrogen, the acidic dihydrogen complex $[M](\eta^2\text{-}H_2)$ transfers a proton to the base (eq 2-4 of the introduction). The proton can then remain associated with the hydride in a 1.7-2.0 Å contact in the ion-pair $\{[M]H\cdots HB^+\}$. This may be an *intramolecular* interaction or an *intermolecular* interaction. In the following sections, our work on *intramolecular* hydridic-protonic bonds will be reviewed first, followed by that on such *intermolecular* non-classical bonds.

There must be a delicate balance of the acid strengths of the dihydrogen complex and the hydrogen bond donor in order to have catalysis or to be able to observe structures like those of eq 2-4. Therefore it is very useful to know approximately the pK_a values of the acids $[M](\eta^2\text{-}H_2)$ and HB^+. To obtain the strongest hydridic-protonic bond, the acidity of the HB^+ donor should probably be as strong as possible and the acidity of the $[M](\eta^2\text{-}H_2)$ form should be as weak as possible so that basicity of the hydrogen bond acceptor $[M]H$ is as strong as possible. If these properties are too extreme then the loss of dihydrogen and formation of [M]-B may occur.

As illustrated by other authors of this book, hydridic-protonic interactions have the strength, IR spectral characteristics, and electronic structure of conventional hydrogen bonds.

1.6 HYDRIDE AS A HYDROGEN BOND ACCEPTOR-INTRAMOLECULAR EXAMPLES

The proposal of *intramolecular* hydridic-protonic bonding dates to 1991 in a paper by Stevens et al. where they reported that the proton on a hydroxide ligand seemed to be oriented to interact with a hydride on iridium 2.4 Å away in the complex cis-$[Ir(H)(OH)(PMe_3)_4]^+$ [73]. Although this distance is of the order of the sum of van der Waals radii of two hydrogen atoms, it shows that electrostatic interactions at this range are important. A corresponding [Ir](SH)(H) system does not show this orientation because the Ir-S bond is longer than the Ir-O bond and the hydrogens cannot get close enough together. As well, S is less electronegative than O so that the hydrogen on S is not as protonic.

Independently in 1993-1994, our group [74] and Crabtree's group [75] identified a much shorter, 1.7-1.8 Å hydridic-protonic bond or "dihydrogen bond" [76]

that forms between ligands in iridium complexes. Our group found short IrH···HN bonds when we were trying to observe proton transfer from η^2-H_2 to a basic site on a ligand. For example the use of mercaptoquinoline (quSH) allowed the observation of the first equilibrium between hydridothiol and (η^2-dihydrogen)thiolato tautomers in the $[Os(H)(quSH)(CO)(PPh_3)_2]BF_4$/$[Os(\eta^2\text{-}H_2)(quS)(CO)(PPh_3)_2]BF_4$ system [77]. When we investigated the use of mercaptopyridine in hydrido complexes of Ir(III) we found several compounds where the protonated nitrogen of the pyridinethione ligand was hydrogen-bonded to the hydride in a HIrSCNH six-membered ring. We found the first evidence [74] that these intramolecular hydrogen bonds were involved in the heterolytic splitting of dihydrogen (eq 2-4 of the introduction) by observing deuteration of the IrH···HN bonds in $[Ir(H\cdots HpyS\text{-}\eta^1)_2(PCy_3)_2]BF_4$ (Figure 6).

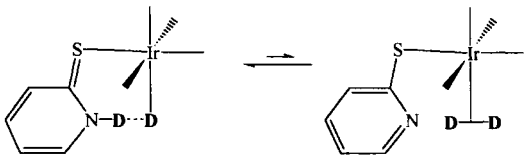

Figure 6. The existence of an equilibrium between $[Ir(D\cdots DpyS\text{-}\eta^1)(H\cdots HpyS\text{-}\eta^1)(PCy_3)_2]BF_4$ and the unobserved η^2-dideuterium (or η^2-dihydrogen) complex $[Ir(\eta^2\text{-}D_2)(\eta^1\text{-}Spy)(H\cdots HpyS\text{-}\eta^1)(PCy_3)_2]BF_4$ is proposed to explain the deuteration by D_2(g) of hydridic-protonic bonds in the complex $[Ir(H\cdots HpyS\text{-}\eta^1)_2(PCy_3)_2]BF_4$

Since that time there have been many reports of *intramolecular* hydridic-protonic bonds [78-86]. Recently an intermediate with an intramolecular RuH···HN interaction has been implicated in the catalytic asymmetric reduction of ketones [87] and another, in the reduction of CO_2 to formic acid [83]. In the last process, the RuH···HN bond is proposed to form via the heterolytic splitting of dihydrogen (see Scheme 4, Section 1.9).

1.6.1 Pyridinethione-iridium tricyclohexylphosphine hydride systems and related systems

1.6.1.1 Synthesis and X-ray structure determination

A good route to the pyridinethione system is the reaction of $Ir(H)_5(PCy_3)_2$ with mercaptopyridine that is protonated with HBF_4 ($HSpyH^+BF_4^-$) (Scheme 2) [68, 74]. First the octahedral complex $[Ir(H\cdots HpyS\text{-}\eta^1)_2(PCy_3)_2]BF_4$ is obtained. Here two hydrides serve as hydrogen bond acceptors from protons donated by cis pyridinethione ligands in the crystalline state or in CD_2Cl_2 solution. The H···H distance is calculated on the basis of T_1 data to be 1.75±0.05 Å.

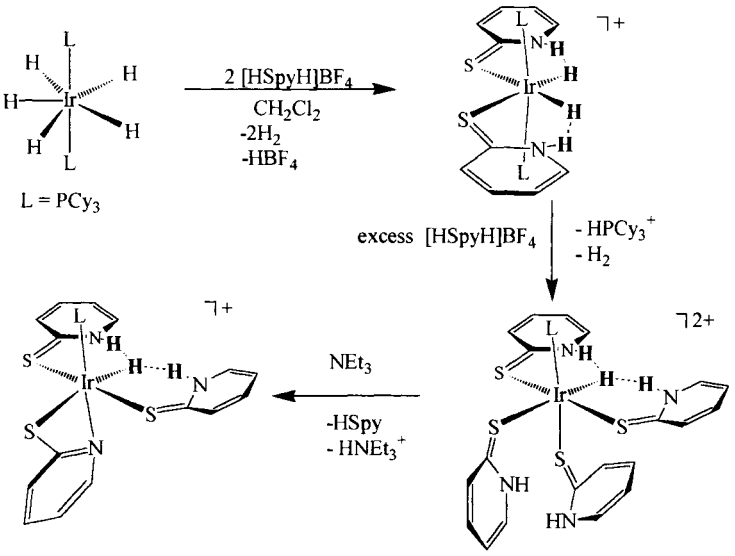

Scheme 2. The synthesis of tricyclohexylphosphine complexes of Ir(III) that contain hydridic-protonic bonds involving the pyridinethione ligand.

Additional $HSpyH^+BF_4^-$ causes the displacement of a phosphine as $HPCy_3^+BF_4^-$ and the production of [(η^1-SpyH···(HIr)···HpyS-η^1) (η^1-SpyH···$FBF_3)_2(PCy_3)$] [68]The subsequent addition of the base NEt^3 resulted in the elimination of HSpy to give [(η^1-SpyH···(HIr)···HpyS-η^1)(η^2-Spy) (PCy_3)]BF_4. [68]. These are unique compounds that contain, in the solid state and in CD_2Cl_2 solution, one hydride that accepts non-classical hydrogen bonds from two NH groups at 1.8 to 1.9 Å in ten-membered bicyclic rings S-C-N-H···H(Ir)···H-N-C-S. This is a very stable configuration. The addition of the strong hydrogen bond acceptor triphenylphosphine oxide fails to disrupt this non-classical hydrogen bonding network.

Analogous 2-thiazolidinethione (SthH) and benzothiazolethione (SbtH) complexes have been prepared [78]. The complexes $[Ir(H\cdots HthS\text{-}\eta^1)_2(PCy_3)_2]BF_4$ and $[Ir(H\cdots HbtS\text{-}\eta^1)_2(PCy_3)_2]BF_4$ have similar structures and chemical reactivity to the pyridinethione derivative described above. The reaction of the complex $[Ir(H)_2(PCy_3)_2(acetone)_2]BF_4$ with an excess of SthH or SbtH in the presence of two equiv. of HBF_4 gives the complexes [(η^1-SthH···(HIr)···HthS-η^1) (η^1-SthH···$FBF_3)_2(PCy_3)$] and [(η^1-SbtH···(HIr)···HbtS-η^1)(η^1-SbtH···$FBF_3)_2$ (PCy_3)]. These compounds have an intramolecular NH···H(Ir)···HN interaction like the SpyH complex described above with H···H distances of about 2.0 Å in both the crystalline solid as determined by X-ray diffraction and in a CD_2Cl_2 solution as determined by the T_1 method. The X-ray structure of the SthH complex reveals a beautiful network of non-classical NH···H(Ir)···HN and classical NH···F···HN hydrogen bonds involving the IrH, two SthH and one FBF_3^- counter-ion (Figure 7).

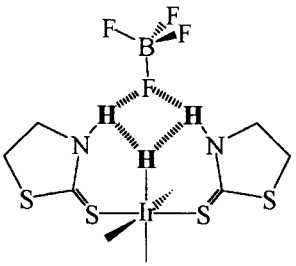

Figure 7. A network of non-classical and classical hydrogen bonds.

1.6.1.2 IR and NMR of IrH···HN bonds and comparison with classical N···HN hydrogen bonds

There are similarities between IrH···HN bonds and classical $R_3N···HNR_3^+$ bonds. It appears that the strength of the hydrogen bonds is similar: 10 to 20 kJ/mol. In a typical hydrogen bond the ν(NH) is decreased in wavenumbers relative to the stretch of the non-hydrogen-bonded acid and there is a broadening and increase in intensity of the peak. The magnitude of the reduction of ν(NH) in the hydridic-protonic bond is comparable to the classical system 100-150 cm^{-1}. In the ^1H NMR spectrum the chemical shift of the proton on nitrogen is shifted downfield. We measure the H···H distance to be about 1.8 Å by X-ray diffraction. The T_1(min) values of the hydride and the proton on nitrogen can also be used to calculate an accurate distance, also of this magnitude. NOE measurements also point to the short distance between the proton and hydride.

1.6.1.3 Calculation of H···H distance from T_1(min)

Both the hydridic and protonic T_1 from ^1H NMR can be used to calculate the MH···HN distance. The hydrogen-bonded pyridinium proton of $[Ir(H···HpyS-\eta^1)_2(PCy_3)_2]BF_4$ in CD_2Cl_2 (see Scheme 2) appears at 12.2 ppm as a broad singlet with a short minimum T_1 of 0.178 s (relaxation rate 5.6 s^{-1}) at 400 MHz, 233 K. This proton is near to only two dipolar nuclei: the ^{14}N nucleus at about 1.0 Å (relaxation rate contribution of about 2.5 s^{-1}) and the hydride which must therefore be at 1.77±0.05 Å (relaxation rate contribution of 3.1 s^{-1}) [74]. Similarly the hydride resonance centered at -18.3 ppm is a broad triplet with a minimum T_1 of 0.168 s at 233 K. When the total relaxation contributions (2.2 s^{-1}) of the cis hydride at about 2.4 Å and two cyclohexyl protons at about 2.2 Å are subtracted from the hydride relaxation rate (5.95 s^{-1}) the calculated hydride to HN distance is 1.72±0.05 Å. Therefore the H···H distance in the IrH···HN unit in CD_2Cl_2 is about 1.75±0.05 Å, consistent with the value of 1.75±0.05 Å obtained by placing the hydrides into the X-ray-derived structure [74]. NOE difference experiments can be used to confirm these short contacts.

1.6.1.4 H/D exchange with D_2(g)

Both the NH and IrH are deuterated rapidly when a solution of [Ir(H···HpyS-η^1)$_2$(PCy$_3$)$_2$]BF$_4$ in CD_2Cl_2 is exposed to 1 atm D_2 gas, presumably via η^2-dihydrogen intermediates as in Figure 6 in Section 1.6, above. The analogues with SthH and SbtH also show this behavior. NMR experiments show that the H···H interaction is disrupted when the complex is dissolved in THF or reacted with two equivalents of $OPPh_3$ in CD_2Cl_2; THF and $OPPh_3$ are better H-bond acceptors than the IrH units in this complex The H/D exchange reaction of D_2 with the complex is "switched off" in THF [74]. Therefore the hydridic-protonic bonding is necessary for the H/D exchange reaction in this case.

1.6.2 Pyridinethione-iridium triphenylphosphine system and the effect of the ancillary ligands on the hydridic-protonic bond strength

Some unique structural types involving hydridic-protonic bonds were observed in triphenylphosphine complexes of iridium(III) [84, 88]. The reaction of $IrH_3(PPh_3)_3$ with HBF_4 in the presence of pyridinethione affords a dihydrido complex with a single hydridic-protonic contact, [IrH(H···HpyS-η^1)(PPh$_3$)$_3$](BF$_4$) (Scheme 3).

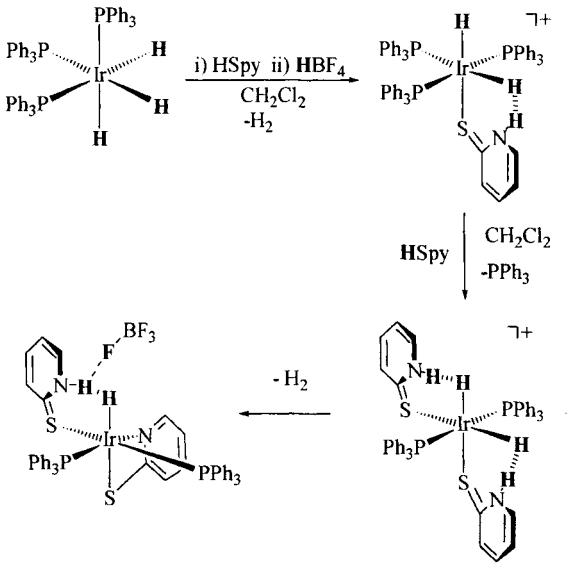

Scheme 3. The synthesis of triphenylphosphine complexes of Ir(III) that contain hydridic-protonic bonds involving the pyridinethione ligand.

The hydridic-protonic bond is weak in this complex as judged by the Ir-N distance and $\Delta\nu$(NH) values from IR; steric crowding by the three bulky PPh_3

ligands may be a factor in this case. This compound undergoes a substitution of one PPh_3 ligand by another SpyH to produce $[Ir(H\cdots HpyS\text{-}\eta^1)_2(PPh_3)_2](BF_4)$, the analogue of the PCy_3 derivative described above in Section 1.6.1.1. The X-ray and IR data suggest that the PPh_3 derivative has longer protonic-hydridic contacts than the PCy_3 derivative. Apparently the more electon-donating PCy_3 ancillary ligand increases the hydridic character and enhances the H···H bond strength relative to the PPh_3 derivative. $[Ir(H\cdots HpyS\text{-}\eta^1)_2(PPh_3)_2](BF_4)$ slowly eliminates dihydrogen to form the monohydrido complex $[IrH(\eta^1\text{-SpyH})(\eta^2\text{-Spy})(PPh_3)_2](BF_4)$. The latter can also be prepared by reacting $Ir(H)_2(\eta^2\text{-Spy})(PPh_3)_2$ with HSpy·HBF_4. This monohydride has a unique bifurcated hydrogen bonding interaction involving Ir-H···H(N)···F-B atoms with the distances of 2.0(1) Å for the H···H unit and of 2.0(1) Å for the F···H unit in the crystalline state. In solution the N-H···H-Ir interaction is maintained according to ^1H T_1(min) and NOE measurements.

1.6.3 Intramolecular MH···HN systems with ring sizes other than six

The intramolecular protonic-hydridic bonds discussed so far are found in 6-member HIrSCNH rings. There are many examples of such 6-member rings reported by others including HIrNCNH [79, 82, 89], HIrNCOH [4, 75, 89, 90], and HRuPCNH [85].

We have attempted to observe rings of size 4 and 5 that are held together by these non-classical hydrogen bonds without success. For example the complexes $[Ir(H)_2(PCy_3)_2(L)_2]BF_4$ with L = NH_3 (potentially a four member HIrNH ring) and L = NH_2NH_2 (potentially a four member HIrNH or five member HIrNNH ring) do not form protonic-hydridic interactions despite the fact that several thione ligands produce six-member rings as discussed above [78]. Similarly $RuHCl(CO)(L)(PPr^i_3)_2$ (L = NH_3, NH_2NH_2) and $IrCl_2(L)(H)(PCy_3)_2$ (L = NH_3, NH_2NH_2, $NH_2(CH_2)_3NH_2$) do not form such hydrogen bonds, although this is not unexpected for the iridium systems which tend to have the amine trans to the hydride [91]. Instead weak M-H···H-C Van der Waals contacts with distances of 2.0 - 2.2 Å are detected in the solid state by X-ray analysis and in solution by NMR T_1 measurements and NOE techniques.

Related intramolecular rings of different sizes have been reported by other groups. Four member rings with relatively long H···H distances have been reported for an HIrOH system [73] as discussed above and for an HOsPH system [92]. A distance of 2.3 Å for an HRuNH interaction was reported by Noyori et coworkers [87]. The H···H distances in HMXH rings are quite long because they are determined by the length of the M-X bond which is almost always greater than 2 Å. A five member HOsOsNH ring has been observed in a triosmium cluster [81]. There are a few examples of larger rings including 7-member HIrNCCOH [93], HIrPCCOH [94], HRuCCCNH [83] and 8-member HRuCCCCNH rings (see Scheme 4, Section 1.9) [83, 86].

1.7 HYDRIDE AS A HYDROGEN BOND ACCEPTOR-INTERMOLECULAR EXAMPLES

The observation of *intermolecular* hydridic-protonic bonds in complexes in solution is more challenging because often these energies are of the same magnitude as the 5 kcal/mol energy penalty for working against entropy at room temperature (eq. 26, $\Delta S<0$). Proton transfer and subsequent loss of H_2 to form M-X is a common reaction that must be avoided to observe eq 26.

$$M\text{-}H + HX \rightleftharpoons M\text{-}H\cdots HX \qquad (26)$$

Crabtree's group first succeeded in observing such *intermolecular* interactions in the solid state between the good hydrogen bond donor, indole, and hydridic hydrogen bond acceptors in the rhenium complex $ReH_5(PPh_3)_3$, with ReH···HN 1.734(8) and 2.212(9) Å [76, 95-97]. Koetzle's and Crabtree's group also showed that this is a general phenomenon that also applies to main-group hydrides like boranes [98, 99]. The existence of equilibria such as eq. 26 was identified in solution by Berke's group by use of hydridic tungsten hydrides and acidic alcohols [100]. Chaudret's [101, 102] and Caulton's groups [103] have taken advantage of the sensitivity of quantum mechanical exchange coupling between hydrides in ruthenium and osmium complexes to second sphere interactions to detect changes to equilibrium 26 in solution. Epstein's group has used low temperature IR spectroscopy to detect the species of equilibrium 26 for several hydride complexes [104-106]. These details are provided in other chapters of this book.

1.8 HYDRIDE AS A HYDROGEN BOND ACCEPTOR IN ION-PAIRS

We were interested in making catalysts that might be activated by intermolecular MH···HN bonds. We thought that the interaction could be enhanced by utilizing anionic hydrides as the hydrogen bond acceptors, counter-cations as the H-bond donors and solvents with low dielectric constants like THF in order to promote ion-pairing.

1.8.1 Use of the (aza-crown)potassium cation as a hydrogen-bond donor

We first showed that hydridic-protonic bonds between ion pairs of anionic hydrides and potassium(aza-crown) cations that have one N-H hydrogen bond donor can be readily observed in solution and the solid state [16, 17]. The anionic

hydrides $[M(H)_3(CO)(P^iPr_3)_2]^-$, M = Ru, Os and $[Re(H)_3(NO)(P^iPr_3)_2]^-$ crystallize with cations $[QNH]^+$ (Table 1.1) and assemble into chains held together with $K^+\cdots OCM$ electrostatic interactions and MH···HN hydridic-protonic bonds with H···H distances estimated to be 1.8 Å (Figure 8).

The N-H absorption is broad for a Nujol mull of $[K(QNH)]^+[M(H)_3(CO)(P^iPr_3)_2]^-$, and is located at 3167 cm^{-1} for M=Os and 3147 cm^{-1} for M=Ru. There is a definite shift and broadening because of hydrogen bonding compared to the sharp N-H absorption of $[K(aza\text{-}crown)]^+BPh_4^-$ at 3283 cm^{-1} where there is no hydrogen bonding. The Ru compound is more basic than the osmium and has the greater reduction in N-H wavenumber. The pK_α^{THF} of the acid form $Ru(\eta^2\text{-}H_2)(H)_2(CO)(P^iPr_3)_2$ is 38 compared to 36 for $Os(\eta^2\text{-}H_2)(H)_2(CO)(P^iPr_3)_2$ (Table 1.3). Therefore the more hydridic hydride is the better hydrogen-bond acceptor.

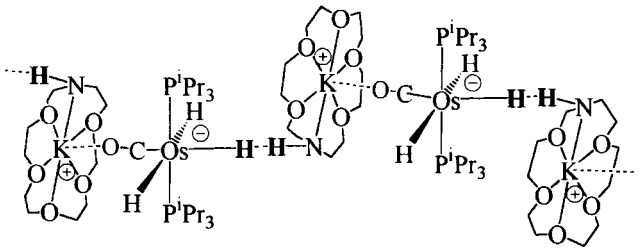

Figure 8. The chain structure of $[K(QNH)][Os(H)_3(CO)(P^iPr_3)_2]$ as revealed by a single crystal X-ray diffraction study.

Similarly the N-H wavenumber for a THF solution of $[K(QNH)]^+[MH_5(P^iPr_3)_2]^-$ is lower for M=Ru (3154 cm^{-1}) than for M=Os (3168 cm^{-1}) and much lower and broader than for $[K(QNH)]^+[BPh_4]^-$ in THF (3296 cm^{-1}) [11]. Again the more basic Ru hydride with the less acidic conjugate acid $(RuH_2(\eta^2\text{-}H_2)_2(P^iPr_3)_2$ with pK_α^{THF} 39 is the better hydrogen bond donor than the Os hydride with the more acidic conjugate acid $(OsH_6(P^iPr_3)_2$ with pK_α^{THF} 35). The MH···HN distances in ion-pairs in solution have been determined by NMR (T_1 and NOE measurements) to be about 1.8 Å while the X-ray structures provide distances of about 1.7 Å. The crystalline structures of these pentahydride complexes are unusual because alternating anions receive hydrogen bonds from the NH (as 1.7 Å NH···HM bonds) and CH on the 5 position of the azacrown (as a 2.2 Å CH···HM bond). This results in a chain structure containing neighbouring NH···HMH···HN and CH···HMH···HC units bridged by the azacrowns (Figure 9).

As noted in Table 1.1, complexes $[K(QNH)]^+$ $[ReH_6(PR_3)_2]^-$ and $[K(QNH)]^+$ $[IrH_4(PR_3)_2]^-$ have also been prepared and studied. Their properties will be described elsewhere.

The M-H absorption in the IR spectrum associated with these inter-ion pair hydrogen bonds $[K(QNH)]^+\cdots HM^-$, is shifted by about 10 cm^{-1} to lower wave-

number and is more intense than that of the corresponding $[K(Q)]^+$ HM^- complex, showing that the hydrogen-bond acceptor is also affected by the formation of this hydrogen bond. Also observed in the ^1H NMR spectra are downfield shifts in the NH resonance and upfield shifts in the hydride resonance, typical behavior for such hydridic-protonic bonds.

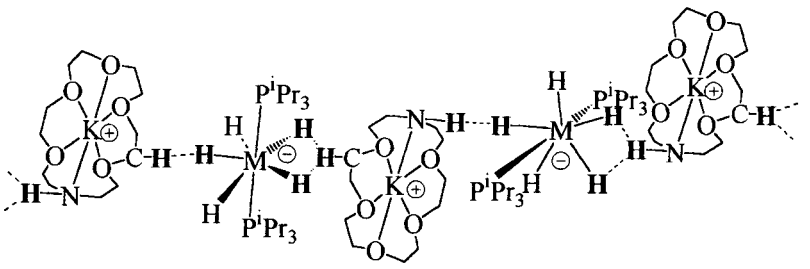

Figure 9. The chain structure of $[K(QNH)(THF)][M(H)_5(P^iPr_3)_2]$, M=Ru, Os, as revealed by a single crystal X-ray diffraction study. The hydride positions were disordered in this structure. A THF is coordinated to each potassium but this is not shown in the Figure.

1.8.2 Use of the (diaza-crown)potassium cation as a dual hydrogen-bond donor for assembling chain structures

The polyhydride anions that we have made have hydrogen-accepting hydrides pointed in opposite directions and so the introduction of cations such as [K(1,10–diaza–18–crown–6)]$^+$ ($[K(HNQNH)]^+$) with divergent hydrogen bond donor N-H groups should encourage the self-assembly of chain structures. Indeed this is the case for $[K(HNQNH)]^+[IrH_4(P^iPr_3)_2]^-$ [17], $[K(HNQNH)]^+[MH_5(P^iPr_3)_2]^-$, M= Ru, Os [11], and $[K(HNQNH)]^+[ReH_6(PR_3)_2]^-$, R=Me, ^{i}Pr [18]. In one rhenium compound with R=Ph, a ring structure was obtained [18].

1.8.2.1 The $[K(HNQNH)]^+[IrH_4(P^iPr_3)_2]^-$ system

The X-ray structure of $[K(HNQNH)]^+[IrH_4(P^iPr_3)_2]^-$ reveals that the NH groups are pointed directly at the hydrides in an almost linear IrH···HN interaction with d(H···H) 1.8 Å [17] in the chain structure shown in Figure 10. This is the distance calculated after the Ir-H and N-H bonds distances as determined by X-ray crystallography are lengthened to values commonly observed in neutron structures. This geometry contrasts with others observed where the MH···H angle is bent. It was postulated that the bent geometry is favorable because the hydrogen bond donor can point its protonic hydrogen at the electron density in the M-H bond. Our structure suggests that this bending may not be required and that the bond is mainly electrostatic in character. This iridium anion is the most basic of

the anionic hydrides that we have prepared as indicated by the pK_α^{THF} of the $IrH_5(P^iPr_3)_2$ form (Table 1.3). It shows the largest reduction compared to the other $[K(HNQNH)]^+$ salts of Table 1.1 in N-H wavenumber, 150 cm^{-1}, from that of the free NH of $[K(diazacrown)]^+BPh_4^-$ at approx. 3280 cm^{-1} (Nujol mulls).

The corresponding $[K(Q)]^+$ salt with no hydrogen bond donors has a completely different structure. $[K(Q)]^+$ $[IrH_4(P^iPr_3)_2]^-$ contains an anion with cis phosphines. A remarkable result of introducing the diazacrown is that the iridium complex is forced to be in the usually unfavorable trans-geometry because of the imposition of the hydridic-protonic bonds in $[K(HNQNH)]^+$ $[IrH_4(P^iPr_3)_2]^-$. The cis isomer has only one set of unfavorable trans hydrides while the trans isomer has two. In the absence of hydrogen bonding, the cis isomer is usually the more stable despite the fact that there will be more steric repulsion between the bulky phosphine ligands.

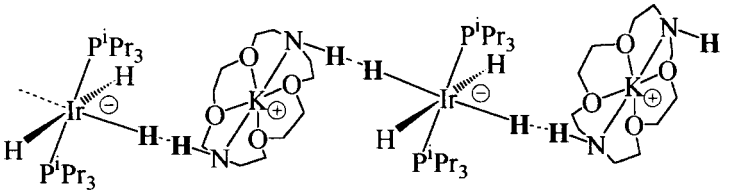

Figure 10. A chain of $[K(HNQNH)]^+$ cations and $[IrH_4(P^iPr_3)_2]^-$ anions held together by hydridic-protonic bonds.

1.8.2.2 $[K(HNQNH)]^+[MH_5(P^iPr_3)_2]^-$, M= Ru, Os, systems

The X-ray structures of these crystalline salts indicate that short intermolecular hydridic-protonic bonds between the hydrides of the anion and the NH moieties of the cation cause the self-assembly of one-dimensional chains of pentagonal bipyramidal $[MH_5(P^iPr_3)_2]^-$ anions and [K(diaza-18-crown-6)]$^+$ cations (Figure 11).

The shortest MH···HN distances are estimated to be 1.9 and 1.8 Å for M=Os and M=Ru, respectively, on the basis of NH···M distances since the positions of the hydrides were not determined because of crystallographic disorder. These distances were calculated by assigning a value of 1.0 Å to the N-H bond length

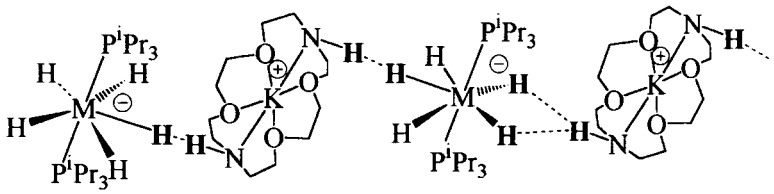

Figure 11. A chain of $[K(HNQNH)]^+$ cations and $[MH_5(P^iPr_3)_2]^-$ anions, M=Ru, Os, held together by hydridic-protonic bonds. The hydride positions were disordered in the structure.

and using the refined average Os-H and Ru-H distances of 1.56(4) and 1.58(3) Å observed for X-ray structures of $[K(Q)][MH_5(P^iPr_3)_2]$. Solution NMR and infrared spectra, and T_1, NOE and NOESY experiments demonstrate that the MH···HN interactions persist in solutions of these complexes.

As in the case of the $[K(QNH)]^+$ salts, the more basic ruthenium anion makes the stronger hydridic-protonic bonds as evidenced by the NMR and infrared spectral characteristics of the ruthenium and osmium salts.

1.8.2.3 $[K(HNQNH)]^+$ $[ReH_6(PMe_3)_2]^-$ system

The structures of the rhenium salts $[K(HNQNH)]^+$ $[ReH_6(PR_3)_2]^-$ are found to depend on the nature of the phosphine. While the P^iPr_3 system gives a zig-zag chain structure related to that of the group 8 metal salts $[K(HNQNH)]^+[MH_5(P^iPr_3)_2]^-$ of Figure 11, the smaller PMe_3 derivative gives a slightly different chain structure that accommodates cis-phosphines as indicated in Figure 12. Again a low ν(NH) at 3214 cm^{-1} signals the presence of protonic-hydridic bonding although the exact structure (whether N-H···HRe or bifurcated N-H···H(Re)···HN) will have to await a single crystal neutron diffraction study. A notable feature of this structure is that all of the rings are in a stack with the metals and hydrides in the middle and the organics lining the walls of a cylinder.

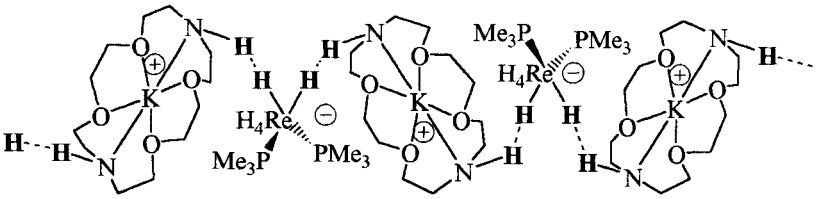

Figure 12. A chain of $[K(HNQNH)]^+$ cations and $[ReH_6(PMe_3)_2]^-$ anions held together by hydridic-protonic bonds.

1.8.2.4 H/D exchange in $[K(HNQNH)]^+$ $[RuH_5(P^iPr_3)_2]^-$

An exciting and mysterious observation is the rapid H/D exchange kinetics caused by these hydridic-protonic bonds. The complex $[K(HNQNH)]^+$

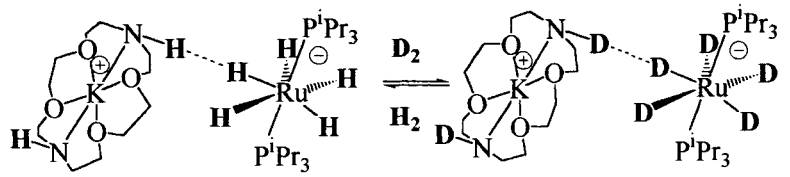

Figure 13. The deuteration of the hydridic-protonic bonds in $[K(HNQNH)]^+$ $[RuH_5(P^iPr_3)_2]^-$ in THF by reaction with D_2 (1 atm).

$[RuH_5(P^iPr_3)_2]^-$ in THF reacts with D_2(g) in less than 5 minutes to produce the isotopomer $[K(DNQND)]^+$ $[RuD_5(P^iPr_3)_2]^-$ that is completely deuterated at the N-H and RuH bonds (Fig. 13) [11]. There was no deuteration of C-H bonds under these conditions. In contrast a complex with a crown with no aza group, $[K(Q)]^+$ $[RuH_5(P^iPr_3)_2]^-$, is inert to D_2 under these conditions.

The obvious mechanism for the exchange with D_2 is proton transfer from the N-H to the Ru-H bond to produce $Ru(\eta^2\text{-}H_2)_2(H)_2(P^iPr_3)_2$ which then exchanges with D_2(g). However we find that this bis-dihydrogen complex undergoes H/D exchange with the incorporation of deuterium into the C-H bonds of the methyls of the phosphine ligands [10]. This is not observed for $[K(HNQNH)]^+$ $[RuH_5(P^iPr_3)_2]^-$. Therefore we come to the surprising conclusion that $Ru(\eta^2\text{-}H_2)_2(H)_2(P^iPr_3)_2$ is not the intermediate that explains the H/D reactivity of this ion pair compound containing a hydridic-protonic bond. The osmium analogue also shows this behavior although the H/D exchange is much slower. Further work is needed to elucidate the mechanism.

1.8.3 Other intermolecular protonic-hydridic bonds supported by ion pairing

Custelcean and Jackson have demonstrated that anionic boron hydrides can also serve as hydrogen bond acceptors to assemble novel lattices held together by hydridic-protonic bonds [107, 108]. Cations with hydrogen bond donors include *N*-[2-(6-aminopyridyl)]acetamidine and triethanolamine(sodium). The former is an NH donor while the latter is an OH donor. These scientists provided evidence for the topochemical conversion of the hydridic-protonic bonds into B-N and B-O covalent bonds, respectively, when the materials are heated and dihydrogen is driven from the H···H bonds.

1.9 CATALYSIS

Conventional soluble catalysts for the hydrogenation of olefins such as Wilkinson's catalyst, $RhCl(PPh_3)_3$, are thought to effectively cleave dihydrogen homolytically into two hydrogen atoms (via oxidative addition to hydrides and then reductive elimination) and pass these from the metal to a coordinated carbon-carbon double bond to give the saturated product. Catalysts that provide an ionic mechanism involving the heterolytic splitting of dihydrogen and step-wise or concerted transfer of the proton and the hydride might display higher activity for the hydrogenation of polar bonds or electron-rich but sterically hindered bonds. Recently such an ionic mechanism has been proposed [109] in the hydrogenolysis of trimethylsilyl enol ethers by the acidic dihydrogen complex $[Ru(\eta^2\text{-}H_2)Cl(dppe)_2]^+$ that has a $pK^{CH_2Cl_2}$ of approx. 6 (not yet corrected for ion-pairing

and referencing errors, see Table 1.2). See the Chapter by M. Hidai of this book for more information on this system.

Another ionic mechanism could involve the hydrogenation of polar C=E bonds from hydridic-protonic bonds (eq 27-29 where R^1, R^2 could be H, alkyl or aryl and E could be O, NR, $CR(OSiR_3)$.

$$[M](\eta^2\text{-}H_2)L \rightleftharpoons {}^-H[M](LH^+) \quad (27)$$

$${}^-H[M](LH^+) + R_1R_2C{=}E \longrightarrow [M]L + R_1R_2HC\text{-}EH \quad (28)$$

$$[M]L + H_2 \rightleftharpoons [M](\eta^2\text{-}H_2)L \quad (29)$$

In reaction 27, the heterolytic splitting of dihydrogen results in a protonated ligand and a metal hydride that might form a ring because of a hydridic-protonic bond. The substrate may form hydrogen bonds with the catalyst but probably does not need to form a metal-substrate bond. The H^+ and H^- are transferred to the substrate in a concerted or stepwise fashion as in eq 28 and then dihydrogen coordinates in eq 29 to regenerate the catalyst. If R_1 and R_2 are different then this could lead to a new mechanism for the asymmetric hydrogenation of ketones (E=O) and imines (E=N).

1.9.1 Catalysts with RuH···HN bonds

In fact Noyori et al. have evidence for reaction 28 [87, 110]. The complexes $Ru^{II}H(\eta^6\text{-arene})(NH_2LNTs)$ such as *R,R*-Ru(cymene)(TsNC*HPhC*HPhNH$_2$)(H) catalyze the transfer of hydrogen from isopropanol to prochiral ketones to produce chiral alcohols in high enantiomeric excess. The X-ray structure of this complex shows an intramolecular RuH···HN distance of 2.3 Å [87]. Recent calculations show that this short distance is maintained in the proposed transition state for concerted dihydrogen transfer to the ketone (Figure 14) [110]. The proton on nitrogen hydrogen-bonds to the oxygen and the hydride attacks the carbonyl in the transition state. The catalyst is regenerated in this case, not from dihydrogen as in eq 29, but from hydrogen transfer from the alcohol solvent.

Lau and coworkers found that heating solutions of $[(\eta^5{:}\eta^1\text{-}C_5H_4(CH_2)_3NMe_2)Ru(dppm)]BF_4$, dppm=$PPh_2CH_2PPh_2$ under H_2/CO_2 (40 atm/40 atm) at 80°C for 16 h gave formic acid in low yields (TON = 8) [83]. They proposed a mechanism similar to eq 27-29 to explain the reaction. Eq 29-27 was demonstrated independently by showing that the Ru complex reacts with 60 atm H_2 to give $[(\eta^5\text{-}C_5H_4(CH_2)_3NHMe_2)RuH(dppm)]BF_4$ that has a hydridic-protonic NH···HRu bond (Scheme 4). The intermediate dihydrogen complex will have a $pK^{CH_2Cl_2}$ of approx. 7 like $[Ru(C_5H_5)(dppm)(\eta^2\text{-}H_2)]BF_4$ (Table 1.2). The hydride and proton are then transferred to the CO_2 to give the formic acid.

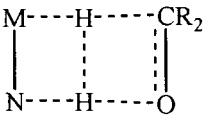

Figure 14. Proposed transition state for the hydrogenation of ketones by the transfer of proton and hydride from nitrogen and the metal, respectively.

Our group has recently reported another possible example of such an ionic mechanism. The complexes $Ru(H)_2(diamine)(PPh_3)_2$, diamine = ethylenediamine or *R,R*–cyclohexyldiamine, were found to be some of the most active catalysts for the hydrogenation of ketones [111]. Such complexes are prepared by first mixing $RuHCl(PPh_3)_3$ with one equiv of the diamine and then reacting the resulting $RuHCl(diamine)(PPh_3)_2$ complex with potassium tri-sec-butylborohydride in THF. This very air-sensitive dihydride has trans phosphines and cis hydrides as revealed by a single crystal X-ray diffraction study. The shortest NH···HRu distances are 2.8 Å, too long for significant hydrogen bonding in the solid state.

Rapid H/D exchange is observed for both the hydrides and NH moieties when a solution of the dihydride is exposed to D_2 gas. This is suggestive of an equilibrium between dihydride and dihydrogen tautomers where the dihydrogen species is in too low a concentration to be observed.

These dihydride complexes readily catalyze the hydrogenation of neat ketones to the alcohols under 1 atm of H_2 gas at 20°. For example neat acetophenone (4.1 g, 34 mmol) was quantitatively hydrogenated to *S*-phenethyl alcohol (60% e.e.) in less than 8 h by use of catalyst containing the chiral diamine (5 mg, 0.0068 mmol). Benzene was used as the solvent for the α,β-unsaturated ketone, benzalacetone, and the product was exclusively the allylalcohol. The hydrogenation of an aldimine and a ketimine in benzene also proceeded under notably mild conditions [111].

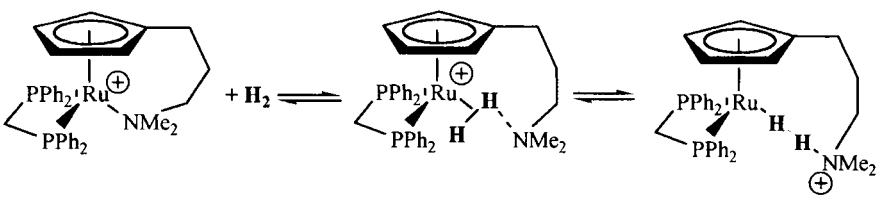

Scheme 4. The heterolytic splitting of dihydrogen at Ru(II) to give a protonic-hydridic bond is proposed by Chu et al. [83] in the mechanism of the homogeneous hydrogenation of carbon dioxide.

A possible mechanism for the hydrogenation of ketones is shown in Scheme 5. The first steps in the catalytic cycle (eq 30, 31) involve the concerted transfer of

the hydride to the carbonyl carbon and NH proton to the oxygen as proposed also for the RuH(η^6-arene)(NH_2LNTs) catalysts [87]. The cycle is completed with the coordination of dihydrogen (eq 32) and its heterolytic cleavage by an amido ligand to yield the hydridoamino complex (eq 33). This direct hydrogenation mechanism, in which the dihydride catalyst is regenerated from H_2 gas, differs from the transfer hydrogenation process reported for the series of Noyori's RuH(η^6-arene)(NH_2LNTs) complexes, in which a hydrogen-donor solvent such as an alcohol is required for the regeneration of the monohydride catalyst. However, in both of these classes of complexes, the presence of a cis-M-H···H-N bifunctional motif seems to be a key feature for the activity of these catalysts.

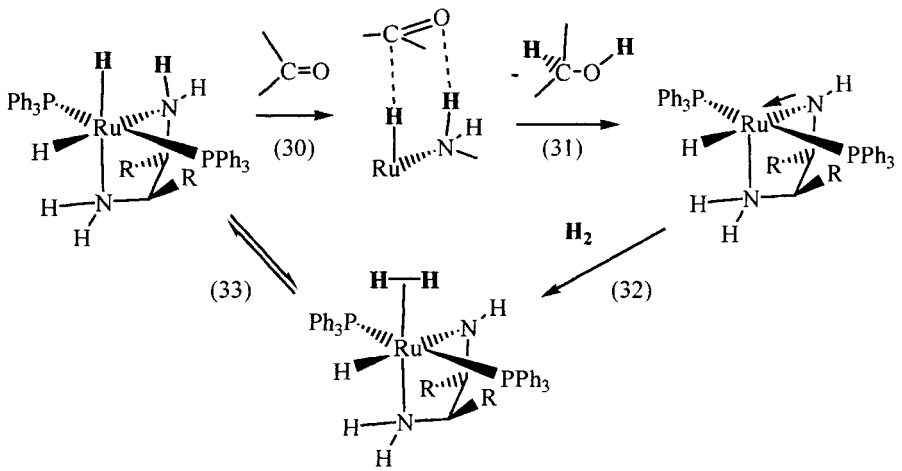

Scheme 5. Proposed mechanism for the homogeneous hydrogenation of ketones catalyzed by Ru(H)$_2$(PPh$_3$)$_2$(diamine) complexes in neat substrate at 3 atm H_2, 20° C.

Preliminary work suggests that the complex $[K(QNH)]^+[RuH_5(P^iPr_3)_2]^-$ is an excellent catalyst for the hydrogenation of nitriles. For example acetonitrile is converted to ethylamine under mild conditions. Again the mechanism illustrated by eq 27-29 may be operative in this case as well.

1.10 CONCLUSIONS

The heterolytic cleavage of dihydrogen at a transition metal complex can have unexpectedly interesting intermediates. These intermediates may have non-classical hydrogen bonding where the η^2-dihydrogen ligand is acting as a hydrogen bond donor or where the hydride ligand is acting as a hydrogen bond acceptor in a hydridic-protonic bond with d(H···H) 1.8 Å. The former non-classical bond is favored by an acidic dihydrogen complex while the latter is promoted by a basic

hydride formed from a weak conjugate acid hydride or dihydrogen complex. A preliminary semiquantitative scale of pK_α^{THF} for many hydride and dihydrogen complexes helps to understand the effect of the metal ion and ligands on the acid strength and the strength of hydridic-protonic interactions. It also helps to unify the various acid-base scales and to predict the outcome of thousands of acid-base reactions. Anionic hydride salts and cationic dihydrogen salts exist as ion-pairs in THF and CH_2Cl_2. Ion-pairing and non-classical hydrogen bonding can greatly affect the chemistry of these species.

Efficient synthetic methods to many types of hydride complexes have been developed including anionic hydrides with (azacrown)potassium counter-cations. The latter display strong 1.7-1.9 Å hydridic-protonic bonding in the solid state and solution. NMR and IR characteristics are documented. The strength of the non-classical bonding can be indirectly related to the basicity of the hydride through the pK_α^{THF} value of the conjugate acid form. This non-classical bonding seems to have an activating effect on the metal hydride toward H/D exchange and possibly also catalytic hydrogenation. The use of (diazacrown)potassium allows the assembly of interesting chain structures held together in the lattice by hydridic-protonic bonds. The solid state structures may then be covalently linked by the elimination of H_2 gas from the lattice. One dimensional chains may form novel hydride-containing polymers with metals and crown ethers in the main chain. Sheet and 3-D networks are also possible. Perhaps the elimination of H_2 may be reversed to provide interesting storage or sensor materials. The use of (diazacrown)potassium turns out to be an excellent strategy for obtaining crystals of difficult-to-crystallize anionic hydrides.

A variety of iridium(III) complexes with intramolecular 1.7-2.0 Å hydridic-protonic bonds can be made by use of pyridinethione and related ligands. The resulting hydrogen-bonded HNCSIrH six-member rings are particularly favorable and can also include interactions with the counter-anion such as BF_4^-. Electron-donating ancillary ligands increase the hydricity of the hydrogen bond acceptor and increase the strength of the IrH···HN bond. Active catalysts containing inter-ion-pair and, possibly, intramolecular RuH···HN bonds are described for the hydrogenation of polar CO and CN bonds.

ACKNOWLEDGMENTS.

The author dedicates this review to all of the excellent students and postdoctoral fellows who have worked with him at the University of Toronto. Their names appear in the references. This work was funded by NSERC Canada and the Petroleum Research Fund, as administered by the American Chemical Society. Johnson-Matthey Ltd is thanked for a loan of platinum-group metals.

REFERENCES

[1] G.J. Kubas, Acc. Chem. Res. 21 (1988) 120.
[2] P.G. Jessop, R.H. Morris, Coord. Chem. Rev. 121 (1992) 155.
[3] R.H. Morris, Can. J. Chem. (1996) 1907.
[4] R.H. Crabtree, O. Eisenstein, G. Sini, E. Peris, J. Organometal. Chem. 567 (1998) 7.
[5] D.M. Heinekey, W.J.J. Oldham, Chem. Rev. 93 (1993) 913.
[6] R.H. Morris, J.F. Sawyer, M. Shiralian, J. Zubkowski, J. Am. Chem. Soc. 107 (1985) 5581.
[7] G.J. Kubas, R.R. Ryan, B.I. Swanson, P.J. Vergamini, H.J. Wasserman, J. Am. Chem. Soc. 106 (1984) 451.
[8] X.-L. Luo, R.H. Crabtree, J. Am. Chem. Soc. 112 (1990) 6912.
[9] M.D. Butts, B.L. Scott, G.J. Kubas, J. Am. Chem. Soc. 118 (1996) 11831.
[10] K. Abdur-Rashid, D. Gusev, A.J. Lough, R.H. Morris, Organometallics 19 (2000) 1652.
[11] K. Abdur-Rashid, D. Gusev, A.J. Lough, R.H. Morris, Organometallics 19 (2000) 834.
[12] D.E. Linn, J. Halpern, J. Am. Chem. Soc. 109 (1987) 2969.
[13] R.A. Grey, G.P. Pez, A. Wallo, J. Chem. Soc., Chem. Commun. (1980) 783.
[14] R.A. Grey, G.P. Pez, A. Wallo, J. Am. Chem. Soc. 103 (1981) 7536.
[15] R. Noyori, S. Hashiguchi, Acc. Chem. Res. 30 (1997) 97.
[16] D.G. Gusev, A.J. Lough, R.H. Morris, J. Am. Chem. Soc. 120 (1998) 13138.
[17] K. Abdur-Rashid, D.G. Gusev, S.E. Landau, A.J. Lough, R.H. Morris, J. Am. Chem. Soc. 120 (1998) 11826.
[18] K. Abdur-Rashid, A.J. Lough, R.H. Morris, in preparation.
[19] D. Alvarez, E.G. Lundquist, J.W. Ziller, W.J. Evans, K.G. Caulton, J. Am. Chem. Soc. 111 (1989) 8392.
[20] D. Gusev, A. Llamazares, G. Artus, H. Jacobsen, H. Berke, Organometallics 18 (1999) 75.
[21] K. Abdur-Rashid, T.P. Fong, B. Greaves, D.G. Gusev, J.G. Hinman, S.E. Landau, R.H. Morris, J. Am. Chem. Soc. (2000) 122 (2000) 9155.
[22] S.E. Landau, R.H. Morris, A.J. Lough, (2000) in preparation.
[23] G.C. Jia, C.P. Lau, Coord. Chem. Rev. 192 (1999) 83.
[24] T.P. Fong, A.J. Lough, R.H. Morris, A. Mezzetti, E. Rocchini, P. Rigo, J. Chem. Soc., Dalton Trans. (1998) 2111.
[25] A.C. Ontko, J.F. Houlis, D.M. Roddick, T.P. Fong, A.J. Lough, R.H. Morris, Organometallics 17 (1998) 5467.
[26] S.E. Landau, R.H. Morris, A.J. Lough, Inorg. Chem. 38 (1999) 6060.
[27] J. Huhmann-Vincent, B.L. Scott, G.J. Kubas, J. Am. Chem. Soc. 120 (1998) 6808.
[28] J.S. Ricci, T.F. Koetzle, M.T. Bautista, T.M. Hofstede, R.H. Morris, J.F. Sawyer, J. Am. Chem. Soc. 111 (1989) 8823.
[29] A. Albinati, W. Klooster, T.F. Koetzle, J.B. Fortin, J.S. Ricci, J. Eckert, T.P. Fong, A.J. Lough, R.H. Morris, A. Golombek, Inorg. Chim. Acta 259 (1997) 351.
[30] P.A. Maltby, M. Schlaf, M. Steinbeck, A.J. Lough, R.H. Morris, W.T. Klooster, T.F. Koetzle, R.C. Srivastava, J. Am. Chem. Soc. 118 (1996) 5396.
[31] A. Albinati, W. Klooster, T.F. Koetzle, J.S. Ricci, P.A. Maltby, A.J. Lough, R.H. Morris, unpublished.
[32] W.T. Klooster, T.F. Koetzle, G. Jia, T.P. Fong, R.H. Morris, A. Albinati, J. Am. Chem. Soc. 116 (1994) 7677.

[33] A. Albinati, V.I. Bakhmutov, K.G. Caulton, E. Clot, J. Eckert, O. Eisenstein, D.G. Gusev, V.V. Grushin, B.E. Hauger, W.T. Klooster, T.F. Koetzle, R.K. McMullan, T.J. O'Loughlin, M. Pelissier, R.S. Ricci, M.P. Sigalas, A.B. Vymenits, J. Am. Chem. Soc. 115 (1993) 7300.
[34] C.L. Gross, D.M. Young, A.J. Schultz, G.S. Girolami, J. Chem. Soc., Dalton Trans. (1997) 3081.
[35] R.M. Chin, R.H. Dubois, L.E. Helberg, M. Sabat, T. Bartucz, R.H. Morris, W.D. Harman, Inorg. Chem. 36 (1997) 3553.
[36] M. Schlaf, A.J. Lough, P.A. Maltby, R.H. Morris, Organometallics 15 (1996) 2270.
[37] A.J. Lough, R.H. Morris, L. Ricciuto, T. Schleis, Inorg. Chim. Acta 270 (1998) 238.
[38] M. Schlaf, A.J. Lough, R.H. Morris, Organometallics 16 (1997) 1253.
[39] B. Chin, A.J. Lough, R.H. Morris, C.T. Schweitzer, C. D'Agostino, Inorg. Chem. 33 (1994) 6278.
[40] R.H. Morris, R. Wittebort, Mag. Res. Chem. 35 (1997) 243.
[41] G. Facey, D. Gusev, S. Macholl, R.H. Morris, G. Buntkowsky, Phys. Chem. Chem. Phys. 2 (2000) 935.
[42] S.S. Kristjánsdóttir, J.R. Norton, in: A. Dedieu, (Ed.) Transition Metal Hydrides: Recent Advances in Theory and Experiment. VCH, New York, 1992, p. 309.
[43] R.T. Weberg, J.R. Norton, J. Am. Chem. Soc. 112 (1990) 1105.
[44] S.S. Kristjánsdóttir, A.E. Moody, R.T. Weberg, J.R. Norton, Organometallics 7 (1988) 1983.
[45] S.S. Kristjánsdóttir, A.J. Loendorf, J.R. Norton, Inorg. Chem. 30 (1991) 4470.
[46] D.E. Berning, B.C. Noll, D.L. DuBois, J. Am. Chem. Soc. 121 (1999) 11432.
[47] M.S. Chinn, D.M. Heinekey, J. Am. Chem. Soc. 109 (1987) 5865.
[48] F.B. Bordwell, Acc. Chem. Res. 21 (1988) 456.
[49] E.P. Cappellani, S.D. Drouin, G. Jia, P.A. Maltby, R.H. Morris, C.T. Schweitzer, J. Am. Chem. Soc. 116 (1994) 3375.
[50] G. Jia, R.H. Morris, J. Am. Chem. Soc. 113 (1991) 875.
[51] G. Jia, A.J. Lough, R.H. Morris, Organometallics 11 (1992) 161.
[52] E. Rocchini, A. Mezzetti, H. Ruegger, U. Burckhardt, V. Gramlich, A. Del Zotto, P. Martinuzzi, P. Rigo, Inorg. Chem. 36 (1997) 711.
[53] D. Wang, R.J. Angelici, J. Am. Chem. Soc. 118 (1996) 935.
[54] R.J. Angelici, Acc. Chem. Res. 28 (1995) 51.
[55] M. Schlaf, A.J. Lough, R.H. Morris, Organometallics 15 (1996) 4423.
[56] C.E. Forde, S.E. Landau, R.H. Morris, J. Chem. Soc., Dalton Trans. (1997) 1663.
[57] A. Streitwieser, J. Am. Chem. Soc. (1993) 8024.
[58] M.J. Kaufman, S. Gronert, A. Streitwieser Jr, J. Am. Chem. Soc. 110 (1988) 2829.
[59] I.S. Antipin, R.F. Gareev, V.V. Ovchinnikov, A.I. Konovalov, Dokl. Phys. Chem. 304 (1989) Eng. Version page 4.
[60] I.S. Antipin, R.F. Gareyev, A.N. Vedernikov, A.I. Konovalov, J. Phys. Org. Chem. 7 (1994) 181.
[61] R.M. Fuoss, J. Am. Chem. Soc. 80 (1958) 5059.
[62] J.F. Coetzee, B.K. Deshmukh, C.-C. Liao, Chem. Rev. 90 (1990) 827.
[63] M.G. Basallote, J. Durán, M.J. Fernández-Trujillo, M.A. Máñez, Organometallics 19 (2000) 695.
[64] E. Buncel, B. Menon, J. Am. Chem. Soc. 99 (1977) 4457.
[65] T.H. Peterson, J.T. Golden, R.G. Bergman, Organometallics 18 (1999) 2005.
[66] X.M. Zhang, J.W. Bruno, E. Enyinnaya, J. Org. Chem. 63 (1998) 4671.

[67] L.S. Van Der Sluys, J. Eckert, O. Eisenstein, J.H. Hall, J.C. Huffman, S.A. Jackson, T.F. Koetzle, G.J. Kubas, P.J. Vergamini, K.G. Caulton, J. Am. Chem. Soc. 112 (1990) 4831.
[68] S. Park, R. Ramachandran, A.J. Lough, R.H. Morris, J. Chem. Soc., Chem. Commun. (1994) 2201.
[69] T.P. Fong, C.E. Forde, A.J. Lough, R.H. Morris, P. Rigo, E. Rocchini, T. Stephan, J. Chem. Soc., Dalton Trans. (1999) 4475.
[70] P.I. Amrhein, S.D. Drouin, C.E. Forde, A.J. Lough, R.H. Morris, J. Chem. Soc., Chem. Commun. (1996) 1665.
[71] Y. Montet, E. Garcin, A. Volbeda, C. Hatchikian, M. Frey, J.C. Fontecilla-Camps, Pure and Appl. Chem. 70 (1998) 25.
[72] R. Cammack, Nature 397 (1999) 214.
[73] R.C. Stevens, R. Bau, D. Milstein, O. Blum, T.F. Koetzle, J. Chem. Soc., Dalton Trans. (1990) 1429.
[74] A.J. Lough, S. Park, R. Ramachandran, R.H. Morris, J. Am. Chem. Soc. 116 (1994) 8356.
[75] J.C. Lee, E. Peris, A.L. Rheingold, R.H. Crabtree, J. Am. Chem. Soc. 116 (1994) 11014.
[76] J. Wessel, J.C. Lee, E. Peris, G.P.A. Yap, J.B. Fortin, J.S. Ricci, G. Sini, A. Albinati, T.F. Koetzle, O. Eisenstein, A.L. Rheingold, R.H. Crabtree, Angew. Chem. Int. Ed. 34 (1995) 2507.
[77] M. Schlaf, R.H. Morris, J. Chem. Soc., Chem. Commun. (1995) 625.
[78] W. Xu, A.J. Lough, R.H. Morris, Inorg. Chem. 35 (1996) 1549.
[79] B.P. Patel, K. Kavallieratos, R.H. Crabtree, J. Organomet. Chem. 528 (1997) 205.
[80] E.S. Subina, N.V. Belkova, L.M. Epstein, J. Organometal. Chem. 536-537 (1997) 17.
[81] S. Aime, R. Gobetto, E. Valls, Organometallics 16 (1997) 5140.
[82] R. Bosque, F. Maseras, O. Eisenstein, B.P. Patel, W.B. Yao, R.H. Crabtree, Inorg. Chem. 36 (1997) 5505.
[83] H.S. Chu, C.P. Lau, K.Y. Wong, W.T. Wong, Organometallics 17 (1998) 2768.
[84] S. Park, A.J. Lough, R.H. Morris, Inorg. Chem. 35 (1996) 3001.
[85] A. Caballero, F.A. Jalon, B.R. Manzano, J. Chem. Soc., Chem. Commun. (1998) 1879.
[86] A. Castellanos, J.A. Ayllon, B. Donnadieu, B. Chaudret, W.B. Yao, K. Kavallieratos, R.H. Crabtree, Comptes Rendus Acad. Sci. Serie ii Fas. c Chimie 2 (1999) 359.
[87] K.J. Haack, S. Hashiguchi, A. Fujii, T. Ikariya, R. Noyori, Angew. Chem. Int. Ed. Engl. 36 (1997) 285.
[88] S.H. Park, A.J. Lough, G.P.A. Yap, R.H. Morris, J. Organometal. Chem. (2000) 609 (2000) 110.
[89] E. Peris, J.C. Lee, J.R. Rambo, O. Eisenstein, R.H. Crabtree, J. Am. Chem. Soc. 117 (1995) 3485.
[90] E. Peris, J.C. Lee, R.H. Crabtree, J. Chem. Soc., Chem. Commun. (1994) 2573.
[91] W. Xu, A.J. Lough, R.H. Morris, Can. J. Chem. 75 (1997) 475.
[92] M.L. Buil, M.A. Esteruelas, E. Onate, N. Ruiz, Organometallics 17 (1998) 3346.
[93] W.B. Yao, R.H. Crabtree, Inorg. Chem. 35 (1996) 3007.
[94] L. Dahlenburg, K. Herbst, M. Kuhnlein, Z. Anorg. Allg. Chem. 623 (1997) 250.
[95] G. Sini, O. Eisenstein, W.B. Yao, R.H. Crabtree, Inorg. Chim. Acta 280 (1998) 26.
[96] B.P. Patel, J. Wessel, W. Yao, J.C. Lee, E. Peris, T.F. Koetzle, G.P.A. Yap, J.B. Fortin, J.S. Ricci, G. Sini, A. Albinati, O. Eisenstein, A.L. Rheingold, R.H. Crabtree, New J. Chem. 21 (1997) 413.

[97] B.P. Patel, W.B. Yao, G.P.A. Yap, A.L. Rheingold, R.H. Crabtree, Chem. Comm. (1996) 991.
[98] R.H. Crabtree, P.E.M. Siegbahn, O. Eisenstein, A.L. Rheingold, Acc. Chem. Res. 29 (1996) 348.
[99] W.T. Klooster, T.F. Koetzle, P.E.M. Siegbahn, T.B. Richardson, R.H. Crabtree, J. Am Chem. Soc. 121 (1999) 6337.
[100] E.S. Shubina, N.V. Belkova, A.N. Krylov, E.V. Vorontsov, L.M. Epstein, D.G. Gusev, M. Niedermann, H. Berke, J. Am. Chem. Soc. 118 (1996) 1105.
[101] J.A. Ayllon, S. Saboetienne, B. Chaudret, S. Ulrich, H.H. Limbach, Inorg. Chim. Acta 259 (1997) 1.
[102] Y. Guari, J.A. Ayllon, S. Sabo-Etienne, B. Chaudret, B. Hessen, Inorg. Chem 37 (1998) 640.
[103] R. Kuhlman, E. Clot, C. Leforestier, W.E. Streib, O. Eisenstein, K.G. Caulton, J. Am. Chem. Soc. 119 (1997) 10153.
[104] L.M. Epstein, E.S. Shubina, E.V. Bakhmutova, L.N. Saitkulova, V.I. Bakhmutov, A.L. Chistyakov, I.V. Stankevich, Inorg. Chem. 37 (1998) 3013.
[105] E.S. Shubina, N.V. Belkova, E.V. Bakhmutova, E.V. Vorontsov, V.I. Bakhmutov, A.V. Ionidis, C. Bianchini, L. Marvelli, M. Peruzzini, L.M. Epstein, Inorg. Chim. Acta 280 (1998) 302.
[106] N.V. Belkova, E.S. Shubina, A.V. Ionidis, L.M. Epstein, H. Jacobsen, A. Messmer, H. Berke, Inorg. Chem. 36 (1997) 1522.
[107] R. Custelcean, J.E. Jackson, Angew. Chem. Int. Ed., Eng. 38 (1999) 1661.
[108] R. Custelcean, J.E. Jackson, J. Am. Chem. Soc. 120 (1998) 12935.
[109] Y. Nishibayashi, I. Takei, M. Hidai, Angew. Chem. Int. Ed., Eng. 38 (1999) 3047.
[110] M. Yamakawa, H. Ito, R. Noyori, J. Am. Chem. Soc. 122 (2000) 1466.
[111] K. Abdur-Rashid, A.J. Lough, R.H. Morris, Organometallics 19 (2000) 2655; 20 (2000) 1047.

Chapter 2

Protonation of Transition Metal Hydrides to Give Dihydrogen Complexes: Mechanistic Implications and Catalytic Applications

Elizabeth T. Papish, Matthew P. Magee, Jack R. Norton

Department of Chemistry, Columbia University, 3000 Broadway, New York, NY 10027, USA

CONTENTS

2.1 INTRODUCTION

Protonation of transition metal hydride complexes plays an important role in many catalytic processes, including ionic hydrogenation and the reduction of H^+ to H_2 [1,2]. Ionic hydrogenation involves the sequential transfer of H^+ and H^- to olefins, ketones, or imines (eq 1). If H_2 addition to a transition metal complex generates an acidic dihydrogen complex [3] capable of transferring H^+ and H^- to a substrate, then the possibility of catalytic ionic hydrogenation exists (eq 2). The mechanism of ionic hydrogenation is intimately related to that of transfer hydrogenation; some of the most effective systems for the latter use 2-propanol as a hydrogen source and transfer H^- to the metal and H^+ to a tethered amino group [4] (eq 3). Transfer of H^+ and H^- to the unsaturated substrate completes the cycle.

$$H^+ + R_2C{=}E \rightleftharpoons R_2\overset{\oplus}{C}{-}EH$$

$$R_2\overset{\oplus}{C}{-}EH + H{-}M \longrightarrow R_2CH{-}EH + M^+ \qquad (1)$$

(E = CR_2, NR or O)

The mechanism of H_2 addition to transition metal complexes goes through a dihydrogen complex. Similarly, upon protonation of transition metal hydrides, an η^2-H_2 complex has been observed prior to H_2 elimination. The kinetic acidity of dihydrogen complexes is much greater than their corresponding dihydrides. By microscopic reversibility, there should be a kinetic preference for protonating a hydride complex at the hydride ligand rather than the metal centre: reaction at the former site will involve less geometric and electronic rearrangement [3e-f, 5, 6]. The resulting dihydrogen complex may not be directly observable, but its presence can be inferred if exchange between the hydride ligand and a Brønsted acid occurs faster than metal protonation. Dihydrogen complex intermediates have been observed during the exchange of metal hydrides with protons of tethered amino groups.

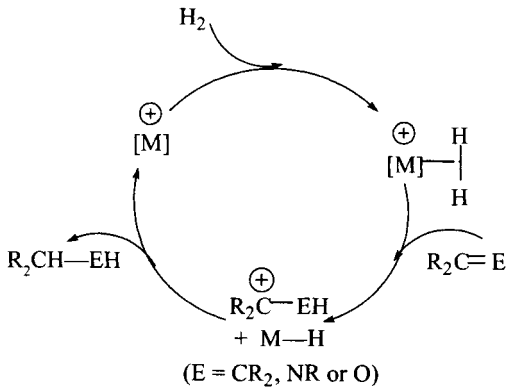

(2)

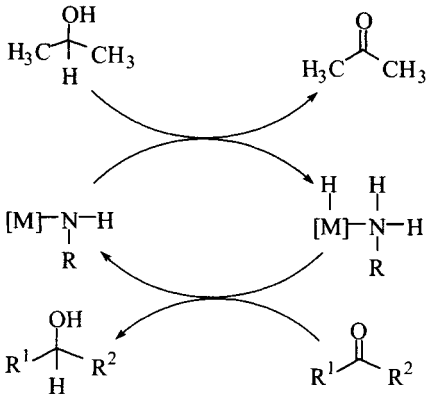

(3)

Spectroscopically, dihydrogen complexes are characterised by T_1 (min) values less than 125 ms [3e-f, 7]. It is important to realise that several factors can affect relaxation, including quadrupolar nuclei and solvent viscosity [8]. The dihydrogen ligand rotates rapidly (making the H's equivalent), so J_{HH} measurements are not possible. Deuterium substitution allows for measurement of J_{HD} — values from 22-36 Hz indicate an H-H bond is present [3c-f]. The only caveat is that quantum mechanical exchange coupling in classical hydrides can produce very large J_{HD} values (in some cases larger than J_{HD} of HD gas) which exhibit a marked temperature dependence [9]. An IR stretching frequency $\nu_{H\text{-}H}$ of 2350-3100 cm^{-1} is also characteristic of dihydrogen complexes [3c-f], but since low temperature IR is rarely practical, short-lived intermediates can be difficult to observe by IR. Neutron diffraction can unequivocally determine whether a non-classical η^2-H_2 ligand is present [3c-f, 10].

A list of abbreviations used in this work is provided in the following endnote [11].

2.2 OBSERVATIONS OF MH/HA EXCHANGE WHICH SUGGEST A DIHYDROGEN INTERMEDIATE

If protonation of a metal hydride by an inter or intramolecular acid (HA) produces a transient dihydrogen complex, rotation about the H-H bond followed by deprotonation can permute the protons of MH and HA. (A dihydrogen complex has been observed during many exchange processes between metal hydrides and acids.) This is of interest because it shows that fast exchange between a metal and an acid prior to metal protonation by the same acid implies a dihydrogen intermediate.

Examples of non traditional hydrogen bonds between MH and HA (due to electrostatic attraction between the δ- of MH and the δ+ of HA) are numerous [12]. In conventional H bonds, O, N, or S serves as the H bond acceptor.

The intramolecular exchange of polyhydride complexes often goes through dihydrogen complexes. It is beyond the scope of this work to discuss the many examples of exchange within polyhydrides [13, 14, 15].

2.2.1 Intramolecular Proton Exchange Between MH and NH

Recently, several transition metal hydrides with a tethered NH group have been studied. MH and NH are often in fast, intramolecular exchange in these complexes, and a dihydrogen complex has been shown to be an intermediate in many cases.

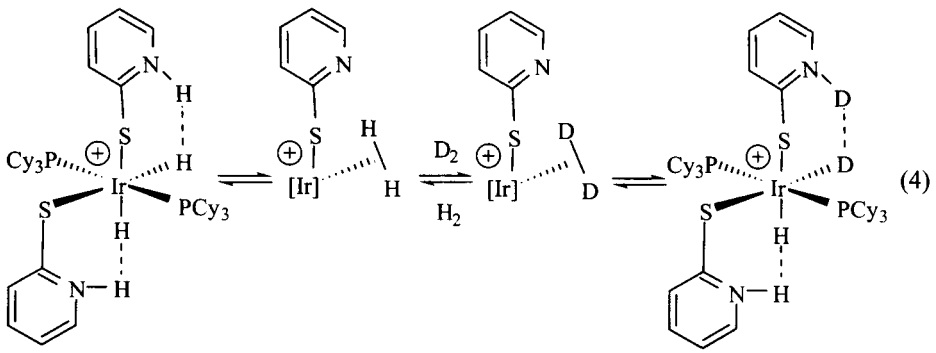

The iridium hydride studied by Morris [16] in eq 4 has an Ir-H···H-N hydrogen bonding interaction. Fast proton exchange between IrH and intramolecular NH presumably goes through an acidic dihydrogen complex intermediate. Though Ir(η^2-H_2) was not spectroscopically observed, its presence is implied from exchange with D_2 gas in CD_2Cl_2. (An η^2-H_2 intermediate has also been proposed for exchange between various Ir(H)(NH_3) complexes and D_2 gas [17].) In THF, IrH/NH hydrogen bonding is disrupted because THF forms a very strong hydro-

gen bond with NH. Thus, in THF the intramolecular NH is no longer free to interact with IrH and formation of the intermediate dihydrogen complex is prevented and exchange with D_2 gas does not occur.

In a similar study by Chaudret [18], the kinetic product of protonation of the iridium dihydride in eq 5 is a piperidinium cation. The resulting NH undergoes fast, intramolecular exchange with IrH (perhaps through an η^2-H_2 intermediate); the exchange can be best explained by a hydrogen-bonding interaction. Hydrogen bonding hinders Cp rotation and holds IrH and NH in close proximity to allow for rapid exchange. The thermodynamic product of protonation in CD_2Cl_2 is the iridium trihydride, which also has a hydrogen-bonding interaction— between the N and the hydrides as evidenced by the downfield shift of the methyl group on N at δ 2.80. The iridium trihydride protons are in an AB_2 spin system and exhibit large, temperature dependent $J_{Ha\text{-}Hb}$ coupling constants due to quantum mechanical exchange coupling [9]. It is interesting to note the thermodynamic product is highly dependent on the strength of hydrogen bonding interactions available— addition of THF or $OPPh_3$ shifts the equilibrium towards the piperidinium form by hydrogen bonding to the NH. In contrast to the system in eq 4, exchange between the IrH and the NH in eq 5 occurs in THF, and the most logical intermediate for this process and metal protonation is an η^2-H_2 complex.

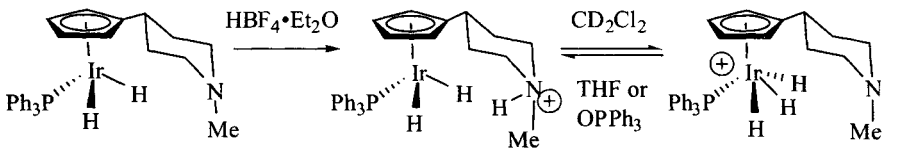

(5)

A dihydrogen complex has been implicated by Caballero in the proton exchange in eq 6 [19]. Addition of CF_3COOH to the ruthenium hydride, which exists as a mixture of isomers, results in a highly downfield shifted NH signal at δ 20 in the ^1H NMR— which can best be explained by rapid exchange between the two basic centres due to kinetic protonation of the pyridine N [20]. A dihydrogen complex was postulated as an intermediate in the exchange and loss of H_2, but it was not observed.

Lau has proposed a dihydrogen complex as the most logical intermediate in exchange between RuH and an intramolecular ammonium proton (eq 7) [21]. Again, the kinetic site of RuH protonation is the pendant amine group to give a complex with broadened hydride and NH signals and downfield shifted $N(CH_3)_2$ in the ^1H NMR— characteristic of a hydrogen-bonding interaction. Also, the T_1 (min)'s are significantly lower upon protonation, for n = 2 the relaxation time drops from 926 ms to 188 ms after protonation in C_6D_5Cl. The exchange was

confirmed by spin saturation transfer experiments; irradiation of the hydride at δ –11.47 produced a decrease in signal of the ammonium (δ 5.48). Although monocationic Ru(η^2-H_2) was not spectroscopically observed, it is implied by reversible loss of H_2 and a dicationic η^2-H_2 complex is observed upon adding two equiv of HBF_4 to RuH (eq 7).

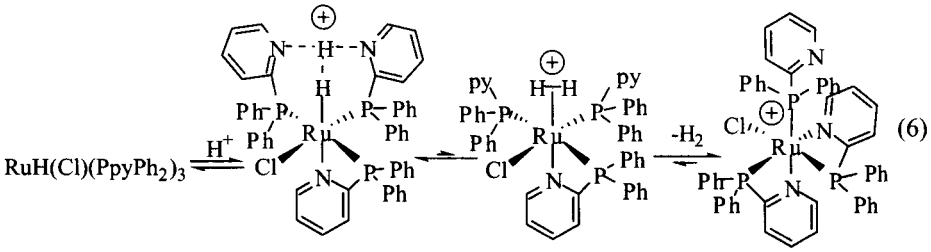

(6)

Chaudret has recently shown that the hydride ligand of **1** {formed by protonation of RuH(η^5-$C_5H_4CH_2CH_2NMe_2$)(PPh_3)$_2$ with $HNEt_3BPh_4$ or $HPBu_3BPh_4$} undergoes intramolecular proton exchange without H_2 loss (eq 8) [22]. In contrast, protonation of RuH(η^5-$C_5H_4CH_2CH_2NMe_2$)(PPh_3)$_2$ with HBF_4 produces facile loss of H_2 (which presumably goes through **2**). This shows that the cationic H_2 complex **2** cannot be an intermediate in RuH/NH exchange.

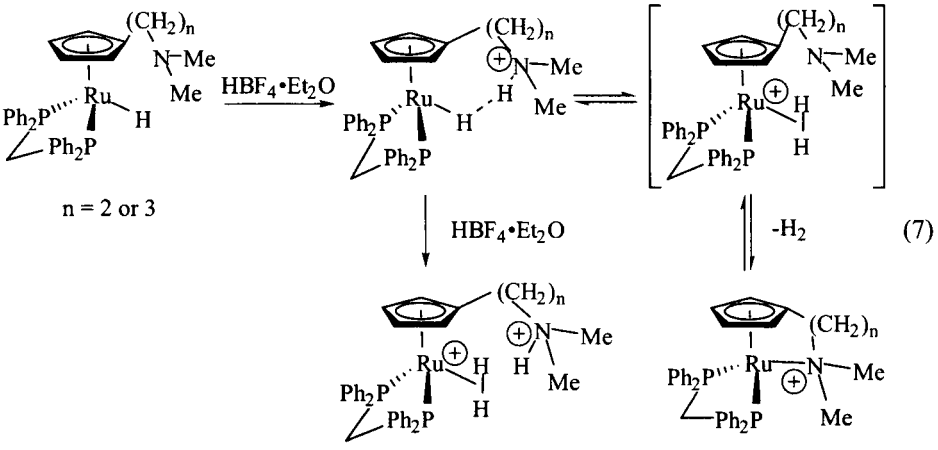

(7)

Chaudret [22] proposed that the exchange occurs through the steps in eq 9: breaking the hydrogen bond, rotation of the Cp ring, followed by dihydride formation as the rate determining step, from which rotation of the Cp ring and repetition of the above steps in reverse could equate the two hydrides. This seems unlikely, especially since the transition state for dihydride formation

could not be located in theoretical calculations despite many attempts [22]. We propose that an intermediate as drawn in eq 8 — with amine coordination stabilising the coordinated H_2 — remains a possibility [23].

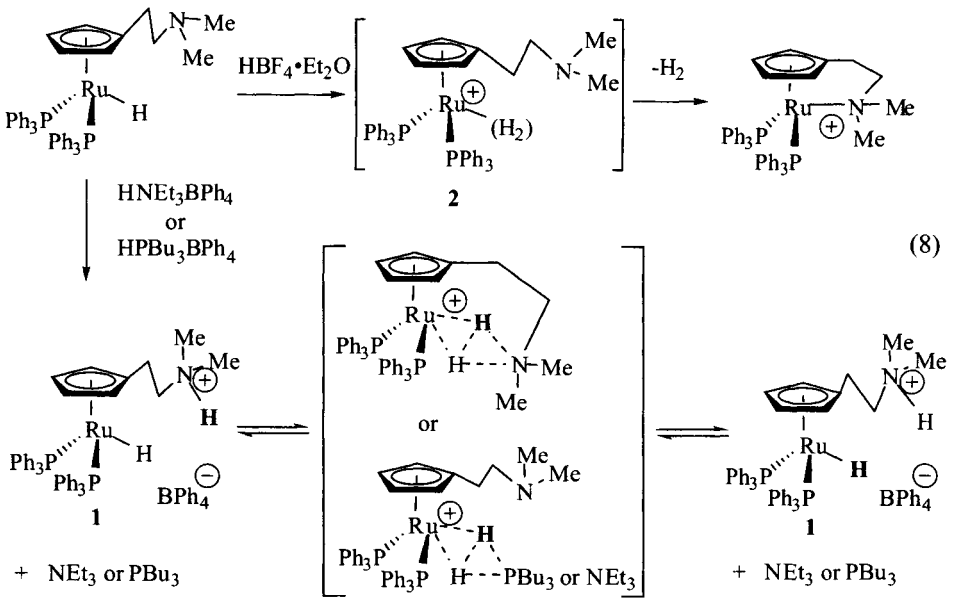

(8)

In conclusion, exchange between metal hydrides and the NH's of tethered amino groups occurs via a dihydrogen intermediate. Hydrogen bonds are often present in these complexes, allowing for an attractive interaction and spatial proximity between MH and intramolecular HA. These compounds undergo facile H_2 loss and addition, and it shall be shown later in this work that dihydrogen complexes are often observed prior to H_2 loss. These complexes bear structural resemblance to hydrogen transfer catalysts that will be discussed later.

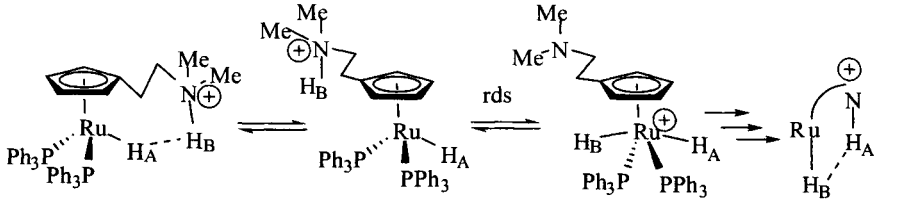

(9)

2.2.2 Intramolecular Proton Exchange Between MH and SH

Another example of a dihydrogen complex serving as an intermediate for an intramolecular exchange process was observed by Bergman with a titanium sul-

fide [24]. Addition of H_2 gas to $Cp^*_2(py)Ti{=}S$ results in the thiol hydride complex shown on the left of eq 10. Since intramolecular exchange (k_{intra}) occurs faster than elimination/readdition of H_2 (k_{inter}), a dihydrogen intermediate must be responsible for the exchange (eq 10). Although d^0 metals are incapable of stabilising dihydrogen complexes through back donation, theoretical calculations have shown that they can still serve as reaction intermediates [25].

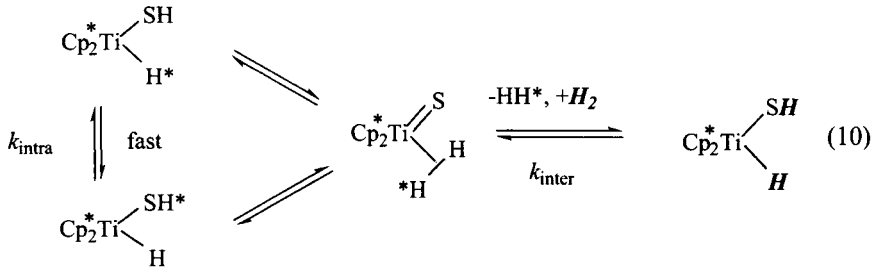

(10)

2.2.3 *Intermolecular Proton Exchange Between MH and OH*

In only one case has a dihydrogen intermediate been directly observed during exchange between a metal hydride and an alcohol. However, a dihydrogen complex intermediate may play a role in other such exchanges between hydrides and alcohols (eg. ROH/D_2 exchange catalysed by $ML_2H(H_2)$ {M = Ru, Ir} [26]). Later, we shall see that such exchanges are important in ionic hydrogenation reactions.

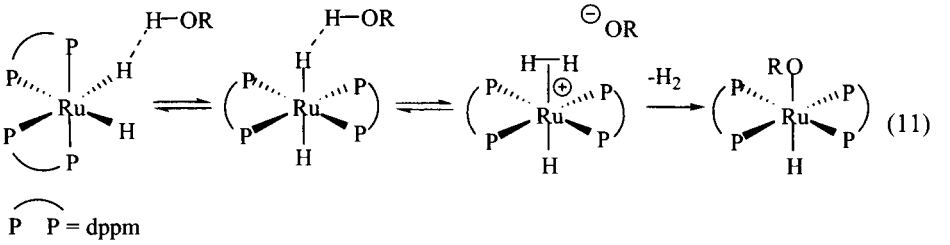

(11)

Chaudret has shown that addition of phenol to $RuH_2(dppm)_2$, for which *cis* and *trans* isomers are in equilibrium, results in a hydrogen bonding interaction between MH and OH (eq 11) [12b]. (A similar hydrogen bonding interaction has been seen between (triphos)$ReH(CO)_2$ and perfluoro-*t*-butyl alcohol prior to $Re(\eta^2\text{-}H_2)$ complex formation [27].) The RuH of the *trans* isomer undergoes rapid proton exchange with the alcohol, as confirmed by magnetisation transfer, whereas the *cis* isomer does not exchange with acid on the NMR timescale.

Preferential protonation of the *trans* isomer illustrates the greater basicity of hydrides that are *trans* to other hydrides. On cooling, a dihydrogen complex was observed with a T_1(min) of 35ms, slower than the relaxation rate of most dihydrogen complexes; its variation with alcohol concentration indicates exchange between the coordinated H_2 and free alcohol. Protonation with hexafluoroisopropyl alcohol results in facile H_2 loss, probably through the same dihydrogen complex that achieves the exchange.

2.3 IS THE METAL OR THE HYDRIDE THE KINETIC SITE OF PROTONATION?

2.3.1 Kinetic Preference for Hydride Ligand Protonation

In order to show a meaningful kinetic preference for protonation of a hydride ligand, the dihydrogen complex cannot be the sole product. Also, if a dihydride complex is the only observable product of protonation, it is still possible that the initial protonation site was the hydride ligand.

The kinetic preference for hydride protonation has been mentioned in existing review articles [3e-f,5,6]. In general, protonation of elements with a stereochemically active lone pair such as N,O, or S tends to be rapid, whereas protonation of metals or carbon involves extensive geometric and electronic rearrangement and tends to be slow (eg. protonation of $Co(CO)_4^-$ (tetrahedral) to give $Co(CO)_4H$ (trigonal bipyramid) [28]). Since hydride protonation involves little change of the coordination sphere, there should be a kinetic preference for hydride ligand protonation, even if the thermodynamic site is the metal centre.

2.3.1.1 Kinetic Protonation of Metal Hydrides to Give Dihydrogen Complexes

There are many cases wherein a dihydrogen complex is suggested but not proven to be the kinetic product of hydride protonation. Addition of H^+ to $(C_5Et_5)MoH_3(dppe)$ gives $(C_5Et_5)MoH_4(dppe)^+$; an η^2-H_2 species has not been seen but is supported by loss of H_2 from the tetrahydride [29].

When $Cp^*_2WH_2$ is protonated by DCl / D_2O, the initial major product ($[Cp^*_2WH_2D]^+$) has a central deuteride ligand (10% formation of tungsten trihydride with an outer deuteride is presumably due to exchange — the amount of outer deuteride eventually increases at a rate faster than formation of $[Cp^*_2WD_2H]^+$ or $[Cp^*_2WD_3]^+$) (eq 12) [30]. This central deuteride product cannot result from direct metal protonation because there is no occupied tungsten orbital between the hydride ligands, so the charge-controlled formation of

an intermediate (η^2-HD)(H) dihydrogen complex has been suggested. The kinetics of the reaction was monitored by stopped flow and the presence of an intermediate was confirmed [31]. Since direct metal protonation can be ruled out and no deuterium incorporation in the Cp* ligands occurs, the only reasonable intermediate that could exchange the inequivalent hydrides is a dihydrogen complex.

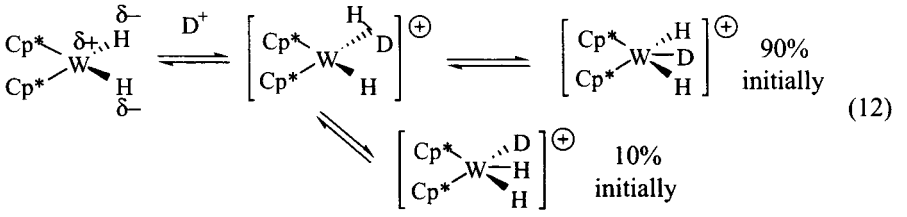

(12)

In one of the first studies to provide clear evidence that the kinetic site of metal hydride protonation is the ligand, Lapinte observed a dihydrogen intermediate at low temperature in the protonation of the iron hydride in eq 13 [32]. The dihydrogen complex was not isolated, but its structure was inferred from a broad ^{1}H NMR hydride peak at δ –12.39 with a T_1 (min) of 7 ms at 223K; the d_1 analogue of the dihydrogen complex had a J_{HD} of 27Hz. Upon warming, the iron dihydride complex is formed as the sole thermodynamic product, with a triplet at δ –7.89 ($^2J_{PH}$ of 68 Hz, consistent with the *trans* structure) and a T_1 (min) of 175 ms in the ^{1}H NMR.

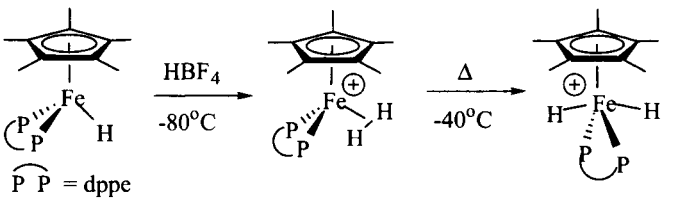

(13)

In a similar study by Morris, protonation of Cp*Ru(dppp)H (eq 14) at -60 °C initially forms a dihydrogen complex as spectroscopically characterised by a broad peak at δ –8.80 with T_1 (min) = 21 ms and J_{HD} = 23.3 Hz by ^{1}H NMR [33]. At room temperature, the dihydrogen complex slowly isomerizes into the *trans* dihydride.

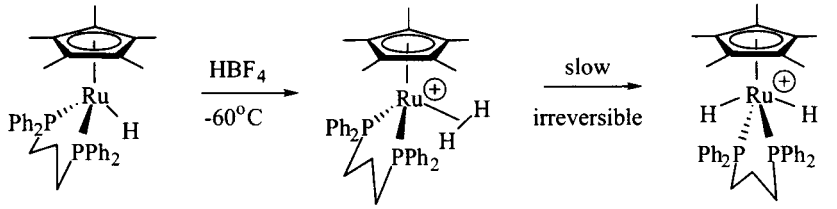

(14)

In eq 15, the kinetic product of hydride complex protonation was a spectroscopically observable dihydrogen complex, which rearranged irreversibly to a dihydride upon warming [14]. The structure of the dihydrogen complex was assigned from a broad signal at δ –6.45 with T_1 (min) 9 ms at 183K in the ^{1}H NMR; in a partially deuterated sample the J_{HD} coupling was 27.7Hz. The phosphorus couplings show that there is no rearrangement of the octahedral structure. Perhaps because σ donation from the *trans* phosphine ligand weakens the dihydrogen σ bond, irreversible formation of the dihydride complex (characterised by NMR and XRD) occurs upon warming to –30°C.

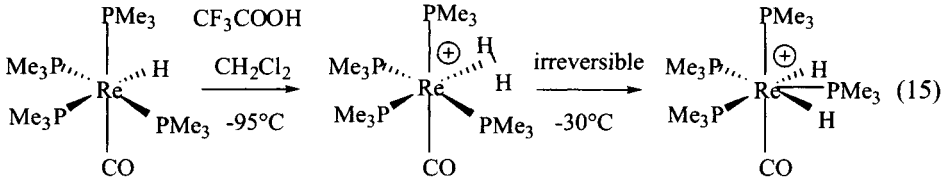

(15)

In another hydride protonation study, kinetic formation of a dihydrogen complex was inferred from the time dependence of the *cis*/*trans* product ratios. Jia investigated the reaction in eq 16, where the chelating phosphine is dppm, dppe, or dppp [34]. Unlike the protonation of analogous Fe/Ru hydrides (eq 13-14), a dihydrogen intermediate was not observed, even at low temperatures. However, the fast, intramolecular exchange of the hydride resonances of the *cis* dihydride can best be explained through a dihydrogen intermediate. A *cis* dihydride structure is consistent with T_1 (min) = 150 ms for the hydrides and the inequivalent methylene protons of the dppm ligand in the ^{1}H NMR; the classical structure is confirmed by J_{HD} = 3.0 Hz for *cis* Os(H)(D). Upon initial protonation of the osmium hydride at –78 °C the percentages of *cis* dihydride (out of total dihydride formed) are 96, 25, and 25% for the dppm, dppe, and dppp complexes respectively. After warming to room temperature, the amount of *trans* dihydride increases; the percentages are then 91, 1, and 0% *cis* respectively. The kinetic preference for formation of the *cis* dihydride may be the result of initial formation of a dihydrogen complex.

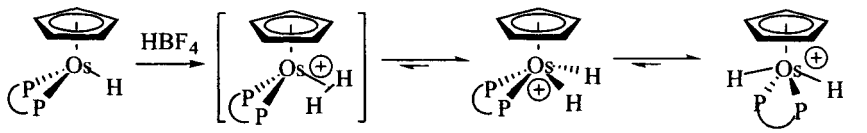

(16)

When the eventual product of a hydride protonation reaction is an equilibrium mixture of MH_2 and $M(\eta^2\text{-}H_2)$, a detailed kinetic study is necessary to determine whether the metal or the hydride is the kinetic site. Roddick and Morris have shown that protonation of the RuH in eq 17 results in a dihydrogen complex and

a dihydride in a ratio of 5:1 [35]. RuH, $Ru(\eta^2\text{-}H_2)^+$, and HOTf rapidly exchange protons, but the dihydride RuH_2^+ has a lower kinetic acidity than $Ru(\eta^2\text{-}H_2)^+$. The $\eta^2\text{-}H_2$ complex is remarkably stable; the product mixture contains only 25% of the H_2 elimination product Cp(dfepe)RuOTf.

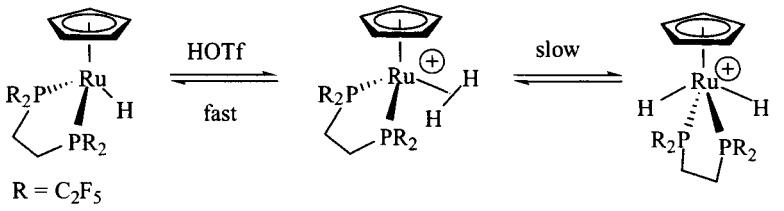

(17)

Basallote has shown that the initial hydride protonation products are the corresponding dihydrogen complexes (eq 18) [36]. For $L=PPh_3$ subsequent rearrangement occurs to give exclusively the dihydride product. The dppe ligand yields a mixture of RuH_2 and $Ru(\eta^2\text{-}H_2)$ as the thermodynamic products. Only the $Ru(\eta^2\text{-}H_2)$ complex is obtained with the dppm ligand. (Similar product mixtures were seen following initial hydride ligand protonation of $(\eta^5\text{-Indenyl})RuHL_2$, L_2 = dppm, dppe, dppp [37]) It is interesting that no correlation between the rate of metal protonation and the pK_a of the resulting dihydrogen complex in THF was obtained. The true acidity in THF may be altered by homoconjugate pair formation or hydrogen bonding interactions [38].

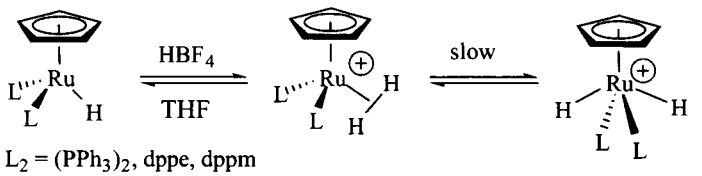

(18)

2.3.1.2 Kinetic Acidity of Dihydrogen Complexes

In some cases, it has not been possible to show that the kinetic site of protonation is the hydride, but that conclusion is implied by microscopic reversibility from the fact that the dihydrogen ligand is selectively deprotonated faster than the dihydride.

For example, in eq 19 the initially formed dihydrogen complex isomerizes to an equilibrium mixture of RuH_2 and $Ru(\eta^2\text{-}H_2)$ [39]. Selective deprotonation of the dihydrogen complex occurs immediately upon addition of base, whereas 30 minutes elapse before deprotonation of the dihydride is complete [33]. Thus the kinetic acidity of the dihydrogen complex is greater than that of the corresponding dihydride, and the kinetic site of protonation of the hydride complex must be the hydride ligand.

The high kinetic acidity of η^2-H_2 complexes is illustrated by the system in eq 20 [40, 41]. For Ru and Os, the dihydrides exist as a mixture of *cis* and *trans* in an equilibrium ratio of 9:1; for Fe, the *cis* form is the only thermodynamically stable isomer. For Ru and Os, deprotonation of the hydride/dihydrogen cation led only to the thermally unstable *trans* dihydride, which rearranged to the *cis*

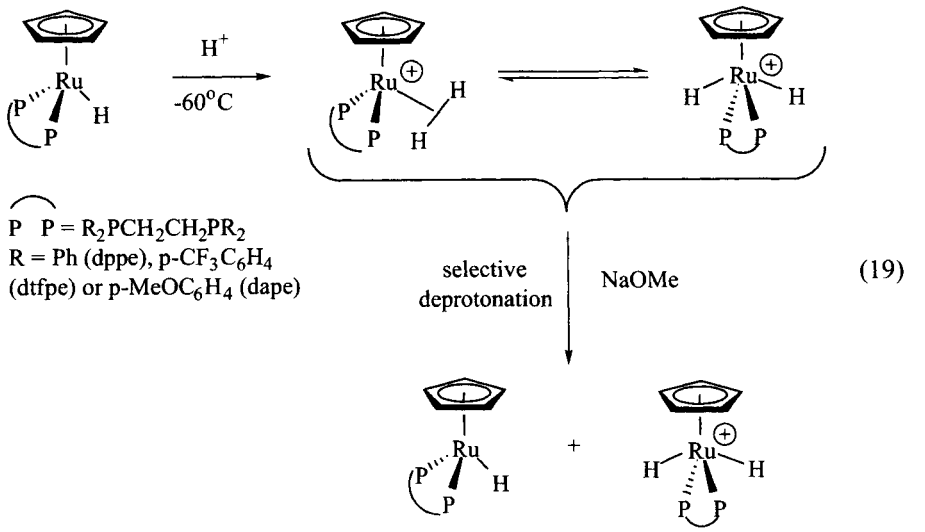

(19)

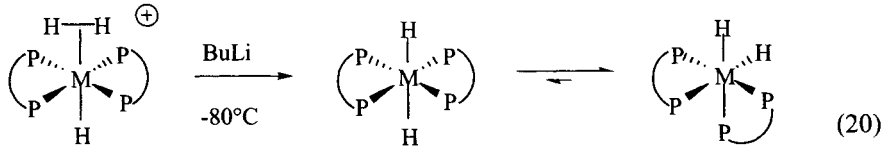

(20)

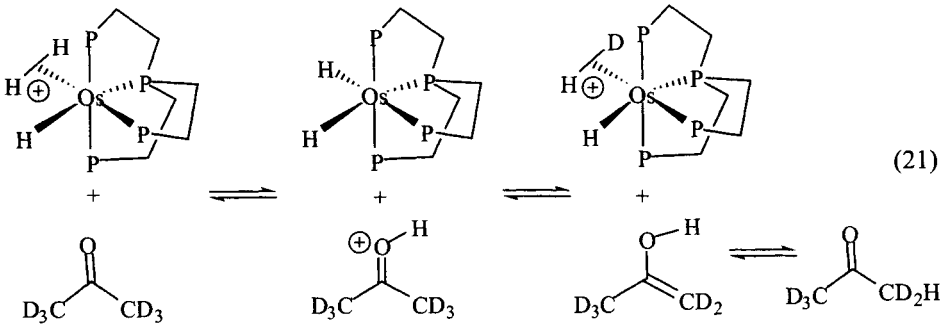

(21)

dihydride at room temperature. For the iron complex, deprotonation led directly to the *cis* dihydride; if the *trans* dihydride was formed, it isomerized too rapidly to be observed.

The high kinetic acidity of dihydrogen complexes is illustrated by the facile exchange between the Os(η^2-H_2) above and various protic solvents, including CD_3OD, D_2O and acetone-d_6 (eq 21); no exchange occurred in CD_2Cl_2 [42]. (Similarly, exchange has been observed between $Ru(H_2)Cl(L)_2^+$ {L = dppe, depe} and acetone-d_6 [43].) Bianchini's proposed mechanism involved protonation of acetone at O, followed by deprotonation at C. Replacement of the (η^2-H_2) with other ligands (N_2 or indirectly $AuHPPh_3$) suppresses exchange with protic solvents, so the hydride ligand cannot itself protonate acetone. Protonation of a polar double bond is a key step in ionic hydrogenation, and dihydrogen complexes play a key role in this process.

Bullock has suggested that fast exchange with TfO^- is responsible for the large line broadening observed for Os(η^2-H_2) by NMR (eq 22) [44]. The hydride peak due to OsH_2 is sharp, as its lower kinetic acidity renders any exchange slow.

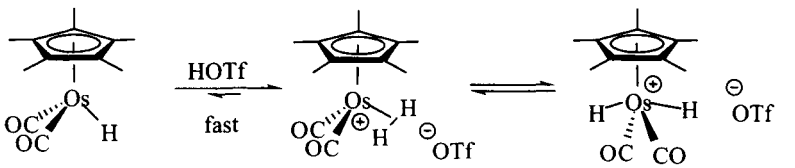

(22)

2.3.2 *Protonation of $CpW(CO)_2(PMe_3)H$: Is the Metal or the Hydride the Kinetic Site?*

We wanted to quantify the kinetic preference for protonation of a hydride ligand over a metal in a case where a dihydride complex was the sole observable product. We decided to search for a dihydrogen intermediate in the protonation of $CpW(CO)_2(PMe_3)H$ (**3**), known eventually to form the cationic dihydride $[CpW(CO)_2(PMe_3)H_2]^+$ (**4**) [44]. Both **3** and **4** had been fully characterised. The hydride complex **3** was first synthesised in 1970 and identified by ^1H and ^{31}P NMR and by IR spectroscopy. It exists in solution in both *cis* (**3c**) and *trans* (**3t**) forms which interconvert rapidly on the NMR timescale (eq 23) [45, 46]. The structure of the cationic dihydride **4** has been determined by x-ray diffraction [44]. The hydride ligands of **4** interconvert rapidly at room temperature, and two inequivalent hydride resonances are not observed until the temperature is lowered to -112 °C [47].

A consequence of eq 24, with kinetic protonation of the hydride ligand, would be that H/D exchange between the hydride complex **3** and an acid would occur faster than protonation of the W to form the dihydride cation **4** (k_{fmp}). We have

therefore compared the rate of H/D exchange between **3** and various acids with the rate at which these acids protonate the metal.

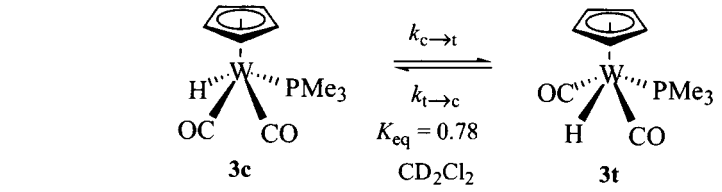

(23)

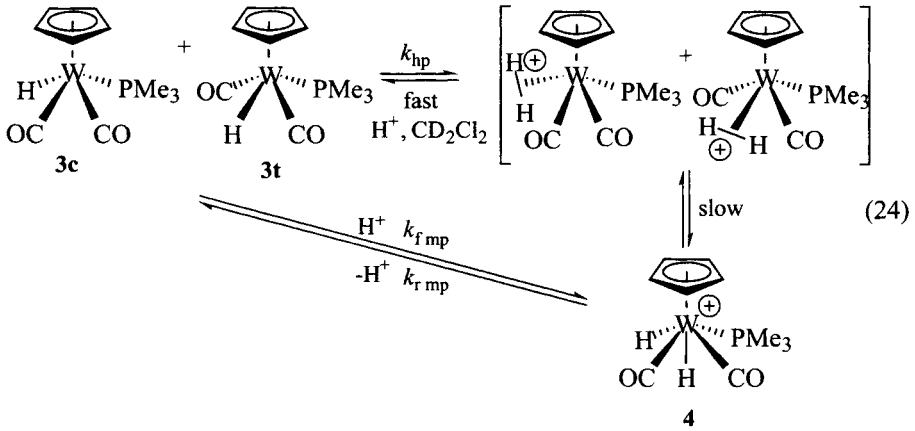

(24)

2.3.2.1 H/D Exchange Between $CpWH(CO)_2(PMe_3)$ and Triflic Acid

Since triflic acid is known to protonate **3** [44], we began our study of the protonation of **3** by examining the rate of isotopic exchange between **3** and TfOD. Preliminary NMR experiments in CD_2Cl_2 at 223K showed that proton exchange was faster than addition of D^+ (or H^+) to the metal. However, both reactions proved to be too fast to quantify even at that temperature [46].

2.3.2.2 Hydride and Metal Protonation of $CpWH(CO)_2(PMe_3)$ by Anilinium

In order to slow down both protonation reactions, and thus to quantify their rates, we replaced TfOH with $PhNH_3^+$ [46]. The PMe_3 resonance of **3** in the ^1H NMR should only be broadened by metal protonation, whereas the H resonance of **3** should be broadened by both exchange with acid and metal protonation, so the excess linebroadening will reflect how much faster hydride ligand protonation is.

Incomplete deprotonation of $[CpWH_2(CO)_2PMe_3][B(Ar^f)_4]$ (**4b**) by aniline (eq 25) gave separate signals for **3**, **4b**, and the acidic hydrogens of the solution. The hydride resonance of **3t** was broadened more (about 60 Hz) than its PMe_3 resonance (2 Hz). The resulting first order rate constants (6.5(7) s^{-1} for metal protonation, 180(30) s^{-1} for exchange) show that the hydride ligand is protonated more rapidly than the tungsten.

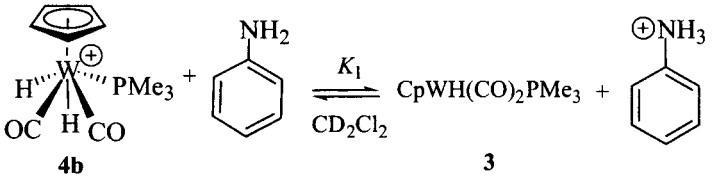

4b **3**

$PhNH_3^+$ should be too weak an acid to protonate **3** according to its pK_a, but protonation of **3** occurs because homoconjugate pair formation between $PhNH_3^+$ and its conjugate base $PhNH_2$ produces $[PhNH_2\cdots H^+\cdots H_2NPh]$ (eq 26) which is the driving force of this reaction (eq 27). The overall reaction is found by combining eq 25 and 26 to yield eq 27, with equilibrium constant K_2 (eq 28). As $[PhNH_2\cdots H^+\cdots H_2NPh]$ = [**3**] and $[PhNH_2] = [PhNH_2]_0 - 2$ [**3**], a linear plot of $([PhNH_2]_0\text{-}2[\mathbf{3}])^2$ versus $([\mathbf{3}]^2/[\mathbf{4b}])$ gives slope $K_2 = K_1K_H = 88.3(4)\ M^{-1}$. Unfortunately, K_H is unknown in CD_2Cl_2, so it is not possible to quantify K_1 or to estimate the value of pK_a(**4b**) in any solvent from this experiment. Since the nature and concentration of the effective acids is uncertain, homoconjugate pair formation makes it impossible to obtain from the line-broadening experiments a meaningful second-order rate constant for either reaction (exchange or protonation at the metal) of **3t**.

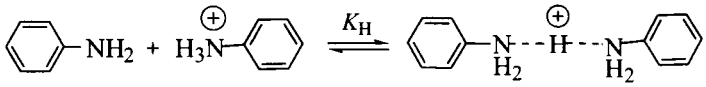

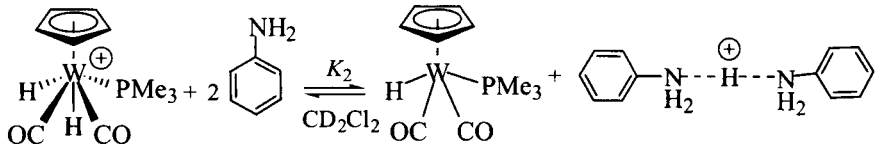

4b **3**

$$K_2 = K_1 \times K_H = \frac{[\mathbf{3}][PhNH_2\cdots H^+\cdots H_2NPh]}{[\mathbf{4b}][PhNH_2]^2} = \frac{[\mathbf{3}]^2}{[\mathbf{4b}]\{[PhNH_2]_0 - 2[\mathbf{3}]\}^2} \quad (28)$$

2.3.2.3 H/D Exchange Between $CpWH(CO)_2(PMe_3)$ and 4-t-Butyl-N,N-dimethylaniline

The substituted anilinium cation **5** was suggested by solubility considerations. The isotopic exchange in eq 29 was studied by ^1H NMR in CD_2Cl_2; as expected, no metal protonation was observed [46]. As anticipated for a bimolecular process, $\Delta S^{\ddagger}$ is ~ –30 e.u., and $k_{f\,ex}$ is $1.8(1) \times 10^{-4}$ $M^{-1}s^{-1}$ at 263 K. K_{eq} was consistently found to be 0.19(2), a surprisingly large equilibrium isotope effect (EIE).

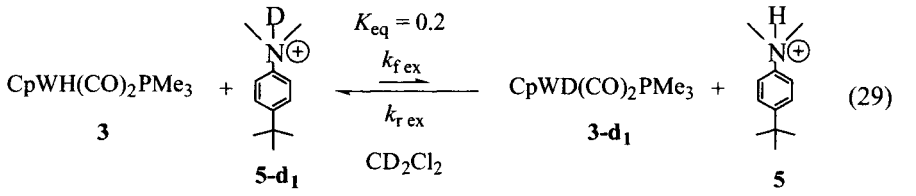

(29)

Equilibrium isotope effects can be calculated from knowledge of the vibrational frequencies of all species involved [48]. While there is precedent [49] for using only the W–H(D) and N–H(D) stretching frequencies to estimate K_{eq}, the stretching frequencies of **3c**, **3c**-d_1, **5**, and **5**-d_1 suggest a K_{eq} of 0.50 at 283 K [46]. Inclusion of one stretching frequency and two bending frequencies leads to a calculated EIE of 0.18 at 283 K, in excellent agreement with the experimentally observed EIE of 0.19 [46]. Since the bending modes of the H(D) ligand of **3** are much lower in frequency than those of the H(D) on the nitrogen in **5**, they have a significant effect on the EIE.

2.3.2.4 Determination of the Rate Constant for Protonation at the W of $CpWH(CO)_2(PMe_3)$ by 4-t-Butyl-N,N-dimethylaniline

We were able to determine the rate constant for protonation by **5** at the metal centre of **3** ($k_{f\,mp}$ in eq 24) only by measuring the reverse rate constant ($k_{r\,mp}$) and considering the equilibrium constant ($K_{eq\,mp}$) [46]. When examined by stopped flow at low temperatures in CH_2Cl_2, the reaction in eq 30 proved quite rapid ($k_{r\,mp}$ = $9.5(3) \times 10^3$ $M^{-1}s^{-1}$ at 263 K) [46]. This rate is not surprising in view of the large thermodynamic driving force for metal deprotonation; **4a** (pK_a = 5.6(1)) is a much stronger acid than **5** (pK_a = 12.2(1)) in CH_3CN [46]. Equilibrium constants for proton transfer between two large bases should not vary appreciably from CH_2Cl_2 to CH_3CN [50], so we can use $K_{eq\,mp}(CH_3CN)$ to solve for $k_{f\,mp}$ = $2.8(1) \times 10^{-4}$ $M^{-1}s^{-1}$. ($K_{eq\,mp}$ at 300 K can be corrected to 263 K by assuming that the variation of ΔG_{mp} with temperature is negligible.)

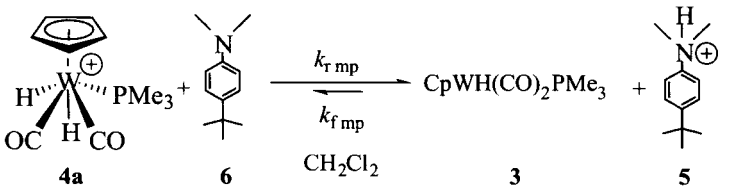

4a 6 3 5 (30)

2.3.2.5 *Comparison of the Rate of Metal Protonation with that of Hydride Protonation of $CpWH(CO)_2(PMe_3)$ by 4-t-Butyl-N,N-dimethylaniline in CH_2Cl_2*

In order to compare the second order rate constant for metal protonation $k_{f\,mp}$ with that for hydride protonation k_{hp} (eq 24), we must calculate the latter from $k_{f\,ex}$. The rate of hydride protonation, k_{hp}, is related to $k_{f\,ex}$ by a primary isotope effect k_H/k_D on $H(D)^+$ transfer to W–H from the anilinium ion and by the fractional probability F that formation of $W(H–D)^+$ will result in detectable rearrangement (to W–D and N–H^+). (F would be 0.5 in the absence of isotope effects.)

If secondary isotope effects are neglected, the ratio k_H/k_D can be estimated as 8.9 from the zero-point energies of the N–H and N–D bonds if we assume a linear transition state for proton transfer [28, 51]. K_{eq} and k_H/k_D can then be used to estimate F = 0.63 [46]. At 263 K, a temperature at which both $k_{f\,ex}$ and $k_{r\,mp}$ were measured, this gives $k_{hp} = 2.7 \times 10^{-3}\ M^{-1}s^{-1}$ and $k_{f\,mp} = 2.8 \times 10^{-4}\ M^{-1}s^{-1}$ [46]. On this basis hydride protonation is ten times faster than metal protonation, thus the kinetic site of protonation of **3** is the hydride ligand [46].

2.3.3 *Kinetic Protonation of a Metal Hydride to Give a Dihydride*

All of the previous examples show that the kinetic site of metal hydride protonation is the hydride ligand. The only evidence to the contrary was found in an attempt to make a silane sigma complex. Brookhart inadvertently generated the iron hydride in eq 31 *in situ* from $CpFe(PEt_3)(SiEt_3)CO$, $H(OEt_2)_2{}^+BAr^f{}_4{}^-$, and adventitious H_2O [52]. Protonation, most likely by $Et_3SiOH_2{}^+$ produced *in situ*, resulted in an iron dihydride which showed a doublet at δ –7.9 (J_{PH} = 70 Hz) in the ^1H NMR. Upon warming, the dihydride isomerized into a dihydrogen complex with a broad doublet in the ^1H NMR (δ –11.8); protonating the iron deuteride gave an η^2-HD complex with J_{HD} = 32 Hz. Loss of H_2 above 10° C precluded isolation of the iron dihydrogen complex. We are aware of no other cases where the kinetic site of protonation of a hydride complex is the metal while the thermodynamic site is the hydride ligand.

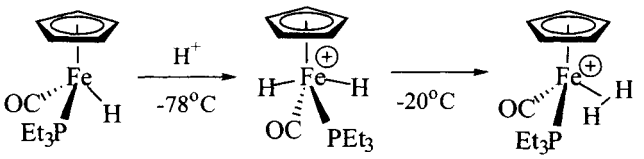

(31)

2.3.4 *Conclusions on Kinetic Protonation of Metal Hydrides*

In the vast majority of studies on the protonation of hydride complexes, the kinetic site was the hydride ligand. This has been proven for many cases in which the thermodynamics of protonation favour a dihydride complex or a mixture of dihydride and dihydrogen complexes. In the case of $CpW(CO)_2(PMe_3)H$ we have shown that hydride protonation (as monitored by exchange) is faster than protonation at the metal; the intermediate dihydrogen complex rearranges too quickly to be observed [46].

The only counterexample, the one discussed in the previous section discovered by Brookhart [52], appears to be due to unique steric and electronic factors acting in concert to favour initial metal protonation. The lack of steric bulk around the iron of $CpFe(CO)(PEt_3)H$ explains why direct metal protonation is possible. In no other examples of hydride ligand protonation followed by H_2 loss (discussed in the next section) has initial metal centre protonation been observed.

2.4 HYDRIDE LIGAND PROTONATION FOLLOWED BY LOSS OF H_2

Of course, H_2 loss can easily occur from H_2 ligands. In many cases a dihydrogen complex has been proposed as an intermediate, but not directly observed, in H_2 loss upon protonation of hydrides by acids [53]. We have already mentioned in Section 2.2 several cases where proton exchange between hydrides and various acids is followed by H_2 loss and both probably occur through a dihydrogen complex intermediate [12b, 16, 18, 19, 21, 22, 24].

In an early investigation of this topic, Berke observed an intermediate dihydrogen complex prior to the loss of H_2 upon treating $Re(NO)(CO)L_2H_2$ with CF_3COOH at low temperature (eq 32) [14, 15]. The resulting dihydrogen ligand

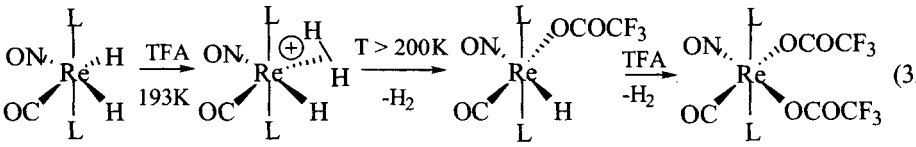

(32)

L = P^iPr_3, $P(O^iPr)_3$, PMe_3

exchanged rapidly with the hydride at all but the lowest temperature (158K) and averaged T_1 (min)'s of 7.3, 4.9, and 9.3 ms for L = P^iPr_3, $P(O^iPr)_3$ and PMe_3, respectively, were observed by ^1H NMR. Above 200 K H_2 gas was evolved and excess acid gave a second equivalent of H_2 gas. When the dihydride was treated with CF_3COOD, the signal of the resulting η^2-HD complex was too broad to resolve J_{HD}.

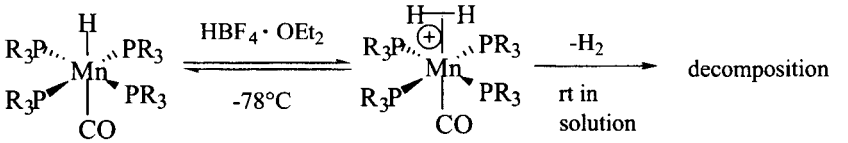

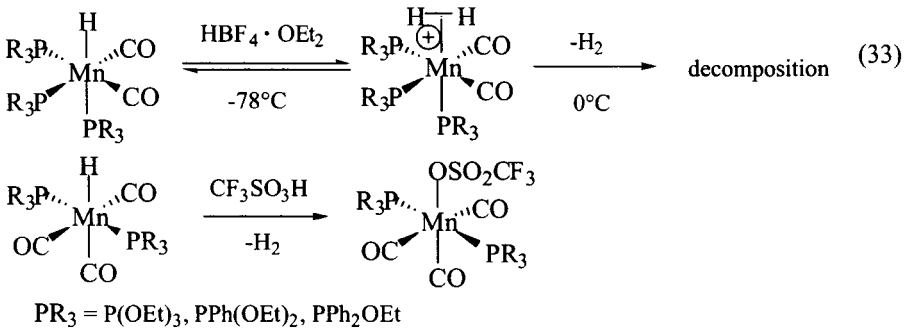

(33)

Similarly, protonation of $MnH(CO)(PR_3)_4$ and $MnH(CO)_2(PR_3)_3$ led to formation of an η^2-H_2 complex prior to H_2 loss and decomposition (eq 33) [54]. The BPh_4^- salts of $Mn(H_2)(CO)(PR_3)_4^+$ are stable in the solid phase and at low temperature in CD_2Cl_2. This allowed characterisation: T_1 (min) was 7 ms and 6 ms and J_{HD} was 32.0 Hz and 32.5 Hz for the $P(OEt)_3$ and $PPh(OEt)_2$ complexes respectively. The dihydrogen complex formulation is also correct for $Mn(H_2)(CO)_2(PR_3)_3^+$: for P = $P(OEt)_3$ T_1 (min) was 5 ms and J_{HD} was 33 Hz. No dihydrogen complex was observed upon protonation of $MnH(CO)_3(PR_3)_2$ with HBF_4, only decomposition and loss of H_2. However, protonation with CF_3SO_3H resulted in loss of H_2 and formation of $Mn(OSO_2CF_3)(CO)_2(PR_3)_2$.

Jia has observed that protonation at room temperature of the iron hydride in eq 34 results in a spectroscopically observable dihydrogen complex (δ −12.5, T_1 (min) = 5 ms, and J_{HD} = 30.7 Hz) prior to thermal loss of H_2 and decomposition [34]. In contrast to the Cp* ligand used by Lapinte (eq 13) [32] which donates electron density into the σ^* of the dihydrogen complex to favour dihydride complex formation, the electron poor Cp disfavours dihydride complex formation.

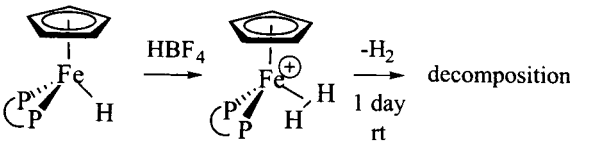

(34)

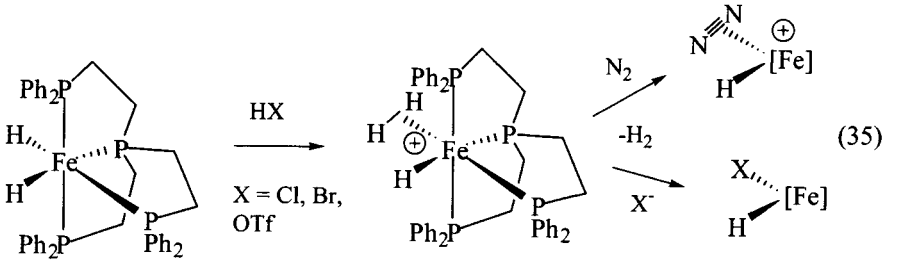

(35)

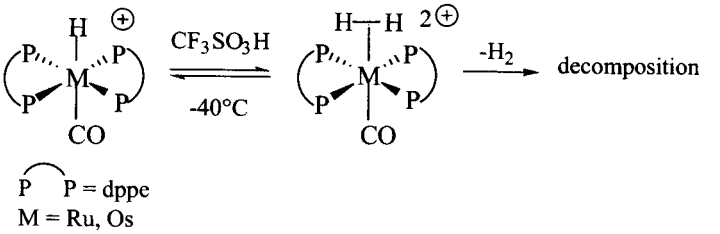

(36)

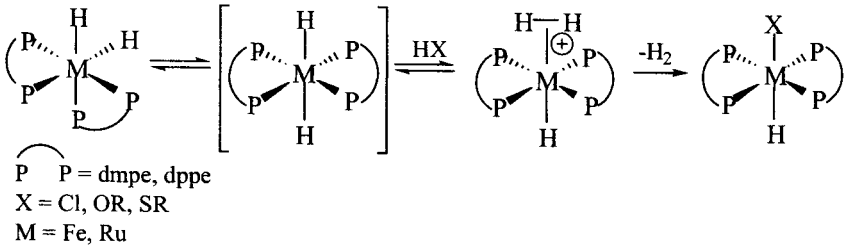

(37)

Basallote has shown that protonation of the hydride in eq 35 results in an Fe(η^2-H_2) complex [55]. The kinetics (monitored electrochemically) showed an inverse kinetic isotope effect consistent with the mechanism shown [56] — normal kinetic isotope effects are expected for metal protonation. Again (eq 18, Section 2.3.1.1) [36], no correlation between the rate of protonation and the apparent pK_a(HX) in THF [38] was observed, possibly due to homoconjugate or ion pairing interactions.

Rocchini has observed that the π acceptor ability of the CO ligand favours formation of an η^2-H_2 complex like the one in eq 36 by decreasing electron

density at the metal and hence reducing donation into the σ* of the H_2 [57]. Attempts to protonate the cationic hydride in eq 36 at room temperature resulted in immediate gas evolution and decomposition, but the dicationic Ru(η^2-H_2) complex could be seen at –40°C. Protonation of the OsH resulted in a dihydrogen complex that was stable in solution at room temperature under H_2 or Ar but lost H_2 on attempted isolation. The dihydrogen complexes were characterised by T_1 (min)'s of 5.0 and 5.5 ms and J_{HD} of 34.2 and 32.0 for Ru and Os, respectively. Similarly, Morris [58] observed that protonation of $Fe(dppe)_2(CO)H$ gave an acidic η^2-H_2 Fe complex that eliminated H_2, resisted isolation, and facilitated H/D scrambling between H_2 and D_2 gas.

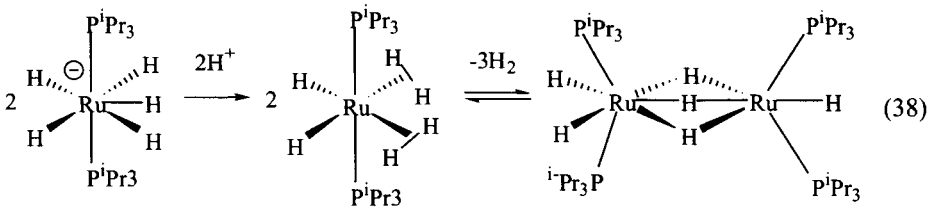

(38)

Protonation of the Fe/Ru dihydrides in eq 37 followed by H_2 evolution was studied by Field [59] and Basallote [60] with dmpe and dppe as phosphines, and thiols, alcohols and HCl as acids. Note that this mechanism (*cis* to *trans* isomerization followed by hydride ligand protonation) is simply the reverse of that proposed by Morris [40, 41] for kinetic deprotonation of a dihydrogen complex (see Section 2.3.1.2, eq 20).

Other metal hydrides which lose H_2 after protonation at the H ligand include $TpM(CO)H(P^iPr_3)$ (M=Ru, Os) (Tp = tris(pyrazolyl)borate) [61] and $TpmRuH(PPh_3)_2$ (Tpm = tris(pyrazolyl)methane) [62]. Protonation of $Os(dppe)_2H(CH_3CN)$ gives a stable η^2-H_2 complex, but transient H_2 loss is implied by exchange with D_2 gas [63]. The same is true for M(bis(bidentate) phosphine)(H)(CN) (M = Fe, Ru, Os) complexes, although protonation at the CN also occurs [64]. Similarly, for Ru/Os complexes containing both an H and an SR ligand, protonation occurs at S as well as at H (followed by H_2 loss) [65].

Some final examples have interesting implications for ionic hydrogenation. Morris [66] investigated the protonation in eq 38 and found an unusual bis(dihydrogen) dihydride complex {non-classical structure confirmed by T_1 (min) = 60ms (η^2-H_2) and J_{HD} = 30Hz (η^2-HD)} which lost H_2 to form a stable Ru dimer under vacuum or Ar. Since loss of H_2 is reversible, the Ru dimer could potentially serve as an *in situ* source of the dihydrogen complex (and thus as a catalyst for ionic hydrogenation).

Jia and Lau have investigated the protonation of Cp*Ru(diene)H complexes [67]. Protonation of the cyclooctadiene complex led to a dihydrogen complex

(T_1 = 9.9 ms at 180K, J_{HD} = 29.3 Hz) which loses H_2 when warmed to room temperature. In contrast, protonation of the norbornadiene complex produced a bimetallic Ru product and partial hydrogenation of the ligand (presumably this reaction also went through an η^2-H_2 complex).

Thus dihydrogen complexes play a key role in the evolution of H_2 gas after protonation of metal hydrides. The reverse of this process, heterolytic H_2 activation to form H^+ and a metal hydride, can be used to hydrogenate polar double bonds.

2.5 IONIC HYDROGENATION

The fact that H_2 loss from MH/HA is reversible means that addition of H_2 to a metal complex to give an acidic dihydrogen complex should be possible. Ionic hydrogenation requires that this dihydrogen complex be acidic enough to protonate the substrate and that the corresponding hydride be capable of transferring H^- to the protonated substrate (eq 2).

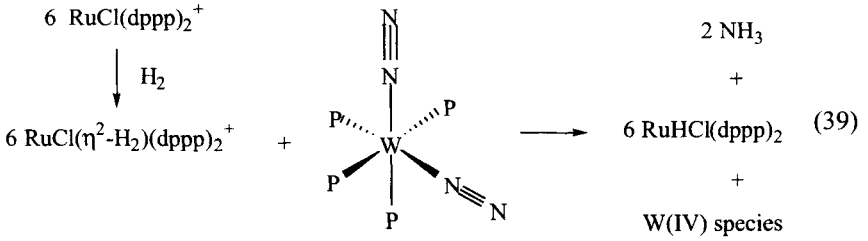

(39)

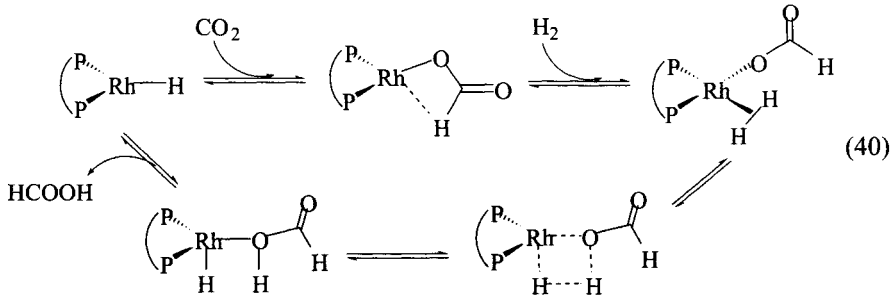

(40)

An early example involves the conversion of coordinated N_2 to NH_3 [68]. Hidai has reported that the Ru(η^2-H_2) complex in eq 39 can carry out this reaction. This process is discussed in greater detail in Chapter 5. Similarly,

Leitner has proposed that dihydrogen complexes play a key role in catalytic hydrogenation of CO_2 (eq 40) [69]. He has suggested that a dihydrogen complex is an intermediate in the hydrogenolysis of the Rh-formate bond; σ bond metathesis yields coordinated formic acid, which is released to complete the catalytic cycle. The reverse of this process explains why formic acid can be used as an H_2 source in transfer hydrogenation [70].

2.5.1 Stoichiometric Ionic Hydrogenation by Transition Metal Complexes

Early reports have shown that transition metals can add the elements of hydrogen across double bonds *stoichiometrically* by an ionic mechanism. In separate papers in 1985 the Darensbourg [71] and Gibson [72] groups reported the reduction of aldehydes (ketones were much less reactive) by Group 6 carbonyl hydrides and CH_3CO_2H (eq 41). In 1987 Vos and co-workers reported the hydrogenation of acetone in eq 42 by a hydride ligand and H^+ in aqueous solution [73]. In 1989 Bullock and Rappoli reported the hydrogenation of tetra-, tri-, and 1,1-disubstituted olefins by $HW(CO)_3Cp$ and CF_3SO_3H (eq 43) [74].

$$\text{RCHO} + \text{H–M} \xrightarrow[\text{THF}]{\text{HOAc}} \text{RCH}_2\text{OH} \qquad (41)$$

$$\text{H–M} = \text{HM(CO)}_4\text{L}^- \text{ (M = Cr, W) or } \text{HMo}_2(\text{CO})_{10}^-$$

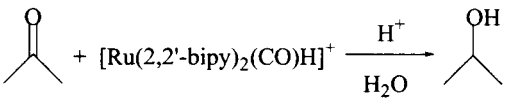

(42)

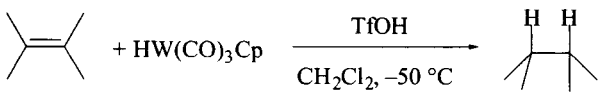

(43)

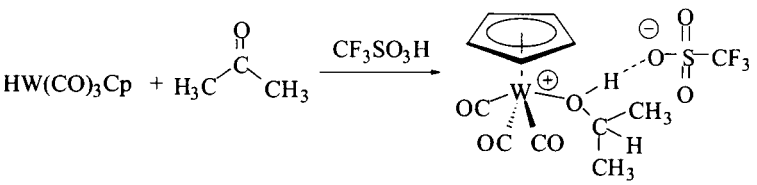

(44)

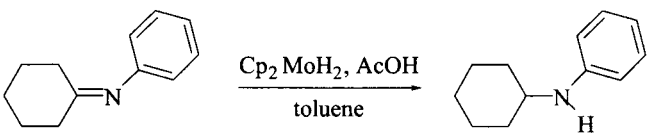

(45)

In 1992 the Bullock and Norton groups reported the reduction of aldehydes and ketones under similar conditions, and isolated an isopropyl alcohol complex formed thereby (eq 44) [75]; similar results have recently been reported with $H_2Re(NO)(CO)(PR_3)_2/CF_3CO_2H$ by Bakhmutov and co-workers [76]. These reactions resemble the "ionic" hydrogenations long known with silanes as hydride donors [77].

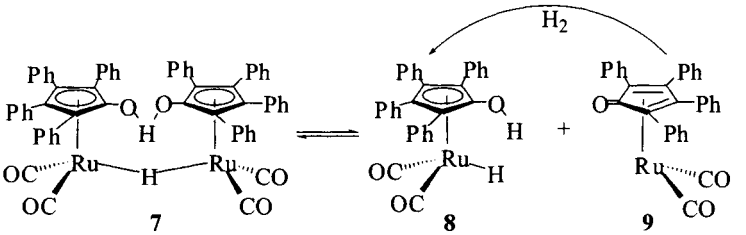

(46)

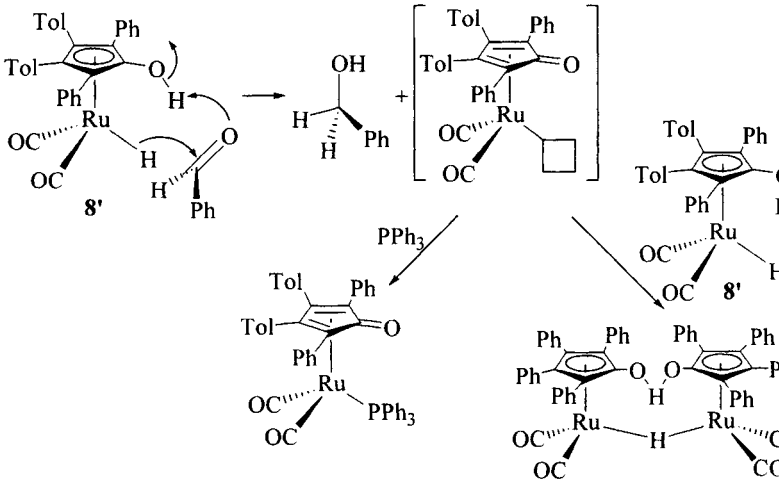

(47)

Such reactions presumably involve the rapid, reversible protonation of the substrate olefin or ketone, followed by hydride transfer from the metal (or the Si of the silane) (eq 1). Several studies have confirmed that metal hydrides transfer H^- in a single step, not by sequential transfer of $H\cdot$ and e^- [78]. As we would expect, the rates of these reactions increase with acidity [73, 74, 75] and are first-order in substrate [75]. When pivaldehyde is used as a substrate with TsOH and $CpRe(NO)(PPh_3)H$ no rearrangement occurs, implying that transfer of hydride to the protonated substrate is efficient [75].

Such ionic hydrogenation reactions mimic biological reductions, which almost always involve the sequential addition of H^+ and H^- [79]. Such hydrogenations are attractive because (1) *they lend themselves to ionising solvents such as water*,

and (2) *they lend themselves to selecting polar C=X double bonds over C=C double bonds*. Noyori has emphasised the need for "preferential hydrogenation of a carbonyl function over olefinic and acetylenic bonds" [80]. He has also noted that "Currently available hydrogenation catalysts, either homogeneous or heterogeneous, are mostly selective for C=C functions over C=O bonds", although he has reported a catalyst system ($RuCl_2L_3$/en/KOH) that reverses that selectivity [81]. Ionic hydrogenation has been extended to C=N double bonds by Ito and co-workers (eq 45) [82].

While stoichiometric ionic hydrogenation reactions are not attractive from a practical standpoint, the Shvo, Hidai, Bullock and Norton groups have shown that these reactions can be done catalytically, from H_2 gas.

2.5.2 *Catalytic Ionic Hydrogenation by Transition Metal Complexes*

2.5.2.1 *$RuH(Ph_4C_5OH)(CO)_2$ as a Catalyst for Ionic Hydrogenation*

Shvo has used complex **7** in eq 46 to catalyse the ionic hydrogenation of ketones, olefins, and acetylenes at moderate temperature and H_2 pressure [83]. A mononuclear hydride with a tethered hydroxyl group (**8**) is believed to be the active catalyst, so dissociation of **7** is necessary [84]. $Ru(Ph_4C_5O)(CO)_2$ (**9**) can be converted to the active catalyst under H_2. The ionic hydrogenation of alkynes occurs with few turnovers because free alkyne coordinates irreversibly to the catalyst precursor (**9**) [85]; similar alkyne complexes have been observed in other hydrogenation studies [86].

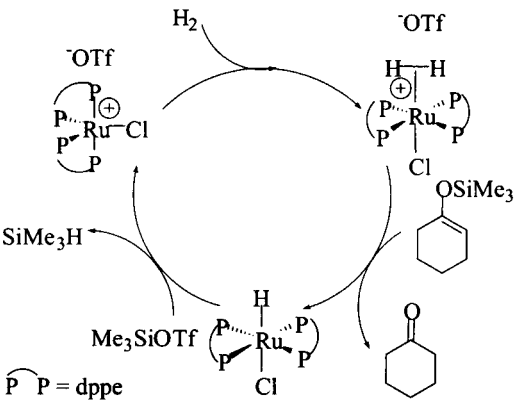

(48)

A mechanistic study by Casey [87] has shown that H_2 is transferred from the catalyst to benzaldehyde in a concerted fashion; the rate law for eq 47 is first order in both hydride and PhCHO, with a $\Delta S^{\ddagger}$ of -28 e.u. indicating an associative pathway. In the absence of donor ligands, the ruthenium hydride

complex **8′** disappears twice as fast as PhCHO. When PPh_3 is present as a trap, the ruthenium hydride disappears at the same rate as PhCHO. The acidic OH group on the substituted Cp is essential to reactivity toward imines: with this hydroxyl the catalyst is selective for the hydrogenation of imines over ketones, whereas similar catalysts without the OH show the reverse selectivity {e.g. Noyori's $RuHAr(NTs\text{-}(C_2H_2Ph_2)\text{-}NH_2)$ does not hydrogenate imines [4]}. Backväll has shown by deuterium labelling that the acidic OH selectively protonates the ketone oxygen, whereas the metal hydride is transferred exclusively to the ketone carbon [88]. Casey has proposed concerted transfer of H^+ and H^- as shown in eq 47 to explain these results [87], thus the Shvo catalyst hydrogenates via an ionic mechanism.

2.5.2.2 $Ru(H_2)(dppe)_2Cl$ as a Catalyst for Hydrogenolysis of Si-O

Hidai has achieved the catalytic hydrogenolysis of silyl enol ethers with H_2 gas via sequential transfer of H^+ and H^- (eq 48) [89]. That the mechanism involves heterolytic H_2 cleavage was shown by treating $Ru(\eta^2\text{-}D_2)^+$ with the corresponding lithium enolate. D^+ transfer from the $\eta^2\text{-}D_2$ complex to the oxygen of the substrate resulted in initial enol formation followed by tautomerization to give ketone with 95% deuterium incorporation in the α position (LiOTf and $RuD(dppe)_2Cl$ were the other products). The second step of hydride transfer was observed by treating $RuH(dppe)_2Cl$ with Me_3SiOTf to give $RuCl(dppe)_2^+(OTf)^-$ and Me_3SiH. The dihydrogen complex catalyst could be regenerated from $RuCl(dppe)_2^+$ under H_2 pressure. Thus Si-O hydrogenolysis occurs via an ionic mechanism.

2.5.2.3 $[CpM(CO)_2(PR_3)(ketone)]^+$ (M = W, Mo) as a Catalyst for Ionic Hydrogenation

Bullock has just reported [90] catalysts for the ionic hydrogenation of ketones that contain inexpensive metals (Mo and W). $[CpM(CO)_2(PR_3)(ketone)]^+A^-$ (M = Mo or W; R = CH_3, Ph, or Cy; and A^- = PF_6^-, BF_4^-, and $BAr^f{}_4^-$) complexes catalyse the slow hydrogenation of diethyl ketone under mild conditions: room temperature and low pressures of H_2 (<4 atm) (eq 49).

$[CpW(CO)_2(PPh_3)(\eta^1\text{-}O{=}CEt_2)]^+BAr^f{}_4^-$ is a relatively poor catalyst, presumably because of formation of the alcohol complex $[CpW(CO)_2(PPh_3)(\eta^1\text{-}OH\text{-}CHEt_2)]^+$ $BAr^f{}_4^-$ at long reaction times. Use of isolated $[CpMo(CO)_2(PPh_3)(\eta^1\text{-}O{=}CEt_2)]^+BAr^f{}_4^-$ produced 2.8 turnovers in 1 day in CD_2Cl_2 solvent. The highest catalytic activity (8.6 turnovers in 6 hours) was found after $CpMo(CO)_2(PCy_3)H$ was treated with $Ph_3C^+BAr^f{}_4^-$.

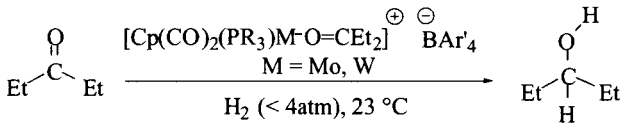

(49)

A catalytic cycle is proposed in eq 50: H_2 displaces the ketone complex to give a dihydrogen or dihydride complex, this dihydrogen complex protonates the ketone, H^- is transferred to the carbon of the substrate, and the 16-electron M^+ complex is coordinated by ketone to complete the cycle. Although $MoH_2^+/Mo(\eta^2\text{-}H_2)^+$ complexes have not been directly observed, some $WH_2^+/W(\eta^2\text{-}H_2)^+$ complexes have been structurally characterised [44] and are known to be acidic [46].

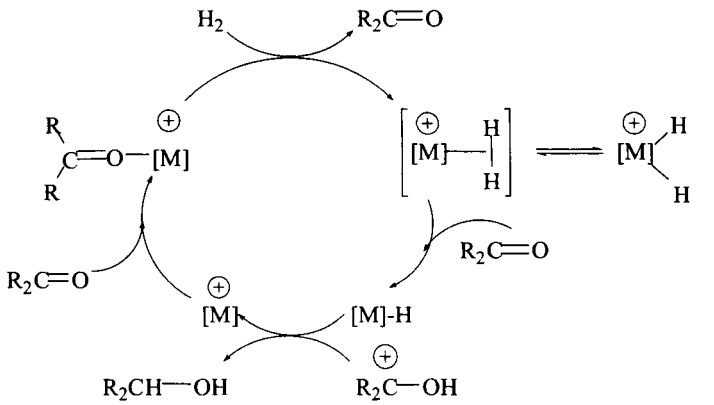

(50)

2.5.2.4 *CpRu(P-P)H as a Catalyst for Ionic Hydrogenation of Iminium Cations*

We have reported that the ionic hydrogenation of iminium cations occurs *catalytically* and with *enantioface selectivity* when a piano-stool ruthenium hydride complex is used [91]; isolated yields range from 60-80% with 2 mol % catalyst. Furthermore, enantiopure bisphosphines give enantioenriched product (eq 51); base workup yields enantioenriched amines (eq 52).

The mechanism undoubtedly involves hydride transfer from Ru to the iminium cation. When run *stoichiometrically* (usually in the presence of two equiv of CH_3CN) the hydride transfer reaction gives the same ee as the catalytic reaction. If the H_2 pressure is varied, there is no change in the rate or enantiomeric excess of the catalytic reaction (eq 53); thus H_2 does not participate in the turnover-limiting or enantio selectivity-determining steps. Transfer of hydride is necessarily the slow, *enantiodetermining* step. It is followed by H_2 coordination to generate an acidic dihydrogen complex, and protonation of the product amine to produce an ammonium cation and complete the catalytic cycle (eq 54). When

catalysis is monitored by ^1H NMR, only the hydride is observed while substrate is still present. Only after complete depletion of substrate is the known [92] ratio of dihydride and dihydrogen complexes observed. Once again, the heterolytic activation of H_2 by a metal complex is ideally suited for hydrogenation of polar double bonds.

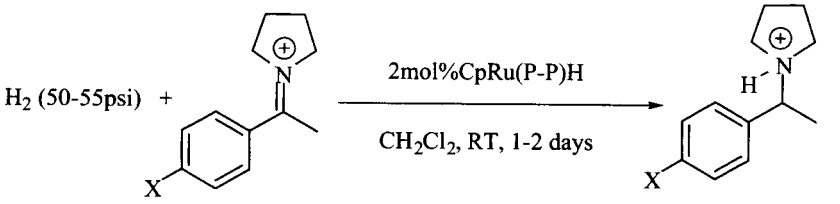

(51)

Hydride	X	ee, configuration of amine
CpRu((*S, S*)-Chiraphos)H	H	35%, (*R*)
CpRu((*S, S*)-Chiraphos)H	Cl	56%, (*R*)
CpRu((*R, R*)-Norphos)H	H	48%, (*S*)
CpRu((*R, R*)-Norphos)H	Cl	60%, (*S*)

(*S, S*)-Chiraphos = 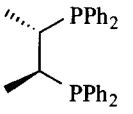

(*R, R*)-Norphos = 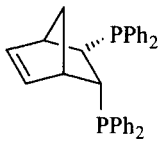

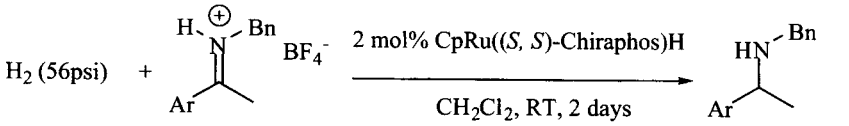

Ar = naphthyl ($C_{10}H_7$)

after base workup
50% yield, 61% ee

(52)

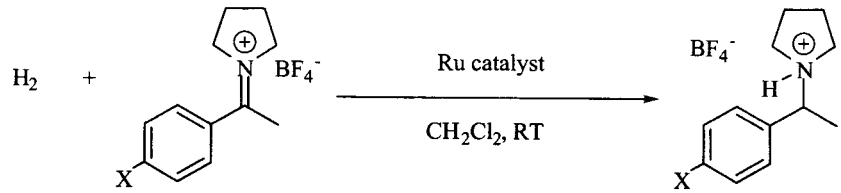

(53)

H_2	X	catalyst	
50 psi	H	4 mol% CpRu(dppe)H, 90 min.	**33% completion**
500 psi	H	4 mol% CpRu(dppe)H, 90 min.	**24% completion**
50 psi	Cl	2 mol% CpRu((*S, S*)-Chiraphos)H, 1 day	**56% ee**
500 psi	Cl	2 mol% CpRu((*S, S*)-Chiraphos)H, 1 day	**50% ee**

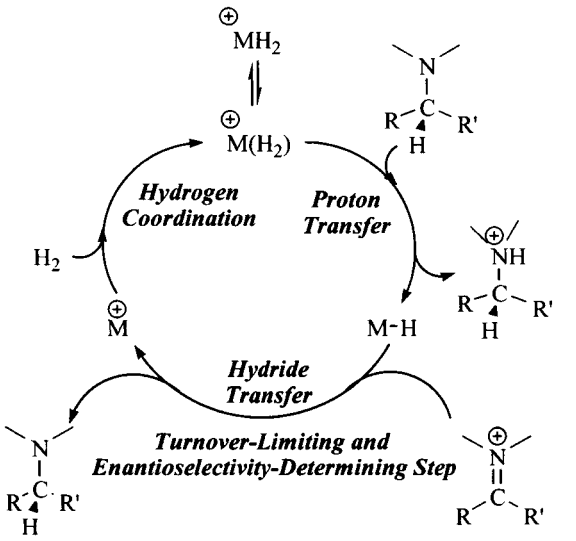

(54)

2.5.3 *Hydrogenation Catalysts Whose Mechanisms may be Ionic*

For many hydrogenation catalysts an ionic mechanism has been suggested but not proven. The selectivity for C=O over C=C of a $Ru(\eta^2\text{-}H_2)_2$ catalyst studied by Chaudret [93] and a CuH catalyst employed by Stryker [94] suggests an ionic hydrogenation mechanism.

Oro has proposed that $OsHCl(PMe^tBu_2)_2$ hydrogenates benzylideneacetone to the saturated ketone by an ionic mechanism. Initial transfer of H^- to coordinated substrate is followed by H_2 addition to give an $Os(\eta^2\text{-}H_2)^+$ complex which can transfer H^+ to complete C=C hydrogenation [95].

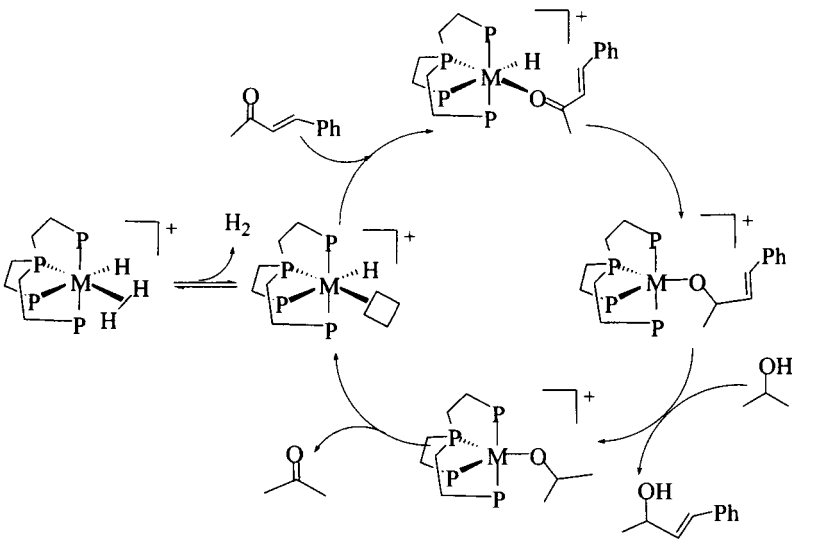

(55)

In contrast, Bianchini has observed the C=O hydrogenation of benzylideneacetone with $(P_3P)M(H)(H_2)^+$ (M = Fe, Ru, Os) catalysts. When run as a transfer hydrogenation (discussed in the next section) with isopropanol as the ultimate source of H_2 (but allowing the H_2 pressure to vary), the catalytic activity proved to depend inversely on H_2 pressure — suggesting that H_2 competes with the ketone for a coordination site (eq 55) [96]. This process is examined in greater detail in Chapter 9.

2.5.4 Transfer Hydrogenation

The same steps involved in ionic hydrogenation — H^+ and H^- transfer to the substrate ketone — are involved in catalysis of hydrogen transfer from isopropyl alcohol to a prochiral ketone (eq 3). Traditionally, ketone coordination to the catalyst was invoked to rationalise the achievement of enantioselectivity. While transfer hydrogenation is usually done under basic conditions, the base is required more for the generation of the active catalyst than for the reaction itself; the dihydride H_2RuL_3 can catalyse the transfer of hydrogen from isopropyl alcohol to various ketones by itself [88, 89].

Recent theoretical [98, 99] and experimental [4, 100] work strongly suggests that, when the catalyst contains a primary or secondary amine ligand, transfer hydrogenation involves H^-/H^+ transfer to/from a Ru-amide bond. (Buchwald [101] has written a similar step for the uptake of H_2 during the asymmetric hydrogenation of imines.) Pictured as structure 56 is a transition state that describes both hydrogen removal from ^{i}PrOH and hydrogen donation to the substrate; coordination of the ketone is not required, and good enantioface selectivity is achieved.

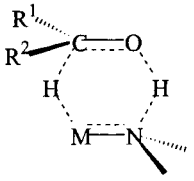

(56)

2.6 CONCLUSION

The heterolytic cleavage of H_2 in ionic hydrogenations is the microscopic reverse of the protonation of a hydride by NH, OH, or SH, and there is often a structural similarity between ionic hydrogenation catalysts (e.g. $RuH(\eta^5\text{-}Ph_4C_5OH)(CO)_2$, Section 2.5.2.1) and hydride complexes that exchange with tethered acids (e.g. $[RuH(\eta^5\text{-}C_5H_4CH_2CH_2NMe_2H)(dppm)]^+$, Section 2.2.1). By comparing the rates of proton exchange and metal protonation of

$CpWH(CO)_2PMe_3$ with various acids, we have shown that the kinetic site of protonation is the hydride ligand, even though a dihydrogen intermediate cannot be directly observed in this case [46]. In general, the initial protonation site is the hydride ligand, even when the thermodynamic product is the dihydride. In only one instance [52], has a kinetic preference for metal centre protonation been demonstrated.

Thus the protonation of hydride complexes often leads to loss of H_2. The reverse of this process, H_2 coordination and formation of a dihydrogen complex that can lose H^+ and yield MH — leads to ionic hydrogenation. Ionic hydrogenation may be done stoichiometrically, but more practical catalytic methods recently developed show great promise for C=O hydrogenation and O-Si hydrogenolysis. Some ionic hydrogenation catalysts employ inexpensive Mo and W metals; modifications of such catalysts have lead to environmentally benign water-soluble catalysts [102] and further investigation of this area is warranted. With chiral CpRu(P-P)H catalysts some enantioface selectivity can be achieved in the hydrogenation of iminium to ammonium cations, with the hydride transfer step determining both the rate and the enantioselectivity. Additional mechanistic understanding should permit the development of better catalysts.

REFERENCES

[1] S. Michaile, M. Hillman, J. J. Eisch Organometallics 7 (1988) 1059–1065, and references therein.

[2] (a) J. P. Collman, P. S. Wagenknecht, R. T. Hembre, N. S. Lewis J. Am. Chem. Soc. 112 (1990) 1294–1295. (b) J. P. Collman, P. S. Wagenknecht, R. T. Hembre, N. S. Lewis J. Am. Chem. Soc. 114 (1992) 5665–5673. (c) J. P. Collman, P. S. Wagenknecht, J. E. Hutchison Angew. Chem. Int. Ed. Engl. 33 (1994) 1537–1554.

[3] (a) G. J. Kubas J. Chem. Soc., Chem. Commun. (1980) 61–2. (b) G. J. Kubas Comments Inorg. Chem. 7 (1988) 17–40. (c) G. J. Kubas Acc. Chem. Res. 21 (1988) 120–8. (d) R. H. Crabtree Acc. Chem. Res. 23 (1990) 95–101. (e) P. G. Jessop, R. H. Morris Coord. Chem. Rev. 121 (1992) 155–284. (f) D. M. Heinekey, W. J. Oldham Chem. Rev. 93 (1993) 913–26. (g) U. Koelle New J. Chem. 16 (1992) 157-169.

[4] R. Noyori, S. Hashiguchi, Acc. Chem. Res. 30 (1997) 97-102

[5] (a) R. F. Jordan, J. R. Norton J. Am. Chem. Soc. 104 (1982) 1255–1263. (b) R. F. Jordan, J. R. Norton ACS Symp. Ser. No. 198 (1982) 403. (c) Inorganic Reactions and Methods; J. J. Zuckerman, Ed.; VCH: New York, 1987, p 207.

[6] (a) S. S. Kristjánsdóttir, J. R. Norton, Acidity of Hydrido Transition Metal Complexes in Solution. In Transition Metal Hydrides; Dedieu, A., Ed.; VCH: New York (1991). (b) R. Kuhlman, Coord. Chem. Rev. 167 (1997) 205–232.

[7] P. J. Desrosiers, L. Cai, Z. Lin, R. Richards, J. Halpern J. Am. Chem. Soc. 113 (1991), 4173-84.

[8] A. E. Derome Modern NMR Techniques for Chemistry Research Pergamon: Oxford, UK (1987).

[9] D. M. Heinekey, J. M. Millar, T. F. Koetzle, N. G. Payne, K. W. Zilm, J. Am. Chem. Soc. 112 (1990) 909.

[10] a) T. F. Koetzle Trans. Am. Crystallogr. Assoc. 31 (1997) 57-68. b) R. Bau, M. H. Drabnis, Inorg. Chim. Acta. 259 (1997) 27-50. c) S. Li, M. B. Hall, J. Eckert, C. M. Jensen, A. Albinati J. Am. Chem. Soc. 122 (2000) 2903-2910. d) D. Braga, P. De Leonardis, F. Grepioni, E. Tedesco, Inorg. Chim. Acta 273 (1998) 116-130.

[11] Cp = cyclopentadienyl; Cp* = pentamethylcyclopentadienyl; py = pyridine; dppm = diphenylphosphinomethane; dppe = diphenylphosphinoethane; dppp = diphenylphosphinopropane; $R_2PCH_2CH_2PR_2$ = dfepe (R = C_2F_5), dtfpe (R = p-CF_3-C_6H_4), or dape (R = p-MeO-C_6H_4); Ar^f = 3,5-bis(trifluoromethyl)phenyl.

[12] a) R. H. Crabtree, J. Organomet. Chem. 577 (1998) 111–115. b) J. A. Ayllon, C. Gervaux, S. Sabo-Etienne, B. Chaudret, Organometallics 16 (1997) 2000–2002. c) E. S. Shubina, N. V. Belkova, A. N. Krylov, E. V. Vorontsov, L. M. Epstein, D. M. Gusev, M. Niedermann, H. Berke, J. Am. Chem. Soc. 118 (1996) 1105–1112.

[13] a) V. Bakhmutov, T. Bürgi, P. Burger, U. Ruppli, H. Berke, Organometallics 13 (1994) 4203–4213. b) D. M. Heinekey, M. van Roon, J. Am. Chem. Soc. 118 (1996) 12134-12140. c) D. M. Heinekey, H. Mellows, T. Pratum, J. Am. Chem. Soc. 122 (2000) 6498-6499.

[14] D. G. Gusev, D. Nietlispach, I. L. Eremenko, H. Berke, Inorg. Chem. 32 (1993) 3628-3636.

[15] S. Feracin, T. Bürgi, V. Bakhmutov, I. Eremenko, E. V. Vorontsov, A. B. Vimenitis, H. Berke, Organometallics 13 (1994) 4194–4202.

[16] A. J. Lough, S. Park, R. Ramachandra, R. H. Morris, J. Am. Chem. Soc. 116 (1994) 8356-8357.

[17] R. Koelliker, D. Milstein, J. Am. Chem. Soc. 113 (1991) 8524-8525.

[18] M. M. Abad, I. Atheaux, A. Maisonnat, B. Chaudret, Chem. Commun. (1999) 359.

[19] A. Caballero, F. A. Jalon, B. R. Manzano; J. Chem. Soc., Chem. Commun. (1998) 1879.

[20] a) M. L. Christ, S. Sabo-Etienne, G. Chung, B. Chaudret, Inorg. Chem. 33 (1994) 5316. b) S. N. Smirnov, R. S. Golnbev, G. S. Demisov, H. Benedict, P. Schah-Mohamendi, H. H. Limbach, J. Am. Chem. Soc. 118 (1996) 4094. c) K. Wozniak, H. H. He, J. Klinowski, T. L. Barr, S. E. Hardcastle, J. Phys. Chem. 100 (1996) 11408.

[21] H. S. Chu, C. P. Lau, K. Y. Wong, W. T. Wong, Organometallics 17 (1998) 2768.

[22] J. A. Ayllon, S. F. Sayers, S. Sabo-Etienne, B. Donnadieu, B., Organometallics 18 (1999) 3981–3990.

[23] This possibility is supported by the effect on the proton exchange rate of the base remaining in solution after **1** is formed (Bu_3P makes exchange faster than does Et_3N). A similar effect (of counterion on H/D exchange rate) was reported by Berke and coworkers with $Re(NO)(CO)L_2H_2$ in ref 15.

[24] a) Z. K. Sweeney, J. L. Polse, R. A. Andersen, R. G. Bergman, Kubinec, M. G. Kubinec, J. Am. Chem. Soc. 119 (1997) 4543-4544. b) Z. K. Sweeney, J. L. Polse, R. G. Bergman, R. A. Andersen, Organometallics 18 (1999) 5502-5510.

[25] a) T. Ziegler, E. Folga, A. Berces, J. Am. Chem. Soc. 115 (1993) 636. b) H. H. Brintzinger, J. Organomet. Chem. 171 (1979) 337. c) A. H. Neuhaus, E. D. Glendening, A. Streitwieser, Organometallics 15 (1996) 3688.

[26] A. C. Albeniz, D. M. Heinekey, R. H. Crabtree, Inorg. Chem. 30 (1991) 3632-3635.

[27] N. V. Belkova, E. V. Bakhmutova, E. S. Shubina, C. Bianchini, M. Peruzzini, V. I. Bakhmutov, L. M. Epstein, Eur. J. Inorg. Chem. (2000) 2163-2165.
[28] R. T. Edidin, J. M. Sullivan, J. R. Norton, J. Am. Chem. Soc 109 (1987) 3945–3953.
[29] D. Morales, R. Poli, J. Andrieu, Inorg. Chim. Acta 300-302 (2000) 709-720.
[30] G. Parkin, J. E. Bercaw, J. Chem. Soc., Chem. Commun. (1989) 255-257.
[31] R. A. Henderson, K. E. Oglieve, J. Chem. Soc., Dalton Trans. (1993) 3431-3439.
[32] P. Hamon, L. Toupet, J. Hamon, C. Lapinte Organometallics 11 (1992) 1429–1431.
[33] G. Jia, A. J. Lough, R. H. Morris Organometallics 11 (1992) 161-171.
[34] G. Jia, W. S. Ng, J. Yao, Organometallics 15 (1996) 5039-5045.
[35] A. C. Ontko, J. F. Houlis, R. C. Schnabel, D. M. Roddick, T. P. Fong, A. J. Lough, R. H. Morris, Organometallics 17 (1998) 5467-5476.
[36] M. G. Basallote, J. Duran, M. J. Fernandez-Trujillo, M. A. Manez, Organometallics 19 (2000) 695-698.
[37] M. Y. Hung, S. M. Ng, Z. Zhou, C. P. Lau, G. Jia, Organometallics 19 (2000) 3692-3699.
[38] A. Streitwieser, Y. J. Kim, J. Am. Chem. Soc. 122 (2000) 11783-11786.
[39] a) G. Jia, R. H. Morris, J. Am. Chem. Soc. 113 (1991) 875-883. b) F. Conroy-Lewis, S. J. Simpson, J. Chem. Soc. Chem. Commun. (1987) 1675-1676.
[40] M. T. Bautista, E. P. Cappellani, S. D. Drouin, R. H. Morris, C. T. Schweitzer, A. Sella, J. Zubkowski, J. Am. Chem. Soc. 113 (1991) 4876-4887.
[41] E. P. Cappellani, S. D. Drouin, G. Jia, P. A. Malthy, R. H. Morris, C. T. Schweitzer, J. Am. Chem. Soc. 116 (1994) 3375-3388.
[42] C. Bianchini, K. Linn, D. Masi, M. Peruzzini, A. Polo, A. Vacca, F. Zanobini, Inorg. Chem. 32 (1993) 2366-2376.
[43] B. Chin, A. J. Lough, R. H. Morris, C. T. Schweitzer, C. D'Agostino, Inorg. Chem. 33 (1994) 6278-6288.
[44] R. M. Bullock, J. S. Song, D. J. Szalda, Organometallics 15 (1996) 2504-2516.
[45] P. Kalck, R. Pince, R Poiblanc, J. Roussel, J. Organomet. Chem. 24 (1970) 445–452.
[46] E. T. Papish, F. C. Rix, N. Spetseris, J. R. Norton, R. D. Williams, J. Am. Chem. Soc. 122 (2000) 12235-12242.
[47] O. B. Ryan, M. Tilset, V. D. Parker, J. Am. Chem. Soc. 112 (1990) 2618–2626.
[48] (a) B.R. Bender, J. Am. Chem. Soc. 117 (1995) 11239–11246. (b) B. R. Bender, G. J. Kubas, L. H. Jones, B. I. Swanson, J. Eckert, K. B. Capps, C. D. Hoff, J. Am. Chem. Soc. 119 (1997) 9179–9190. (c) F. Abu-Hasanayn, K. Krogh-Jespersen, A. S. Goldman, J. Am. Chem. Soc. 115 (1993) 8019–23. (d) D. Rabinovich, G. Parkin, J. Am. Chem. Soc. 115 (1993) 353–4. (e) C. D. Ritchie, Physical Organic Chemistry: The Fundamental Concepts; Marcel Dekker: New York, 1975; Chapter 8. (f) T. H. Lowry, K. S. Richardson, Mechanism and Theory in Organic Chemistry, 3rd ed.; Harper: New York, 1987; p 255. (g) M. Wolfsberg, Acc. Chem. Res. 5 (1972) 225.
[49] (a) R. M. Bullock, C. E. L. Headford, K. M. Hennessy, S. E. Kegley, J. R. Norton, J. Am. Chem. Soc. 111 (1989) 3897–3908. (b) W. D. Jones, F. J. Feher, J. Am. Chem. Soc. 108 (1986) 4814.
[50] G. Jia, R. H. Morris, Inorg. Chem. 29 (1990) 581–582.
[51] T. Y. Cheng, R. M. Bullock, J. Am. Chem. Soc. 121 (1999) 3150-3155.

[52] E. Scharrer, S. Chang, M. Brookhart, Organometallics 14 (1995) 5686-5694.
[53] B. Pleune, R. Poli, J. C. Fettinger, Organometallics 16 (1997) 1581-1594.
[54] G. Albertin, S. Antoniutti, M. Bettiol, E. Bordignon, F. Busatto, Organometallics 16 (1997) 4959-4969.
[55] M. G. Basallote, J. Duran, M. J. Fernandez-Trujillo, M. A. Manez, J. R. de la Torre, J. Chem. Soc., Dalton Trans. (1998) 745-750.
[56] Unfortunately, the two situations (a single elementary step with a late transition state and a rapidly maintained thermodynamic equilibrium) that can give inverse kinetic isotope effects are kinetically indistinguishable.
[57] E. Rocchini, A. Mezzetti, H. Rüegger, U. Burckhardt, V. Gramlich, A. Del Zotto, P. Martinuzzi, P. Rigo, Inorg. Chem. 36 (1997) 711-720.
[58] S. E. Landau, R. H. Morris, A. J. Lough, Inorg. Chem. 38 (1999) 6060-6068.
[59] L. D. Field, T. W. Hambley, B. C. K. Yau, Inorg. Chem. 33 (1994) 2009-2017.
[60] (a) M. G. Basallote, J. Duran, M. J. Fernandez-Trujillo, M. A. Manez, J. Chem. Soc., Dalton Trans (1998) 2205-2210. (b) M. G. Basallote, J. Duran, M. J. Fernandez-Trujillo, M. A. Manez, Inorg. Chem. 38 (1999) 5067-5071.
[61] C. Bohanna, M. A. Esteruelas, A. V. Gomez, A. M. Lopez, M. P. Martinez, Organometallics 16 (1997) 4464-4468.
[62] H. S. Chu, Z. Xu, S. M. Ng, C. P. Lau, Z. Lin, Eur. J. Inorg. Chem.(2000) 993-1000.
[63] M. Schlaf, A. J. Lough, P. A. Malby, R. H. Morris, Organometallics 15 (1996) 2270-2278.
[64] T. P. Fong, C. E. Forde, A. J. Lough, R. H. Morris, P. Rigo, E. Rocchini, T. Stephan, J. Chem. Soc., Dalton Trans. (1999) 4475-4486.
[65] M. Schlaf, A. J. Lough, R. H. Morris, Organometallics 15 (1996) 4423-4436.
[66] K. Abhur-Rashid, D. G. Gusev, A. J. Lough, R. H. Morris, Organometallics 19 (2000) 1652-1660.
[67] G. Jia, W. S. Ng, C. P. Lau, Organometallics 17 (1998) 4538-4540.
[68] (a) Y. Nishibayashi, S. Iwai, M. Hidai, Science 279 (1998) 540-542. (b) Y. Mizobe, Y. Yokobayashi, H. Oshita, T. Takahashi, M. Hidai, Organometallics 13 (1994) 3764-3766. (c) G. Jia, R. H. Morris, C. T. Schweitzer, Inorg. Chem. 30 (1991) 594-596.
[69] (a) T. Burgemeister, F. Kastner, W. Leitner, Angew, Chem. Int. Ed. 32 (1993) 739-741. (b) F. Hutschka, A. Dedieu, M. Eichberger, R. Fornika, W. Leitner, J. Am. Chem. Soc. 119 (1997) 4432-4443.
[70] T. Mizugaki, Y. Kanayama, K. Ebitani, K. Kaneda, J. Org. Chem. 63 (1998) 2378-2381.
[71] P. L. Gaus, S. C. Kao, K. Youngdahl, M. Y. Darensbourg, J. Am. Chem. Soc. 107 (1985) 2428-2434.
[72] D. H. Gibson, Y. S. El-Omrani, Organometallics 4 (1985) 1473-1475.
[73] S. M. Geraty, P. Harkin, J. G. Vos, Inorganica Chimica Acta 131 (1987) 217-220.
[74] (a) R. M. Bullock, B. J. Rappoli, J. Chem. Soc., Chem. Commun. (1989) 1447-1448. (b) R. M. Bullock, J. S. Song, J. Am. Chem. Soc. 116 (1994) 8602-8612.
[75] J. S. Song, D. J. Szalda, R. M. Bullock, C. J. C. Lawrie, M. A. Rodkin, J. R. Norton, Angew. Chem. Int. Ed. 31 (1992) 1233-1235.
[76] V. I. Bakhmutov, E. V. Vorontsov, D. Y. Antonov, Inorganica Chimica Acta 278 (1998) 122-126.

[77] For a review see D. N. Kursanov, Z. N. Parnes, N. M. Loim, Synthesis (1974) 633-651.
[78] (a) R. M. Bullock, T. Y. Cheng, Organometallics 14 (1995) 4031-4033. (b) K. T. Smith, J. R. Norton, M. Tilset, Organometallics 15 (1996) 4515-4520. (c) R. T. Hembre, S. McQueen, J. Am. Chem. Soc. 116 (1994) 2141-2142.
[79] A. L. Lehninger, Biochemistry; Worth Publishers, Inc.: New York, 1975; Chapter 13.
[80] (a) R. Noyori, Acta Chem. Scand. 50 (1996) 380-390. (b) R. Noyori, T. Ohkuma, Pure Appl. Chem. 71 (1999) 1493-1501.
[81] T. Ohkuma, H. Oka, T. Ikariya, R. Noyori, J. Am. Chem. Soc. 117 (1995) 10417-10418.
[82] (a) M. Minato, Y. Fujiwara, T. Ito, Chem. Lett.(1995) 647-648.
(b) M. Minato, Y. Fujiwara, M. Koga, N. Matsumoto, S. Kurishima, M. Natori, N. Sekizuka, K. Yoshioka, T. Ito, J. Organomet. Chem. 569 (1998) 139-145.
[83] Y. Shvo, D. Czarkie, Y. Rahamim, J. Am. Chem. Soc. 108 (1986) 7400-7402.
[84] N. Menashe, Y. Shvo, Organometallics 10 (1991) 3885-3891.
[85] Y. Shvo, I. Goldberg, D. Czerkie, D. Reshef, Z. Stein, Organometallics 16 (1997) 133-138.
[86] (a) G. Albertin, S. Antoniutti, E. del Ministro, E. Bordignon, J. Chem. Soc., Chem. Commun. (1992) 3203-3208. (b) A. J. Lough, R. H. Morris, L. Ricciuto, T. Schleis, Inorg. Chim. Acta 270 (1998) 238-246.
[87] C. P. Casey, S. W. Singer, D. R. Powell, R. K. Hayashi, M. Kavana, J. Am. Chem. Soc. 123 (2001) 1090-1100.
[88] Y. R. Santosh Laxmi, J. E. Backvall, J. Chem Soc., Chem. Commun. (2000) 611-612.
[89] Y. Nishibayashi, I. Takei, M. Hidai, Angew. Chem. Int. Ed. 38 (1999) 3047-3050.
[90] R. M. Bullock, M. H. Voges, J. Am. Chem. Soc. 122 (2000) 12594-12595.
[91] M. P. Magee, J. R. Norton, J. Am. Chem. Soc. 123 (2001) 1778-1779.
[92] G. Jia, R. H. Morris, J. Am. Chem. Soc. 113 (1991) 875-883.
[93] C. Vicente, G. B. Shul'pin, B. Moreno, S. Sabo-Etienne, B. Chaudret, J. Mol. Catal. A 98 (1995) L5-L8.
[94] J. X. Chen, J. F. Daeuble, D. M. Brestensky, J. M. Stryker, Tetrahedron 56 (2000) 2153-2166.
[95] M. A. Esteruelas, L. A. Oro, C. Valero, Organometallics 11 (1992) 3362-3369.
[96] C. Bianchini, E. Farnetti, M. Graziana, M. Peruzzini, A. Polo, Organometallics 12 (1993) 3753-3761.
[97] A. Aranyos, G. Csjernyik, K. J. Szabo, J. E. Backvall, J. Chem Soc., Chem. Commun. (2000) 351-352.
[98] M. Yamakawa, H. Ito, R. Noyori, J. Am. Chem. Soc. 122 (2000) 1466-1478.
[99] D. A. Alonso, P. Brandt, S. J. M. Nordin, P. G. Andersson, J. Am. Chem. Soc. 121 (1999) 9580-9588.
[100] (a) K. J. Haack, S. Hashiguchi, A. Fujii, T. Ikariya, R. Noyori, Angew. Chem. Int. Ed. Engl. 36 (1997) 285-288. (b) S. Hashiguchi, A. Fujii, K. J. Haack, K. Matsumura, T. Ikariya, R. Noyori, Angew. Chem. Int. Ed. Engl. 36 (1997) 288-290.
[101] C. A. Willougby, S. L. Buchwald, J. Am. Chem. Soc. 116 (1994) 11703-11714.
[102] L. Y. Kuo, Abstr. Pap. - Am. Chem. Soc. 220th (2000) INOR-489.

Chapter 3

Hydrides and Hydrogen Bonding: Combining Theory with Experiment

Eric Clot,[a] Odile Eisenstein,[a] Dong-Heon Lee[b] and Robert H. Crabtree[c]

a LSDSMS (UMR 5636), Case Courrier 14, Univ. de Montpellier 2, Montpellier Cedex 5, France.
b Dept. of Chemistry, Chonbuk National University, Chonju, 561-756, Korea.
cYale Chemistry Laboratory, 225 Prospect St., New Haven, CT 06520-8107, USA.

CONTENTS

3.1 INTRODUCTION

Many metal hydrides can be protonated to give dihydrogen complexes [1]. In some cases, kinetic protonation takes place on an M-H bond of a complex to give an M-(H_2) complex, even when the thermodynamically most favored protonation site is the metal itself. An early example was protonation of CpFeH(dppe), where the dihydrogen complex was formed at low temperature, followed by rearrangement to the dihydride on warming [1b]. The more facile kinetic proto-

nation at the metal hydride can now be understood in relation to the newly discovered phenomenon of dihydrogen bonding. On this idea, any acid AH forms a precursor adduct of type A-H···H-M with the metal hydride. Subsequent proton transfer directly yields the dihydrogen complex. Subsequent rearrangement to the dihydride is much slower than simple proton transfer because it implies motion of the heavy atoms [1c]. Dihydrides derived from dihydrogen complexes tend not to have cis-hydrides [1d]. In the case of $[CpFe(H)_2(dppe)]^+$, the hydrides are indeed trans.

In a number of recent studies, metal hydrides have been shown to act as the weak base (proton acceptor) component of a hydrogen bond. Classical hydrogen bonds [2a] of type A-H···B, show a weak electrostatic attraction between a weak acid, AH, and a weak base, B, requiring the presence of a lone pair on the base, B. Both A and B are electronegative atoms or groups. In the dihydrogen bond, A-H···H-M, the role of the weak base is taken by M-H. As Morris [2b] has noted, these interactions can also be considered as arising from an attractive interaction between a proton and a hydride: hence the alternative term, proton-hydride interaction.

3.2 IS A-H···H-E HYDROGEN BONDING REAL?

In early examples of A-H···H-E hydrogen bonding, found by our own group [2c] and by Morris [2d], the weak acid AH was an NH or OH bond and E was a d^6 transition metal such as Re(I) or Ir(III). A typical example is shown as **1.** The problem that arose at this point was one of interpretation, because a d^6 metal such as Ir(III) has d_π nonbonding electrons in a position that allows them to interact with the A-H bond (Fig. 1). A Devil's advocate could argue that the reason the AH proton is close to the MH hydride is nothing to do with a proton-hydride interaction. The AH might in fact interact with the d_π nonbonding electrons, the effective equivalent of the base lone pair in the classical A-H···B hydrogen bond. The reason this takes place adjacent to the M-H bond is simply that H is the sterically smallest ligand. On this idea, the H···H interaction would be *repulsive.*

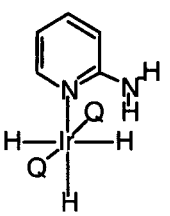

1 (Q = PPh_3)

To resolve this ambiguity, we decided to look at boron hydrides, which have no nonbonding electrons. This seemed promising because the simplest example, BH_3NH_3, is known to have a melting point of +104°C, very much higher than its isoelectronic analogue, CH_3CH_3, with a melting point of -183°C. This large elevation of m.pt. is reminiscent of the situation with H_2O versus CH_4. We felt that data on interactions of the O,N-H···H-B type (B = boron) probably existed unsuspected in the literature. The Cambridge Crystallographic Database (CSD), giving access to both intramolecular and intermolecular interactions, seemed the best resource. In our first such study, we provided evidence for the existence of intermolecular N-H···H-B hydrogen bonds [3a] in a series of amine-boranes. The key result was that the nature of the interaction was essentially identical in the transition metal and main group examples and so we argued that the d_π nonbonding electrons play no more than a minor role.

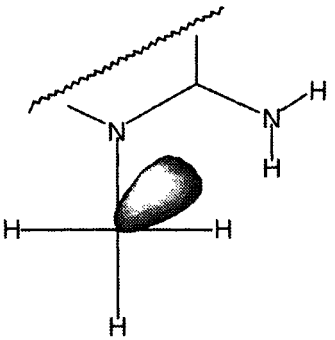

Figure 1. The nature of the interaction in **1** was at first ambiguous: it could have been direct M···HN interaction but experimental and theoretical work discussed here suggests it is best described as a true H···H interaction.

The typical range of H···H distances found is 1.7-2.2 Å, although the upper limit is not sharp because very weak dihydrogen bonds shade imperceptibly into close nonbonding contacts. These H···H distances should be compared with 2.4 Å [5], the sum of the van der Waals (vdW) radii for two hydrogens. The typical geometry, shown in Fig. 2, involves a side-on approach of the weak acid AH group (such as NH or OH) to the weak base EH bond (such as M-H or B-H) to give E-H···H angles of 90-120°.

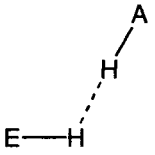

Figure 2. The typical geometry of a dihydrogen bond, showing the side-on approach of the weak acid AH group to the weak base EH bond. (AH = NH or OH; EH = MH or BH).

Another problem arose at this point. Of all the boron hydrides for which CSD data was collected, the archetypal case, BH_3NH_3 proved to have a configuration entirely different from that shown in Fig. 1. This species had been examined by X-ray crystallography on several occasions but the BHHN configuration found was the reverse of the one in Fig. 1: B-H···HN appeared to be almost linear and N-H···HB appeared strongly bent. Thanks to a collaboration with Wim Klooster and Thomas Koetzle at Brookhaven National Labs, we were able to look at this case by neutron diffraction. By comparison of the neutron data with the published X-ray work it was found that the B and N had previously been misassigned as N and B, respectively, and the true assignments produced a normal BHHN configuration as in Fig. 2.

Theoretical work was very valuable in this area [3a]. A DFT calculation on the BH_3NH_3 dimer shows a conformation for the BH···HN group that is very similar to that of Fig. 1. The calculated H···H bond energy was found to be 6.6 kcal/mol for each bond, again in line with dihydrogen bonding. Finally, the calculated charge distribution suggested that the BH bonds are polarized on forming the H···H interaction, as expected from the soft character of the BH bond. This polarization may help explain the relatively high interaction energy.

Calhorda et al [3b] found a large number of complexes in the CSD database with short MH···H(O,N) distances and carried out a DFT study for $[(H_3P)_4IrH(OH)]PF_6$ that concluded that the counterion needed to be included to obtain good agreement with experiment. Lledos, Eisenstein et al. [1d] have reviewed recent applications of theoretical methods to hydride complexes.

Another objection to our interpretation that we considered was that in many cases, such as **1**, the NH or OH bond is held in a chelate manner and is not free to adopt any conformation, so the similarity of the metric parameters for a range of systems might be an artefact.

To resolve this problem, we attempted to cocrystallize an acid AH with a hydride (B), where both AH and B are independent molecules. The usual result was the formation of separate crystals of AH and the hydride, as would be expected on the principle of recrystallization. We solved this problem by choosing an acid, indole (**1**), that is a liquid and therefore cannot crystallize, and a base, $ReH_5(PPh_3)_3$ (**2**) that forms powders rather than good quality crystals on attempted crystallization. This implies that **2** does not have good crystallization kinetics. An X-ray study by Arnie Rheingold confirmed the formulation and suggested the H···H distance was short. In one crystallization attempt, large, very high quality crystals were formed and the adduct between **1** and **2** were obtained. These allowed Tom Koetzle and Alberto Albinati to obtain a high quality neutron diffraction structure [4]. This showed essentially the same conformation (Fig. 2) previously seen and confirmed that it was not a result of the constraints of chelation. The H···H distance of 1.73 Å in this

structure remains the smallest to have been reliably determined. The value is much smaller than the sum of the van der Waals radii for two hydrogens (2.4 Å) [5].

DFT (B3LYP) work on the $ReH_5(PH_3)_3$ + NH_3 model system by Eisenstein and coworkers showed, however, that the PE surface is very flat and so the tendency for a bent E-H···HA is not strong [4]. Indeed, linear B-H···H-N cases had been identified in the early CSD study where the intermolecular arrangement precluded adoption of the usual conformation of Fig. 2. There was no significant attractive interaction between $ReH_5(PH_3)_3$ and weak acids like CH_4, C_2H_4, or HCCH [4b].

3.3 EARLY WORK

Two 1990 papers were important precursors to the work described here. Attractive A-H···H-M interactions were suggested to account for the close contact (H···H, 2.4 Å) found between the OH proton and the Ir-H hydrogen in a n-diffraction study of *cis*-$[Ir(OH)H(PMe_3)_4]$ [6], although in this case the H···H distance is equal to the sum of the vdW radii and the interaction must be relatively weak. A d(H···H) of 1.86 Å was found by n-diffraction in the crystal structure [7a] of *mer*-$[Fe(H)_2(H_2)(PEt_2Ph)_3]$, a study originally carried out to test the earlier spectroscopic assignment [8] of this species as a dihydrogen complex. The H_2 ligand was unexpectedly found to be in an orientation that represents a compromise (**B**) between **A** (⊥ to cis-Fe-H) which leads to the strongest metal to ligand back donation and **C** (|| to cis-Fe-H) which leads to the maximal attractive interaction between the protonic H2 hydrogen and the hydridic Fe-H.

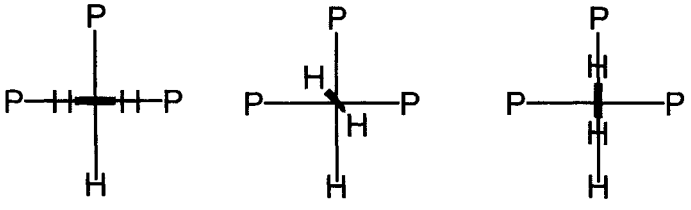

A **B** **C**

One of the present authors (OE) recognized the origin of the attractive interaction from an extended Hückel analysis [7a] and from an ab initio calculation [7b] and used the term 'cis-effect' for this phenomenon. This can now be alternatively seen as a particular case of dihydrogen bonding because dihydrogen ligands are known to have acidic character and the short H···H distance (1.86 Å) puts this squarely into the dihydrogen bonding range.

3.4 ENERGETICS

From the decrease in hydrogen bonding energies [2] on moving from the classical lone pair type, N-H···(lone pair) {4-8 kcal/mol}, to the N-H···π case in which the proton acceptor is an arene, {≤2 kcal/mol}, one might expect that any N-H···σ type would have a negligable bond energy {<1 kcal/mol}. In contrast, we find NH···HE interaction energies of 4-7 kcal/mol which are almost as large as for the N-H···(lone pair) case. This requires E to be an electropositive element such as B or a transition metal, so that the hydride has significant hydridic character. The reasons for the energies being quite so large are still not entirely clear, however.

Approximate bondstrengths were first obtained via IR spectroscopy using the Iogansen equation [9] which relates the low energy shift of the ν(NH) or ν(OH) band in the IR spectrum to the interaction energy. Applied [4] to $[ReH_5(PPh_3)_3 \cdot indole]$ (3.6 kcal/mol), and $[ReH_5(PPh_3)_3 \cdot ArOH]$ (5.6-5.8 kcal/mol.), the results seem reasonable. They agree quite well with UV-VIS data from equilibrium studies [10], which give a ΔG of 5 kcal/mol binding energy for $[ReH_5(PPh_3)_2(C_5H_5N)]$ + indole (Table 1).

Epstein, Berke et al. [11] have used the Iogansen method to obtain intermolecular association energies of ca. 5.5 kcal/mol between acidic alcohols such as $(CF_3)_2CHOH$ and the hydridic hydride, $[WH(CO)_2(NO)(PMe_3)_2]$. Equilibrium constants for the same systems gave an interaction energy of 4.9 kcal/mol.

Table 1. Some dihydrogen bond strengths (kcal/mol), deduced from Δν(NH) and Δν(OH) IR spectroscopic data, for adducts of the d^0 and d^2 complexes shown with typical proton donors, indicating that direct X-H···M hydrogen bonding is not predominant; data taken from ref 4.

H-bond donor	$[ReH_5(PPh_3)_3]$	$[ReH_7(dppe)]$
indole	4.3	3.3
$2,4,6\text{-}Me_3C_6H_2OH$	4.5	4.7
d^n configuration	d^2	d^0

dppe = $Ph_2PCH_2CH_2PPh_2$

We introduced an NMR method for estimating the H···H bond energy by estimating the C-NH_2 rotation barrier in species like **1** from VT NMR. For example, in the case of complex **1a** (eq. 1), the barriers to exchange between H_a and H_b were determined and associated with relative values of H···H interaction energies [12]. By estimating the intrinsic C-N rotation barrier in the absence of dihydrogen bonding using a combination of experimental data and Hartree-Fock calculations, it was possible to estimate the absolute values of the hydrogen bond strengths.

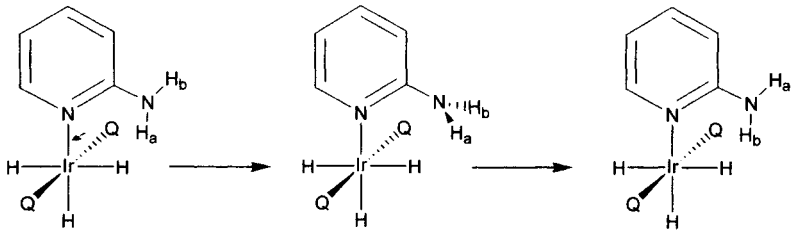

(1)

For **3a** the C-N rotation barriers were strongly dependent on the nature of the trans ligand, Y, indicating the presence of a substantial trans effect on the H···H interaction (eq. 2). Where Y is H^-, the H···H bond energy was highest, estimated to be 5.0 kcal/mol. When Y becomes more electron withdrawing, the H···H interaction energy falls until for Y = F^-, the energy is <2.9 kcal/mol (Table 2). The presence of the other isomer, **3b**, allowed the N-H···Y hydrogen bondstrengths to be determined and even for Y = F^-, this proved to be only just a little more (5.2 kcal/mol) than for the N-H···H-Ir bond where Y = H^- (5.0 kcal/mol). The system was designed to be most favorable for formation of an N-H···H-Ir dihydrogen bond, however, so there is probably some size mismatch for the larger Y groups. Fluoride being very similar in size to hydride, however, a valid comparison is probably possible in this case.

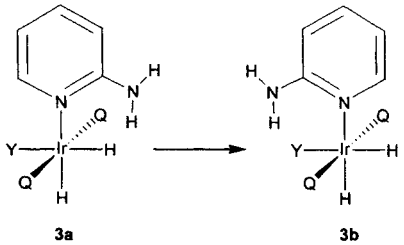

(2)

While calculations can confirm that H···H bonding occurs, they do not yet give quantitative energetics [1d].

Table 2. Some Dihydrogen bond strengths of **1** taken from ref 13.

Y	H···H bond strength (kcal/mol)
H^-	5.0
CO	3.7
CN^-	3.4
I^-	3.3
MeCN	3.1
Br^-	3.0
Cl^-	2.9
F^-	<2.9

3.5 SPECTROSCOPY

We suggested fast T_1 relaxation as a criterion for the presence of close H···H distances in dihydrogen complexes, and Morris et al. [2b] and our own group [2c] have detected a substantial excess relaxation. Making the usual assumptions, the excess T_1 can be interpreted in terms of an H···H distance of about 1.8 Å in all the cases studied, a value consistent with the structural data.

Chaudret, Limbach and coworkers [13] have recently shown that dihydrogen bonding effects can alter the quantum exchange coupling observed in the NMR spectrum of $[Cp^*(PCy_3)RuH_3]$.

3.6 REACTIVITY

Using the information discussed above, protonation of metal hydrides can now be considered as going via the following pathway (eq. 3).

Chaudret and coworkers [14a] have recently detected an equilbrium between $RuH_2(dpm)_2$ {dpm = $Ph_2PCH_2PPh_2$} and the corresponding dihydrogen complex as a result of proton transfer from an acidic alcohol such as $(CF_3)_2CHOH$ (eq. 4). Other related reactions exist. [14b]

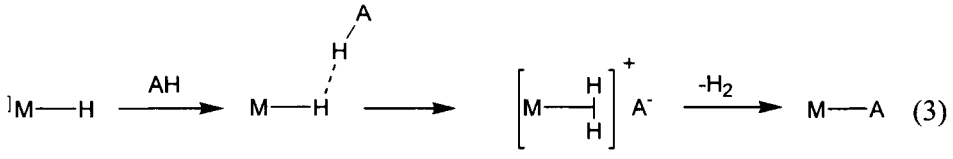

(3)

$$RuH_2(dpm)_2\,HOR \rightleftharpoons [RuH(H_2)(dpm)_2]^+[OR]^- \qquad (4)$$

3.7 PENDANT GROUP EFFECTS

These developments led us to look at the effect of adding pendant groups to our complexes to see if we could observe reversible protonation/deprotonation of an H_2 complex via a dihydrogen bonded system. The rigid benzoquinolinate ligand was chosen because a variety of groups G can easily be appended at the 2-position, where both electronic and pendant group effects are expected, and in the 4-position, where only electronic effects should occur. In this way we have a control for the substituent electronic effect. Cyclometallation of the bq ligand gives species of type 4, where the group G is adjacent to the labile binding site where a variety of ligands L can be bound.

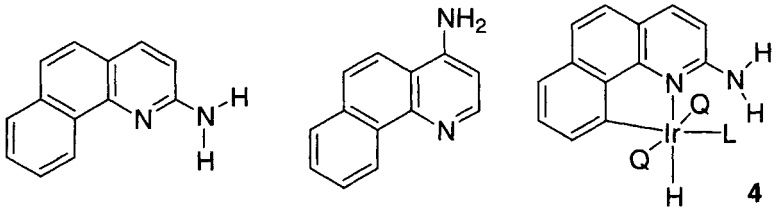

The case of **4** (L = H_2O) [15a] was significant because the experimental data, including an X-ray crystal structure, failed to characterize the hydrogen bonding pattern: among **5a, 5b** and **5c, 5a** was only weakly preferred.

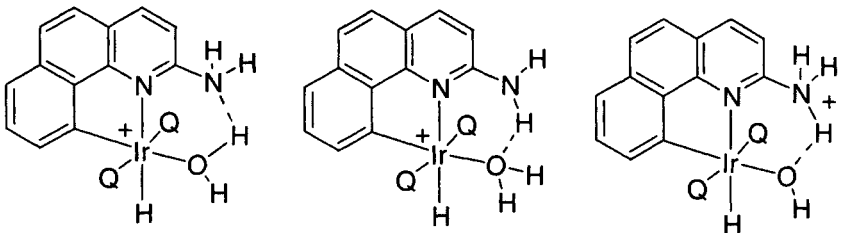

The DFT (B3PW91) calculations [15b] make the clear prediction that **5a** should be preferred and indeed cooling to -80 °C allowed the water peak in the proton NMR to be resolved into a 1:1 decoalesced pair of signals, consistent with structure **5a**.

In another application [15] of the bq-NH_2 system, we showed that hydrogen bonding could stabilize HF complex, **6**, a type of ligand not previously observed. This was synthesized from the fluoride by the route shown in eq. 5. NMR observations at -80 °C showed the presence of a J(H,F) of 440 Hz, unambiguously indicating the presence of a hydrogen bonded HF group. The persistance of a J(F,P) and J(F,H) couplings with reduced values relative to the parent fluoride, **5**, suggested that the HF was still bound to the metal. The J(H,F) in the parent **5** is a mere 52 Hz.

Unfortunately, the HF compound was too thermally unstable to be isolated for a crystal structure and so the detailed conformation of this system remained conjectural. In an application of computational methods, DFT (B3PW91) calculations [15b] predict the structure (Fig. 3) and suggest that the HF binds to the complex as in **6** with a binding energy of 28.2 kcal/mol, a much larger value than when the NH_2 pendant group is replaced by H (18.0 kcal/mol) when no HF complex is detectable experimentally. The HF distance of 1.042 Å is only slightly elongated from free HF (0.922 Å) but the IrF distance elongates significantly from 2.123 Å in the fluoride to 2.262 Å in the HF complex. The N···HF distance of 1.43 Å indicates a very strong H-bond. The calculations suggest that the total binding is approximately equally shared between the coordinate and hydrogen bonds.

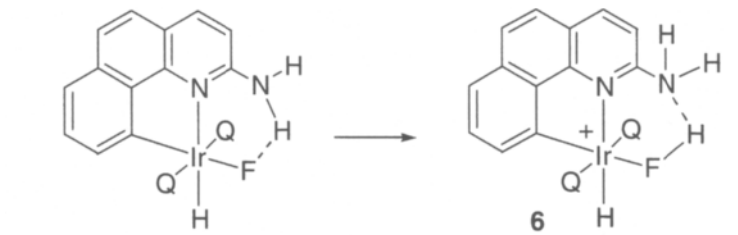

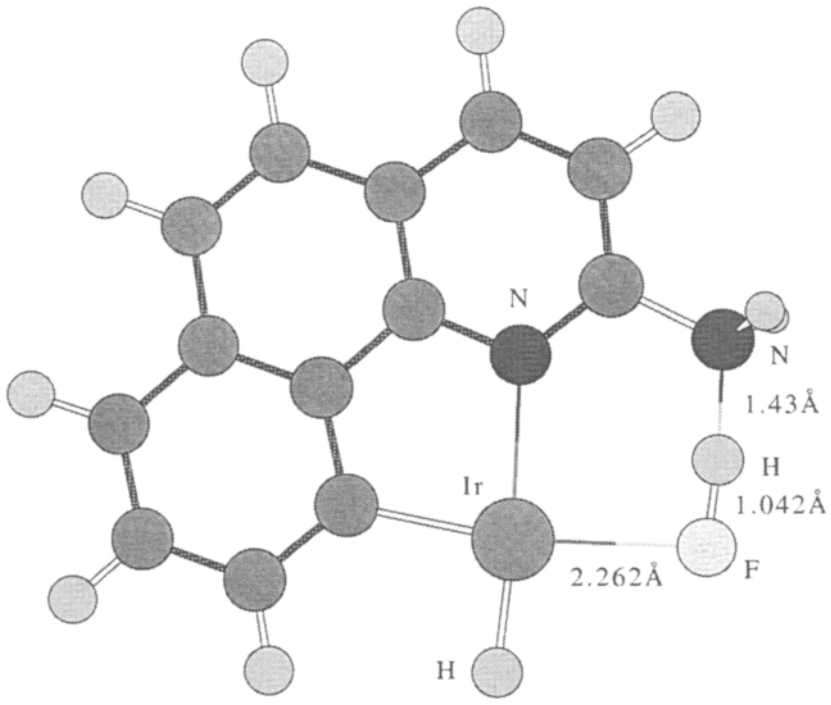

Figure 3. The calculated structure for the HF complex from DFT (B3PW91) calculations [15b].

3.8 HETEROLYTIC H-H ACTIVATION

The behavior of the bq complexes that lack a pendant group can usefully be compared with that of the bq-NH_2 system. For example, in eq. 6, H_2 displaces water from the precursor to give a molecular hydrogen complex that is deprotonated by external base. In eq. 7, the corresponding situation with bq-NH_2 and Q = PPh_3 yields the hydride **8b** where the coordinated H_2 has been deprotonated by the pendant amino group [16].

DFT calculations on a model system with Q = PH_3 gave the prediction that **8a** (Q = PH_3) should be stabler than **8b**, in contrast with experiment. In an initial attempt to reconcile theory and experiment, we replaced the experimental

PPh_3 with the more basic phosphine $P(n\text{-}Bu)_3$ with the result that the dihydrogen complex, **8a**, was now the stable isomer. The same dihydrogen form was also observed for Q = $PMePh_2$ and PMe_2Ph. Likewise, when the theoretical model PH3 was replaced by weaker donors PFH_2, PF_2H and PF_3, **8b** became the most stable isomer in line with the experimental situation for the least electron-donor phosphine PPh_3. Absolute values are not the key issue in such work; the trends are the important features.

Other factors may well be at work here and we are continuing our studies on the problem to resolve the situation, but the results to date are already striking. In the absence of the theoretical result, we would not have tried the other experimental ligands, $PMePh_2$ and PMe_2Ph, and would not have seen the second isomer.

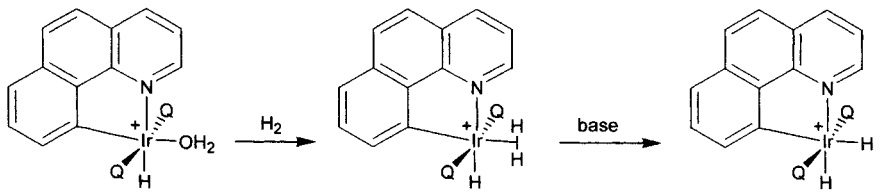

(6)

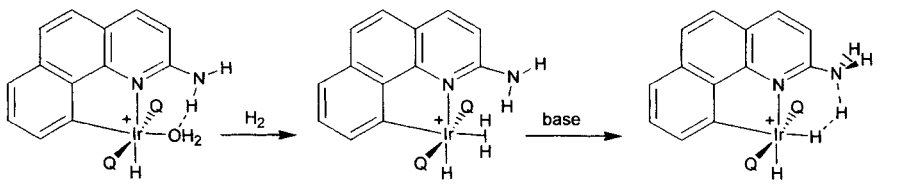

(7)

8a **8b**

The theoretical results in this case prove to be remarkably sensitive to the model chosen, probably because the pK_a of an H_2 complex is very dependent on the phosphine. The preference for **8a** or **8b** is essentially the result of the pK_a of coordinated H_2 changing as Q is varied. A basic phosphine causes greater back donation into the H_2 σ^* orbital leading to a decrease in the acidity and a lower tendency to give heterolytic splitting. This is probably related to the very large acidification that takes place when H_2 binds. In the free state (eq. 8), the pK_a of H_2 is about 35, but on binding pK_as in the range 15 to -5 have been reported. The acid dissociation for free H_2 is presumably greatly perturbed on binding (eq. 9) because H_2 is weakly bound but H^- is very strongly bound to the metal. The tighter binding of the acid dissociation product favors the acid dissociation. Changing the ligand is expected to make a bigger difference to H_2 binding than to H^-, hence the large pK_a dependence on Q.

$$H_2 + :B \rightleftharpoons H^- + [BH]^+ \quad (8)$$

$$M\text{-}(H_2) + :B \rightleftharpoons [M\text{-}H]^- + [BH]^+ \quad (9)$$

3.9 ALKYL TO CARBENE REARRANGEMENT

One of us (DHL) has found a very interesting rearrangement of an alkylamine to an aminocarbene (eq. 10) by double geminal CH activation. [17]

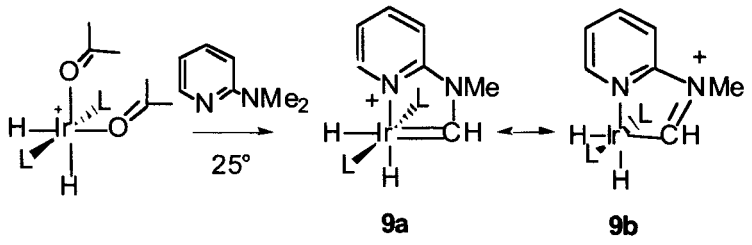

(10)

Resonance form **9b** is preferred, as expected for this Fischer carbene. At -80 °C, an intermediate agostic species (**10**) is seen, leading to the mechanistic proposal shown in Fig. 4. The cis-hydride is proposed to have the role of promoting departure of H_2, an observed (NMR) product of the reaction.

3.10 CONCLUSION

A combination of theoretical and experimental approaches gives an improved understanding of several aspects of hydride chemistry. A new type of hydrogen

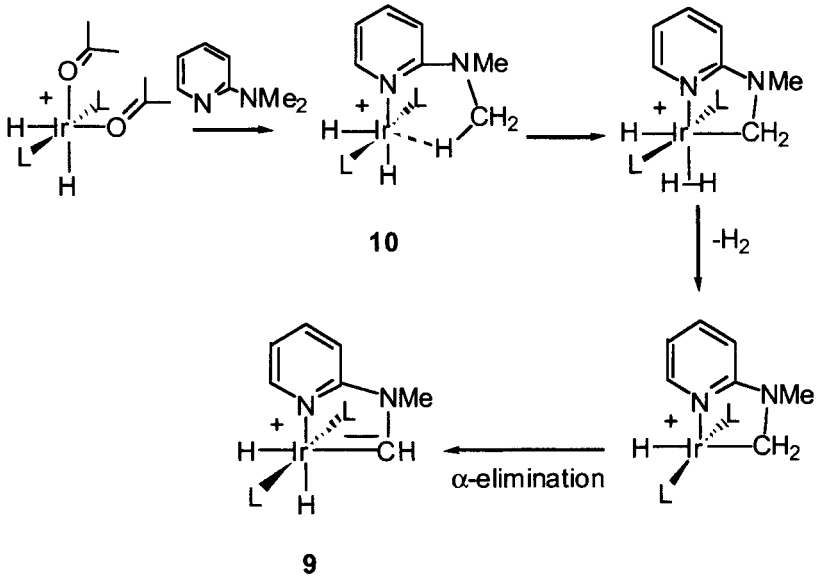

Figure 4 The proposed mechanism for the carbene formation, showing the proposed role of the cis-hydride.

bond between a proton and a hydride is shown to influence the properties of a number of main group and transition metal compounds. It seems to be important in cases of protonation of hydrides by acids AH. Pendant group effects are described that allow stabilization of an HF complex and observation of heterolytic H_2 activation.

ACKNOWLEDGEMENTS

We thank our coworkers and collaborators, as well as Arnie Rheingold and Per Siegbahn, for their insights on the problems described here, the NSF and the Université de Montpellier 2 and CNRS for funding.

REFERENCES AND NOTES

[1] a) P.G. Jessop, R.H. Morris, Coord. Chem. Rev. 121 (1992) 155; R.H. Crabtree, Angew. Chem. Int. Engl. Ed., 32 (1994) 789. b) P. Hamon, L. Toupet, J.-R. Hamon, C. Lapinte, J. Organomet. Chem., 428 (1992) 49. c) R.H. Crabtree, X.-L. Luo, D. Michos, Chemtracts Inorg. Chem., 3 (1991) 245. d) F. Maseras, A. Lledós, E. Clot, O. Eisenstein, Chem. Rev., 100 (2000) 601.

[2] a) G.A. Jeffrey, W Saenger, «Hydrogen Bonding in Biological Structures», Springer, Berlin, 1994. b) R.H. Morris, Can. J. Chem. 74 (1996) 1907. c) R.H. Crabtree, P.E.M. Siegbahn, O. Eisenstein, A.L. Rheingold, Acc. Chem. Res., 29 (1996) 348. d) W. Xu, A.J. Lough, R.H. Morris, Inorg. Chem. 35 (1996) 1549.

[3] a) T. Richardson, S. deGala, R.H. Crabtree, P.E.M. Siegbahn, J. Am. Chem. Soc., 117 (1995) 12875. b) D. Braga, F. Grepioni, E. Tedesco, M.J. Calhorda. P.E.M. Lopes, New J. Chem., 23 (1999) 219.

[4] a) J. Wessel, J.C. Lee, E. Peris, G.P.A. Yap, J.B. Fortin, J.S. Ricci, G. Sini, A. Albinati, T.F. Koetzle, O. Eisenstein, A.L. Rheingold, R.H. Crabtree, Angew. Chem. Int. Eng. Ed., 34 (1995) 2507; B.P. Patel, J. Wessel, W. Yao, J.C. Lee, E. Peris, T.F. Koetzle, G.P.A. Yap, J.B. Fortin, J.S. Ricci, G. Sini, A. Albinati, O. Eisenstein, A.L. Rheingold, R.H. Crabtree, New. J. Chem., 21 (1997) 413. b) G Sini, O. Eisenstein, W. Yao, R.H Crabtree, Inorg. Chim. Acta, 280 (1998) 26.

[5] A. Bondi. J. Phys. Chem., 68 (1964) 441.

[6] R. Stevens, R. Bau, D. Milstein, O. Blum, T.F. Koetzle, J.C.S., Dalton, (1990) 1429.

[7] a) L.S. Van der Sluys, J. Eckert, O. Eisenstein, J.H. Hall, J.C. Huffman, S.A. Jackson, T.F. Koetzle, G.J. Kubas, P.J. Vergamini, K.G. Caulton, J. Am. Chem. Soc., 112 (1990) 4831. b) J-F. Riehl, M. Pélissier, O. Eisenstein Inorg. Chem. 31 (1992) 3344.

[8] R.H. Crabtree, D.G. Hamilton, J. Am. Chem. Soc., 108, (1986) 124.
[9] A.V. Iogansen, G.A. Kurchi, V.M. Furman, V.P. Glazunov, S.E. Odinokov, Zh. Prikl. Spectrosk., 33 (1980) 460. S.G. Kazaian, P.A. Hamley, M. Poliakoff, J. Am. Chem. Soc., 115 (1993) 460.
[10] P. Desmurs, K. Kavallieratos, W. Yao, R. H. Crabtree, New J. Chem., 23 (1999) 1111.
[11] E.S. Shubina, N.V. Belkova, A.N. Krylov, E.V. Vorontsov, L.M. Epstein, D.G. Gusev, M. Niedermann, H. Berke, J. Am. Chem. Soc., 118 (1996) 1105.
[12] E. Peris, J.C. Lee Jr., J.R. Rambo O. Eisenstein, R.H. Crabtree, J. Am. Chem. Soc., 117 (1995) 3485.
[13] J.A. Ayllon, S. Sabo-Etienne, B. Chaudret, S. Uhlrich, H.-H. Limbach, Inorg. Chim. Acta, 259 (1997) 1.
[14] a) J.A. Ayllon, C. Gervaux, S. Sabo-Etienne, B. Chaudret, Organometallics, 16 (1997) 2000. b) A.J. Toner, S. Grundemann, E. Clot, H.H. Limbach, B. Donnadieu, S. Sabo-Etienne, B. Chaudret, J. Am. Chem. Soc., 122 (2000) 6777; J.A. Ayllon, S.F. Sayers, S. Sabo-Etienne, B. Donnadieu, B. Chaudret, E. Clot Organometallics 18 (1999) 3981.
[15] a) D.H. Lee, H.J. Kwon, B.P. Patel, L.M. Liable-Sands, A.L. Rheingold, R.H. Crabtree, Organometallics, 18 (1999) 1615. b) E. Clot, O. Eisenstein, R.H. Crabtree, New J. Chem., (2001), 25, 66.
[16] D.-H. Lee, B.P. Patel, E. Clot, O. Eisenstein, R.H. Crabtree, Chem. Comm., (1999) 297.
[17] D.-H. Lee, J. Chen, R.H. Crabtree, Chem. Comm., (2001), 213.

Chapter 4

Hydridicity of Transition Metal Hydrides and its Implications for Reactivity

Heiko Jacobsen and Heinz Berke

Anorganisch-chemisches Institut, Universität Zürich, Winterthurerstr. 190, CH-8057 Zürich, Switzerland

CONTENTS

4.1 INTRODUCTION

The chemistry of transition metal hydride (TMH) complexes started back in 1931 with the discovery of $H_2Fe(CO)_4$ by Hieber and coworkers [1]. This compound indeed contains two single iron-hydrogen bonds. In subsequent years, related metal carbonyl hydrides appeared, such as $HCo(CO)_4$ [2,3]. During the same period of time, the industrially important hydrofomylation process was discovered [4,5]. Back then, it was not clear that these two findings were directly related to each other. As we know nowadays, $HCo(CO)_4$ plays an important role in the hydrofomylation process [6], and constitutes probably the first application of TMHs in catalytic processes.

$HCo(CO)_4$ acts in the hydroformylation reaction more as a hydride rather than a proton donor. This behavior strongly contrasts the acidic properties of all the mentioned carbonyl hydride species, since in solution, and especially in water, they function as strong acids, with sometimes even very low pK_a values. The discrepancy that the very same transition metal hydrides may act as either hydride or proton sources, gave rise to controversial discussions in the literature for many years. Thus, $HCo(CO)_4$ not only provides the prototypical example for the ambivalence of the TM-H bond, but also an early example of TMH complexes in homogeneous catalysis.

In this article, we are going to identify the characteristic features of TMHs, which connect their unique bonding properties with their synthetic potential as useful reagents in stoichiometric or catalytic transformations. To this end, it is necessary to examine the nature of the TM-H bond in greater detail. As we shall see, the TM-H bond is best described as a polar covalent linkage, in which a charge distribution is imposed on an essentially covalent bond between the transition metal and the hydrogen atoms. In connection with the basic electronic picture of the transition metal-hydride bond, we will also discuss its thermodynamic properties. For a discussion of the acidic or basic properties of TMH complexes, it is crucial to include the influence of solvent effects. In this context, a strong emphasis is placed on the so called hydridicity of TMH systems. Here, we tie back into the earlier efforts of Labinger [7], to describe the specific hydridic properties of TM-H bonds. Finally, we present examples from the recent work of our group, which illustrate how the concepts developed for the nature of the TM-H bond can be utilized to control and tune its reactivity. These new experiments not only provide further understanding of the TM-H bond and its hydridicity, but also open up new directions for synthetic applications including catalytic transformations.

4.2 ELECTRONIC STRUCTURE OF TRANSITION METAL HYDRIDES

Qualitative molecular orbital considerations derived from perturbation theory [8] provide a useful picture of the L_nM-H bond (Scheme 1).

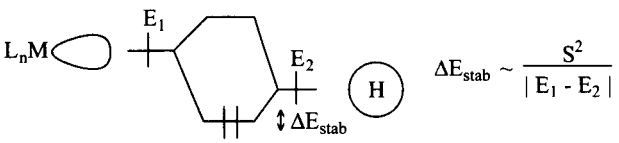

Scheme 1

In a first order approximation, one can view the TM-H bond as the result of a -type interaction of an orbital of the L_nM fragment, which is dominated by metal-d_σ contributions, with the 1*s* orbital of the hydrogen ligand. The splitting, or stabilization energy ΔE_{stab} contributes prevailingly to the thermodynamic strength of this interaction, and may therefore be taken as an approximate measure of the L_nM-H bond strength. The expression for ΔE_{stab} as shown above tells us how this particular bond might be influenced. An increase of the overlap between the orbitals of both bonding partners should lead to a strengthening of this bond, while an increase of the energy gap between the interacting fragment orbitals causes the opposite effect. These factors therefore provide a rational basis for an electronic tuning of the L_nM-H bond.

To illustrate the picture as given above, selected mean bond dissociations energies (BDE) for various TMHs are sketched in Figure 1 [9].

The BDE values of this rather limited listing span a considerable range from 200 to 400 kJ/mol, which apparently is typical for the TM-H bond. Not only

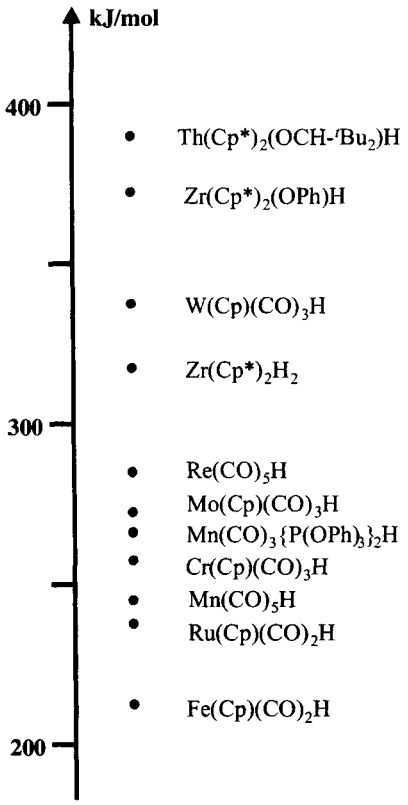

Figure 1. Mean bond dissociation energies for selected TMHs (in kJ/mol; Cp* = C_5Me_5). Data taken from ref. 9.

the transiton metal center, but also the ligand sphere influences the strength of the M-H interaction. When changing the transition metal center in comparable ligand environments, we see partly strong effects in the BDEs, where the heavier elements have the higher values. Examples are found in the comparison $FeCp(CO)_2H$ vs. $RuCp(CO)_2H$, and $Mn(CO)_5H$ *vs.* $Re(CO)_5H$; and along the triad of compounds $MCp(CO)_3H$, M = Cr, Mo, W. The same trend is also observed for the related systems $ZrCp_2^*(OPh)H$ and $ThCp_2^*(OCH^tBu_2)H$. Similarly, a ligand influence can be traced, when for instance a CO group of $HMn(CO)_5$ is replaced by a phosphite donor to give $HMn(CO)_3\{P(OPh)_3\}_2$, or when one of the H ligands in $ZrCp^*_2H_2$ is substituted by a phenoxy group.

To quantify our perturbational picture of the TM-H bond, we performed Density Functional calculations for a variety of complexes. For the optimized molecular geometries, we did a fragment molecular orbital analysis, as outlined in Scheme 1. The HOMO energies E_1 for the L_nM fragment, as well as the nd_σ-$1s_H$ overlap terms *S* are displayed in Figure 2.

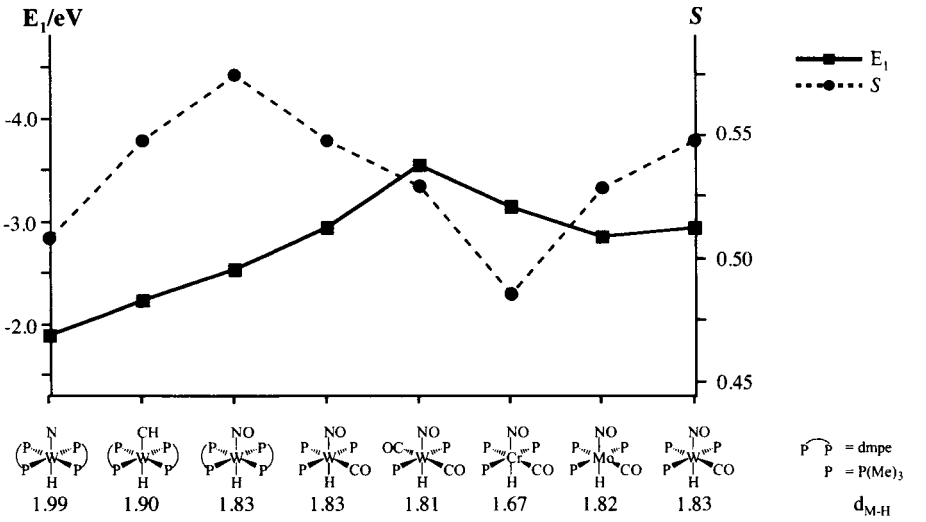

Figure 2. Spin-restricted metal fragment orbital energies, and overlap values for L_nM-H complexes. (Calculated M-H distances (in Å) are also reported.)

When we compare the three complexes $LW(H)(dmpe)_2$, L = NO, CH, N, we can analyze how different *trans* ligands influence the TM-H bond. From Figure 2, we see that the *trans* ligand has a strong influence on the orbital energy E_1. The fragment with the strong π–accepting nitrosyl ligand has the lowest E_1 value, followed by the carbyne and nitride systems. Thus, the term $|E_1\text{-}E_2|$ for

$LW(H)(dmpe)_2$ fragments increases as NO < CH < N, suggesting an decrease in the TM-H bond strength as NO > CH > N. The trend is paralleled by the values of the overlap integral *S*. This is understandable, since a stronger interaction causes a shorter metal-hydride bond, which in turns leads to an enhanced orbital overlap. Variation of the *trans* ligand therefore allows a tuning of the TM-H bond via the energy term E_l for the HOMO of the L_nM fragment.

A different trend is observed when the three complexes $M(CO)H(NO)(PMe_3)_3$, M = Cr, Mo, W, are compared. As can be seen from Figure 2, the major changes, when going down this triad, are found in the overlap term *S*, rather than in the HOMO energy E_l. We find the smallest overlap for the chromium complex, and the largest one for the tungsten system. Two reasons are responsible for this effect. Going from the first to the second row elements, the core expansion [10] causes a greater spatial extent of the 4*d* orbitals on Mo, compared to the 3*d* orbitals on Cr. This leads not only to a significant elongation of the M-H bond (compare Figure 2), but also to an enhanced M-H overlap. The further increase of the *S* value, when going from Mo to W, is mainly caused by relativistic effects [11]. From this analysis we can expect that the nitrosyl hydride complexes will follow the general trend that the M-H bond strength increases, when going from the lighter to the heavier metals [12]. Variation of the transition metal center thus allows for a tuning of the TM-H bond via changes in the orbital overlap *S*.

Lastly, we want to investigate the influence of the ligand sphere on the TM-H bond. To this end, we compare the series of molecules $W(CO)_{2-n}(H)(NO)(PR_3)_{2+n}$, n = 0,1,2. We see that an increase of the number of phosphine ligands raises the orbital energy E_l, which should induce a bond weakening. However, we also observe an increase of the overlap integral *S*, which in turn should cause a strengthening of the M-H bond. Thus, the two trends in E_l and in *S* have opposing influences on the metal hydride bond strength. Following our perturbational analysis, it is not clear what the effect of a higher phosphine substitution will be. At this point, we need to turn to a more detailed bond analysis.

In our decomposition scheme, the metal hydride bond is built up from two fragments, which possess both the right electronic, as well as geometric structure to form the final molecule [10]. The energy associated with this process is called the bond snapping energy $BE_{snap,}$ and can be decomposed into a term for steric interaction ΔE^0 and orbital interaction ΔE_{int} (Eq. 1).

$$BE_{snap} = -[\Delta E^0 + \Delta E_{int}] \quad (1)$$

Depending on whether Pauli repulsion or electrostatic attraction represents the dominant contribution to ΔE^0, this term is either destabilizing or bonding in nature. Although BE_{snap} values are not defined in the same way as bond dissociation enthalpies ΔH, they are reasonable approximations of bond enthalpy terms, which in turn provide a good description for the bond strength [9].

The results of our analysis are gathered into Table 1.

Table 1. Bond energy terms[a] and Mulliken charges[b] for TMH complexes.

	ΔE^0	ΔE_{int}	BE_{snap}	Q
H-W(dmpe)$_2$(N)	-14	-281	295	-0.37
H-W(dmpe)$_2$(CH)	-29	-294	323	-0.35
H-W(dmpe)$_2$(NO)	-39	-309	348	-0.36
H-W(CO)(NO)(PMe$_3$)$_3$	-23	-313	336	-0.27
H-W(CO)$_2$(NO)(PMe$_3$)$_2$	-9	-312	321	-0.16
H-Cr(CO)(NO)(PMe$_3$)$_3$	8	-309	301	-0.18
H-Mo(CO)(NO)(PMe$_3$)$_3$	-20	-299	319	-0.29

[a]in kJ/mol; [b]in a.u.

First, we look at the term ΔE_{int}, which is closely related to the term ΔE_{stab} from the perturbational analysis. The trend predicted for the influence of the *trans*-ligand is reflected in the ΔE_{int} values. We also note that the orbital interaction energy for the tungsten nitrosyl hydride systems is essentially the same, independent of the number of phosphine ligands. For all three compounds, the steric contribution ΔE^0 is stabilizing, and therefore dominated by attractive electrostatic interactions. Increasing the number of P-donors further increases the absolute value of ΔE^0, and strengthens the TM-H bond.

In addition, the larger number of P-donors increases the polarity of the TM-H bond, and thus enhances the reactivity of the compounds. This trend is reflected in the familiar Mulliken charges Q (Table 1), which do not provide an absolute measure for the physical value of the local charge, but rather are good indicators of qualitative trends.

Comparing the three compounds of the chromium triad, we observe that molybdenum and tungsten show similar bonding characteristics, and similar bond polarities. The tungsten compound possessing a TM-H bond, which is stronger by about 10 kJ/mol. The chromium complex differs in that we now have a destabilizing contribution from ΔE^0 to BE_{snap}, and a less polar M-H bond. Again, relativistic effects and core expansion are the key factors which, are responsible for the stronger bond in the tungsten complex, and for the different bonding characteristics of the hypothetical chromium compound.

The different polarity of transition metal hydrogen bonds is reflected in the hydridic-protonic preference (ΔH_{hp}) scheme developed by Pearson [13]. The basis for ΔH_{hp} is the following gas phase redox equilibrium, in which the protonic and hydridic dissociations of transition metal hydrides are considered.

$$L_nM^- + H^+ \rightleftharpoons LnM^+ + H^- \quad : \quad \Delta H \tag{2}$$

According to Pearson, ΔH_{hp} can be obtained from the difference in the Mulliken electronegativity χ_H of H and the Mulliken orbital electronegativity χ_{L_nM} of L_nM, as shown in Eq.3:

$$\Delta H_{hp}\,(\text{kJ/mol}) = -193\cdot(\chi_H - \chi_{L_nM}) \tag{3}$$

If ΔH_{hp} is positive, the L_nM-H bond is acidic in character, and if ΔH_{hp} is negative, the hydridic dissociation is favored in the above equilibrium. The triad of the binary transition metal hydrides MH, M = Cu, Ag, Au, provides an illustrative example for this concept. The relvant Mulliken electronegativies are χ_{Cu} = 4.48, χ_{Ag} = 4.44, χ_{Au} = 5.80, and χ_H = 7.17 [13]. All three hydrides thus display hydridic behavior.

Our considerations of hydridic or protonic dissociation of the L_nM–H bond have to be viewed as somewhat artificial, since they refer to the gas phase, whereas most of the chemistry of transition metal hydrides takes place in solution. For a more realistic discussion of the polar behavior of transition metal hydrides, it is necessary to include solvent effects. This aspect will be dealt with in the following section.

4.3 SOLVENT EFFECTS

To make a connection between ΔH_{hp} as defined in the gas phase, to the chemistry in solution, correction increments for solvation enthalpies have to be included. For the example of water, the above gas phase equilibrium (equation 2) is formulated for the hydrated species, eq. 4:

$$L_nM^-(aq) + H^+(aq) \rightleftharpoons L_nM^+(aq) + H^-(aq)\,;\quad \Delta H_{hp}^{(aq)} \tag{4}$$

Under these circumstances, $\Delta H_{hp}^{(aq)}$ can be calculated as

$$\Delta H_{hp}^{(aq)} = \Delta H_{hp} + \Delta\Delta H(aq) \tag{5}$$

In equation 5, $\Delta\Delta H$(aq) stands for the difference in the enhalpies of hydration ΔH(aq) for the species on the right and on the left side of equation 4. If one assumes that the ΔH(aq) values in the cases of large ions are similar for both the L_nM^+ and L_nM^-, these terms might be neglected in the calculation of $\Delta\Delta H$(aq), and one is left with the difference of the enthalpies of hydration for the proton and the hydride. These values amount to -1117 and -452 kJ/mol, respectively [13], and one obtains the following relation:

$$\Delta H_{hp}^{(aq)}\ (\text{kJ/mol}) = 193 \cdot (\chi_H - \chi_{L_nM}) + 665 \qquad (6)$$

Compared to the expression for the gas phase equilibrium (eq 3), the increment of +665 kJ/mol leads to a protonic shift in the the hydridic-protonic preference. However, for monoatomic ions, like those involved in reactions of the hydrides of the copper triade, the simplifications, which led to eq 6, are no longer valid. The protonic shift as a consequence of solvation is nevertheless prominent, as can be seen from the values in Table 2. AuH thus behaves as an acid, AgH is expected to be a borderline case, and CuH is a hydride.

Table 2. Acidic and hydridic properties of the binary hydrides MH, M = Cu, Ag, Au, in the gaseous and aqueous phase.

	Au-H	Ag-H	Cu-H
Mulliken electronegativity, χ(M)	5.80	4.44	4.48
$\Delta H_{hp}^{(gas)}$[a]	-264	-527	-519
gas phase behavior	weakly hydridic	hydridic	hydridic
$\Delta H_{hp}^{(aq)}$[a]	351	0	-84
solution behavior	acidic	borderline	hydridic

[a]in kJ/mol

Transition metal hydrides, which are weakly basic as isolated molecules, are expected to display acidic properties in solution. With an appropriate choice of solvent we are thus able to induce 'Umpolung' of the acid-base behavior of certain transition metal hydrides. The break-even point of a TMH in water would be reached with $\chi_{LnM} \approx 3.7$. This relatively low value indicates that most transition metal hydrides will dissociate protons in water.

In order to conclude these considerations about the nature of the L_nM-H bond, it is appropriate to say that the L_nM-H bond is normally intrinsically basic at the hydrogen site, although most of the known species are potential acids in solution. It is therefore better to talk about hydridicity, when describing the intrinsic basic features of TMH complexes.

4.4 HYDRIDICITY OF TRANSITION METAL HYDRIDES

In the previous section it was demonstrated that transition metal hydrides may change their naturally basic character at the hydride site into acid behavior in solution. The latter aspect however strongly depends on the nature of the solvent. Those with only minor solvation properties are expected to retain the original features of the hydrides to a great extent, and thus allow them to react as bases.

One should mention that these basicities or hydridcities are understood in a thermodynamic sense. For any further consideration we will exclude any effect which may be caused by barriers of proton transfer processes. Given these assumptions, bond ionicities may be taken as indicators for the basic or hydridic character of the L_nM-H bond, provided that the polarization of this bond leads to accumulation of negative charge at the H atom. Bond ionicities of transition metal deuterides were determined by us earlier [14]. They were deduced from T_{1min} measurements of the ^2H nucleus, which subsequently allowed for the calculation of Deuterium Quadrupole coupling Constants (DQCC) [15]. The DQCCs depend on the electrical field gradient, which is zero for isotropic conditions as for an isolated deuteride, and which is at maximum (227 kHz) for the ideally covalent D_2 molecule. These two extreme cases define 100 % and 0 % bond ionicity, and the value for any intermediate case might be obtained by linear interpolation. If the ^2H nucleus is replaced by the ^1H nucleus being more relevant for TMH chemistry, we expect that the ionicities remain similar, and that the derived general trends are completely transferable. Selected values of DQCC's and the corresponding bond ionicities are presented in Table 3.

A closer inspection of these values reveals that the TM-H bond is rather variable in its ionic character. The determined ionicities span a range from 70 % to 85 %, depending mainly on the natural properties of the metal center and on the influence of the ligand sphere. Many of the complexes investigated were nitrosyl species. Compared to related carbonyl compounds their bond ionicities can be found in the upper range of the ionicity scale. In a similar way, an increasing number of phosphine ligands will also lead to an increase in bond ionicities. Both of these observations stress the various possibilities that exist for a ligand tuning of the ionic or covalent character of the TM-H bonds.

We should mention that the values in Table 3 marked with an asterix are derived from solid state determinations of DQCCs. Up to now not many DQCC values have been determined by such methods. However, due to the major strides that have been made in the field of solid state NMR spectroscopy, DQCCs for the solid state will become more easily available. We have initiated such investigations for a series of transition metal deuterides, and it will be interesting to see whether the solution and solid state results are comparable. This might provide another possibility to study solvent influences on the transition metal hydride bond.

Table 3. Deuterium quadrupole coupling constants DQCC and bond ionicities *i* for selected TMDs, determined from ^2H T_{1min} measurements in toluene. Starred values refer to solid state determinations.

	T_{1min}[a]	DQCC[b]	*i*[c]
$WD(CMes)(dmpe)_2$	45 (-60)	34.1	85
	-	34.8*	85
$WD(CO)(NO)(PMe_3)_3$	45.0 (-95)	39.1	83
	-	56.8*	75
$WD(CO)_2(NO)(PMe_3)_2$	22.7 (-95)	55.0 ± 0.6	76
$WD(CO)_2(NO)(PPh_3)_2$	22.5 (-70)	55.2 ± 0.6	76
$MnD(NO)_2(PEt_3)_2$	21.5 (-87)	56.4 ± 0.6	75
$MnD(CO)_3(PMe_3)_2$	15.4 (-90)	66.7 ± 1.0	71
$ReD_2(CO)(NO)\{P(O^iPr)_3\}_2$	14.5 (-80)[d]	68.8 ± 1.0	70
	15.6 (-80)	66.3 ± 1.0	71
$ReD_2(CO)(NO)(PMe_3)_2$	14.0 (-100)[d]	70.0 ± 1.0	69
	16.1 (-100)	65.3 ± 1.0	71
$ReD_2(CO)(NO)(PCy_3)_2$	14.2 (-70)[d]	69.5 ± 1.0	69
	15.4 (-70)	66.7 ± 1.0	71
$ReD_2(CO)(NO)(P^iPr_3)_2$	13.1 (-87)[d]	71.0 ± 1.0	69
	14.5 (-87)	68.8 ± 1.0	70
cis-$ReD(CO)(PMe_3)_4$	12.4 (-110)[e]	74.4 ± 1.0	67
trans-$ReD(CO)(PMe_3)_4$	15.3 (-110)[e]	66.8 ± 1.0	71
cis,mer-$ReD(CO)_2(PMe_3)_3$	17.0 (-87)	63.5 ± 1.0	72
trans,mer-$ReD(CO)_2(PMe_3)_3$	16.4 (-95)	64.7 ± 1.0	71
fac-$ReD(CO)_3(PMe_3)_2$	15.7 (-90)	66.1 ± 1.0	71

[a]in ms. Temperature (in °C) given in parentheses. [b]in kHz. [c]in %. [d] *trans* NO. [e] in CH_2Cl_2

In connection with these studies we have recently measured the solid state DQCC of a carbyne species $W(\equiv CMes)(dmpe)_2D$ (Mes = mesityl) and a nitrosyl compound [16] $W(CO)(NO)(PMe_3)_3D$. It came to a surprise that in both cases only at lower temperatures the expected double modal Pake curve could be noticed. At room temperature, just a residual Pake pattern could be observed, while otherwise a strong singlet resonance developed for the ^2H nucleus of the above complexes. This can only be interpreted in terms of deuteride mobility in the solid state. Even though the mechanism for this process is not clear yet at the present time, this experiment points to the general propensity for deuteridic, or hydridic cleavage of hydridic L_nM-D(H) bonds.

For both deuteride complexes, the bond ionicities have been determined in solution as well. They show the same value of $i = 85\%$ for the carbyne species in solution as well as in the soldid state, but for the nitrosyl compound amount to i(solid) = 75 %, and. *i*(liquid) = 83%, respectively. This effect that a solvent may induce additional polarization of the metal hydride bond, has been observed for the first time. At the moment it is not possible to present a clear-cut interpretation of this result. However, we believe that it may provide an important step towards

the understanding of polar reactivity of transition metal hydrides in chemical transformations, which are to a major extent carried out in solution.

Other approaches to classify the L_nM-H bond in terms of hydridicity are based on kinetic or thermodynamic studies of hydride transfer reactions. Selected examples can be found in the work of Cheng, Brunschwig and Bullock [17], who determined kinetic hydridicities by the reaction of TMHs with the trityl cation, and in the work of Sarker and Bruno [18], who used the equilibration of both types of species to establish a thermodynamic scale of hydridicities.

As we have seen so far, there exist different methodologies to characterize hydridicities of transition metal hydrides, namely the electronic, kinetic, and thermodynamic approaches. However, up to now there is no unified view, which could combine all aspects of these different methods. It would be valuable to have in hand a general concept of hydridicity in the same way as it was established for electrophylicity in carbocation chemistry by Mayr and coworkers [19].

4.5 DIHYDROGEN BONDING AND LEWIS ACID ADDUCT FORMATION

L_nM-H complexes normally display different basic sites. Among the various possibilities there are the ancillary ligands L, the metal centers M, or the hydrides. If a too great steric hindrance can be ruled out, the hydride site is normally the kinetically preferred position for interaction with protons [20]. A more sensitive probe to describe the basicity of transiton metal hydrides is presumably their interaction with protic substrates. This new bonding phenomenon L_nM-H···HX is strongly connected to a novel type of hydrogen bond termed *dihydrogen bonding* [21-23]. We can assume that a proton transfer to the hydride site of a TMH is normally proceeded by dihydrogen bonding, which then might also have implication for the reactivity of TMHs in general.

The main bond characteristics of dihydrogen bonding is anticipated to be of electrostatic nature. Thus, the ability of L_nM-H complexes to interact with protic compounds is expected to be directly related to the basicity of transition metal hydrides, as we have defined them above. This in our mind provides an excellent additional method to quantify the basicity of TMH complexes by the strength of the L_nMH···HX bonding.

We would like to note that a related Lewis acid/base interaction with hydrides may also suffice the purpose of the assessment of basicity. The thermodynamic analyses of the hydride adduct formation with protic substrate is usually accomplished by spectroscopic investigations of their equilibria of formation (eq 7).

$$L_nMH + HX \rightleftharpoons L_nMH\cdots HX \qquad (7)$$

There are three superior methodologies [24] to examine these reactions:

i) VT-IR investigations allow for direct observation of all involved species, and the required equilibrium concentrations are obtained by integration of appropriate IR bands.

ii) VT-NMR titration of equilibrium reactions with acidic substrates HX, observing the shift of the hydride resonances. Since the equilibrium reactions are normally fast on the NMR time scale, respective resonances of species that appear on the left or on the right side of the above equilibrium cannot be resolved. Only an averaged chemical shift for the hydride ligand is observed, and the dependence of this $\delta_{Hydride}$ from the amount of HX allows one to extract the equilibrium constants.

iii) The IR investigations of the red-shift or of half-height widths of ν(OH) bands upon hydrogen bonding enables one to extract the strength of H···H interactions based on empirical correlations.

In our group we have applied all three methods to study dihydrogen bonding of transition metal nitrosyl hydrides [25-27] These studies led to an overall consistent picture of the general phenomenon of dihydrogen bonding, and of the basic character of transition metal hydrides.

In this manner, we have established for nitrosyl hydride complexes that the hydride ligand behaves very basic, and undergoes relatively strong interactions with protic substrates. The strength of these bonds ranges from 8 to 30 kJ/mol, and depend on the metal center, the nature of the ligand sphere, as well as on the steric requirements of the whole molecule. In these experiments it was also recognized that the strength of $L_nMH\cdots H$ interaction is also related to the acidity of the protic substrate. Via T_{1min} relaxation time measurements of the hydride ligand, it was possible to calculate H···H distances, which take on values between 1.7 and 2.0 Å. In the extreme case of highly acidic protic substrates, and at low temperatures, even double dihydrogen bonding, in which two basic sites of the TMH molecule are involved, could be traced. It was found that thermodynamically the hydride site is favored in the interaction with HX. However, if an increasing bulk of neighboring ligands provides steric shielding of the H site, HX interaction takes place at thermodynamically less favored basic positions. Typically, the O_{NO} atom becomes the site of interaction, which is now rather weak (8 - 12 kJ/mol).

During the course of these studies, it was observed that a solvent may influence the interaction strength significantly. NMR measurements in deuterated methylcyclohexane yielded values which were about 8 - 12 kcal/mol higher than those obtained in deuterated toluene. This difference was attributed to aromatic hydrogen bonding of the protic compounds ($(CF_3)_2CHOH$, $(CF_3)_3COH$) with d^8-toluene.

We should mention here that the basic behavior and consequently the ability of dihydrogen bonding is not restricted to the class of transition metal nitrosyl

hydrides, but seems to be a more general feature of TMHs, which takes place the solid state and also in solution. While in the group of Crabtree mainly solid state H···H interactions were studied [28,29], other research groups have investigated in great detail this kind of bonding in solution [30-32].

It is further possibe to probe the basicity of transition metal hydrides by the interaction with Lewis acids. Here, one has to take into account that due to the relatively strong sensitivity of the H···H interaction toward steric congestion, the addition of Lewis acids, which *a priori* are of sizable steric demand, could be relatively weak. However, in these cases it is expected that the addition of Lewis acids to TMHs leads to full covalent bonds, with generally higher interaction energies. In this way, we have studied - mainly by VT-IR - the site preference of boranes (BH_3·THF, 9-boranorbonane) in their reactions with a series of phosphine substituted rhenium carbonyl hydrides, $Re(CO)_n(PMe_3)_{5-n}H$ [33]. It was interesting to see in these investigations that the sterically less cumbersome BH_3 always goes for the hydride position, independent of the degree of phosphine substitution. In contrast to this, the sterically more demanding 9-boranorbonane attacks in the cases of the higher substituted rhenium carbonyl hydrides a O_{CO} atom. When reducing the number of phospines ligands, the 9-boranorbonane then interacts with the hydride ligand, if at all.

4.6 REACTIVITY OF HYDRIDIC TRANSITION METAL HYDRIDES

To this point, we have characterized the basicity of TMH complexes, and in the previous chapter dihydrogen bonding was described as a special interaction, which is directly related to this property. This directional bonding may also have implications for the reactivity of hydride complexes in the sense that it may be a pre-stage to protonation of TMHs, leading to dihydrogen complexes [34]. This type of reactivity is characterized by bond formation with the hydride ligand, which in this way however remains in the coordination sphere of the metal.

In the following, we turn our attention to reactivities which involve cleavage of the L_nM-H bond, inducing hydrogen or hydride transfer reactions. These processes can normally be viewed as insertion reactions into the metal-hydride bond and represent valuable elementary steps of homogeneous catalysis. It is very important to note at this point that such insertions do not require precoordination of the inserting substrate.

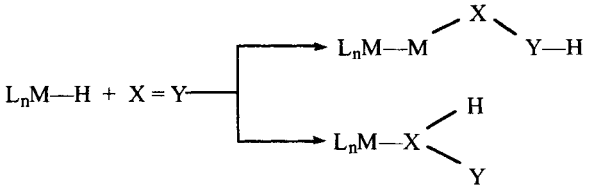

(8)

This, however, does not necessarily mean that hydride transfer can exclusively occur with attack on external substrates. As the example of hydride transfer to a carbyne ligand demonstrated, it is well possible to also direct a hydride transfer to internal unsaturated substrates [35].

Mechanistically, the essential step of the hydride transfer reactions with TMHs may be characterized according to one of the following categories:

i) Full hydride transfer

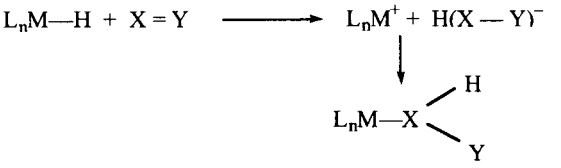

(9)

ii) Single electron transfer SET

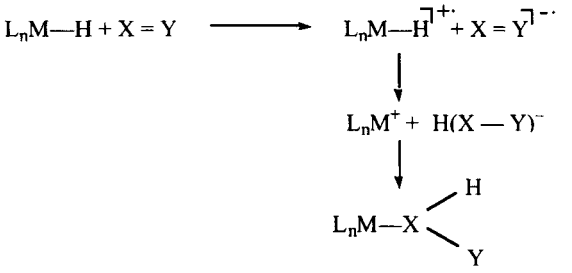

(10)

iii) Synchronous hydride transfer SHT

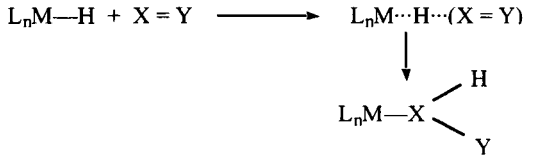

(11)

iv) Hydride tunnelling onto the substrate

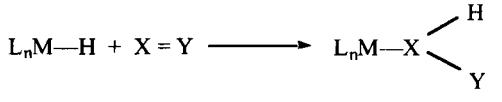

(12)

As demonstrated by various reactions in the field of organic chemistry, it is often not easy to distinguish route i) from ii). The radical type SET mechanism may proceed as solvent-caged reaction, and as such it may show very similar

kinetic characteristics as reactions of type i). We will return to this point in the last chapter, in connection with ionic hydrogenations. Only the appearance of tunnelling [36] may clearly be identified by a temperature independent kinetic term, or by deuterium substitution studies. Hydridic TMHs are especially proned for insertion reaction for two reasons, which are i) the nucleophilicity of the hydridic hydride, and ii) a reduced metal hydride bond strength.While i) provides a mainly kinetic argument, so does ii) aim at the thermodynamics of such reactions.

As mentioned before, we have studied in our group various types of insertion reactions with phosphine substituted transition metal nitrosyl hydrides [37]. In general, these compounds appear to have a very hydridic L_nM-H bond, but also a very reactive one. In a series of complexes $W(NO)(CO)_{4-n}(PR_3)_nH$, (n = 2,3), it was seen that there is increased propensity for insertion with an increasing number of phosphine substituents. For instance, $W(NO)(CO)_2(PR_3)_2H$ complexes react with CO_2 and aldehydes to afford formate and alkoxide compounds. These species, however, do not undergo transformations with ketones, or metal carbonyl compounds. Increasing the number of PMe_3 ligands by one considerably enhances the reactivity. $W(NO)(CO)(PMe_3)_3H$ inserts not only CO_2 and aldehydes, but also several ketones, for example acetone, acetophenone and benzophenone [38].

Fixated carbon monoxide in form of metal carbonyl complexes like $Fe(CO)_5$ and $Re_2(CO)_{10}$ inserts in equilibrium reactions, equation 13, for which we were able to determine ΔH values. They amount to ΔH = -26 kJ/mol (M = Re, n = 2), and -46 kJ/mol (M = Fe, n = 1), respectively.

$$W(NO)(CO)(PMe_3)_3H + OC\text{–}M_n(CO)_{5n-1} \rightleftharpoons W(NO)(CO)(PMe_3)_3\text{–}OHC\text{–}M_n(CO)_{5n-1} \quad (13)$$

A very related molybdenum system [39] $Mo(NO)(CO)(PMe_3)_3H$ qualitatively revealed the same reaction patterns, but showed an enhanced reactivity. In particular, the reactions with metal carbonyls do not only require shorter reaction times, but also have significantly higher K values of the corresponding insertion equilibria. According to equation 14, the reaction with $Fe(CO)_5$ is completely irreversible in this case, while the reaction with $Re_2(CO)_{10}$ is still at equilibrium, however lying much more on the product side as compared to the insertion reaction with the tungsten compound. The value for the equilibrium with $Re_2(CO)_{10}$ could be determined as ΔH = -47 kJ/mol.

$$(CO)_{2n}M_n\text{-}CO + Mo(NO)(CO)(PMe_3)_3H \underset{M = Re}{\overset{M = Fe,Re}{\rightleftharpoons}} Mo(NO)(CO)(PMe_3)_3\text{-}OHC\text{-}M_n(CO)_{2n-1} \quad (14)$$

The difference in behavior of the tungsten and molybdenum compounds is related to the thermodynamics of the insertion equilibrium, and thus to the M–H bond strengths. As we have seen in our analysis above, the tungsten compound indeed possesses the somewhat stronger metal-hydride bond. The difference in the BE_{snap} values for $W(NO)(CO)(PMe_3)_3H$ and $Mo(NO)(CO)(PMe_3)_3H$, 17 kJ/mol, comes close to the experimental $\Delta\Delta H$ value of 21 kJ/mol for the insertion reactions with $Re_2(CO)_{10}$. Furthermore, Density Functional calculations suggest that the main difference in the reaction of $W(NO)(CO)(PMe_3)_3H$ with the iron and the rhenium carbonyl compounds is not of electronic nature, but is governed by the different stereochemistry of the insertion products [38].

Our group then has turned to study systems with four phosphorus donors, which were established by introducing two dmpe ligands into the coordination sphere of molybdenum or tungsten nitrosyl complexes. Again, an increase in the reactivity of the hydride ligand is observed. The compound $Mo(NO)(dmpe)_2H$ even undergoes addition reactions with the normally quite reluctant imine reagents to afford amido compounds, Scheme 2 [40].

This transformation could not be accomplished with bis- or tris-phosphine substituted complexes. In a special case, namely when inserting a phenyl (naphtyl)imine, an equilibrium was observed.

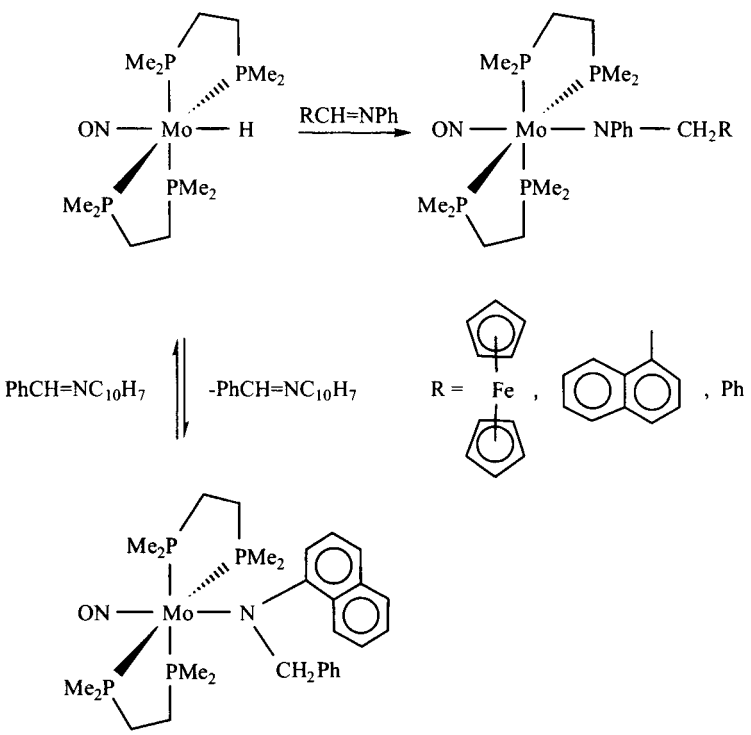

Scheme 2

For the mono-insertion step with metal carbonyl compounds, very fast reactions were noticed, which led to complete formation of the μ-formyl complexes, as displayed in Scheme 3. The hydride $Mo(NO)(dmpe)_2H$ showed even such a high activity that it inserted into a Re–(CO) bond of $Re_2(CO)_{10}$ twice. The second insertion step, however, again represents an equilibrium reaction, lying far on the product side.

By isoelectronic replacement of the nitrosyl ligand with a carbyne unit, we derived a new type of system, which was realized in the form of the complex $W(\equiv CMes)(dmpe)_2H$ [41]. A strong π-accepting ability is also attributed to the carbyne ligand, so that a electronically related environment of the hydride could be expected, compared to related nitrosyl substituted species. It turns out that $W(NO)(dmpe)_2H$ reacts with excess benzophenone about five times faster than the corresponding carbyne complexes. This factor of enhancement, however, is in kinetic terms a minor one, which means that these complexes have overall comparable reactivity. For the insertion of benzophenone into the W-H bond of $W(CMes)(dmpe)_2H$, an inverse and very pronounced deuterium isotope effect is observed (k_H/k_D = 1/3). This points to existence of a late transition state in the rate determining step, which must have to do with the actual H-transfer.

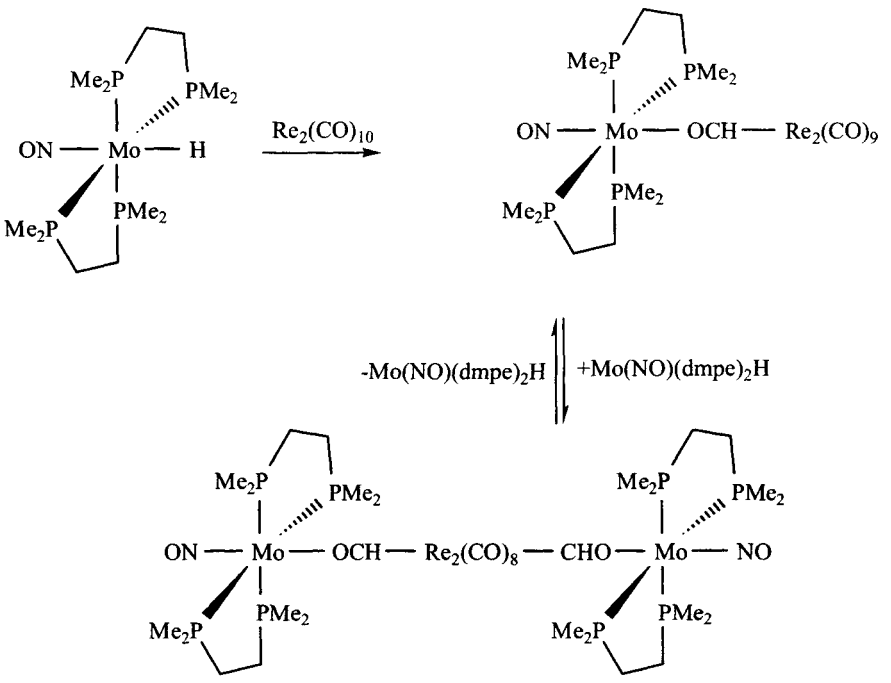

Scheme 3

The mainly qualitative reactivity studies revealed that the hydride activity is tied to three major factors:

i) The presence of an activating *trans* influence ligand is essential;

ii) The increase in the number of phosphine substituents parallels an increase in the insertion potential;

iii) Second row transition metal given rise to enhanced hydride activity.

All of these three features do not only cause an increase in hydridicity of the L_nM-H bond, but also stabilize the corresponding $16e^-$-species, L_nM^+, by delocalizing σ orbital character via the *trans* influence, and raising the orbital energy via electron donation mainly of the phosphorus ligands. One might thus pose the question whether these L_nM^+ cations might be able to undergo interaction with H_2. It is anticipated that the newly formed dihydrogen complex could be deprotonated, either by an internal basic site of the molecule, or by an external base. This process would then lead to heterolytic splitting of the H_2 molecule, leaving behind a hydridic TMH complex, and a weak acid. Both of these components are the essential ingredients for the very useful ionic hydrogenation reactions. In the remaining two chapters we will discuss these aspects in more detail.

4.7 HETEROLYTIC SPLITTING OF DIHYDROGEN

The reaction of dihydrogen with transition metal complexes leading to a splitting of the H_2 molecule, is an important step in many catalytic reactions. For the example of the above mentioned hydroformylation, this process closes the catalytic cycle by liberating the final product, and regenerating the catalyst [42]. In general, these reactions proceed as oxidative additions, and correspond to a homolytic splitting of the dihydrogen bond. The activation of H_2 itself by oxidative addition to form a transition metal dihydride is closely related to the discovery of dihydrogen complexes by Kubas [43-45]. The dichotomy between the dihydrogen and dihydride complex illustrates the activating potential of the transition metal hydride center. Comparing a series of related complexes, one can actually trace out the oxidative addition of H_2 [46], when only the ligand sphere around one specific metal center is varied. On the other hand, one might also compare related complexes with the same ligand environment, to assess the role of the transition metal in detail [47-49].

The oxidative addition or homolytic splitting of H_2 does activate the dihydrogen molecule, since it strongly changes the acid or basic characteristics of the H sites. However, both of the H atoms possess the same reaction potential. All Wilkinson-type hydrogenation catalysts induce homolysis of H_2. On the other side, the process of heterolytic splitting, which occurs with formal generation of H^- and H^+, in general creates a TMH complex and a corresponding protonated base.

Thus, two active H sites with complementary reaction potential are generated, which is a necessity for certain transformations, like the so-called ionic hydrogenation reactions.

Our investigations of the reactivity of transition metal nitrosyl hydrides guided us to speculate how a potential system for heterolytic splitting might look like. On the one hand, the cationic 16e$^-$ species are expected to have a great propensity to pick up a hydride ligand, forming a TMH complex. On the other hand, we have seen that these nitrosyl hydrides themselves possesses various basic sites, and thus could also act as base, taking up the forming proton. The process of H_2 activation via heterolytic splitting might be feasible without the addition of an external base.

The cationic rhenium complexes $[Re(NO)_2(PR_3)_2]^+$ (R = Cy, ^{i}Pr) [50] indeed show great potential for hydrolytic activation of dihydrogen. When $[Re(NO)_2(PR_3)_2]^+$ is treated with a mixture of H_2 and D_2 in toluene or chlorobenzene, hydrogen-deuterium scrambling is observed, and HD can be traced in the NMR spectrum of the reaction mixture [51]. The proposed mechanism for this catalytic exchange is illustrated in Scheme 4.

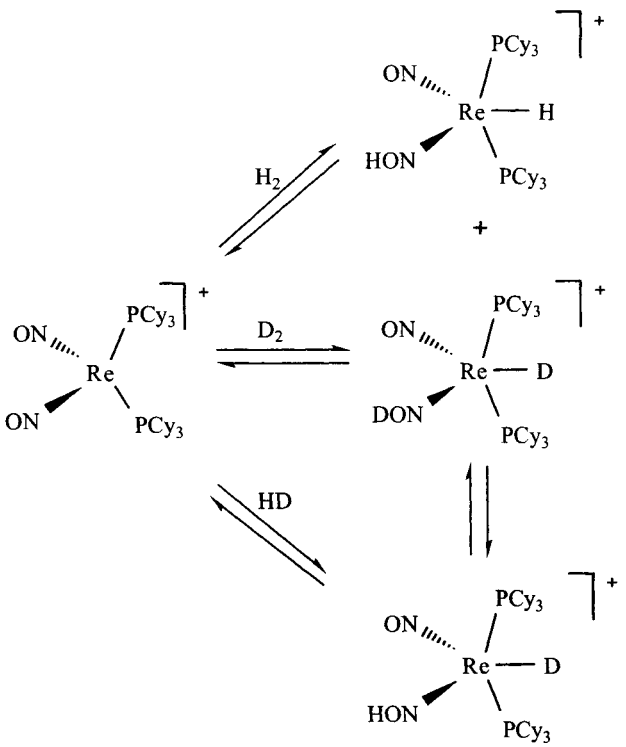

Scheme 4

We suggest that the initial step is heterolytic splitting of H_2 or D_2, leading to the protonated or deuterated transition metal nitrosyl hydrides or deuterides, respectively. H/D exchange via the second nitrosyl ligand might lead to the mixed hydride-deuteride complex, which in a reverse reaction forms HD, and regenerates the cationic catalyst.

Although the protonated TMH or TMD complexes as formulated above have so far never been observed directly, and are just postulated intermediates, there exists experimental evidence that the dinitrosyl hydride complexes posses a strong basic site at the O_{NO} atom. For example, we were able to characterize A···ON-ReH(NO)(P^iPr_3)$_2$ adducts, A representing a Lewis acid like BF_3 [52] or even the cationic metal fragment [Re(NO)$_2$(P^iPr_3)$_2$]$^+$ itself [50]. The formation of these adducts not only illustrates the basicity of the nitrosyl group, but also the strong Lewis acidity of the 16e$^-$ cation. We also found that the bimetallic complex shows a similar reactivity as the free cationic species itself. Further evidence for the proposed heterolytic splitting was obtained when the reaction with H_2 or D_2 is performed in the presence of an external base (Scheme 5).

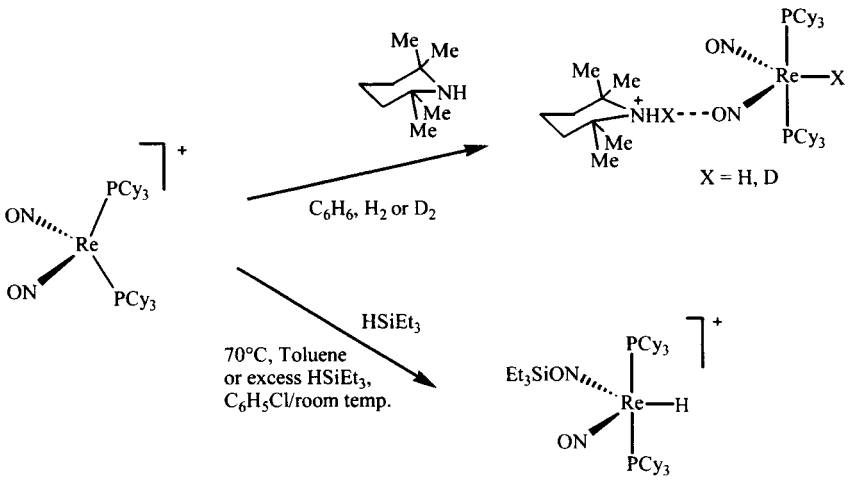

Scheme 5

Although the proton that is formed during heterolytic splitting, is taken up by the external base, one clearly observes additional interactions with an O_{NO} atom of ReH(NO)$_2$(P^iPr_3)$_2$. This unusual kind of hydrogen bonding, [R_3N···H···ON-ReL_4]$^+$, where a proton bridges two basic sites, points to the possibility that the rhenium hydride itself is indeed able to serve as a proton acceptor, as indicated above. The role taken by the external base might also be that of cocatalyst, assisting the heterolytic cleavage of H_2. In a theoretical study, Dedieu and Hutschka evaluate this possibility for the model system

$Rh(H_2)(PH_3)_2(HCO_2)/NH_3$, and present a possible pathway for base assisted heterolytic cleavage [53]. Similar mechanisms might be at work in our case, and are currently under investigation. We have further provided synthetic access to another type of bifunctional systems containing pyridyl functionalized phosphine ligands. In the tungsten cations $[W(CO)_2(NO)(R_2Ppy)]^+$ (R = Me, Ph; py = 2-pyridyl, 2-(6-Me-pyridyl), 2-(6-^{t}Butyl-pyridyl)), the N-site of the pyridyl substitutents is supposed to take on the role of the external base, potentially providing assistance in the heterolytic cleavage of H_2 [54].

Lastly, we should mention that the possibility of the $[Re(NO)_2(PR_3)_2]^+$ cations to cleave σ-bonds in a heterolytic fashion, is not restricted to dihydrogen only. When these systems are reacted with triethylsilane, either stoichiometrically at 70°C in toluene, or with an excess at room temperature in chlorobenzene, the Si-H bond is cleaved, leading to a cationic TMH, in which the silicon moiety is bound to an O_{NO} atom (Scheme 5). This reaction offers various possibilities for the design of catalytic hydrosilylation cycles, which are explored in our laboratories [51].

4.8 IONIC HYDROGENATION

The last topic that we are going to address is the potential application of TMH complexes in ionic hydrogenation reactions. As we shall see, stoichiometric reactions of this type can indeed be carried out utilizing TMH. Together with heterolytic splitting reactions, catalytic cycles can be envisioned, which open up the possibility of hydrogenation of unsaturated functional groups using molecular hydrogen. Adequately designing the ligand sphere of the transition metal catalyst, stereocontrol of the reaction can be exercised. This principle has already been demonstrated, for example, in the ionic hydrogenation of sterically demanding alcohols to the corresponding methanes [55]. Furthermore, using chiral TMHs, enantioselective reactions may become possible. This opens up an entry into asymmetric transfer hydrogenation [56-58], thus greatly expanding the synthetic capacity and possible use of such potentially catalytic systems.

Ionic hydrogenation reactions have been known for a long time in organic chemistry [59]. The basic mechanism is displayed in Scheme 6. In a first step, a carbenium ion is formed by i) protonation or ii) bond hydrolysis, which then reacts with hydride donors to the hydrogenation product. For an effective reaction it is required that the single components must not react with each other, that no side reactions take place with the substrate, and that the product evolution must not be hindered.

We already mentioned the different mechanistic possibilities for the hydride transfer step. Fundamental work dealing with the nature of the H transfer has

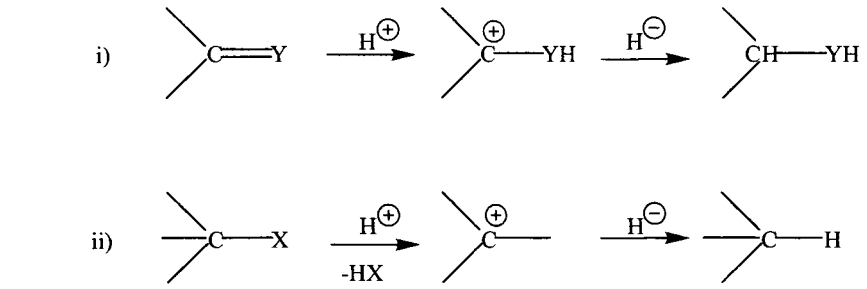

Scheme 6

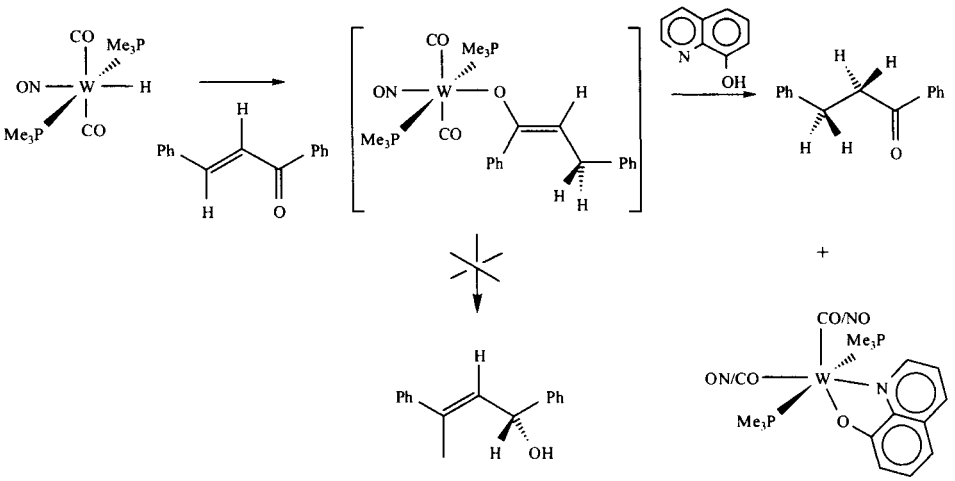

Scheme 7

been carried out in a series of studies for the hydride shift reactions from hydrosilanes to carbenium ions. The kinetic study of Chojnowski and co-workers [60] lead to the result that and SET mechanism is followed, involving radical intermediates, whereas Mayr and co-workers present experimental evidence for the SHT mechanism [61]. The computational work of Apeloig and co-workers provides further evidence for the SHT mechanism, in particular since these authors could show that SHT exhibits certain characteristics of an electron transfer process without actually being a SET process [62]. These studies illustrate the difficulties which may arise when assessing the reaction mechanism for hydrogen transfer.

In the field of transition metal mediated stoichiometric ionic hydrogenation, the prototypical system $Cp(CO)_3WH/CF_3SO_3H$ has been introduced by Bullock and co-workers [63], who systematically investigated the range of its potential

application for hydrogenation of a variety of sterically hindered olefins [64] and alkynes [65]. During the course of these investigations, a solvent effect has also been observed; not in the sense that different solvents cause different basicities of the TMH complex, but rather that solvent coordination to the transition metal center might inhibit product evolution [66]. In the same way as found in the case of hydrosilanes as hydride donors, the hydride transfer step follows a SHT mechanism [67].

In the context of ionic hydrogenations, our group has studied insertion reactions into the transition metal hydride bond for a variety of tungsten systems. Our first example of an activated TMH molecule was the complex $W(NO)(CO)_2(P(O^iPr)_3)_2H$, which inserts carbon dioxide and electron poor acetylenes [68,69]. The same complex also reduces a variety of aldehydes to the corresponding alcohols, in the presence of acetic acid or phenol, acting as proton sources [70]. Enhancing the hydridicity of the tungsten complex by exchanging the phosphite ligands for more electron rich phosphine groups, we could effectively use the complex $W(NO)(CO)_2(PMe_3)_2H$ in the reduction of salicylaldehyde or o-hydroxyacetophenone, in which the substrate also serves as proton source [71]. An interesting example of for a stoichiometric ionic hydrogenation is shown in Scheme 7.

The hydrogenation pair $W(NO)(CO)_2(PMe_3)_2H$ together with 8-hydroxyquinoline selectively reduces the olefin functionality, and does not attack the C=O double bond, when reacted with the enone HPhC=CH(C(O)Ph) [72].

So far, we have encountered ionic hydrogenation reactions, which have been described as two step reactions, and for which the mechanistic characteristics are closely related to the nature of the second step, namely the H transfer process. However, one has to keep in mind that the ionic hydrogenation is essentially a three component reaction. There might exist the possibility that all three components work together in certain steps of the hydrogenation reaction. Already in our early studies we observed that the insertion into the metal hydride bond of a particular substrate, which under normal reaction conditions took place with a reaction time of one day, was greatly accelerated in the presence of a proton donor [71]. The same cooperative effect could be established for the trisphosphine-substituted nitrosyl complexes $W(NO)(CO)(PMe_3)_3H$ [73] and $Re(NO)(PMe_3)_3H_2$ [74]. An exemplary reaction is given in Scheme 8.

At room temperature, the complex $W(NO)(CO)(PMe_3)_3H$ does not react with acetone, and the reaction with phenol under the same conditions, leading to evolution of molecular hydrogen and formation of the phenoxy complex, is slow, lasting one day. If, however, all three components are reacted together, the formation of isopropanol can be observed, which is complete already after 15 minutes. For the above mentioned Re complex, no reaction is observed neither with phenol, nor with acetophenone, in refluxing toluene. When mixing the carbonyl compound together with the hydride and the proton source at room

temperature, the formation of benzyl alcohol immediately takes place. The rhenium dihydride can utilize both its H ligands in the reduction process, and $Re(NO)(OPh)_2(PMe_3)_3$ is formed during the course of this reaction.

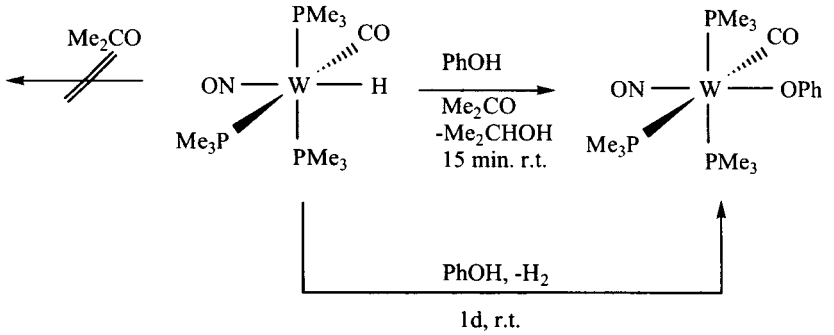

Scheme 8

This observation points to the possibility that dihydrogen bonding precedes the actual hydrogen transfer. In the interaction with the proton donor, the L_nM-H bond is activated, and the hydride transfer step is facilitated. This interaction then provides one possibility to introduce chirality into the reaction. Preliminary investigations of the dihydrogen bond between $W(NO)(CO)(PMe_3)_3H$ and the chiral Pirkle alcohol (9-anthryl)(CF_3)CH(OH), reveal an induction of chirality at the tungsten hydride, as could be observed by NMR spectroscopy. This chiral information might then be transferred to the substrate in the further steps of the hydrogenation process. Ongoing work in our group [51] is concerned with the exploration of a catalytic ionic hydrogenation cycle with the mentioned $[Re(NO)_2(PCy_3)_2]^+$ cation as catalyst. Preliminary explorations of these reactions have shown that hydrogenations and hydrosilations might proceed as depicted in Scheme 9.

The challenge that remains in ionic hydrogenation is the development of a catalytic cycle, including the activation of molecular hydrogen. The biological paragon is the [FeNi]-hydrogenase from the bacterium *Desulfovibrio gigas* [75,76], a metallaprotein which catalyzes the heterolytic splitting of molecular hydrogen [77]. A first example how hydrogenase enzyme reactivity might be modeled was provided by Hembre and McQueen. The complex Cp*(dppm)RuH ($Cp^* = C_5(CH_3)_5$; dppm = $Ph_2PCH_2PPh_2$) is active in the catalytic reduction of NAD^+ model compounds with H_2 [78]. Sellmann and co-workers gave an example for the mechanism and the complete cycle for the heterolytic H_2 cleavage with rhodium hydrides, containing sulfur based ligands [79]. Only very recently an effective catalytic cycle for synthetic purposes has been found by Noyori and co-workers, using ruthenium diamine complexes [80-82]. This transfer hydro-

genation reaction shows similarities to the ionic hydrogenation, although the mechanism of the catalysis is not fully established yet. Generally, valuable insights into this class of reactions might not only be gained from continued, detailed investigations of the role played by transition metals sites in hydrogenases [83-85], which recently have also become the subject of computational studies [86,87], but also by identifying the basic principles and mechanisms at work in novel enzymes, which mediate the reaction with molecular hydrogen, and do not contain transition metal centers [88].

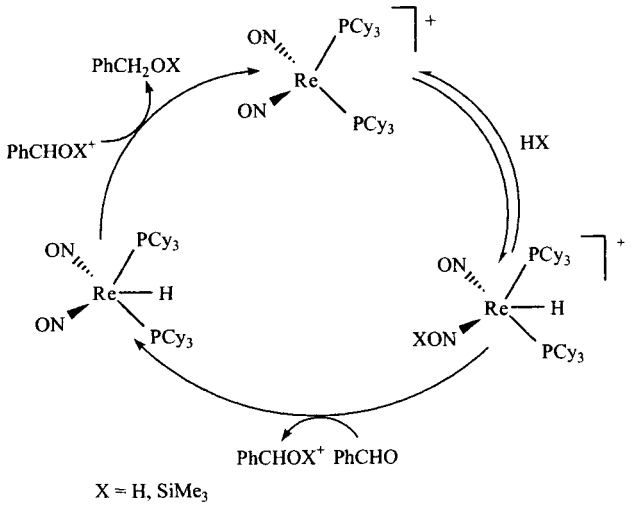

Scheme 9

4.9 CONCLUSION

We hope that in the present review we have drawn a consistent picture of the nature of the TMH bond as a polar covalent linkage. This description is supported by spectroscopic investigations, reactivity studies, and a theoretical analysis. Variation of the transition metal center, as well as of the ligand sphere, especially the *trans* ligand, allows for thermodynamic or kinetic tuning of the TM-H bond. Selected reactions demonstrate the versatility of TMH in hydrogen transfer reactions, and open up new and promising ways into catalytic conversions.

ACKNOWLEDGMENTS

During the last 10 years, numerous co-workers have contributed with their skills and efforts to the development of the transition metal hydride chemistry in our group. Space does not permit a full mention of all the individuals. The

most relevant contributors demand special naming, although we are equally as grateful to all the others. We are indebted to Adolphus van der Zeijden, Andreas Messmer, Fupei Liang, Angela Llamazares, Jürgen Höck, Dmitry Gusev, and Franck Furno, whose work constitutes major parts of the present review. This work also benefited from fruitful cooperations with the Institute of Organoelement Compounds in Moscow. Financial support from the Swiss National Science Foundation (SNSF) and the University of Zürich is gratefully acknowledged.

REFERENCES

[1] W. Hieber, H. Schulten Z. Anorg. Allg. Chem. 232 (1937) 29.
[2] W. Hieber, F. Leutert Ber. Dtsch. Chem. Ges. 64 (1931) 2832.
[3] W. Hieber, F. Leutert Naturwissenschaften 19 (1931) 360.
[4] B. Cornils, W. A. Herrmann, M. Rasch Angew. Chem. Int. Ed. Engl. 33 (1994) 2144.
[5] B. Cornils, W. A. Herrmann, M. Rasch Angew. Chem. Int. Ed. Engl. 33 (1994) 2348.
[6] B. Cornils, W.A Herrmann: Applied Homogenous Catalysis with Organometallic Compounds, VCH, Weinheim, 1996.
[7] J. A. Labinger, in A. Dedieu (Ed.), Transition Metal Hydrides. VCH, Weinheim, 1992, p. 361.
[8] D. K. Seo, G. Papoian, R. Hoffmann Int. J. Quantum Chem. 77 (2000) 408.
[9] J. A. M. Simões, J. L. Beauchamp Chem. Rev. 90 (1990) 629.
[10] H. Jacobsen, T. Ziegler Comments Inorg. Chem. 17 (1995) 301.
[11] N. Kaltsoyannis J. Chem. Soc. Dalton Trans. (1997) 1.
[12] T. Ziegler, V. Tschinke, A. Becke J. Am. Chem. Soc. 109 (1987) 1351.
[13] R. G. Pearson Chem. Rev. 85 (1985) 41.
[14] D. Nietlispach, V. I. Bakhmutov, H. Berke J. Am. Chem. Soc. 115 (1993) 9191.
[15] See also chapter 13 in this book.
[16] J. Höck, H. Berke manuscript in preparation.
[17] T. Y. Cheng, B. S. Brunschwig, R. M. Bullock J. Am. Chem. Soc. 120 (1998) 13121.
[18] N. Sarker, J. W. Bruno J. Am. Chem. Soc. 121 (1999) 2174.
[19] H. Mayr, M. Patz Angew. Chem. Int. Ed. Engl. 33 (1994) 938.
[20] P. G. Jessop, R. H. Morris Coord. Chem. Rev. 121 (1992) 155.
[21] R. H. Crabtree, P. E. M. Siegbahn, O. Eisenstein, A. L. Rheingold Acc. Chem. Res. 29 (1996) 348.
[22] R. H. Crabtree, O. Eisenstein, G. Sini, E. Peris J. Organomet. Chem. 567 (1998) 7.
[23] R. H. Crabtree J. Organomet. Chem. 557 (1998) 111.
[24] See chapter 1, 13 and 14 in this book.
[25] E. S. Shubina, N. V. Belkova, A. N. Krylov, E. V. Vorontsov, L. M. Epstein, D. G. Gusev, M. Niedermann, H. Berke J. Am. Chem. Soc. 118 (1996) 1105.

[26] N. V. Belkova, E. S. Shubina, A. V. Ionidis, L. M. Epstein, H. Jacobsen, A. Messmer, H. Berke Inorg. Chem. 36 (1997) 1522.
[27] A. Messmer, H. Jacobsen, H. Berke Chem.Eur. J. 5 (1999) 3341.
[28] W. B. Yao, R. H. Crabtree Inorg. Chem. 35 (1996) 3007.
[29] W. T. Klooster, T. F. Koetzle, P. E. M. Siegbahn, T. B. Richardson, R. H. Crabtree J. Am. Chem. Soc. 121 (1999) 6337.
[30] S. Gründemann, S. Ulrich, H. H. Limbach, N. S. Golubev, G. S. Denisov, L. M. Epstein, S. Sabo-Etienne, B. Chaudret Inorg. Chem. 38 (1999) 2550.
[31] E. S. Shubina, N. V. Belkova, L. M. Epstein J. Organomet. Chem. 536 (1997) 17.
[32] E. S. Shubina, N. V. Belkova, E. V. Bakhmutova, L. N. Saitkulova, A. V. Ionidis, L. M. Epstein Russ. Chem. Bull. 47 (1998) 817.
[33] X.-Y. Liu, S. Bouherour, H. Jacobsen, H. W. Schmalle, H. Berke submitted for publication.
[34] S. Feracin, T. Bürgi, V. I. Bakhmutov, I. Eremenko, E. V. Vorontsov, A. B. Vimenits, H. Berke Organometallics 13 (1994) 4194.
[35] E. Bannwart, H. Jacobsen, F. Furno, H. Berke Organometallics 19 (2000) 3605.
[36] R. P. Bell: The Tunnel Effect in Chemistry, Chapman and Hall, London, 1980.
[37] H. Berke, P. Burger Comments Inorg. Chem. 16 (1994) 279.
[38] J. Höck, H. Jacobsen, H. W. Schmalle, G. Artus, T. Fox, J. I. Amor, F. Bäth, H. Berke Organometallics 20 (2001) 1533.
[39] F. P. Liang, H. Jacobsen, H. W. Schmalle, T. Fox, H. Berke Organometallics 19 (2000) 1950.
[40] F. P. Liang, H. Berke manuscript in preparation.
[41] F. Furno, T. Fox, H. W. Schmalle, H. Berke Organometallics 19 (2000) 3620.
[42] L. Versluis, T. Ziegler Organometallics 9 (1990) 2985.
[43] G. J. Kubas, R. R. Ryan, B. I. Swanson, P. J. Vergamini, H. J. Wasserman J. Am. Chem. Soc. 106 (1984) 451.
[44] G. J. Kubas Acc. Chem. Res. 21 (1988) 120.
[45] G. J. Kubas Comments Inorg. Chem. 7 (1988) 17.
[46] R. H. Morris Can. J. Chem. 74 (1996) 1907.
[47] D. G. Gusev, R. Hübener, P. Burger, O. Orama, H. Berke J. Am. Chem. Soc. 119 (1997) 3716.
[48] H. Jacobsen, H. Berke Chem. Ber.-Recl. 130 (1997) 1273.
[49] H. Jacobsen, H. Berke Chem. Eur. J. 3 (1997) 881.
[50] H. Jacobsen, K. Heinze, A. Llamazares, H. W. Schmalle, G. Artus, H. Berke J. Chem. Soc.-Dalton Trans. (1999) 1717.
[51] A. Llamazares, H. W. Schmalle, H. Berke Organometallics submitted for publication.
[52] D. Gusev, A. Llamazares, G. Artus, H. Jacobsen, H. Berke Organometallics 18 (1999) 75.
[53] F. Hutschka, A. Dedieu, W. Leitner Chem. Soc.-Dalton Trans. (1997) 1899.
[54] J. Baur, H. Jacobsen, P. Burger, G. Artus, H. Berke, L. Dahlenburg Eur. J. Inorg. Chem. (2000) 1411.
[55] J. S. Lomas, J. Vaissermann J. Chem. Soc. Perkin Trans. 2 (1997) 2589.
[56] K. J. Haack, S. Hashiguchi, A. Fujii, T. Ikariya, R. Noyori Angew. Chem. Int. Ed. Engl. 36 (1997) 285.

[57] S. Hashiguchi, A. Fujii, K. J. Haack, K. Matsumura, T. Ikariya, R. Noyori Angew. Chem. Int. Ed. Engl. 36 (1997) 288.
[58] R. Noyori, S. Hashiguchi Acc. Chem. Res. 30 (1997) 97.
[59] D. N. Kursanov, Z. N. Parnes, N. M. Loim Synthesis (1974) 633.
[60] J. Chojnowski, W. Fortuniak, W. Stanczyk J. Am. Chem. Soc. 109 (1987) 7776.
[61] H. Mayr, N. Basso, G. Hagen J. Am. Chem. Soc. 114 (1992) 3060.
[62] Y. Apeloig, O. Merinaharoni, D. Danovich, A. Ioffe, S. Shaik Isr. J. Chem. 33 (1993) 387.
[63] J.-S. Song, D. J. Szalda, R. M. Bullock, C. J. C. Lawrie, M. A. Rodkin, J. R. Norton Angew. Chem. Int. Ed. Engl. 31 (1992) 1233.
[64] R. M. Bullock, J.-S. Song J. Am. Chem. Soc. 116 (1994) 8602.
[65] L. Luan, J.-S. Song, R. M. Bullock J. Org. Chem. 60 (1995) 7170.
[66] J.-S. Song, D. J. Szalda, R. M. Bullock J. Am. Chem. Soc. 118 (1996) 11134.
[67] K. Smith, J. R. Norton, M. Tilset Organometallics 15 (1996) 4515.
[68] P. Kundel, H. Berke J. Organomet. Chem. 314 (1986) C31.
[69] P. Kundel, H. Berke J. Organomet. Chem. 339 (1988) 297.
[70] P. Kundel, H. Berke J. Organomet. Chem. 335 (1987) 353.
[71] A. A. H. van der Zeijden, H. W. Bosch, H. Berke Organometallics 11 (1992) 2051.
[72] A. A. H. van der Zeijden, H. Berke Helv. Chim. Acta 75 (1992) 513.
[73] J. Höck, T. Fox, H. Schmalle, H. Berke Chimia 53 (1999) 350.
[74] A. Messmer: Rhenium-Nitrosyl-Hydride mit aktivierten Metall-Wasserstoff-bindungen, Dissertation University of Zurich, 1999, Hartung-Gorre, Konstanz, 2000.
[75] A. Volbeda, M. H. Charon, C. Piras, E. C. Hatchikian, M. Frey, J. C. Fontecilla-Camps Nature 373 (1995) 580.
[76] A. Volbeda, E. Garcia, C. Piras, A. L. deLacey, V. M. Fernandez, E. C. Hatchikian, M. Frey, J. C. Fontecilla-Camps J. Am. Chem. Soc. 118 (1996) 12989.
[77] R. Cammack Nature 373 (1995) 556.
[78] R. T. Hembre, S. McQueen J. Am. Chem. Soc. 116 (1994) 2141.
[79] D. Sellmann, G. H. Rackelmann, F. W. Heinemann Chem. Eur. J. 3 (1997) 2071.
[80] T. Ohkuma, D. Ishii, H. Takeno, R. Noyori J. Am. Chem. Soc. 122 (2000) 6510.
[81] T. Ohkuma, M. Koizumi, M. Yoshida, R. Noyori Org. Lett. 2 (2000) 1749.
[82] M. Yamakawa, H. Ito, R. Noyori J. Am. Chem. Soc. 122 (2000) 1466.
[83] S. P. J. Albracht Biochim. et Biophys. Acta (1994) 167.
[84] C. M. Goldman, P. K. Mascharak Comments Inorg. Chem. 18 (1995) 1.
[85] M. J. Maroney Comments Inorg. Chem. 17 (1995) 347.
[86] M. Pavlov, P. E. M. Siegbahn, M. R. A. Blomberg, R. H. Crabtree J. Am. Chem. Soc. 120 (1998) 548.
[87] P. Amara, A. Volbeda, J. C. Fontecilla-Camps, M. J. Field J. Am. Chem. Soc. 121 (1999) 4468.
[88] R. K. Thauer, A. R. Klein, G. C. Hartmann Chem. Rev. 96 (1996) 3031.

Chapter 5

Heterolytic Cleavage of Dihydrogen by Ruthenium and Molybdenum Complexes

Masanobu Hidai[a] and Yoshiaki Nishibayashi[b]

[a]*Department of Materials Science and Technology, Faculty of Industrial Science and Technology, Science University of Tokyo, Noda, Chiba 278-8510, Japan*
[b]*Department of Energy and Hydrocarbon Chemistry, Graduate School of Engineering, Kyoto University, Sakyo-ku, Kyoto 606-8501, Japan*

CONTENTS

5.1 INTRODUCTION

Since the first discovery of dihydrogen complexes by Kubas and co-workers in 1984 [1], extensive studies on this unique class of complexes have been carried out to reveal structural and chemical properties of coordinated dihydrogen [2]. The results show that dihydrogen complexes are more than intermediates for oxidative addition of molecular dihydrogen (H_2). Thus, they have their own reactivities, and participate in interesting stoichiometric and catalytic reactions, although this aspect has been less explored until recently [3]. In this article, we summarize our

recent results concerning heterolytic cleavage of dihydrogen by using ruthenium dihydrogen complexes and sulfido-bridged dinuclear molybdenum complexes to protonate coordinated dinitrogen and cleave the Si-O bond in silyl enol ethers.

5.2 PROTONATION OF COORDINATED DINITROGEN WITH ACIDIC RUTHENIUM DIHYDROGEN COMPLEXES

Nitrogen is one of the essential elements for life and for various chemicals and materials. The Haber-Bosch process has long been used industrially to produce ammonia from dinitrogen and dihydrogen gases. Although dinitrogen is readily available from the atmosphere, the synthesis of ammonia by this process requires quite drastic conditions due to the extreme chemical inertness of dinitrogen. Therefore, development of alternatives to this energy-consuming process has long been awaited.

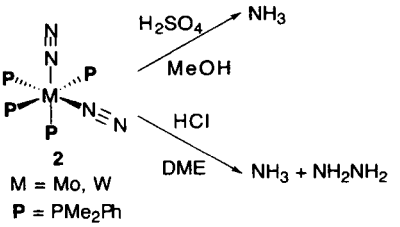

Scheme 1

It is well-known that low valent metal centers coordinated with adequate ancillary ligands can bind dinitrogen to form dinitrogen complexes [4]. Among a variety of dinitrogen complexes known to date, molybdenum and tungsten dinitrogen complexes of the type $[M(N_2)_2(L)_4]$ (M = Mo, W; L = tertiary phosphine) are outstanding because they are readily prepared and show a variety of reactivities. Since the first discovery of *trans*-$[Mo(N_2)_2(dppe)_2]$ [dppe = 1,2-bis(diphenylphosphino)ethane] (**1a**) in our laboratory [5], extensive studies on the preparation and reactivity of these dinitrogen complexes have been performed by Chatt's group, our group, and many other researchers because of, at least in part, their possible relevance to the active site of nitrogenase [6,7]. The coordinated dinitrogen undergoes protonation by treatment with strong protonic acids under mild reaction conditions [8]. Thus, when molybdenum and tungsten dinitrogen complexes *cis*-$[M(N_2)_2(PMe_2Ph)_4]$ (M = Mo, W) (**2**) are treated with excess amounts of sulfuric acid in methanol at ambient temperature, ammonia is formed in 68% and 198% yields, respectively, based on the metal atom (Scheme 1) [8]. Interestingly, hydrazine is significantly produced along with ammonia from the reactions of dinitrogen complexes **2** with excess hydrochloric acid in 1,2-dimethoxyethane (DME) (Scheme 1) [9]. In contrast, dinitrogen complexes

with diphosphine ligands *trans*-$[M(N_2)_2(dppe)_2]$ (M = Mo, W) (**1**) react with strong protonic acids to give hydrazido(2-) complexes in high yields (Scheme 2) [10]. A detailed mechanism for the protonation of the coordinated dinitrogen leading to the formation of ammonia and hydrazine has been proposed on the basis of the reactivities of isolable intermediate complexes such as hydrazido(2-) complexes. The protonation of coordinated dinitrogen proceeds in a stepwise manner via hydrazido(2-) intermediates, accompanied by the transfer of necessary electrons from the central metal to the nitrogenous ligands.

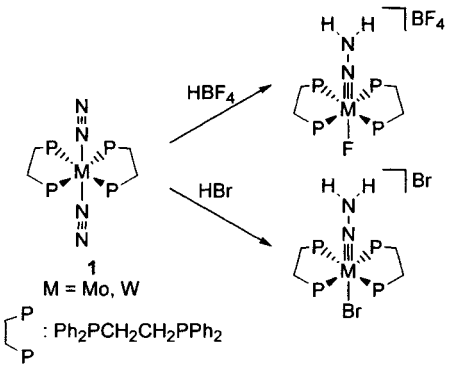

Scheme 2

The N-H bond formation is not achieved by treatment of those dinitrogen complexes with dihydrogen because dihydrogen replaces the coordinated dinitrogen to form hydride complexes $[MH_4L_4]$ [11]. However, some strongly acidic metal carbonyl hydrides such as $[HCo(CO)_4]$, $[H_2Fe(CO)_4]$, and $[HFeCo_3(CO)_{12}]$ react with *cis*-$[W(N_2)_2(PMe_2Ph)_4]$ (**2b**) to give ammonia in substantial yields after base treatment of the reaction mixture [12,13]. It is to be noted that $[HCoCO_4]$ is formed from $Co_2(CO)_8$ and dihydrogen under some reaction conditions. Interestingly, hydrazido(2-) complexes *trans*-$[W(OMe)(NNH_2)(dppe)_2][X]$ [X = $Co(CO)_4$, $FeCo_3(CO)_{12}$] are isolated from the reaction of **1b** and $[HCo(CO)_4]$ or $[HFeCo_3(CO)_{12}]$ in methanol [13] (Scheme 3). Table 1 shows typical results of the reactions of dinitrogen complex (**2b**) with various protonic acids.

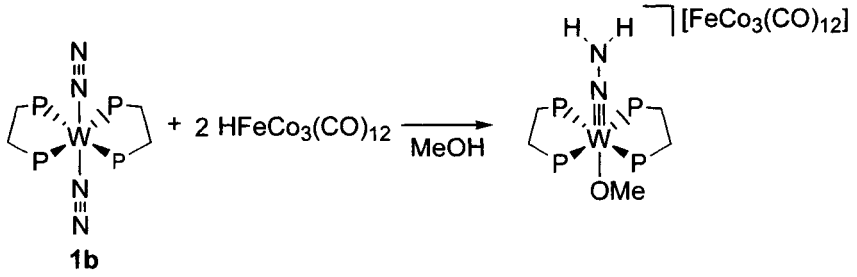

Scheme 3

One of the most important properties of dihydrogen complexes [$M(\eta^2\text{-}H_2)$] is reflected in the heterolytic cleavage of coordinated dihydrogen by bases; thus dihydrogen complexes exhibit acidic property [2a,15]. In this context, dihydrogen complexes with relatively high acidities are expected to protonate coordinated dinitrogen because dinitrogen complex (**2b**) reacts in methanol (pK_a = 15) at 50 °C to form ammonia [8b,14]. Actually, Morris and co-workers employed an acidic ruthenium dihydrogen complex [$CpRu(\eta^2\text{-}H_2)(dtfpe)]BF_4$ [dtfpe = $(p\text{-}CF_3C_6H_4)_2PCH_2CH_2P(p\text{-}CF_3C_6H_4)_2$] with pK_a = 4.3 to protonate the coordinated dinitrogen in **1b** (Eq. 1) [16]. Although the dihydrogen complex is not obtained from the reaction with dihydrogen gas, protonation of the coordinated dinitrogen proceeds to form a hydrazido(2-) complex. On the other hand, no reaction occurs between tungsten dinitrogen complex (**1b**) and *trans*-[$RuH(\eta^2\text{-}H_2)(Et_2PCH_2CH_2PEt_2)_2$] with pK_a = 16. The (pseudo-aqueous) pK_a values of dihydrogen complexes are determined from the K_{eq} of Eq. 2 by using the relationship pK_a ($M(\eta^2\text{-}H_2)^+$) = pK_a (BH^+ in water) + pK_{eq}, where K_{eq} is the equilibrium constant and BH^+ is the conjugate acid of B (base). Measurement of the K_{eq} is usually performed in THF or dichloromethane. Details are found in excellent comprehensive reviews on the acidic properties of dihydrogen complexes [2a,15] and in Chapter 1 of this Monograph.

Table 1. Reactions of *cis*-[$W(N_2)_2(PMe_2Ph)_4$] (**2b**) with various protonic acids

protonic acid	pK_a value of acid	yield of NH_3 (%)[a]	reference[b]
H_2SO_4	-9	198	8b
HCl	-7	64[c]	9
$[HCo(CO)_4]$	(-7)	16	13
$[HFeCo_3(CO)_{12}]$	(-7)	32	13
H_3PO_4	2.2	151	8b
MeCOOH	4.7	94	8b
$[H_2Fe(CO)_4]$	6.9	28	13
MeOH	15	101	8b,14
H_2O	15.7	86	14
EtOH	16	24	14

[a]Yield of NH_3 was based on the W atom. [b]See reference for experimental details. [c]NH_2NH_2 was formed in 33% yield.

Previously, Morris and co-workers systematically investigated effects of the ligands and metals on the acidity of dihydrogen complexes such as [$MX(\eta^2\text{-}H_2)L_4]^{n+}$ and [$Cp'M(\eta^2\text{-}H_2)L_2]^+$ (M = Fe, Ru, Os; L = tertiary phosphine; X = H, halogen, CO, CH_3CN etc.; Cp' = $\eta^5\text{-}C_5H_5$, $\eta^5\text{-}C_5Me_5$; n = 1, 2) [17]. Typical acidic dihydrogen complexes together with their pK_a values are shown

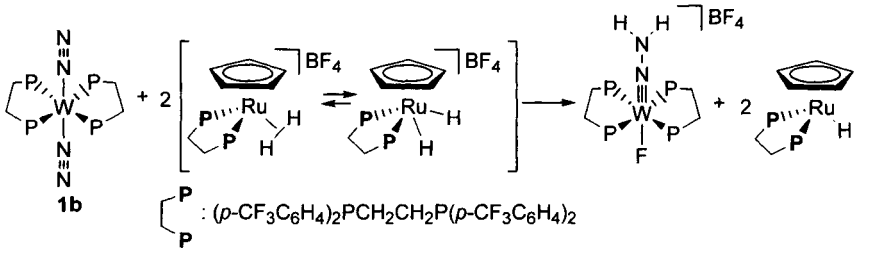

(1)

(2)

in Table 2 [17-19]. Relatively strong acidic dihydrogen complexes directly derived from molecular dihydrogen gas are quite limited in number. Among the dihydrogen complexes shown in Table 2, an acidic ruthenium dihydrogen complex, *trans*-[RuCl(η^2-H_2)(dppp)$_2$]PF_6 [dppp = 1,3-bis(diphenylphosphino)-propane] (**3a**), prepared by Mezzetti and co-workers [19] seems to be one of the most suitable dihydrogen complexes for the protonation of coordinated dinitrogen because the ruthenium dihydrogen complex is readily prepared from dihydrogen and [RuCl(dppp)$_2$]PF_6, and the pK_a value of **3a** is almost the same as that of [CpRu(η^2-H_2)(dtfpe)]BF_4 employed by Morris for the protonation of coordinated dinitrogen (vide supra) [16]. This has recently prompted us to investigate the reaction of the ruthenium dihydrogen complex with tungsten dinitrogen complex (**2b**) and eventually led to our finding of ammonia formation. Thus, treatment of dinitrogen complex (**2b**) with an equilibrium solution of [RuCl(dppp)$_2$]X and *trans*-[RuCl(η^2-H_2)(dppp)$_2$]X [X = PF_6, BF_4, or OTf] (**3**) containing 10 equiv of the Ru atom at 55 °C for 24 h under H_2 affords ammonia in

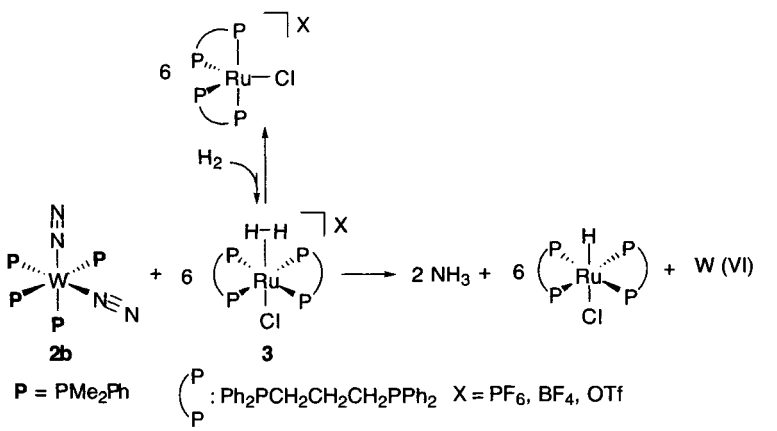

(3)

45~55% yields based on tungsten, together with *trans*-[RuHCl(dppp)$_2$] [20]. The presumed stoichiometry for the formation of ammonia is shown in Eq. 3. It is to be noted that heterolytic cleavage of dihydrogen proceeds at the Ru center in this reaction, and a proton is used for the N-H bond formation while a hydride remains on the Ru atom [20].

Table 2. Acidic dihydrogen complexes with their pK_a values

Structure of M(η^2-H_2) complex				pK_a value of M(η^2-H_2) complex
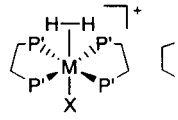	: $Ar_2PCH_2CH_2PAr_2$	M = Ru Ar = Ph	X = CNH^+	< -2.4
		M = Ru Ar = Ph	X = Cl	6.0
		M = Ru Ar = p-$CF_3C_6H_4$	X = H	9.0
		M = Ru Ar = Ph	X = H	15.0
		M = Ru Ar = p-$CH_3OC_6H_4$	X = H	16.4
		M = Fe Ar = Ph	X = H	12.1
		M = Os Ar = Ph	X = Cl	7.4
		M = Os Ar = Ph	X = H	13.6
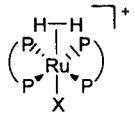	: $Ph_2PCH_2CH_2CH_2PPh_2$		X = Cl	4.4
			X = H	10.2
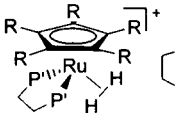	: $R'_2PCH_2CH_2PR'_2$	R = H R' = C_2F_5		-5
		R = Me R' = C_2F_5		0~-3
		R = H R' = p-$CF_3C_6H_4$		4.3
		R = H R' = Ph		7.0
		R = H R' = p-$CH_3OC_6H_4$		8.1
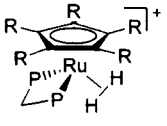	: $Ph_2PCH_2PPh_2$	R = H		7.5
		R = Me		9.2
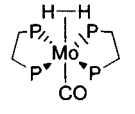	: $Ph_2PCH_2CH_2PPh_2$			>24
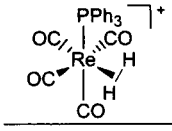				-2

We also employed other ruthenium dihydrogen complexes for the protonation of the coordinated dinitrogen in complex (**2b**). Typical results are shown in Table 3 [21]. Ammonia is formed in higher yields (up to 79% based on tungsten) when dinitrogen complex (**2b**) is similarly treated with *trans*-[RuCl(η^2-H_2)(dppe)$_2$]X

with pK_a = 6.0 [X = PF_6, BF_4, or OTf] (**4**), which is quantitatively formed from the reaction of [RuCl(dppe)$_2$]X with dihydrogen under ambient conditions. However, the ruthenium dihydrogen complex [CpRu(η^2-H_2)(dppm)]OTf [dppm = bis(diphenylphosphino)methane] with pK_a = 7.5 is less effective for the formation of ammonia compared with **3a**. Furthermore, employment of ruthenium dihydrogen complexes such as *trans*-[RuH(η^2-H_2)(dppp)$_2$]X (X = BF_4, OTf) and *trans*-[RuH(η^2-H_2)(dppe)$_2$](X = BF_4, OTf) with pK_a = 10.2 and 15.0, respectively, results in the remarkable decrease in the yields of ammonia.

Table 3 Reactions of *cis*-[W(N_2)$_2$(PMe_2Ph)$_4$] (**2b**) with Ru(η^2-H_2) complexes[a]

Ru(η^2-H_2) complex	pK_a value of Ru(η^2-H_2) complex	yield of NH_3 (%)[b]
trans-[RuCl(η^2-H_2)(dppp)$_2$]PF_6 (**3a**)[c]	4.3	55
trans-[RuCl(η^2-H_2)(dppp)$_2$]BF_4 (**3b**)[c]	(4.3)	54
trans-[RuCl(η^2-H_2)(dppp)$_2$]OTf (**3c**)[c]	(4.3)	45
trans-[RuCl(η^2-H_2)(dppe)$_2$]PF_6 (**4a**)	6.0	55
trans-[RuCl(η^2-H_2)(dppe)$_2$]BF_4 (**4b**)	(6.0)	71
trans-[RuCl(η^2-H_2)(dppe)$_2$]BF_4 (**4b**)[d]	(6.0)	79
trans-[RuCl(η^2-H_2)(dppe)$_2$]OTf (**4c**)	(6.0)	74
trans-[RuCl(η^2-H_2)(dppe)$_2$]BAr_4[e]	(6.0)	3
[CpRu(η^2-H_2)(dppm)]OTf	7.5	34
trans-[RuH(η^2-H_2)(dppp)$_2$]BF_4	10.2	0
trans-[RuH(η^2-H_2)(dppe)$_2$]BF_4	15.0	0

[a]All of the reactions were carried out in benzene–dichloroethane using 0.10 mmol of *cis*-[W(N_2)$_2$(PMe_2Ph)$_4$] (**2b**) and 1.00 mmol of Ru(η^2-H_2) complex under H_2 at 55 °C for 24 h unless otherwise stated. [b]Yield of NH_3 was based on the W atom. [c]An equilibrium mixture of *trans*-[RuCl(η^2-H_2)(dppp)$_2$]$^+$ and *trans*-[RuCl(dppp)$_2$]$^+$ derived from 10 equiv of *trans*-[RuCl(dppp)$_2$]$^+$. [d]This yield of NH_3 was observed in the water extract of the reaction mixture. [e]Ar = 3,5-(CF_3)$_2$$C_6H_3$.

Noticeably, when the dinitrogen complex *trans*-[W(N_2)$_2$($PMePh_2$)$_4$] (**2c**) is analogously treated with dihydrogen complex **4c**, the yield of ammonia is considerably decreased compared with that of the reaction with dinitrogen complex (**2b**). On the other hand, the reactions of both of dinitrogen complexes (**2b**) and (**2c**) with trifluoromethanesulfonic acid (HOTf) give ammonia in almost the same yields (Scheme 4) [21]. Furthermore, the latter reactions proceed even at ambient temperature to produce ammonia in ca. 100% yield based on tungsten, whereas the reaction temperature has to be raised up to 55 °C to obtain ammonia from the former reactions. These results support the view that the N-H bond formation proceeds through the direct nucleophilic attack of the coordinated dinitrogen on tungsten upon the coordinated dihydrogen on ruthenium, as shown in Eq. 4. The remote nitrogen of the coordinated dinitrogen behaves as a base for the

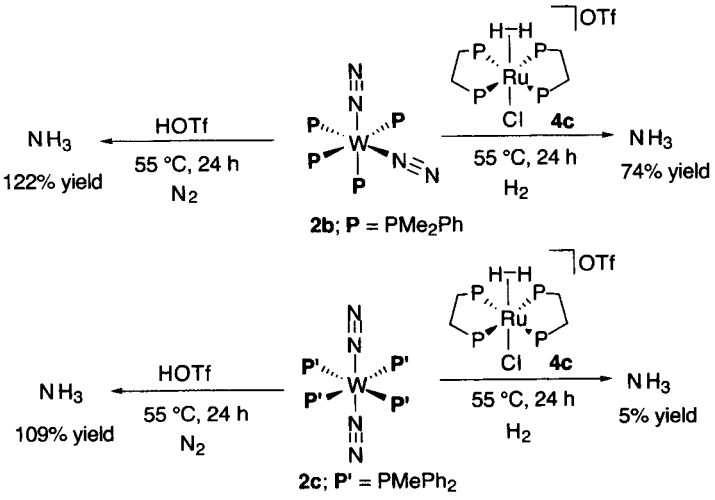

Scheme 4

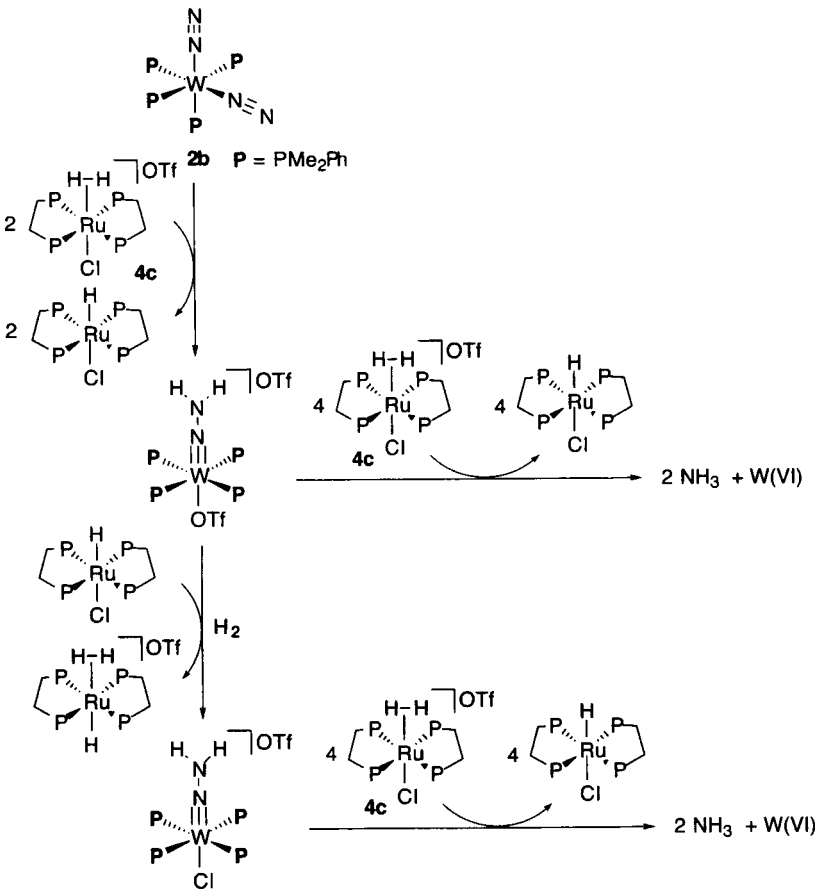

Scheme 5

heterolytic splitting of the coordinated dihydrogen. Recently, numerous compounds containing intramolecular or intermolecular non-classical hydrogen bonds between a metal hydride and a hydrogen bond donor like a N-H group have been reported which might correspond to intermediates for the heterolytic cleavage of coordinated dihydrogen [22-24]. In this book, Morris and Crabtree describe recent advances on this subject in chapter 1 and 3, respectively.

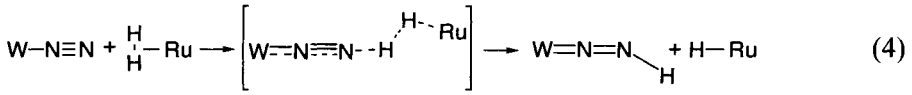

(4)

Scheme 5 summarizes a plausible reaction mechanism for the formation of ammonia from dinitrogen complex (**2b**) and an excess of dihydrogen complex **4c** at 55 °C [21]. The first step is the formation of the hydrazido(2-) complex *trans*-[W(OTf)(NNH_2)(PMe_2Ph)$_4$]OTf. Actually, if the reaction is performed at ambient temperature, the hydrazido(2-) complex is obtained together with *trans*-[RuHCl(dppe)$_2$]. Interestingly, the hydrazido(2-) complex initially formed further reacts with *trans*-[RuHCl(dppe)$_2$] to form another hydrazido(2-) complex *trans*-[WCl(NNH_2)(PMe_2Ph)$_4$]OTf. Further protonation of these hydrazido(2-) complexes with the ruthenium dihydrogen complex **4c** results in the formation of ammonia and ammonium salt. It is to be noted that all the electrons required for the reduction of the coordinated dinitrogen are supplied from the tungsten atom.

5.3 CATALYTIC HYDROGENOLYSIS OF TRIMETHYLSILYL ENOL ETHERS BY ACIDIC RUTHENIUM DIHYDROGEN COMPLEXES

In the reaction of coordinated dinitrogen with acidic ruthenium dihydrogen complexes shown in the previous section, only one of the two hydrogen atoms of the coordinated dihydrogen is used for the N-H bond formation, while the other is not used for the product formation and remains at the Ru center. However, several examples are now known where both of the hydrogen atoms of coordinated dihydrogen are catalytically transferred to products via the heterolytic splitting.

Treatment of tetramethylpiperidine and *N*-methylacridinium salt $[MA]^+$ in the presence of a catalytic amount of the ruthenium complex [Cp*RuH(dppm)] under D_2 gives monodeuterated products MAD and piperidinium salt in quantitative yields, respectively (Eq. 5). The stoichiometric reactions of [Cp*RuH(dppm)] with *N*-methylacridium salt $[MA]^+$ in CH_3CN or THF afford $[Cp^*Ru(S)(dppm)]^+$ (S = CH_3CN or THF) and MAH in high yields, respectively. This shows that the hydride at the Ru center is readily transferred to the acridium salt. A catalytic cycle proposed by Hembre and co-worker is shown in Scheme 6, where tetramethylpiperidine behaves as a base and the acridinium salt as a hydride

acceptor. This is the first well-characterized catalytic reaction by using the heterolytic cleavage of molecular dihydrogen [25].

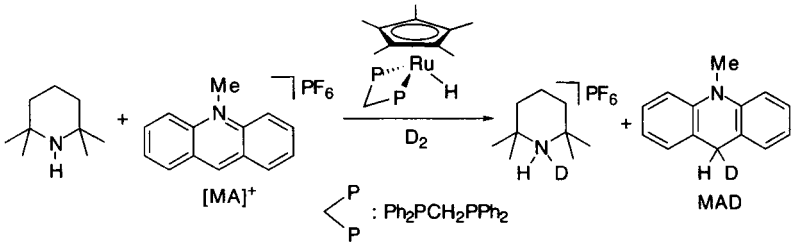

(5)

Dihydrogen complexes $[M(\eta^2\text{-}H_2)R]$ with a hydrocarbon ligand undergo intramolecular proton transfer from the coordinated dihydrogen to the hydrocarbon ligand to form M-H and R-H (Eq. 6). This reaction is regarded as an intramolecular acid-base reaction. Intramolecular protonation reactions of an alkynyl ligand and an aryl ligand with coordinated dihydrogen are shown in Eq. 7 [26] and 8 [27]. A similar type of intramolecular proton transfer is believed to be involved in the hydrogenation of phenylacetylene catalyzed by the iron dihydrogen complex $[FeH(\eta^2\text{-}H_2)\mathbf{PP_3}]^+$ ($\mathbf{PP_3}$ = $P(CH_2CH_2PPh_2)_3$) [28]. A proposed mechanism is shown in Scheme 7. A key step is proton transfer from the coordinated dihydrogen to the σ-vinyl ligand which is derived from the insertion of the alkyne into the Fe-H bond. Similar proton transfer reactions are proposed in the hydrogenation of acetylenes and olefins catalyzed by $[RuH(\eta^2\text{-}H_2)\mathbf{PP_3}]^+$ [29] and $[OsHCl(CO)(P^iPr_3)_2]$, respectively [30].

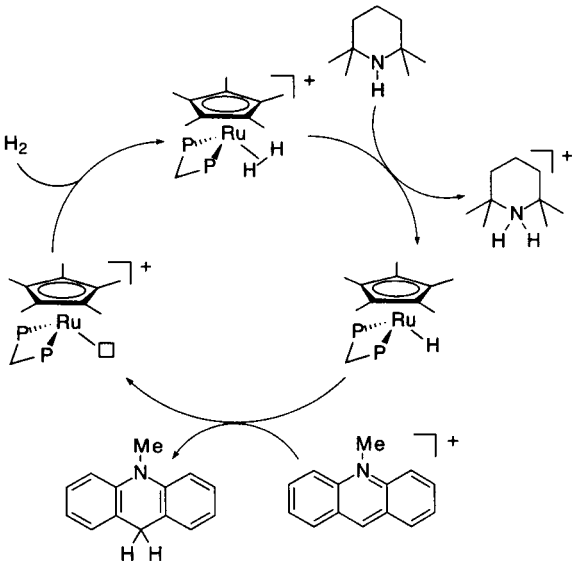

Scheme 6

During our study on reactivities of acidic ruthenium dihydrogen complexes, we have recently found that some ruthenium dihydrogen complexes catalyze the hydrogenolysis of the Si-O bond in trimethylsilyl enol ethers to afford the corresponding ketones and trimethylsilane (Scheme 8, *type A*) [31]. In this reaction, dihydrogen is heterolytically cleaved into a proton and a hydride on the Ru center, which are transferred to the enol oxygen and the trimethylsilyl silicon atom, respectively. This provides a conceptually new type of hydrogenation, in sharp contrast to the conventional hydrogenation where trimethylsilyl enol ethers are converted into saturated trimethylsilyl ethers (Scheme 8, *type B*).

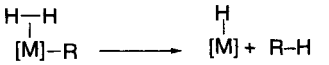

(6)

R = alkynyl, aryl, σ-vinyl

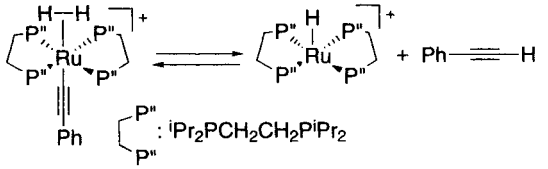

(7)

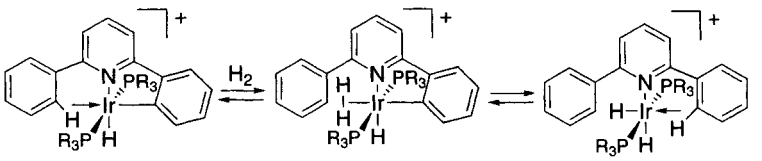

(8)

PR_3 = PPh_3 etc.

Acidic ruthenium dihydrogen complexes such as **4c** with pK_a = 6.0 and **3c** with pK_a = 4.4 catalyze the hydrogenolysis of silyl enol ethers, whereas [RuH(η^2-H_2)(dppe)$_2$]OTf with much lower acidity (pK_a = 15.0) is not effective for the hydrogenolysis. These results indicate that relatively high acidic dihydrogen complexes are required to promote this hydrogenolysis. Scheme 9 shows a plausible mechanism for the formation of cyclohexanone and Me_3SiH from 1-trimethylsilyloxy-1-cyclohexene and dihydrogen catalysed by **4c** [31]. The initial step is the protonation of the trimethylsilyl enol ether probably at the oxygen atom with the coordinated dihydrogen on the Ru atom, where cyclohexanone and Me_3SiOTf are formed together with [RuHCl(dppe)$_2$]. The subsequent reaction

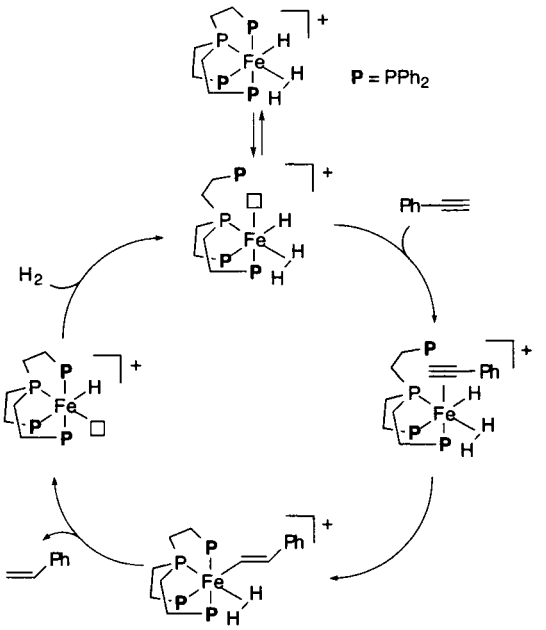

Scheme 7

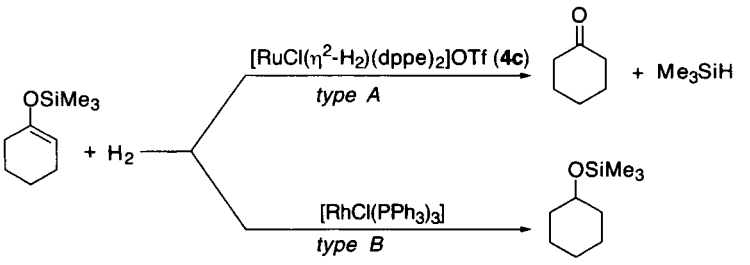

Scheme 8

of Me_3SiOTf with $[RuHCl(dppe)_2]$ under H_2 results in the formation of the starting dihydrogen complex **4c** *via* $[RuCl(dppe)_2]OTf$, concurrent with Me_3SiH. In fact, the reaction of $[RuHCl(dppe)_2]$ with 1 equiv of Me_3SiOTf under H_2 rapidly gives **4c** in quantitative NMR yield together with Me_3SiH. Thus, Me_3SiOTf works as a hydride acceptor. It is presumed that a delicate balance of the acidity of dihydrogen complex **4c** and the nucleophilicity of the hydride complex $[RuHCl(dppe)_2]$ might realize this novel hydrogenolysis. The present reaction mechanism is quite similar to the Hembre's reaction catalysed by [Cp*RuH(dppm)] (vide supra) [25], where tetramethylpiperidine and an acridinium salt work as proton and hydride acceptors, respectively. The heterolytic splitting of dihydrogen developed by Hembre et al. seems to proceed quite smoothly in the presence of only a small amount of

the ruthenium complex (<0.1 mol% catalyst). In contrast, a larger amount of the ruthenium complexes (5 or 10 mol% catalyst) are necessary to complete the catalytic hydrogenolysis of silyl enol ethers.

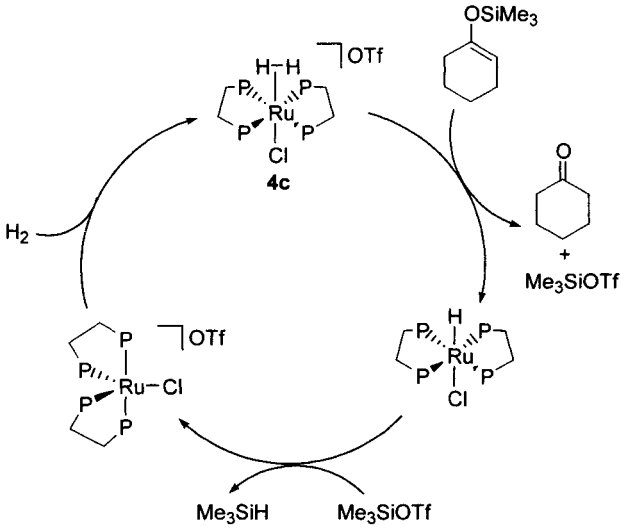

Scheme 9

Another intriguing fact is that the ruthenium dihydrogen complex with chiral diphosphine ligands *trans*-[RuCl(η^2-H_2)(BINAP)$_2$]OTf protonates a prochiral lithium enolate to afford a chiral ketone in high chemical yield with high enantioselectivity, together with a ruthenium hydride (Eq. 9) [31]. This asymmetric reaction is considered to proceed through the direct protonation of the prochiral enolate with the coordinated dihydrogen. In contrast, no enantioselectivity is induced by the stoichiometric and catalytic protonation reactions of silyl enol ethers with the chiral ruthenium dihydrogen complex. These results indicate that the carbon of the lithium enolate is directly protonated by the coordinated dihydrogen while the oxygen of silyl enol ethers is attacked by the coordinated dihydrogen [32].

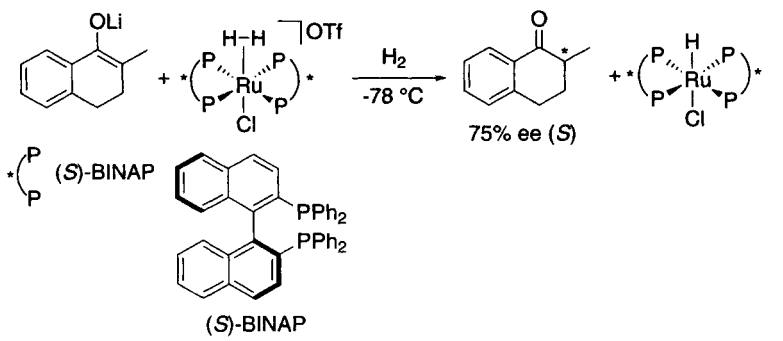

(9)

5.4 PROTONATION OF COORDINATED DINITROGEN WITH DIHYDROGEN MEDIATED BY SULFIDO-BRIDGED DINUCLEAR MOLYBDENUM COMPLEXES

Heterolytic cleavage is not only realized on a single metal center, but also on a metal-heteroatom bond (M-X: X = S, N, O) as shown in Eq. 10. The latter reaction is mostly presumed to proceed through an intramolecular acid-base reaction similar to Eq. 6.

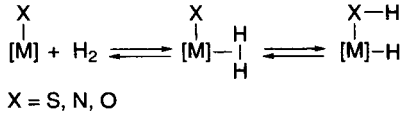

(10)

Bianchini and co-workers reported the reversible reaction of a sulfido-bridged dinuclear rhodium complex with dihydrogen at atmospheric pressure to produce hydrosulfido-bridged hydrido complex (Eq. 11). This is the first clear-cut example of heterolytic cleavage of dihydrogen on a metal-sulfur bond [33]. Later, Sellmann and co-workers found the D_2/H^+ exchange reaction catalyzed by transition metal sulfur complexes such as $[RhH(L)(S_4)]$ (L = CO, PCy_3), $[RuH(PCy_3)(S_4)]^-$, and $[(\mu\text{-}N_2H_2)\{Ru(PCy_3)(S_4)\}_2]$ (S_4 = 1,2-bis((2-mercaptophenyl)thio)ethane(2-)) (Eq. 12) [34]. A proposed reaction mechanism is shown in Scheme 10, which includes heterolytic cleavage of dihydrogen on a metal-sulfur bond as a key step. More recently, Bergman and co-workers have reported that a titanocene sulfido complex reacts reversibly with dihydrogen to give $Cp^*_2Ti(H)SH$ (Eq. 13) [35].

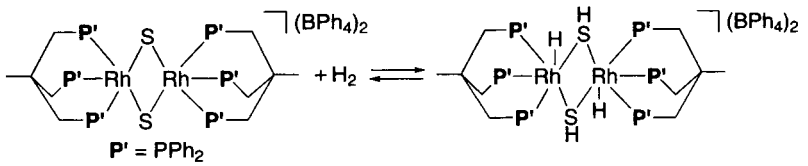

(11)

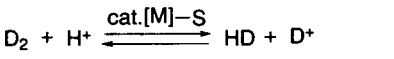

(12)

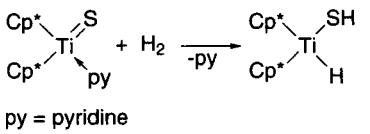

(13)

On the other hand, extensive studies on synthesis and reactivities of dinuclear molybdenum complexes with bridging sulfur ligands have been carried out by Rakowski DuBois and co-workers [36]. Interestingly, hydrogenolysis of the C≡N triple bond in nitriles proceeds in the presence of dinuclear molybdenum complexes under H_2 to afford ammonia and dinuclear molybdenum complexes incorporating the hydrocarbon fragment of the nitriles (Eq. 14) [37]. Furthermore, heterolytic splitting of dihydrogen occurs when a sulfido-bridged dinuclear molybdenum complex is treated with pyridine under H_2 (Eq. 15) [38]. These results have prompted us to investigate the protonation of tungsten dinitrogen complex (**2b**) with dihydrogen in the presence of sulfido-bridged dinuclear molybdenum complexes [39].

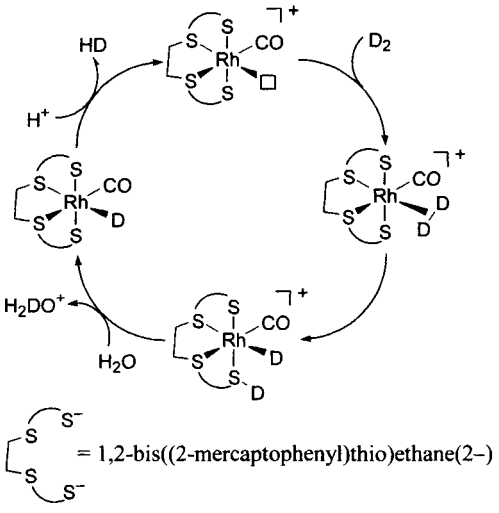

Scheme 10

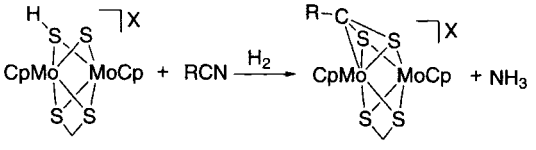

(14)

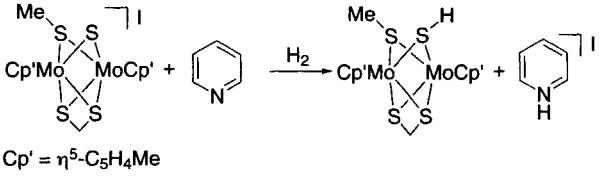

(15)

When complex (**2b**) is treated with 10 equiv of $[(\eta^5\text{-}C_5H_5)Mo(\mu_2\text{-}S_2CH_2)(\mu\text{-}S)(\mu\text{-}SH)Mo(\eta^5\text{-}C_5H_5)]OTf$ under H_2 in THF at 25 °C and then 55 °C for 24 h each, ammonia is formed in 38% yield based on tungsten atom (Eq. 16) [39]. In contrast to the reaction of tungsten dinitrogen complex (**2b**) with acidic ruthenium dihydrogen complexes (vide supra), the present reaction gives rise to the formation of ammonia even at ambient temperature if the reaction is carried out for a longer time. On the other hand, the reaction of tungsten dinitrogen complex (**1b**) with 2 equiv of $[(\eta^5\text{-}C_5H_4Me)Mo(\mu_2\text{-}S_2CH_2)(\mu\text{-}S)(\mu\text{-}SMe)Mo(\eta^5\text{-}C_5H_4Me)]OTf$ under H_2 gives the hydrazido(2-) complex *trans*-$[W(OTf)(NNH_2)(dppe)_2]OTf$ and a hydrosulfido- and methylsulfido-bridged dimolybdenum complex in almost quantitative yields, respectively (Eq. 17) [39]. In the absence of dihydrogen gas, no reaction occurs, and both tungsten and molybdenum complexes are recovered quantitatively. This demonstrates that heterolytic splitting of dihydrogen proceeds on the molybdenum complex, where one H atom is used for the N-H bond formation at the coordinated dinitrogen on tungsten and the other H atom is bound to the bridging-sulfido ligand. The formal oxidation state of the starting and product molybdenum complexes is +IV and +III, respectively, and the two electrons required for the reduction come from the activated dihydrogen. On the other hand, the four electrons for the formation of the hydrazido(2-) complex are supplied from the starting zero-valent tungsten. However, the detailed mechanism for activation of dihydrogen on sulfido-bridged dinuclear molybdenum complexes is not clear at present.

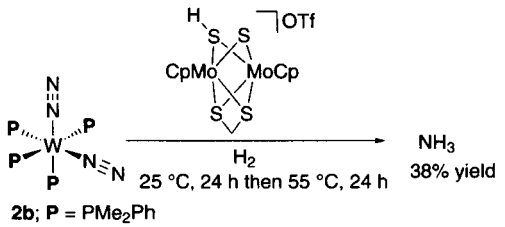

(16)

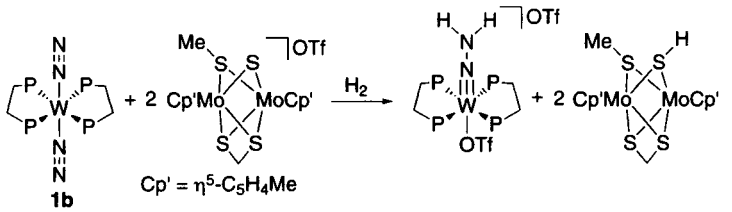

(17)

The pK_a values of hydrosulfido complexes have never been investigated in detail, although a huge number of hydrosulfido complexes are known [40]. During our continuous study on the reactivities of coordinated dinitrogen, we have

recently found that the coordinated dinitrogen in complex (**2b**) is protonated to afford ammonia by treatment with hydrosulfido-bridged dinuclear iridium and iron complexes, although PhSH (pK_a = 6.6) and H_2S (pK_a = 7.0) do not protonate the coordinated dinitrogen (Scheme 11) [41]. This result indicates the important role of bridging sulfur ligands in biological nitrogen fixation. Actually, in a theoretical model proposed by Dance [42], the bridging sulfido ligands mediate proton transfer to the coordinated dinitrogen bound to the Fe_4 face of the Fe/Mo sulfido cluster via μ-SH intermediates, as shown in Scheme 12.

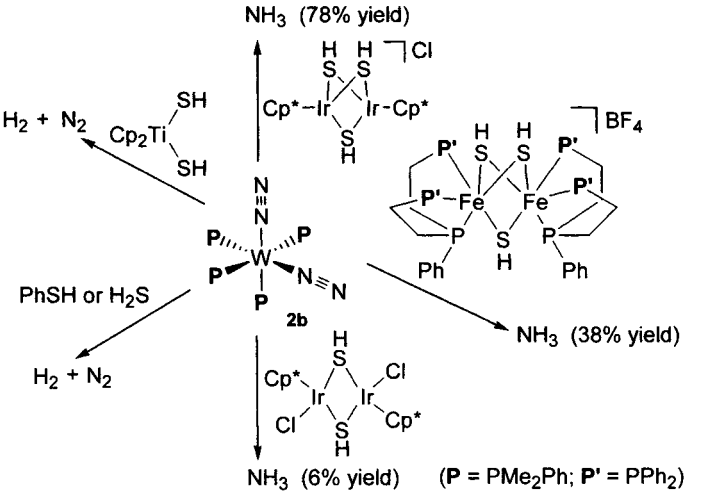

Scheme 11

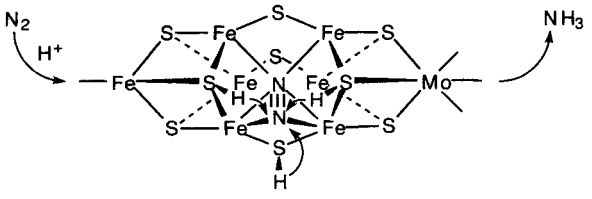

Scheme 12

Heterolytic cleavage of dihydrogen on metal-nitrogen bonds is also well known [43]. Recently, Noyori and coworkers have reported that the heterolytic dihydrogen splitting on a Ru-N bond is a key step in the asymmetric hydrogenation of ketones to produce chiral alcohols with high enantioselectivities [44]. A proposed catalytic cycle is shown in Scheme 13. The mechanism involves the concerted dihydrogen transfer from a hydride and a N-H group bound *cis* to Ru(II) to the ketone, which is followed by heterolytic dihydrogen splitting on the Ru-N

bond to accomplish the catalytic cycle [44b, 44d, 44e]. Quite recently, Morris and co-workers have proposed a similar reaction mechanism for the hydrogenation of ketones and imines catalysed by [$RuH_2(PPh_3)_2$(cyclohexyldiamine)] [45]. On the other hand, Brothers previously claimed that the heterolytic splitting of dihydrogen on a Pd-O bond is a key step in the catalytic hydrogenation of alkenes catalysed by palladium salen complex [46].

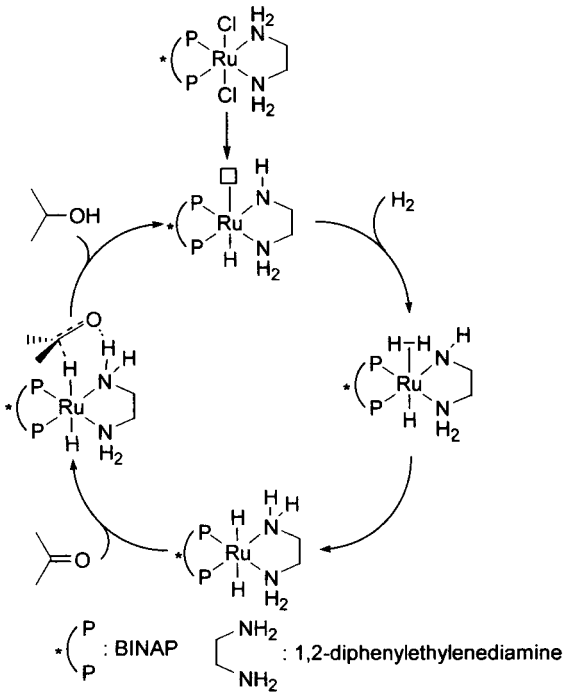

Scheme 13

5.5 PERSPECTIVE

As described above, ammonia is formed by protonation of the coordinated dinitrogen on tungsten with acidic ruthenium dihydrogen complexes under mild reaction conditions. In this bimetallic system, the heterolytic cleavage of dihydrogen occurs at the ruthenium centre where a proton is used for the protonation of the coordinated dinitrogen and a hydride ion remains at the ruthenium atom. The coordinated dinitrogen is further protonated by dihydrogen with the aid of sulfido-bridged dinuclear molybdenum complexes to form ammonia. In this reaction, the heterolytic splitting of dihydrogen takes place on the molybdenum complexes, where a proton is used for the N-H bond formation at the coordinated dinitrogen and the other hydrogen is bound to the bridging-

sulfido ligand. Both the protonation reactions by dihydrogen are stoichiometric, and the yields of ammonia are at present 30~80% based on tungsten. In these reactions, only one proton formed by the heterolytic cleavage of dihydrogen is used for the N-H bond formation and all of the electrons required for the formation of ammonia are supplied from the zero-valent tungsten. However, in the hydrogenolysis of the Si-O bond of trimethylsilyl enol ethers catalyzed by acidic ruthenium dihydrogen complexes, both a proton and a hydride derived from the heterolytic dihydrogen splitting are used for the product formation. Several other catalytic reactions involving heterolytic cleavage of dihydrogen as a key step are also known which include the splitting on a metal-nitrogen bond. These results encourage us to develop multimetallic systems where both the hydrogen atoms of activated dihydrogen are effectively and catalytically used for the synthesis of ammonia from dinitrogen and dihydrogen under mild conditions.

ACKNOWLEDGMENT

This work was supported by a Grant-in-Aid (09102004 and 12750747) from the Ministry of Education, Science, Sports, and Culture of Japan.

REFERENCES AND NOTES

[1] (a) G. J. Kubas, R. R. Ryan, B. I. Swanson, P. J. Vergamini, H. J. Wasserman, J. Am. Chem. Soc. 106 (1984) 451. (b) G. J. Kubas, Acc. Chem. Res. 21 (1988) 120.

[2] (a) P. G. Jessop, R. H. Morris, Coord. Chem. Rev. 121 (1992) 155. (b) D. M. Heinekey, W. J. Oldham, Chem. Rev. 93 (1993) 913. (c) R. H. Crabtree, Angew. Chem., Int. Ed. Engl. 32 (1993) 789. (d) S. Sabo-Etienne, B. Chaudret, Chem. Rev. 98 (1998) 2077.

[3] M. A. Esteruelas, L. A. Oro, Chem. Rev. 98 (1998) 577.

[4] (a) M. Hidai, Y. Mizobe, Chem. Rev. 95 (1995) 1115. (b) M. Hidai, Y. Ishii, Bull. Chem. Soc. Jpn. 69 (1996) 819.

[5] M. Hidai, K. Tominari, Y. Uchida, A. Misono, J. Chem. Soc., Chem. Commun. (1969) 1392.

[6] (a) J. Kim, D. C. Rees, Science 257 (1992) 1677. (b) J. Kim, D. C. Rees, Nature 360 (1992) 553. (c) M. K. Chan, J. Kim, D. C. Rees, Science 260 (1993) 792.

[7] (a) J. B. Howard, D. C. Rees, Chem. Rev. 96 (1996) 2965. (b) B. K. Burgess, D. J. Lowe, Chem. Rev. 96 (1996) 2983.

[8] (a) J. Chatt, A. J. Pearman, R. L. Richards, Nature, 253 (1975) 39. (b) J. Chatt, A. J. Pearman, R. L. Richards, J. Chem. Soc., Dalton Trans. (1977) 1852.

[9] T. Takahashi, Y. Mizobe, M. Sato, Y. Uchida, M. Hidai, J. Am. Chem. Soc. 102 (1980) 7461.

[10] (a) M. Hidai, T. Kodama, M. Sato, M. Harakawa, Y. Uchida, Inorg. Chem. 15 (1976) 2694. (b) J. Chatt, G. A. Heath, R. L. Richards, J. Chem. Soc., Dalton Trans. (1974) 2074. (c) J. C. Chatt, A. J. Pearman, R. L. Richards, J. Chem. Soc., Dalton Trans. (1976) 1520.

[11] Quite recently, Fryzuk and co-workers observed the N-H bond formation when a dinuclear zirconium complex with a side-on bridging dinitrogen ligand was treated with molecular dihydrogen. However, no ammonia was formed; (a) M. D. Fryzuk, J. B. Love, S. J. Rettig, V. G. Young, Science 275 (1997) 1445. (b) H. Basch, D. G. Musaev, K. Morokuma, M. D. Fryzuk, J. B. Love, W. W. Seidel, A. Albinati, T. F. Koetzle, W. T. Klooster, S. A. Mason, J. Eckert, J. Am. Chem. Soc. 121 (1999) 523.

[12] M. Hidai, T. Takahashi, I. Yokotake, Y. Uchida, Chem. Lett. (1980) 645.

[13] H. Nishihara, T. Mori, Y. Tsurita, K. Nakano, T. Saito, Y. Sasaki, J. Am. Chem. Soc. 104 (1982) 4367.

[14] A. Watakabe, T. Takahashi, D.-M. Jin, I. Yokotake, Y. Uchida, M. Hidai, J. Organomet. Chem. 254 (1983) 75.

[15] (a) R. H. Morris, Inorg. Chem. 31 (1992) 1471. (b) R. H. Morris, Can. J. Chem. 74 (1996) 1907. (c) R. H. Morris, Chapter 1 of this book

[16] G. Jia, R. H. Morris, C. T. Schweitzer, Inorg. Chem. 30 (1991) 594.

[17] (a) M. T. Bautista, E. P. Cappellani, S. D. Drouin, R. H. Morris, C. T. Schweitzer, A. Sella, J. Zubkowski, J. Am. Chem. Soc. 113 (1991) 4876. (b) E. P. Cappellani, S. D. Drouin, G. Jia, P. A. Maltby, R. H. Morris, C. T. Schweitzer, J. Am. Chem. Soc. 116 (1994) 3375. (c) G. Jia, R. H. Morris, J. Am. Chem. Soc. 113 (1991) 875. (d) G. Jia, A. J. Lough, R. H. Morris, Organometallics 11 (1992) 161. (e) B. Chin, A. J. Lough, R. H. Morris, C. T. Schweitzer, C. D'Agostino, Inorg. Chem. 33 (1994) 6278.

[18] (a) J. Huhmann-Vincent, B. L. Scott, G. J. Kubas, J. Am. Chem. Soc. 120 (1998) 6808. (b) T. P. Fong, A. J. Lough, R. H. Morris, A. Mezzetti, E. Rocchini, P. Rigo, J. Chem. Soc., Dalton Trans. (1999) 4475. (c) A. C. Intko, J. F. Houlis, R. C. Schabel, D. M. Roddick, Organometallics 17 (1998) 5467.

[19] E. Rocchini, A. Mezzetti, H. Rüegger, U. Burckhardt, V. Gramlich, A. Dal Zotto, P. Martinuzzi, P. Rigo, Inorg. Chem. 36 (1997) 711.

[20] Y. Nishibayashi, S. Iwai, M. Hidai, Science 279 (1998) 540.

[21] Y. Nishibayashi, S. Takemoto, S. Iwai, M. Hidai, Inorg. Chem. 39 (2000) 5946.

[22] (a) J. C. Jr. Lee, A. L. Rheingold, B. Muller, P. S. Pregosin, R. H. Crabtree, J. Chem. Soc., Chem. Commun. (1994) 1021. (b) J. C. Jr. Lee, E. Peris, A. L. Rheingold, R. H. Crabtree, J. Am. Chem. Soc. 116 (1994) 11014. (c) S. Park, R. Ramachandran, A. J. Lough, R. H. Morris, J. Chem. Soc., Chem. Commun. (1994) 2201. (d) A. J. Lough, S. Park, R. Ramachandran, R. H. Morris, J. Am. Chem. Soc. 116 (1994) 8356.

[23] (a) E. Peris, J. Wessel, B. P. Patel, R. H. Crabtree, J. Chem. Soc., Chem. Commun. (1995) 2175. (b) J. Wessel, J. C. L. Jr. Lee, E. Peris, G. P. A. Yap, J. B. Fortin, J. S. Ricci, G. Sini, A. Albinati, T. F. Koetzle, O. Eisenstein, A. L. Rheingold, R. H. Crabtree, Angew. Chem., Int. Ed. Engl. 34 (1995) 2507.

[24] (a) R. H. Crabtree, P. E. M. Siegbahn, O. Eisenstein, A. L. Rheingold, T. Koetzle, Acc. Chem. Res. 29 (1996) 348. (b) E. S. Shubina, N. V. Belkova, L. M. Epstein, J. Organomet. Chem. 536-537 (1997) 17. (c) R. H. Crabtree, Science 282 (1998) 2000. (d) R. H. Crabtree, O. Eisenstein, G. Sini, E. J. Peris, J. Organomet. Chem. 567 (1998) 7. (e) R. H. Crabtree, J. Organomet. Chem. 577 (1998) 111.

[25] R. T. Hembre, S. McQueen, J. Am. Chem. Soc. 116 (1994) 2141.
[26] M.J. Tenorio, M. C. Puerta, P. Valerga, J. Chem. Soc., Chem. Commun. (1993) 1750.
[27] A. C. Albéniz, G. Schulte, R. H. Crabtree, Organometallics 11 (1992) 242.
[28] (a) C. Bianchini, A. Meli, M. P. Peruzzini, P. Frediani, C. Bohanna, M. A. Esteruelas, L. A. Oro, Organometallics 11 (1992) 138. (b) C. Bianchini, F. Laschi, D. Masi, F. M. Ottaviani, A. Pastor, M. Peruzzini, P. Zanello, F. Zanobini, J. Am. Chem. Soc. 115 (1993) 2723.
[29] C. Bianchini, C. Bohanna, M. A. Esteruelas, P. Frediani, A. Meli, L. A. Oro, M. Peruzzini, Organometallics 11 (1992) 3837.
[30] M. A. Esteruelas, L. A. Oro, C. Valero, Organometallics 11 (1992) 3362.
[31] Y. Nishibayashi, I. Takei, M. Hidai, Angew. Chem., Int. Ed. Engl. 38 (1999) 3047.
[32] (a) A. Yanagisawa, K. Ishihara, H. Yamamoto, Synlett (1997) 411. (b) C. Fehr, Angew. Chem., Int. Ed. Engl. 35 (1996) 2566. (c) M. Sugiura, T. Nakai, Angew. Chem., Int. Ed. Engl. 36 (1997) 2366. (d) A. Yanagisawa, H. Inanami, H. Yamamoto, Chem. Commun. (1998) 1573. (e) K. Ishihara, H. Nakamura, S. Nakamura, H. Yamamoto, J. Org. Chem. 63 (1998) 6444. (f) G. Asensio, P. Aleman, J. Gil, L. R. Domingo, M. Medio-Simon, J. Org. Chem. 63 (1998) 9342. (g) S. Nakamura, M. Kaneeda, K. Ishihara, H. Yamamoto, J. Am. Chem. Soc. 122 (2000) 8120.
[33] (a) C. Bianchini, C. Mealli, A. Meli, M. Sabat, Inorg. Chem. 25 (1986) 4618. (b) C. Bianchini, A. Meli, Inorg. Chem. 26 (1987) 4268.
[34] (a) D. Sellmann, G. H. Rackelmann, F. W. Heinemann, Chem. Eur. J. 3 (1997) 2071. (b) D. Sellmann, T. Gottschalk-Gaudig, F. W. Heinemann, Inorg. Chem. 37 (1998) 3982. (c) D. Sellmann, A. Fürsattel, Angew. Chem., Int. Ed. 38 (1999) 2023. (d) D. Sellmann, F. Geipel, M. Moll, Angew. Chem., Int. Ed. 39 (2000) 561.
[35] (a) Z. K. Sweeney, J. L. Polse, R. A. Anderson, R. G. Bergman, M. G. Kubinec, J. Am. Chem. Soc. 119 (1997) 4543. (b) Z. K. Sweeney, J. L. Polse, R. G. Bergman, R. A. Anderson, Organometallics 18 (1999) 5502.
[36] (a) M. Rakowski DuBois, Chem. Rev. 89 (1989) 1. (b) M. Rakowski DuBois, B. Jagirdar, B. Noll, S. Dietz, Transition Metal Sulfur Chemistry; E. I. Stiefel, K. Matsumoto, Eds.; ACS Symposium Series 653, Washington, 1996.
[37] P. Bernatis, J. C. V. Laurie, M. Rakowski DuBois, Organometallics 9 (1990)1607.
[38] J. C. V. Laurie, L. D. Duncan, R. C. Haltiwanger, R. T. Weberg, M. Rakowski DuBois, J. Am. Chem. Soc. 108 (1986) 6234.
[39] Y. Nishibayashi, I. Wakiji, K. Hirata, M. Rakowski DuBois, M. Hidai, Inorg. Chem. 40 (2001) 578.
[40] (a) S. Kuwata, M. Hidai, Coord. Chem. Rev. 213 (2001) 211. (b) M. Peruzzini, I. de los Rios, A. Romerosa, Prog. Inorg. Chem. 49 (2001) 169
[41] Y. Nishibayashi, S. Iwai, M. Hidai, J. Am. Chem. Soc. 120 (1998) 10559.
[42] (a) I. G. Dance, Aust. J. Chem. 47 (1994) 979. (b) I. G. Dance, Transition Metal Sulfur Chemistry; E. I. Stiefel, K. Matsumoto, Eds.; ACS Symposium Series 653, Washington, 1996. (c) I. Dance, Chem. Commun. (1997) 165. (d) I. Dance, Chem. Commun. (1998) 523.
[43] (a) M. D. Fryzuk, P. A. MacNeil, Organometallics 2 (1983) 682. (b) M. D. Fryzuk, P. A. MacNeil, S. J. Rettig, Organometallics 4 (1985) 1145. (c) M. D. Fryzuk, P. A. MacNeil, S. J. Rettig, J. Am. Chem. Soc. 109 (1987) 2803. (d) M. D. Fryzuk, K.

Bhangu, J. Am. Chem. Soc. 110 (1988) 961. (e) M. D. Fryzuk, C. D. Montgomery, S. J. Rettig, Organometallics 10 (1991) 467.

[44] (a) T. Ohkuma, H. Ooka, T. Ikariya, R. Noyori, J. Am. Chem. Soc. 117 (1995) 10417. (b) T. Ohkuma, H. Doucet, T. Pham, K. Mikami, T. Korenaga, M. Terada, R. Noyori, J. Am. Chem. Soc. 120 (1998) 1086. (c) T. Ohkuma, M. Koizumi, H. Doucet, T. Pham, M. Kozawa, K. Murata, E. Katayama, T. Yokozawa, T. Ikariya, R. Noyori, J. Am. Chem. Soc. 120 (1998) 13529. (d) T. Ohkuma, J. Synth. Org. Chem. Japan 57 (1999) 667. (e) R. Noyori, T. Ohkuma, Angew. Chem., Int. Ed. Engl. 40 (2001) 40.

[45] K. Abdur-Rashid, A. J. Lough, R. H. Morris, Organometallics 19 (2000) 2655.

[46] P. Brothers, Prog. Inorg. Chem. 28 (1981) 1.

Chapter 6

Paramagnetic Mono- and Polyhydrides of the Transition Metals

Rinaldo Poli

Laboratoire de Synthèse et d'Electrosynthèse Organométalliques, Université de Bourgogne, 6 boulevard Gabriel, 21100 Dijon, France

CONTENTS

6.1 INTRODUCTION

Although hydrogen is the simplest element in the periodic table, it binds transition metals in a wide variety of modes, including terminal, doubly bridging, triply bridging (capping), as a η^2-H_2 ligand to provide so-called σ-complexes (or nonclassical hydrides), as part of intra- or intermolecular η^2-C-H σ-complexes (agostic), etc. Some of these binding modes are similar to those found in boranes, and are discussed in other chapters of this book. The simple $1s^1$ electronic configuration, however, insures that each H atom provides only one orbital and one electron for bonding no matter what the binding mode. In particular, hydrogen cannot establish π bonding or back-bonding interactions, thereby behaving as a π-neutral ligand. It is, perhaps, the only truly π-neutral ligand commonly encountered in coordination chemistry, since even alky ligands may establish in principle π-interactions with transition metals via symmetry-adapted combinations of the α-C-H and/or α-C-C σ and σ^* orbitals. In addition, like alkyl ligands, the H atom has an electronegativity which is comparable to the transition metal partner. This leads to strong covalent interactions and, therefore, to a strong stabilization for the M-H σ-bonding orbital and a strong destabilization for the corresponding σ^* orbital.

Because of the above factors, the 18-rule dominates the chemistry of transition metal hydride complexes. Open-shell complexes obtained by ligand dissociation or by redox processes from 18-electron precursors are usually high-energy, reactive molecules or ions (we shall neglet here the effectively saturated square planar d^8 complexes) unless other ligands in the coordination sphere are capable of providing a stabilizing contribution by π-donation or by a hapticity increase. For instance, one-electron oxidation of saturated $WH_2Cl_2(PMe_3)_4$ provides the 17-electron $[WH_2Cl_2(PMe_3)_4]^{+\bullet}$ product, whose stability may be attributed at least in part to the π-donating properties of the chloride ligands [1]. As an additional example, the saturated $IrClH_2(H_2)(PR_3)_2$ (R = Pr^i, Cy, Bu^t) complexes, unlike the related $IrH_5(PR_3)_2$ molecules, readily lose dihydrogen to afford

the corresponding π-stabilized (by the chloride ligand) 16-electron $IrClH_2(PR_3)_2$ derivatives [2].

An additional reason that makes hydride compounds more reactive than alkyl analogues, also valid for saturated complexes, but *a fortiori* further limiting the stability of open-shell hydrides, is the spherical shape of the H 1s orbital. Thus, orbital rearrangements on the way to transition states are much less pronounced for reactions involving hydride ligands and consequently the activation free energies are lower because of a more positive (or less negative) activation entropy. A splendid example of this principle is shown by the rapid ($1.8 \cdot 10^4$ $M^{-1}s^{-1}$) protonolysis of the 15-electron transient $[CrH(H_2O)_5]^{2+}$, while the analogous decomposition rates for alkyl analogues are lower than 10^2 $M^{-1}s^{-1}$ and as low as $<1.6 \cdot 10^{-6}$ $M^{-1}s^{-1}$ for the CH_2COOH derivative [3].

A greater understanding in the area of open-shell hydride complexes has relevance to important applications such as building models for hydrogenase enzymes (eq. 1, MV = methyl viologen; B = Bronsted base) [4] and electrocatalysts for the reverse hydrogen evolution process [5-7], the electro-catalytic hydrogenation of different substrates (eq. 2), [8-11] the electrocatalytic reduction of CO_2 (eq. 3) [12, 13], and the electrochemical functionalization of saturated hydrocarbons (eq. 4). Catalysts for the electrolytic oxidation of organic materials for fuel cell applications are known, although these accomplish a total oxidation to CO_2 rather than a selective functionalization process [14, 15]. In addition, the established implication of paramagnetic hydrides as intermediates in reactions such as the photochemical hydrogenation of electron-deficient olefins [16], where one would normally not predict a radical mechanism, constitutes another reason for exploring the fundamental properties of this class of compounds.

$$H_2 + 2MV^{2+} + 2B \xrightarrow{[Cat]} 2MV^{+} + 2BH^{+} \quad (1)$$

$$[X] + 2H^{+} + 2e^{-} \xrightarrow{[Cat]} [X]H_2 \quad (2)$$

$$CO_2 + nH^{+} + ne^{-} \xrightarrow{[Cat]} CO, HCOOH, HCHO, CH_3OH, CH_4 \quad (3)$$

$$R\text{-}H + H_2O \xrightarrow{[Cat]} R\text{-}OH + 2H^{+} + 2e^{-} \quad (4)$$

In this chapter, we shall first briefly survey the methods used for the synthesis or generation of paramagnetic hydride complexes, subsequently survey the known classes of stable open-shell hydride complexes, then review our current knowledge on the fundamental properties of the M-H bond in open-shell compounds, and finally examine the various established decomposition modes. No review articles specifically focusing on paramagnetic hydride compounds and their chemical reactivity appear to have been previously published. With few exceptions, this chapter will be limited to the analysis of monometallic species of the d elements. The f elements are treated in a separate chapter in this

Monograph. To facilitate reading of this article, all radical species (17, 19, and 15-electron with a single unpaired electron) are explicitely marked with a "dot".

6.2 SYNTHESES OF PARAMAGNETIC HYDRIDE COMPLEXES

Since, as a general rule, paramagnetic hydride complexes are thermally sensitive compounds and are unstable toward a variety of decomposition pathways (see section 6.5), all methodologies for their preparation/generation should in principle be carried out under mild conditions. Certain products, however, have proven sufficiently stable to be isolated under normal laboratory conditions (see section 6.3).

6.2.1 Oxidation of diamagnetic precursors

This is by far the most common method for generating 17-electron hydride complexes, starting from stable, saturated hydride compounds. The vast majority of reported examples employ a neutral precursor for the generation of cationic products, *e.g.* equation 5 [17]. However, the oxidation of anionic precursors to neutral species, for instance $[MH(Porph)(L)]^-$ (M = Ru, Os) [4], and of cationic precursors to 2+ charged products, *viz.* $[WClH_2(PMe_4)_4(MeCN)]^+$ [1], and even of doubly charged precursors to 3+ products, *viz.* $[ReH(MeCN)_3(PPh_3)_2(py)]^{2+}$ [18], have been reported.

$$CpMoH(PMe_3)_3 + Cp_2Fe^+ \longrightarrow [CpMoH(PMe_3)_3]^{+\bullet} + Cp_2Fe \qquad (5)$$

It has been shown that, for certain particular classes of compounds where an ambiguity may exist between classical and nonclassical tautomeric forms of the saturated precursor, the oxidation potential may be a valuable structural gauge. Thus, while $[M(H_2)\{P(CH_2CH_2PPh_2)_3\}]^+$ (M = Co, Rh) which exhibit the nonclassical dihydrogen structure undergo irreversible one-electron oxidation processes at relatively accessible potentials (characteristic of analogous d^8 M(I) species), the corresponding $[RhH_2\{N(CH_2CH_2PPh_2)_3\}]^+$ and $[IrH_2\{E(CH_2CH_2PPh_2)_3\}]^+$ (E = N, P) complexes which adopt the classical arrangement and are therefore better described as d^6 M(III) species show no redox activity within the potential window of THF [19]. However, other classical polyhydride species have been shown to be oxidized at remarkably low potentials, *e.g.* $Cp^*RuH_3(PPh_3)$ [20] and $OsH_6(P^iPr_3)_2$ [21].

One could naïvely predict that only compounds where the metal has a d^n ($n \geq 1$) configuration may be oxidized. However, the $M^{\delta+}$-$H^{\delta-}$ bond is itself a source of electrons. Removal of one electron from the hydride ligand may then lead

to direct hydrogen evolution or even deprotonation with electron redistribution resulting in a formal metal *reduction* (see Scheme 1). In addition, when oxidizing a d^0 *poly*hydride complex, it is conceivable that an internal rearrangement to a nonclassical structure may be triggered upon oxidation, again with formal metal reduction (Scheme 1). An example of the oxidation of a d^0 polyhydride complex, namely Cp_2TaH_3, has recently been reported [22]. However, no *stable* paramagnetic hydride product was obtained from this reaction.

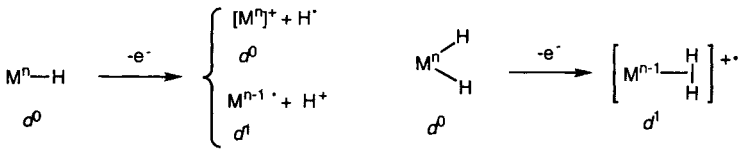

Scheme 1

6.2.2 Reduction of diamagnetic precursors

Starting from an 18-electron precursor, a formally 19-electron product is expected to form. No stable product nor well-characterized reaction intermediate wich such electronic configuration appears to have been obtained by this method. However, this reaction may be followed by loss of a 2-electron donor ligand to afford a 17-electron product. For instance, sodium reduction of $FeHCl(dppe)_2$ induces chloride expulsion, see eq. 6 [23].

$$FeHCl(dppe)_2 + Na \longrightarrow FeH(dppe)_2^{\bullet} + NaCl \qquad (6)$$

On the other hand, one electron reduction of other substrates, for instance $[MH(CO)_2(L\text{-}L)_2]^+$ (M = Cr, Mo, W; L-L = dppm, dppe) [24] and $[CpCoH(PR_3)_2]^+$ [25], leads to expulsion of H_2. This type of reaction is of fundamental importance in the electrocatalytic reduction of protons to dihydrogen [7] and could play a fundamental role in other electrocatalytic reduction processes.

6.2.3 Hydrogen atom abstractions

Numerous atom transfer reactions in transition metal hydride chemistry have been documented and early reviews on the subject are available [26, 27]. Reagents such as the trityl radical are readily available and are effective at the abstraction of hydrogen atoms from organometallic hydrides. The BDE of Ph_3C-H (75 kcal/mol) is greater than that of most transition metal - hydrogen bonds. The majority of these processes, however, involve monohydride complexes such as $CoH(CO)_4$, $MnH(CO)_5$, or $CpWH(CO)_3$ [28, 29], the radical product being therefore a nonhydridic, highly reactive species [26]. The conversion of some alkyl

halides to alkanes by monohydride complexes, especially anionic ones, may also take place via an initial hydrogen atom transfer [30, 31]. This synthetic route holds considerable promise for the generation of neutral 17-electron hydride complexes when carried out on a polyhydride material, although it has so far been applied only in a limited number of cases.

The earliest example seems that provided by Kochi for Cp_2NbH_3 [32]. The low-temperature interaction of this compound with photolytically generated *tert*-butoxy radicals yields an unstable species which is interpreted as $Cp_2NbH_2^{\bullet}$ by its EPR properties. The half-life of this species is > 10 min in benzene-cyclopropane at -70°C.

The trityl radical is able to abstract a hydrogen atom from $OsH_2(CO)_4$, yielding the 17-electron $OsH(CO)_4^{\bullet}$, which rapidly dimerizes to $Os_2H_2(CO)_8$ [33]. Although this intermediate was not directly observed, kinetic evidence is in agreement with the proposed hydrogen atom transfer mechanism [34, 35].

6.2.4 *Dihydrogen oxidative addition*

This reaction has only been rarely documented for paramagnetic complexes, in contrast to the wide variety of H_2 oxidative addition to 16-electron complexes, especially of d^8 type, to afford saturated products. A rare example is shown in Scheme 2 [36], the M(IV) d^1 product having a 17-electron configuration.

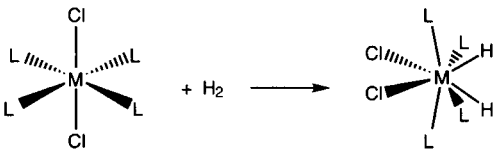

(M = Nb, Ta; L = PMe_3 or L_2 = dmpe)

Scheme 2

6.2.5 *From paramagnetic alkyl complexes*

6.2.5.1 *By β-hydrogen elimination.*

Alkyl ligands containing β-hydrogen substituents are susceptible to β-hydrogen elimination to afford hydride products. This reaction is difficult for electronically saturated compounds because it would involve the formation of a 20-electron intermediate having two electrons in a metal-ligand antibonding orbital. Therefore, the transformation usually involves the preliminary dissociation of a ligand to afford a reactive 16-electron intermediate. 17-electron compounds, on the other hand, could involve 19-electron intermediates where only one electron is located in a metal-ligand antibonding orbital and the barrier to this process is

therefore expected to be reduced. Alternatively, a preliminary ligand dissociation may again take place to afford a 15-electron intermediate. If this intermediate adopts a spin doublet configuration, then an empty metal orbital is available and the β-hydrogen elimination process may occur rapidly, whereas a larger barrier is expected if each of the three remaining metal orbitals is singly occupied to afford a spin quartet ground state. Indeed, the relative inertness of $[CrR(H_2O)_5]^{2+}$ complexes is largely associated to their spin quartet configuration [37].

In spite of the predicted facile β-hydrogen elimination from paramagnetic alkyl complexes, this transformation is little documented, probably because the final hydride product is in most cases more reactive than its alkyl precursor and decomposes further. A rare example of this pathway is illustrated in equation 7 [38].

$$Cp_2TiCl^{\bullet} + 2\ EtMgCl \longrightarrow Cp_2TiH_2^{\bullet} \qquad (7)$$

6.2.5.2 By hydrogenolysis

The reaction of metal alkyl compounds with dihydrogen, leading to hydride species with elimination of alkanes, is commonly observed for Lewis acidic metal centers. This reaction has been used to prepare hydride complexes of the lanthanides, and of titanium(III), see equation 8 [39].

$$Cp^*_2Ti(CH_3)^{\bullet} + H_2 \longrightarrow Cp^*_2TiH^{\bullet} + CH_4 \qquad (8)$$

6.2.6 Other methods

The hydride ligand originates either from water of from 1-butanol in the synthesis of $[CoH(triphos)(PEt_3)]BPh_4$ [triphos = $CH_3C(CH_2PPh_2)_3$] from a mixture of $Co(ClO_4)_2$, triphos, and PEt_3, reaction 9. The reaction is carried out in 1-butanol and the outcome is highly dependent on the hydration of the cobalt source. The best yields were obtained when the salt was dehydrated by reflux with triethyl orthoformate in 1-butanol, while the reaction using $Co(ClO_4)_2{\cdot}6H_2O$ yielded a dinuclear bis-μ-OH product. A rigorously anhydrous salt, however, could not be prepared. It seems likely that the hydride originates from a butoxy ligand via a β-hydrogen elimination process [40].

$$Co^{2+} + triphos + PEt_3 \xrightarrow{1\text{-butanol}} [CoH(triphos)(PEt_3)]^{+\bullet} \qquad (9)$$

6.3 SURVEY OF STABLE PARAMAGNETIC HYDRIDE COMPLEXES.

For the purpose of this section, the attribute "stable" is not restricted to those compounds that are sufficiently inert to be isolated and fully characterized, but is also extended to sufficiently long-lived products in solution under any kind of experimental conditions (including low temperature) to allow an unambiguous spectroscopic characterization. Most of the reported stable paramagnetic hydride complexes have a 17-electron configuration, while those having 19, 16 and 15 electrons are much less represented. Paramagnetic hydride complexes of the f elements are not considered in this chapter.

6.3.1 19-electron complexes

This a very rare class of compounds. The first example has apparently been reported only in 1992 by Lapinte and co-workers [41]. Carbonylation of the stable 17-electron hydride complex $[Cp^*FeH(dppe)]^{+\bullet}$ affords the adduct $[Cp^*FeH(CO)(dppe)]^{+\bullet}$. CO binding is reversible and the 17-electron precursor is reobtained upon warming above -60°C (Scheme 3). The 19-electron nature of the product is indicated by the EPR properties, while the IR spectrum shows the CO coordination and the Mössbauer spectrum is characteristic of a Fe(III) species.

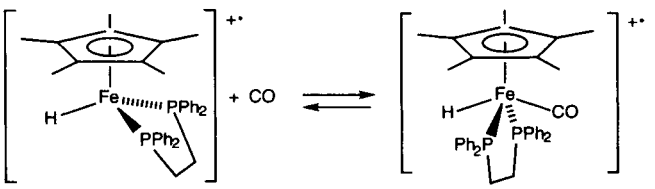

Scheme 3

Complex $[Cp^*MoH(dppe)(CH_2Cl_2)]^{+\bullet}$ is obtained from the spontaneous H_2 elimination from $[Cp^*MoH_3(dppe)]^{+\bullet}$ in CH_2Cl_2. The EPR spectrum shows coupling to one H, two equivalent P, and two equivalent Cl nuclei. Under the assumption that the Cp* has maintained the usual η^5 coordination mode, the complex has a 19-electron count [42].

Reversible reduction of complexes $[Cp^*IrH(bipy)]^+$ and $[(C_6Me_6)OsH(bipy)]^+$ affords EPR active species that have been characterized by EPR spectroscopy [43, 44]. According to these spectroscopic analyses, however, the compounds are best described as derivatives of Ir(III) and Os(II) with a reduced bipy ligand. Compounds $[CpCoH(L\text{-}L)]^+$ (L-L = dppe, $Ph_2PCH{=}CHPPh_2$), on the other hand, display one-electron reduction waves with observable return waves in cyclic vol-

tammetric studies at high scan rates, but the reduced species could not be observed spectroscopically, while analogous complexes with monodentate ligands display completely irreversible reduction processes [25].

6.3.2 17-electron complexes

6.3.2.1 Group 4

Treatment of titanocene dichloride or monochloride with excess alkyl (ethyl or isopropyl) Grignard affords the $[Cp_2TiH_2]^{-\bullet}$ anion, fully identified by EPR spectroscopy in comparison with the deuteriated analogue [38]. More extensive EPR studies have also been reported later [45]. In a preliminary communication, this species had been incorrectly formulated as the dinuclear $[Cp_2Ti(\mu\text{-}H)]_2$ [46]. The use of a reduced quantity of Grignard reagent affords a monohydride species, interpreted as a 17-electron solvate $Cp_2TiH(S)^{\bullet}$. The use of methyl Grignard, on the other hand, produced stable mono- or dimethyl analogues [38]. The anionic dihydride complex is stable at room temperature, and reacts rapidly with protic substances including water with dihydrogen evolution. The Cp* analogue of this compound has been isolated as an ion-paired lithium complex, $Cp^*_2Ti(\mu\text{-}H)_2Li(tmed)$, and crystallographically characterized [47]. Its reaction with water yields compound $\{Cp^*_2TiOLi(THF)\}_2$.

The dinuclear complex $[Cp_2Ti(\mu\text{-}H)]_2$ was eventually obtained by reacting dimethyl titanocene, $Cp_2Ti(CH_3)_2$, with dihydrogen in the absence of solvent [48]. The compound is diamagnetic and reacts with 1,3-pentadiene to afford π-(1,3-dimethylallyl)titanocene, or with diborane to afford $Cp_2Ti(BH_4)^{\bullet}$, and with 2-electron ligands to form $Cp_2TiH(L)^{\bullet}$ (L = THF, PPh_3). An *ansa*-indenyl analogue of this compound has also been synthesized and structurally characterized [49]. The Cp* analogue of this compound is a 15-electron monomeric species [47].

6.3.2.2 Group 5

The first 17-electron complexes of niobium and tantalum, namely Cp_2MH_2 and $TaH_4(dmpe)_2$, were obtained from the corresponding M(V) hydrides and photogenerated *tert*-butoxy radicals. They were, however, not sufficiently stable for isolation and were only characterized by EPR spectroscopy at low temperature [32]. Replacement of two hydrido ligands with halides, however, leads to isolable products. Compounds $MCl_2H_2(PMe_3)_4^{\bullet}$ and $MCl_2H_2(dmpe)_2^{\bullet}$ (M = Nb, Ta) have been obtained by H_2 oxidative addition to the corresponding M(II) dichloride complexes, see Scheme 2, and have been characterized by IR and EPR spectroscopies and by magnetic susceptibility. In addition, the structures of $TaCl_2H_2(PMe_3)_4^{\bullet}$ and $TaCl_2H_2(dmpe)_2^{\bullet}$ have been confirmed by X-ray crystallography [36, 50].

Controlled potential oxidation (1 F) of the niobiocene complex $(C_5H_4SiMe_3)_2NbH\{P(OMe)_3\}$ yields the stable one-electron oxidation product, which has been characterized by EPR spectroscopy. This material decomposes only upon heating to 60°C in the presence of $P(OMe)_3$ [51]. One-electron oxidation of $(\eta^5\text{-}C_5H_4R)_2NbH_3$ (R = $SiMe_3$, *t*-Bu), correspondingly give stable solutions whose EPR spectra indicate coupling to a single Nb atom and to a single H atom. The products, on the other hand, have been formulated as dihydride-bridged dimers, $[(\eta^5\text{-}C_5H_4R)_2NbH(\mu\text{-}H)]_2$. Unfortunately, these materials could not be isolated [52]. One-electron oxidation of $MH(CO)_2(dppe)_2$ (M = Nb, Ta) gives the corresponding 17-electron cations. These are sufficiently stable at room temperature to be characterized by IR and EPR spectroscopies and have been quantitatively reduced back to the corresponding neutral precursors, but have not been isolated [53].

6.3.2.3 Group 6

Species $[Cp_2WH(Ph)]^{+\bullet}$ has been detected in an EPR spectroelectrochemistry experiment at -45°, but the signal disappears as soon as the current is turned off. A doublet splitting of 12 G is unambiguously assigned to the hydride ligand, since deuterium substitution leads to a singlet resonance with unresolved D coupling [54]. The cation derived from Cp_2WH_2 is too transient to be observed directly, reversibility for the oxidation wave being attained only at 5000 V s^{-1} [16]. However, trapping by phenantroquinone (PQ) affords an EPR spectrum consistent with the formation of $Cp_2WH(PQ)^{\bullet}$, see equation 10.

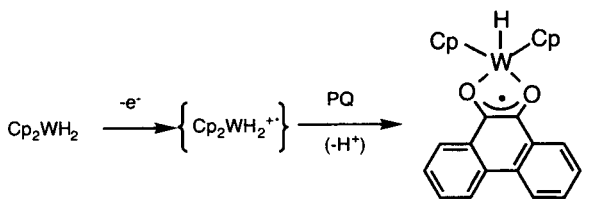

(10)

One-electron chemical (Ag^+ or Cp_2Fe^+) or electrochemical oxidation of $WCl_2H_2(PMe_3)_4$ and $[WClH_2(PMe_3)_4(MeCN)]^+$ affords the corresponding 17-electron W(V) products. IR, ^1H NMR and EPR spectra are reported for these compounds, and the structure of $[WCl_2H_2(PMe_3)_4]^{+\bullet}$ as the BF_4^- salt has also been confirmed by X-ray crystallography [1]. Although the hydride positions were not located, the rest of the structure is consistent with a dodecahedral geometry for the cation.

The cyclic voltammetric study of complexes $[M(CO)_2(L\text{-}L)H]^+$ (M = Cr, Mo, W; L-L = dppm, dppe), shows an irreversible one-electron oxidation at room temperature, reversibility being attained only for the two W complexes and for

the Mo-dppe complex at lower temperatures (down to -60° in butyronitrile). The corresponding $[MH(CO)_2(L\text{-}L)]^{2+\bullet}$ products were not identified spectroscopically [24]. In contrast, complex $CpMoH(PMe_3)_3$ undergoes a reversible one-electron oxidation at room temperature. The EPR spectrum of the $[CpMoH(PMe_3)_3]^{+\bullet}$ product shows unambiguously the presence of one H and three P nuclei in the coordination sphere [17].

The chemical or electrochemical oxidation of $Cp^*MH_3(dppe)$ (M = Mo, W) affords the corresponding monocations, $[Cp^*MH_3(dppe)]^{+\bullet}$, that are fully identified by the EPR coupling to the three H (not present for the corresponding trideuterides) and two P nuclei, see Figure 1.

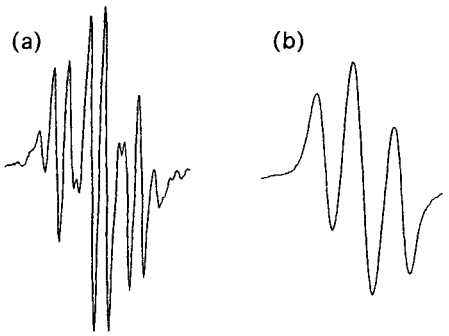

Figure 1. EPR spectrum of the $[CpMoX_3(dppe)]^{+\bullet}$ species [(a): X = H; (b) X = D] in THF (T = 193 K). Reprinted in part with permission from ref. [42]. Copyright 1999 American Chemical Society.

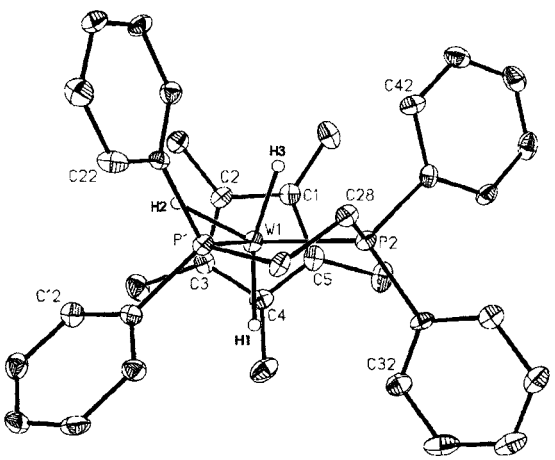

Figure 2. ORTEP view of the $[Cp^*WH_3(dppe)]^{+\bullet}$ cation. Reprinted with permission from ref. [42]. Copyright 1999 American Chemical Society.

The tungsten compound is sufficiently stable to be isolated and an X-ray structure has been determined (Figure 2) [42, 55]. The unusual positions of two of the three hydride ligands, half-way between those expected for a pseudo trigonal prism (as observed for the starting neutral system) and for a pseudo octahedron (as observed for other compounds with the same stoichiometry) is matched by DFT geometry optimations on the model $[CpWH_3(H_2PCH_2CH_2PH_2)]^{+\bullet}$ system [42].

6.3.2.4 Group 7

Compounds $ReH(PPh_3)_2(acac)X_2^{\bullet}$ (X = Cl, Br, I) are apparently the first isolated and stable paramagnetic hydride compounds ever reported [56]. They were obtained by oxidation of $ReH_2(PPh_3)_3(acac)$, see Scheme 4. Besides elemental analyses, they have been characterized by magnetic susceptibility and IR spectroscopy. In addition, further oxidation or protonation reactions leas to the liberation of H_2.

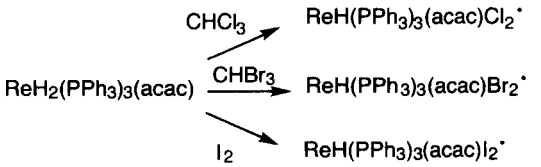

Scheme 4

The bulk electrolysis of $[ReH(MeCN)_3(PPh_3)_2(py)]^{2+}$ has afforded the corresponding 17-electron trication, which has subsequently been electrolyzed back to the dication precursor proving the stability of the paramagnetic complex [18]. No characterization data are provided, however, for this product. The oxidation of $ReH_5(PPh_3)_3$ and other $ReH_5(PPh_3)_2L$ compounds, on the other hand, is chemically irreversible in the cyclic voltammogram [57].

The oxidation of $CpReH_2\{P(p\text{-}XC_6H_4)_3\}_2$ (X = H, Me, F, OMe) and the decomposition mechanism of the oxidation product have been investigated in detail [58]. The paramagnetic products of the one-electron oxidation, $[CpReH_2\{P(p\text{-}XC_6H_4)_3\}_2]^{+\bullet}$, are stable and the reversible potential shows a linear dependence with Hammett's σ_p parameter. These compounds, however, have not been isolated and have only been characterized, besides their cyclic voltammetric properties, by UV-visible spectroscopy for X = H and by the nature of the chemical decomposition products (see section 6.5.2). Two isolated members of this class were described later by Herrmann. The silver oxidation of $Cp^*ReH(X)(PMe_3)_2$ (X = H or Cl) yield salts of the corresponding cations, isolated as the triflate for X = H and the hexafluoroantimonate for X = Cl. No characterization other than elemental analysis and IR (no mention of Re-H frequencies) was given, however [59].

6.3.2.5 Group 8

The reduction of $FeClH(dppe)_2$ or $[FeH(dppe)_2]^+$ with 1 equiv of Na powder in toluene or benzene gives $FeH(dppe)_2^{\bullet}$, a Curie-Weiss paramagnet (one unpaired electron) [23]. Cryoscopy in benzene proves its monomeric nature. A subsequent study has described an improved synthetic route by bulk electrolysis of $[FeH(MeCN)(dppe)_2]^+$ in acetonitrile, and has shown that the compound displays reversible one-electron oxidation and one-electron reduction processes [60]. An isoelectronic compound, $FeH\{P(CH_2CH_2PPh_2)_3\}^{\bullet}$, has been generated by reversible coulometric reduction of $[FeH\{P(CH_2CH_2PPh_2)_3\}]^+$ and characterized by EPR spectroscopy [19].

Oxidation of $FeClH(dppe)_2$ with $AgClO_4$ or with trityl salts gives the paramagnetic Fe(III) hydride complex $[FeClH(dppe)_2]^{+\bullet}$, with an IR Fe-H stretching vibration at 1865 cm^{-1}. The low-temperature EPR spectrum is consistent with a d^5 Fe(III) system, although the resolution does not allow to discern the hydride coupling [23]. The reaction of this complex with HCl in ethanol leads to hydrogen evolution, according to eq. 11.

$$[FeClH(dppe)_2]^{+\bullet} + HCl \longrightarrow FeCl_2(dppe) + dppe + 1/2\ H_2 \qquad (11)$$

Paramagnetic ruthenium complexes containing only phosphines and hydrides do not appear to be known. There is, on the other hand, a report of one such osmium complex, $[OsH_4(PMe_2Ph)_2]^{-\bullet}$ [61]. While no EPR data on this complex was reported, and the hydride ligands were not located by the X-ray structural determination, a reaction with Bu_3SnH afforded $[OsH_5(PMe_2Ph)_2]^-$, which could be fully identified by NMR spectroscopy. Anionic porphyrin derivatives of Ru(II) and Os(II) have been oxidized to afford relatively stable neutral products (the Os compound has a half life of ca. 1 day in THF), but no spectroscopic characterization of these materials was presented [4].

Cyclopentadienyl complexes containing hydride ligands have also been described for Fe(III) and Ru(III). Treichel first reported the reversible oxidation of CpFeX(dppe) for a variety of X groups including H, but his isolation attempts of the oxidized hydride product from CH_2Cl_2/Et_2O only gave $[CpFeCl(dppe)]PF_6$ [62]. Lapinte *et al.* later noted similar reversible oxidations for Cp* analogues [63], and succeded in the isolation of the 17-electron hydride complex, $[Cp^*FeH(dppe)]^{+\bullet}$ [64]. Steric protection in this compound prevents deprotonation by PPh_3, PMe_2Ph or NEt_3. Similar compounds with 1,2-bis(diisopropylphosphino)ethane have also been described by Puerta *et al.* [65].

The stability of ruthenium analogues of the Lapinte compound depends on the cyclopentadienyl substitution. Cyclic voltammetric studies of neutral CpRu(II) precursors by the Tilset group show near-reversibility but the oxidation pro-

ducts decompose rapidly and have not been observed directly [66]. The substituted compounds $(C_5H_4R)RuH(PPh_3)_2$ show reversible oxidations and the 17-electron product with R = $CTol_3$ could be identified by ESR spectroscopy [67]. A stable complex of this class, containing the Cp* ligand and the ferrocenyl ligand $(\eta^5\text{-}C_5H_4PPh_2)_2Fe$ (dppf), namely $[Cp^*RuH(dppf)]^{+\cdot}$, has been described by Hembre *et al.* [68].

6.3.2.6 Group 9

Oxidation of the cobalt(I) compounds $CoHL_4$ [L = $P(OEt)_2Ph$, $P(OMe)_2Ph$, $P(OPh)_3$] with $Ph_3C^+X^-$ (X = PF_6 or BF_4) affords the corresponding $[CoHL_4]X$ salts, characterized by magnetic suceptibility, electrical conductivity, and IR spectroscopy [69]. The presence of the hydride ligand is further evidenced by the result of the sodium reduction reaction, which gives back the parent compound $CoHL_4$ in an essentially quantitative yield. In addition, compound *trans*-$[CoHCl\{P(OEt)_2Ph\}_4]PF_6$ with a characteristic quintet ^1H NMR hydride resonance is obtained by Cl abstraction from CCl_4. Further oxidation also occurs with ferrocenium in the presence of additional ligands L' to afford doubly cationic Co(III) hydride complexes, $[CoH\{P(OEt)_2Ph\}_4L']^{2+}$ [L' = MeCN, PhCN, $ClCH_2CN$, $PPh(OEt)_2$] [70]. An example of this class with the tripodal polyphosphine $P(CH_2CH_2PPh_2)_3$ has been crystallographically characterized [19, 71, 72]. This X-ray structure (Figure 3) is one of the earliest reported for a mononuclear 17-electron hydride complex. Another example of this class, $[CoH(triphos)(PEt_3)]BPh_4$ [triphos = $CH_3C(CH_2PPh_2)_3$], has more recently been obtained from $Co(ClO_4)_2$, triphos and PEt_3 in 1-butanol [40], see equation 9.

Electrochemical experiments in MeCN have shown that the oxidation of $MH(dppe)_2$ (M = Co, Rh, Ir), $CoHL_4$ [L = $P(OMe)_3$, $P(OEt)_3$], and $MHCO(PPh_3)_3$ (M = Rh, Ir), proceeds in two one-electron steps and that the Rh(II) and Ir(II) are unstable, decomposing through a disproportionation pathway [73, 74]. Complexes $[MH(CO)(PPh_3)_3]^{+\cdot}$ (M = Rh, Ir) show M-H stretching vibrations at 2100 cm^{-1} for both M = Rh and Ir and magnetic moments of 1.65 (Rh) and 1.6 (Ir) μ_B in solution, but attempts to isolate them have been unsuccessful. Subsequent studies in CH_2Cl_2, on the other hand, have allowed a full spectroscopic investigation of both Rh [75] and Ir [76] complexes. The EPR spectra suggest that the system rearranges upon oxidation from a trigonal bipyramid to a square pyramid.

Cyclopentadienyl hydrido complexes of the group 9 metals have received little attention in terms of their redox behaviour. An exeption is $[Cp^*IrH(bipy)]^+$, which shows a reversible one-electron *reduction* at -1.65 V *vs.* ferrocene. The narrow EPR line of the product at 2.003, however, seem to indicate that the reduction process has involved the bipy ligand, the product being formulated as $[Cp^*Ir^{I}H^{+I}(bipy^{-\cdot})]$ [43].

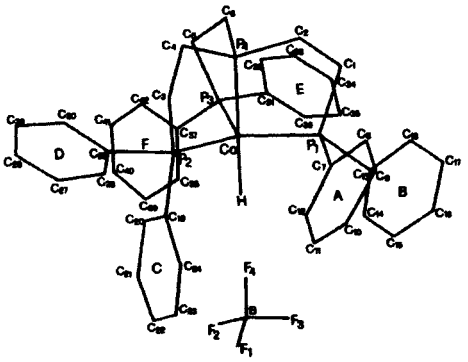

Figure 3. Line drawing of the structure of $[CoH\{P(CH_2CH_2PPh_2)_3\}]BF_4$. Reproduced with permission from ref. [71].

Higher oxidation state paramagnetic group 9 hydride derivatives have led to controversy. An initial report of an Ir(IV) hydride compound [77, 78] was later disclaimed by the same authors, the observed paramagnetism of $IrCl_2H_x(PPr^i_3)_2$ being attributed to cooperative surface phenomena, while the bulk of the material is diamagnetic [79].

6.3.3 16-electron complexes

We shall exclude from this section all square planar hydride derivatives of the d^8 transition metals, since these are effectively saturated systems and diamagnetic. For other d^n systems, compounds such as $MXH(CO)(PR_3)_2$ (M = Ru, Os; X = π donating group such as halide) are diamagnetic and stable, because of the effective saturation ascribed to the π donation from X, whereas the corresponding $MH_2(CO)(PR_3)_2$ complexes are very reactive and non isolable transient species [80].

Complex $[FeH(dppe)_2]^+$ was first reported by Sacco *et al.* [81, 82]. It was obtained from $FeClH(dppe)_2$ by chloride abstraction with NaY (Y = BPh_4 or ClO_4) in THF. Its THF solutions are bright red below 0°C and blue above 40°C, according to the easy reversible equilibrium of eq. 12, while the isolated solid is deep blue. The compound has also been obtained later by Pilloni *et al* by controlled potential electrolysis in DME of the 17-electron $FeH(dppe)_2^{\bullet}$. The DME solutions are red-violet, with a reduced temperature dependence relative to the THF solutions [60]. The addition of a number of ligands L immediately produces yellow solutions of the stable 18-electron adducts $[FeH(dppe)_2(L)]^+$ (L = Me_2CO, N_2, H_2, py, NH_3, MeCN, PhCN, $P(OR)_3$, CO). Although the magnetic properties of this 16-electron species do not appear to have been investigated, it seems likely that the ion carries two unpaired electrons, in order to rationalize

its relative resistance to achieving a saturated configuration by ligand coordination [37]. The related complex $[FeH\{P(CH_2CH_2PPh_2)_3\}]^+$ was first described by Sacconi [83] as yellow and diamagnetic, but a later study by Bianchini reports it as a violet paramagnetic compound ($\mu_{eff} = 3.05\ \mu_B$) [19].

$$[FeH(dppe)_2]^+ + THF \rightleftharpoons [FeH(dppe)_2(THF)]^+ \quad (12)$$

6.3.4 15-electron complexes

Compound Cp_2TiH was shown to exist in two forms, a violet dimer with a symmetrical $Ti_2(\mu\text{-}H)_2$ bridge and a gray-green form, thought to be polymeric. The use of Cp*, on the other hand, allows stabilization of the monomeric species. $Cp^*_2TiH^\cdot$ was first mentioned to result from the decomposition of $Cp^*_2TiH_2$ [84], but a better synthesis is the reaction of $Cp^*_2Ti(CH_3)^\cdot$ with H_2 [39]. Its molecular structure has been reported [47] as well as that of the corresponding $(C_5Me_4Ph)_2TiH^\cdot$ [85a].

The complex $[CrH(H_2O)_5]^{2+}$ briefly mentioned in the introduction is obtained by pulse radiolysis from aqueous Cr^{2+}, but this is an unstable species which decomposes by protonolysis. Its spectroscopic properties are similar to those of the analogous alkyl species, known to adopt a spin quartet configuration [3]. On the other hand, the isoelectronic, sterically protected $Tp^{t\text{-}Bu,Me}CoH$ complex [$Tp^{t\text{-}Bu,Me}$ = hydrotris(3-*tert*-butyl-5-methylpyrazolyl)borate], also having a spin quartet ground state, could be isolated and characterized by X-ray crystallography [85b].

6.4 FUNDAMENTAL PROPERTIES OF THE METAL-HYDROGEN BOND

In many cases, the reactivity of paramagnetic hydrides can be traced to changes in the fundamental properties of the metal-hydrogen bond relative to the 18-electron compounds from which they are prepared or generated *in situ*. Before examining the various reactivity pathways of paramagnetic hydride complexes, it is therefore necessary to review our current knowledge in this area.

The classical picture of the terminal M-H bond is that shown in Scheme 5, where the hydrogen atom 1s orbital combines with an appropriate metal fragment hybrid orbital to generate the bonding and antibonding combinations. A more detailed description of the M-H bond properties according to this scheme is provided in the Chapter by Jacobsen and Berke in this Monograph. While the energy of the H 1s orbital is constant, the energy of the metal fragment orbital is tunable by appropriate choice of metal, ligand, and *metal oxidation state*. We

are concerned here with how a variation of the oxidation state reflects on the fundamental bond properties.

6.4.1 Metal-hydrogen bond polarity

Although this has been a topic of some controversy, it is now widely accepted that electronically saturated hydride complexes have a $M^{\delta+}$-$H^{\delta-}$ bond polarity, even for those hydride complexes undergoing facile acid dissociation in water. This situation is indicative of the predominance of H 1s character in the bonding combination of Scheme 5 and to the common view that hydrogen is more electronegative than the transition metals. Ligands having a strong donating power tend to raise the energy of the metal fragment orbital, lowering the metal electronegativity, and increasing the hydride "hydridicity", while strongly π accepting ligands should have the opposite effect. Therefore, the established $M^{\delta+}$-$H^{\delta-}$ bond polarity of compounds such as $CoH(CO)_4$ suggests that most if not all electronically saturated metal hydride compounds should indeed have this kind of electronic distribution.

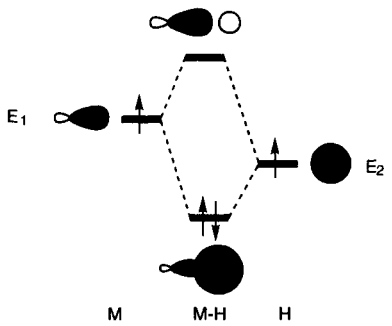

Scheme 5

The energy of a metal fragment orbital, however, can be changed in a much more dramatic way by a redox process. Removal of one electron from a mainly metal based orbital lowers the energy of the metal fragment orbital participating in M-H bonding. This change has the predictable effect of lowering the hydridic ($H^{\delta-}$) character and may even lead to an inversion of polarity, yielding a hydride ligand carrying a partial positive charge in the ground state. To our knowledge, neither experimental nor theoretical studies have addressed so far this issue that constitutes, on the other hand, knowledge or paramount importance to analyze chemical reactivity on a quantitative basis. On the other hand, the effects of this predicted bond polarity change on chemical reactivity, notably on the thermodynamic acidity, have been analyzed in detail at the experimental level. The

effects on hydrogen atom transfer reactivity (homolytic bond strength) have also received some attention, while nothing is known about oxidation state effects on the hydridicity.

6.4.2 Thermodynamic acidity

A seminal work by Ryan, Tilset and Parker has established that one-electron oxidation of a number of 18-electron monohydride complexes increases the thermodynamic acidity by a factor of approximately 10^{20}, see equation 13 [86]. Subsequent work on related compounds has shown acidity increases up to 30 orders of magnitude upon oxidation [24] (see Table 1).

$$pK_a([MH]^{+\bullet}) \approx pK_a(MH) - 20 \quad (13)$$

Table 1. Differences in thermodynamic acidity of redox-related 18- and 17-electron hydrides

M^nH complex[a]	$E_{1/2}(M^{n-1/n})$ (V)	$E_{1/2}(M^{n/n+1}H)$ (V)	$pK_a(M^nH)$-$pK_a(M^{n+1}H)$	ref.
$CpCrH(CO)_3$	-0.688	0.668	22.8	[86]
$Cp^*CrH(CO)_3$	-0.83	0.55	23.3	[87]
$CpCrH(CO)_2\{P(OMe)_3\}$	-1.11	0.28	23.5	[87]
$CpCrH(CO)_2(PPh_3)$	-1.29	0.12	23.9	[87]
$CpCrH(CO)_2(PEt_3)$	-1.51	0.00	25.5	[87]
$CpMoH(CO)_3$	-0.385	0.800	19.9	[86]
$Cp^*MoH(CO)_3$	-0.603	0.561	19.6	[86]
$CpWH(CO)_3$	-0.379	0.758	19.1	[86]
$CpWH(CO)_2(PMe_3)$	-1.119	0.195	21.5	[86]
$TpMoH(CO)_3$	-0.521	0.596	18.9	[88]
$Tp^*MoH(CO)_3$	-0.583	0.297	19.2	[88]
$TpWH(CO)_3$	-0.582	0.246	19.8	[88]
$Tp^*WH(CO)_3$	-0.652	0.208	19.6	[88]
$[CrH(CO)_2(dppm)_2]^+$	-1.25	0.52	30.0	[24]
$[CrH(CO)_2(dppe)_2]^+$	-1.04	0.70	29.5	[24]
$[MoH(CO)_2(dppm)_2]^+$	-0.92	0.73	27.9	[24]
$[MoH(CO)_2(dppe)_2]^+$	-0.68	0.87	26.2	[24]
$[WH(CO)_2(dppm)_2]^+$	-0.95	0.75	28.8	[24]
$[WH(CO)_2(dppe)_2]^+$	-0.68	0.82	25.4	[24]

[a]Abbreviations: Tp = hydrotris(pyrazolyl)borate; Tp* = hydrotris(3,5-dimethylpyrazolyl)-borate

These results derive from experimental measurements of the MH acidity and the MH and M^- oxidation potentials, see Scheme 6. It is important to underline that the absolute thermodynamic acidity of a compound is a parameter that depends on the choice of solvent. The pK_a value of a given hydride complex

in, say MeCN will be different than the pK_a in water. However, the formula given in Scheme 6 should be solvent independent, provided the solvent does not directly participate in the given equilibria other than by their solvation effect (*e.g.* by coordination). This is a rather critical point, because 17-electron species have been shown to establish rapid and reversible equilibria to afford 19-electron species [89]. If the equilibrium constant of this coordination process lies far on the 19-electron side, a significant shift of the redox potential will result. The formula in Scheme 6 is nevertheless a good first approximation, because compensation effects will operate if the two 17-electron species $M^{\bullet}$ and $M\text{-}H^{+\bullet}$ establish similar solvent coordination equilibria. More accurate thermodynamic information can only be obtained by carrying out detailed investigations of the solvent coordination process.

			$^2G^\circ$	
M-H	$\rightleftharpoons$	$M^- + H^+$	$2.301(RT)[pK_a(M\text{-}H)]$	
M^-	$\rightleftharpoons$	$M^{\bullet} + e^-$	$FE^\circ_{ox}(M^-)$	$pK_a(M\text{-}H^{+\bullet}) - pK_a(M\text{-}H) =$
$M\text{-}H^{+\bullet} + e^-$	$\rightleftharpoons$	M-H	$-FE^\circ_{ox}(M\text{-}H)$	$[F/2.301(RT)][E^\circ_{ox}(M^-) - E^\circ_{ox}(M\text{-}H)]$
$M\text{-}H^{+\bullet}$	$\rightleftharpoons$	$M^{\bullet} + H^+$	$2.301(RT)[pK_a(M\text{-}H^{+\bullet})]$	

Scheme 6

6.4.3 Metal-hydrogen homolytic bond strength

From the bonding picture in Scheme 5 and from perturbation theory, one can predict that the homolytic bond strength will be proportional to the orbital overlap and inversely proportional to the energy difference $|E_1\text{-}E_2|$ between the two participating orbitals. The prediction of the effect of a variation of oxidation state on the homolytic bond strength is not an easy excercise. The reason is that a change of oxidation state will independently affect $|E_1\text{-}E_2|$ and the orbital overlap.

We shall examine the effect of oxidation. As already mentioned, oxidation lowers the energy of the metal fragment orbital. The $|E_1\text{-}E_2|$ term will therefore decrease with the effect of increasing the bond strength, unless of course the bond polarity is inversed and the $|E_1\text{-}E_2|$ term (absolute value) is in the end greater. As for the effect on overlap, oxidation contracts the metal fragment orbital, leading to a decreased orbital overlap. However, the resulting decrease of metal covalent radius also allows a closer approach of the hydrogen atom to the metal and an opposite effect on overlap. The overall effect is not easily predictable. Corresponding arguments may be presented for a metal reduction process.

Table 2. Variation of M-H stretching frequencies for redox-related 18- and 17-electron hydride complexes

Compound[a]	M-H stretching frequencies (cm^{-1}) M^nH	$M^{n+1}H$	Ref.
$[CoH(dppe)_2]^{0/+\bullet}$	1884	1885	[74, 94]
$[CoH\{P(OEt)_3\}_4]^{0/+\bullet}$	1964	1930	[74, 93]
$[CoH\{P(CH_2CH_2PPh_2)_3\}]^{0/+\bullet}$	1780	1815	[72, 95]
$[RhH(CO)(PPh_3)]^{0/+\bullet}$	2004	2100	[74, 96]
$[IrH(CO)(PPh_3)]^{0/+\bullet}$	2068	2100	[74, 96]
$[WCl_2H_2(PMe_3)_4]^{0/+\bullet}$	1940 (br)	1940 (m), 1920 (m)	[1]
$[WCl_2H(MeCN)(PMe_3)_4]^{+/2+\bullet}$	1960 (sh), 1920 (m, br)	1950 (m), 1930 (sh)	[1]
$[Cp^*FeH(dppe)]^{0/+\bullet}$	1869	1886[b]	[63, 64]
$[Cp^*FeH(dppp)]^{0/+\bullet}$	1800	1845	[92]
$[CpFeH(dippe)]^{0/+\bullet}$	1911	1939	[65]
$[Cp^*FeH(dippe)]^{0/+\bullet}$	1901	1915	[65]
$[Cp^*WH_3(dppe)]^{0/+\bullet}$	1885 (m-w, br), 1815 (m, br)	1897 (m, br), 1830 (w, br)	[42]

[a]Abbreviations: dppp = $Ph_2PCH_2CH_2CH_2PPh_2$; dippe = $^iPr_2PCH_2CH_2P^iPr_2$. [b]This value was incorrectly reported in the original paper [90].

The little availability of stable paramagnetic hydrides has limited the spectroscopic investigations with relevance to the M-H bond nature and strength. A few redox-related pairs of 18- and 17-electron hydride complexes have been studied by IR spectroscopy. While some compounds exhibit low-frequency shifts for the M-H stretching vibrations upon oxidation, other systems show the opposite effect (see Table 2). Some of these variations should be taken with caution, since some redox pairs were examined independently by different authors under sometimes unspecified and likely different conditions of phase (solid, solution) and solvent. The high-frequency shifts observed for $[Cp^*WH_3(dppe)]^{0/+\bullet}$ and the $[Cp^*FeH(L\text{-}L)]^{0/+\bullet}$ systems have been reproduced by DFT calculations on the model $[CpWH_3(PH_2CH_2CH_2PH_2)]^{+\bullet}$ (see Figure 4) and $[CpFeH(PH_2CH_2CH_2PH_2)]^{+\bullet}$ systems [42, 90]. The simple bonding theories tell us that a bond force constant is directly related to the bond strength [91], thus the data in Table 2 would seem to indicate M-H bond strengthening for most hydride compounds upon oxidation.

Electrochemical studies on cyclopentadienylchromium and hydrotris-(pyrazolyl)borate group 6 metal carbonyl hydride derivatives have allowed an estimate of the activation toward homolytic M-H bond cleavage upon one-electron oxidation, by use of the thermodynamic cycle in Scheme 7 [87, 88].Rapid radical dimerization usually precludes the determination of $E°_{ox}(M^{\bullet})$. However, the radicals $CpCr(CO)_2(PR_3)^{\bullet}$, $Cp^*Fe(dppe)^{\bullet}$, $TpM(CO)_3^{\bullet}$ and $Tp^*M(CO)_3^{\bullet}$ (Tp = hydrotris(pyrazolyl)borate; Tp* = hydrotris(3,5-dimethyl pyrazolyl) borate; M = Cr, Mo, W) are stable enough for their oxidation

potentials to be measured, upon *in situ* electrochemical generation from the corresponding anions. The result of these studies (see Table 3) is that the BDE of the M-H bond becomes 6-11 kcal/mol *weaker* upon one-electron oxidation. For the iron system, the availability of two consecutive oxidation potentials for both the hydride complex and the radical species, and the extension of Scheme 7, allow the calculation of a further BDE decrease of 23.9 kcal/mol upon going from Fe(III) to Fe(IV) [97].

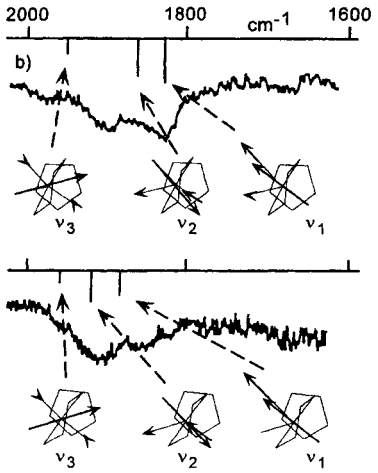

Figure 4. Room temperature IR spectra of $Cp^*WH_3(dppe)$ (top) and $[Cp^*WH_3(dppe)]^{+\bullet}$ (bottom) in THF. The normal modes and relative intensities corresponding to the frequencies ν_1, ν_2 and ν_3 are obtained from DFT calculations on geometry optimized $[CpWH_3(H_2PCH_2CH_2PH_2)]^{0/+\bullet}$. Reprinted in part with permission from ref. [42]. Copyright 1999 American Chemical Society.

			$\Delta G°$	
M-H	$\rightleftharpoons$	$M^\bullet + H^\bullet$	BDE(M-H)	
$M^\bullet$	$\rightleftharpoons$	$M^+ + e^-$	$FE°_{ox}(M^\bullet)$	$BDE(M\text{-}H^{+\bullet}) - BDE(M\text{-}H) =$
$M\text{-}H^{+\bullet} + e^-$	$\rightleftharpoons$	M-H	$-FE°_{ox}(M\text{-}H)$	$F[E°_{ox}(M^\bullet)\text{-}E°_{ox}(M\text{-}H)]$
$M\text{-}H^{+\bullet}$	$\rightleftharpoons$	$M^+ + H^\bullet$	$BDE(M\text{-}H^{+\bullet})$	

Scheme 7

The same electrochemical studies indicate that the same bonds are activated towards heterolysis (see previous section, Scheme 6) by at least 32-35 kcal/mol [87, 88]. The equations of Schemes 6 and 7 can be combined and rearranged

to give $\Delta\Delta G_{het} - \Delta\Delta G_{hom} = F(E_{ox}(M^-) - E_{ox}(M^\bullet))$. This implies that the heterolytic activation will be greater than the homolytic activation if $E_{ox}(M^\bullet) > E_{ox}(M^-)$, which is the expected trend. These results should be taken with caution since, once again, as for the case of the thermodynamic acidity examined in the previous section, neglet is made of the possible solvent coordination to $M^\bullet$, $M\text{-}H^{+\bullet}$ and especially M^+ with consequent significant potential shifts. At the very least, it would seem necessary to verify that the measured potentials are solvent independent. However, the results of these investigations do agree with the experimental evidence that proton transfer rather than H atom transfer follows one-electron oxidation in most cases (see section 6.5).

Table 3. Difference in homolytic bond dissociation energies of redox-related 18- and 17-electron hydrides[a]

M^nH complex	$E_{1/2}(M^{n/n+1})$ (V)	$BDE(M^nH)$-$BDE(M^{n+1}H)$ (kcal/mol)	ref.
$Cp^*CrH(CO)_3$	0.19	8	[87]
$CpCrH(CO)_2\{P(OMe)_3\}$	-0.21	11	[87]
$CpCrH(CO)_2(PPh_3)$	-0.29	10	[87]
$CpCrH(CO)_2(PEt_3)$	-0.37	9	[87]
$TpMoH(CO)_3$	0.311	6.4	[88]
$Tp^*MoH(CO)_3$	0.297	6.0	[88]
$TpWH(CO)_3$	0.246	7.9	[88]
$Tp^*WH(CO)_3$	0.208	6.9	[88]
$Cp^*FeH(dppe)$	-1.272[b]	12.2	[97]

[a]The necessary values of $E_{1/2}(M^{n/n+1}H)$ for the calculation of Δ(BDE) according to the equation in Scheme 7 are listed in Table 1. [b]$E_{1/2}(M^{n/n+1}H) = -0.747$ V.

It may be noted that for the same system, $Cp^*FeH(dppe)$, the IR studies indicate M-H bond strengthening while the electrochemical data lead to the calculation of a bond weakening upon oxidation. Theoretical investigations have attempted to throw light onto this matter. System $[Cp^*WH_3(dppe)]^{0/+\bullet}$ has been modelled by the corresponding $[CpWH_3(PH_2CH_2CH_2PH_2)]^{0/+\bullet}$ [42]. The DFT calculations yield a BDE of 66.1 kcal/mol for the neutral system and 65.1 kcal/mol for the cation (relative to the optimized ground state triplet minimum for the 16-electron $[CpWH_2(PH_2CH_2CH_2PH_2)]^+$). On the other hand, dissociation to the singlet excited state is more costly, 77.2 kcal/mol. In addition, the optimized $[CpWH_3(PH_2CH_2CH_2PH_2)]^{n+}$ geometries show a slight W-H bond contraction on going from n = 0 to n = 1. Thus, the available experimental and theoretical evidence points to a M-H bond strengthening upon oxidation. Unfortunately, the unavailability of the 17-electron complex $Cp^*WH_2(dppe)^\bullet$ makes it impossible

to apply the electrochemical method of Scheme 7 to this system.

A model system of the $[Cp^*FeH(dppe)]^{0/+\bullet}$ redox pair, $[CpFeH(PH_2CH_2CH_2PH_2)]^{0/+\bullet}$, has also been investigated theoretically with DFT [90]. These calculations, like those of the above mentioned tungsten system, reveal a slight Fe-H bond shortening and an increase of the Fe-H stretching frequency, in agreement with the experimental IR data. On the other hand, a calculation of BDE (without the consideration of geometry relaxation effects) indicates bond weakening. Thus, while the theory appears to match again the experiment, a conflict remains between the M-H stretching frequencies and the electrochemical results for this system. One consideration that may be advanced [98] is the possible lack of a direct relationship between the BDE (which describes the homolytic spitting of the bond to leave one electron on each partner) and the M-H stretching frequency which reflects on the other hand the actual covalent polar characteristics of the bond. Thus, the normal mode force constant (curvature of the energy surface at the minimum) would reflect the bond charge distribution or ionic component of the M-H interaction but not necessarily the bond strength in a homolytic dissociation sense.

From the above studies, it is evident that the effect of an oxidation state change on the M-H homolytic bond strength is far from being clear, and results obtained on a specific system may not lend themselves to extrapolation or generalization. Further investigations on this deceptively simple chemical bonding topic are most definitely necessary.

6.5 DECOMPOSITION MECHANISMS OF 17-ELECTRON HYDRIDE COMPLEXES

6.5.1 Deprotonation

Early work by Pilloni *et al.* has shown that neutral hydride complexes readily lose protons following oxidation to cationic products. Electrolysis of $IrH(CO)(PPh_3)_3$ on the second oxidation wave in dichloroethane produces a 1:1 ratio of $[Ir(CO)(PPh_3)_3]^+$ and $[IrH_2(CO)(PPh_3)_3]^+$, while electrolysis of the stable first oxidation product $[IrH(CO)(PPh_3)_3]^+$ produces $[Ir(CO)(PPh_3)_3]^+$ and H^+ [74]. This shows that the coordinatively unsaturated $[IrH(CO)(PPh_3)_3]^{2+}$ complex is unstable in dichloroethane and loses a proton, which is captured by $IrH(CO)(PPh_3)_3$ when this is present. While deprotonation does not occur, in this case, on the paramagnetic first oxidation product, this study was probably the first one to highlight an increase of acidity upon oxidation. A similar phenomenon was described for the 2-electron oxidations of $PtClH(PEt_3)_2$ [99] and of the group 8 complexes $MClH\{P(CH_2CH_2PPh_2)_3\}$ (M = Fe, Ru, Os), these being

interpreted as EEC processes [100].

A reversible deprotonation for a 17-electron hydride complex was shown for the stable cationic cobalt(II) hydride complex $[CoH\{CH_3C(CH_2PPh_2)_3\}(PEt_3)]BPh_4$, yielding a presumed Co(0) neutral species. Although the latter species could not be isolated and fully characterized, it was shown that it can be reprotonated to yield the Co(II) hydrido species back [40]. Polyhydride complexes have also been shown to readily lose protons. Early examples have been provided by Walton on rhenium compounds, *e.g.* $ReH_5(PR_3)_3$ derivatives [101], on the basis of electrochemical investigations.

Following oxidation, a rearrangement of a classical polyhydride to a dihydrogen complex is possible (Scheme 1). However, dihydrogen complexes are kinetically more acidic than the corresponding classical tautomers. In addition, the starting neutral complex may already adopt a nonclassical form. Oxidation is again followed by deprotonation, as in the electrochemical investigation of $[M(H_2)\{P(CH_2CH_2PPh_2)_3\}]^+$ (M = Co, Rh) [19].

When 17-electron complexes generated by oxidation decompose by deprotonation, the overall stoichiometry is highly dependent on the nature of the base capturing the proton, on the stability of the proton transfer products, and on the rate of oxidation. Equation 14 shows proton capture by an external base (e.g. pyridine or lutidine, often used for this kind of studies). The resulting 17-electron deprotonated radical may in principle evolve by either dimerization (equation 15), or by reaction with the paramagnetic hydride precursor, (equation 16), or by subsequent oxidation, which is usually assumed to be preceded by solvent coordination (equations 17-18) [86]. The oxidation potential of $M(S)^\bullet$ may be less positive than that of the MH precursor, resulting in an overall two-electron process for the oxidation of MH.

$$[MH]^{+\bullet} + B \longrightarrow M^\bullet + BH^+ \quad (14)$$

$$M^\bullet + M^\bullet \longrightarrow M\text{-}M \quad (15)$$

$$M^\bullet + [MH]^{+\bullet} \longrightarrow [M(\mu\text{-}H)M]^+ \quad (16)$$

$$M^\bullet + S \rightleftharpoons M(S)^\bullet \quad (17)$$

$$M(S)^\bullet \xrightarrow{-e^-} [M(S)]^+ \quad (18)$$

The observed overall stoichiometry involves consumption of one or two oxidizing equivalents per mole, as indicated in equations 19 and 20 on one side, and equation 21 on the other side. The choice between equations 19 and 20 is determined by the relative basicity of B and the metal-metal bonded system.

$$2\,MH + 2\,B - 2\,e^- \longrightarrow M\text{-}M + 2\,BH^+ \quad (19)$$

$$2\,MH + B - 2\,e^- \longrightarrow [M(\mu\text{-}H)M]^+ + BH^+ \quad (20)$$

$$MH + B + S - 2e^- \longrightarrow [M(S)]^+ + BH^+ \quad (21)$$

Kochi *et al.* [54] had reported that the controlled-potential electrolysis of $CpMoH(CO)_3$ at 0.50 V vs. SCE required 1.08±0.05 electrons per molybdenum and that the dimer $[CpMo(CO)_3]_2$ was the isolated product, in agreement with equation 19. Tilset *et al.*, however, reported a different result under apparently identical conditions, both in terms of stoichiometry (2.1±0.1 F/mol) and oxidation product, $[CpMo(CO)_3(MeCN)]^+$, in agreement with equation 21 [86]. Kochi's report appears puzzling in view of the easier oxydation of $[CpMo(CO)_3]_2$ (+0.55 V) relative to $CpMoH(CO)_3$ (+0.80 V) in the acetonitrile solvent used for the experiment. No other oxidation process following the stoichiometry of eq. 19 appears to have been documented.

The formation of hydride-bridged dimers according to equation 20, on the other hand, has been established more than once. Electrolysis of Cp_2WH_2 in acetonitrile leads, after workup, to purple crystals of $[(Cp_2W)_2H_3][ClO_4]$, which have been characterized by ^1H NMR and X-ray crystallography. The three hydride ligands could not be located and the ^1H NMR shows a single hydride resonance, but a rapid fluxional process averaging chemically inequivalent hydride positions cannot be excluded. The $[(Cp_2WH)_2(\mu\text{-}H)]^+$ formulation appears most consistent with a space filling analysis [54]. Oxidation of $CpRuH(CO)(PMe_3)$ leads to a hydride-bridged dimer in the presence 2,6-lutidine, while the stronger base pyrrolidine requires the consumption of two oxidizing equivalents according to eq 21 (see Scheme 8) [102].

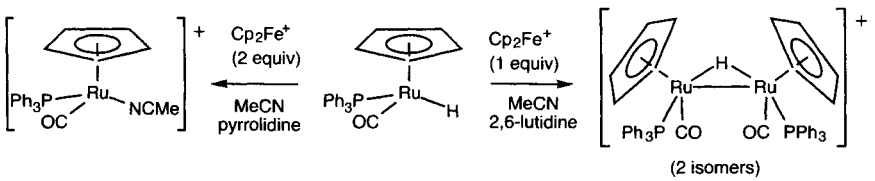

Scheme 8

The stoichiometry of equation 21 is the most common one, whenever a strong base is added to the system being oxidized or electrolyzed. Other examples are provided by $CpMoH(CO)_2(PPh_3)$, $CpWH(CO)_2(PMe_3)$ and $CpRuH(CO)(PMe_3)$ in the presence of 2,6-lutidine [86, 102, 103]. For complexes loaded with π acceptor ligands, thus leading to extremely acidic oxidized species, even the water present in the electrolytic cell often leads to consumption of two oxidizing equivalents [86, 104]. A stoichiometry corresponding to equation 21 has also been observed during the anodic scan at low rates of *trans*-$[FeH(CNMe)(dppe)_2]^+$, although in this case the product of the second oxidation step is able to abstract a fluoride ion from the BF_4^- electrolyte, to afford *trans*-$[FeF(CNMe)(dppe)_2]^+$ as the final product [105].

Under favourable circumstances, the 17-electron product of deprotonation, M•, may be sufficiently stabilized by addition of a molecule S (spin trap) which is capable of delocalizing the unpaired electron density and allow the direct observation of the adduct M(S)•. An example was shown in eq. 10 [54].

Yet additional possibilities arise from proton capture by the unoxidized complex M-H. This species has basic properties by virtue of metal lone pairs (only for d^n configurations with $n \geq 2$), other ligands lone pairs, or even the hydride itself (leading to the formation of a H_2 σ-complex). It has been shown in many cases, in fact, that a M-H complex has a greater kinetic basicity at the hydride ligand, even when the thermodynamically stable protonation product is a classical polyhydride [106-110]. The proton transfer step to MH is shown in equation 22. The fate of M• is in principle the same as above (equations 15, 16 or 17-18), leading to the possible overall stoichiometries of equations 23, 24 and 25, respectively.

$$[MH]^{+\bullet} + MH \longrightarrow M^{\bullet} + [MH_2]^+ \quad (22)$$

$$2MH - e^- \longrightarrow 1/2\ M\text{-}M + [MH_2]^+ \quad (23)$$

$$3MH - 2e^- \longrightarrow [M(\mu\text{-}H)M]^+ + [MH_2]^+ \quad (24)$$

$$2MH + S - 2e^- \longrightarrow [M(S)]^+ + [MH_2]^+ \quad (25)$$

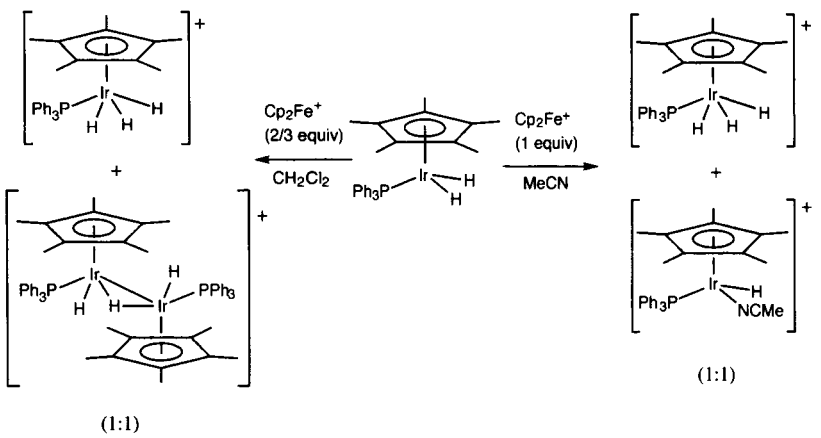

Scheme 9

For instance, the ferrocenium oxidation of $Cp^*IrH_2(PPh_3)$ follows the stoichiometry of equation 24 in dichloromethane and that of equation 25 in MeCN (see Scheme 9) [111]. Equation 24 is also found for the oxidation of $CpRuH(CO)(PMe_3)$ in MeCN in the absence of an external base, except that the $[CpRuH_2(CO)(PMe_3)]^+$ product further reacts under these conditions with

loss of cyclopentadiene and generation of $[RuH(CO)(PMe_3)(MeCN)_3]^+$ which is observed together with $[\{CpRu(CO)(PMe_3)\}_2(\mu\text{-}H)]^+$ in a 1:1 ratio [102].

Reaction 22 is deceptive in that it could proceed by H^+ transfer from the radical to MH or by H atom transfer from MH to the radical. Is the 17-electron $[MH]^{+\bullet}$ species a proton donor or a H atom acceptor in this case? Studies by Caulton have shown that the oxidation of $IrH_3(PMe_2Ph)_3$ in CH_2Cl_2 consumes 1 equivalent of ferrocenium according to the stoichiometry of eq. 25, yielding an unstable solvent adduct $[IrH_2(CH_2Cl_2)(PMe_2Ph)_3]^+$ and the tetrahydrido derivative $[IrH_4(PMe_2Ph)_3]^+$, while when the same experiment is conducted in acetone in the presence of excess pyridine or Et_3N, two equivalents of ferrocenium are required (equation 21), leading to the sole product $[IrH_2(L)(PMe_2Ph)_3]^+$ (L = py or Me_2CO, respectively) [112]. This result is in favour of a proton transfer mechanism for eq. 22. Under favourable circumstances, however, 17-electron hydride compounds may indeed behave as H atom scavengers (see Section 6.5.6).

In addition, the deprotonation process allows additional stoichiometric variations depending on the stability of the protonated hydride complex MH_2^+, which may prefer either the classical or the nonclassical tautomeric form. In the latter case, the product may be unstable, depending on the reaction conditions, toward replacement of H_2 by a solvent molecule, leading to the possible alternative stoichiometries of equations 26-28.

$$2MH + S - e^- \longrightarrow 1/2\ M\text{-}M + [M(S)]^+ + H_2 \quad (26)$$

$$3MH + S - 2e^- \longrightarrow [M(\mu\text{-}H)M]^+ + [M(S)]^+ + H_2 \quad (27)$$

$$2MH + 2S - 2e^- \longrightarrow 2\,[M(S)]^+ + H_2 \quad (28)$$

The above mentioned $IrH_3(PMe_2Ph)_3$ is oxidized according to eq. 25 in CH_2Cl_2 and according to eq. 28 in MeCN when no extended base is added [112]. The ferrocenium oxidation of $CpMH(CO)_2(PR_3)$ (M = Mo, W; R = Me, Ph) in *dry* acetonitrile requires only one equivalent of oxidant for both metal systems. The observed difference in the reaction products ($[CpMo(CO)_2(PR_3)(MeCN)]^+$ and H_2 for Mo, eq 28, and a 1:1 mixture of $[CpW(CO)_2(PR_3)(MeCN)]^+$ and $[CpWH_2(CO)_2(PR_3)]^+$ for W, eq 25) [86, 104], is easily ascribed to the greater ability of the heavier metal to oxidatively add H_2 and yield a stable classical dihydride product, while an analogous product is unstable for Mo. Indeed, attempts to protonate $CpMoH(CO)_2(PMe_3)$ at -80°C in pentane have resulted in an immediate H_2 evolution from the putative $[CpMo(\eta^2\text{-}H_2)(CO)_2(PMe_3)]^+$ intermediate [104], while an isolobal $Au(PPh_3)^+$ model of this complex, $[CpMo\{\eta^2\text{-}Au_2(PPh_3)_2\}(CO)_2(PMe_3)]^+$, has been crystallographically characterized [113]. Other oxidations requiring one equivalent of oxidant in the absence of an external base are those of $CpRuH(PPh_3)_2$ [114], $Cp^*RuH_3(PPh_3)$ [20], and $OsH_6(PPr^i_3)_2$ [21].

It will be noted that, in reactions 23-28, compound MH is consumed by two competitive processes, namely oxidation and protonation. Thus, these stoichiometries will be observed when the following two conditions are satisfied: (*i*) the unoxidized complex MH is the strongest available base in the reaction medium and (*ii*) the rate of proton transfer is fast relative to the rate of oxidation of MH. When, on the other hand, the proton transfer is much slower than the electron transfer, then the oxidizing agent can finish its job and no more MH will be available to capture the proton from $[MH]^{+\bullet}$. Under these conditions, $[MH]^{+\bullet}$ can only deliver its proton (slowly) to an external base, if a sufficiently strong one is present, otherwise the product becomes kinetically stabilized toward deprotonation and can sometimes be isolated. However, other decomposition pathways may remain available, see following sections.

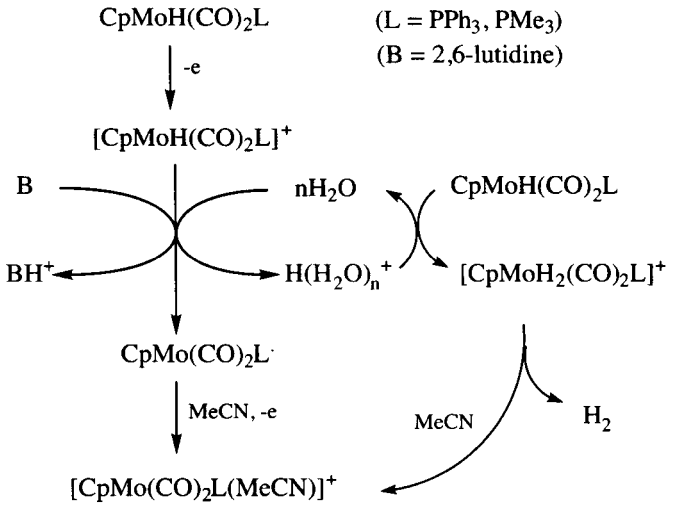

Scheme 10

The stabilization of an oxidized hydride against deprotonation can therefore be achieved by ensuring that its pK_a lies above those of the conjugate acids of the available external bases. This is easily accomplished by selecting a strongly donating coordination sphere (*e.g.* $PR_3 > PAr_3 > CO$; Cp* > Cp, etc.). However, the same modification increases the basicity of MH at the same time, so that the driving force of the proton transfer from $MH^{+\bullet}$ to MH remains unaltered at a first approximation. In brief, ligand modification may render a proton transfer *thermodynamically* unfavourable toward an external base but not toward the starting material itself. Therefore, it is always imperative to impose a low *kinetic acidity* in order to permit complete oxidation. This is easily achieved by increasing the ligand steric encumberance, rendering a close contact between the oxidized

hydride and the base more difficult. A steric protection of deprotonation has been shown, for instance, for complexes $[Cp^*FeH(dppe)]^{+\bullet}$ and $[CpMoH(PMe_3)_3]^{+\bullet}$ [17, 64]. Steric protection has also been invoked to rationalize a lack of proton transfer during the decomposition of $[CpRuH(PR_3)_2]^{+\bullet}$, which decomposes by disproportionation instead (see next section) [66].

Although the rates of outer-sphere electron transfer processes are usually quite fast for chemical oxidations in a homogenous phase, oxidation rates are low in bulk electrolysis experiments, being limited by the diffusive process. A bulk electrolysis study of $CpMoH(CO)_2(PR_3)$ (R = Me, Ph) has highlighted a competition between water as an external base and the starting material for the proton of the oxidized product. Water is the stronger base, as verified by a control protonation experiment. However, since the basicity difference is not too large, a small amount of protonated hydride is present at equilibrium. The latter, on the other hand, is unstable and irreversibly decomposes by H_2 loss (see Scheme 10). Therefore, the proton is slowly transferred from the stronger base (water), which acts as a "proton shuttle", to the weaker one. Under slow oxidation rate conditions, the shuttle has sufficient time to operate and the electrolysis consumes 1 F/mol according to eq. 28, whereas 2 F/mol are consumed under fast oxidation conditions [104]. With a stronger external base B (e.g. 2,6-lutidine), on the other hand, the consumption of 2 F/mol is measured even under slow oxidation conditions.

Water is a hardly avoidable external base in bulk electrolysis experiments, in view of the large amounts of supporting electrolyte added to the solution. The above "proton shuttle" scheme with the intervention of water allows the rationalization of several ambiguous literature reports. The reported consumption of 1.70±0.11 F/mol for the oxidation of $CpRuH(CO)(PPh_3)$ [115] (whereas 1.93±0.15 F/mol are consumed in the presence of 2,6-lutidine) can be attributed to an effective competition between oxidation and proton shuttle rates. On the other hand, in agreement with the expected trends of metal basicity, the oxidation of $CpRuH(CO)(PMe_3)$ and $CpRuH(PPh_3)_2$ requires only 1 F/mol [102, 114].

6.6.2 Disproportionation

When a 17-electron $[MH]^{+\bullet}$ species cannot deprotonate (because MH or other external bases of sufficient strength are not present, see previous section), a disproportionation may take place according to the processes indicated in equations 29 and 30.

$$[MH]^{+\bullet} + S \rightleftharpoons [MH(S)]^{+\bullet} \quad (29)$$

$$[MH(S)]^{+\bullet} + [MH]^{+\bullet} \longrightarrow [MH(S)]^{2+} + MH \quad (30)$$

An equilibrium coordination of a solvent molecule to afford a 19-electron species may occur, by analogy with the coordination to species $M^\bullet$ in eq. 17. Now,

the metal electron richness may be sufficiently increased by the coordination of S that the metal center in the 19-electron species $[MH(S)]^{+\bullet}$ becomes a sufficiently strong reductant, capable of reducing the 17-electron precursor $[MH]^{+\bullet}$ back to MH (equation 30). In many cases, the 18-electron $[MH(S)]^{2+}$ product is quite acidic and transfers a proton to its co-product MH, according to eq. 31.

$$[MH(S)]^{2+} + MH \longrightarrow [M(S)]^{+} + [MH_2]^{+} \qquad (31)$$

It is to be noted that the products of equation 31 are identical with those of equation 25. Thus, the nature of the decomposition products alone does not permit a distinction between the decomposition mechanisms by deprotonation and by disproportionation when the 17-electron hydride species is obtained by oxidation of a 18-electron precursor. The same stoichiometry of equation 25 (and also 28) is obtained from either mechanism.

Proton transfer

$$[MH]^{+\bullet} + B \xrightarrow{k} M^{\bullet} + BH^{+} \qquad \text{rate} = k[[MH]^{+\bullet}][B]$$

Disproportionation

$$[MH]^{+\bullet} + S \underset{}{\overset{K_{eq}}{\rightleftharpoons}} [MH(S)]^{+\bullet}$$

$$[MH(S)]^{+\bullet} + [MH]^{+\bullet} \xrightarrow{k} [MH(S)]^{2+} + MH \qquad \text{rate} = \frac{2K_{eq}k[[MH]^{+\bullet}]^2[S]}{1 + K_{eq}[S]}$$

Scheme 11

A distinction, however, is possible from kinetic studies (see Scheme 11). The slow step of the proton transfer mechanism is the proton transfer process (eqs. 14 and 22), thus the rate law should be first order in the radical species and first order in the base. The slow step of the disproportionation mechanism, on the other hand, is the electron transfer process following the solvent coordination pre-equilibrium, thus the rate law should be second order in the radical species and first order in the solvent under the conditions in which $K_{eq}[S] << 1$ (pre-equilibrium favouring the 17-electron species). In addition, stronger donor solvents leads to faster disproportionation processes (*e.g.* MeCN >> CH_2Cl_2, THF), while the proton transfer process should be much less solvent dependent.

This mechanism, however, presents a subtlety like that discussed in the previous section for the proton transfer mechanism. The solvent addition to the 17-electron hydride must establish a pre-equilibrium but this equilibrium must be shifted on the side of the 17-electron species, or else it must be slow relative to the rate of oxidation. If the 19-electron $[MH(S)]^{+\bullet}$ species is a stronger reductant than MH and forms extensively and rapidly relative to the rate of oxidation

(i.e. during a slow bulk electrolysis), then a direct 2-electron oxidation of MH to produce $[MH(S)]^{2+}$ is predicted to become the prevalent process and the one-electron oxidation product $[MH]^{+\bullet}$ should never accumulate in solution.

The first report of a disproportionation process for a 17-electron hydride complex was apparently that of Pilloni *et al.* [74], showing that the electrolysis of $MH(dppe)_2$ (M = Rh, Ir) on the plateau of the first one-electron oxidation wave consumes one Faraday per mole to yield a 2:1 mixture of $[Rh(dppe)_2]^+$ and H_2, or a 1:1 mixture of complexes $[Ir(dppe)_2]^+$ and $[IrH_2(dppe)]^+$, respectively. The carbonyl derivative $IrH(CO)(PPh_3)_3$ correspondingly yields a stable solution of the $[IrH(CO)(PPh_3)_3]^{+\bullet}$ product at -35°C, which decomposes upon warming to room temperature to yield a 1:1 mixture of $IrH(CO)(PPh_3)_3$ and $[IrH(CO)(PPh_3)_3(MeCN)]^{2+}$. Incidentally, it is interesting to note that the nature of the final products depends on the metal and the ancillary ligands: $2M^+ + H_2$ vs. $M^+ + MH_2^+$ for the dppe complexes of Rh and Ir, respectively, and $MH(S)^{2+}$ + MH in the carbonyl-triphenylphosphine Ir case. These variations can be fully understood on the basis of the lower metal basitity of Rh vs. Ir, and the stronger electron-withdrawing properties of CO, increasing at the same time the acidity of MH_2^+ and the tendency of M^+ to coordinate a solvent molecule (electronic unsaturation). Kinetic measurements in MeCN/toluene (50% v/v) by controlled potential coulometry coupled with amperometry at various temperatures have confirmed a second-order rate law for the decay of the 17-electron species, and have yielded activation energies of 12.5±1, 10.0±1, and 11.5±1 kcal/mol for the complexes $[IrH(dppe)_2]^{+\bullet}$, $[RhH(dppe)_2]^{+\bullet}$, and $[IrH(CO)(PPh_3)_3]^{+\bullet}$, respectively. Furthermore, kinetic measurements for the decay of $[IrH(CO)(PPh_3)_3]^{+\bullet}$ in dichloromethane/MeCN mixtures at variable [MeCN] shows that k_{obs} depends linearly on [MeCN], in agreement with the disproportionation mechanism shown in Scheme 11. The linearity and the zero intercept of the k_{obs} vs. [MeCN] line further imply that $K_{eq}[MeCN] << 1$, namely the equilibrium between the 17-electron hydride and its 19-electron MeCN solvate largely favours the former.

A disproportionation was suggested amongst various possibilities for the decomposition following the silver oxidation of $MoH_4(PMe_2Ph)_4$, but kinetic and mechanistic studies were not reported in that case [116]. The effect of concentration on the cyclic voltammograms points to decompositions by disproportionation also for the anodic studies of $[ReClH(NCR)(dppe)_2]^+$ (R = 4-XC_6H_4; X = H, Cl, F) [117] and $CpRuH(PR_3)_2$ [$(PR_3)_2$ = $(PPh_3)_2$, dppm, dppe, dppp)] [66]. The latter study also confirms the solvent dependence of this mechanism, the decomposition being faster in MeCN relative to THF.

The decomposition of $[CpMoH(PMe_3)_3]^{+\bullet}$ has been extensively investigated in our own laboratory [17]. The decomposition in THF has been kinetically assessed by EPR spectroscopy, providing the following results. In the absence of the neutral precursor, $CpMoH(PMe_3)_3$, a second order decay affords the rate constant for the disporportionation pathway: rate = $k_{disprop}[M\text{-}H^+]^2$; $k_{disprop}$ =

$7.5(8)\cdot10^{-3}$ $s^{-1}M^{-1}$. In the presence of unoxidized hydride M-H, however, the decomposition is faster and proceed by a two-term rate law: rate = $k_{disprop}[MH^{+\bullet}]^2$ + $k_{deprot}[MH^{+\bullet}][MH]$; k_{deprot} = $4.4(3)\cdot10^{-2}$ $s^{-1}M^{-1}$. The ratio of the two constants (k_{deprot}/k_{disp} = 5.8(7)) provides the comparative reactivity of $[CpMoH(PMe_3)_3]^{+\bullet}$ toward proton transfer (to the neutral hydride) and electron transfer (to another hydride radical) in THF. In acetonitrile, on the other hand, a faster decomposition takes place, presumably via a pure disproportionation mechanism [17]. The use of one equivalent of oxidant (ferrocenium) initially affords a 50:50 mixture of $[CpMoH(PMe_3)_3(MeCN)]^{2+}$ (isolated and characterized by X-ray crystallography) and unreacted starting material. This mixture rearranges slowly (>24 hours) to a 1:1 mixture of $[CpMo(PMe_3)_3(MeCN)]^{+}$ and $[CpMoH_2(PMe_3)_3]^{+}$ (Scheme 12). The initial result can be easily rationalized either by a rapid solvent coordination to the first oxidation product, yielding the 19-electron and even more easily oxidizable $[CpMoH(PMe_3)_3(MeCN)]^{+}$ intermediate, or by a rapid disproportionation of $[CpMoH(PMe_3)_3]^{+\bullet}$. The astounding inertness of $[CpMoH(PMe_3)_3(MeCN)]^{2+}$ toward deprotonation by $CpMoH(PMe_3)_3$ (a control study from isolated pure reagents requires over 24 h at room temperature to reach completion) illustrates the paramount importance of steric effects in proton transfer reactions.

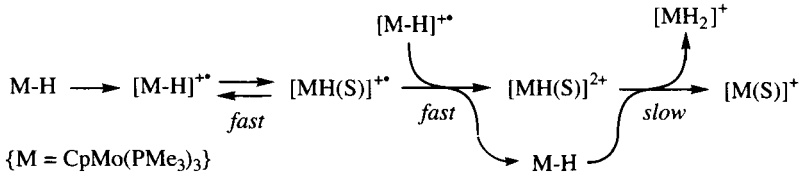

Scheme 12

A cyclic voltammetric study of $Cp^*MoH_3(dppe)$ in MeCN has allowed another kinetic assessment of the competition between deprotonation and disproportionation pathways. The oxidation wave is chemically reversible in MeCN at scan rates greater than ca. 100 mV s^{-1} but it loses reversibility at lower scan rates. The slopes of the $E_{p,a}$ vs. log v and $E_{p,a}$ vs. log c straight lines (v = scan rate, c = concentration) is consistent with a DISP2 mechanism (*i.e.* the disproportionation mechanism in Scheme 11) and furnishes k_{disp} = $3.98(9)\cdot10^{3}$ s^{-1} M^{-1}. Thin-layer cyclic voltammetric studies, however, yield slopes for the $E_{p,a}$ vs. log v and $E_{p,a}$ vs. log c straight lines in agreement with a proton transfer mechanism and yield k_{deprot} = $2.8(2)\cdot10^{2}$ s^{-1} M^{-1}. The two results are not inconsistent with each other, because the two experiments are carried out in different time domains such that disproportionation is rate limiting in CV and deprotonation is rate limiting in TLCV, as confirmed by subsequent simulations. In this case, k_{disp} is 14(1) times greater than k_{deprot} [42].

Steric protection has been shown to increase the inertness of paramagnetic hydrides not only toward deprotonation, but also toward disproportionation. While the one electron oxidation of $Cp^*MoH_3(dppe)$ in a cyclic voltammetric experiment in MeCN is chemically reversible only a rates greater than 0.1 V s^{-1}, the same process for $(C_5Et_5)MoH_3(dppe)$ remains chemically reversible even at a rate of 10 mV s^{-1} [109].

Complex $[Cp^*RuH(dppf)]^{+\bullet}$ is unusual in that it disproportionates in THF, according to eq. 32, with the expected second order rate law ($k_{disp} = 3.5 \cdot 10^{-2}$ $M^{-1}s^{-1}$ at 23°). However, the decomposition is retarded over 10-fold by the addition of 4 equivalents of the neutral species $Cp^*RuH(dppf)$ [68]. This observation means two things. Firstly, the proton transfer decomposition pathway (section 6.5.1) for this system is not as competitive as it is for $[CpMoH(PMe_3)_3]^{+\bullet}$ [17], undoubtedly because of the even greater steric encumberance which limits the approach between the acid and the base. Secondly, the electron transfer process (eq. 30) must be reversible and precede the rate determining step, which is likely to be the proton transfer raction. The reversibility of the electron transfer process may be attributed to either the poor donor ability of the THF solvent (making the 19-electron solvent adduct an insufficiently strong reductant), or to the inability of THF to coordinate to the 17-electron Ru(III) center, thereby requiring passage through a 16-electron Ru(IV) intermediate. As may be expected, the disproportionation is accelerated by the presence of small amounts of MeCN [68].

$$2[Cp^*RuH(dppf)]^{+\bullet} + THF \longrightarrow [Cp^*Ru(dppf)(THF)]^{+} + [Cp^*RuH_2(dppf)]^{+} \quad (32)$$

A disproportionation pathway has also been highligthed by Detty and Jones for complexes $[CpReH_2(PAr_3)_2]^{+\bullet}$ (Ar = *p*-C_6H_4X, X = H, Me, F, OMe) [58]. In that case, however, the disproportionation is catalyzed by further oxidation, with current efficiencies up to 20. For instance, passage of only 0.12 Faradays per mole of $[CpReH_2(PPh_3)_2]^{+\bullet}$ completely converted this species to a 1:1 mixture of $[CpReH(PPh_3)_2(MeCN)]^{+}$ and $[CpReH_3(PPh_3)_2]^{+}$, as also confirmed by chemical oxidation experiments. The 17-electron complexes are stable in both CH_2Cl_2 and MeCN solutions for extended periods of time in the absence of further oxidation.

An interesting variant of the disproportionation mechanism is provided by the use of water as a ligand. The protons of water become more acidic upon coordination to a metal center, especially when this is in a high oxidation state, thus getting involved in the overall decomposition stoichiometry with the eventual formation of hydroxo or oxo species. We have shown that the oxidation of compound $CpMoH(PMe_3)_3$ in wet acetonitrile leads to quite different products relative to the same process, described above, in dry acetonitrile [17]. The products and the proposed mechanism are shown in Scheme 13, all boxed spe-

cies being observed by ^1H NMR or EPR spectroscopy, or isolated and characterized by X-ray crystallography [118]. After the disproportionation step, the $[CpMoH(PMe_3)_3(OH_2)]^{2+}$ compound (observed by NMR) slowly transfers two protons consecutively (the hydride proton and one of the water ligand protons, in whichever order) to the starting material. The intermediate $CpMo(OH)(PMe_3)_n$ (n = 2 or 3) is not observed experimentally in this process, but can be accessed (as a spin triplet bis-PMe_3 complex) upon metathesis from $CpMoCl(PMe_3)_3$ and KOH [119, 120]. Oxidation of this hydroxo-Mo(II) intermediate by the $[CpMoH(PMe_3)_3]^{+\bullet}$ complex that has not yet disproportionated affords the isolated and structurally characterized $[CpMo(OH)(PMe_3)_3]^{+\bullet}$. Depending on the experimental conditions (amount of oxidizing agent, solvent and crystallization conditions), subsequent deprotonation and oxidation steps take place. The overall stoichiometries for the production of these three observed products are shown in equations 33-35. The likelyhood of this mechanism is further indicated by DFT calculations on a model system where PMe_3 is replaced by PH_3 [118].

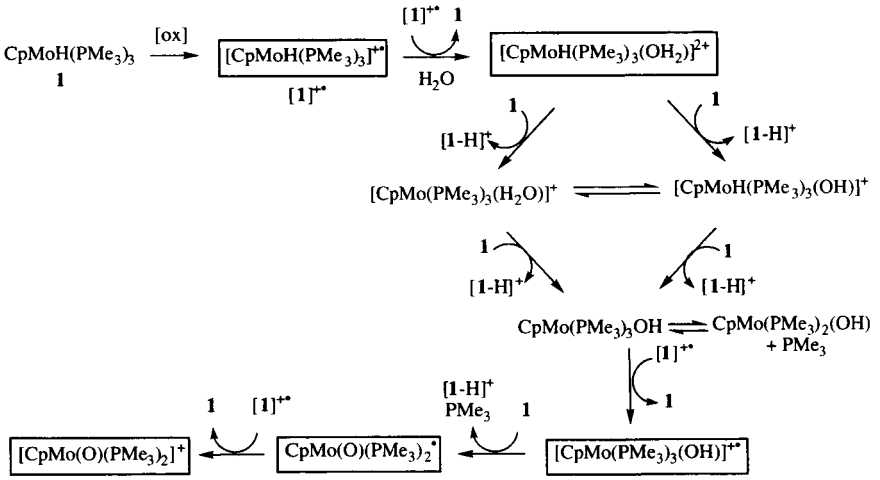

$$3\ CpMoH(PMe_3)_3 - 3e^- + H_2O \longrightarrow 2\ [CpMoH_2(PMe_3)_3]^+ + [CpMo(OH)(PMe_3)_3]^{+\bullet} \quad (33)$$

$$4\ CpMoH(PMe_3)_3 - 3e^- + H_2O \longrightarrow 3\ [CpMoH_2(PMe_3)_3]^+ + CpMo(O)(PMe_3)_2^{\bullet} + PMe_3 \quad (34)$$

$$4\ CpMoH(PMe_3)_3 - 4e^- + H_2O \longrightarrow 3\ [CpMoH_2(PMe_3)_3]^+ + [CpMo(O)(PMe_3)_2]^+ + PMe_3 \quad (35)$$

Scheme 13

The involvement of water as a ligand has been further exploited by us for the preparation or a bis-hydroxo species, $CpMo(OH)_2(dppe)^{\bullet}$, by oxidation of $CpMoH_3(dppe)$ [121].

6.5.3 *Dihydrogen reductive elimination*

Although the oxidatively induced alkyl-alkyl reductive elimination is a well established phenomenon [111, 122-125], the analogous oxidatively induced dihydrogen reductive elimination is not as widely documented, although it has been proposed to occur in a number of cases. It is know that a decrease of metal electron density favors the rearrangement of a classical polyhydride complex to the nonclassical tautomer. Therefore, it is reasonable to expect that metal oxidation triggers the same phenomenon leading to dihydrogen evolution. The concept of oxidatively induced H_2 elimination was even proposed as the basis for the development of an assay of hydrides in transition metal complexes via outer-sphere oxidation [126]. The situation, however, is greatly complicated by the two alternative decomposition mechanisms discussed in the previous sections, each of which may lead to the evolution of H_2 (vide supra). Therefore, the mere observation of H_2 evolution does not prove that an oxidatively induced reductive elimination has occurred. Metal reduction, on the other hand, is not expected to lead to the rearrangement of a classical to a nonclassical polyhydride. However, a complex which is already nonclassical in the 18-electron configuration may remain so in the reduced state, while the extra electron may reside in an orbital with M-(H_2) antibonding component and promote dihydrogen evolution. Notably, no stable or transient paramagnetic dihydrogen complex has been identified with certainty as yet [20].

We shall distinguish cases where the two hydrogen atoms are originating from the same metal (mononuclear, or 2-electron reductive elimination, equation 36) from those where each H atom is provided by a different metal (binuclear, or 1-electron reductive elimination, equation 37). The latter class of reactions is treated here, although some ambiguity may persist relative to the H atom transfer mechanism treated in the section that will follow. A bimolecular reductive elimination is meant to consist in the *direct* formation of H_2, while the H atom transfer process involves transfer of a H atom to a different site. The confusion arises from the fact that when the accepting site is a metal atom bearing other hydride ligands, the reaction may ultimately lead to H_2 evolution.

$$\longrightarrow \quad [M] + H_2 \tag{36}$$

$$[M]\text{-}H + H\text{-}[M] \longrightarrow 2\,[M] + H_2 \tag{37}$$

The [M] product is formally a 15- or 17-electron species when starting from a 17- or 19-electron complex for reaction 36, while it is a 16- or 18-electron species (from a 17-or 19-electron M-H species, respectively) for reaction 37.

Stabilization by solvent coordination or by other processes may accompany these reactions.

6.5.3.1 Mononuclear

The thermally unstable niobiocene dihydride, $Cp_2NbH_2^{\bullet}$ [32], has been proposed to decompose by H_2 reductive elimination to afford niobiocene, Cp_2Nb, on the basis of EPR spectroscopic evidence [127].

Oxidatively induced H_2 reductive eliminations have been proposed in a few cases, such as for instance the oxidation of $ReH_7(PPh_3)_2$ to ultimately yield $[ReH_6(PPh_3)_3]^+$ [101]. An anambiguous case of a dihydrogen reductive elimination from a paramagnetic polyhydride complex comes from our own mechanistic studies of the $[Cp^*MoH_3(dppe)]^{+\bullet}$ decomposition [42]. The compound undergoes competitive H_2 reductive elimination, deprotonation and disproportionation depending on the choice of solvent and other conditions. The overall decomposition mechanism is summarized in Scheme 14. All decomposition pathways occur after rearrangement of the oxidized material to the nonclassical form. This is the reason for the stability of the corresponding tungsten system, for which this rearrangement is energetically more costly. Addition of solvents to the classical form does occur, but even MeCN cannot bring the reduction potential to sufficiently low values, thus complex $[Cp^*MoH_3(dppe)(MeCN)]^{+\bullet}$ (classical isomer) is not capable of triggering the disproportionation pathway [128]. After rearrangement to the nonclassical form, however, the metal becomes electron-richer. Coordination of the poorer donors THF or CH_2Cl_2 is again not sufficient to trigger the disproportionation pathway, thus leading to an associative H_2 substitution by the solvent, whereas MeCN coordination leads to disproportionation by reduction of the 17-electron *classical* trihydride which remains the major species at equilibrium. In all solvents, however, proton transfer remains the preferred pathway in the presence of unoxidized $Cp^*MoH_3(dppe)$.

6.5.3.2 Binuclear

Binuclear H_2 reductive elimination processes from *saturated* hydride complexes to yield 17-electron products have been established for electrocatalytic dihydrogen evolution systems [6, 129]. Analogous processes have been shown to occur from 19-electron hydride complexes to yield saturated products. Compounds $[CpCoH(PR_3)_2]^+$ (R = Ph, Et, OMe) and $[CpCoH(L\text{-}L)]^+$ (L-L = dppe, dmpe, and $Ph_2PCH{=}CHPPh_2$), undergo one-electron reduction processes followed by the production of H_2 and the expected 18-electron Co(I) bis-phosphine products. In the presence of protons, catalytic H_2 evolution was shown [25]. Although the one electron reduction process for the monophosphine derivatives is irreversible at all investigated scan rates (possibly due to phosphine decoordination from the

19-electron reduction product), the reduction of $[CpCoH(dppe)]^+$ begins to show the reverse wave at scan rates greater than 1 V s^{-1}. The i_a/i_c ratio at 10 V s^{-1} was shown to be concentration dependent, indicating a second order component for the decomposition of $CpCoH(dppe)^{\bullet}$. However, direct first order decomposition by protonation competes with this process [25].

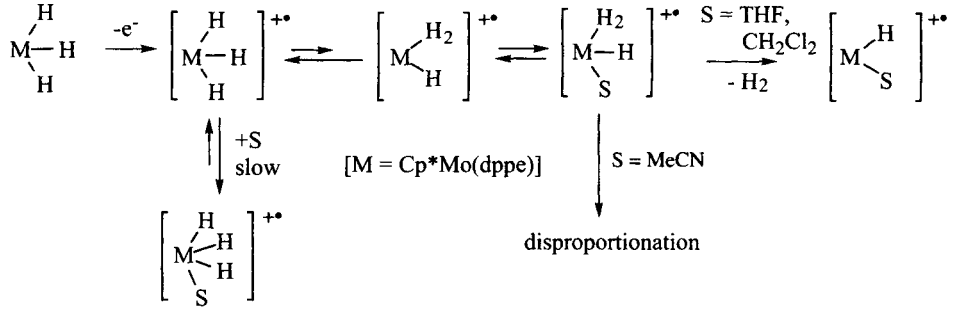

Scheme 14

The one electron reduction of $[FeH(H_2)\{P(CH_2CH_2PPh_2)_3\}]^+$ is irreversible and leads to the formation of the dihydride complex $FeH_2\{P(CH_2CH_2PPh_2)_3\}$ [19], with presumed dihydrogen evolution. It is unclear, however, whether a binuclear H_2 reductive elimination is involved in this case. The irreversible reduction of the corresponding $[FeH(N_2)\{P(CH_2CH_2PPh_2)_3\}]^+$ occurs at a slightly lower potential (-1.6 V *vs.* -1.1 V) and leads to $FeH\{P(CH_2CH_2PPh_2)_3\}^{\bullet}$ via explusion of dinitrogen [19]. Therefore, it is possible to imagine an alternative mononuclear H_2 elimination from 19-electron $FeH(H_2)\{P(CH_2CH_2PPh_2)_3\}^{\bullet}$, followed by a hydrogen atom (or the alternative coupled proton/electron) transfer (see Sections 6.5.5-6) from a second molecule of the dihydrogen complex, see Scheme 15.

A few processes reported in the literature have been interpreted as binuclear H_2 reductive elimination from 17-electron hydride complexes. This process requires, of course, the formation of 16-electron products or intermediates, unless it is preceded by coordination of a 2-electron donor to afford 19-electron complexes which then undergoes the reductive elimination process. In most cases, however, mechanistic studies (*e.g.* rate law determinations, kinetic isotope effects, use of different solvents, etc.) in support of this proposal have not been carried out. In particular, in no case can the observed process be unambiguously distinguished from a disproportionation process. Proof of the viability of a truly bimolecular one-electron reductive elimination process from 17-electron hydride complexes requires, in our opinion, additional investigations.

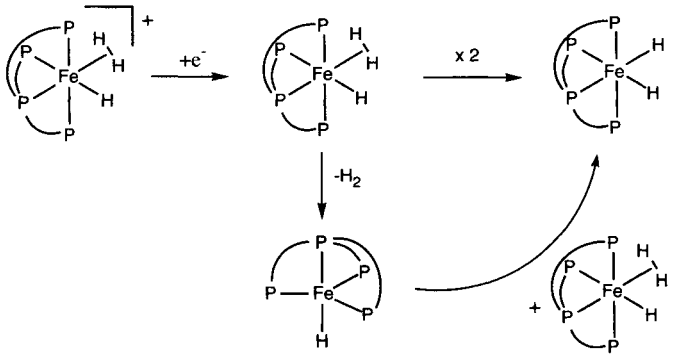

Scheme 15

Warming $[(C_5H_4SiMe_3)_2NbH\{P(OMe)_3\}]^{+\bullet}$ in the presence of $P(OMe)_3$ produces a complex which has not been isolated nor characterized spectroscopically. However, subsequent bulk electrolysis shows the consumption of 1 Faraday per mole with production of $[(C_5H_4SiMe_3)_2Nb\{P(OMe)_3\}_2]^{2+\bullet}$, as confirmed by EPR spectroscopy [51]. The formation of dihydrogen has not been confirmed experimentally, but only inferred from the stoichiometry of the follow-up oxidation process according to the proposed mechanism in Scheme 16 [Cp' = $C_5H_4SiMe_3$, L = $P(OMe)_3$].

$$2\,[Cp'_2NbHL]^{+\bullet} + 2L \longrightarrow 2\,[Cp'_2NbL_2]^{+} + H_2$$
$$[Cp'_2NbL_2]^{+} \longrightarrow [Cp'_2NbL_2]^{2+\bullet} + e^-$$

Scheme 16

Controlled potential reduction of $[ReClH(NCR)(dppe)_2]^+$ (R = 4-XC_6H_4; X = H, Cl, F) on the plateau of the first, almost reversible one-electron reduction wave affords *trans*-$ReCl(NCR)(dppe)_2$ with consumption of 1F/mole. In this case, again, neither the formation of H_2, nor the intimate details of the decomposition mechanism have been established [117].

A recent reinvestigation of the electrochemistry of $IrH(CO)(PPh_3)_3$, using dichloromethane as solvent [76], has shown slightly different results relative to the previous investigation in dichloroethane (which were the basis for the first proposal of a disproportionation mechanism, see Section 6.5.2) [74]. Bulk electrolysis on the plateau of the first oxidation wave requires one Faraday per mole and affords an approximately equimolar mixture of $[IrH(CO)(PPh_3)_3]^{+\bullet}$ and $[Ir(CO)(PPh_3)_3]^+$. These data have been interpreted with the fact that $[IrH(CO)(PPh_3)_3]^{+\bullet}$ is not completely stable on long time scales, decomposing primarily as shown in equation 38 [76].

$$2\ [IrH(CO)(PPh_3)_3]^{+\bullet} \longrightarrow 2\ [Ir(CO)(PPh_3)_3]^{+} + H_2 \qquad (38)$$

The kinetically best characterized system for which a bimolecular reductive elimination has been proposed is a neutral hydrido porphyrin derivative of Ru(III) [4]. Cyclic voltammetry and double potential step chronoamperometry afford data that are more consistent with a second order than with a first order decay for the 17-electron RuH(OEP)(L)$^{\bullet}$ (OEP = octaethylporphyrin; L = THF, 1-*tert*-bytyl-5-phenylimidazole) complexes in THF as solvent. The second order dependence of the rate constant and the independence on the parent 18-electron anion concentration exclude the proton transfer mechanism. The possibility of a disproportionation mechanism (which would afford the same second order dependence, see section 6.5.2), however, has not been considered, nor were studies in solvents other than THF carried out. In the light of the gathered information, the mechanism shown in Scheme 17 was proposed.

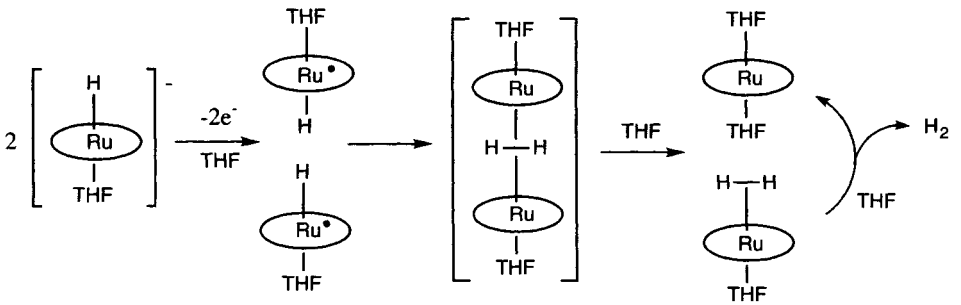

Scheme 17

Consistent with this mechanism, the derivative containing the imidazole ligand (having a stronger *trans* effect) decomposes at a faster rate, while the bulkier tetramesitylporphyrin derivative retards the dihydrogen elimination. In addition, a stable dinuclear dihydrogen complex could be obtained by use of a "puckman" porphyrin [130]. We note, however, that the same effects could be anticipated for a disproportionation mechanism. A possible difficulty for the disproportionation alternative might be related to the rigidity of the porphyrin ring, disfavouring the addition of a solvent (S) molecule to afford the putative 19-electron RuH(OEP)(L)(S)$^{\bullet}$ intermediate.

6.5.4 Alkane elimination from alkyl hydrides

The oxidation of Cp*IrH(CH_3)(PMe_3) in MeCN requires two equivalents of ferrocenium and leads to the formation of [Cp*Ir(PMe_3)($MeCN)_2$]$^{2+}$ and CH_4. The reductive elimination is intramolecular, as shown by a labelling crossover

experiment. The corresponding oxidation in CH_2Cl_2, on the other hand, requires only one equivalent of oxidant and CH_4 is again detected. Therefore, the reductive elimination process is probably taking place at the 17-electron level [111].

6.5.5 *Hydrogen atom transfer **from** the hydride radical*

Hydrogen atom transfer reactions involving 17-electron hydrides have been considered in a number of cases [54, 58, 86, 99, 112] as alternatives to proton and electron transfers, on the basis of the known atom transfer processes of hydride compounds of tin, germanium, and silicon. In addition, as discussed in section 6.4.3, there is some evidence for M-H bond weakening upon oxidation, suggesting that the homolytic rupture of this bond may take place under favourable circumstances.

Transfer of a hydrogen atom from a 17-electron hydride complex to the trityl radical has been considered as an alternative pathway to the direct hydride abstraction from a saturated hydride complex by the trityl cation (Scheme 18) [27]. The first step of this process would consist of an electron transfer, which is a likely possibility given the reduction potential of -0.08 V *vs.* Cp_2Fe/Cp_2Fe^+ for the perchlorate salt in MeCN [131], making the trityl cation a relatively strong oxidizing agent. A mechanism of this kind was shown to operate for the hydride abstraction by the trityl cation from an α-C-H bond of a rhenium alkyl complex, to afford a carbene product [132]. In addition, it is well established that C-H bonds are stronger than most transition metal - hydrogen bonds and the trityl radical is known to act as a H atom abstractor from certain 18-electron hydride complexes (see Section 6.2.3). Investigations have shown that a direct hydride transfer is in fact preferred when the oxidation potential of the hydride complex is high, *e.g.* for $CpMoH(CO)_2(PPh_3)$ [86]. More easily oxidizable hydrides, on the other hand, indeed undergo electron transfer processes with the trityl radical. However, in all reported cases the 17-electron hydride product is either stable [23, 69] or prefers to undergo other transformations than to transfer a hydrogen atom to the trityl radical. An example is provided by $CpRuH(PPh_3)_2$ [114], where the trityl radical adds to the Cp ring of the paramagnetic hydride species in the major follow-up process (see Section 6.5.9). In our laboratory, we have probed the reaction of the trityl cation with compounds $CpMoH(PMe_3)L_2$ (L = CO, PMe_3) in MeCN as solvent. While the less easily oxidizable dicarbonyl compound ($E_{1/2}$ = 0.19 V *vs.* Cp_2Fe/Cp_2Fe^+) leads to a clean hydride abstraction process [133], the tris-phosphine compound ($E_{1/2}$ = -1.46 V *vs.* Cp_2Fe/Cp_2Fe^+) leads to products resulting from disproportionation of the oxidized species (a 1:1 mixture of $[CpMoH_2(PMe_3)_3]^+$ and $[CpMo(PMe_3)_3(MeCN)]^+$) and the double oxidation product, $[CpMoH(PMe_3)_3(MeCN)]^{2+}$ [17]. It seems, therefore, that the hydrogen atom transfer from cationic 17-electron hydride complexes to the trityl radical is kinetically less viable than other reactivity pathways.

$$\{[M]\text{-}H\}^{+\bullet} + Ph_3C^{\bullet} \longrightarrow [M]^{+} + Ph_3C\text{-}H$$

Scheme 18

A direct hydrogen atom transfer has been shown to occur, on the other hand, from neutral 19-electron transients obtained by one-electron reduction of saturated cationic hydrides. These derivatives apparently have a reduced acidity relative to cationic 17-electron complexes, while the presence of an unpaired electron in an orbital which may have an M-H σ^* component may further contribute to weaken the M-H bond homolytically. An example is provided by complex $CpCoH(dppe)^{\bullet}$, which forms as a transient by one-electron reduction of $[CpCoH(dppe)]^{+}$. Cobaltocene is a strong radical scavenger, and has sufficient reducing power to carry our the reduction of the cationic cobalt hydride. Thus, reaction of the Co(III) hydride complex with *two* equivalents of cobaltocene affords $CpCo(C_5H_6)$ in 80 % isolated yields, according to the proposed mechanism of Scheme 19 [25].

$$[CpCoH(dppe)]^{+} + Cp_2Co^{\bullet} \longrightarrow CpCoH(dppe)^{\bullet} + [Cp_2Co]^{+}$$
$$CpCoH(dppe)^{\bullet} + Cp_2Co^{\bullet} \longrightarrow CpCo(dppe) + CpCo(C_5H_6)$$

Scheme 19

*6.6.6 Atom transfer **to** the hydride radical*

Atom transfer processes to organometallic radicals (17-electron), thereby generating stable 18-electron species, are widely known [134]. These processes, however, have less frequently been documented for hydride-containing species. An early example is provided by the oxidation product of $[ReH_6(PMePh_2)_2]^{-}$, the putative radical $ReH_6(PMePh_2)_2^{\bullet}$, which quantitatively reacts with the H atom donor 1,4-cyclohexadiene to afford a quantitative yield of $ReH_7(PMePh_2)_2$. In the absence of 1,4-cyclohexadiene, a slower H atom abstraction from the solvent competes with a dimerization reaction [135]. Labelling studies on this process could not be carried out, but indirect evidence for H abstraction from the solvent rather than from a second molecule of hexahydride radical or from the anionic precursor is the observation that this H atom transfer pathway is not disfavoured by low reactant concentrations.

Another example is provided by complex $[Cp^*RuH(dppf)]^{+\bullet}$, see reaction 38 [dppf = $(\eta^5\text{-}C_5H_4PPh_2)_2Fe$] [68]. This process, however, competes with the more common disproportionation pathway of decomposition (vide supra). A similar reaction is that of Cp^*_2TiH with $PbCl_2$, yielding Cp^*_2TiClH [136].

$$[Cp^*RuH(dppf)]^{+\bullet} + XY \longrightarrow [Cp^*RuH(X)(dppf)]^{+} + Y^{\bullet} \quad (38)$$
$$(XY = HSnBu_3,\ CCl_4,\ BrMn(CO)_5,\ I_2)$$

The photochemical hydrometallation reaction of electron deficient olefins (fumaronitrile, maleic anhydride, etc.) by Cp_2MH_2 (M = Mo, W) was shown to occur via electron transfer, followed by proton transfer from $[Cp_2MH_2]^+$ to the reduced olefin, and final radical recombination (scheme 20) [16].

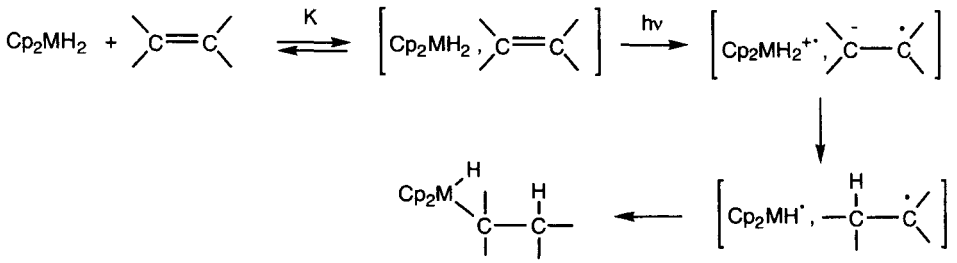

Scheme 20

6.5.7 *Dimerization*

The direct dimerization of a 17-electron hydride has rarely been documented. One example is provided by the high yield synthesis of $[OsH(CO)_4]_2$ (*Os-Os*), upon hydrogen atom abstraction from $OsH_2(CO)_4$ by $Ph_3C^{\bullet}$. Although the 17-electron $OsH(CO)_4^{\bullet}$ intermediate was not directly observed, stopped-flow kinetic and isotope effect evidence is consistent with the slow step being a H atom abstraction [33-35].

Oxidation of $[ReH_6(PMePh_2)_2]^-$ in THF leads to two different products, $ReH_7(PMePh_2)_2$ and $Re_2H_8(PMePh_2)_2$. Studies at different concentrations have shown that the two products arise from independent and competitive pathways, the first involving H atom transfer (section 6.5.6), and the latter involving dimerization of the $ReH_6(PMePh_2)_2^{\bullet}$ intermediate species with H_2 evolution. The intimate mechanism of this dimerization process could not be established. The sequence favoured by the authors (Scheme 21), however, involves combination between the radical and an additional molecule of starting material, followed by one-electron oxidation, rather than direct radical dimerization [135].

$$ReH_6(PMePh_2)_2 + [ReH_6(PMePh_2)_2]^- \longrightarrow [Re_2H_x(PMePh_2)_4]^- + (6\text{-}x/2)\ H_2$$
$$[Re_2H_x(PMePh_2)_4]^- - e^- \longrightarrow Re_2H_8(PMePh_2)_4 + (x/2\text{-}4)\ H_2$$

Scheme 21

6.5.8 *Protonation*

When a paramagnetic hydride is obtained by a one-electron reduction process starting from a saturated precursor, the electron density on the hydride ligand increases, resulting in a decrease of its acidity and an increase of its basicity

(section 6.4). An electrophilic attack at the hydride ligand becomes therefore a predictable process. One-electron reduction processes have been shown to be followed by protonation and subsequent H_2 evolution, as a step of the electrocatalytic reduction of H^+ to H_2. This reaction may compete with the binuclear one-electron reductive elimination from the 19-electron [M]-H complex (section 6.5.3). An example of this process is provided by the electrocatalyzed reduction of protons by complexes $[CpCoH(PR_3)_2]^+$ (R = Ph, Et, OMe), see Scheme 22 [25]. Susceptibility to protonation has also been found, however, for some cationic 17-electron compounds, *i.e.* $[FeClH(dppe)_2]^+$ [23].

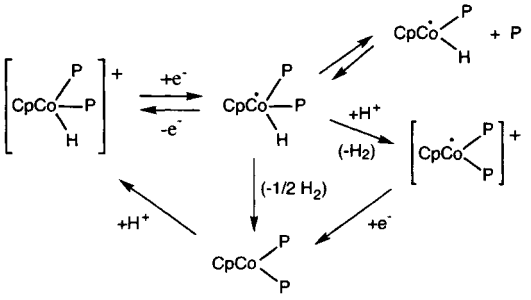

[P = PR_3, $P(OR)_3$; P-P = $R_2P(CH_2)_nPR_2$]

Scheme 22

6.5.9 Other reactivity pathways

Organometallic compounds with a 17-electron configuration are often labile toward associative ligand exchange. Radical chain mechanisms are well established for phosphine substitution on metal carbonyl hydrides (Scheme 23), the 17-electron chain carrier being in most cases non hydridic. This mechanism, however, was also shown to operate for $OsH_2(CO)_4$ via the 17-electron hydride complex $OsH(CO)_4^{\bullet}$ [137]. Thus, phosphine addition to the radical prevails over the dimerization, which indeed occurs in the absence of phosphine [33] (section 6.5.7), and over other possible decomposition pathways. The second step of the chain propagation process in Scheme 23, for this osmium system, is another example of atom transfer *to* a hydride radical (section 6.5.6).

If an olefin ligand is present, oxidation of a diamagnetic hydride complex may induce olefin insertion into the M-H bond. The oxidation of complex (triphos)RhH(π-DMFU) [triphos = $MeC(CH_2PPh_2)_3$; DMFU = dimethyl fumarate] consumes two electrons and affords the stable olefin insertion product $[(triphos)Rh\{CH(COOMe)CH_2(COOMe)\}]^{2+}$. This is shown to undergo a reversible one-electron reduction at a less positive potential with respect to the 2-electron oxidation of the Rh(I)-hydride complex, to afford the corresponding Rh(II) monocation, which has been spectroscopically characterized (Scheme 24)

[138].

$$In^{\bullet} + H\text{-}M(L) \longrightarrow In\text{-}H + M(L)^{\bullet} \qquad \textit{initiation}$$

$$M(L)^{\bullet} + L' \longrightarrow M(L')^{\bullet} + L$$

$$M(L')^{\bullet} + H\text{-}M(L) \longrightarrow H\text{-}M(L') + M(L)^{\bullet} \qquad \textit{propagation}$$

Scheme 23

Other insertions into M-H bonds of paramagnetic complexes have been proposed to occur during the reactions of a few saturated hydride complexes with electron poor acetylenes, the first step being an electron transfer process. A characteristic of this mechanism is an E- rather than Z-addition stereochemistry. Examples of this phenomenon have been described for PtH_2L_2 (L = tertiary phosphine) [139], Cp_2ReH and Cp_2WH_2 [140].

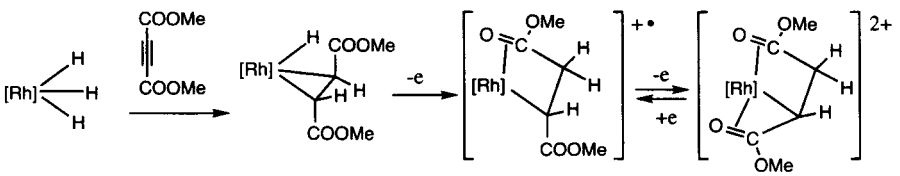

Scheme 24

Following one electron oxidation of $CpRuH(PPh_3)_2$ by Tol_3C^+, the resulting 17-electron hydride radical yields the product of addition of the trityl radical to the Cp ring as the major product (Scheme 25), in addition to the expected products of disproportionation [114].

6.6 CONCLUSIONS

Paramagnetic hydride chemistry is still a relatively young and unexplored research area. Although the first stable paramagnetic hydride complexes were prepared in the mid-70s, most advances in this field of chemistry have been made during the last 10 years. These, however, have been the result of scattered studies, bringing together pieces of a large puzzle which still remains largely incomplete. On the other hand, learning more about the properties and reactivity of this class of materials holds great promise for the development of a large number of applications, especially in electrocatalysis, as outlined in the introduction.

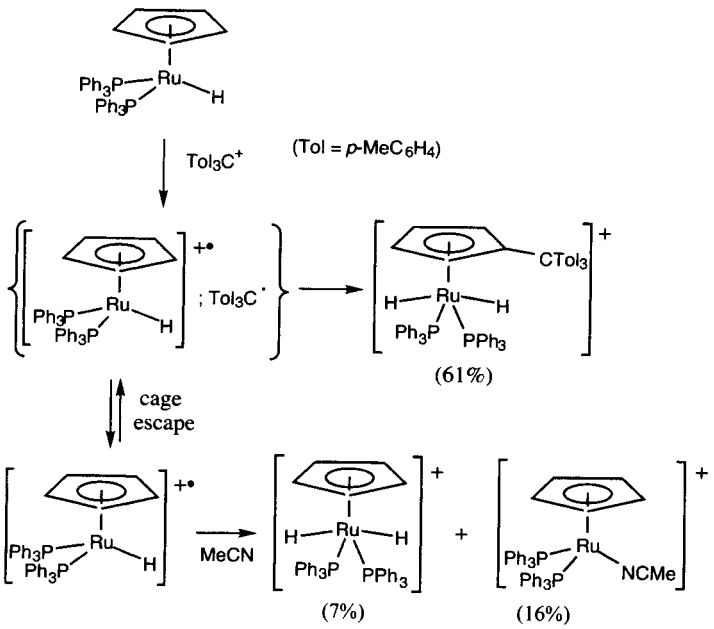

Scheme 25

Further investigations will be needed to sort out the stereoelectronic requirements that can make the hydride complex selectively chose amongst the several different reactivity pathways (deprotonation, disproportionation, dihydrogen reductive elimination, hydrogen atom transfer, dimerization, etc.) at its disposal. Some fundamental reactions have not yet been fully assessed from the kinetic point of view. The choice of solvent appears critical for diverting the reactivity from a more favoured path to a less favoured one, and a detailed study of complex-solvent interactions appears particularly important. Although oxidation processes of hydride compounds have been investigated in some detail, a lot less is known about the reductive chemistry and electrochemistry, which may on the other hand lead to the development of interesting reductive electrocatalytic processes. In conclusion, this area of chemistry has enormous potential for significant advances at both the fundamental and applicative levels.

ACKNOWLEDGEMENTS

I am grateful to the students and postdocs who have contributed to advancing the area of paramagnetic hydride chemistry in my laboratory. My activities in this area have mostly been carried out at the University of Maryland at College

Park with funding from the US Department of Energy. Current work is funded by the French Ministery of Research and by the French National Center of Scientific Research (CNRS). I also wish to thank the European Commission for financially supporting the organization of the EURO-Hydrides 2000 meeting.

REFERENCES

[1] P. R. Sharp, K. G. Frank, Inorg. Chem. 24 (1985) 1808-1813.
[2] M. Mediati, G. N. Tachibana, C. M. Jensen, Inorg. Chem. 31 (1992) 1827-1832.
[3] H. Cohen, D. Meyerstein, J. Chem. Soc., Dalton Trans. (1974) 2559-2564.
[4] J. P. Collman, P. S. Wagenknecht, N. S. Lewis, J. Am. Chem. Soc. 114 (1992) 5665-5673.
[5] G. Schiavon, S. Zecchin, G. Pilloni, M. Martelli, J. Electroanal. Chem. 93 (1978) 141-144.
[6] P. Connolly, J. H. Espenson, Inorg. Chem. 25 (1986) 2684-2688.
[7] U. Koelle, New J. Chem. 16 (1992) 157-169.
[8] A. Deronzier, J.-C. Moutet, E. Saint-Aman, J. Electroanal. Chem. 327 (1992) 147-158.
[9] I. M. F. de Oliveira, J.-C. Moutet, J. Mol. Catal. 81 (1993) L19-L24.
[10] H. Cano Yelo Bettega, J.-C. Moutet, S. Tingry, J. Electroanal. Chem. 391 (1995) 51-61.
[11] S. Chardon-Noblat, I. M. F. de Oliveira, J.-C. Moutet, S. Tingry, J. Mol. Catal. A 99 (1995) 13-21.
[12] C. J. Stalder, S. Chao, M. S. Wrighton, J. Am. Chem. Soc. 106 (1984) 3673-3675.
[13] K. Ogura, K. Mine, J. Yano, H. Sugihara, J. Chem. Soc., Chem. Commun. (1993) 20-21.
[14] B. Folkesson, R. Larsson, J. Zander, J. Electroanal. Chem. 267 (1989) 149-161.
[15] S. Park, J. M. Vohs, R. J. Gorte, Nature 404 (2000) 265-267.
[16] J. J. Ko, T. M. Bockman, J. K. Kochi, Organometallics 9 (1990) 1833-1842.
[17] J. C. Fettinger, H.-B. Kraatz, R. Poli, E. A. Quadrelli, R. C. Torralba, Organometallics 17 (1998) 5767-5775.
[18] J. D. Allison, R. A. Walton, J. Chem. Soc., Chem. Commun. (1983) 401-403.
[19] C. Bianchini, F. Laschi, M. Peruzzini, F. Ottaviani, A. Vacca, P. Zanello, Inorg. Chem. 29 (1990) 3394-3402.
[20] A. A. Zlota, M. Tilset, K. G. Caulton, Inorg. Chem. 32 (1993) 3816-3821.
[21] K.-T. Smith, M. Tilset, R. Kuhlman, K. G. Caulton, J. Am. Chem. Soc. 117 (1995) 9473-9480.
[22] P. Sauvageot, A. Sadorge, B. Nuber, M. M. Kubicki, J. C. Leblanc, C. Moïse, Organometallics 18 (1999) 2133-2138.
[23] M. Gargano, P. Giannoccaro, M. Rossi, G. Vasapollo, A. Sacco, J. Chem. Soc., Dalton Trans. (1975) 9-12.
[24] F. Marken, A. M. Bond, R. Colton, Inorg. Chem. 34 (1995) 1705-1710.

[25] U. Koelle, S. Ohst, Inorg. Chem. 25 (1986) 2689-2694.
[26] D. C. Eisenberg, J. R. Norton, Isr. J. Chem. 31 (1991) 55-66.
[27] R. M. Bullock, Comm. Inorg. Chem. 12 (1991) 1-33.
[28] F. Ungváry, L. Markó, J. Organomet. Chem. 193 (1980) 383-387.
[29] N. N. Turaki, J. M. Huggins, Organometallics 5 (1986) 1703-1706.
[30] R. J. Kinney, W. D. Jones, R. G. Bergman, J. Am. Chem. Soc. 100 (1978) 7902-7915.
[31] C. E. Ash, P. W. Hurd, M. Y. Darensbourg, M. Newcomb, J. Am. Chem. Soc. 109 (1987) 3313-3317.
[32] I. H. Elson, J. K. Kochi, U. Klabunde, L. E. Manzer, G. W. Parshall, F. N. Tebbe, J. Am. Chem. Soc. 96 (1974) 7374-7375.
[33] R. T. Edidin, K. M. Hennessy, A. E. Moody, S. J. Okrasinski, J. R. Norton, New J. Chem. 12 (1988) 475-477.
[34] D. C. Eisenberg, C. J. C. Lawrie, A. E. Moody, J. R. Norton, J. Am. Chem. Soc. 113 (1991) 4888-4895.
[35] M. A. Rodkin, G. P. Abramo, K. E. Darula, D. L. Ramage, B. P. Santora, J. R. Norton, Organometallics 18 (1999) 1106-1109.
[36] M. L. Luetkens, Jr., W. L. Elcesser, J. C. Huffman, A. P. Sattelberger, Inorg. Chem. 23 (1984) 1718-1726.
[37] R. Poli, Chem. Rev. 96 (1996) 2135-2204.
[38] H. H. Brintzinger, J. Am. Chem. Soc. 89 (1967) 6871-6876.
[39] G. A. Luinstra, J. H. Teuben, J. Am. Chem. Soc. 114 (1992) 3361-3367.
[40] C. Bianchini, D. Masi, C. Mealli, A. Meli, M. Sabat, Gazz. Chim. Ital. 116 (1986) 201-206.
[41] P. Hamon, J.-R. Hamon, C. Lapinte, J. Chem. Soc., Chem. Commun. (1992) 1602-1603.
[42] B. Pleune, D. Morales, R. Meunier-Prest, P. Richard, E. Collange, J. C. Fettinger, R. Poli, J. Am. Chem. Soc. 121 (1999) 2209-2225.
[43] M. Ladwig, W. Kaim, J. Organomet. Chem. 439 (1992) 79-90.
[44] W. Kaim, R. Reinhardt, M. Sieger, Inorg. Chem. 33 (1994) 4453-4459.
[45] J. G. Kenworthy, J. Myatt, M. C. R. Symons, J. Chem. Soc. (A) (1971) 1020-1024.
[46] H. Brintzinger, J. Am. Chem. Soc. 88 (1966) 4305-4307.
[47] W. W. Lukens, Jr., P. T. Matsunaga, R. A. Andersen, Organometallics 17 (1998) 5240-5247.
[48] J. E. Bercaw, H. H. Brintzinger, J. Am. Chem. Soc. 91 (1969) 7301-7306.
[49] S. Xin, J. F. Harrod, E. Samuel, J. Am. Chem. Soc. 116 (1994) 11562-11563.
[50] M. L. Luetkens, Jr., W. L. Elcesser, J. C. Huffman, A. P. Sattelberger, J. Chem. Soc., Chem. Commun. (1983) 1072-1074.
[51] L. Roullier, D. Lucas, Y. Mugnier, A. Antiñolo, M. Fajardo, A. Otero, J. Organomet. Chem. 396 (1990) C12-C16.
[52] L. Roullier, D. Lucas, Y. Mugnier, A. Antiñolo, M. Fajardo, A. Otero, J. Organomet. Chem. 412 (1991) 353-362.
[53] C. A. Blaine, J. E. Ellis, K. R. Mann, Inorg. Chem. 34 (1995) 1552-1561.
[54] R. J. Klinger, J. C. Huffman, J. K. Kochi, J. Am. Chem. Soc. 102 (1980) 208-216.
[55] B. Pleune, R. Poli, J. C. Fettinger, J. Am. Chem. Soc. 120 (1998) 3257-3258.

[56] M. Freni, P. Romiti, D. Giusto, J. Inorg. Nucl. Chem. 32 (1970) 145-153.
[57] J. D. Allison, C. J. Cameron, R. E. Wild, R. A. Walton, J. Organomet. Chem. 218 (1981) C62-C66.
[58] M. R. Detty, W. D. Jones, J. Am. Chem. Soc. 109 (1987) 5666-5673.
[59] W. A. Herrmann, H. G. Theiler, E. Herdtweck, P. Kiprof, J. Organomet. Chem. 367 (1989) 291-311.
[60] G. Pilloni, G. Zotti, Q. G. Mulazzani, P. G. Fuochi, J. Electroanal. Chem. 137 (1982) 89-102.
[61] J. W. Bruno, J. C. Huffman, M. A. Green, J. D. Zubkowski, W. E. Hatfield, K. G. Caulton, Organometallics 9 (1990) 2556-2567.
[62] P. M. Treichel, D. C. Molzahn, K. P. Wagner, J. Organomet. Chem. 174 (1979) 191-197.
[63] C. Roger, P. Hamon, L. Toupet, H. Rabaâ, J.-Y. Saillard, J.-R. Hamon, C. Lapinte, Organometallics 10 (1991) 1045-1054.
[64] P. Hamon, L. Toupet, J.-R. Hamon, C. Lapinte, Organometallics 11 (1992) 1429-1431.
[65] M. Jiménez-Tenorio, M. C. Puerta, P. Valerga, Organometallics 13 (1994) 3330-3337.
[66] K.-T. Smith, C. Rømming, M. Tilset, J. Am. Chem. Soc. 115 (1993) 8681-8689.
[67] C. Rømming, K.-T. Smith, M. Tilset, Inorg. Chim. Acta 259 (1997) 281-290.
[68] R. T. Hembre, J. S. McQueen, V. W. Day, J. Am. Chem. Soc. 118 (1996) 798-803.
[69] J. R. Sanders, J. Chem. Soc., Dalton Trans. (1973) 748-749.
[70] J. R. Sanders, J. Chem. Soc., Dalton Trans. (1975) 2340-2342.
[71] A. Orlandini, L. Sacconi, Cryst. Struct. Commun. 4 (1975) 157-161.
[72] C. Bianchini, P. Innocenti, A. Meli, M. Peruzzini, F. Zanobini, P. Zanello, Organometallics 9 (1990) 2514-2522.
[73] S. Valcher, G. Pilloni, M. Martelli, J. Electroan. Chem. Interfac. Electrochem. 42 (1973) App. 5-6.
[74] G. Pilloni, G. Schiavon, G. Zotti, S. Zecchin, J. Organomet. Chem. 134 (1977) 305-318.
[75] D. Menglet, A. M. Bond, K. Coutinho, R. S. Dickson, G. G. Lazarev, S. A. Olsen, J. R. Pilbrow, J. Am. Chem. Soc. 120 (1998) 2086-2089.
[76] A. M. Bond, D. G. Humphrey, D. Menglet, G. G. Lazarev, R. S. Dickson, T. Vu, Inorg. Chim. Acta 300-302 (2000) 565-571.
[77] P. Mura, A. Segre, A. Sostero, Inorg. Chem. 28 (1989) 2852-2858.
[78] D. Attanasio, P. Mura, A. Maldotti, S. Sostero, O. Traverso, New J. Chem. 16 (1992) 347-350.
[79] D. Capitani, P. Mura, Inorg. Chim. Acta 258 (1997) 169-181.
[80] K. G. Caulton, New J. Chem. 18 (1994) 25-41.
[81] P. Giannoccaro, M. Rossi, A. Sacco, Coord. Chem. Rev. 8 (1972) 77-79.
[82] P. Giannoccaro, A. Sacco, Inorg. Synth. 17 (1977) 69-71.
[83] P. Stoppioni, F. Mani, L. Sacconi, Inorg. Chim. Acta 11 (1974) 227-230.
[84] J. E. Bercaw, J. Am. Chem. Soc. 96 (1974) 5087-5095.
[85a] J. M. de Wolf, A. Meetsma, J. H. Teuben, Organometallics 14 (1995) 5466-5468.
[85b] J. D. Jewson, L. M. Liable-Sands, G. P. A. Yap, A. L. Rheingold, K. H. Theopold, Organometallics 18 (1999) 300-305.

[86] O. B. Ryan, M. Tilset, V. D. Parker, J. Am. Chem. Soc. 112 (1990) 2618-2626.
[87] M. Tilset, J. Am. Chem. Soc. 114 (1992) 2740-2741.
[88] V. Skagestad, M. Tilset, J. Am. Chem. Soc. 115 (1993) 5077-5083.
[89] D. R. Tyler, Acc. Chem. Res. 24 (1991) 325-331.
[90] K. Costuas, Ph. Thesis. University of Rennes, 2000.
[91] R. S. Berry, S. A. Rice, J. Ross, "Physical Chemistry," p. 266-268. Wiley, New York, (1980).
[92] J.-R. Hamon, C. Lapinte, personal communication.
[93] W. Kruse, J. H. Atalla, Chem. Commun. (1968) 921-922.
[94] A. Sacco, R. Ugo, J. Chem. Soc. (1964) 3274-3278.
[95] C. A. Ghilardi, S. Midollini, L. Sacconi, Inorg. Chem. 14 (1975) 1790-1795.
[96] S. S. Bath, L. Vaska, J. Am. Chem. Soc. 85 (1963) 3500-3501.
[97] M. Tilset, J.-R. Hamon, P. Hamon, J. Chem. Soc., Chem. Commun. (1998) 765-766.
[98] Discussion with M. Tilset and J.-Y. Saillard.
[99] L. Chen, J. A. Davies, Inorg. Chim. Acta 175 (1990) 41-45.
[100] C. Bianchini, M. Peruzzini, A. Ceccanti, F. Laschi, P. Zanello, Inorg. Chim. Acta 259 (1997) 61-70.
[101] M. T. Costello, R. A. Walton, Inorg. Chem. 27 (1988) 2563-2564.
[102] O. B. Ryan, M. Tilset, J. Am. Chem. Soc. 113 (1991) 9554-9561.
[103] K.-T. Smith, M. Tilset, J. Organomet. Chem. 431 (1992) 55-64.
[104] E. A. Quadrelli, H.-B. Kraatz, R. Poli, Inorg. Chem. 35 (1996) 5154-5162.
[105] M. A. N. D. A. Lemos, A. J. L. Pombeiro, J. Organometal. Chem. 332 (1987) C17-C20.
[106] G. Parkin, J. E. Bercaw, J. Chem. Soc., Chem. Commun. (1989) 255-257.
[107] M. S. Chinn, D. M. Heinekey, J. Am. Chem. Soc. 112 (1990) 5166-5175.
[108] G. Jia, A. J. Lough, R. H. Morris, Organometallics 11 (1992) 161-171.
[109] D. Morales, R. Poli, J. Andrieu, Inorg. Chim. Acta 300-302 (2000) 709-720.
[110] J. R. Norton, in "EURO-Hydrides 2000" (R. Poli, ed.), Dijon, 2000. (see also chapter 2 of this book)
[111] A. Pedersen, M. Tilset, Organometallics 13 (1994) 4887-4894.
[112] D. E. Westerberg, L. F. Rhodes, J. Edwin, W. E. Geiger, K. G. Caulton, Inorg. Chem. 30 (1991) 1107-1112.
[113] R. Galassi, R. Poli, E. A. Quadrelli, J. C. Fettinger, Inorg. Chem. 36 (1997) 3001-3007.
[114] O. B. Ryan, K.-T. Smith, M. Tilset, J. Organomet. Chem. 421 (1991) 315-322.
[115] O. B. Ryan, M. Tilset, V. D. Parker, Organometallics 10 (1991) 298-304.
[116] L. F. Rhodes, J. D. Zubkowski, K. Folting, J. C. Huffman, K. G. Caulton, Inorg. Chem. 21 (1982) 4185-4192.
[117] C. Amatore, J. J. R. Fraústo da Silva, M. F. C. Guedes da Silva, A. J. L. Pombeiro, J.-N. Verpeaux, J. Chem. Soc., Chem. Commun. (1992) 1289-1291.
[118] J. C. Fettinger, H.-B. Kraatz, R. Poli, E. A. Quadrelli, J. Chem. Soc., Dalton Trans. (1999) 497-508.
[119] J. C. Fettinger, H.-B. Kraatz, R. Poli, E. A. Quadrelli, Chem. Commun. (1997) 889-890.
[120] R. Poli, E. A. Quadrelli, New J. Chem. 22 (1998) 435-450.
[121] D. Morales, B. Pleune, R. Poli, P. Richard, J. Organometal. Chem. 596 (2000)

64-69.
[122] T. T. Tsou, J. K. Kochi, J. Am. Chem. Soc. 100 (1978) 1634-1635.
[123] W. Lau, J. C. Huffman, J. K. Kochi, Organometallics 1 (1982) 155-169.
[124] A. Pedersen, M. Tilset, Organometallics 12 (1993) 56-64.
[125] A. Pedersen, M. Tilset, K. Folting, K. G. Caulton, Organometallics 14 (1995) 875-888.
[126] T. H. Lemmen, L. F. Lundquist, B. R. Sutherland, D. E. Westerberg, K. G. Caulton, Inorg. Chem. 25 (1986) 3915-3917.
[127] I. H. Elson, J. K. Kochi, J. Am. Chem. Soc. 97 (1975) 1262-1264.
[128] R. Meunier-Prest, R. Poli, (to be published) .
[129] R. M. Kellett, T. G. Spiro, Inorg. Chem. 24 (1985) 2373-2377.
[130] J. P. Collman, J. E. Hutchison, P. S. Wagenknecht, N. S. Lewis, M. A. Loperz, R. Guilard, J. Am. Chem. Soc. 112 (1990) 8206-8208.
[131] T.-Y. Cheng, R. M. Bullock, Organometallics 14 (1995) 4031-4033.
[132] G. S. Bodner, J. A. Gladysz, M. Folmer Nielsen, V. D. Parker, J. Am. Chem. Soc. 109 (1987) 1757-1764.
[133] E. A. Quadrelli, R. Poli, Organometallics 17 (1998) 5776-5781.
[134] D. Astruc, (Ed), "Electron Transfer and Radical Processes in Transition Metal Chemistry." VCH, Weinheim, (1995).
[135] J. W. Bruno, K. G. Caulton, J. Organomet. Chem. 315 (1986) C13-C16.
[136] G. A. Luinstra, J. Teuben, J. Chem. Soc., Chem. Commun. (1990) 1470-1471.
[137] R. T. Edidin, J. R. Norton, J. Am. Chem. Soc. 108 (1986) 948-953.
[138] C. Bianchini, F. Laschi, A. Meli, M. Peruzzini, P. Zanello, P. Frediani, Organometallics 7 (1988) 2575-2577.
[139] H. C. Clark, G. Ferguson, A. B. Goel, E. G. Janzen, H. Ruegger, P. Y. Siew, C. S. Wong, J. Am. Chem. Soc. 108 (1986) 6961-6972.
[140] G. E. Herberich, W. Barlage, Organometallics 6 (1987) 1924-1930.

Chapter 7

Ruthenium- and Osmium- Hydride Compounds Containing Triisopropylphosphine as Precursors for Carbon-Carbon and Carbon-Heteroatom Coupling Reactions

Miguel A. Esteruelas and Ana M. López

Departamento de Química Inorgánica, Universidad de Zaragoza, 50009 Zaragoza, Spain

CONTENTS

7.1 INTRODUCTION

Owing to the increasing demand for the products of organic synthesis, the development of highly efficient and selective synthetic methods is one of the most urgent tasks for the chemical science. In this respect, the formation of carbon-carbon and carbon-heteroatom bonds mediated by transition metal complexes has emerged on its own right over the last years as an important step in organic synthesis [1].

In an effort to develop new models for homogeneous systems effective in the synthesis of functionalized organic molecules from basic hydrocarbon units, our group is carrying out a research program centered in the use of hydrido and hydrido-chloro ruthenium- and osmium-triisopropylphosphine compounds as precursors of carbon-carbon and carbon-heteroatom bonds. The program is based on the hypothesis summarized in Scheme 1: The process would involve the entry, in a consecutive and controlled way, of organic fragments (A, B, etc) into a coordination transition-metal complex (M) to give an organometallic compound (MA···B). It could react with an organic function (F) to afford the functionalized organic molecule (FA···B) and regenerate the coordination transition-metal complex.

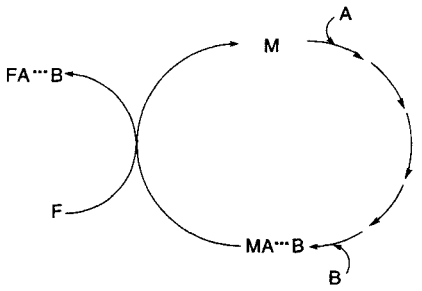

Scheme 1

The choice of the system could give rise to three questions from the readership, which are answered in the following paragraphs.

Why ruthenium and osmium? These elements lie in a relatively centered position within the Periodic Table, forming stable compounds in a wide range of oxidation states. For example, $Os(\eta^2\text{-}C_2Ph_2)(CO)(P^iPr_3)_2$ (d^8) and $OsH_6(P^iPr_2Ph)_2$ (d^2) are known and sufficiently stable to be characterized, even by X-ray [2] and neutron diffraction [3] techniques, respectively. This allows, with only two elements, to have a first forecast about the behavior of a wide range of metallic ions, from the point of view of the Scheme 1.

Why triisopropylphosphine? This ligand is a bulky phosphine with a large cone angle (160°) [4], which allows the stabilization of saturated and

unsaturated transition-metal compounds in low and high oxidations states [5]. Although recently a few *cis*-triisopropylphosphine complexes have been reported [6], in bis(phosphine) compounds the usual arrangement of the triisopropylphosphine ligands is mutually *trans* [5,7]. As a result of this disposition, the M-bis(triisopropylphosphine) fragment leaves available a wide region in the perpendicular plane to the P-M-P direction for the entry of the organic substrates.

Why hydride and chloride ligands? The hydrides are the best anchorages to nail unsaturated organic molecules in transition-metal compounds. Furthermore, the addition of X-H bonds to olefins and alkynes are well known processes in organic chemistry. In addition, the reaction of chloro-transition-metal complexes with main group organometallic complexes is an early developed method to prepare tansition metal organometallic compounds containinig η^1-carbon ligands.

The design of new catalysts and new processes requires a basic knowledge of the leading factors of the catalytic cycles, that is, the stoichiometric steps of the catalysis. Thus, from the point of view of Scheme 1, in the following pages we revise the most important stoichiometric features of the chemistry of the complexes $MHCl(CO)(P^iPr_3)_2$ (M = Ru, Os), $[Ru(\eta^5\text{-}C_5H_5)(CO)(\eta^2\text{-}H_2)(P^iPr_3)]BF_4$, $OsH_2Cl_2(P^iPr_3)_2$, $[OsH_2(\kappa^2\text{-}O_2CCH_3)(H_2O)(P^iPr_3)_2]BF_4$, $OsH_3Cl(P^iPr_3)_2$, $[OsH(CO)(\eta^2\text{-}H_2)(P^iPr_3)_2]BF_4$, and $OsH_2(CO)(\eta^2\text{-}H_2)(P^iPr_3)_2$, where the number of hydrogen atoms bonded to the metallic center is increased from one to four.

7.2 THE HYDRIDE-CHLORO-RUTHENIUM COMPLEX $RuHCl(CO)(P^iPr_3)_2$ AS A PRECURSOR FOR CARBON-CARBON AND CARBON-SULFUR COUPLING REACTIONS

Complex $RuHCl(CO)(P^iPr_3)_2$ (**1**) is prepared in 70% yield upon boiling a solution of triisopropylphosphine and $RuCl_3.xH_2O$ in methanol under argon for 24 h. It is an orange very air sensitive solid, stable for a long time at room temperature if kept under argon. The spectroscopic data of this compound support a rigid square-pyramidal structure in solution with the mutually *trans* phosphines, the chloride and carbonyl group occupying the basal sites, and the hydride ligand located at the apex, *trans* to the coordination vacancy [8].

In spite of its rigid structure in solution and the *trans* disposition of the hydride and the coordination vacancy, complex **1** reacts with terminal alkynes to afford alkenyl derivatives, as a result of the addition of the Ru-H bond to the carbon-carbon triple bond of the alkynes [9]. In all cases, the alkenyl ligands have an *E*-stereochemistry and lie in the apex of a square pyramid similar to that of **1**. This property along with the presence of the chloride ligand allows the entry to C_1, C_2, C_4, and SH fragments into the coordination sphere of the ruthenium.

The subsequent manipulation of the resulting organometallic products, under the appropiate conditions, gives rise to η^4-butadiene, acyl, η^3-hexadienyl and monothio-β-diketonato derivatives by means of $C_2 + C_2$, $C_1 + C_1$, $C_4 + C_2$, and C_2 + SH coupling processes, respectively.

7.2.1 Formation of Ru(η⁴-C₄H₅Ph)(CO)(P^{i}Pr₃)₂

The addition of 1.2 equiv of phenylacetylene to hexane solutions of **1** results in an almost instantaneous formation of the styryl compound Ru{(*E*)-CH=CHPh}Cl(CO)(P^{i}Pr$_3$)$_2$ (**2**). Treatment of this complex with CH_2=CHMgBr in hexane, at room temperature, gives the styryl-vinyl intermediate Ru{(*E*)-CH=CHPh}(CH=CH$_2$)(CO)(P^{i}Pr$_3$)$_2$ (**3**), which by reductive carbon-carbon coupling leads to the π-(phenyl)butadiene Ru(η^4-C$_4$H$_5$Ph)(CO)(P^{i}Pr$_3$)$_2$ (**4**), after 15 h stirring in hexane at 50 °C (Scheme 2) [10].

The coordination number 6 for **3** can be achieved by reaction with carbon monoxide. By passage of a slow stream of this gas through an hexane suspension of **3**, the dicarbonyl complex Ru{(*E*)-CH=CHPh}(CH=CH$_2$)(CO)$_2$(P^{i}Pr$_3$)$_2$ (**5**) is obtained. Complex **5** can be also prepared by reaction of Ru{(*E*)-CH=CHPh}Cl(CO)$_2$(P^{i}Pr$_3$)$_2$ (**6**) with CH_2=CHMgBr.

In contrast to the behavior of **3**, reductive carbon-carbon coupling between styryl and vinyl fragments of the saturated complex **5** is not observed, suggesting that the unsaturated ligand environment around the metallic center is a determinant factor for the coupling.

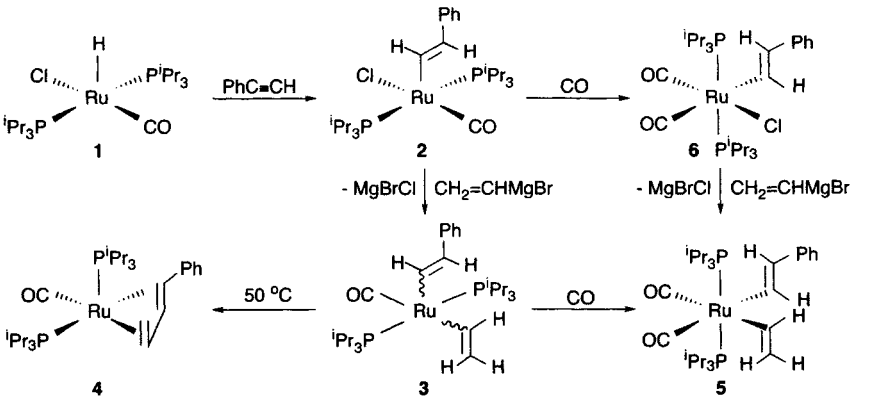

Scheme 2

7.2.2 Formation of acyl compounds [11]

The chloride ligand of **6** can be replaced not only by a vinyl group, but also by a methyl one. Thus, the reaction of **6** with LiCH$_3$ in toluene at room temperature

affords the methyl-styryl derivative $Ru(CH_3)\{(E)\text{-}CH{=}CHPh\}(CO)_2(P^iPr_3)_2$ (**7**), which is also stable, and does not evolve by reductive carbon-carbon coupling of the methyl and styryl fragments.

Although, at a first glance, complex **7** should have three centers (the metal, the methyl group, and the β-carbon atom of the styryl ligand) with a stronger nucleophilic power than that of the α-carbon atom of the styryl group, the addition of $HBF_4{\cdot}OEt_2$ to acetone solutions of **7** affords styrene and the five-coordinate methyl compound $[Ru(CH_3)(CO)_2(P^iPr_3)_2]BF_4$ (**8**), as a result of the attack of the proton from the acid to the α-carbon atom of the styryl ligand of **7** (Scheme 3).

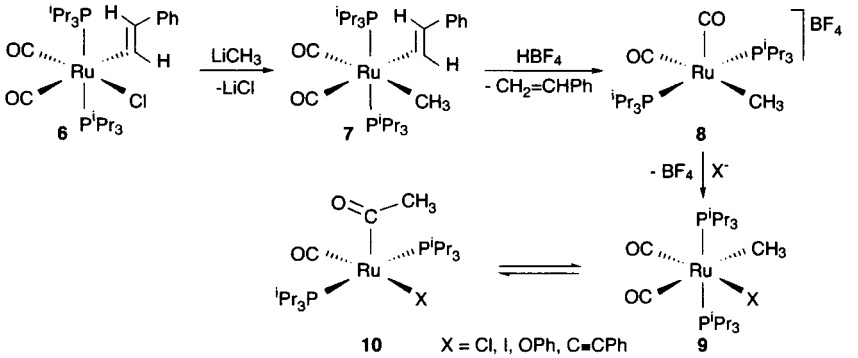

Scheme 3

In solution complex **8** rapidly decomposes to unidentified products. However, the addition of anionic monodentate nucleophilic reagents to toluene suspensions of **8** affords six-coordinate methyl dicarbonyl compounds of the type $Ru(CH_3)X(CO)_2(P^iPr_3)_2$ (**9**), in equilibrium with the corresponding acyl derivatives $Ru\{C(O)CH_3\}X(CO)(P^iPr_3)_2$ (**10**; X = Cl, I, OPh, C≡CPh). The position of the equilibrium is markedly dependent on X, increasing the tendency toward the migration in the sequence C≡CPh < OPh < I < Cl. For X = OPh, the values of ΔH (2.31 ± 0.07 kcal·mol^{-1}) and ΔS (10.04 ± 0.28 cal·K^{-1}·mol^{-1}) have been determined. They suggest that the factors underlying the migration are the higher number of molecular degrees of freedom in the acyl-carbonyl complexes than in the methyl dicarbonyl derivatives. The acyl compounds coordinate the acyl ligand in a η^1-fashion, in contrast to the η^2-coordination mode observed by Roper and co-workers for related complexes containing triphenylphosphine [12]. The study of the structure of $Ru\{C(O)CH_3\}Cl(CO)_2(P^iPr_3)_2$, determined by X-ray investigations, suggests that the steric demands of the triisopropylphosphine ligands play a main role in the stabilization of the five-coordination for these compounds. Thus, 4 of the 12 methyl groups of the phosphines surround the metal like an umbrella.

7.2.3 Formation of $Ru\{\eta^3\text{-}CH_2CHCHCH{=}C(CH_3)_2\}Cl(CO)_2(P^iPr_3)$

Similarly to the reaction of **1** with phenylacetylene to afford **2**, the addition of 1 equiv of 2-methyl-1-buten-3-yne to toluene solutions **1** leads to the butadienyl complex $Ru\{(E)\text{-}CH{=}CHC(CH_3){=}CH_2\}Cl(CO)(P^iPr_3)_2$ (**11**) as a result of the selective addition of the Ru-H bond of **1** to the carbon-carbon triple bond of the enyne (Scheme 4).

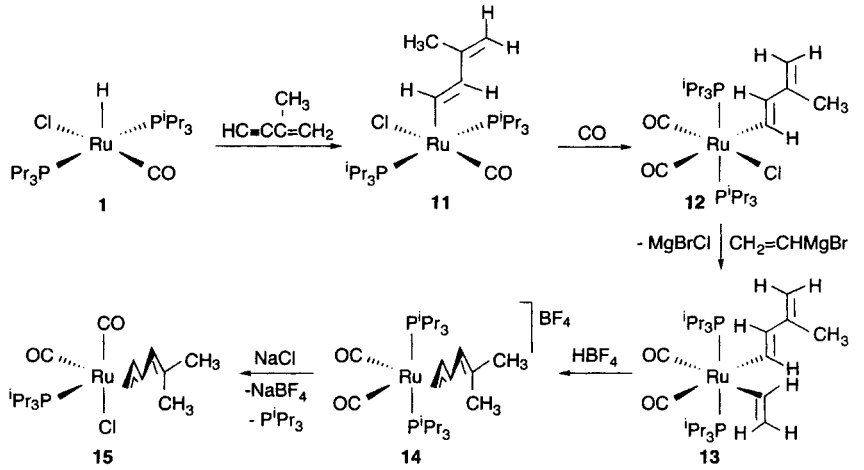

Scheme 4

The coordination number 6 for **11** can be achieved by coordination of carbon monoxide. Thus, bubbling carbon monoxide through hexane suspensions of **11** results in the formation of $Ru\{(E)\text{-}CH{=}CHC(CH_3){=}CH_2\}Cl(CO)_2(P^iPr_3)_2$ (**12**), which reacts with $CH_2{=}CHMgBr$ to give $Ru\{(E)\text{-}CH{=}CHC(CH_3){=}CH_2\}(CH{=}CH_2)(CO)_2(P^iPr_3)_2$ (**13**). Like the saturated complexes **5** and **7**, complex **13** is stable towards the reductive carbon-carbon coupling of the butadienyl and vinil fragments, even at high temperature (refluxing toluene).

Although the reductive elimination of 2-methylhexatriene from **13** is not thermally activated, in contrast to **7**, the carbon-carbon coupling of the η^1-carbon donor ligands can be carried out in the presence of HBF_4 [13].

The protonation of **13** with $HBF_4{\cdot}Et_2O$ leads to a mixture of products containing about 50% of the hexadienyl compound $[Ru\{\eta^3\text{-}CH_2CHCHCH{=}C(CH_3)_2\}(CO)_2(P^iPr_3)_2]BF_4$ (**14**). Treatment of this mixture with an excess of NaCl in methanol affords $Ru\{\eta^3\text{-}CH_2CHCHCH{=}C(CH_3)_2\}Cl(CO)_2(P^iPr_3)$ (**15**) as a microcrystallline yellow solid, which was characterized by X-ray diffraction analysis, and where the η^3-ligand has w-shape *syn* geometry.

Deuterium labeling experiments indicate that the formation of the η^3-ligand of **15** involves the electrophilic attack of the proton of the acid to the δ-carbon atom in the butadienyl ligand of **13**, and the subsequent vinyl migration from the

ruthenium to the α-carbon atom in the resulting α,β-unsaturated carbene ligand. This is a consequence of the high electron density situated on the δ-carbon atom of the butadienyl ligand, as is suggested by the X-ray diffraction analysis of **11** and proved by the reaction of this complex with $HBF_4 \cdot Et_2O$ to afford $[Ru\{=CHCH=C(CH_3)_2\}Cl(CO)(P^iPr_3)_2]BF_4$ (**16**).

7.2.4 *Formation of monothio-β-diketonato derivatives*

Treatment at room temperature of tetrahydrofuran solutions of **1** with NaHS affords the five coordinate hydride-metallothiol derivative $RuH(SH)(CO)(P^iPr_3)_2$ (**17**), which reacts with acetylenedicarboxylic methyl ester by insertion of the carbon-carbon triple bond of the alkyne into the S-H bond of **17** (Scheme 5) [14]. In the resulting monothio-β-diketonato complex **18**, the hydride ligand lies *trans* to the sulfur atom. In toluene at room temperature, complex **18** is unstable and evolves into the isomer **19** after 15 min. This compound contains the hydride ligand *trans* to the oxygen atom of the chelate group.

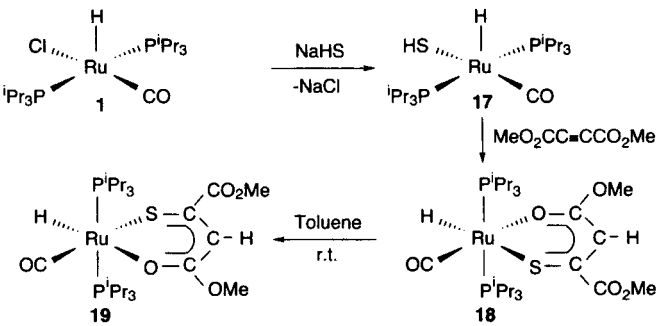

Scheme 5

7.3 THE HYDRIDE-CHLORO-OSMIUM COMPLEX $OsHCl(CO)(P^iPr_3)_2$ AS A PRECURSOR FOR CARBON-CARBON, CARBON-OXYGEN, AND CARBON-SULFUR COUPLING REACTIONS

The red complex $OsHCl(CO)(P^iPr_3)_2$ (**20**) has been one of the cornerstones in the development of the modern organometallic osmium chemistry [5]. It is prepared in nearly quantitative yield (about 90%), on boiling a solution of triisopropylphosphine and $OsCl_3 \cdot xH_2O$ in methanol, under argon, for 48 h. As the ruthenium counterpart, complex **20** is a very air sensitive solid, stable for long time at room temperature if kept under argon [8].

The structure, the properties in solution and the coordination chemistry of **1** and **20** are similar. However, the intrinsically higher basicity of the osmium atom

in comparison with ruthenium [15] gives some special features to the chemistry of the species derived from **20**, as for example their higher tendency to undergo oxidative addition processes, in particular C-H activation reactions.

The presence of the hydride and chloro ligands in **20** allows to introduce two different fragments into the osmium atom, which gives rise to butadiene, 2-(*E*-1'-styryl)phenyl, 2-(*E*-1'-propenyl)phenyl, β-diketonato, and monothio-β-diketonato ligands, by means of reductive carbon-carbon coupling and subsequent C-H activation processes, and C_2 + OH and C_2 + SH addition reactions.

7.3.1 Formation of Os(η⁴-C₄H₅R)(CO)(PⁱPr₃)₂ (R = H, Ph)

Similarly to **1**, complex **20** reacts with terminal alkynes such as acetylene and phenylacetylene to give the corresponding alkenyl derivatives Os{(*E*)-CH=CHR}Cl(CO)(P^iPr_3)$_2$ (R = H (**21a**), Ph (**21b**)) (Scheme 6). The structure of the styryl derivative **21b** has been determined by X-ray diffraction analysis [9]. The most remarkable features are, first, the square pyramidal coordination of the metal with the alkenyl ligand in the apex and, second, the *E*-stereochemistry of the styryl group.

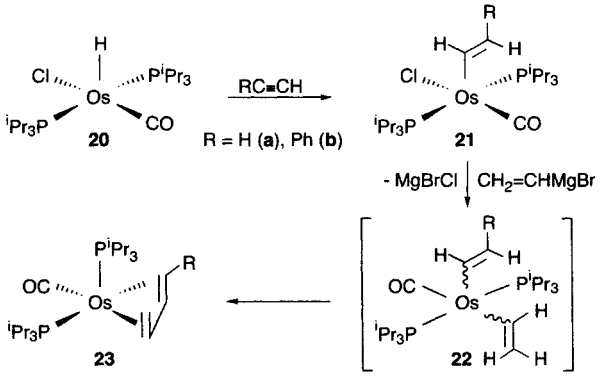

Scheme 6

Treatment of these alkenyl compounds with CH_2=CHMgBr in toluene at room temperature affords the butadienyl complexes Os(η⁴-C_4H_5R)(CO)(P^iPr_3)$_2$ (R = H (**23a**), Ph (**23b**)). Although reaction intermediates are not isolated, the reaction of **2** with CH_2=CHMgBr to give **3** (Scheme 2) suggests that the formation of the η⁴-butadiene complexes **23** involves the replacement of the chlorine ligand by the vinyl group to give bis(vinyl) (**22a**) or styryl-vinyl (**22b**) intermediates that evolve by reductive carbon-carbon coupling.

The structure of the η^4-butadiene complexes **23** has been established by an X-ray investigation on a monocrystal of **23b**. The phenyl-butadiene ligand coordinates in a predominant η^4-π-fashion but with significant σ^2-π-contribution [10].

7.3.2 *Formation of 2-(E-1'-styryl)phenyl, 2-(E-1'-propenyl)phenyl, and phenylallyl ligands*

Reactions of the five coordinate styryl complex **21b** with LiPh, $LiCH_3$, and $LiCD_3$ give the aryl derivatives $OsH\{C_6H_4\text{-}2\text{-}E\text{-}CH{=}CHR\}(CO)(P^iPr_3)_2$ (R = Ph (**24a**), CH_3 (**24b**), CD_3 (**24c**)), containing an agostic interaction between the metallic center and the CHR-hydrogen atom (Scheme 7). This interaction has been proved by X-ray diffraction on a single crystal of **24a**. The separation between the atoms involved in the agostic bond is 2.05(7) Å, whereas the Os···H-C angle is 118(6)° [16].

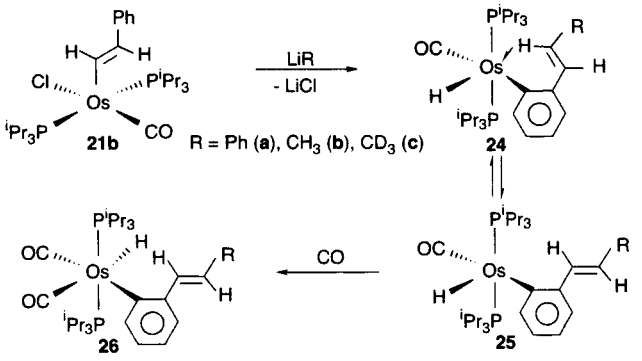

Scheme 7

In solution, complexes **24** are in equilibrium with the corresponding nonagostic isomers **25**. For R = Ph, the thermodynamic magnitudes involved in the equilibrium as well as the activation parameters for the conversion between the two isomers have been determined in toluene-d_8 by ^1H NMR spectroscopy. The values obtained for the formation of the agostic isomer are ΔH^o = -1.6 (± 0.1) kcal·mol^{-1} and ΔS^o = -9.6 (± 0.6) cal·K^{-1}·mol^{-1}, whereas the activation parameters for the breaking of the agostic interaction are $\Delta H^{\neq}$ = 7.6 (± 0.2) kcal·mol^{-1} and $\Delta S^{\neq}$ = -1.0 (± 0.7) cal·K^{-1}·mol^{-1}.

The negative entropy increment is consistent with the less ordered character of **25**, which are always the major species in the temperature range studied. The value of ΔH^o reveals the small stabilization achieved by means of the agostic interaction. This value could be justified to be not only due to the weakness of

the agostic bond but also to the destabilization imposed by the steric repulsion between the R substituent of the olefinic unit and the bulky phosphines.

The activation entropy, nearly zero, is in agreement with an intramolecular process, whereas the activation enthalpy lies in the range of other reported exchange processes in which agostic interactions are breaking and reforming [17]. As expected from the lability of the agostic bond, the reactions of **24a** and **24b** with carbon monoxide give the *cis*-dicarbonyl complexes $OsH\{C_6H_4$-2-*E*-$CH{=}CHR\}(CO)_2(P^iPr_3)_2$ (R = Ph (**26a**), CH_3 (**26b**)), in which the incoming ligand coordinates *trans* to the hydride position, releasing the C-H bond from the metal coordination sphere.

The exclusive formation of **24c**, by reaction of **21b** with $LiCD_3$, and the *trans* position of the two substituents at the carbon-carbon double bond of **24** suggests that the reactions of **21b** with LiR (R = Ph, CH_3, CD_3) follow the steps shown in Scheme 8. The reactions appear to involve the replacement of the chlorine by the R group to give the R-styrylosmium(II) species **27**. Subsequently, the carbon-carbon reductive coupling should afford the osmium(0) intermediates **28**, containing a coordinated olefin ligand. Because the reductive carbon-carbon coupling is a concerted process, the stereochemistry at the carbon-carbon double bond is retained, thus, the phenyl and R groups are mutually *trans*. Finally, the C-H activation of the *ortho*-CH bond of the phenyl group should lead to the reaction products [16].

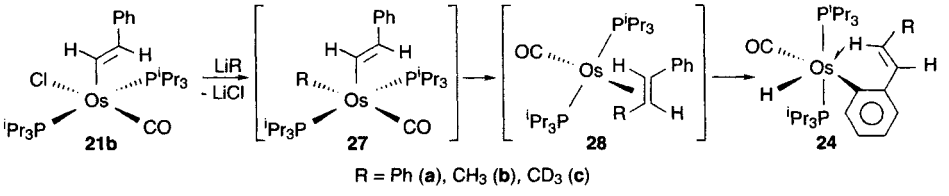

Scheme 8

In solution, complexes **24b** and **24c** transform into the allyl compounds $OsH(\eta^3$-$CH_2CHCHPh)(CO)(P^iPr_3)_2$ (**29b**) and $OsD(\eta^3$-$CD_2CHCHPh)(CO)(P^iPr_3)_2$ (**29c**), according to Scheme 9. The isomerization is a first order process with activation parameters for the conversion of **24b** into **29b** of $\Delta H^{\neq} = 20.8$ (± 1.7) kcal·mol^{-1} and $\Delta S^{\neq} = -2.8$ (± 2.0) cal·K^{-1}·mol^{-1}, and a primary isotope effect of 3.6 at 30 °C.

The near zero activation entropy is consistent with an intramolecular process, whereas the primary isotope effect suggests that the rate-determining step of the isomerization involves the cleavage of one C-H bond of the methyl group.

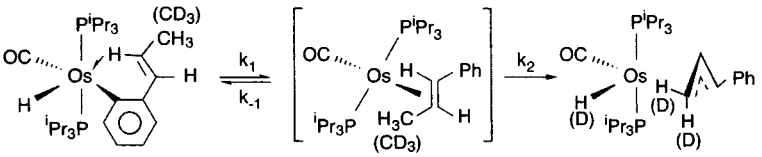

24b (24c) **28b (28c)** **29b (29c)**

Scheme 9

In view of the *trans* relative position of the metallated phenyl ring and the methyl substituent at the carbon-carbon double bond, the methyl C-H activation step seems unlikely to occur in **24b**. Thus, the isomerization reaction might involve an initial step consisting of the reductive elimination of 1-phenylpropene from **24b** to give the unsaturated osmium(0) intermediate **28b**. This intermediate is consistent with the observation that no H/D scrambling occurs between the *ortho* phenyl position and the methyl group during the isomerization of **24c**. The second and slow step of the reaction would consist in the C-H activation of the methyl group of the 1-phenylpropene in **28b** to give **29b**.

Despite the fact that the C-H activation of the methyl group in **28b** (k_2) is the slow step of the isomerization, no signal corresponding to **28b** can be spectroscopically detected in the course of the isomerization. Moreover, the only signals observable during the reaction are those corresponding to **24b** and **29b**. The fact that **28b** does not accumulate in solution suggests that the C-H activation process in **28b** to reform **24b** (k_{-1}) is faster than the conversion of **28b** into **29b**. This is also in agreement with the formation of complexes **24** via Scheme 8.

The reactions shown in Scheme 9 may be considered as two competitive C-H activation processes in an undetected osmium(0) complex. One of them, kinetically favored and reversible at room temperature, consists of the activation of the *ortho*-C-H of the phenyl ring to give the product of kinetic control **24b**. The other, which requires a large activation enthalpy leads to the isomer **29b**. Because the η^3-allyl coordination is expected to give a more stable complex than the η^1-phenyl coordination, complex **29b** is the product of thermodynamic control.

Products from the oxidative addition of the olefinic C-H bonds are not observed. This appears to be due to the higher thermodynamic stability of the aryl product with regard to the alkenyl species. Thus, it has been observed that the reaction of **21b** with Li^{n}Bu affords OsH{C_6H_4(CH=CH_2)}(CO)(P^{i}Pr$_3$)$_2$ (**33**), according to Scheme 10. Interestingly, however, the reactivity of **33** can be easily understood as a result of the reactions of the more labile isomer OsH{(*E*)-CH=CHPh}(CO)(P^{i}Pr$_3$)$_2$ (**31**). For example, passing a slow stream of carbon dioxide through an hexane solution of **33** affords the formato-styryl complex Os{(*E*)-CH=CHPh}(κ^2-O_2CH)(CO)(P^{i}Pr$_3$)$_2$ (**34**), which can be rationalized as the insertion of carbon dioxide into the Os-H bond of **31** [18].

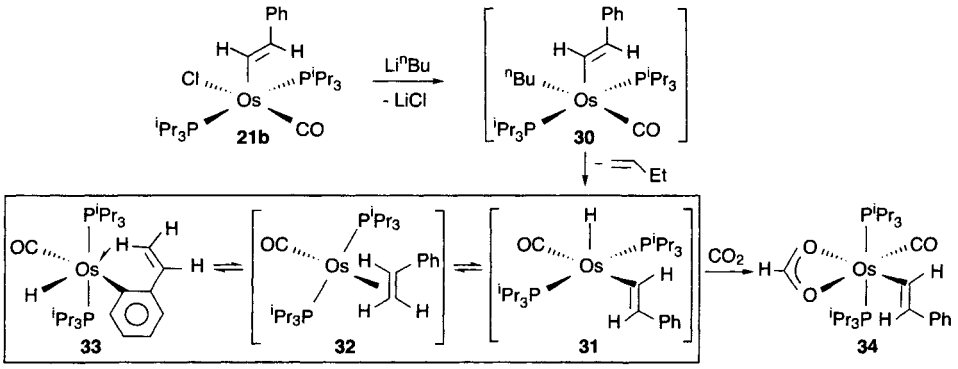

Scheme 10

7.3.3 Formation of β-diketonato and monothio-β-diketonato derivatives

Treatment of tetrahydrofuran solutions of the hydride-chloro complex **20**, at room temperature, with the stoichiometric amount of another methanol solution of KOH gives the five-coordinate hydride-hydroxo derivative $OsH(OH)(CO)(P^iPr_3)_2$ (**35**). The addition of the stoichiometric amount of acetylendicarboxylic methyl ester to diethyl ether solutions of **35** affords a red solution, from which orange crystals of the β-diketonato complex **36** are isolated in 95% yield, after crystallization from pentane at -20 °C (Scheme 11). The formation of **36**, which has been characterized by X-ray diffraction analysis, is the result of the *trans*-addition of the O-H bond of **35** to the carbon-carbon triple bond of the alkyne [19].

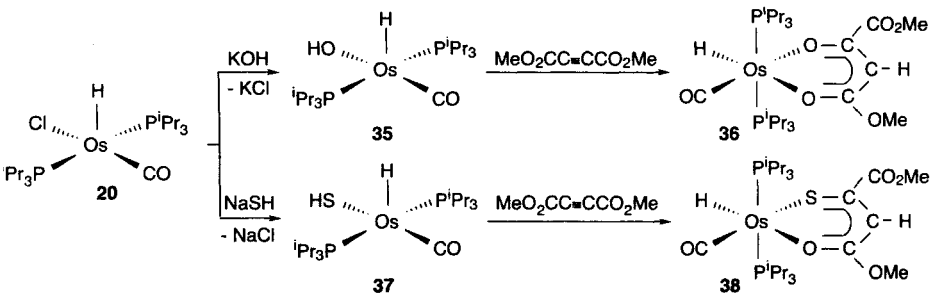

Scheme 11

Similarly to its ruthenium counterpart, complex **20** reacts with NaHS to give the hydride-metallothiol derivative $OsH(SH)(CO)(P^iPr_3)_2$ (**37**), which reacts with acetylendicarboxylic methyl ester to afford the monothio-β-diketonato **38** with the hydride ligand *cis* to the sulfur atom of the chelate group [14].

7.4 THE DIHYDROGEN-RUTHENIUM COMPLEX $[Ru(\eta^5\text{-}C_5H_5)(CO)(\eta^2\text{-}H_2)(P^iPr_3)]BF_4$ AS A PRECURSOR FOR CARBON-CARBON, CARBON-OXYGEN, CARBON-NITROGEN, CARBON-SULFUR, AND CARBON-PHOSPHORUS COUPLING REACTIONS

This dihydrogen compound is prepared according to Scheme 12 [20]. Treatment of a refluxing suspension of **1** in methanol with freshly distilled cyclopentadiene in a 1:22 molar ratio for 4 h gives the hydride-cyclopentadienyl derivative $RuH(\eta^5\text{-}C_5H_5)(CO)(P^iPr_3)$ (**39**). The addition of 1 equiv of $HBF_4{\cdot}OEt_2$ to dichloromethane solutions of **39** affords the dihydrogen compound $[Ru(\eta^5\text{-}C_5H_5)(CO)(\eta^2\text{-}H_2)(P^iPr_3)]BF_4$ (**40**), with a hydrogen-hydrogen separation of 0.94 Å, in equilibrium with traces of the dihydride tautomer $[RuH_2(\eta^5\text{-}C_5H_5)(CO)(P^iPr_3)]BF_4$ (**41**). In agreement with the lability of the dihydrogen ligands, the addition of acetone to the dichloromethane solutions of **40** produces the displacement of the coordinated hydrogen molecule, and the formation of the solvated complex $[Ru(\eta^5\text{-}C_5H_5)(CO)\{\eta^1\text{-}OC(CH_3)_2\}(P^iPr_3)]BF_4$ (**42**), which can be directly obtained by protonation of **39** in acetone as solvent.

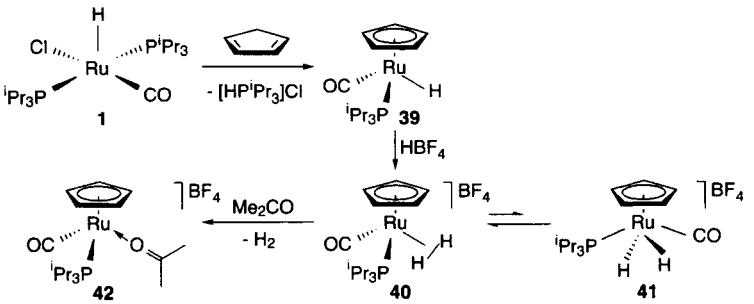

Scheme 12

Complex **42** reacts with 1,1-diphenyl-2-propyn-1-ol to give the allenylidene compound $[Ru(\eta^5\text{-}C_5H_5)(C{=}C{=}CPh_2)(CO)(P^iPr_3)]BF_4$ (**43**), according to Eq. 1.

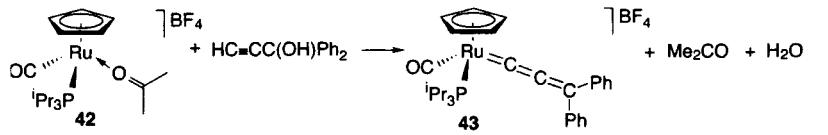

(1)

EHT-MO calculations indicate that allenylidenes coordinate to metal centers as σ-donor and π-acceptor ligands. The interaction between the HOMO of the allenylidene and LUMO of the metallic fragment produces a lower charge transfer than the interaction between the HOMO of the metallic fragment and

the LUMO of the allenylidene. Then, the π-acceptor component of the metal-allenylidene bond is stronger than the σ-donor one [21].

The majority of allenylidene complexes have only donor ligands which somewhat reduce the electrophilicity of the allenylidene [22]. The presence of a carbonyl ligand in **43** may seem trivial, however its π-acidic nature enhances the reactivity associated with the allenylidene spine. According to a Mulliken population analysis of the model complex $[Ru(\eta^5\text{-}C_5H_5)(C{=}C{=}CH_2)(CO)(PH_3)]^+$, the 60% of the LUMO of **43** is located on the allenylidene ligand with a distribution on the carbon atoms of 23% (C_α), 6% (C_β), and 31% (C_γ), whereas the 20% of the HOMO is located on the β-carbon atom. Furthermore, from the same analysis it is inferred that the net charges on each carbon are -0.36 (C_α), -0.13 (C_β), and -0.05 (C_γ) [23]. The above mentioned implies that the α- and γ-carbon atoms of the allenylidene of **43** are electrophilic centers, while the β-carbon atom is nucleophilic. This, together with the enhancement of the reactivity of the allenylidene, associated to the presence of a carbonyl group in **43**, gives rise to a C_3-organic fragment with three reactive centers, which are active for a wide range of carbon-carbon and carbon-heteroatom coupling processes. As a consequence, the introduction of the allenylidene ligand into the ruthenium atom, and the addition of organic molecules with one, two, and three reactive centers to the C_3-fragment, allow the synthesis of a new generation of organometallic ligands and the formation of organic skeletons, difficult to be prepared by the traditional organic methods.

7.4.1 Addition of phenylacetylene and methane to the allenylidene ligand of $[Ru(\eta^5\text{-}C_5H_5)(C{=}C{=}CPh_2)(CO)(P^iPr_3)]BF_4$

Although complex **43** does not react with phenylacetylene and methane, the products resulting from the formal addition of H-C bonds of these molecules to the C_α-C_β and C_β-C_γ bonds of the allenylidene ligand of **43** can be easily obtained [23]. Because in the allenylidene ligand of **43**, the C_α and C_γ atoms are electrophilic centers, and the C_β atom is nucleophilic, the synthetic strategy involves the initial nucleophilic attack of the corresponding carbanion at the C_α or C_γ atoms and the subsequent protonation of the resulting allenyl or alkynyl derivatives.

Treatment of tetrahydrofuran solutions of **43** with 1.1 equiv of lithium phenylacetylide, between -40 and 0 °C, leads to a mixture of the alkynyl complex $Ru(\eta^5\text{-}C_5H_5)\{C{\equiv}CCPh_2C{\equiv}CPh\}(CO)(P^iPr_3)$ (**44**) and its allenyl isomer $Ru(\eta^5\text{-}C_5H_5)\{C(C{\equiv}CPh){=}C{=}CPh_2\}(CO)(P^iPr_3)$ (**45**). The allenyl complex **45**, which is a result of the attack of the acetylide at the C_α atom of the allenylidene of **43**, is the main product of the reaction. The isomer **44**, which is a result of the attack of the acetylide at the C_γ atom, is obtained in 18% yield.

Complex **45** reacts with $HBF_4{\cdot}OEt_2$ in dichloromethane to give the unusual carbene complex $[Ru(\eta^5\text{-}C_5H_5)\{C(C{\equiv}CPh)CH{=}CPh_2\}(CO)(P^iPr_3)]BF_4$ (**46**), where the substituted carbene ligand has two unsaturated groups, the acetylide -C≡CPh and the alkenyl -CH=CPh_2 (Scheme 13). This ligand is a result that one should expect if the insertion of the C_α-C_β double bond of the allenylidene ligand of **43** into the H-C(sp) bond of the alkyne had taken place. Its formation suggests that the inertia of **43** towards the alkyne is kinetic in origin.

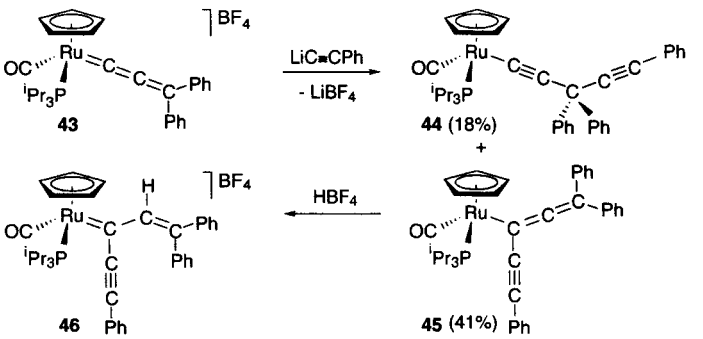

Scheme 13

Similarly to the reaction of **43** with LiC≡CPh, the addition of $LiCH_3$ to tetrahydrofuran solutions of **43** leads to a mixture of the allenyl complex $Ru(\eta^5\text{-}C_5H_5)\{C(CH_3){=}C{=}CPh_2\}(CO)(P^iPr_3)$ (**47**) and the alkynyl compound $Ru(\eta^5\text{-}C_5H_5)\{C{\equiv}CCPh_2(CH_3)\}(CO)(P^iPr_3)$ (**48**). In this case the main product of the reaction is the alkynyl species, resulting from the addition of the carbanion at the C_γ atom of the allenylidene. Complex **48** reacts with $HBF_4{\cdot}OEt_2$ in diethyl ether to give the vinilydene derivative $[Ru(\eta^5\text{-}C_5H_5)\{C{=}CHC(Ph)_2CH_3\}(CO)(P^iPr_3)]BF_4$ (**49**), which is a result of the formal addition of a H-C bond of methane to the C_β-C_γ double bond of the allenylidene ligand of **43** (Scheme 14).

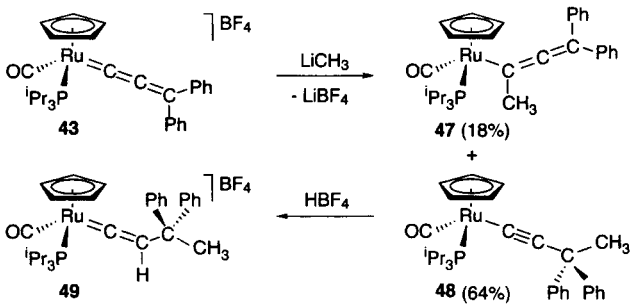

Scheme 14

7.4.2 Addition of acetone to the allenylidene ligand of [Ru(η⁵-C_5H_5)(C=C=CPh_2)(CO)(P^iPr_3)]BF_4

The allenylidene complex **43** is stable in acetone solution. However, the addition of potassium hydroxide gives rise to the functionalized alkynyl derivative Ru(η⁵-C_5H_5){C≡C$C(Ph)_2CH_2C(O)CH_3$}(CO)(P^iPr_3) (**50**), which is a result of the selective attack of the enolate of the ketone to the C_γ atom of the allenylidene ligand of **43**. Complex **50** reacts with HBF_4·OEt_2 to afford the unsaturated cyclic carbene complex **51** in 86% yield (Scheme 15) [23].

Complex **50** also reacts with 2 equiv of CF_3CO_2D to give **51-*d*$_2$** and CF_3CO_2H, and the reaction of Ru(η⁵-C_5H_5){C≡C$C(Ph)_2CD_2C(O)CD_3$}(CO)(P^iPr_3) (**50-*d*$_5$**) with 2 equiv of HBF_4 leads to **51-*d*$_4$** and DBF_4 (Scheme 16).

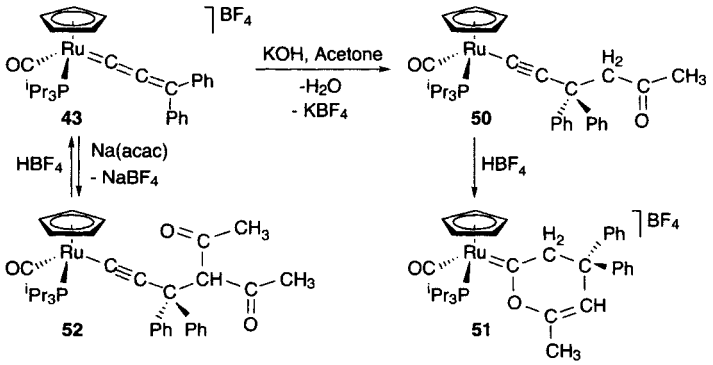

Scheme 15

On the basis of these isotope labeling experiments, the formation of **51** has been rationalized according to Scheme 17. One equivalent of acid protonates the alkynyl group of **50** to afford a vinylidene intermediate, whereas the other equivalent catalyzes the keto-enol conversion. Finally, the addition of the enol to the carbon-carbon double bond of the vinylidene intermediate yields the unsaturated cyclic carbene ligand.

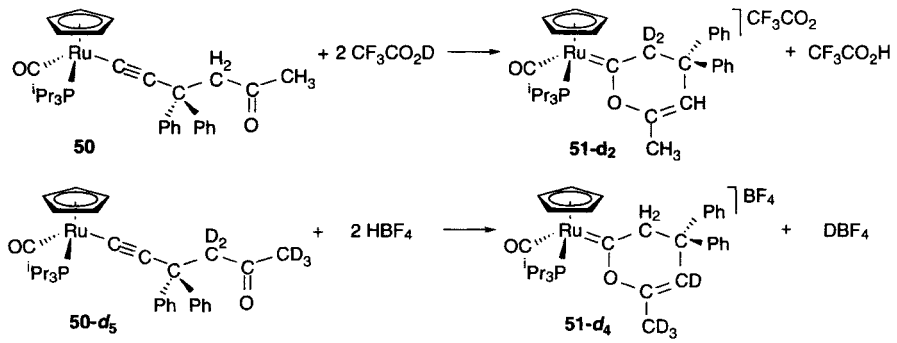

Scheme 16

From a methodological point of view, it should be pointed out the formation of **51**, which is a result of the addition of acetone to an allenylidene ligand. Heteroatom-containing cyclic metal-carbene complexes [24] have been conveniently prepared via metal ω-haloacyl, carbamoyl, alkoxycarbonyl, or imido intermediates [25], opening of epoxides by deprotonated Fischer-type carbene complexes [26], and activation of homopropargylic alcohols with low-valent d^6 complexes [27], including ruthenium(II) derivatives [28]. In general, the preparation of unsaturated cyclic carbene complexes requires the previous preparation of functional carbenes to react with β-dicarbonyl derivatives, acrylates, and enol ethers [29].

Complex **43** also reacts with sodium acetylacetonate. The reaction leads to the derivative $Ru(\eta^5\text{-}C_5H_5)\{C{\equiv}CC(Ph)_2CH[C(O)CH_3]_2\}(CO)(P^iPr_3)$ (**52**), related to **50**. However, in contrast to the latter, the protonation of **52** with $HBF_4{\cdot}OEt_2$ regenerates **43** (Scheme 15).

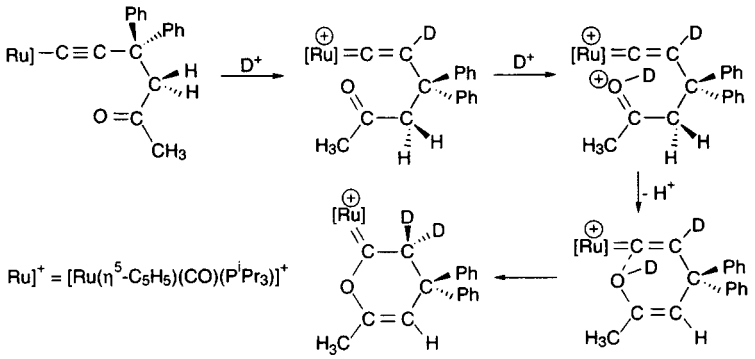

Scheme 17

7.4.3 *Addition of water and alcohols to the allenylidene ligand of* $[Ru(\eta^5\text{-}C_5H_5)(C{=}C{=}CPh_2)(CO)(P^iPr_3)]BF_4$

In contrast to the C-H bonds of phenylacetylene, methane and acetone, the O-H bonds of water and alcohols are added at the C_α-C_β double bond of the allenylidene ligand of **43** (Scheme 18) [20]. The reaction with water leads to the α,β-unsaturated hydroxycarbene $[Ru(\eta^5\text{-}C_5H_5)\{C(OH)CH{=}CPh_2\}(CO)(P^iPr_3)]BF_4$ (**53**), which affords the acyl derivative $Ru(\eta^5\text{-}C_5H_5)\{C(O)CH{=}CPh_2\}(CO)(P^iPr_3)$ (**54**), when its dichloromethane solutions are passed through an Al_2O_3 column. The reaction with alcohols give the α,β-unsaturated-alcoxycarbenes $[Ru(\eta^5\text{-}C_5H_5)\{C(OR)CH{=}CPh_2\}(CO)(P^iPr_3)]BF_4$ (R = Me (**55**), Et (**56**), $CH_2CH{=}CH_2$ (**57**)). Treatment of these complexes with sodim methoxide in tetrahydrofuran produces the deprotonation of the olefinic group of the alkoxycarbene ligands and the formation of the alkoxyallenyl derivatives $Ru(\eta^5\text{-}C_5H_5)\{C(OR){=}C{=}CPh_2\}(CO)(P^iPr_3)$ (R = Me (**58**), Et (**59**), $CH_2CH{=}CH_2$ (**60**)).

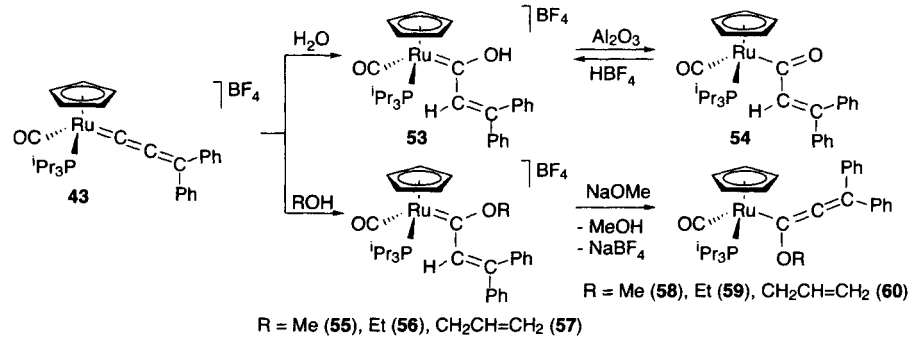

Scheme 18

Because the EHT-MO calculations on the model cation $[Ru(\eta^5\text{-}C_5H_5)(C{=}C{=}CH_2\}(CO)(PH_3)]^+$ indicate that the C_α and C_β atoms of the allenylidene unit are electrophilic and nucleophilic centers, respectively, and the H-O hydrogen atoms of water and alcohols are electrophilic, it has been proposed that the transition states for the above mentioned additions require heteroatom-C_α interactions, which labilize the O-H bonds, favouring the migration of the H-O hydrogen atoms to the C_β atom of the allenylidene. Thus, the lower nucleophilicity of the H-C(sp)carbon atom of phenylacetylene and H-C(sp^3) carbon atoms of methane and acetone could explain why the additions of the latter substrates to the allenylidene ligand are kinetically disfavored processes [23].

Attempts to obtain alkoxyallenyl compounds by attack of alkoxy groups at the C_α atom of the allenylidene have been unsuccessful. The nucleophiles OMe^- and OH^- add at the C_γ atom of **43**, leading to the alkynyl complexes $Ru(\eta^5\text{-}C_5H_5)\{C{\equiv}CC(Ph)_2OR\}(CO)(P^iPr_3)$ (R = Me (**61**), R = H (**62**)) (Scheme 19). Isomerization of **61** into the alkoxyallenyl **58** is not observed. This is in agreement with theoretical calculations on the model compounds $Ru(\eta^5\text{-}C_5H_5)\{C(OMe){=}C{=}CH_2\}(CO)(PH_3)$ and $Ru(\eta^5\text{-}C_5H_5)\{C{\equiv}CC(OMe)H_2\}(CO)(PH_3)$, which indicate that the second model complex is 9.29 kcal·mol^{-1} more stable than the first one [30].

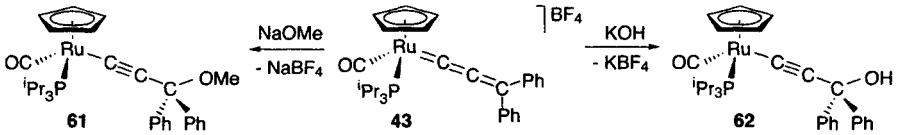

Scheme 19

In solution, the alkoxyallenyl complex **60** is stable at low temperature. At room temperature, it evolves into the tricyclic tetraenyl derivative $Ru(\eta^5\text{-}C_5H_5)$(9-phenyl-3,3a,4,4a-tetrahydronaphto[2,3-*c*]-1-furanyl)(CO)(P^iPr_3) (**63**) by

an intramolecular Diels-Alder reaction, where the C_β-C_γ double bond and one of the two phenyl groups of the allenyl unit act as an inner-outer ring diene and the $CH=CH_2$ double bond of the alkoxy fragment acts as a dienophile. The isomerization is highly stereospecific due to the chiral nature of **60**. Thus, the approach of the dienophile to the diene is determined by the *R* or *S* configuration of the metallic center of **60** (Scheme 20). The C_β atom of the tetraenyl ligand of **63** is the nucleophilic center of the molecule. As a consequence, the reaction of **63** with HBF_4 leads to the tricyclic carbene [Ru(η^5-C_5H_5)(9-phenyl-1,3,3a,4,4a,9a-hexahydronaphtho[2,3-*c*]-1-furanylidene)(CO)(P^iPr_3)]BF_4 (**64**) by direct attack of the proton of the acid to the C_β atom of the tetraenyl unit of **63**. The attack is also stereospecific, and the proton makes its entry in the direction pointed by the carbonyl group of **63**. In solution, complex **64** is also unstable and evolves into the acyclic alkoxycarbene [Ru(η^5-C_5H_5){C(OCH_2[1-phenyl-3,4-dihydro-3-naphthyl])H}(CO)(P^iPr_3)]BF_4 (**65**) by a concerted intramolecular hydrogen transfer reaction. At room temperature, in methanol as the solvent, complex **65** losses the alkoxy group to afford the alcohol 3-hydroxymethyl-1-phenyl-3,4-dihydronaphthalene (**66**) and the methoxycarbene organometallic salt [Ru(η^5-C_5H_5){C(OCH_3)H}(CO)(P^iPr_3)]BF_4 (**67**) (Scheme 20) [31].

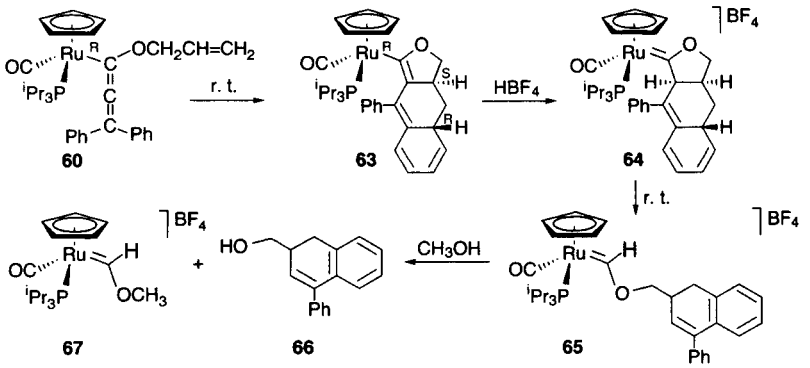

Scheme 20

Complex **43** also adds propargyl alcohol. The reaction is similar to those with the previously mentioned alcohols (Scheme 18), and the α,β-unsaturated propargyloxy-carbene [Ru(η^5-C_5H_5){$C(OCH_2C{\equiv}CH)CH{=}CPh_2$}(CO)($P^iPr_3$)]$BF_4$ (**68**) is obtained according to Eq. 2.

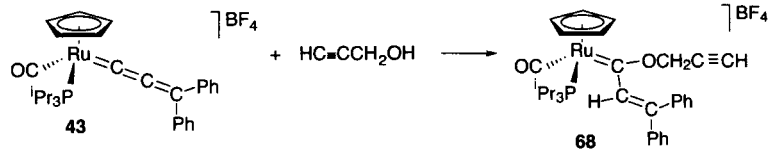

(2)

However, in basic medium, there are marked differences in behaviour between **68** and **55-57**. The treatment of **68** with bases does not afford an allenyl derivative, but a mixture of six different cycloaddition products. The main component of the mixture depends on the nature of the base used (Scheme 21) [32]. In the presence of 1 equiv of sodium carbonate the polycyclic carbene complex [Ru(η^5-C_5H_5){9-phenyl-1,3-dihydronaphtho-[2,3-*c*]-1-furanylidene}(CO)(P^iPr_3)]BF_4 (**69**) is obtained, which by reaction with $NaBH_4$ affords [Ru(η^5-C_5H_5){CH_2(1-phenyl-3-hydroxymethyl-2-naphthyl)}(CO)(P^iPr_3) (**70**). Treatment of **68** with 3 equiv of sodium methoxide gives rise to the Ru_R, C_R; Ru_S, C_S racemic mixture of the dihydronaphtho-furanyl complex Ru(η^5-C_5H_5){9-phenyl-1,3-dihydronaphtho-[2,3-*c*]-1-furanyl}(CO)(P^iPr_3) (**71**), which within a chromatography column epimerizes to the corresponding Ru_R, C_S; Ru_S, C_R racemic form (complex **72** in Scheme 21), or is transformed into its isomer Ru(η^5-C_5H_5){CH_2(1-phenyl-3-carboxa-2-naphthyl}(CO)(P^iPr_3) (**73**), depending upon the polarity of the eluent used. When **68** is passed through an alumina column using a tetrahydrofuran/dichloromethane (5:1) mixture as eluent, the isomer of **71**, Ru(η^5-C_5H_5){9-phenyl-3,3a-dihydronaphtho-[2,3-*c*]-1-furanyl}(CO)(P^iPr_3) (**74**), is formed.

The formation of **69**, **71**, and **74** has been rationalized according to Scheme 22. Since the formation of these compounds occurs under basic conditions, and it is well known that bases catalyze the isomerization of propargylic into allenic

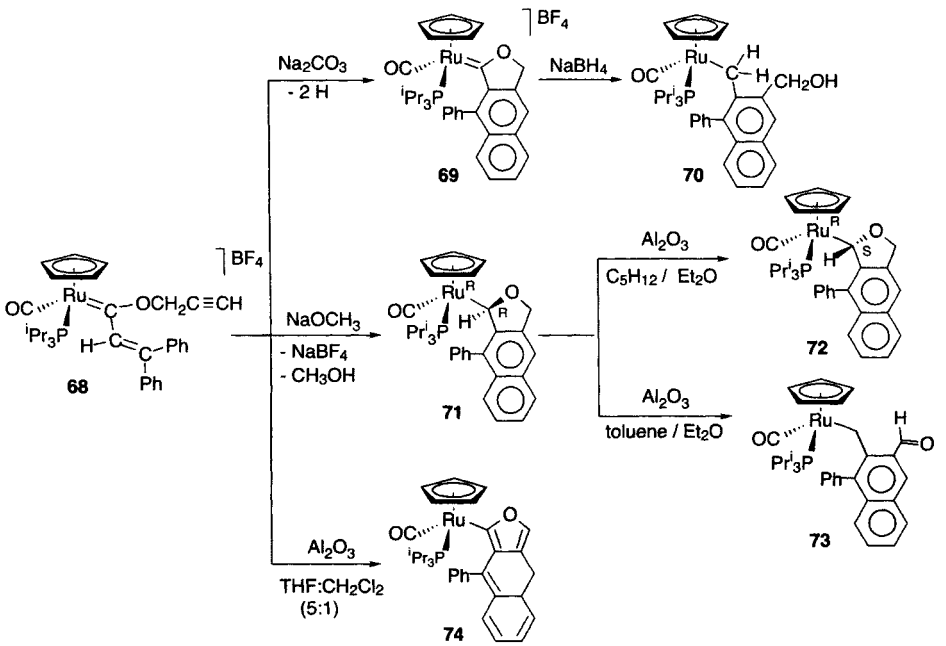

Scheme 21

moieties, it has been proposed an alkyne-allene rearrangement to give **B** as the first step of the reaction. This intermediate **B** could evolve via an intramolecular Diels-Alder reaction similar to that shown in Scheme 20, where the C_β-C_γ double bond and one of the two phenyl groups of the alkenyl-carbene unit of **B** act as an inner-outer ring diene, while the terminal C-C double bond of the allene moiety should act as a dienophile. Subsequently, a 1,3-hydrogen shift from the CH_2 group of the central six-membered ring to the OCH- carbon atom in the resulting intermediate **C** would give **D**. A further step of aromatization of **D** should afford complex **69**. Deprotonation of intermediate **D** at the carbon C_{9a} would give intermediate **E**, which could evolve into **71** by a 1,5-hydrogen shift from carbon C_{4a} to C_1, or alternatively into **74** by 1,3-hydrogen migration from C_3 to C_4. Complex **71** could be also formed by deprotonation of **D** at C_{4a} and a hydrogen migration from C_{9a} to C_1.

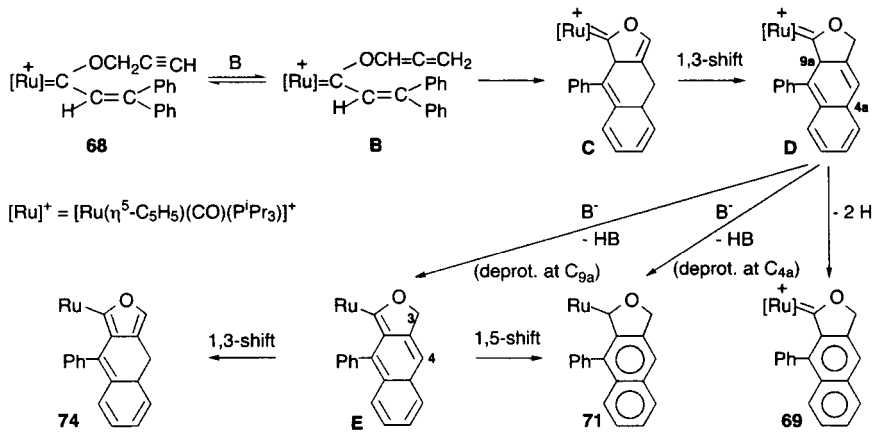

Scheme 22

7.4.4 *Addition of secondary and primary amines to the allenylidene ligand of* $[Ru(\eta^5\text{-}C_5H_5)(C{=}C{=}CPh_2)(CO)(P^iPr_3)]BF_4$

The diphenylallenylidene ligand of **43** also adds at the C_α-C_β double bond the N-H bond of secondary and primary amines, to afford azoniabutadienyl derivatives of the types $[Ru(\eta^5\text{-}C_5H_5)\{C(CH{=}CPh_2){=}NR_2\}(CO)(P^iPr_3)]BF_4$ (**75**, **76**) and $[Ru(\eta^5\text{-}C_5H_5)\{C(CH{=}CPh_2){=}NHR\}(CO)(P^iPr_3)]BF_4$ (**77**, **78**), respectively (Scheme 23) [33]. Although, at a first glance, an important contribution of the aminocarbene resonance form to the structure of these compounds should be expected, the X-ray structure determination of the complex **75** and the analysis of the ellipticities of the Ru-C_α and C_α-N bonds of the model cation $[Ru(\eta^5\text{-}C_5H_5)\{C(CH{=}CH_2){=}NH_2\}(CO)(PH_3)]^+$ indicate that the contribution of this resonance form is not relevant. According to the values of the

ellipticities 0.07, for the Ru-C_α bond, and 0.12, for the C_α-N bond, the respective single and double characters of the Ru-C_α and C_α-N bonds are unanswerable.

There is a marked difference, in the presence of bases, in behavior between the tertiary azoniabutadienyl complexes **75** and **76** and the secondary azoniabutadienyl compounds **77** and **78**. Treatment of **75** and **76** with sodium methoxide produces the deprotonation of the $CH{=}CPh_2$ group of the unsaturated η^1-carbon donor ligand, and the formation of the corresponding aminoallenyl derivatives $Ru(\eta^5\text{-}C_5H_5)\{C(NR_2){=}C{=}CPh_2)\}(CO)(P^iPr_3)$ (**79**, **80**). Under the same conditions, the deprotonation of **77** and **78** does not occur at the $CH{=}CPh_2$ group, but at the nitrogen atom. Thus, the reactions of the latters with sodium methoxide lead to the azabutadienyl derivatives $[Ru(\eta^5\text{-}C_5H_5)\text{-}\{C(CH{=}CPh_2){=}NR\}(CO)(P^iPr_3)$ (**81**, **82**).

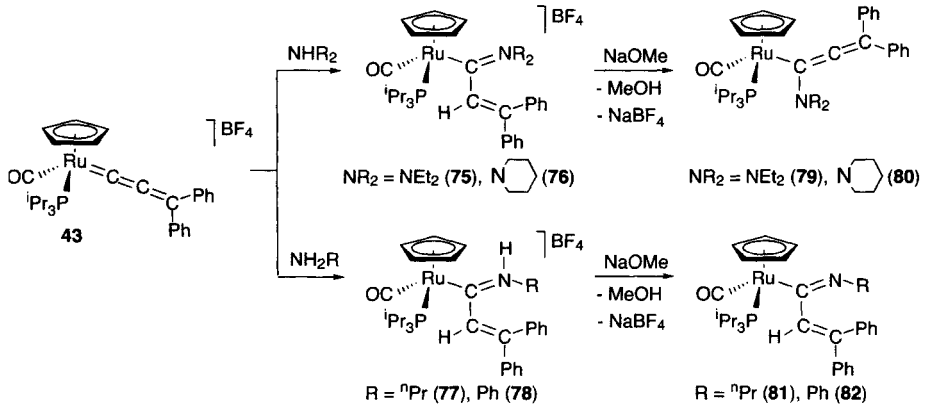

Scheme 23

Similarly to secondary and primary amines, the N-H bond of benzophenone imine is added at the C_α-C_β double bond of **43**, to give the α,β-unsaturated-2-azaallenyl derivative $[Ru(\eta^5\text{-}C_5H_5)\{C(CH{=}CPh_2){=}N{=}CPh_2)\}(CO)(P^iPr_3)]BF_4$ (**83**), which has been characterized by X-ray diffraction. By deprotonation, this compound yields the allenyl derivative $Ru(\eta^5\text{-}C_5H_5)\{C(N{=}CPh_2){=}C{=}CPh_2\}$ $(CO)(P^iPr_3)$ (**84**) (Scheme 24) [20].

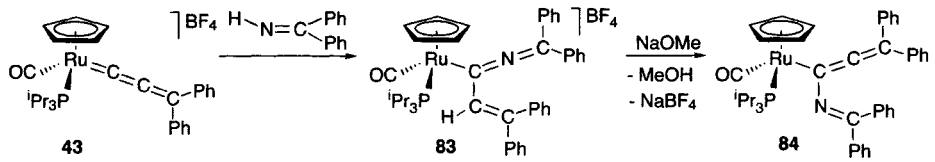

Scheme 24

In reactions with secondary amines containing a second nitrogen atom, the diphenylallenylidene ligand of **43** is active not only at the C_α-C_β double bond but also at the C_γ atom. Thus, the addition of pyrazoles to solutions of **43** leads to the pyrazolo[1,2-*a*]pyrazolyl complexes **85-87** (Scheme 25). Complexes **85** and **87** yield the functionalized alkynyl derivatives **88** and **89** by treatment with sodium methoxide. The formation of **85-87** involves novel 1,2,3-diheterocyclization reactions, where an organometallic complex is used for the first time [34].

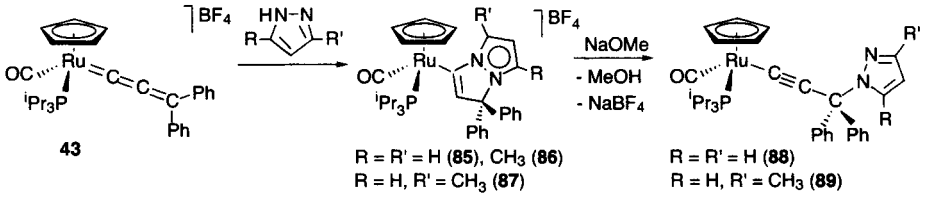

Scheme 25

Pyrido[1,2-*a*]pyrimidinyl complexes can be prepared according to Scheme 26 [35]. The reaction of **43** with 2-aminopyridine gives a mixture of the pyridinium[1,2-*a*]pyrimidinyl compound $[Ru(\eta^5\text{-}C_5H_5)\{2,2\text{-diphenyl-}2H\text{-pyridinium[1,2-}a\text{]pyrimidin-4-yl}\}(CO)(P^iPr_3)]BF_4$ (**90**) and its azoniabutadienyl isomer $[Ru(\eta^5\text{-}C_5H_5)\{C(CH{=}CPh_2){=}NH(o\text{-pyridinyl})\}(CO)(P^iPr_3)]BF_4$ (**91**). The molar ratio of the isomers in the mixture depends on the reaction temperature. At temperatures lower than -30 °C, isomer **90** is the main reaction product, while at 0 °C an inverse relationship is observed.

At a first glance, the formation of **90** could be rationalized as the addition of one of the two NH bonds of the amine to the C_β-C_γ double bond of the allenylidene ligand of **43** and the subsequent coordination of the nitrogen atom of the pyridine

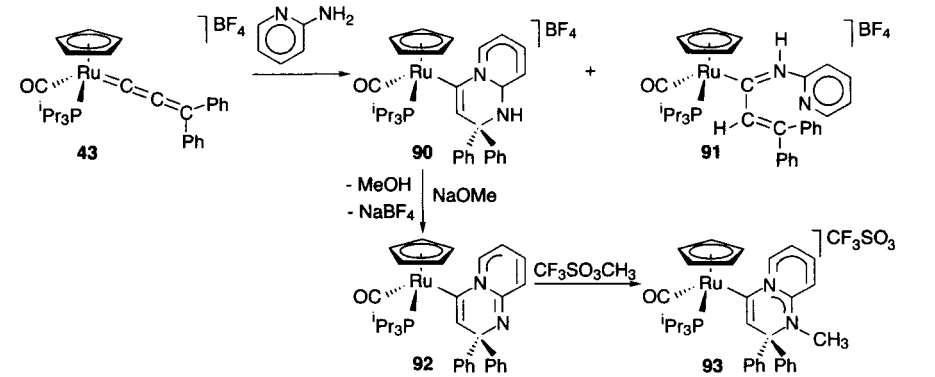

Scheme 26

group to the C_α atom. The formation of **91** can be rationalized as the addition of one of the two NH bonds of the amine to the C_α-C_β double bond of the allenylidene. According to this, one could think that the addition of primary amines containing a second nitrogen atom occurs not only at the C_α-C_β double bond of the allenylidene but also at the C_β-C_γ double bond. The first addition should be favored at high temperatures, while the second one should be favored at low temperatures. This trivial conclusion is probably incorrect. It should be noted that 2-aminopyridine also exists in the imino tautomeric form, and that this tautomeric equilibrium is highly dependent on the temperature [36]. On this basis, the formation of **90** can be rationalized as the addition of the endocyclic NH bond of the imino form at the C_α-C_β double bond of the allenylidene ligand, and the subsequent coordination of the exocyclic nitrogen atom to the C_γ atom. In addition, it should be noted that the pyridinic nitrogen atom of **91** is not coordinated to the C_γ atom of the azoniabutadienyl ligand. It could be argued that this is due to the large steric hindrance experienced by the phenyl and pyridinyl groups. However, it has been observed that the allenylidene of **43** reacts with pyridine-2-thiol to give a bicycle containing a N(pyridinyl)-CPh_2 bond (vide infra). Therefore, the instability of the product resulting from the intramolecular cyclization of **91** should be related to the electronic structure of its condensed heterocycles.

Treatment of **90** with sodium methoxide results in the deprotonation of the NH group of the heterocycle to give the pyrido[1,2-*a*]pyrimidinyl derivative $Ru(\eta^5\text{-}C_5H_5)$\{2,2-diphenyl-2*H*-pyrido[1,2-*a*]pyrimidin-4-yl\}$(CO)(P^iPr_3)$ (**92**), which reacts with methyl trifluoromethanesulfonate to afford $[Ru(\eta^5\text{-}C_5H_5)$\{1-methyl-2,2-diphenyl-2*H*-pyridinium[1,2-*a*]pyrimidin-4-yl\}$(CO)(P^iPr_3)]CF_3SO_3$ (**93**). The deprotonation of **90** produces a high electronic perturbation in the bycycle of this compound, as is shown in Scheme 26.

7.4.5 Addition of S-H bonds to the allenylidene ligand of $[Ru(\eta^5\text{-}C_5H_5)(C{=}C{=}CPh_2)(CO)(P^iPr_3)]BF_4$

In a similar way to that shown in Scheme 18, it is also possible to obtain thioallenyl derivatives (Scheme 27). Treatment of dichloromethane solutions of **43** with the stoichiometric amount of 1-propanethiol leads to the α,β-unsaturated (alkylthio)carbene $[Ru(\eta^5\text{-}C_5H_5)$\{$C(S^nPr)CH{=}CPh_2$\}$(CO)(P^iPr_3)]BF_4$ (**94**), which reacts with sodium methoxide to afford the (alkylthio)allenyl $Ru(\eta^5\text{-}C_5H_5)$\{$C(S^nPr){=}C{=}CPh_2$\}$(CO)(P^iPr_3)$ (**95**) [20]. The allenylidene ligand of **43** also adds pyridine-2-thiol. In this case, the reaction product is the bicycle compound **96**, which yields the allenyl derivative $Ru(\eta^5\text{-}C_5H_5)$\{C(Spy)=C=CPh_2\}$(CO)(P^iPr_3)$ (**97**) by reaction with sodium methoxide [34].

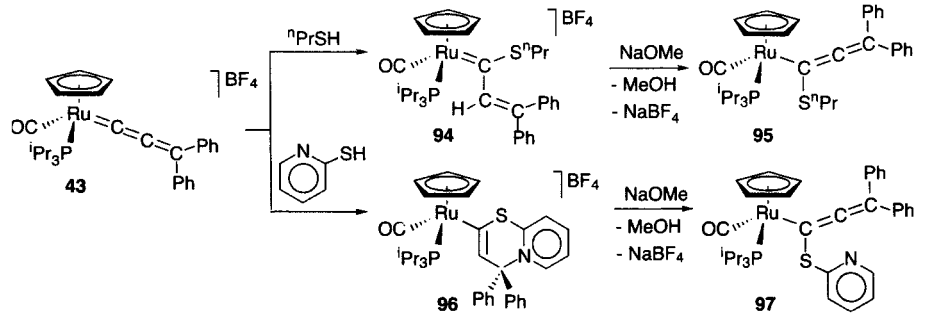

Scheme 27

1,3-Thiazinyl complexes can be obtained by reaction of **43** with thioisonicotinamide (Scheme 28) [35]. Treatment of dichloromethane solutions of **43** with stoichiometric amounts of this thioamide, under reflux, affords [Ru(η^5-C_5H_5){4,4-diphenyl-2-(*p*-pyridinyl)-4H-1,3-thiazinium-6-yl}(CO)(P^iPr_3)]BF_4 (**98**). The formation of **98** can be rationalized, formally, as the addition of one of the two NH bonds of the thioamide at the C_β-C_γ double bond of the allenylidene ligand of **43**, followed by the coordination of the sulfur atom to the C_α atom of the resulting vinylidene. However, it should be taken into account that primary and secondary thioamides have the tautomeric forms shown in Eq. 3 [37].

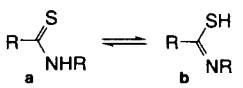

(3)

So, the reactions shown in Scheme 23 and 27 suggest that the addition of the S-H bond of the imidothiol form **b** to the C_α-C_β double bond of the allenylidene ligand of **43**, followed by the coordination of the nitrogen atom to the C_γ atom of the resulting thiocarbene intermediate is the most reasonable way to explain the formation of **98**. Moreover, since the formation of an isomer of **98** containing the nitrogen atom bonded to the RuC carbon atom is not observed, Scheme 28 suggests that the addition of SH bonds to the the C_α-C_β double bond of the allenylidene ligand of **43** is favored with regard to the addition of NH bonds.

Similarly to **90**, the nitrogen atom of **98** undergoes deprotonation in basic medium. The treatment of tetrahydrofuran suspensions of **98** with sodium methoxide leads to the thiazinyl derivative Ru(η^5-C_5H_5){4,4-diphenyl-2-(*p*-pyridinyl)-4H-1,3-thiazin-6-yl}(CO)(P^iPr_3) (**99**), which reacts with methyl trifluoromethanesulfonate to yield [Ru(η^5-C_5H_5){3-methyl-4,4-diphenyl-2-(*p*-pyridinyl)-4H-1,3-thiazinium-6-yl}CO)(P^iPr_3)]CF_3SO_3 (**100**).

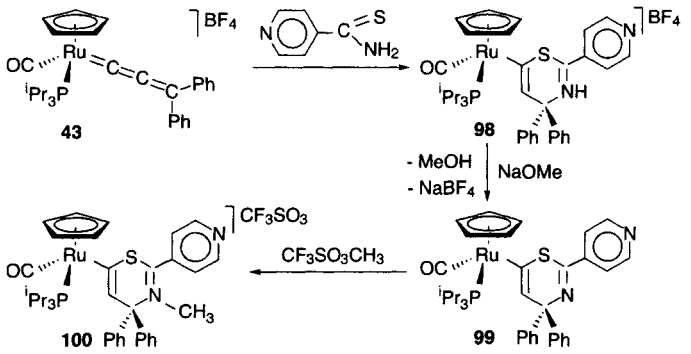

Scheme 28

7.4.6 *Addition of phosphines to the allenylidene ligand of [Ru(η⁵-C_5H_5)(C=C=CPh_2)(CO)(P^iPr_3)]BF_4*

Diphenylphosphine adds regioselectively to the C_α atom of the allenylidene ligand of **43** to afford [Ru(η⁵-C_5H_5){C($PHPh_2$)=C=CPh_2}(CO)(P^iPr_3)]BF_4 (**101**), according to Scheme 29. Complex **101** reacts with NEt_3 in toluene to give the neutral allenyl-phosphine derivative Ru(η⁵-C_5H_5){C(PPh_2)=C=CPh_2}(CO)(P^iPr_3) (**102**), which regenerates **101** by protonation with HBF_4·OEt_2. Complex **102** reacts with MeI to afford the iodide salt of the allenyl-phosphonio cation [Ru(η⁵-C_5H_5){C($PMePh_2$)=C=CPh_2}(CO)(P^iPr_3)]⁺ (**103**). The tetrafluoroborate salt is obtained by direct reaction of **43** with $PMePh_2$ in dichloromethane as solvent. Similarly, treatment of **43** with PPh_3 gives [Ru(η⁵-C_5H_5){C (PPh_3)=C=CPh_2}(CO)(P^iPr_3)]BF_4 (**104**) [30].

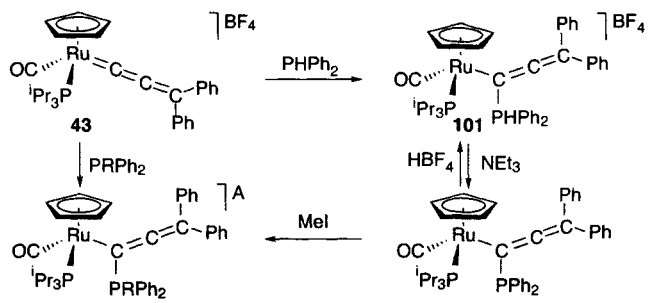

Scheme 29

The exclusive formation of **103** starting from **102** and **43** suggests that the addition of bulky phosphines to the C_α atom of the allenylidene ligand is kinetic and thermodinamically favored over the addition at the C_γ atom. The

origin of this preference may be the steric congestion due to the phenyl groups on the C_γ atom [38]. In fact, theoretical calculations at the MP2 level on the model cations $[Ru(\eta^5\text{-}C_5H_5)\{C(PH_3)=C=CH_2\}(CO)(PH_3)]^+$ and $[Ru(\eta^5\text{-}C_5H_5)\{C\equiv CC(PH_3)H_2\}(CO)(PH_3)]^+$ indicate that both isomers are minima on the potential energy surface and that the difference of energy between them is not greater than 3 kcal·mol^{-1}.

7.4.7 *Addition of ethyl diazoacetate to the allenylidene ligand of* $[Ru(\eta^5\text{-}C_5H_5)(C=C=CPh_2)(CO)(P^iPr_3)]BF_4$

Heteroatom-containing cyclic metal-carbene complexes can be also prepared by reaction of **43** with ethyl diazoacetate. Unlike the complexes of this type previously mentioned, they are doubly unsaturated with endocyclic and exocyclic carbon-carbon double bonds [39]. Treatment of dichloromethane solutions of **43** with ethyl diazoacetate at 40 °C leads to the cyclic carbene complex **105**, according to Eq. 4.

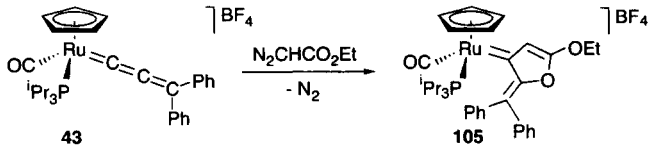

(4)

An X-ray diffraction study on **105** indicates that for an adequate description of the bonding situation in this compound a second resonance form such as **b** (Scheme 30) should be considered.

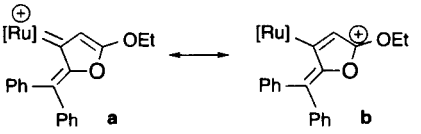

Scheme 30

In agreement with a significant contribution of the resonance form **b** to the structure of **105**, the C-OEt carbon atom of this complex shows a marked electrophilic character, adding nucleophiles (Scheme 31). The treatment of **105** with methyllithium at -60 °C affords the cyclic alkenyl compound **106**, while the reaction of **105** with sodium methoxide at room temperature gives **107**, which possesses an ortho ester alkenyl ligand. In agreement with the trend shown by organic ortho esters to eliminate ethers [40], complex **107** affords the lactonyl derivative **108** when its tetrahydrofurane solutions are passed through an Al_2O_3 column. Treatment at room temperature of the ortho ester alkenyl complex

107 with 1 equiv of $HBF_4{\cdot}OEt_2$ in diethyl ether as solvent regenerates **105**, by selective protonation of the methoxy group. However, under the same conditions, complex **106** leads to the new cyclic carbene **109** by protonation of the ethoxy group. The lactonyl complex **108** also reacts with $HBF_4{\cdot}OEt_2$. The addition, at -60 °C, of 4 equiv of $HBF_4{\cdot}OEt_2$ to dichloromethane solutions of **108** yields **110**.

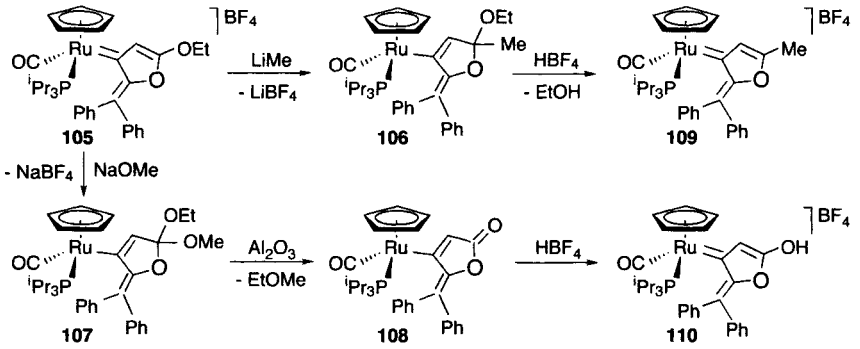

Scheme 31

7.4.8 Formation of azetidine and hexahydroquinoline skeletons

Azetidines are an interesting class of four-membered heterocyclic compounds, with various biological activities. These derivatives are difficult to synthetize due to ring strain. The allenylidene complex **43** has shown to be a useful substrate to generate this skeleton and to study its evolution into hexahydroquinoline [41]. Treatment of dichloromethane solutions of **43** with 1 equiv of dicyclohexylcarbodiimide at room temperature affords the iminiumazetidinylidenemethyl complex **111**, which is isolated as a 4:1 mixture of the isomers *Z* and *E* shown in Eq. 5.

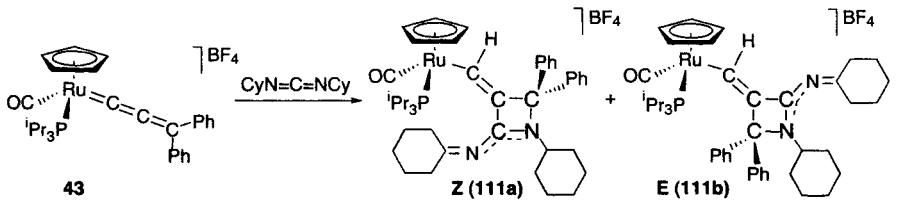

(5)

The formation of **111** (Scheme 32) has been rationalized as a [2+2] cycloaddition of one of the two carbon-nitrogen double bonds of the dicyclohexylcarbodiimide to the C_β-C_γ double bond of the allenylidene of **43** to give the intermediate **113**, which rapidly evolves into **114**, by an Alder-ene reaction, where the C_α-C_β double bond of **113** acts as an enophile. The presence

of the isomers *Z* (**111a**) and *E* (**111b**) in the reaction product suggests that the intermediate **114** exists as an equilibrium mixture of the isomers **114a** and **114b**. The [2+2] cycloaddition possibly occurs via a polar mechanism by attack of one of the nitrogen atoms of the carbodiimide on the allenylidene C_γ atom to give intermediate **112**.

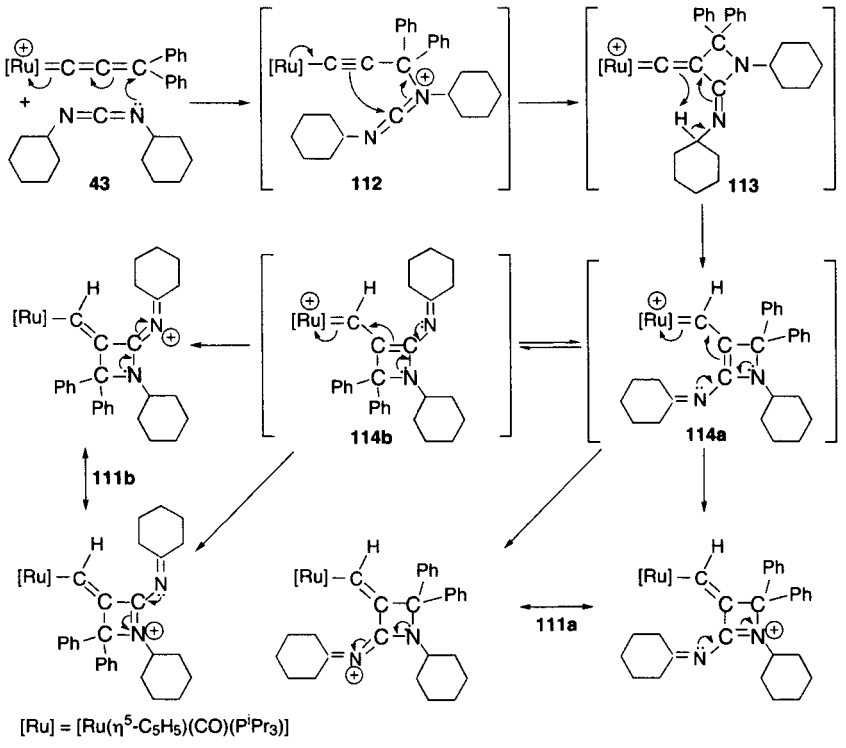

Scheme 32

Treatment of the isomeric mixture of **111** with sodium methoxide in tetrahydrofuran at room temperature affords the iminoazetidinylidenemethyl complex **115** as a result of the deprotonation of a CH_2CN proton of the cyclohexylidene group of **111** (Eq. 6).

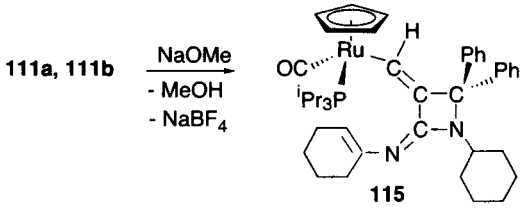

(6)

Although from the isomeric mixture of **111**, two stereochemistries at the carbon-carbon double bond of the unsaturated η^1-carbon ligand of **115** could result, *E* and *Z*, according to Eq. 6, only one of them, *Z*, is obtained. This appears to be related with the steric requirements of the triisopropylphosphine and azetidinylidenemethyl ligands, which are mutually *cis* disposed. Thus, both phenyl groups of the unsaturated η^1-carbon ligand are away from the bulky phosphine ligand.

Complex **115** reacts with 1 equiv of $HBF_4 \cdot OEt_2$ in diethyl ether at -78 °C to give compound **116** as a result of the protonation of the exocyclic nitrogen atom of the unsaturated η^1-carbon ligand of **115** (Scheme 33). Complexes **111** and **116** are isomers. Formally, complex **116** is a result of the migration of a $CH_2C{=}N$ proton of the cyclohexylidene group to the exocyclic nitrogen atom in **111**. This isomerization is not spontaneous even at high temperature in chloroform. The isomerization of **116** into **111** is also not observed. In dichloromethane and in chloroform, complex **116** is stable at low temperatures. At room temperature, it evolves into a 9:1 mixture of a new isomer, **117**, and a minor product, which was not identified. When a dichloromethane solution of the above mentioned mixture is passed through an Al_2O_3 column, the hexahydroquinolinylidenemethyl complex **118** is obtained as a result of the deprotonation of the endocyclic nitrogen atom of **117**. The protonation of **118** again affords **117**.

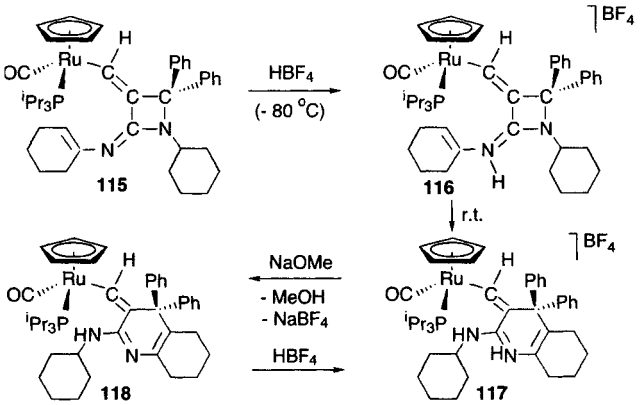

Scheme 33

In a similar manner to **111**, **116**, and **117**, complexes **118** and **115** are isomers. Although the isomerization of **115** into **118** is not spontaneous, the sequence of reactions shown in Scheme 33 indicates that it can be easily carried out by protonation of **115** and subsequent deprotonation of **117**. In addition, it should be noted that during the process the stereochemistry at the C-C double bond of the RuCH=C unit is retained.

Scheme 34 shows a possible mechanism for the isomerization of **115** to **118**, where the species **116** and **117** are intermediates. The process involves the split of the $NCPh_2$ bond of the azetidine skeleton and subsequent electrophilic attack of the resulting carbocation to the olefin of the cyclohexenyl group. Although, as a result of the protonation of **115**, complex **116** is the only one isolated species, in solution this compound should be in equilibrium with a non detectable concentration of its tautomer **116a**, which is produced by hydrogen transfer from the exocyclic nitrogen atom to the endocyclic nitrogen atom. Thus, the coordination of the lone electron pair of the azetidine nitrogen atom to the proton should promote the N-CPh_2 bond breakage to form the carbocation.

With regard to the result of the attack of the carbocation to the olefin of the cyclohexenyl group, it should be mentioned that the formation of the six-membered heterocycles of **117** and **118** is determined by the disposition of the substituents at the nitrogen atom of the imine group, during the process. Thus, using a molecular model, it can be easily established that a change in the position of the substituents at this nitrogen does not allow the formation of **117**. In other words, the rearrangement of the azetidine skeleton to the six-membered heterocycle is due not only to the presence of the cyclohexenylimino substituent in the azetidine but also to the stereochemistry at the C=N double bond.

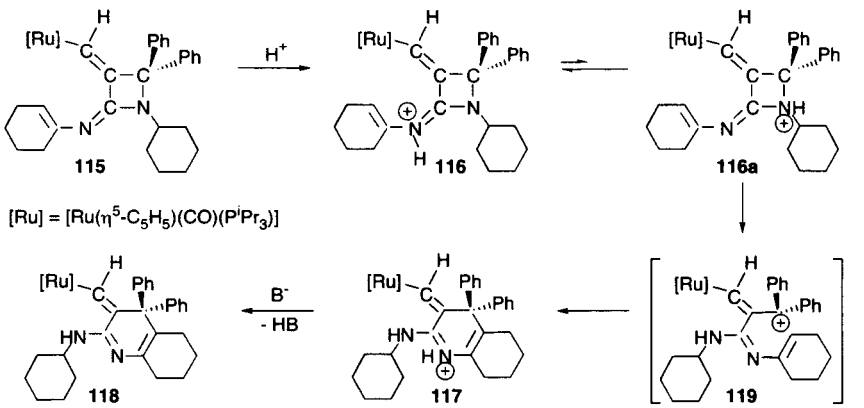

Scheme 34

7.5 THE DIHYDRIDE-OSMIUM(IV) COMPLEX $OsH_2Cl_2(P^iPr_3)_2$ AS A PRECURSOR FOR CARBON-CARBON, CARBON-NITROGEN, CARBON-PHOSPHORUS, CARBON-GERMANIUM, AND CARBON-SILICON COUPLING REACTIONS

The complex $OsH_2Cl_2(P^iPr_3)_2$ (**120**) is an unusual example of a six-coordinate osmium(IV) molecule, which is prepared by reaction of $OsCl_3.xH_2O$ with triisopropylphosphine in refluxing 2-propanol. Its solid state structure,

significantly distorted from octahedral, has only C_2 symmetry and can be described as a square antiprism with two missing vertices [42]. In solution, it exists as two rapidly interconverting isomers, one having C_2 symmetry and the other with no symmetry [43].

In recent years, it has been proved that complex **120** is a unique species with a completely different chemical behaviour than that of previously reported compounds [44]. Its reactions with diolefins, oximes, and cyclopentadienyl thallium give rise to interesting organometallic compounds containing organic fragments, which are activated to afford carbon-carbon and carbon-heteroatom coupling reactions.

7.5.1 Reactions of $OsH_2Cl_2(P^iPr_3)_2$ with diolefins

The reactions of **120** with diolefins leads to osmium products which result from C-H and C-C activation and C-C and C-P bond formation processes. They are competitive and depend upon the nature of the diolefin (Scheme 35) [45]. When the diene is 1,5-cyclooctadiene (COD), the dehydrogenation of an isopropyl

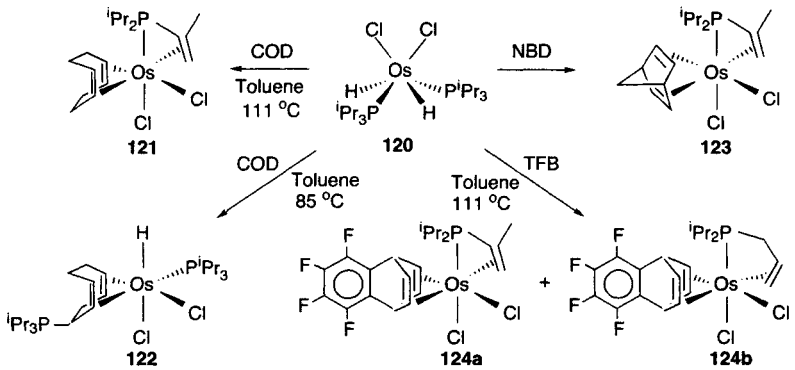

Scheme 35

group of triisopropylphosphine affords the isopropenylphosphine complex $OsCl_2(cod)\{^iPr_2PC(CH_3)=CH_2\}$ (**121**), under refluxing toluene. However, at 85 °C, the C-H activation of a coordinated 1,5-cyclooctadiene molecule occurs, and the reaction produces, by a subsequent C-P bond formation, the derivative $OsHCl_2(\eta^4\text{-}C_8H_{11}P^iPr_3)(P^iPr_3)$ (**122**) containing the carbocyclic ligand $[C_8H_{11}P^iPr_3]^+$. In the presence of 2,5-norbornadiene (NBD), the activation of the triisopropylphosphine ligand leads to the isopropenylphosphine complex $OsCl_2(nbd)\{^iPr_2PC(CH_3)=CH_2\}$ (**123**), while the activation of the diolefin is not observed. During the reaction of **120** with tetrafluorobenzobarrelene (TFB), the diene is not activated either. However, the C-H activation of the

triisopropylphosphine leads to a mixture of two propenyl phosphine isomers, as a result of two competitive β-elimination process on one metallated group of a metallated triisopropylphosphine ligand. The β-elimination of hydrogen leads to the isopropenylphosphine complex $OsCl_2(tfb)\{^iPr_2PC(CH_3)=CH_2\}$ (**124a**), while the β-elimination of the CH_3 group affords the allylphosphine derivative $OsCl_2(tfb)(^iPr_2PCCH_2CH=CH_2)$ (**124b**) by a subsequent C-C bond formation process.

7.5.2 Preparation of 2-aza-1,3-dienes

Complex **120** is not only useful to modify and generate ligands within the coordination sphere of the osmium but also allows the synthesis of 2-aza-1,3-dienes of the type $R_2C=NC(Ph)=CH_2$ ($CR_2 = C(CH_2)_4CH_2$, CMe_2), starting from oximes and phenylacetylene (Scheme 36).

The dihydride-dichloro complex **120** reacts with cyclohexanone oxime and acetone oxime in the presence of NEt_3 to give the dihydride derivatives $OsH_2Cl\{\kappa\text{-}N,\kappa\text{-}O\text{-}[ON=CR_2]\}(P^iPr_3)_2$ ($CR_2 = C(CH_2)_4CH_2$ (**125a**), CMe_2 (**125b**)) [46], which react with HCl to afford the hydride-azavinylidene compounds $OsHCl_2(N=CR_2)(P^iPr_3)_2$ (CR_2 = $C(CH_2)_4CH_2$ (**126a**), CMe_2 (**126b**)) and water [47].

Complexes **126** are rare examples of hydride-azavinylidene osmium(IV) species. In these compounds, the hydride and azavinilydene ligands are mutually

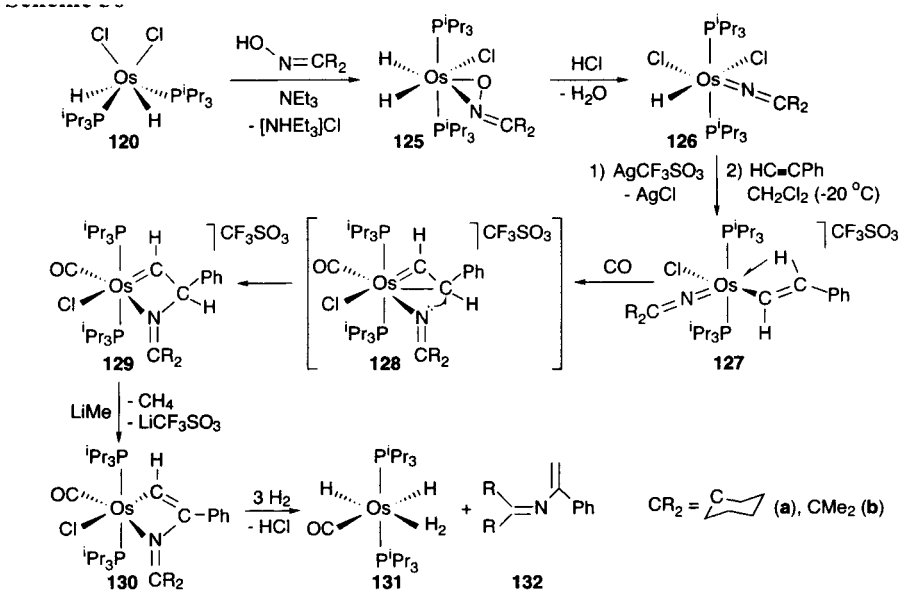

Scheme 36

cis disposed. Despite this, they are stable and do not evolve by 1,3- or 1,2-hydride shifts into the corresponding $OsCl_2(NCHR_2)(P^iPr_3)_2$ or $OsCl_2(NH{=}CR_2)(P^iPr_3)_2$ isomers. Theoretical calculations prove that the reason for their stability is both thermodynamic and kinetic in origin [47].

Complexes **126** do not react with phenylacetylene due to their saturated character. However, the treatment at room temperature of dichloromethane solutions of these compounds with 1.0 equiv of $Ag[CF_3SO_3]$, and the subsequent addition of 1.2 equiv of phenylacetylene at -20 °C affords, after 5 hours, the alkenyl-azavinylidene complexes $[Os\{(E)\text{-}CH{=}CHPh\}Cl(N{=}CR_2)(P^iPr_3)_2][CF_3SO_3]$ (CR_2 = $C(CH_2)_4CH_2$ (**127a**), CMe_2 (**127b**)), as a result of the extraction of a chloride ligand from **126** and the insertion of the carbon-carbon triple bond of the alkyne into the Os-H bonds of the resulting unsaturated intermediates [48].

In solution at room temperature, the alkenyl compounds **127** evolve into mixtures of five products. However, under carbon monoxide atmosphere, they lead to the cyclic heterocarbene derivatives **129**, probably, via the intermediates **128**. Treatment of tetrahydrofuran solutions of **129** with $LiCH_3$ at room temperature produces the deprotonation of the central CHPh carbon atom of the hetero-metalacycle and the formation of **130**. In benzene as solvent, complexes **130** react with molecular hydrogen to yield the corresponding azabutadienes **132** and the well known dihydride-dihydrogen complex $OsH_2(\eta^2\text{-}H_2)(CO)(P^iPr_3)_2$ (**131**) [49].

7.5.3 Generation of functionally substituted cyclopentadienyl ligands

Half-sandwich pentamethylcyclopentadienyl- and cyclopentadienylruthenium complexes exhibit a particularly rich and interesting chemistry, which has formed one of the cornerstones in the development of the organometallic field [28a, 50]. The chemistry of the related half-sandwich osmium complexes has attracted comparatively less attention, in particular those containing the $Os(\eta^5\text{-}C_5H_5)$ unit [51]. This is in part due to the lack of convenient osmium synthetic precursors [52] and the higher kinetic inertia of the $CpOsL_3$ compounds in comparison with the related iron and ruthenium complexes [53].

The dihydride-dichloro complex **120** is also a starting point for the cyclopentadienylosmium chemistry. Thus, it reacts with cyclopentadienylthallium to give $Os(\eta^5\text{-}C_5H_5)Cl(P^iPr_3)_2$ (**133**) [54]. Despite the high inertia of the $CpOsL_3$ compounds, this complex is a labile starting material for the development of new cyclopentadienyl-osmium chemistry. Thus, in pentane and toluene, the dissociation of a phosphine ligand is favored and the resulting metallic fragment $Os(\eta^5\text{-}C_5H_5)Cl(P^iPr_3)$ is capable of activating $HEPh_3$ molecules by oxidative addition. The reactions afford the osmium(IV) hydride derivatives $OsH(\eta^5\text{-}$

$C_5H_5)Cl(EPh_3)(P^iPr_3)$ (E = Ge (**134**), Si (**135**)) with a distribution of ligands around the metallic fragment that can be described as a four legged piano stool geometry (Scheme 37) [55].

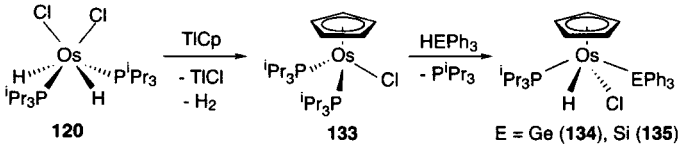

Scheme 37

Several types of substituted cyclopentadienyl osmium(IV) complexes can be obtained by reaction of **134** and **135** with LiNu (Nu = R, NR_2, PPh_2) reagents. These compounds are formed via $EPh_3(Os)/H(C_5H_5)$ or $Nu(Os)/H(C_5H_5)$ exchanges [56]. Treatment of tetrahydrofuran solutions of **134** and **135** with LiNu produces the replacement of the chlorine ligand by the Nu group, to afford $OsH(\eta^5\text{-}C_5H_5)Nu(EPh_3)(P^iPr_3)$. These intermediates are unstable and evolve in three different manners depending on the nature of E and the Nu group (Scheme 38).

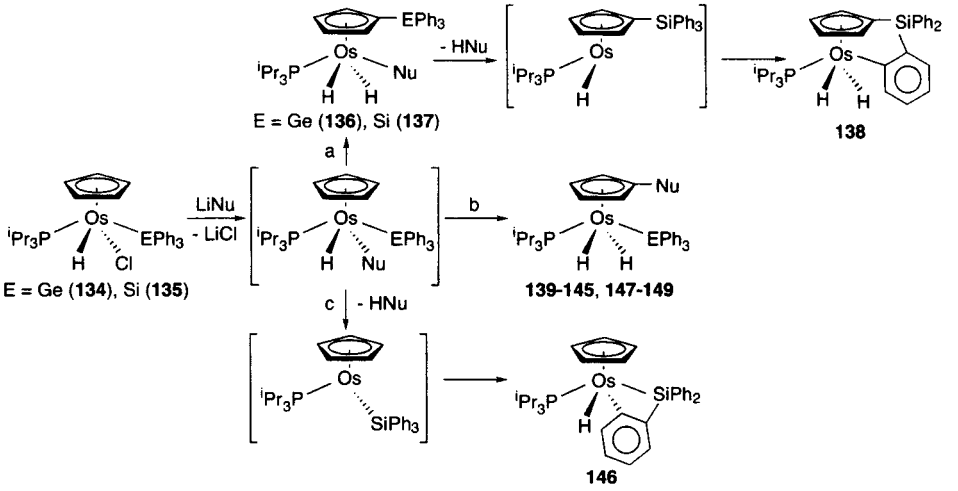

Scheme 38

(a) $EPh_3(Os)/H(C_5H_5)$ exchange. This process affords $OsH_2(\eta^5\text{-}C_5H_4EPh_3)Nu(P^iPr_3)$ derivatives, and occurs selectively when the atom E is Ge and the Nu group is CH_2N, and when E is Si and the Nu group is CH_2N, CH_3, and ^{n}Bu. Complexes $OsH_2(\eta^5\text{-}C_5H_4EPh_3)(CH_2N)(P^iPr_3)$ (E = Ge (**136**), Si (**137**)) are stable towards the reductive elimination of CH_3CN and can be isolated in high yields. However, the species $OsH_2(\eta^5\text{-}C_5H_4SiPh_3)R(P^iPr_3)$ (R = CH_3, ^{n}Bu) are unstable

towards the reductive elimination of alkane. As a result, the metallic center of the unsaturated formed intermediate $OsH(\eta^5\text{-}C_5H_4SiPh_3)(P^iPr_3)$ is capable of a C-H activation reaction on one of the phenyl groups of the $SiPh_3$ fragment, to give the dihydride-cyclometallated compound **138**.

(b) Nu(Os)/H(C_5H_5) exchange. This behaviour is selectively observed when the atom E is Ge and the Nu group is alkyl, amide or phosphide, and when E is Si and the Nu group is phosphide. In this case, the dihydride germyl derivatives $OsH_2(\eta^5\text{-}C_5H_4Nu)(GePh_3)(P^iPr_3)$ (Nu = CH_3 (**139**), ^{n}Bu (**140**), ^{sec}Bu (**141**), NEt_2 (**142**), $N(allyl)_2$ (**143**), PPh_2 (**144**)) and the dihydride silyl complex $OsH_2(\eta^5\text{-}C_5H_4PPh_2)(SiPh_3)(P^iPr_3)$ (**145**) are isolated.

(c) Reductive elimination of H-Nu. This occurs in the reaction of **135** with $LiCH_2C(O)CH_3$. The loss of acetone from $OsH(\eta^5\text{-}C_5H_5)(SiPh_3)\{CH_2C(O)CH_3\}(P^iPr_3)$ affords the $Os(\eta^5\text{-}C_5H_5)(SiPh_3)(P^iPr_3)$ intermediate, which has the same behaviour as the $Os(\eta^5\text{-}C_5H_5)(P^iPr_3)(LPh)$ systems [57] and evolves by aryl C-H activation into the hydride-cyclometallated compound **146**.

The reactions of **135** with $Li^{sec}Bu$ and $LiNR_2$ (R = Et, allyl) lead to mixtures of **138** and $OsH_2(\eta^5\text{-}C_5H_4Nu)(SiPh_3)(P^iPr_3)$ (Nu = ^{sec}Bu (**147**), NEt_2 (**148**), $N(allyl)_2$ (**149**)). This suggests that on the species $OsH(\eta^5\text{-}C_5H_5)(SiPh_3)Nu(P^iPr_3)$ (Nu = ^{sec}Bu, NEt_2, $N(allyl)_2$) both $SiPh_3(Os)/H(C_5H_5)$ and $Nu(Os)/H(C_5H_5)$ exchanges take place in a competitive manner.

The comparison of the products from the reactions previously mentioned indicates that the trend of the ligands H, Nu, and EPh_3 for exchanging their positions with the hydrogen atoms of the cyclopentadienyl group in the $OsH(\eta^5\text{-}C_5H_5)(EPh_3)Nu(P^iPr_3)$ species decreases in the sequence $PPh_2 > N(allyl)_2 > NEt_2 > SiPh_3 > {}^{sec}Bu > CH_3, {}^nBu > GePh_3 > H, CH_2CN, CH_2C(O)CH_3$.

7.5.4 Other coupling reactions using the Os(η^5-C_5H_5)(P^iPr_3) unit as a support

The chemical behaviour of **133** is a result of two factors: the high basicity of the metallic center, as a consequence of the presence of the strong donor phosphine and the chloride ligands in the complex, and the large steric hindrance experienced by the triisopropylphosphine groups, which are mutually *cis* disposed. This mixture allows access to reactive points on the osmium center by activation of Os-P and Os-Cl bonds.

In agreement with the tendency shown by **133** to release a phosphine ligand, the treatment of this compound with 1 equiv of 1,1-diphenyl-2-propyn-1-ol in pentane at room temperature leads to the π-alkynol complex $Os(\eta^5\text{-}C_5H_5)Cl\{\eta^2\text{-}HC{\equiv}C(OH)Ph_2\}(P^iPr_3)$ (**150**). In toluene at room temperature, this compound is stable. However, at 85 °C, it evolves into the allenylidene derivative $Os(\eta^5\text{-}C_5H_5)Cl(C{=}C{=}CPh_2)(P^iPr_3)$ (**151**), which has a very remarkable nucleophilic character [58].

The marked nucleophilic character of **151** is revealed by its inert behaviour towards alcohols, diphenylphosphine, benzophenone imine, pyrazole and acetate, and by its reactions with HBF_4 and dimethyl acetylenedicarboxylate, which afford $[Os(\eta^5\text{-}C_5H_5)Cl(CCH{=}CPh_2)(P^iPr_3)]BF_4$ and $Os(\eta^5\text{-}C_5H_5)Cl\{C{=}C(CO_2Me)C(CO_2Me){=}C{=}CPh_2\}(P^iPr_3)$ (**152**), respectively. The latter complex, which is a result of a novel $C_3 + C_2$ reaction, involves the insertion of the electron-withdrawing alkyne into the C_α-C_β double bond of the allenylidene ligand of **151**. The insertion can be rationalized as a stepwise cycloaddition to form an η^1-cyclobutenyl intermediate, which rapidly ring-opens to form the allenylvinylidene product (Scheme 39).

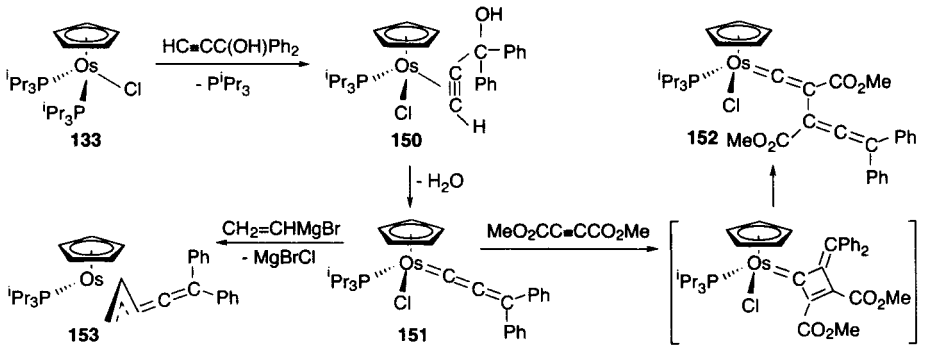

Scheme 39

Not only is the reactivity of **151** limited to the nucleophilic power of the C_β carbon atom of the allenylidene, but the chloro ligand is also activated toward the nucleophilic substitution, as is revealed by its reaction with KI to give $Os(\eta^5\text{-}C_5H_5)I(C{=}C{=}CPh_2)(P^iPr_3)$. This property is most probably responsible for the formation of the pentatrienyl complex $Os(\eta^5\text{-}C_5H_5)\{3\text{-}5\text{-}\eta\text{-}CH_2CHC{=}C{=}CPh_2\}(P^iPr_3)$ (**153**), as a result of the reaction of **151** with $CH_2{=}CHMgBr$, which is another $C_3 + C_2$ coupling reaction. In this respect, complex **151** shows a behaviour similar to that reported for the complexes $MCl(C{=}C{=}CPh_2)(P^iPr_3)_2$ (M = Rh, Ir) [7], which are related to the Vaska compound and, therefore, are also strong Lewis bases.

Treatment of **133** at room temperature with a suspension containing 1 equiv of $TlPF_6$ and 1.52 equiv of 1,1,-diphenyl-2-propyn-1-ol produces the activation of the Os-Cl of the starting complex, and the oxidative addition of the H-C(sp) bond of the alkynol to the resulting unsaturated metallic fragment $[Os(\eta^5\text{-}C_5H_5)(P^iPr_3)_2]^+$. As a result the hydroxyalkynyl-osmium(IV) derivative $[OsH(\eta^5\text{-}C_5H_5)\{C{\equiv}C(OH)Ph_2\}(P^iPr_3)_2]PF_6$ (**154**) is obtained (Scheme 40) [59].

In agreement with the null tendency of this type of osmium-systems to isomerize into hydroxyvinylidene derivatives, complex **154** is stable in the

solid state and in solution. Even the metallic center can be deprotonated without affecting the alkynyl unit. Thus, the addition of 2.7 equiv of KOH to methanol solutions of **154** affords the neutral hydroxyalkynyl compound $Os(\eta^5\text{-}C_5H_5)\{C{\equiv}CC(OH)Ph_2\}(P^iPr_3)_2$ (**155**), which reacts with HPF_6 to give the allenylidene $[Os(\eta^5\text{-}C_5H_5)(C{=}C{=}CPh_2)(P^iPr_3)_2]PF_6$ (**156**).

The reactivity of this allenylidene is a particular case in the chemistry of the diarylallenylidene complexes of the iron triad. The behaviour of its C_3-chain is intermediate between those observed for nucleophilic (*i. e.* complex **151**) and γ-electrophilic (ruthenium compounds of the type $[Ru(\eta^5\text{-}C_5R_5)(C{=}C{=}CPh_2)(PR_3)_2]^+$) derivatives. In agreement with the nucleophilic diarylallenylidene compounds, complex **156** reacts with HPF_6 to give $[Os(\eta^5\text{-}C_5H_5)(CCH{=}CPh_2)(P^iPr_3)_2](PF_6)_2$. However, in contrast to nucleophilic diarylallenylidene compounds, but in agreement with the γ-electrophiles, it undergoes the regioselective addition of nucleophilic reagents at the C_γ atom of the allenylidene. Thus, complex **156** reacts with $LiCH_3$ and acetone and methanol solutions of KOH to give the functionalized alkynyl compounds $Os(\eta^5\text{-}C_5H_5)\{C{\equiv}CC(Nu)Ph_2\}(P^iPr_3)_2$ (Nu = CH_3 (**57**), $CH_2C(O)CH_3$ (**158**), OCH_3 (**159**)).

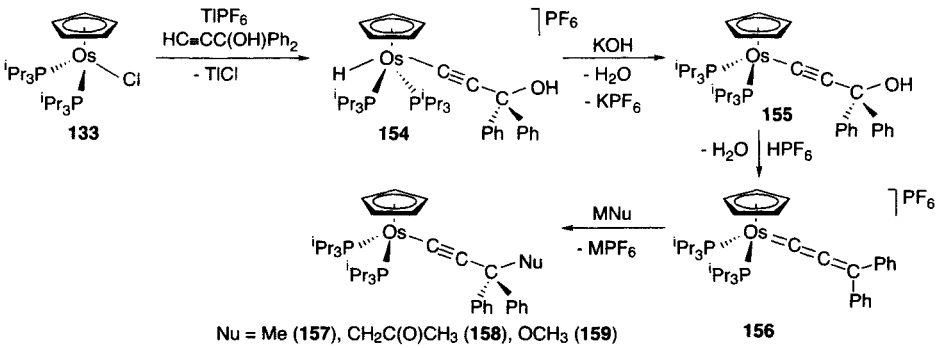

Scheme 40

EHT-MO calculations indicate that the electron density on the C_3-chain of the allenylidene ligand of **156** is similar to that on the C_3-chain of **151**, while it is significantly higher than that on the allenylidene ligands of the γ-electrophiles. This suggests that the behaviour of **156** as nucleophile is a consequence of the high electron density of its allenylidene ligand, while the behavior as γ-electrophile is due to the cationic nature of the complex.

A novel $Os(\eta^5\text{-}C_5H_5)$- mediated acetato-plus-1,1-diphenyl-2-propyn-1-ol coupling reaction leading to a 2-{(*Z*)-3-acetoxy-1-hydroxy-1-phenyl-2-propenyl} aryl complex has been also reported (Scheme 41) [60]. Complex **133** reacts with thallium acetate in dichloromethane as solvent to give $Os(\eta^5\text{-}C_5H_5)\{\kappa^1\text{-}$

$OC(O)CH_3\}(P^iPr_3)_2$ (**160**). Although this compound is soluble in pentane and its solutions are stable for a few days, similarly to **133**, a triisopropylphosphine ligand is easily displaced by 1,1-diphenyl-2-propyn-1-ol to afford the π-alkyne $Os(\eta^5\text{-}C_5H_5)\{\kappa^1\text{-}OC(O)CH_3\}(\eta^2\text{-}HC{\equiv}CC(OH)Ph_2\}(P^iPr_3)$ (**161**). In the solid state, complex **161** is stable for 2 days if kept under argon at -20 °C. However, in solution at temperatures higher than -40 °C, it rapidly evolves into $Os(\eta^5\text{-}C_5H_5)\{C_6H_4[C(OH)(Ph)CH{=}CHOC(O)CH_3]\}(P^iPr_3)$ (**162**). The aryl ligand of **162** is formally the result of the *trans* anti-Markovnikov addition of acetic acid to the carbon-carbon triple bond of 1,1-diphenyl-2-propyn-1-ol. In addition, it should be noted that the formation of this aryl ligand involves the C-H activation of an *ortho*-CH bond of one of the two phenyl groups of the prop-2-yn-1-ol, in the presence of weaker H-C(sp) and H-O bonds.

Although reaction intermediates have not been isolated, it has been proposed that the catalytic addition of carboxylic acids to prop-2-yn-1-ols, in the presence of transition-metal compounds, requires the initial π-coordination of the alkynol to the metallic center, with subsequent attack of the carboxylato group at the coordinated carbon-carbon triple bond of the alkyne [61]. The reactions shown in Scheme 41 are strong evidence in favour of this proposal by isolating complexes which are examples of species proposed as intermediates in these catalytic transformations.

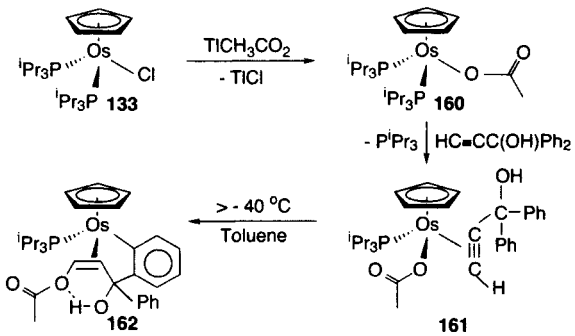

Scheme 41

Another interesting catalytic transformation involving alkynes is the hydro phosphinylation, which affords alkenylphosphine oxides [62]. The formation of hydride-phosphinito compounds is one of the key steps of the reaction. These species are formed by oxidative addition of the P-H bond of diphenylphosphine oxide to platinum(0) and palladium(0) complexes, which act as catalytic precursors. In this context, it should be mentioned that a novel method to prepare hydride-phosphinito compounds has been recently reported. The new strategy starts from **133** and involves the oxidative addition of the P-H bond of

a secondary phosphine, followed by the addition of water and deprotonation of the resulting $P(OH)R_2$ ligand (Scheme 42) [63].

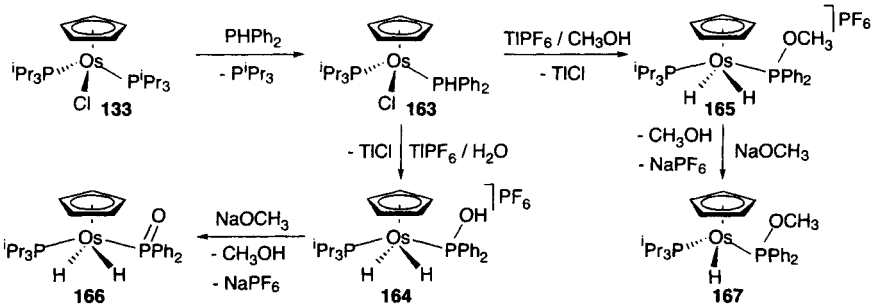

Scheme 42

In agreement with the tendency shown by **133** to release a triisopropylphosphine ligand, the addition of $PHPh_2$ to pentane solutions of **133** leads to $Os(\eta^5\text{-}C_5H_5)Cl(PHPh_2)(P^iPr_3)$ (**163**). Treatment of acetone solutions of **163** with $TlPF_6$ in the presence of water produces the release of the chlorine ligand and the formation of $[OsH_2(\eta^5\text{-}C_5H_5)\{P(OH)Ph_2\}(P^iPr_3)]PF_6$ (**164**). This compound is obtained via the hydride-phosphido intermediate of $[OsH(\eta^5\text{-}C_5H_5)(PPh_2)(P^iPr_3)]^+$, which is generated by intramolecular P-H oxidative addition of diphenylphosphine in the unsaturated $[Os(\eta^5\text{-}C_5H_5)(PHPh_2)(P^iPr_3)]^+$ metallic fragment. Once the hydride-phosphido species is formed the HO-H addition to the Os-phosphido bond affords **164**. The generality of the process is evident in the synthesis of $[OsH_2(\eta^5\text{-}C_5H_5)\{P(OMe)Ph_2\}(P^iPr_3)]PF_6$ (**165**), which is prepared by reaction of **163** with $TlPF_6$ in methanol.

Treatment of **164** with NaOMe in tetrahydrofuran produces its deprotonation and the formation of the dihydride-phosphinito-osmium(IV) derivative $OsH_2(\eta^5\text{-}C_5H_5)\{P(O)Ph_2\}(P^iPr_3)$ (**166**). Under the same conditions, the deprotonation of **165** yields $OsH(\eta^5\text{-}C_5H_5)\{P(OMe)Ph_2\}(P^iPr_3)$ (**167**), as a result of the extraction of one of the two hydrides.

7.6 THE DIHYDRIDE-OSMIUM(IV) COMPLEX $[OsH_2(\kappa^2\text{-}O_2CCH_3)(H_2O)(P^iPr_3)_2]BF_4$ AS A PRECURSOR FOR CARBON-CARBON COUPLING REACTIONS

The title complex is prepared starting from **120**, according to the reaction sequence shown in Scheme 43. The reaction of **120** with 2 equiv of $Ag[CH_3CO_2]$ leads to the bis(acetate) complex $OsH_2(\kappa^2\text{-}O_2CCH_3)\{\kappa^1\text{-}OC(O)CH_3\}(P^iPr_3)_2$ (**168**). In the solid state, the structure of **168** is as fascinating as that of its

precursor and can also be described as a square antiprism but with only one missing vertex. In solution, it exists as two rapidly interconverting isomers. One of them has no symmetry elements other than a C_1 axis, while the other one has a high simmetry, consistent with a pentagonal bipyramid arrangement of ligands around the metallic center, with the monodentate acetate ligand located in the equatorial plane between the hydride ligands [64].

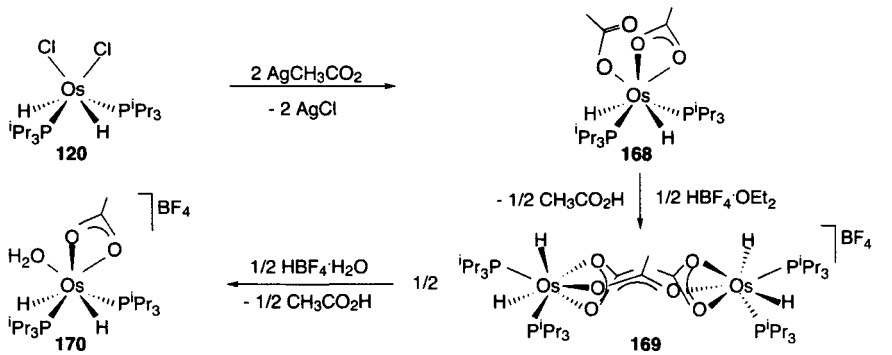

Scheme 43

Treatment of 7:1 diethyl ether/dichloromethane solutions of **168** with 0.5 equiv of $HBF_4{\cdot}OEt_2$ leads to the cationic tetrahydride compound $[\{OsH_2(\kappa^2\text{-}O_2CCH_3)(P^iPr_3)_2\}_2(\mu\text{-}OCOCH_3)]BF_4$ (**169**). The formation of **169** can be rationalized as the result of the protonation of an acetate ligand of 0.5 equiv of **168** and the subsequent coordination of the monodentate acetate ligand of the other 0.5 equiv of **168** to the resulting fragment $[OsH_2(\kappa^2\text{-}O_2CCH_3)(P^iPr_3)_2]^+$. In agreement with this, it has been observed that the addition of 0.5 equiv of water to chloroform-*d* solutions of **169** regenerates 0.5 equiv of **168** and 0.5 equiv of the cationic mononuclear complex $[OsH_2(\kappa^2\text{-}O_2CCH_3)(H_2O)(P^iPr_3)_2]BF_4$ (**170**), which can be also obtained by protonation of **169** with 0.5 equiv of $HBF_4{\cdot}OH_2$ [65].

Complex **169** has been characterized by an X-ray crystallographic study. Although the related structural parameters of the two $[OsH_2(\kappa^2\text{-}O_2CCH_3)(P^iPr_3)_2]^+$ fragments are not strictly equal, they can be considered equivalent due to the presence of a pseudo-C_2 axis, which contains the C-C bond of the acetate bridge. The two fragments have no symmetry elements other than a C_1 axis. At a first glance, the coordination polyhedron around each osmium atom could be described as a capped trigonal prism. The two trigonal faces are made up by an oxygen atom of the bidentate acetate ligand, a hydride, and the phosphorous atom of a phosphine. The remaining vertex is occupied by the oxygen atom of the bridging acetate. In solution, at room temperature, complex **169** is fluxional.

At -100 °C, at least four environments around the osmium atoms coexist, three of them are rigid, while the fourth one is fluxional even at -100 °C.

Complex **170** is a useful precursor for catalytic and stoichiometric carbon-carbon coupling reactions including the polymerization of acetylene, the synthesis of dimethyl-1,4-cyclohexadiene-1,2-dicarboxylate, and the formation of novel organometallic derivatives which act as synthetic intermediates in the above mentioned processes. These organometallic species are carbene, butadienyl, cyclohexadienyl, and dioxo-hexahydroisobenzofuranyl compounds [66].

7.6.1 Polymerization of acetylene

At 0 °C, under one atmosphere of acetylene, dichloromethane solutions of **170** give *trans*-polyacetylene, and a yellow solution. From this solution the vinyl-carbyne complex $[Os(CH{=}CH_2)(\kappa^2\text{-}O_2CCH_3)(CCH_3)(P^iPr_3)_2]BF_4$ (**171**) is obtained in 75% yield (Scheme 44).

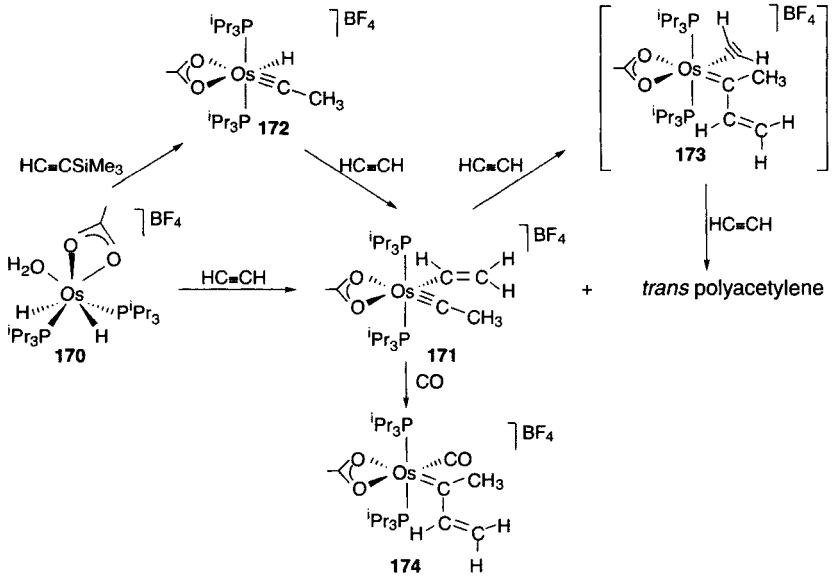

Scheme 44

The formed amount of polyacetylene increases by increasing the exposure time of **170** to acetylene, in a slow but constant manner. This suggests that **170** is a catalyst precursor for the polymerization of acetylene. The active species appears to be **171** or a derivative of this compound. Thus, the stirring of dichloromethane solutions of **171** under one atmosphere of acetylene affords polyacetylene and a yellow solution from which complex **171** is recovered in high yield.

The catalytic formation of polyacetylene and the stoichiometric formation of **171** is also observed when dichloromethane solutions of the hydride-carbyne complex $[OsH(\kappa^2\text{-}O_2CCH_3)(CCH_3)(P^iPr_3)_2]BF_4$ (**172**) [65] are stirred under one atmosphere of acetylene at 0 °C. This agrees with the proposal that the reaction of **170** with acetylene to give **171** is a two-step process, which involves the initial formation of **172** and the subsequent insertion of the alkyne into the Os-H bond of this intermediate. Once complex **171** has been formed, the migratory insertion of the carbyne ligand into the Os-vinyl bond should afford a carbene derivative, **173**. The polymerization of alkynes in a living manner via alkylidene compounds is a well-known process [67]. In favour of the formation of an alkylidene species from **171** under an acetylene atmosphere, it has been observed that, under a carbon monoxide atmosphere, complex **171** evolves into $[Os(\kappa^2\text{-}O_2CCH_3)\{C(CH{=}CH_2)CH_3\}(CO)(P^iPr_3)_2]BF_4$ (**174**), which is unstable under these conditions and affords, finally, the well known compound $[Os(\kappa^2\text{-}O_2CCH_3)(CO)_2(P^iPr_3)_2]BF_4$ [64].

7.6.2 Synthesis of dimethyl 1,4-cyclohexadiene-1-2-dicarboxylate

Dimethyl 1,4-cyclohexadiene-1,2-dicarboxylate has been traditionally prepared by three methods: (i) dimethyl 3-vinyl-1,2-dichlorocyclobutane-1,2-dicarboxylate undergoes a ring expansion, with concomitant loss of the chlorine atoms to give the cyclohexadiene in 52% yield, upon treatment with $Ni(CO)_4$ in refluxing benzene-dimethylformamide [68], (ii) butadiene sulfone and dimethyl acetylenedicarboxylate have been allowed to reflux in xylene for 150 min, and (iii) butadiene and dimethyl acetylendicarboxylate have been mixed in dioxane in a sealed tube, and allowed to stand at room temperature for 5 days [69].

Scheme 45 summarizes a novel method to prepare dimethyl 1,4-cyclohexadiene-1,2-dicarboxylate. The method starts from 2 equiv of acetylene and 1 equiv of dimethyl acetylendicarboxylate, and uses the $Os(O_2CCH_3)(P^iPr_3)_2$ unit as a template. This unit is introduced in the form of the dihydride-acetate complex **170** [66].

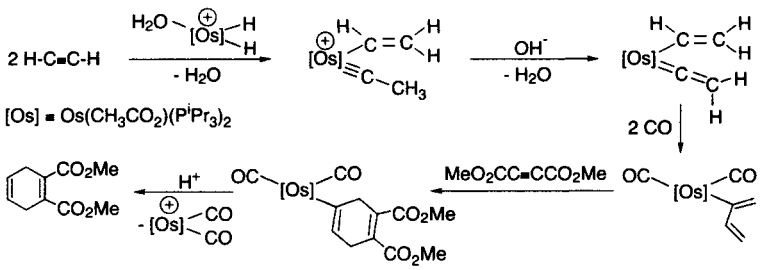

Scheme 45

Complex **170** reacts with acetylene to afford **171**. Once this vinyl-carbyne compound is formed, its deprotonation with a stoichiometric amount of KOH in methanol yields the vinyl-vinylidene $Os(CH{=}CH_2)(\kappa^2\text{-}O_2CCH_3)(C{=}CH_2)(P^iPr_3)_2$ (**175**), as a result of the deprotonation of the carbyne ligand (Scheme 46). Like **171**, under carbon monoxide atmosphere, complex **175** evolves by migratory insertion. In this case, the migration of the vinylidene into the Os-vinyl bond takes place, to afford the butadienyl compound $Os\{C(CH{=}CH_2){=}CH_2\}\{\kappa^1\text{-}OC(O)CH_3\}(CO)_2(P^iPr_3)_2$ (**176**), which in solution exists as a mixture of the isomers **a** and **b** shown in Scheme 46.

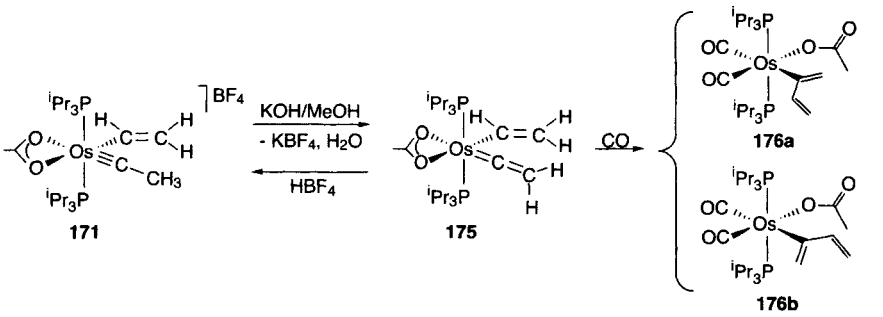

Scheme 46

At 45 °C, the benzene solutions of the isomeric mixture of **176a** and **176b** reacts with dimethyl acetylenedicarboxylate to give the cyclohexenyl derivative **177**, as a result of a Diels-Alder reaction between the butadienyl ligands of **176** and the activated alkyne. In solution, complex **177** also exists as a mixture of the isomers **a** and **b** shown in Scheme 47. This isomeric mixture reacts in chloroform with $HBF_4{\cdot}OEt_2$ to give the $[Os\{\kappa^2\text{-}O_2CCH_3\}(CO)_2(P^iPr_3)_2]BF_4$ and dimethyl 1,4-cyclohexadiene-1,2-dicarboxylate in quantitative yield.

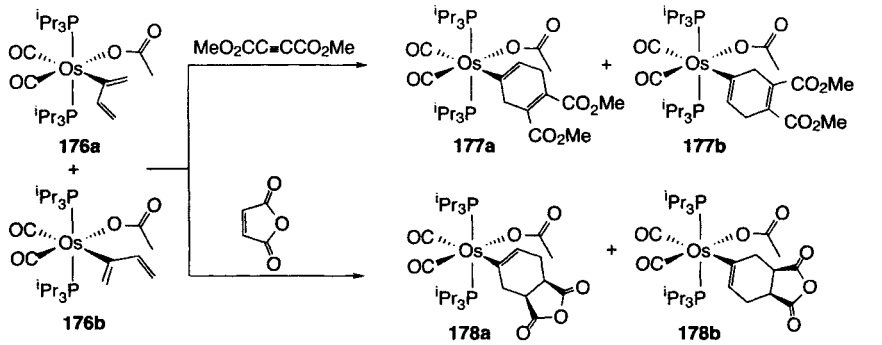

Scheme 47

Complex **176** also reacts with maleic anhydride. In this case, the cycloaddition reaction leads to an isomeric mixture of **178** in quantitative yield after one week. The reaction is carried out in benzene as solvent at room temperature, using 2 equiv of maleic anhydride. Under reflux, the reagents give rise to an ill-defined straw-colored solid. Attempts to separate the bicycle from the metallic fragment, by reaction of the isomeric mixture with H_2 or I_2, have been unsuccessful.

7.7 THE TRIHYDRIDE-OSMIUM(IV) COMPLEX $OsH_3Cl(P^iPr_3)_2$ AS A PRECURSOR FOR THE SYNTHESIS OF $OsCl\{C(CH{=}CHSiMe_3){=}CHSiMe_3\}(CO)_2(P^iPr_3)_2$

Complex $OsH_3Cl(P^iPr_3)_2$ (**179**) has been prepared by reaction of **120** with molecular hydrogen, in toluene as solvent, and in the presence of water or triethylamine [70]. Analytical gradient with *ab initio* Hartree-Fock calculations on the model compound $OsH_3Cl(PH_3)_2$ suggest that **179** has a C_{2v} structure. The phosphine groups remain perpendicular to the plane containing the other ligands. The hydrogen-hydrogen distance is about 1.55 Å and the H-Os-H angle is about 58°. In solution, the hydride ligands undergo thermally activated site exchange and quantum exchange coupling processes.

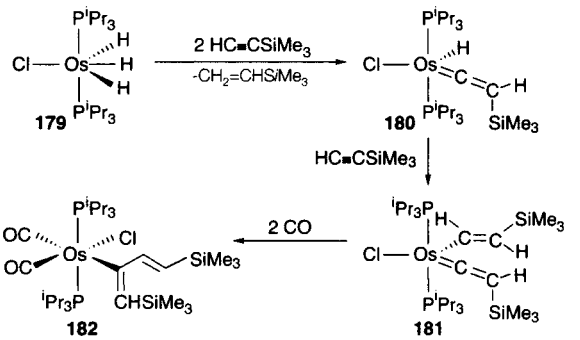

Scheme 48

Complex **179** is dehydrogenated in the presence of 2 equiv of trimethyl silylacetylene to give the silylated olefin and the hydride-vinylidene derivative $OsHCl(C{=}CHSiMe_3)(P^iPr_3)_2$ (**180**) [71], according to Scheme 48. The reaction of **180** with a new molecule of trimethylsilylacetylene affords the alkenyl-vinylidene $OsCl\{(E)\text{-}CH{=}CHSiMe_3\}\{(C{=}CHSiMe_3)(P^iPr_3)_2$ (**181**). The single-crystal X-ray structure of **181** reveals a distorted trigonal bibyramid (Y shape, considering the alkenyl, vinylidene and chlorine ligands on the equatorial plane). Similarly to **175**, carbon monoxide induces migration of the

vinylidene ligand into the Os-alkenyl bond to give the butadienyl derivative $OsCl\{C(CH{=}CHSiMe_3){=}CHSiMe_3\}(CO)_2(P^iPr_3)_2$ (**182**). Reaction of **181** with equimolecular carbon monoxide yields a mixture of unreacted **181** and the dicarbonyl complex **182**. This means that any 1:1 CO adduct reacts more rapidly with CO than does **181** itself [72].

7.8 THE FIVE-COORDINATE HYDRIDE-DIHYDROGEN COMPLEX $[OsH(\eta^2\text{-}H_2)(CO)(P^iPr_3)_2]BF_4$ ACTING AS A TEMPLATE FOR THE CARBON-CARBON COUPLING BETWEEN METHYL PROPIOLATE AND 1,1-DIPHENYL-2-PROPYN-1-OL

Complex $[OsH(\eta^2\text{-}H_2)(CO)(P^iPr_3)_2]BF_4$ (**183**) is a rare example of a 16-electron hydride-dihydrogen compound. It is obtained starting from **20** according to the reaction sequence shown in Scheme 49.

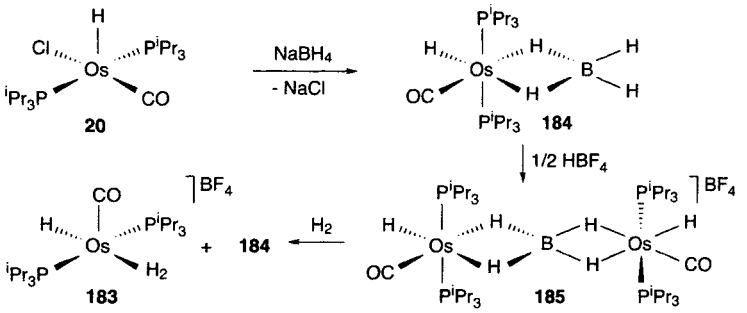

Scheme 49

The reaction of **20** with $NaBH_4$ in methanol leads to the octahedral compound $OsH(\kappa^2\text{-}H_2BH_2)(CO)(P^iPr_3)_2$ (**184**), which has a rigid structure in solution at low temperatures. Above ca. -30 °C an exchange process takes place, which involves the bridging hydrogen atoms and the terminal hydrogens attached to boron but not the metal hydride ligand [73]. Complex **184** reacts with 0.5 equiv $HBF_4{\cdot}OEt_2$ to give the binuclear compound $[\{OsH(CO)(P^iPr_3)_2\}_2(\mu\text{-}\kappa^4\text{-}H_2BH_2)]BF_4$ (**185**) consisting of two $OsH(CO)(P^iPr_3)_2$ fragments bridged by a tetrahedral BH_4 unit. The six donor atoms around each metal define two octahedra with the CO and the hydride ligands trans to the BH_4 unit [74].

Complex **185** can be considered as the result of the stabilization of the unsaturated fragment $[OsH(CO)(P^iPr_3)_2]$ by **184**. So, the mononuclear tetrahydroborate complex is a metalloligand that can be displaced by other

coordinating molecules. Thus, under normal conditions (25 °C, 1 atm of hydrogen), the binuclear tetrahydroborate complex reacts with molecular hydrogen to afford **183**.

This hydride-dihydrogen complex allows the access of methyl propiolate and 1,1-diphenyl-2-propyn-1-ol into the osmium atom, and the carbon-carbon coupling between the resulting carbon-donor ligands [75] (Scheme 50).

In an initial stage the alkyne molecules are introduced in a sequential manner. Thus, complex **183** reacts with methyl propiolate in acetone to give the alkenyl derivative **186**, which by addition of 1,1-diphenyl-2-propyn-1-ol affords the alkenyl-allenylidene compound **187**.

Despite the fact that **187** is stable in solution and does not evolve by migratory insertion of the allenylidene ligand into the Os-C(alkenyl) bond, in the subsequent stage of the process, it is shown that the addition of NaCl produces the carbon-carbon coupling to give the allenyl derivative **188**, via the intermediate $Os\{C(CO_2Me)=CH_2\}Cl(C=C=CPh_2)(CO)(P^iPr_3)_2$ (**189**), which is isolated as the mixture of isomers shown in Scheme 50.

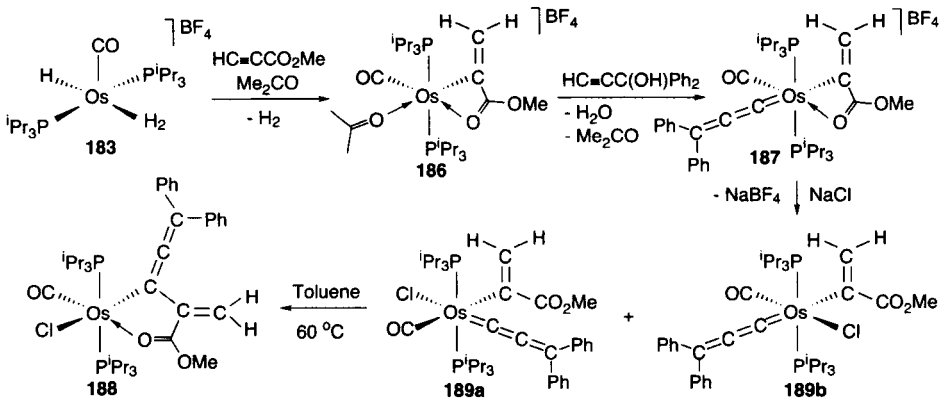

Scheme 50

7.9 HE DIHYDRIDE-DIHYDROGEN COMPLEX $OsH_2(\eta^2\text{-}H_2)(CO)(P^iPr_3)_2$ AS A PRECURSOR FOR CARBON-CARBON AND CARBON-HETEROATOM COUPLING REACTIONS

The dihydride-dihydrogen complex $OsH_2(\eta^2\text{-}H_2)(CO)(P^iPr_3)_2$ (**190**) can be prepared by stirring of the borohydride compound **184** in methanol at room temperature. If the treatment is prolonged or the temperature is increased, the *cis*-dihydride-*cis*-dicarbonyl derivative $OsH_2(CO)_2(P^iPr_3)_2$ is formed instead of **190** [73]. So, the most suitable method to prepare **190** is that shown in Scheme 51.

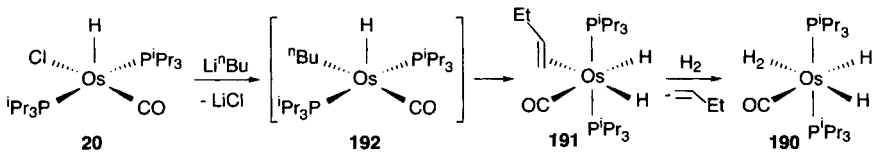

Scheme 51

Complex **20** reacts with Li^{n}Bu in hexane at room temperature to give the dihydride $OsH_2(CO)(\eta^2\text{-}CH_2{=}CHEt)(P^iPr_3)_2$ (**191**), which is isolated as a colorless oil in quantitative yield. The reaction most probably involves the replacement of the chlorine by a butyl group to give initially $OsH^nBu(CO)(P^iPr_3)_2$ (**192**), which evolves into the dihydride derivative by a β-elimination reaction [76].

Under a hydrogen atmosphere, complex **191** affords **190**, which shows a nonclassical interaction between two of the four hydrogen atoms bonded to the osmium atom. In solution, these atoms exchange their positions giving in the ^1H NMR spectra only one resonance, which has $T_{1\ min}$ of 32 ms at -67 °C [77].

Ab initio DFT calculations on the model compound $OsH_2(\eta^2\text{-}H_2)(CO)(PH_3)_2$ indicate that the dihydrogen ligand lies trans to a hydride, and that the separation between the hydrogen atoms of the dihydrogen is 0.87 Å. On the basis of separate optimization of the 16-electron $OsH_2(CO)(PH_3)_2$ species and free molecular hydrogen, an Os-H_2 bond dissociation energy of 18.9 kcal·mol^{-1} is calculated. The preferred conformation of the dihydrogen ligand is found to be when the H-H vector eclipses the Os-H bond (*i. e.*, lies in the XZ plane). However, the barrier to rotation is calculated to be very small, 0.54 kcal·mol^{-1}. This comes from the fact that back-bonding is better in the plane containing the phosphines, since π^*_{CO} in the orthogonal plane stabilizes the d_{xz} orbital. However, the interaction with the *cis* hydride compensates the loss of backbonding in the plane of the carbonyl group and favours the conformation with the lesser back-donation. The observed dihydrogen alignment is also sterically favored, especially when considering the additional bulk of the phosphines used experimentally [78].

The dihydride-dihydrogen complex permits not only the introduction, in a sequential manner, of two organic molecules into the metallic center, but also the selective transformation of one of them, and the coupling of the resulting ligands to afford new organic fragments.

7.9.1 *Formation of and* $\overline{Os\{C(CH_2Ph){=}CHC_6H_4\}}$ *Os{η³-CH(Ph)CHCHPh} fragments*

The behaviour of the dihydride-dihydrogen complex **190** towards phenylacetylene is as expected for the 16-electron dihydride $OsH_2(CO)(P^iPr_3)_2$, suggesting that in solution the hydride-dihydrogen compound dissociates the dihydrogen molecule [79]. Thus, the reaction of **190** with 1 equiv

of phenylacetylene affords the alkynyl-hydride-dihydrogen $OsH(C_2Ph)(\eta^2\text{-}H_2)(CO)(P^iPr_3)_2$ (**193**), which can be spectroscopically characterized under hydrogen atmosphere. When the hydrogen atmosphere is evacuated and the system refilled with argon, the 16-electron derivative $OsH(C_2Ph)(CO)(P^iPr_3)_2$ (**194**) is formed (Scheme 52). The latter reacts with a second molecule of phenylacetylene to give molecular hydrogen and the bis-alkynyl derivative $Os(C_2Ph)_2(CO)(P^iPr_3)_2$ (**195**), which can be also obtained by reaction of the tetrahydroborate complex **184** with an excess of phenylacetylene. Similarly, the reaction of $RuH(\kappa^2\text{-}H_2BH_2)(CO)(P^iPr_3)_2$ with phenylacetylene leads to $Ru(C_2Ph)_2(CO)(P^iPr_3)_2$ (**196**) [80].

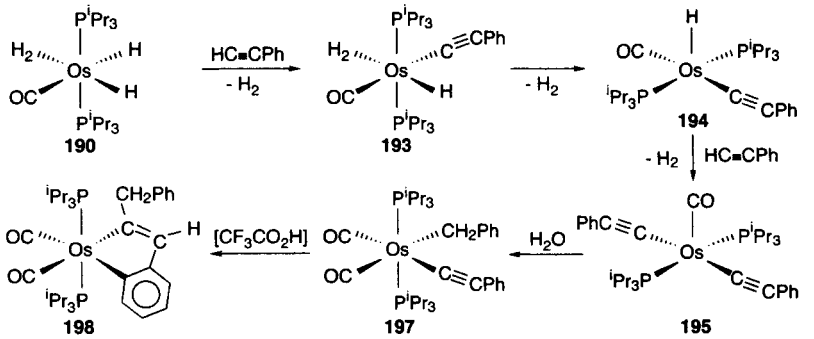

Scheme 52

In 2-propanol as solvent, the carbon-carbon triple bond of one of the two alkynyl ligands of **195** can be selectively broken by reaction with water to afford $Os(C_2Ph)(CH_2Ph)(CO)_2(P^iPr_3)_2$ (**197**). The reaction involves a metal-promoted hydration-disproportionation of the transformed alkynyl ligand catalyzed by the solvent. In methanol, trifluoroacetic acic catalyzes the isomerization of **197** into **198**, which contains an ortho-metallated phenyl group [81].

According to the results from isotope labeling experiments, the isomerization involves the initial attack of the proton from the acid to the C_β atom of the alkynyl ligand of **197**. The subsequent migratory insertion of the resulting vinylidene into the metal-benzyl bond gives an alkenyl intermediate containing a coordinated trifluoroacetate anion, which evolves into **198** by trifluoroacetic acid elimination (Scheme 53).

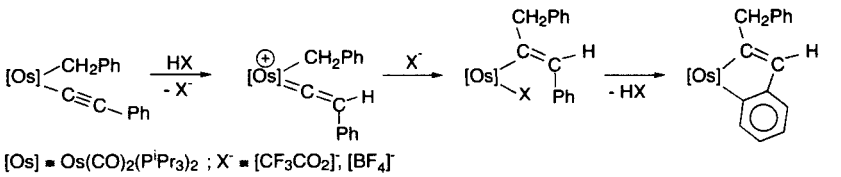

Scheme 53

In the presence of tetrafluoroboric acid, complex **197** also isomerizes into **198** but, furthermore, it produces the π-allyl derivative $[Os\{\eta^3\text{-}CH(Ph)CHCHPh\}(CO)_2(P^iPr_3)_2]BF_4$ (**199**), which is a result of the addition of the proton from the acid and the carbon-carbon-coupling of the benzyl and alkynyl fragments of **197** (Eq. 7).

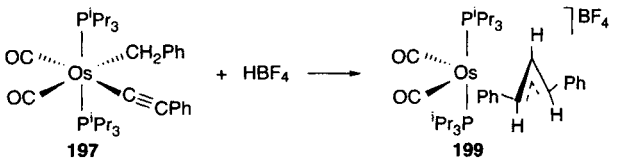

(7)

In this case the isotope labeling experiments suggest that the formation of **199** involves the unsaturated alkenyl intermediate $Os\{C(CH_2Ph)=CHPh\}(CO)_2(P^iPr_3)_2]^+$, which by 1,2-hydrogen shift evolves into **199** (Scheme 54).

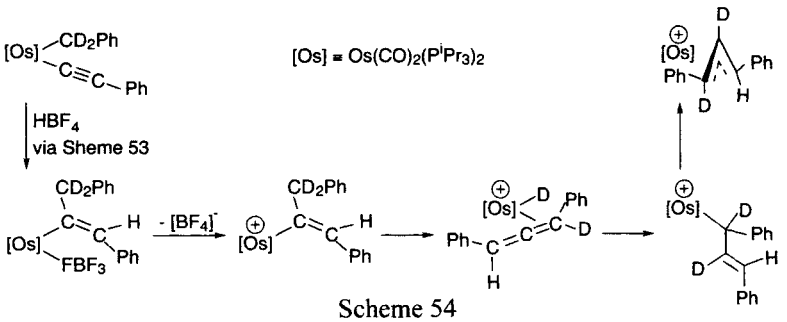

Scheme 54

The different behaviour of **197** towards trifluoroacetic and tetrafluoroboric acids can be rationalized in terms of different coordination powers of the corresponding anions. The trifluoroacetate, which has a stronger coordination power than the tetrafluoroborate, prevents the formation of the unsaturated intermediate $Os\{C(CH_2Ph)=CHPh\}(CO)_2(P^iPr_3)_2]^+$, which is the key for the formation of **199**. Thus, complex **198** is the only species formed from **197**, in the presence of this acid.

7.9.2 Formation of the butadienyl complex Os{C(CH=CHC)$_2$Me)=CHC(O)OMe}Cl(CO) (P^{i}Pr$_3$)$_2$

In contrast to the reaction with phenylacetylene, the treatment of **190** with 2 equiv of methyl propiolate leads to the alkenyl-alkynyl compound **200** (Scheme 55). The use of a 1:1 molar ratio of alkyne to osmium complex gives the same product along with unreacted dihydride-dihydrogen complex [79]. The addition of a toluene solution of HCl to a toluene solution of **200** produces the carbon-carbon coupling of the alkynyl and alkenyl fragments to give selectively the

butadienyl derivative **201**. The reaction proceeds by protonation of the C_β atom of the alkynyl ligand of **200** and subsequent migratory insertion of the resulting vinylidene into the Os-alkenyl bond. The insertion appears to be promoted by the entry of chloride into the coordination sphere of the osmium [82].

In agreement with the above mentioned proposal, it has been observed that the addition of 1 equiv of $HBF_4{\cdot}OEt_2$ to diethyl ether solutions of **200** affords the alkenyl-vinylidene complex **202** as a yellow solid in 65% yield and that the treatment of **202** with NaCl gives **201** in 91% yield.

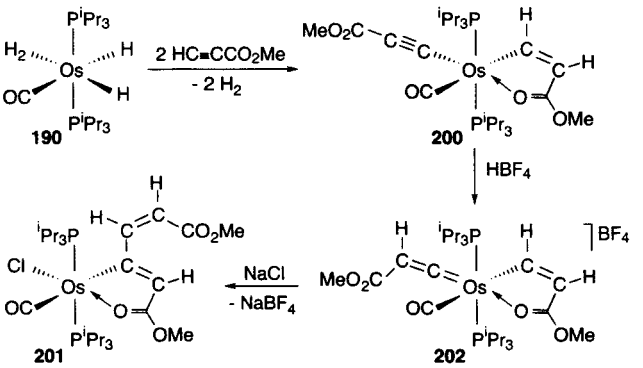

Scheme 55

In addition, it should be noted that the selective protonation of the alkynyl group of **200**, in the presence of the alkenyl ligand, elegantly proves that under the same conditions, the C_β atom of an alkynyl ligand has a stronger nucleophilic character than the C_β atom of an alkenyl ligand.

7.9.2 Formation of alkenyl ester compounds

Treatment of **195** with a stoichiometric amount of acetic acid in methanol leads to the alkynyl-alkenyl ester complex **203**, as a result of the addition of the acid to the carbon-carbon triple bond of one of the two alkynyl ligands of **195** (Scheme 56). Complex **203** reacts with $HBF_4{\cdot}OEt_2$ in diethyl ether to give the alkynyl-carbene compound **204**. The formation of **204** involves the addition of the proton of the acid to the C_β atom of the alkenyl ester ligand of **203**. This suggests that the C_β atom of a vinyl ester ligand has a stronger nucleophilic character than the C_β atom of both alkenyl and alkynyl groups [83].

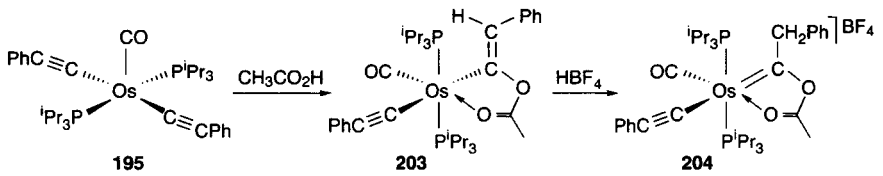

Scheme 56

The bis(alkynyl) ruthenium complex **196**, in contrast to **195**, reacts with a stoichiometric amount of acetic acid in methanol to give the alkynyl-acetate derivative $Ru(C_2Ph)(\kappa^2\text{-}O_2CMe)(CO)(P^iPr_3)_2$ (**205**) and phenylacetylene (Scheme 57). In contrast to the trend shown by **196**, the alkynyl ligand of **205** undergoes electrophilic attack at the C_β atom. Thus, the addition of $HBF_4{\cdot}OEt_2$ to acetone solutions of **205** leads to the alkenyl ester compound **206**, which can be rationalized as the result of the nucleophilic attack of the acetate group at the C_α atom of a vinylidene intermediate.

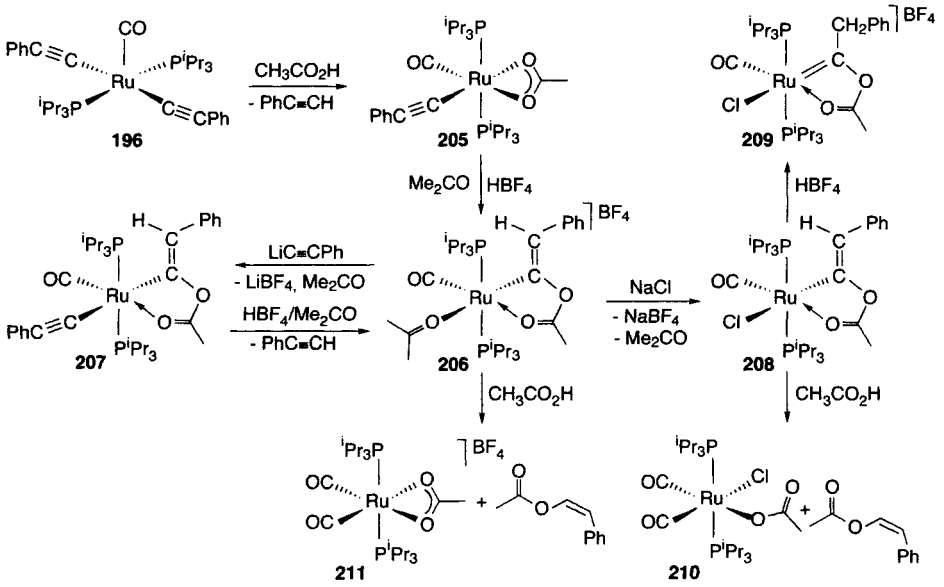

Scheme 57

The acetone molecule of **206** can be displaced by anions such as $[PhC{\equiv}C]^-$ and Cl^- to give the alkenyl-alkynyl complex **207** and the alkenyl-chloro derivative **208**, respectively. The osmium and ruthenium complexes **203** and **207** are isoelectronic. Furthermore, they contain the same ligands in the same positions. However, there is a pronounced difference between them in reactivity towards HBF_4. The osmium complex **203** reacts with HBF_4 by electrophilic attack at the C_β atom of the alkenyl ester group to give **204**, while complex **207** regenerates **206**, as a consequence of the electrophilic attack at the C_α atom of the alkynyl ligand. Complex **208**, in contrast to **207**, shows the same behaviour as **203**. Thus, the addition of $HBF_4{\cdot}OEt_2$ to dichloromethane solutions of **208** leads to the carbene complex **209**. Complex **208** also reacts with acetic acid under reflux. The reaction leads to *cis*-PhCH=CHOC(O)Me and the monodentate acetate compound $Ru\{\kappa^1\text{-}OC(O)Me\}Cl(CO)_2(P^iPr_3)_2$ (**210**). Complex $[Ru(\kappa^2\text{-}O_2CMe)(CO)_2(P^iPr_3)_2]BF_4$ (**211**) and *cis*-PhCH=CHOC(O)Me are similarly obtained by reaction of **206** and acetic acid in acetone as solvent.

The reactions collected in Schemes 56 and 57 contain overwhelming evidence proving that the direction of the H^+ addition to alkynyl and alkenyl acetate complexes of osmium and ruthenium is determined by the electronic nature of the metallic center (Os or Ru), by the electronic properties of the ancillary ligands of the complexes, and also by the source of the electrophile.

Although the catalytic activity of the alkenyl acetate compounds previously mentioned have not been studied, Kawano et al. have recently shown that the triphenylphosphine derivative $Ru\{C(=CHPh)OC(O)Et\}Cl(CO)(PPh_3)_2$ catalyzes the addition of propanoic acid to phenylacetylene to give (*Z*)-2-phenylethenyl propanoate, selectively. This complex is prepared by reaction of $RuCl(\kappa^2\text{-}O_2CEt)(CO)(PPh_3)_2$ with phenylacetylene [84].

7.10 FINAL REMARKS

The study of the reactivity of transition metal hydride compounds towards unsaturated organic molecules, mainly olefines and alkynes, has been traditionally centered in monohydrides. In general, the reactions lead to the insertion products, alkyl or alkenyl, which have a limited chemistry. Furthermore, the generation of subsequent carbon-carbon or carbon-heteroatom bonds requires the presence of other active ligands, such as halogen or carbon monoxide, in the coordination sphere of the metallic center of the alkyl or alkenyl intermediates.

In the previous pages, we have shown that the field offers more chances. The increase of the number of hydrogen atoms bonded to the metallic center, firstly, allows the access of several organic molecules into the metal; second, this access can be sequential and selective; and third, a wide range of organometallic functional groups can be obtained. All this facilitates the different types of coupling reactions and the generation of organic fragments with a rich organic chemistry, which permits the growth of the ligands.

The field needs much more research effort, mainly in the initial stage, the control of the products from the reactions of the polyhydrides with the organic molecules. Today, their prediction presents severe limitations, wich hinder to design *a priori* the steps to obtain a particular ligand or molecule, and even to know the most useful polyhydride for the process. For instance, the six-coordinate dihydride-osmium(IV) complex **120** reacts with phenylacetylene, cyclohexylacetylene, 1-(trimethylsilyl)-1,4-pentadiyne or trimethylsilylacetylene to give hydride-carbyne compounds of the type $OsHCl_2(CCH_2R)(P^iPr_3)_2$ [85], while the reaction of the dihydrogen derivative $OsCl_2(\eta^2\text{-}H_2)(CO)(P^iPr_3)_2$ with phenylacetylene affords the carbene $OsCl_2(CHCH_2Ph)(CO)(P^iPr_3)_2$ [86], and the addition of 2-methyl-1-buten-3-yne- to the solutions of the dihydride-bis(acetate) **168** gives the alkenylvinylidene $OsH(\kappa^2\text{-}O_2CMe)\{C=CHC(CH_3)=CH_2\}(P^iPr_3)_2$

[64]. Even, recently, it has been found that hydride-carbynes, hydride-osmacyclopropenes, or mixtures of both types of compounds can be formed by reaction of the dihydride-acetate **170** with terminal alkynes [65] and alkynols [87]. With olefins, the situation starts to point out in the same direction. Caulton and co-workers [88] have observed that complex **120** reacts with propene and styrene to give equimolecular amounts of $OsHCl_2(CCH_2R)(P^iPr_3)_2$ (R = Me, Ph) and the hydrogenated olefins, and our group has observed that complex **170** reacts with ethylene to afford the novel tetraethylene dimer complex $[\{(P^iPr_3)(\eta^2\text{-}C_2H_4)_2Os\}_2(\mu\text{-}OH)_2(\mu\text{-}O_2CCH_3)]BF_4$, while under the same conditions styrene is inert [89].

In spite of the above mentioned limitations, it should be noted that a lot of carbon-carbon and carbon-heteroatom coupling reactions have been summarized in this review. These reactions have given rise to about 200 new compounds in recent years. Complexes **111**, **115**, and **116** containing an azetidine skeleton or the 1,3-thiazinyl derivatives **98-100** are of particular interest. In this respect, it should be mentioned that as a consequence of the discovery of the cephalosporins and the enormous development occurring in the chemistry of these antibiotics since the 1940s, the 1,3-thiazine nucleus has became one of the most important six-membered heterocycles [90].

The scope of the review is limited to ruthenium- and osmium- triisopropylphosphine polyhydrides. Under the point of view of Scheme 1, many more polyhydride systems have not been studied. If one takes into account that there are certain properties characteristic for each metal, the development of new types of coupling reactions and the formation of novel ligands should be observed in the near future, by using polyhydrides of metals different from ruthenium and osmium.

Why should you, the person in charge of a chemical or pharmaceutical industry, sponsor this field? Because each reaction can open the door towards different organic fragments and there are a lot of doors to be opened, as many as polyhydrides. Although, we do not yet know how to control the result of the reaction in the first stage, in the near future, we will learn. Then, we will have the key to build novel and sophisticated organic molecules.

ACKNOWLEDGMENTS

The authors express their sincere thanks to their coworkers, whithout whose contributions this article could not have been written: their names are cited in the references.

REFERENCES

[1] (a) J.K. Stille, in: F.R. Hartley, S. Patai (Eds.), Chemistry of the Metal-Carbon Bond, vol 2, Wiley, Chichester, UK, 1985. (b) T. Hagashi, M. Kumada, in: J.D. Morrison (Ed.), Asymmetric Synthesis, vol 5, Academic Press, New York, 1985. (c) A. Yamamoto, Organotransition Metal Chemistry, Willey, New York, 1986. (d) J.P. Collman, L.J. Hegedus, J.R. Norton, R.G. Finke, Principles and Applications of Organotransition Metal Chemistry, University Science Books, Mill Valley, CA, 1987. (e) J.M. Brown, N.A. Cooley, Chem. Rev. 88 (1988) 1031. (f) M. Brookhart, A.F. Volpe, Jr., J. Yoon, in: B.M. Trost, Y. Fleming (Eds.), Comprehensive Organic Synthesis, vol. 4, Pergamon Press, Tarrytown, NY, 1991. (g) H.G. Schmalz, Angew. Chem. Int. Ed. 34 (1995) 1833. (h) T. Naota, H. Takaya, S.-I. Murahashi, Chem. Rev. 98 (1998) 2599.

[2] J. Espuelas, M.A. Esteruelas, F.J. Lahoz, A.M. López, L.A. Oro, C. Valero, J. Organomet. Chem. 468 (1994) 223.

[3] J.A.K. Howard, O. Johnson, T.F. Koetzle, J.L. Spencer, Inorg. Chem. 26 (1987) 2930.

[4] C.A. Tolman, Chem. Rev. 77 (1977) 313.

[5] M.A. Esteruelas, L.A. Oro, Adv. Organomet. Chem. 47 (2001) 1.

[6] (a) H. Werner, M. Schäfer, O. Nürnberg, J. Wolf, Chem. Ber. 127 (1994) 27. (b) W. Chen, M.A. Esteruelas, J. Herrero, F.J. Lahoz, M. Martín, E. Oñate, L.A. Oro, Organometallics 16 (1997) 6010.

[7] H. Werner, Chem. Commun (1997) 903.

[8] M.A. Esteruelas, H. Werner, J. Organomet. Chem. 303 (1986) 221.

[9] H. Werner, M.A. Esteruelas, H. Otto, Organometallics 5 (1986) 2295.

[10] C. Bohanna, M.A. Esteruelas, F.J. Lahoz, E. Oñate, L.A. Oro, E. Sola, Organometallics 14 (1995) 4825.

[11] C. Bohanna, M.A. Esteruelas, F.J. Lahoz, E. Oñate, L.A. Oro, Organometallics 14 (1995) 4685.

[12] W.R. Roper, G.E. Taylor, J.M. Waters, L.J.Wright, J. Organomet. Chem. 182 (1979) C46.

[13] M.A. Esteruelas, F. Liu, E. Oñate, E. Sola, B. Zeier, Organometallics 16 (1997) 2919.

[14] M.L. Buil, S. Elipe, M.A. Esteruelas, E. Oñate, E. Peinado, N. Ruiz, Organometallics 16 (1997) 5748.

[15] R.J. Angelici, Acc. Chem. Res. 28 (1995) 51.

[16] M.A. Esteruelas, F.J. Lahoz, E. Oñate, L.A. Oro, E. Sola, J. Am. Chem. Soc. 118 (1996) 89.

[17] P.M. Morse, M.O. Spencer, S.R. Wilson, G.S. Girolami, Organometallics 13 (1994) 1646, and references therein.

[18] M.J. Albéniz, M.A. Esteruelas, A. Lledós, F. Maseras, E. Oñate, L.A. Oro, E. Sola, B. Zeier, J. Chem. Soc., Dalton Trans. (1997) 181.

[19] A.J. Edwards, S. Elipe, M.A. Esteruelas, F.J. Lahoz, L.A. Oro, C. Valero, Organometallics 16 (1997) 3828.

[20] M.A. Esteruelas, A.V. Gómez, F.J. Lahoz, A.M. López, E. Oñate, L.A. Oro, Organometallics 15 (1996)3423.

[21] (a) H. Berke, G. Huttner, J. Von Seyerl, Z. Naturforsch. 36B (1981) 1277. (b)

A.J. Edwards, M.A. Esteruelas, F.J. Lahoz, J. Modrego, L.A. Oro, J. Schrickel Organometallics 15 (1996) 3556. (c) V. Cadierno, M.P. Gamasa, J. Gimeno, M. González-Cueva, E. Lastra, J. Borge, S. García-Granda, E. Pérez-Carreño, Organometallics 15 (1996) 2137.

[22] (a) M.I. Bruce, Chem. Rev. 98 (1998) 2797. (b) V. Cadierno, M.P. Gamasa, J. Gimeno, Eur. J. Inorg. Chem. (2001) 571.

[23] M.A. Esteruelas, A.V. Gómez, A.M. López, J. Modrego, E. Oñate, Organometallics 16 (1997) 5826.

[24] B. Weyershausen, K.H. Dötz, Eur. J. Inorg. Chem. (1999) 1057.

[25] (a) R.B. King, J. Am. Chem. Soc. 85 (1963) 1922. (b) C.P. Casey, R.L. Anderson, J. Am. Chem. Soc. 93 (1971) 3554. (c) H. Motschi, R.J. Angelici, Organometallics 1 (1982) 343. (d) R.A. Michelin, L. Zanotto, D. Braga, P. Sabatino, R.J. Angelici, Inorg. Chem. 27 (1988) 93.

[26] (a) C.P. Casey, W.R. Brunsvold, D.M. Scheck, Inorg. Chem. 16 (1977) 3059. (b) L. Lattuada, E. Licandro, S. Maiorana, H. Molinari, A. Papagni, Organometallics 10 (1991) 807. (c) C. Baldoli, L. Lattuada, E. Licandro, S. Maiorana, A. Papagni, Organometallics 12 (1993) 2994.

[27] (a) A. Parlier, H. Rudler, J. Chem. Soc., Chem. Commun. (1986) 514. (b) K.H. Dötz, W. Sturm, H.G. Alt, Organometallics 6 (1987) 1424. (c) P. Quayle, S. Rahman, E.L.M. Ward, J. Herbert, Tetrahedron Lett. 35 (1994) 3801.

[28] (a) S.G. Davies, J.P. McNally, A.J. Smallridge, Adv. Organomet. Chem. 30 (1990) 1. (b) H. Le Bozec, K. Ouzzine, P.H. Dixneuf, Organometallics 10 (1991) 2768. (c) N. Ruiz, D. Perón, P.H. Dixneuf, Organometallics 14 (1995) 1095.

[29] (a) F. Camps, J.M. Moretó, S. Ricart, J.M. Viñas, E. Molins, C. Miravitlles, J. Chem. Soc., Chem. Commun. (1989) 1560. (b) K.N. Juneau, L.S. Hegedus, F.W. Roepke, J. Am. Chem. Soc. 111 (1989) 4762. (c) S.L.B. Wang, W.D. Wulff, J. Am. Chem. Soc. 112 (1990) 4550. (d) K.L. Faron, W.D. Wulff, J. Am. Chem. Soc. 112 (1990) 6419. (e) A. Segundo, J.M. Moretó, J.M. Viñas, S. Ricart, E. Molins, Organometallics 13 (1994) 2467.

[30] M.A. Esteruelas, A.V. Gómez, A.M. López, J. Modrego, E. Oñate, Organometallics 17 (1998) 5434.

[31] M.A. Esteruelas, A.V. Gómez, A.M. López, E. Oñate, N. Ruiz, Organometallics 17 (1998) 2297.

[32] M.A. Esteruelas, A.V. Gómez, A.M. López, M. Oliván, E. Oñate, N. Ruiz, Organometallics 19 (2000) 4.

[33] D.J. Bernad, M.A. Esteruelas, A.M. López, J. Modrego, M.C. Puerta, P. Valerga, Organometallics 18 (1999) 4995.

[34] M.A. Esteruelas, A.V. Gómez, A.M. López, E. Oñate, Organometallics 17 (1998) 3567.

[35] D.J. Bernad, M.A. Esteruelas, A.M. López, M. Oliván, E. Oñate, M.C. Puerta, P. Valerga, Organometallics 19 (2000) 4327.

[36] (a) A.R. Katritzky, J.M. Lagowski, Adv. Heterocycl. Chem. 1 (1963) 341. (b) J. Elguero, C. Marzin, A.R. Katritzky, P. Linda, in: The Tautomerism of Heterocycles: Advances in Heterocyclic Chemistry, Academic Press, New York, 1976, Supplement 1, Chapter 2.

[37] W. Walter, J. Voss, in: S. Patai (Ed.), The Chemistry of Amides, Interscience, London, 1970, Chapter 8.

[38] V. Cadierno, M.P. Gamasa, J. Gimeno, M.C. López-González, J. Borge, S. García-Granda, Organometallics 16 (1997) 4453.
[39] M.A. Esteruelas, A.V. Gómez, A.M. López, M.C. Puerta, P. Valerga, Organometallics 17 (1998) 4959.
[40] R.H. De Wolfe, Synthesis (1974) 153.
[41] M.A. Esteruelas, A.V. Gómez, A.M. López, E. Oñate, N. Ruiz, Organometallics 18 (1999) 1606.
[42] M. Aracama, M. A. Esteruelas, F.J. Lahoz, J.A. López, U. Meyer, L.A. Oro, H. Werner, Inorg. Chem. 30 (1991) 288.
[43] D.G. Gusev, R. Kuhlman, J.R. Rambo, H. Berke, O. Eisenstein, K.G. Caulton, J. Am. Chem. Soc. 117 (1995) 281.
[44] M. Bourgault, A. Castillo, M.A. Esteruelas, E. Oñate, N. Ruiz, Organometallics 16 (1997) 636, and references therein.
[45] A. J. Edwards, M.A. Esteruelas, F.J. Lahoz, A.M. López, E. Oñate, L.A. Oro, J.I. Tolosa, Organometallics 16 (1997) 1316.
[46] R. Castarlenas, M.A. Esteruelas, E. Gutiérrez-Puebla, Y. Jean. A. Lledós, M. Martín, J. Tomàs, Organometallics 18 (1999) 4296.
[47] R. Castarlenas, M.A. Esteruelas, E. Gutiérrez-Puebla, Y. Jean. A. Lledós, M. Martín, E. Oñate, J. Tomàs, Organometallics 19 (2000) 3100.
[48] R. Castarlenas, M.A. Esteruelas, E. Oñate, Organometallics, 20 (2001) 2294.
[49] R. Castarlenas, M.A. Esteruelas, E. Oñate, XIX Reunión del Grupo Especializado de Química Organometálica de la Real Sociedad Española de Química, Valladolid, 2000, P28.
[50] M.O. Albers, D.J. Robinson, E. Singleton, Coord. Chem. Rev. 79 (1987) 1.
[51] (a) M.I. Bruce, F.S. Wong, J. Organomet. Chem. 210 (1981) C5. (b) J.K. Hoyano, C.J. May, W.A.G. Graham, Inorg. Chem. 21 (1982) 3095. (c) M.I. Bruce, I.B. Tomkins, F.S. Wong, B.W. Shelton, A.H. White, J. Chem. Soc., Dalton Trans. (1982) 687. (d) T. Wilczewski, J. Organomet. Chem. 317 (1986) 307. (e) M.I. Bruce, M.G. Humphrey, G.A. Koutsantonis, M. J. Liddell, J. Organomet. Chem. 326 (1987) 247. (f) M.I. Bruce, G.A. Koutsantonis, M. J. Liddell, B.K. Nicholson, J. Organomet. Chem. 320 (1987) 217. (g) Y. Kawano, H. Tobita, H. Ogino, Organometallics 13 (1994) 3849. (h) G. Jia, W.S. Ng, J. Yao, C. Lau, Y. Chen, Organometallics 15 (1996) 5039. (i) P.A. Shapley, J.M. Shusta, J.L. Hunt, Organometallics 15 (1996) 1622. (j) D.A. Freedman, T.P. Gill, A.M. Blough, R.S. Koefod, K.R. Mann, Inorg. Chem. 36 (1997) 95. (k) J.L. Koch, P.A. Shapley, Organometallics 18 (1999) 814.
[52] (a) M.I. Bruce, N.J. Windsor, Aust. J. Chem. 30 (1977) 1601. (b) W. A. Hermann, E. Herdtweeck, A. Schäfer, Chem. Ber. 121 (1988) 1907. (c) S. Dev, J.P. Selegue, J. Organomet. Chem. 469 (1994) 107.
[53] J.D. Atwood, Inorganic and Organometallic Reaction Mechanisms, VCH Publishers, New York, 1997, Chapter 3.
[54] M.A. Esteruelas, A.M. López, N. Ruiz, J.I. Tolosa, Organometallics 16 (1997) 4657.
[55] M. Baya, P. Crochet, M.A. Esteruelas, E. Gutiérrez-Puebla, N. Ruiz, Organometallics 18 (1999) 5034.
[56] M. Baya, P. Crochet, M.A. Esteruelas, E. Oñate, Organometallics, 20 (2001) 240.
[57] M.A. Esteruelas, E. Gutiérrez-Puebla, A.M. López, E. Oñate, J.I. Tolosa, Organometallics 19 (2000) 275.

[58] P. Crochet, M.A. Esteruelas, A.M. López, N. Ruiz, J.I. Tolosa, Organometallics 17 (1998) 3479.
[59] M. Baya, P. Crochet, M.A. Esteruelas, E. Gutiérrez-Puebla, A.M. López, J. Modrego, E. Oñate, N. Vela, Organometallics 19 (2000) 2585.
[60] P. Crochet, M.A. Esteruelas, E. Gutiérrez-Puebla, Organometallics 17 (1998) 3141.
[61] (a) C. Bruneau, Z. Kabouche, M. Neveux, B. Seiler, P.H. Dixneuf, Inorg. Chim. Acta 222 (1994) 155. (b) H. Doucet, B. Martin-Vaca, C. Bruneau, P.H. Dixneuf, J. Org. Chem. 60 (1995) 7247. (c) M. Picquet, C. Bruneau, P.H. Dixneuf, Chem. Commun (1997) 1201.
[62] L.-B. Han, M. Tanaka, Chem. Commun. (1999) 395.
[63] M.A. Esteruelas, A.M. López, J.I. Tolosa, N. Vela, Organometallics, 19 (2000) 4650.
[64] P. Crochet, M.A. Esteruelas, A.M. López, M.-P. Martínez, M. Oliván, E. Oñate, N. Ruiz, Organometallics 17 (1998) 4500.
[65] M.L. Buil O. Eisenstein, M.A. Esteruelas, C. García-Yebra, E. Gutiérrez-Puebla, M. Oliván, E. Oñate, N. Ruiz, M.A. Tajada, Organometallics 18 (1999) 4949.
[66] M.A. Esteruelas, C. García-Yebra, M. Oliván, E. Oñate, M.A. Tajada, Organometallics 19 (2000) 5098.
[67] R.R. Schrock, S. Luo, J.C. Lee, Jr, N.C. Zanetti, W.M. Davis, J. Am. Chem. Soc. 118 (1996) 3883, and references therein.
[68] (a) H.D. Scharf, F. Korte, Chem. Ber. 99 (1966) 1299. (b) H.D. Scharf, F. Korte, Chem. Ber. 99 (1966) 3925.
[69] D. Di Francesco, A.R. Pinhas, J. Org. Chem. 51 (1986) 2098.
[70] D.G. Gusev, R. Kuhlman, G. Sini, O. Eisenstein, K.G. Caulton, J. Am. Chem. Soc. 116 (1994) 2685.
[71] M. Oliván, O. Eisenstein, K.G. Caulton, Organometallics 16 (1997) 2227.
[72] D. Huang, M. Oliván, J.C. Huffman, O. Eisenstein, K.G. Caulton, Organometallics 17 (1998) 4700.
[73] H. Werner, M.A. Esteruelas, U. Meyer, B. Wrackmeyer, Chem. Ber. 120 (1987) 11.
[74] M.A. Esteruelas, M.P. García, A.M. López, L.A. Oro, N. Ruiz, C. Schlünken, C. Valero, H. Werner, Inorg. Chem. 31 (1992) 5580.
[75] C. Bohanna, B. Callejas, A.J. Edwards, M. A. Esteruelas, F.J. Lahoz, L.A. Oro, N. Ruiz, C. Valero, Organometallics 17 (1998) 373.
[76] M.J. Albéniz, M.L. Buil, M.A. Esteruelas, A.M. López, L.A. Oro, B. Zeier, Organometallics 13 (1994) 3746.
[77] M.L. Buil, Ph. D. Dissertation, University of Zaragoza, 1997.
[78] D.G. Gusev, R.L. Kuhlman, K.B. Renkema, O. Eisenstein, K.G. Caulton, Inorg. Chem. 35 (1996) 663.
[79] J. Espuelas, M.A. Esteruelas, F.J. Lahoz, L.A. Oro, C. Valero, Organometallics 12 (1993) 663.
[80] H. Werner, U. Meyer, M.A. Esteruelas, E. Sola, L.A. Oro, J. Organomet. Chem. 366 (1989) 187.
[81] M.L. Buil, M.A. Esteruelas, A.M. López, E. Oñate, Organometallics 16 (1997) 3169.

[82] C. Bohanna, M.L. Buil, M.A. Esteruelas, E. Oñate, C. Valero, Organometallics 18 (1999) 5176.
[83] M.A. Esteruelas, F.J. Lahoz, A.M. López, E. Oñate, L.A. Oro, Organometallics 13 (1994) 1669.
[84] H. Kawano, Y. Masaki, T. Matsunaga, K. Hiraki, M. Onishi, T. Tsubomura, J. Organomet. Chem. 601 (2000) 69.
[85] J. Espuelas, M.A. Esteruelas, F.J. Lahoz, L.A. Oro, N. Ruiz, J. Am. Chem. Soc. 115 (1993) 4683.
[86] M.A. Esteruelas, F.J. Lahoz, E. Oñate, L.A. Oro, B. Zeier, C. Valero, J. Am. Chem. Soc. 117 (1995) 7935.
[87] M.L. Buil, M.A. Esteruelas, C. García-Yebra, E. Gutiérrez-Puebla, M. Oliván, Organometallics 19 (2000) 2184.
[88] G.J. Spivak, J.N. Coalter, M. Oliván, O. Eisenstein, K.G. Caulton, Organometallics 17 (1998) 999.
[89] M.A. Esteruelas, C. García-Yebra, M. Oliván, E. Oñate, Organometallics 19 (2000) 3260.
[90] H. Quiniou, O. Guilloton, Adv. Heterocycl. Chem. 50 (1990) 85.

Chapter 8

New Trends in Organolanthanide Hydride Chemistry

Denise Barbier-Baudry, Alain Dormond

Laboratoire de Synthèse et d'Electrosynthèse Organométallique, L. S. E. O., UMR 5632, Faculté des Sciences Mirande, 9 Avenue Alain Savary, BP 47870, 21000 Dijon France

CONTENTS

8.1 INTRODUCTION

Organometallic lanthanide hydride chemistry has undergone a relatively recent development [1]. Except for rare examples, this chemistry was born with the pioneering works published in the early 80ths [2]. This delay, in comparison with the late d-element hydride chemistry, has several reasons, the main one being the difficulty to apply the usual synthetic methods, *i.e.* the displacement of a halide by a metallic hydride, MH, or borohydride, MBH_4, to the synthesis of lanthanide hydrides. In contrast, β-hydrogen elimination from alkyl compounds of the *f* elements is uncommon. Therefore, the hydrogenolysis of alkyl complexes remains by far the most used route to obtain lanthanide hydrides.

A very important point which was not well understood during the first investigations of organolanthanides was the necessity to rigorously exclude oxygen and moisture and, in some cases, to also avoid the presence of solvents bearing oxygenated functions such as ethers. All the lanthanide hydride complexes are exceedingly reactive, even with the usual solvents or with themselves. Thus, their synthesis has needed more sophisticated methods than the Schlenk techniques.

The characterisation of the hydride function in organolanthanide hydrides by the classical spectroscopic methods remains difficult. The frequent paramagnetism of the lanthanide ion causes both a broadening and a significant shift of the hydride NMR signal away from the diamagnetic region. In the IR spectra, the Ln-H bond absorption falls in a non characteristic region and has a scarce diagnostic value.

The major part of these drawbacks has been solved during the last fifteen years. Nowadays, the synthesis of the lanthanide hydrides is less challenging, the experimental conditions for their formation are known and their reactivity has been widely investigated.

During the last two decades, lanthanide catalysis has been extensively explored [3], considering the unique properties and the absence of toxicity of these "heavy" metals which make them environmentally friendly. Olefin transformations catalysed by organolanthanides such as oligomerisation, hydrogenation, hydrosilylation, hydroamination, polymerisation, have attracted much attention. The two latter reactions can be initiated by hydrides (which act as precatalysts, such as for MMA polymerisation [4]), but do not involve hydrides as intermediates in the catalytic cycle and therefore will not be considered in the present review.

At first, different hydride families will be briefly presented together with the currently adopted synthetic strategies, the most useful characterisation methods, and their reactivity. As the use of these complexes in stoichiometric processes is aprioristically forbidden by their very high cost, only their catalytic applications will be, in a second part, reviewed. Finally, in the third part of the review, some of the more important and characteristic features of the organolanthanide hydrides will be summarised.

For clarity, the following abbreviations are used throughout the text and schemes: [Ln] = bis(cyclopentadienyl, substituted or not, or related ligands)lanthanide

moieties, Cp = C_5H_5, Cp* = C_5Me_5, A = anionic ligand, generally cyclopentadienyl, L = neutral ligand, generally an ether.

8.2. SYNTHESIS AND GENERAL PROPERTIES OF LANTHANIDE HYDRIDES

8.2.1 General properties of the lanthanide ions

Lanthanides have large ionic radii and, as a consequence, a wide range of co-ordination numbers (3 to 12) are possible. The most common oxidation state is +3. The 4*f* orbitals do not participate intensely in bonding. The bonding in organometallic complexes remains highly ionic and the complexes undergo facile ligand exchange. The adopted co-ordination geometry is strongly related to steric factors. The lanthanide ions are hard Lewis acids and exhibit a high affinity for anionic ligands, especially for oxygen donors. The group III metals yttrium and scandium are generally considered together with the lanthanides. The yttrium ionic radius (0.88 Å for six co-ordination) is close to the corresponding values of the late lanthanides, erbium and holmium (0.881 and 0.894 Å). Scandium has a smaller ionic radius (0.68 Å) [5], and its chemistry is somewhat different, showing intermediate properties between those of the lanthanides and aluminium.

8.2.2 The different families of lanthanide hydrides

The hydrides of the early lanthanides may be stabilised by bulky substituted cyclopentadienyl ligands, such as 1,3-di-*tert*-butylcyclopentadienyl and pentamethylcyclopentadienyl. The late lanthanide hydrides $[(C_5H_4R)_2LnH(L)]_2$, Ln = Lu, Er and Y, may be obtained with less bulky cyclopentadienyl ligands. Only monocyclopentadienyl hydrides of scandium and yttrium of general formula $[(C_5Me_4R)LnH(L)]$ have been reported [6]. Most of the lanthanide hydrides

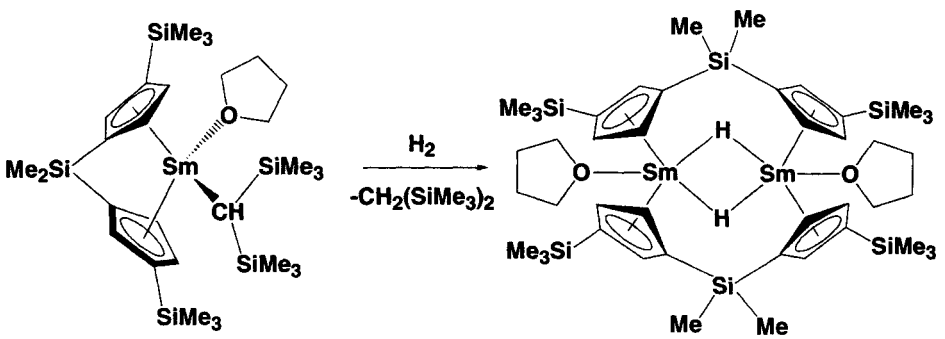

Scheme 1

are bis(cyclopentadienyl) complexes. The Cp_2LnH unit may be isolated as an unsolvated monomer, as a solvate Cp_2LnH(solvent), or as a bridged dimer. The latter structure, with H atoms providing strong intermetallic bridges, is by far the most common. Non-cyclopentadienyl ligands, benzamidinate and tris(pyrazolyl)borate have also been used.

A recent exhaustive review [1] presents the known and well characterised lanthanide hydrides. Recently, a few additional original complexes have been synthesised. These include phospholyl [7] and indenyl derivatives [8], a bimetallic metallocenic structure (Scheme 1) [4], a samarium hydride supported by a calix-tetrapyrrolyl ring, with a triply bonded hydride ligand (Scheme 2) [9], metallocenes with chiral groups which has been used for the asymmetric hydrogenation [10], a tris(pyrazolyl)borate ytterbium(II) hydride [11], Cp amido- [12] and bis(amido)yttrium hydrides [13]. The latter was not isolated but obtained *in situ* from the methyl derivative (Scheme 2).

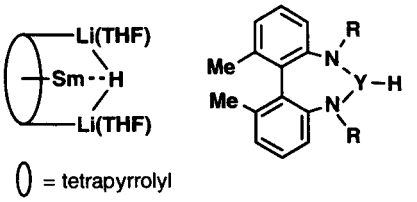

Scheme 2

8.2.3 Syntheses

In general, lanthanide hydrides cannot be successfully synthesised by using conventional hydride reagents, such as MH, MBH_4, $MHBR_3$ (M = Li, Na or K) (eq. 1).

$$[Ln]{-}Cl + NaBH_4 \longrightarrow [Ln]{-}BH_4 \not\longrightarrow [Ln]{-}H + BH_3 \qquad (1)$$

Insoluble MH hydrides react very slowly, they must be used in large excess and rearrangements often occur. In some cases, however, the addition of the hydride ion H^- was observed, and the formation of anionic complexes of poor stability, Cp_3LnH^-, was mentioned [14]. Nevertheless, an yttrium hydride could be structurally characterised [15]. Owing to the high electropositive character of the lanthanide atoms, the use of borohydride (or aluminohydrides) reagents leads to stable borohydrides (or to bimetallic Ln-Al complexes) [1]. The spontaneous elimination of the borane (or alane), which is commonly observed for the late transition metals, does not occur.

Superhydride, $MHBEt_3$, has been widely used in the chemistry of 5*f* elements, (actinides), [16], but for the harder 4*f* elements, only one example of hydride

formation was reported by using superhydride, namely the moderately solution stable $[Cp'_2SmH]_2$ (Cp' = *tert*-butylcyclopentadienyl) [17].

The normal way to access the LnH function is hydrogenolysis of a convenient alkyl precursor [18] (Scheme 3). The choice of the alkyl precursor depends on the ease of its synthesis, on its stability, and on the hydrogenolysis conditions. Useful alkyl precursors are typically methyl derivatives, generally obtained as stable dimers, or monomeric $CH(SiMe_3)_2$ compounds. The hydrogenolysis of dimers may require more drastic conditions than that of monomeric complexes, because two Ln-C bonds must be cleaved and the intermediate mixed alkyl-hydride complex is often less reactive than the starting alkyl. Medium hydrogen pressure and smooth heating can therefore be necessary for disrupting the dimeric structure, whereas atmospheric hydrogen pressure and room temperature conditions usually allow the cleavage of terminal Ln-alkyl groups.

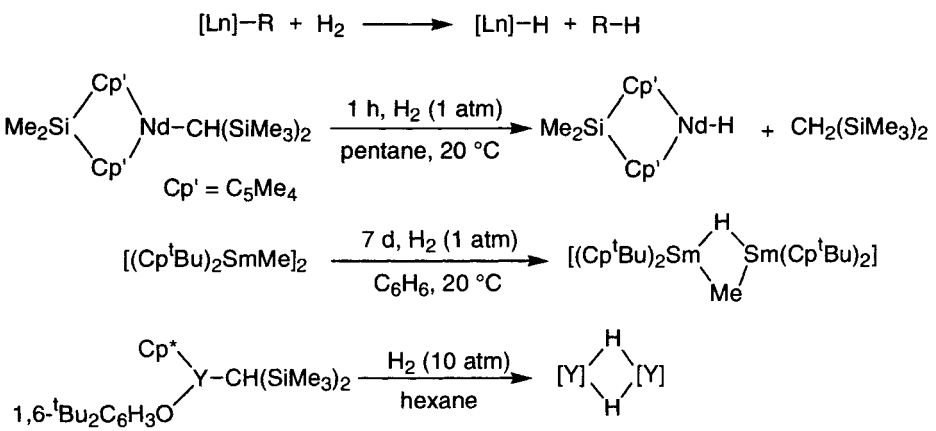

Scheme 3

8.2.4 Characterisation

It is nowadays well established that the hydrogenolysis of an alkyl complex involves the initial formation of the corresponding hydride. This may be an unstable transient species, especially when the alkyl precursor includes non-bulky ligands. A monomeric stable [Ln]R complex can lead to an unstable [Ln]H moiety, because the smaller size of the hydride ligand may not ensure the saturation of the co-ordination sphere about the lanthanide. The rearrangement into tris(cyclopentadienyl) derivative may also compete with both dimerisation or reduction (Scheme 4).

The formation of the RH molecule during the hydrogenolysis is not sufficient evidence for the generation of a stable hydride. In addition, the detection of

the Ln-H function is not a simple task. IR spectroscopy does not bring a lot of information: the Ln-H absorbtion is located in the range 1100 - 1300 cm^{-1} [2] and many bands, especially those of the THF ligand which is frequently contained in these complexes, also appear in this range. The unambiguous assignment of the Ln-H vibration requires the synthesis of the corresponding Ln-D complex and the observation of the Ln-D frequency at the theoretical lower value.

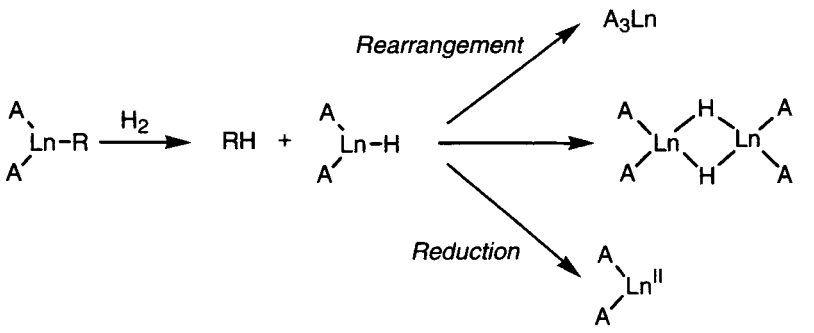

Scheme 4

The characterisation of the hydride function by NMR is not easy, except in the case of yttrium derivatives. In this case, the presence of the Y-H bond can be established by the observation of the J(Y,H) coupling constant. For the other diamagnetic elements, the Ln-H signals are located in the broad range 2 - 9 ppm, and their assignment requires the preparation of samples of high purity. Hydride chemical shifts of lutetium complexes were published, and few data were reported for scandium and lanthanum. The other elements are paramagnetic and, even for those accessible by NMR such as Nd, Sm and Yb (narrow signals and moderate paramagnetic shifts), the data so far published remain quite rare [1]. The reasons of the difficulties in localising the paramagnetic Ln-H signals are not clear. A great broadening of the H signal under the influence of the paramagnetic metal centre, and/or the possibility of H/D exchange with the deuterated solvent have been considered. Unusually high chemical shifts, due to a strong contact contribution, might also be postulated. In the neodymium series, the Ln-H-B signal (C_6D_6 solution) of the metallocene monomeric tetrahydroborate [$(^tBuC_5H_4)_2Nd(BH_4)$] is found at 90 ppm, (the infrared data suggest a tridentate structure [19]) while the corresponding tris(alkyl)borohydride signal is found at 210 ppm. The signal of a dimeric hydride, under the influence of two paramagnetic centres may be expected to resonate at even lower fields (Scheme 5).

There exists, however, a chemical correlation that readily allows one to establish the presence of a lanthanide hydride complex, even in a crude mixture. Hindered ketones can insert into Ln-H bonds but do not react within a few hours with the alkyl precursor complexes. After hydrogenolysis in the presence of pivalone

resulting in the formation of an alkoxide, the NMR spectrum indirectly proves the formation of the Ln-H intermediate. When the pivalone is added after the hydrogenation step, the formation of the alkoxide demonstrates the fair stability of the initially formed hydride monomer. The detection, in the alkoxide, of the LnOCH signal additionally excludes the occurrence of H/D exchange for [Ln]H, which is as a common process.

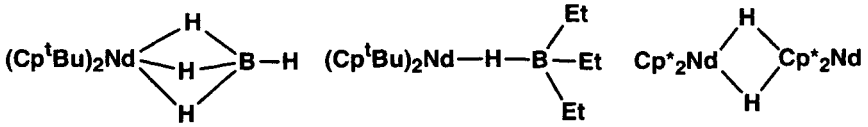

$\delta_H = 90$ $\delta_H = 210$ δ_H = not located

Scheme 5

8.2.5 Reactivity and stability

The stability of lanthanide hydrides is strongly controlled by steric factors. In particular, the small size of the hydride ion requires the presence of bulky ancillary ligands, usually ethers and/or anionic coligands, in order to prevent the rearrangement to more stable derivatives.

In organometallic lanthanide complexes, the bonds are partially covalent but remain largely ionic in nature and both associative and dissociative mechanisms may play a relevant part in the ligand scrambling. Considering the electrophilic nature of the lanthanides, dissociative pathways are only possible in co-ordinating solvent (Scheme 6).

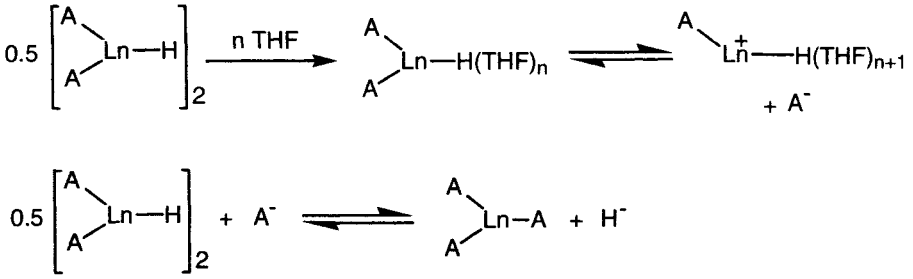

Scheme 6

In non co-ordinating solvent, this process is not favoured, and the ligand exchange occurs by formation and dissociation of a binuclear structure. The presence of bulky ligands markedly slows down this process (Scheme 7).

A bimolecular route is also postulated to explain the reduction of less electron rich hydrides when the lower oxidation state is accessible (samarium and ytterbium). Thus, the hydrogenolysis of analogous neodymium and samarium hydrides bearing tetramethylphospholyl ligands leads to the stable neodymium hydride and to the reduced samarium(II) metallocene, respectively (Scheme 8).

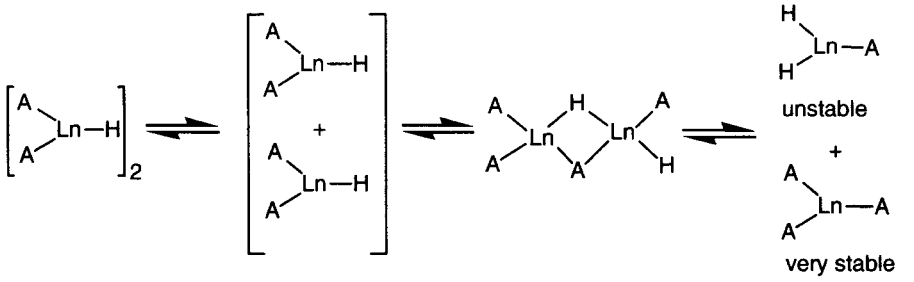

Scheme 7

It is noteworthy that while the electron rich Cp^*_2SmH is only moderately stable in solution, the analogous more strained dinuclear bridging complex is less stable and must be kept under hydrogen in order to record the NMR spectrum [2]. The synthesis of a samarium hydride supported by a calix-tetrapyrrolyl system was recently published [9] (Scheme 2), with the hydride ligand bonded to one samarium and to two lithium atoms. This cage affords an efficient protection against bimolecular collisions and the complex is described as thermally robust.

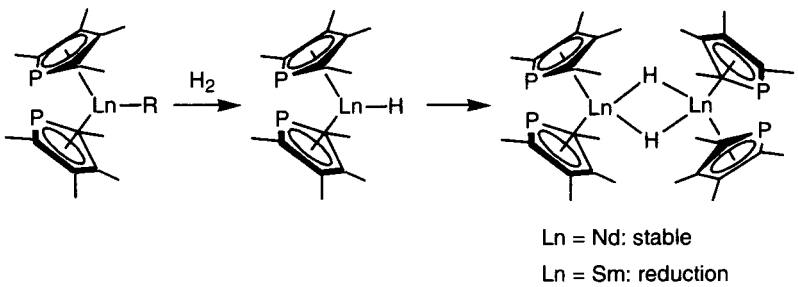

Scheme 8

The lanthanide hydrides are exceedingly sensitive towards air and moisture. In the absence of added reagents, the electron-rich pentamethylcyclopentadienyl hydrides, Cp^*_2LnH, react with themselves by intermolecular H abstraction from a Cp* ligand. Aromatic solvents and a large variety of unsaturated substrates (carbon monoxide, aldehydes, ketones, imines, alkynes, olefins) also readily react with these hydrides (Scheme 9) [20]. The high electrophilic nature of these metals

leads to fast reactions with many organic molecules (halogenoalkanes, amines, alcohols, oxiranes), allowing the formation of the very stable Ln-O, Ln-N, and Ln-Cl bonds.(Scheme 9)

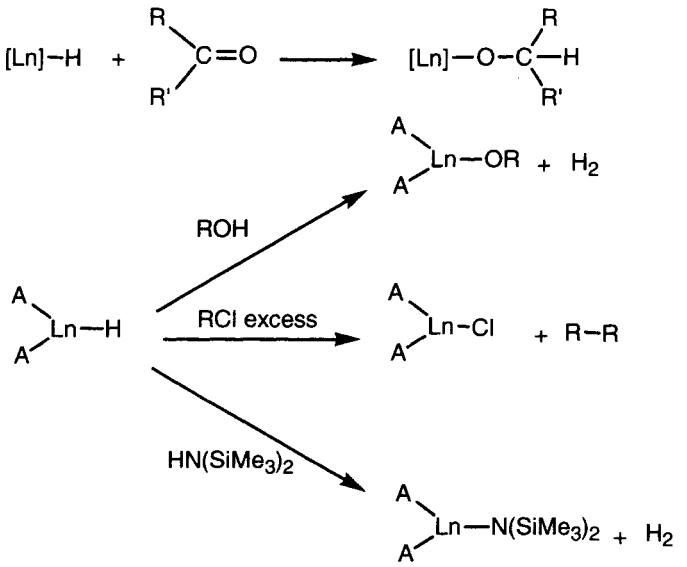

Scheme 9

8.3. LANTHANIDE HYDRIDES IN CATALYSIS

8.3.1 Hydrogenation

Cyclopentadienyl lanthanide hydrides were reported to behave as hydrogenation catalysts of alkenes since the eighties. The permethylcyclopentadienyl hydrides $[Cp^*_2LnH]_2$ (Ln=La, Nd, Sm, Lu) and $[\{Me_2Si(C_5Me_4)_2\}LnH]_2$ (Ln=Nd, Sm, Lu) were described as being among the most active homogeneous olefin hydrogenation catalysts yet discovered [21, 2]. The catalytic cycle is initiated by the dissociation of the dimeric hydrides (Scheme 10).

The hydrogenation of hex-1-ene was found to be extremely rapid, with a turnover Nt = 120,000 h^{-1} at 25 °C under 1 atm of H_2 (3000 h^{-1} for $RuHCl(PPh_3)_3$). The relative order of catalytic activity was found to be approximately inversely proportional to the metal ionic radius, Lu > Sm > Nd > La. The olefin addition is rapid and exothermic and the rate limiting step is the hydrogenolysis of the Ln-C bond. Hydrogenation of internal olefins is slower, and the order of the activities for cyclohexene hydrogenation is the opposite: La > Nd > Sm > Lu. In this case the rate limiting step is the addition of the lanthanide hydride to the hindered olefin. Molander and co-workers [22] took advantage of this difference of reactivity

to accomplish the selective hydrogenation of substituted non conjugated dienes by [Cp*YH] obtained *in situ* by hydrogenolysis of the corresponding methyl derivative. In some cases, competing cyclisation reactions occurred (Scheme 11).

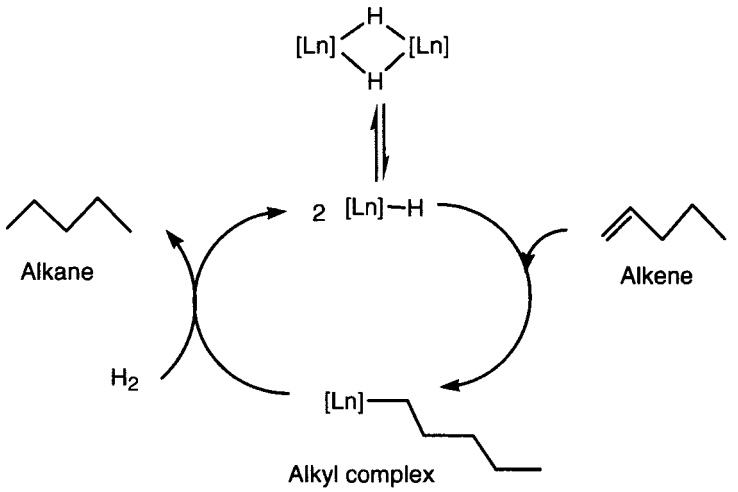

Scheme 10

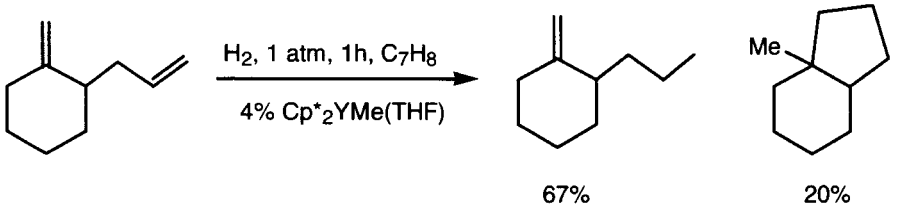

Scheme 11

Recently, after the synthesis of more sophisticated organolanthanide complexes, enantioselective hydrogenations and deuteriations were described. Thus, by using (*S,R*)-$Me_2Si(3\text{-}Me_3SiC_5H_3)[3\text{-}(-)\text{-}menthylC_5H_3]LnCH(SiMe_3)_2$, Ln=Y or Lu, as precatalyst, moderate enantiomeric excesses were obtained in the hydrogenation of α-ethyl styrene and 2-ethylhex-1-ene [23]. A new chelating ligand bearing a chiral neomenthyl group allowed the preparation of diastereomerically pure $[(R,S)\text{-}Me_2Si(^tBuC_5H_3[(+)\text{-}neomenthylC_5H_3]LuH]_2$, precatalyst for asymmetric hydrogenation (or deuteriation) of functionalised olefins.

The deuteriation of pent-1-ene could be accomplished with the highest *ee* value (63 %) so far reported [24]. Although the authors claimed excellent yield and selectivity, no important development of these catalysts has occurred. Perhaps the

complexity of the experiments, the required rigorous exclusion of oxygen and moisture and the incompatibility of the organolanthanide hydrides with several functional groups constitute obstacles to their practical utilisation.

8.3.2 Hydrosilylation

The first hydrosilylation reaction catalysed by organolanthanide hydrides was described at the beginning of the nineties (eq. 2) by using metallocene neodymium hydrides as catalysts [25-27]. Nowadays, the more stable and more soluble alkyls dimers with methyl bridges or monomers with $CH(SiMe_3)_2$ substituents have been demonstrated to be especially convenient precatalysts and are generally used [28-30].

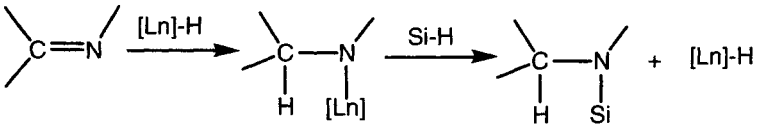

(2)

The mechanism of the reaction was studied for cyclopentadienyl lanthanide complexes, [26, 29, 31]. A monomeric metal hydride is proposed to be the active species. The catalytic cycle turns via a fast and irreversible insertion of the olefin into the metal hydrogen bond to form an alkyl species which reacts with the silane in the rate determining step with regeneration of the hydride (Scheme 12).

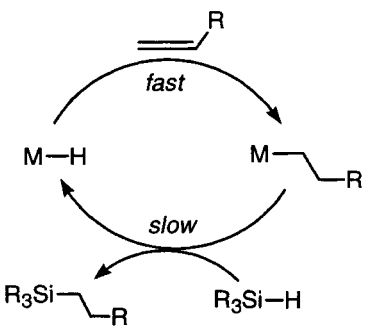

Scheme 12

Owing to the encumberance of the ligands, the reaction generally proceeds with high selectivity and the hydrosilylation products of terminal olefins are generally obtained in high yields. The selectivity depends on the size of the metal radius: the smallest metal ions (Lu, Yb, Y) are totally selective for the linear silyl products, whereas larger lanthanides provide higher yields of both regioisomers.

An illustrative example of this situation is presented in Scheme 13 and refers to the hydrosilylation of 1-decene with phenylsilane [30, 31]. The ratio between the two regioisomers (**1/2**) as a function of the organolanthanide used as precatalyst is summarised in table 1.

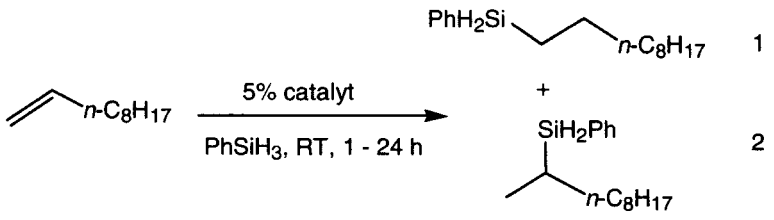

Scheme 13

TABLE 1. Ratio (**1/2**) between the regioisomers for the hydrosilylation of 1-hexene as a function of the ionic radius of the lanthanide

Precatalyst	Yield %	1/2 Ratio
[Cp*$_2$LuMe(THF)]	98	100/0
[Cp*$_2$YMe(THF)]	84	100/0
[Cp*$_2$YbCH(SiMe$_3$)$_2$]	91	100/0
[Cp*$_2$NdCH(SiMe$_3$)$_2$]	85	3.2/1
[Cp*$_2$LaCH(SiMe$_3$)$_2$]	90	1.9/1

With the exception of norbornene, internal olefins do not undergo hydrosilylation. Hydrosilylation of 3-phenylpropene with $PhSiD_3$ forms a unique product and the process tolerates a variety of functional groups, halides, ethers and acetals, despite the well known strong Lewis acidity of the catalysts. Cyclisation/silylation of 1,5-dienes or 1,6-enynes has been reported to give a single product (Scheme 14) [26]. In the case of metallocene complexes bearing a menthyl substituent, *ee* values near 70% were obtained for the asymmetric hydrosilylation of 2-phenyl-but-1-ene [31].

A unique example of non metallocenic catalyst [(DADMB)YMe], [(DADMB)$^{2-}$ = 2,2'-bis(*tert*-butyldimethylsilylamido)-6,6'-dimethyldiphenyl], was recently reported [13]. It was assumed that the methyl complex first reacts with the silane to give a small concentration of a monomeric highly reactive hydride (Scheme 2). The yttrium hydride was not detected by NMR spectroscopy, probably because its concentration is very low. Nevertheless, precipitation of the insoluble yttrium dimer [(DADMB)YH]$_2$ occurred at the end of the reaction. The bulky ligand

$[DADMB]^{2-}$ did not impede the reaction with secondary silanes. Thus, both 1,2- and 2,1-addition of silane across the double bond were observed: aliphatic olefins gave terminal addition as the major process, while conjugated (styrenic) olefins led to mixtures in which the benzylsilanes predominated. For these olefins, the catalyst $[\{Me_2Si(C_5Me_4)_2\}SmCH(SiMe_3)_2]$, remains the most selective and the 2,1 addition product is formed in nearly quantitative yield. Complexes of metals with large ionic radius and with open co-ordination spheres favour the 2,1 addition [33].

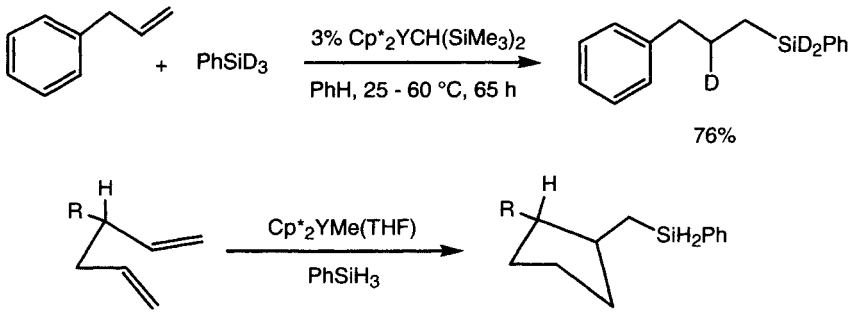

Scheme 14

In the presence of the ytterbium(II) imino complex, $[Yb(\eta^2\text{-}Ph_2CNAr)(HMPA)_n]$, imines react with triphenylsilane to give aminosilanes in good yields. Primary and secondary amines undergo a dehydrogenative silylation. The two reactions proceed through common intermediates, and present similar selectivity and yields. The possible catalytic cycle involves the formation of the intermediate ytterbium hydride $Y(H)\{(Ar)CHPh_2\}$ [34] (Scheme 15). In the proposed mechanism, imine inserts into the Yb-H bond, whereas the amine acts as a nucleophilic reagent to give the correspondent (amido)ytterbium species. In both cases, the hydride is regenerated by the cleavage of the Si-H bond.

8.3.3 Olefin polymerisation

Olefin polymerisation can be initiated by lanthanide hydrides, but the active species of the catalytic cycle is an alkyl complex, which reacts with the monomer. The β-H elimination is not a favoured reaction for lanthanide compounds, and in these pseudo-living polymerisations, very high molecular weights are obtained. It is of interest for some applications to synthesise polymers of lower molecular weight and this is usually done by adding a small percentage of hydrogen to the feed in order to hydrogenate the alkyl chain. The formed hydride would initiate the growing of a new polymer chain and the chain length would be modulated by competition between the hydrogenolysis of the Ln-C bond and the monomer insertion.

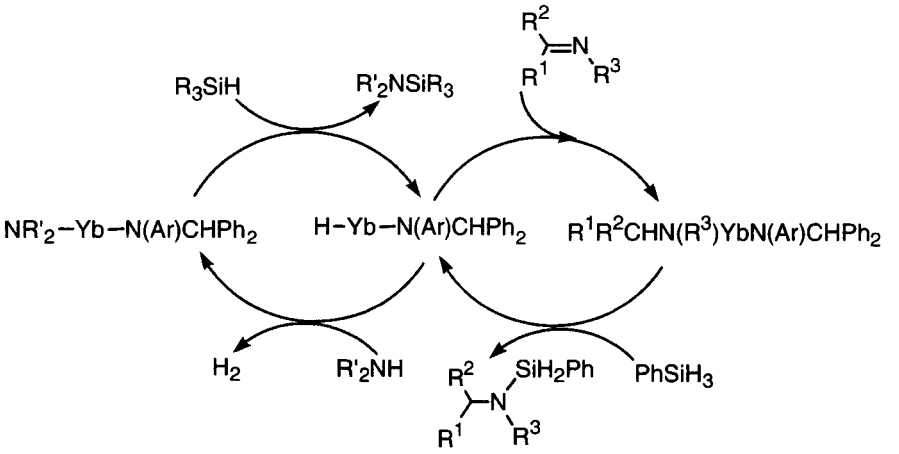

Scheme 15.

8.3.4 Olefin oligomerisation

Oligomerisation of ethylene and α-olefins are important industrial processes, providing useful added value products. Olefin oligomerisation is generally carried out by using homogeneous late-transition metal catalysts, particularly nickel-based catalysts [35, 36]. Lanthanide hydrides can, however, initiate the polymerisation of both ethylene and higher olefins; with the latter substrates oligomers or polymers with low molecular weight can be obtained [1]. The formation of dimers is usually not favoured and seldom occurs, involving in any case the hydride in the catalytic cycle.

The sterically hindered hydride $[(Indenyl)_2YH]_2$ [8] is an effective catalyst to accomplish homo- and co-dimerisation of a wide range of terminal olefins CH_2=CHR, R=Ph, *n*-Bu, *i*-Pr, *t*-Bu, $SiMe_3$, CH_2Ph. The presence of substituents and functionalities in the monomer are usually tolerated. An induction period of *ca.* 30 min may be necessary to cleave the dimeric structure of the catalyst precursor; the yields are nearly quantitative within two days. Co-dimerisation of α-olefins with styrene proceeds via initial insertion of the α-olefin into the Y-H bond, followed by a 2,1-insertion of styrene into the Y-C bond of the alkyl intermediate. Subsequent β-H abstraction leads to the releasing of the dimer (Scheme 16).

The controlling feature for this uncommon reaction is likely to be the steric hindrance around the metal: β-H elimination of the hydrogen atom on the tertiary carbon is therefore more favoured than further co-ordination - insertion of the monomers in the Ln-C bond [8].

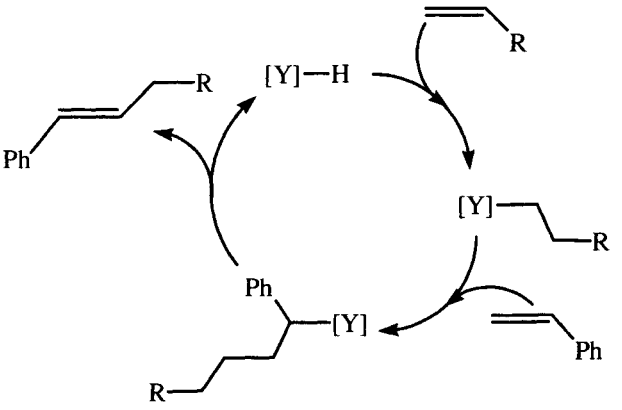

Scheme 16

8.4. NEW TRENDS AND IMPORTANT FACTS

8.4.1 The importance of the monomeric hydrides

Lanthanide hydrides are usually isolated in the form of dimeric or, more seldom, as trimeric species. In a few cases [37], monomeric complexes with a terminal hydride and ancillary ligands may be isolated. However, it is worth stressing that lanthanide hydrides playing an active role in a catalytic cycle may be formed *in situ* by cleavage of a Ln-C bond. This may be accomplished by hydrogenation (olefin hydrogenation), by reaction with a silane (hydrosilylation), or by β-H elimination (olefin dimerisation). Once these transient monomeric hydrides are formed they may undergo different transformations such as addition to the substrate (at the very beginning of a new catalytic cycle), or redistribution during the catalytic process leading to inactive species. This last reaction reduces the amount of the active species in the catalytic cycle, thus leading to partial or complete deactivation of the system after some time. Moreover, dimerisation of the active species may in some cases lead to the precipitation of the insoluble dimer. Thus, before synthesising a new catalyst, it would be of great importance to predict which pathway among the competitive reactions is the favoured one. Alternatively, if a lanthanide precatalyst is chosen for catalytic reactions, its structure should allow the formation of a hydride whose existence has been previously established by a parallel synthesis. Nevertheless, a transient hydride which does not lead to a stable and isolable complex could exhibit new and interesting reactivity. The search of new reactive hydride species could be a profitable operation, but how to do that?

One of the keys for understanding the reactivity of transient species is the study of their behaviour in solution. As an example, during the attempts to synthesise non hindered metallocenic hydrides, the synthesis of $(C_5H_4{}^tBu)_2SmH$

was unsuccessfully attempted. No stable complex could be isolated in the solid state, and the sole formation of the tris(cyclopentadienyl) compound $[(C_5H_4{}^tBu)_3Sm]$ occurred. Nevertheless, the formation of the moderately stable unsolvated dimer $[(C_5H_4{}^tBu)_2SmH]_2$ could be established. Its formation occurred in variable yields depending on the adopted synthetic route. By hydrogenolysis of a terminal bulky monomeric alkyl complex, low yields (20 - 30%) were obtained. However, by treating the dimeric chloride with $NaHBEt_3$, the hydrido-chloride intermediate forms, leading to the dinuclear hydride in 80% yield. [15] (Scheme 17).

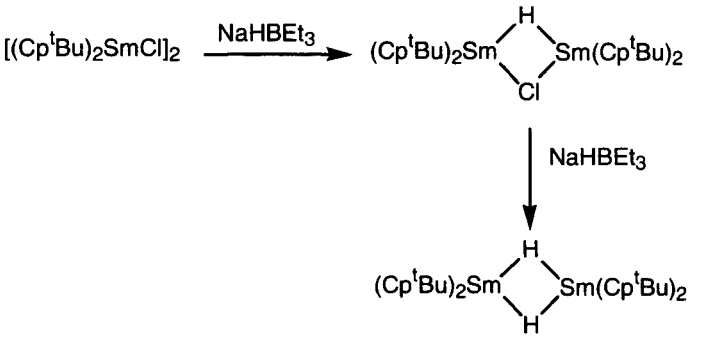

Scheme 17

Obviously, a bridging structure is an important factor for stability and it is of great importance to preserve this dimetallic assembly. For example, hydrogenolysis of the dimeric methyl complex (Scheme 18) leads to the stable mixed hydrido-methyl complex, which within a week converts only in traces to the dinuclear dihydride [17]. Such uncrowded hydrides could be useful reagents to be used in reactions involving hindered olefins.

8.4.2 Steric effects

By considering the typical decrease of the lanthanide ionic radius (1.06 to 0.85 Å) [5] due to the lanthanide contraction, a difference in the molecular formula of non-hydrido complexes is observed for comparable species on moving from early to late lanthanides. As a general rule, the number of ancillary ligands necessary to ensure the saturation of the co-ordination sphere is higher for the early lanthanides, the borderline case being generally samarium. The situation is slightly different for the hydride complexes, as a consequence of the minimal dimensions of the H ligand. For those complexes devoid of bulky coligands, the series of analogous complexes are not accessible. Thus, the bis(pentamethylcyclopentadienyl) series, $[Cp^*_2LnH]_2$, is complete, whereas bis(cyclopentadienyl) complexes, $[Cp_2LnH(THF)]_2$, have

been obtained only for lutetium and yttrium. In many cases, when $[Cp_2LnH(THF)]_2$ complexes are involved in a reaction, a disproportionation occurs resulting in the formation of the very stable homoleptic derivative $[Cp_3Ln]$. As a consequence, only organolanthanide hydrido complexes bearing bulky coligands are used in synthesis, a typical example being the yttrium complex $[Cp^*_2YH]$ which is readily obtained *in situ* by hydrogenolysis of the methyl or $CH(SiMe_3)_2$ derivatives. In spite of this limitation, new catalytic systems in which the metal centre would be largely accessible could be designed and synthesised. The use of chelating ligands, especially bridged metallocenes or hemimetallocenes containing amido or alkoxy ligands, is highly promising as it strongly hampers the rearrangements. Syntheses of such hydride complexes were recently published [12].

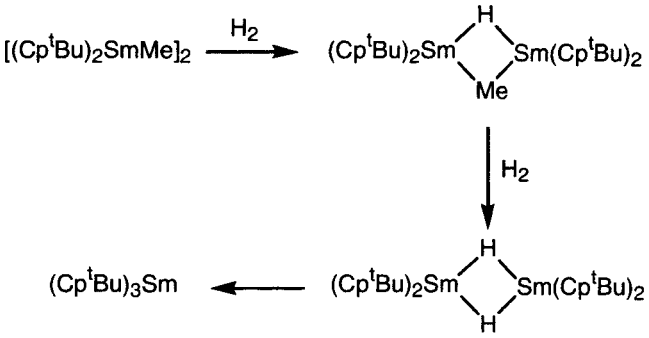

Scheme 18

8.4.3 Electronic effects

For a long time, it has been assumed that the stability of organometallic complexes of the lanthanides, on the basis of their ionic character, is mainly governed by electrostatic factors and by steric requirements. The recent preparation of under-coordinated samarium(II) and samarium(III) complexes (Scheme 19) [38, 39] has raised the question of a possible electronic control in organolanthanide chemistry.

Any modification of a complex, in order to increase or decrease its reactivity towards a substrate for catalytic purposes, can be easily accomplished by modulating the steric effects, even though modification of the electronic properties of the reactive site may also be necessary to render the catalyst more efficient. The evaluation of such electronic influence requires a comparison of complexes bearing ligands of the same size (isosteric ligands) but different in their chemical nature. The organometallic chemistry of the hard lanthanide elements is dominated by the soft cyclopentadienyl type ligands, while the number of non cyclopentadienyl hydrides is really modest. Due to the paucity of the published syntheses of

non metallocene hydrides, it is not possible to address any valuable conclusion. Carrying out these comparative studies would represent an interesting contribution in this field. Of particular interest would be the study of pairs of analogous complexes sharing the same geometry and differing for the nature of the ligands, which would allow one to establish rules of reactivity. More efforts should be made to synthesise hydrides bearing sterically demanding ligands such as benzamidinates, diketiminates, or tris(pyrazolyl)borates. It is noteworthy that the electron donating ability of these ligands varies with the transition metal. Data concerning early d-metals, particularly titanium and vanadium, are available. For example, the tris(pyrazolyl)borate ligand is apparently more donating than Cp towards vanadium and conversely Cp is a better electron donor for titanium complexes [40]. Similar conclusions are, however, not yet extended to the lanthanide series.

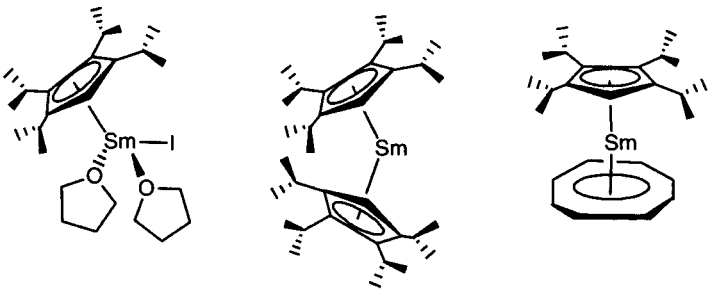

Scheme 19

8.4.4 The importance of the f electrons.

During the first studies of the organometallic chemistry of *f* elements, considering the high number of available orbitals, it was expected that lanthanide complexes could exhibit an original reactivity. In contrast, it is currently thought that the f-electrons of the organometallic core are relatively uninvolved in bonding and do not play a significant role in determining the reactivity. However, if one includes in the "lanthanide chemistry" the extensive non-lanthanide yttrium chemistry, it may be remarked that among the known lanthanide hydrides [1], those of yttrium are by far the most common ones, being about twice as many as those of lutetium and twice as many as those of all the early lanthanides (La-Sm) combined. Of course, the paucity of early lanthanide hydrides reflects the well known difficulties encountered in their synthesis and is a consequence of the large size of the metal radius. Conversely, the relative abundance of lutetium complexes could be explained by the easier synthetic work associated with these complexes.

It is not obvious to compare the properties of yttrium and analogous lanthanide complexes. The ionic radius of yttrium is close to the radius of erbium, holmium,

terbium and dysprosium, but the organometallic chemistry of these elements remains relatively unexplored. The chemistry of the smaller ytterbium is more developed. Despite the smaller size of this element (0.858 vs 0.88 Å [5]), it is noteworthy that ytterbium analogues of stable yttrium complexes are not so easily obtained. These two elements show some differences of reactivity but there is no simple explanation for this fact. In particular, ligand scrambling processes are observed to a larger extent for ytterbium than yttrium. For example, the bis(benzamidinate) $[\{Ph(NSiMe_3)_2\}_2YH]$ has been described [41], whereas attempted syntheses of the corresponding Yb compounds failed [14].

In view of the known complexes, the presence of f-electrons might appear as a factor of destabilisation for ytterbium and late lanthanides derivatives. An exhaustive comparative study of analogous complexes of yttrium and late lanthanides appears necessary to establish a sound comparison of the stability and reactivity between these complexes. This would allow us to bring new light on the role played by the *f* electrons.

8.4.5 The agostic interaction.

The agostic interaction, Ln···H-X can be considered as the step preceding the formation of a hydride species (Scheme 20).

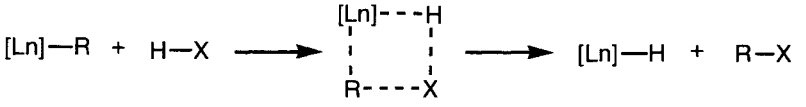

Scheme 20

For the lanthanide complexes, the β-H elimination leading to an unsaturated organic substrate and an hydrido complex is not a common process. As a consequence, organolanthanides are efficient catalysts for olefin polymerisation, and it is assumed that strong α-H and β-H agostic interactions play a significant role in the stabilisation of the reactive species in the catalytic reactions [42]. The importance of the Ln···H-Si agostic interactions in the dehydrogenative polymerisation of hydrosilanes has been discussed [43]. Recently, the importance of the agostic contribution to the stability of an indenyl derivative bearing a bis(dimethylsilyl) amido ligand has also been suggested. A strong Sm···H-Si bis(agostic) interaction has been proposed as the early step of the oxidative addition of a Si-H bond to the metal centre (Scheme 21) [44].

The search of such interactions could be possible by a careful re-examination of the known published crystal structures and could help to search further examples of agostic interactions in lanthanide chemistry; a better knowledge of these weak

bonding effects would, eventually, permit a more precise understanding of the factor governing the stability and probably the reactivity of organolanthanide complexes.

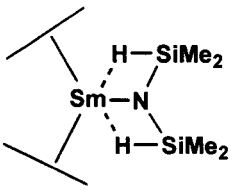

Scheme 21

8.5. CONCLUSION

Although remarkable progress in vacuum line and glove-box techniques has allowed an easier handling of these exceedingly air and moisture sensitive complexes, lanthanide hydrides still remain hardly accessible compounds, in spite of their interest. As stoichiometric reagents, they can only be used for academic work devoted to the development of new concepts and fundamental knowledge. As catalysts, they can only operate in hydrogenation or hydrosilylation processes. This limitation is likely due to the difficult regeneration of the hydride function in a catalytic cycle. Therefore, more stable and more easily synthesised alkyl complexes are generally used instead of the hydrides. These are, at the same time, precursors of the hydrides in hydrogenation experiments and are themselves active catalysts for olefin and diene polymerisation processes.

REFERENCES

[1] M. Ephritikhine, Chem. Rev. 97 (1997) 2193.
[2] (a) W. J. Evans, J. H. Meadows, A. L. Wayda, W. E. Hunter, J. L Atwood, J. Am. Chem. Soc. 104 (1982) 2008. (b) P. L. Watson, D. C. Roe, J. Am. Chem. Soc. 104 (1982) 6471. (c) W. J. Evans, J. H. Meadows, A. L. Wayda, W. E. Hunter, J. L Atwood, J. Am. Chem. Soc. 104 (1982) 2008. (d) G. Jeske, H. Lauke, H. Mauermann, P. N. Swepston, H. Schumann, T. J. Marks, J. Am. Chem. Soc. 107 (1985) 8091. (e) G. Jeske, L. E. Schock, P. N. Swepston, H. Schumann, T. J. Marks, J. Am. Chem. Soc 107 (1985) 8103.
[3] G.A. Molander, E. D. Dowdy, Topics Organomet. Chem. 2 (1999) 119.
[4] G. Desurmont, Y. Li, H. Yasuda, T. Maruo, N. Kanehisa, Y. Kai, Organometallics 19 (2000) 1811.
[5] F. A. Cotton, G. Wilkinson, Advanced Inorganic Chemistry, 4th Ed., J. Wiley and Sons, New York (1980).
[6] (a) P. J. Shapiro, E. Bunel, W. P. Schaefer, J. E. Bercaw, Organometallics 9 (1990)

867. (b) C. J. Schaverien, Organometallics 13 (1994) 69.
[7] F. Nief, P. Riant, L. Ricard, P. Desmurs, D. Baudry-Barbier, Eur. J. Inorg. Chem. (1999) 1041.
[8] W. P. Kretschmer, S. I. Troyanov, A. Meetsma, B. Hessen, J. H. Teuben, Organometallics 17 (1998) 284.
[9] T. Dube, S. Gambarotta, G. P. A. Yap, Organometallics 19 (2000) 817.
[10] M. A. Giardello, V. P. Conticello, L. Brard, M. R. Gagné, T. J. Marks, J. Am. Chem. Soc. 116 (1994) 10241.
[11] (a) G. M. Ferrence, R. Mc Donald, M. Morissette, J. Takats, J. Organomet. Chem. 596 (2000) 95. (b) G. M. Ferrence, M. Gregory, R. Mc Donald, J. Takats, Angew. Chem. Int. Ed. Engl. 38 (1999) 2233.
[12] K. C. Hultzsch, P.Voth, K. Beckerle, T. P. Spaniol, J. Okuda, Organometallics 19 (2000) 228.
[13] T. I. Gountchev, T. D. Tilley, Organometallics 18 (1999) 5661.
[14] M. Visseaux, unpublished results.
[15] B. Wang, D. Deng, C. Qian, New. J. Chem. 19 (1995) 515.
[16] (a) J. C. Berthet, M. Ephritikhine, New. J. Chem. 16 (1992) 767. (b) D. Baudry, A. Dormond, I. Alaoui Abdallaoui, J. Organomet. Chem. 476 (1994) C15.
[17] D. Baudry, A. Dormond, B. Lachot, M. Visseaux, G. Zucchi, J. Organomet. Chem. 547 (1997) 157.
[18] C. J. Schaverien, Organometallics 13 (1994) 69.
[19] D. Baudry, A. Dormond, M. Visseaux, J. Organomet. Chem. 609 (2000) 21.
[20] (a) W. J. Evans, Adv. Organomet. Chem. 24 (1985) 131. (b) W. J. Evans, T. A. Ulibarri, J. W. Ziller, Organometallics 10 (1991) 134. (c) I. N. Parshina, A. K. Shestakova, K. P. Butin, I. P. Beletskaya, L. G. Kuz'mina, J. A. K. Howard, Organometallics 16 (1997) 4041.
[21] H. Schumann, G. Jeske, Angew. Chem. Int. Ed. Engl. 24 (1985) 225.
[22] G. A. Molander, J. O. Hoberg, J. Org. Chem. 57 (1994) 3266.
[23] C. M. Aar, C. L. Stern, T. J. Marks, Organometallics 15 (1996) 1765.
[24] H. W. Roesky, U. Denninger, C. L. Stern, T. J. Marks, Organometallics 16 (1997) 4486.
[25] T. Sakakura, H. J. Lautenschlager, M. Tanaka, J. Chem. Soc. Chem. Comm. (1991) 40.
[26] G. A. Molander, M. Julius, J. Org. Chem. 57 (1992) 6347.
[27] G. A. Molander, J. Winterfeld, J. Organomet. Chem. 524 (1996)) 275.
[28] G. A. Molander, C. P. Corrette, Organometallics 17 (1998) 5504.
[29] P. F. Fu, T. J. Marks, J. Am. Chem. Soc. 117 (1995) 10747.
[30] H. G. Schumann, M. R. Keitsch, J. Demtschuk, G. A. Molander, J. Organomet. Chem. 582 (1999) 70.
[31] G. A. Molander, E. D. Dowdy, B. C. Noll, Organometallics 17 (1998) 3754.
[32] G.A. Molander, E .E. Knigth, J. Org. Chem. 63 (1998) 7009.
[33] P. F. Fu, L. Brard, Y. Li, T. J. Marks, J. Am. Chem. Soc. 117 (1995) 7157.
[34] K.Tanaki, T. Kamata, Y. Miura, T. Shishido, K. Takehira, J. Org. Chem. 64 (1999) 3891.
[35] F. Benvenuti, C. Carlini, M. Marchionna, A. M. Galetti, G. Sbrana, Polym. Adv. Technol. 10 (1999) 554.

[36] S. A. Svejda, M. Brookhart, Organometallics 18 (1999) 65.
[37] M. E. Thompson, S. M. Baxter, A. R. Bulls, B. J. Burger, M. C. Nolan, B. D. Santarsiero, W. P. Schaefer, J. E. Bercaw J. Am. Chem. Soc. 109 (1987) 203.
[38] D. Barbier-Baudry, O. Blacque, A. Hafid, A. Nyassi, H. Sitzmann, M. Visseaux, Eur. J. Inorg. Chem. (2000) 2333.
[39] M. Visseaux, D. Barbier-Baudry, O. Blacque, A. Hafid, P. Richard, F. Weber, New J. Chem. 24 (2000) 939.
[40] D. M. Tellers, S. J. Skoog, R. G. Bergman, Organometallics 19 (2000)) 2428.
[41] R. Duchateau, C. T. van Wee, P. T. van Duijnen, J. H. Teuben, Organometallics, 15 (1996) 2279.
[42] D. G. Musaev, R .D. J. Froese, K. Morokuma, New J. Chem. 21 (1997) 1269.
[43] C. M. Forsyth, S. P. Nolan, T. J. Marks, Organometallics 10 (1991) 2543.
[44] J. Eppinger, M. Spiegler, W. Hieringer, W. A. Herrmann, R. Anwander, J. Am. Chem. Soc. 122 (2000) 3080.

Chapter 9

Dihydrogen Metal Complexes in Catalysis

Claudio Bianchini and Maurizio Peruzzini

Istituto per lo Studio della Stereochimica ed Energetica dei Composti di Coordinazione, Consiglio Nazionale delle Ricerche, ISSECC-CNR, Via J. Nardi 39, 50132 Firenze, Italy

CONTENTS

9.1 INTRODUCTION

Transition metal complexes containing an "intact" dihydrogen ligand (η^2-H_2, 3 centre bonding at one metal coordination site) constitute an ubiquitous class of transition metal compounds. Since the description of $[W(\eta^2\text{-}H_2)(CO)_3(PCy_3)_2]$ by Kubas et al. in 1984 [1], more than 400 η^2-H_2 metal complexes have been prepared and characterized [2-11]. This number is destined to increase considerably as new members of the family are being discovered at an impressive rate, especially due

to the application of innovative synthetic and spectroscopic techniques allowing for the interception and identification of compounds with a fleeting existence (e. g. laser flash photolysis [12], *p*-hydrogen NMR [13], high-pressure NMR [14] and IR spectroscopy [15]).

In addition to oriented reactions, many η^2-H_2 metal complexes can be generated, as either stable species or elusive intermediates, in the course of both hydrogenation and dehydrogenation processes. Indeed, the η^2-H_2 ligand does not necessarily need the intervention of molecular hydrogen to be formed as it may also be obtained from a terminal hydride by treatment with various proton donors, including many solvents of common use in organometallic synthesis and homogeneous catalysis (e. g. alcohols) [16]. The formation of η^2-H_2 complexes in homogeneous processes is therefore a facile route and should always be considered in the mechanistic elaboration of any reaction involving either H_2 and a metal complex or a metal-hydride and a Brønsted acid.

The physical and chemical properties of η^2-H_2 metal complexes have been amply reviewed over the last ten years [2-9]. Reviews on homogeneous hydrogenation reactions catalysed by η^2-H_2 precursors or involving η^2-H_2 intermediates have also appeared [17-18], while biocatalytic cycles involving dihydrogen metal complexes are covered by a specific monograph in this book [19]. Hence, it is not the aim of this article to provide a comprehensive account of the chemistry of η^2-H_2 metal complexes. We have exclusively focussed our attention on some recent or intriguing homogeneous and heterogeneous reactions that "see" the participation of an η^2-H_2 metal complex as either catalyst precursor or catalytic intermediate. Another catalytically relevant issue of η^2-H_2 metal complexes is their acidity [20-23]. This aspect too is not specifically covered here as a detailed account of the factors that control the acidity of the dihydrogen ligand, hence its heterolytic splitting, is provided by Morris in this book [24].

9.1.1 Roles of η^2-H_2 metal complexes in catalysis

Recognized roles of η^2-H_2 ligands in homogeneously metal-catalysed reactions are: i) creation of free coordination sites for incoming substrates *via* either H_2 decoordination or entrapment of a ligand by intramolecular protonation; ii) capability to transfer a proton to either a substrate or a proximal nucleophilic centre leaving a hydride ligand on the metal (heterolytic splitting). When H_2 behaves exclusively as a weakly bound ligand, it can generally be replaced in the parent metal complex by other weak ligands (N_2, solvent molecules, etc) with no change in the chemical reactivity. There are some cases, however, in which H_2 serves to create a free coordination site, but its presence is of mandatory importance for the stabilization of catalytic precursors and/or intermediates. These cases are much more numerous than it is generally realized and will specifically be considered here.

9.2 HYDROGENATION OF C=C AND C≡C BONDS IN EITHER HOMOGENEOUS OR HETEROGENEOUS PHASE SYSTEMS

9.2.1 Homogeneous reactions

Homogeneous hydrogenation reactions of alkenes and alkynes involving η^2-H_2 metal complexes as either catalyst precursors or intermediates are relatively numerous [17]. In most instances, the dihydrogen ligand is easily displaced by the incoming unsaturated substrate, which then inserts into a pre-existing M-H bond to give either M-alkyl or M-alkenyl. By doing so, a new free coordination site is generated for the activation of further H_2 that ultimately brings about the hydrogenolysis of the M-C bond yielding either alkane or alkene and M-H. In non-selective alkyne hydrogenations, the alkene is successively reduced to alkane by the same mechanism. The activation of H_2 at the coordinatively unsaturated M-σ-organyl complex may proceed by either oxidative addition or η^2 coordination. In the latter case, the following M-C hydrogenolysis step involves the heterolytic splitting of the coordinated H_2 (*vide infra*).

A catalytic cycle for the hydrogenation of a generic alkyne is illustrated in Scheme 1.

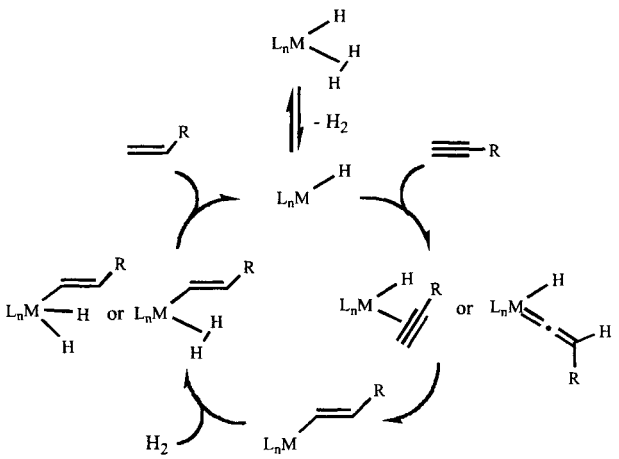

Scheme 1

A real example following the H_2-decoordination mechanism is provided by the selective hydrogenation of 1-alkynes to alkenes with the ruthenium(II) complex $[(PP_3)RuH(\eta^2\text{-}H_2)]BPh_4$ [PP_3 = $P(CH_2CH_2PPh_2)_3$] [25]. A kinetic study of the hydrogenation of phenylacetylene at ambient or sub-ambient pressure showed that the reaction is first-order in catalyst concentration, second order in H_2 pressure and independent of substrate concentration. At very low 1-alkyne concentration (< 0.12 M), a first order dependence with respect to the substrate was observed,

while the hydrogenation rate was found to decrease with the H_2 pressure due to the stabilization of the η^2-H_2 catalyst precursor.

The selective hydrogenation of 1-alkynes to alkenes has also been achieved with the iron(II) precursor $[(PP_3)FeH(\eta^2\text{-}H_2)]BPh_4$ [26], which differs from $[(PP_3)RuH(\eta^2\text{-}H_2)]BPh_4$ only for the strength of the Ru-H_2 bond [27-28]. Indeed, the dihydrogen ligand in the Fe complex is much more strongly bound than in the Ru analogue, which leads to completely different kinetics and mechanism for the hydrogenation of 1-alkynes. The rate of reduction of phenylacetylene to styrene was actually found to be first order in both catalyst and substrate concentration whereas a zero order dependence was observed with respect to the H_2 pressure [26]. Based on the kinetic study as well as various independent reactions and spectroscopic experiments, a mechanism was proposed in which the dihydrogen ligand remains coordinated to the metal centre during the migratory insertion of the alkyne into the Fe-H bond, and the following Fe-alkenyl bond cleavage occurs *via* intramolecular protonolysis (heterolytic splitting of the H_2 ligand) (Scheme 2).

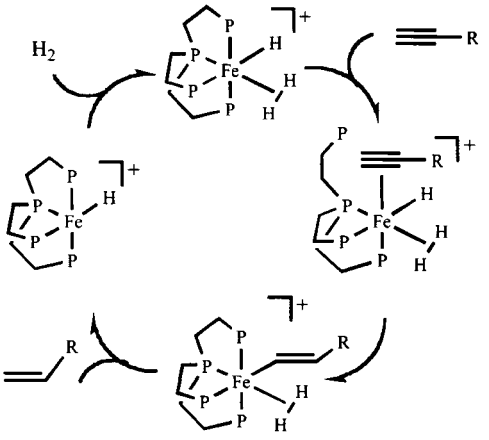

Scheme 2

The intramolecular heterolytic splitting mechanism shown in Scheme 2 has also been proposed by Lau, Jia and co-workers to account for the hydrogenation of styrene with the η^2-H_2 complexes $[Ru\{HB(pz)_3\}(PPh_3)_2(H_2)]BF_4$ and $[Ru\{HB(pz)_3\}(PPh_3)(CH_3CN)(H_2)]BF_4$ that, unlike most η^2-H_2 precursors [17], do not contain classical M-H bonds [$HB(pz)_3$ = hydridotris(1-pyrazolyl)borate] [29]. In these high-pressure hydrogenations (40 bar H_2), the alkene has been suggested to displace either triphenylphosphine or acetonitrile before being converted to σ-alkyl *via* a concerted five-membered transition state (**A**) (Scheme 3).

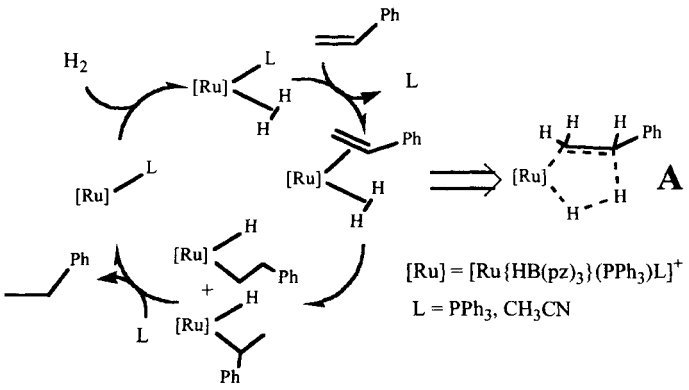

Scheme 3

Recent reports highlight a number of intriguing roles for the H_2 ligand in catalytic hydrogenation reactions that are not considered in the mechanisms shown in Schemes 1-3.

Creation of a free coordination site by intramolecular heterolytic splitting of a dihydrogen ligand has been reported by Yi and coworkers to occur in the hydrogenation of alkenes catalysed by $[RuH(CO)Cl(PCy_3)_2]/HBF_4.OEt_2$ [30]. As shown in Scheme 4, the dihydrogen ligand protonates a tricylclohexylphosphine leading to the formation of the 14e- species $[RuH(CO)Cl(PCy_3)]$ that has been suggested to be the effective hydrogenation catalyst.

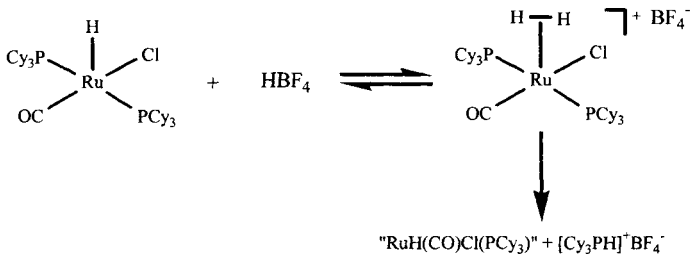

Scheme 4

A 16e- η^2-H_2 complex has also been suggested to play a relevant role in the hydrogenation of alkenes catalysed by 14e- rhodium(I) precursors with bulky β-diiminate ligands [31]. On the basis of both theoretical and experimental evidence, it has been postulated that the formation of the 16e- η^2-H_2 adduct precedes the oxidative addition yielding the dihydride complex. A crucial role of dihydrogen ligands in stabilizing unstable metal intermediates as well as in controlling kinetic access to isomeric reaction pathways has been reported by some authors. For the mechanism of H_2 oxidative addition at iridium, Crabtree

has proposed that the observed stereochemical isomer distributions correlate with the stabilities of five-coordinate η^2-H_2 complexes [32]. More recently, a theoretical work by Landis and co-workers on the enantioselective hydrogenation of enamides using the model compound $[Rh(PH_3)_2(\alpha\text{-acetoamidoacrylonitrile})]^+$ has confirmed the potential role of the H_2 ligand in discriminating the kinetics of different reaction paths. In particular, DFT calculations have indicated that a Rh(I) η^2-H_2 complex is formed before oxidative addition and that "the stereochemical isomer distribution correlates with the stabilities of five-coordinate molecular H_2 complexes" [33].

The hydrogenation of norbornadiene (NBD) ligand in $MH(OTf)(NBD)(PPh_3)_2$ (M = Ru, Os OTf = triflate) has been proposed by Lau and Jia to proceed with the intermediacy of $[MH(H_2)(NBD)(PPh_3)_2]^+$ [34]. DFT calculations on the reaction paths leading to the conversion of $[RuH(H_2)(NBD)(PH_3)_2]^+$ to $[RuH(H_2)(NBE)(PH_3)_2]^+$ (NBE = norbornene), indicate that path **a** in which the first hydrogen transfer is from the hydride ligand is favoured over path **b** in which the first transfer is from the dihydrogen ligand (Scheme 5).

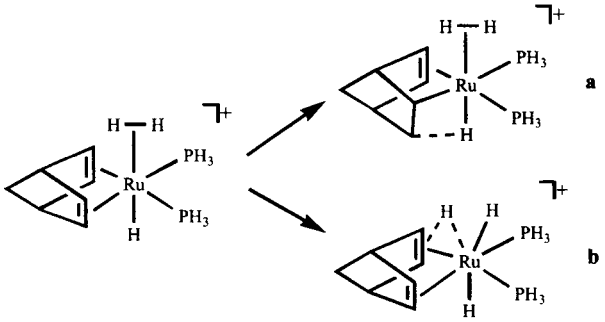

Scheme 5

Binuclear complexes containing at least one H_2 ligand have often been employed to catalyse the hydrogenation of alkenes and alkynes [17]. In most instances, the de-oligomerisation of the precursor occurs in catalytic conditions leading to mononuclear catalysts. In at least two cases, however, the maintenance of the dimeric structure all over the hydrogenation reaction was supported by experimental evidence. The first well-documented example has been described by Joshi and James for the hydrogenation of styrene with $[(\eta^2\text{-}H_2)(dppb)Ru(\mu\text{-}Cl)_3RuCl(dppb)]$ [dppb = bis-1,4-(diphenylphosphino)butane] [35-37]. A kinetic study in N,N-dimethylacetamide (DMA) is consistent with a catalytic mechanism involving a basic hydride route (Scheme 6); the hydrogen transfer was proposed to proceed in two steps *via* a μ-Cl_2 intermediate.

A dimeric η^2-H_2 metal complex has also been proposed as intermediate species in the selective hydrogenation of diphenylacetylene to *cis*-stilbene catalysed by the diiridium compound $[Ir_2(\mu\text{-}H)(\mu\text{-}Pz)_2H_3(NCCH_3)(P\textit{i}\text{-}Pr_3)_2]$ [38-40]. As shown

in Scheme 7, the dihydrogen ligand acts as a reservoir of hydrogen atoms that are delivered to the catalytically active iridium centre through a hydride bridge.

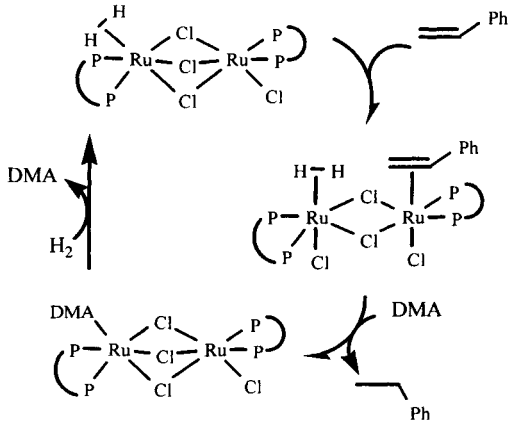

Scheme 6

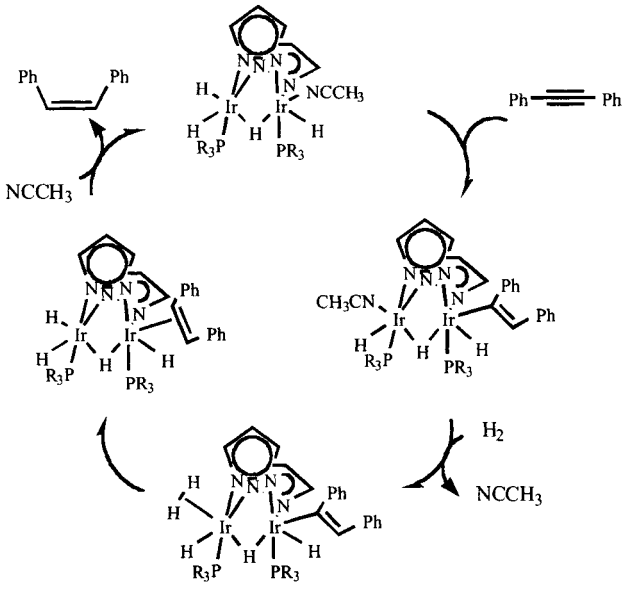

Scheme 7

Homogeneous modelling studies applying soluble metal complexes are emerging as a powerful tool to elucidate the mechanism of H_2 activation over single metal sites capable of hydrogenating S- and N-heterocycles contained in

petroleum [41-42]. Heteroaromatic substrates like thiophenes, quinolines, and indoles are removed from fossil fuels by catalytic hydrodesulphurization (HDS) and hydrodenitrogenation (HDN) over supported Mo-Ni and Mo-Co sulphides [43]. The modes of activation of H_2 over these catalysts are the object of much current research as they are related to the nature of the metal site and therefore to the HDS and HDN mechanisms [43]. It is worthwhile to report here that η^2-H_2 metal complexes have been found to play a role in some catalytic hydrogenation reactions of S- and N-heteroaromatics.

The reduction of various S- and N-heterocycles to give the corresponding cyclic thioethers and amines has been achieved by Chaudret and co-workers with the catalyst precursor $[RuH_2(H_2)_2(PCy_3)_2]$ [44]. In particular, the regioselective hydrogenation of the C_2-C_3 double bond in thiophene, benzo[*b*]thiophene, indole, quinoline and isoquinoline has been obtained in condensed arenes (naphthalene, anthracene) under very mild reaction conditions (80 °C, 3 bar H_2). In contrast, dibenzo[*b,d*]thiophene, pyridine and pyrrole were not reduced in the presence of $[RuH_2(H_2)_2(PCy_3)_2]$ which exclusively underwent the displacement of one H_2 ligand by the heterocycle to form η^1-heteroatom adducts.

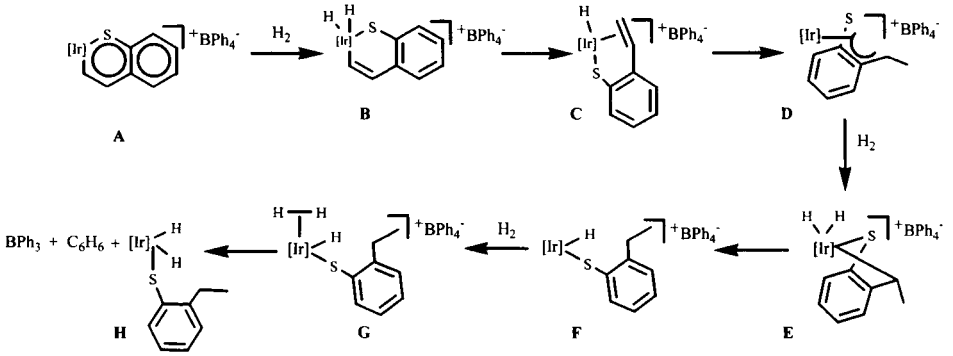

Scheme 8

An η^2-H_2 complex has also been detected along the pathway of hydrogenation of C-S inserted benzo[*b*]thiophene to ethylthiophenol with the [(triphos)Ir] fragment [triphos = $MeC(CH_2PPh_2)_3$] [45]. As is shown in Scheme 8, of the 3 molecules of H_2 which are necessary to convert the iridabenzothiabenzene complex [(triphos)Ir(η^2-*C,S*-C_8H_6S)]BPh_4 (**A**) into the (2-ethylthiolate)dihydride [(triphos)Ir(H)$_2${*o*-S-(C_6H_4)C_2H_5}] (**H**), the first two are cleaved homolytically, while the third molecule forms an η^2-H_2 adduct which is so acidic to decompose the tetraphenylborate counter-anion to BPh_3 and benzene [46]. On the other hand, DFT calculations have suggested that adsorbed molecular hydrogen is most likely involved in the hydrogenation of thiophenic substrates by Ni_xS_y clusters (x = 3,

4) [47]. According to the theoretical analysis, intact H_2 adsorbed on the nickel centres of the metallo-sulphido cluster can readily undergo a heterolityc activation yielding both MSH and MH species.

9.2.2 Heterogeneous reactions

The reduction of unsaturated C-C bonds constitutes one of the largest applications of heterogeneous catalysis [48]. On the surface of a metal particle, hydrogen is either cleaved homolytically to give M-H units or is adsorbed in the intact form. The metal sites that are responsible for either activation path of H_2 on the catalyst surface as well as the chemical-physical characteristics of the adsorbed H_2 are still a matter of debate. In this respect, molecular systems mimicking the activation of H_2 on a single metal site without the cooperation of a solvent are expected to provide valuable information on the mechanism of H_2 adsorption/release over heterogeneous metal catalysts.

Evidence of η^2-H_2 metal adducts in solvent-free systems was primarily obtained by phototolysis of $Cr(CO)_6$ in hydrogen-containing matrices [49], while the formation of both η^2- and η^1-H_2 $Pd(H_2)$ moieties was proposed to occur in the reaction of $4d^{10}$ Pd atoms with H_2 in rare gas matrices [50].

Several Pt-Au clusters stabilized by phosphine ligands have been shown to catalyse the H_2-D_2 equilibration ($H_2 + D_2 \rightleftharpoons 2\ HD$) in heterogeneous conditions with turn-over rates for HD production comparable to those of activated Pt surfaces [51].

Some examples of heterogeneous hydrogenation of alkenes catalysed by η^2-H_2 complexes in either solid-gas or solid-liquid systems have been reported. The first of such reactions regards the hydrogenation of ethylene catalysed by crystals of the iridium(III) complex $[(triphos)Ir(H)_2(C_2H_4)]BPh_4$ in a tubular flow reactor [52].

In the temperature range from 60 to 70 °C under 1 bar H_2, ethylene (1 bar) was selectively and steadily hydrogenated to ethane, whereas at higher temperature slow deactivation of the catalyst occurred due to the formation of the inactive dimer $[(triphos)IrH(\mu\text{-}H_2)HIr(triphos)]^{2+}$. On the basis of kinetic studies and the isolation of some intermediate species, a mechanism was proposed in which the (ethylene)dihydride precursor **A** thermally rearranges to the unsaturated (ethyl)hydride complex **B** and then reacts with H_2 to give either a classical iridium(V) trihydride **C** or an η^2-H_2 complex **D** (Scheme 9). Following the reductive elimination of ethane and the addition of another H_2 molecule, the tetrahydride $[(triphos)Ir(H_2)(\eta^2\text{-}H_2)]^+$ (**E**) is formed, which regenerates the precursor **A** by displacement of H_2 by ethylene. A concomitant catalytic cycle involves the reaction of intermediate **B** with ethylene to give an (ethyl)(ethylene)hydride complex (**F**), which eliminates ethane to give the unsaturated ethylene complex **G** and then closes the cycle by picking up further ethylene. The rate inhibiting effect

observed at C_2H_4 pressure higher than 1 bar was just attributed to the stabilization of the bis(ethylene) complex **H** [53].

Unambiguous characterization of intermediate **E** as a highly fluxional, nonclassical tetrahydride was obtained by high-pressure NMR spectroscopy and by low temperature ^1H and ^2H NMR relaxation experiments in CD_2Cl_2 [46, 54]. A rather short ^1H T_1 value of 13 ms (163 K, 300 MHz) for **E**, a rather long ^2H T_1 value of 32.6 Hz (190 K, 76.753 MHz) for the perdeuterated isotopomer [(triphos)Ir(D_2)(η^2-D_2)]$^+$, and a J(HD) constant of 26-29 Hz for partially deuterated isotopomers were all consistent with a nonclassical structure.

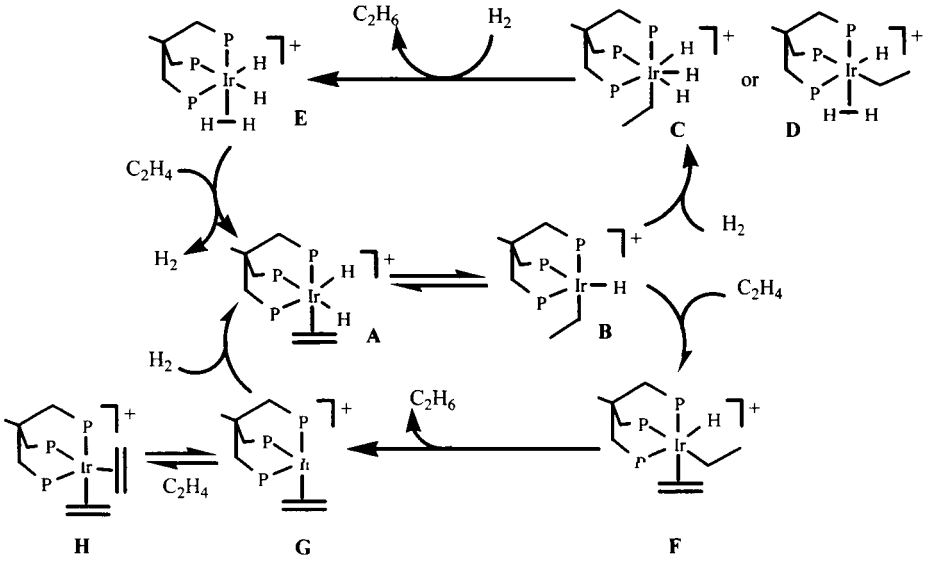

Scheme 9

Interestingly, when the C_2H_4/H_2 feed through the flow reactor was temporarily interrupted and replaced by N_2, the catalyst underwent irreversible deactivation due to the formation of the catalytically inactive dimer [(triphos)IrH(μ-H_2)HIr(triphos)]$^{2+}$ [52]. In the solid-gas hydrogenation of ethylene by [(triphos)Ir(H)$_2$(C_2H_4)]BPh_4, H_2 is therefore of mandatory importance for the stabilization of the catalytically active species.

It is worth mentioning that [(triphos)Ir(H_2)(η^2-H_2)]$^+$ contains a very acidic H_2 ligand, which is capable of decomposing the tetraphenylborate counter-anion to BPh_3 and benzene when dissolved in a polar solvent like THF [46].

The formation of an η^2-H_2 complex has also been proposed to occur in the solid-liquid hydrogenation of alkenes with the supported hydrogen-bonded (SHB) catalyst [(sulphos)Rh(cod)]/SiO_2 (sulphos = $^-O_3S(C_6H_4)CH_2C(CH_2PPh_2)_3$; cod = cyclo-octa-1,5-diene) (Scheme 10) [55-56].

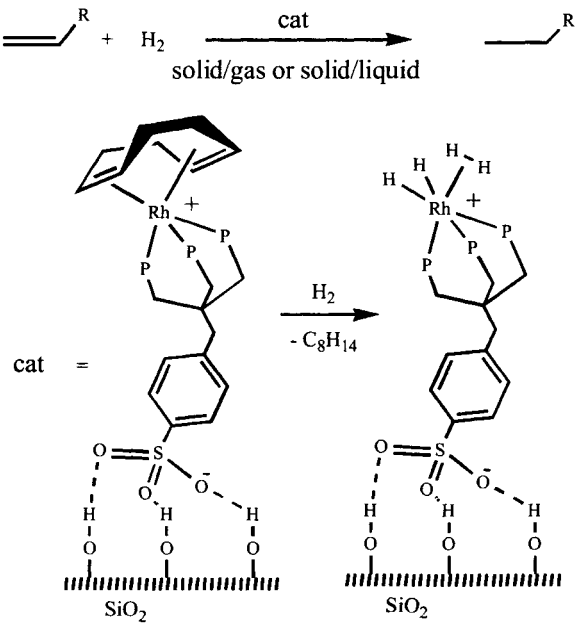

Scheme 10

The silica-grafted Rh precursor was found to be active for the hydrogenation of alkenes in either flow reactors (ethylene, propene) or batch reactors (styrene) in hydrocarbon solvents. EXAFS experiments on the terminal metal product after reaction of [(sulphos)Rh(cod)]/SiO_2 with H_2 or C_2H_4/H_2 showed the disappearance of COD and the formation of Rh polyhydride and Rh-ethyl(ethylene) species, respectively. A low-temperature NMR analysis of the Rh complex freed from the silica surface by means of MeOH-d_4 showed the formation of an η^2-H_2 species. This was unambiguously authenticated through an in-depth NMR study of the more stable triphos analogue $[(triphos)Rh(H)_2(\eta^2\text{-}H_2)]^+$, obtained by protonation of the classical trihydride $[(triphos)RhH_3]$ at low temperature [54]. The rhodium(III) tetrahydride contains a fast-spinning H_2 ligand featured by a T_{1min} of 38.9 ms (CD_2Cl_2, 220 K, 400 MHz and by a T_{1min} value of 32.6 ms for the D_2 ligand in the perdeuterated isotopomer $[(triphos)Rh(D)_2(\eta^2\text{-}D_2)]^+$, which corresponds to a two-fold elongation as compared to the classical trideuteride $[(triphos)RhD_3]$ (16.5 ms at 76.75 MHz) [54].

The potential of $M(\eta^2\text{-}H_2)$ moieties in the heterogeneous hydrogenation of aromatics has been demonstrated for $[RuH_2(H_2)_2(PCy_3)_2]$, which, in temperature-programmed decomposition under hydrogen, has been found to convert benzene into cyclohexane [57].

9.3 REDUCTION OF KETONES, β-DIKETONES AND α,β-UNSATURATED KETONES

The reduction of ketones to alcohols catalysed by metal precursors containing dihydrogen ligands has been reported to occur in either hydrogenation and hydrogen-transfer conditions [17, 18, 58]. A great variety of ketonic substrates have successfully and selectively been reduced, including aliphatic, aromatic and cyclic ketones, β-diketones and α,β-unsaturated ketones. In all known cases, the η^2-H_2 ligand is displaced by the ketone, which may also form an isolable η^1-*O*-ketone adduct [59].

In hydrogenation conditions, a residual hydride ligand migrates to the C=O carbon atom forming a metal-alkoxy which undergoes M-O hydrogenolysis to give the alcohol and re-generate the metal-hydride (Scheme 11**A**). The hydrogen transfer mechanism (e.g. using 2-propanol as hydrogen donor) is quite similar, the main difference being that the metal hydride is re-generated by β-H elimination involving the conjugate base of the hydrogen donor (Scheme 11**B**).

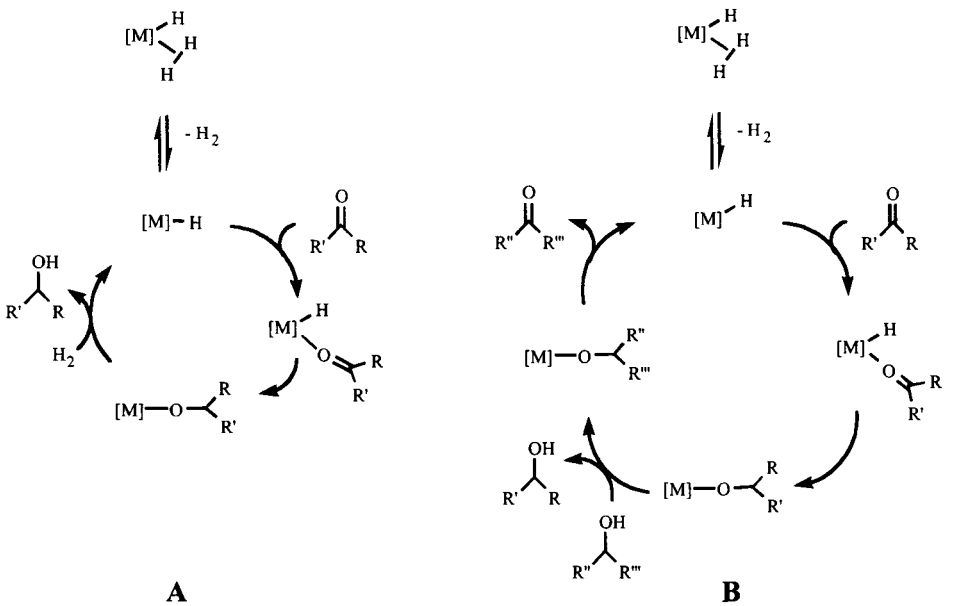

Scheme 11

In most catalytic hydrogenation reactions of the keto functional group by rhodium and iridium complexes, H_2 is cleaved homolytically by the metal which then assists the reductive elimination of the alcohol. In contrast, ruthenium catalysts generally reduce ketones to alcohols with ionic mechanisms involving the heterolytic splitting of H_2 [60] (Scheme 12). Obviously this is only a general

classification as other metals can promote the reduction of ketones via an ionic mechanism and even for rhodium there are cases that are difficult to assess [61]. For example the very acidic h^2-H_2 complex $[ReH(H_2)(CO)(NO)(PR_3)_2](CF_3COO)$ (R = O^{i}Pr) (pKa = -1.8 in CD_2Cl_2) has been shown to reduce benzaldehyde or acetone with the intermediacy of an alcohol complex [62]. As a general trend, it may be said here that the propensity of the dihydrogen ligand to heterolysis depends on several factors, which include the nature of the ancillary ligands in the catalyst precursor and the presence of additives in the reaction mixture [20-23, 61].

An interesting example of heterolytic activation of a dihydrogen ligand at a metal-heteroatom bond has been described by Morris and co-workers who have been able to hydrogenate chemo- and stereoselectively ketones, α,β-unsaturated ketones and imines with the ruthenium(II) precursor $[RuH_2(PPh_3)_2(R,R\text{-cydn})]$ (cydn = cyclohexyldiamine) [63]. In the proposed catalytic mechanism (Scheme 13), the reduction of the substrate occurs *via* a concerted transfer of a hydride from the metal to the carbonyl carbon atom and of a proton from an amino group to the oxygen, while the heterolytic splitting of H_2 occurs on a metal-nitrogen bond. The formation of an equilibrium concentration of an η^2-H_2 intermediate (**D**) under catalytic conditions was inferred from the occurrence of rapid H/D exchange for both the hydrides and NH moieties of **A** when this precursor was exposed to D_2 gas.

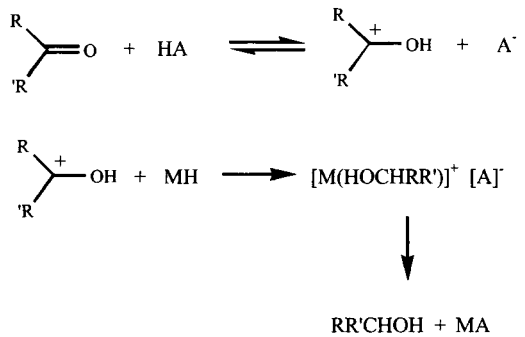

Scheme 12

A mechanism involving heterolytic splitting of H_2 by an amido ligand is most likely at work also in the hydrogenation reactions of prochiral ketones reported by Noyori et al. in which 2-propanol is used as hydrogen donor in the presence of a variety of Ru(II) catalysts with chiral diphosphines and 1,2-diamine ligands [64-65]. On the other hand, the heterolytic splitting of H_2 on a Pd-O bond has been suggested by Brothers to occur in the hydrogenation of alkenes catalysed by Pd salen complexes [66].

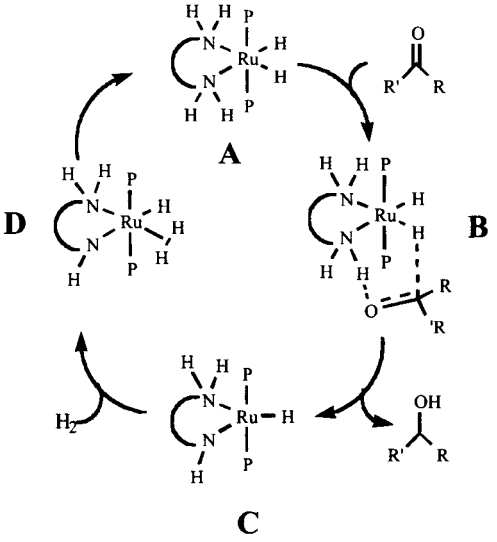

Scheme 13

The enantioselective hydrogenation of acetylacetone to (*S*)-(*S*)-2,4-pentanediol with $[RuCl_2(PPh_3)\{(S)\text{-biphemp}\}]/NEt_3$ has been proposed by Mezzetti and co-workers to involve an ionic mechanism in which the metal centre and a C=O group in the substrate cooperate to heterolytically cleave H_2 (biphemp = 2,2'-bis(diphenylphosphino)-6,6'-dimethylbiphenyl) [67]. In particular, the double stereodifferentiation process leading to the diastereo- and enantioselective production of (*S*)-(*S*)-2,4-pentanediol was explained by taking into account the transfer of a proton to a ketonic oxygen, followed by hydride migration to the carbon atom. This catalytic mechanism is illustrated in Scheme 14 for the production of (*S*)-4-hydroxypentan-2-one.

The η^2-H_2 dinuclear complex $[\{(S)\text{-biphemp}\}ClRu(\mu\text{-}Cl)_3Ru(\eta^2\text{-}H_2)\{(S)\text{-biphemp}\}]$ was spectroscopically detected in an independent study of the hydrogenation of the catalyst precursor $[RuCl_2(PPh_3)\{(S)\text{-biphemp}\}]$. However, any role of this dihydrogen complex in the catalytic hydrogenation reaction was ruled out on the basis of the observation that the hydrogenation rate drops at high H_2 pressures at which the dihydrogen complex predominates [67].

Unlike the reaction catalysed by $[RuCl_2(PPh_3)\{(S)\text{-biphemp}\}]$, a dimeric η^2-H_2 complex has been reported to play a direct role in the enantioselective conversion of acetylacetone to (*R*)-(*R*)-2,4-pentanediol with the catalyst precursor [(BDPzP)(DMSO)Ru(μ-Cl)$_3$RuCl(BDPBzP)] (BDPBzP = (*R*)-(*R*)-3-benzyl-2,4-bis(diphenylphosphino)pentane) (MeOH, 50 bar H_2, 50 °C) [68]. The binuclear complex $[(BDPzP)Cl(\eta^2\text{-}H_2)Ru(\mu\text{-}H)_2Ru(\eta^2\text{-}H_2)(BDPBzP)]$ was actually detected by high-pressure NMR spectroscopy as the only ruthenium compound in the course of the catalytic reaction yielding (*R*)-(*R*)-2,4-pentanediol (Scheme 15).

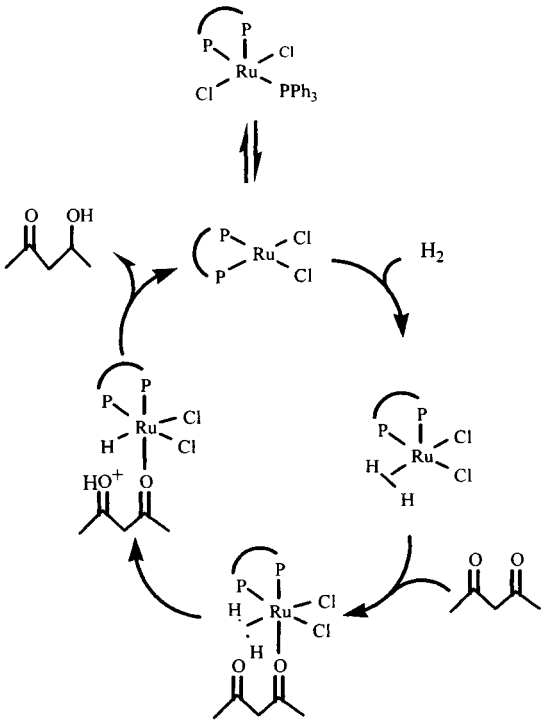

Scheme 14

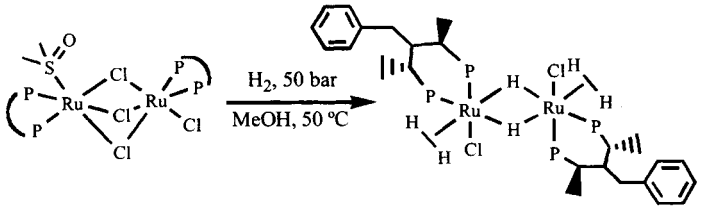

Scheme 15

The quantitative and selective transformation of the precursor into the dinuclear η^2-H_2 complex in catalytic conditions, the different catalytic performance of the mononuclear derivative [(BDPBzP)Ru($CH_3CN)_3$]OTf (lower activity and enantioselectivity), the identical catalytic performance of the precursor and of the η^2-H_2 complex, and the recognized capability of the structurally related Ru(II) complex [(η^2-H_2)(dppb)Ru(μ-Cl)$_3$RuCl(dppb)] to maintain the dimeric structure in olefin hydrogenation reactions [35-37] were taken as proofs for the direct involvement of [(BDPzP)(DMSO)Ru(μ-Cl)$_3$Ru(η^2-H_2)(BDPBzP)] in the enantioselective hydrogenation of acetylacetone [68].

9.4 HYDROGENATION OF CARBON DIOXIDE TO FORMIC ACID AND DECOMPOSITION OF FORMIC ACID TO DIHYDROGEN AND CARBON DIOXIDE

The catalytic hydrogenation of CO_2 to formic acid by transition-metal complexes [69-72] and its reverse reaction, *i. e.* the decomposition of formic acid to H_2 and CO_2 [73], are processes of considerable interest for hydrogen storage as well as the development of efficient and clean hydrogen-transfer reductions. The involvement of nonclassical polyhydrides in such processes dates back to 1991 when the iron trihydride, $[(PP_3)FeH(H_2)]BPh_4$ was prepared by treating a mixture of PP_3 and $[Fe(H_2O)_6](BF_4)_2$ with an excess of formic acid under argon in tetrahydrofuran (Scheme 16) [74]. A mechanistic investigation showed the intermediacy of the η^2-formate complex $[(PP_3)Fe(O_2CH)]BPh_4$ which was isolated at room temperature under a protective CO_2 atmosphere. In the absence of CO_2, the formate complex rapidly decomposes to give the unsaturated hydride $[(PP_3)FeH]BPh_4$ and CO_2. Reaction with further formic acid restores the formate complex releasing H_2. After some dehydrogenation cycles of the acid at room temperature, the H_2 accumulated in the reaction mixture traps the transient iron monohydride to give the stable complex $[(PP_3)FeH(H_2)]BPh_4$. At reflux temperature in tetrahydrofuran, the η^2-H_2 complex reacts with formic acid producing H_2 catalytically according to the cycle shown in Scheme 16.

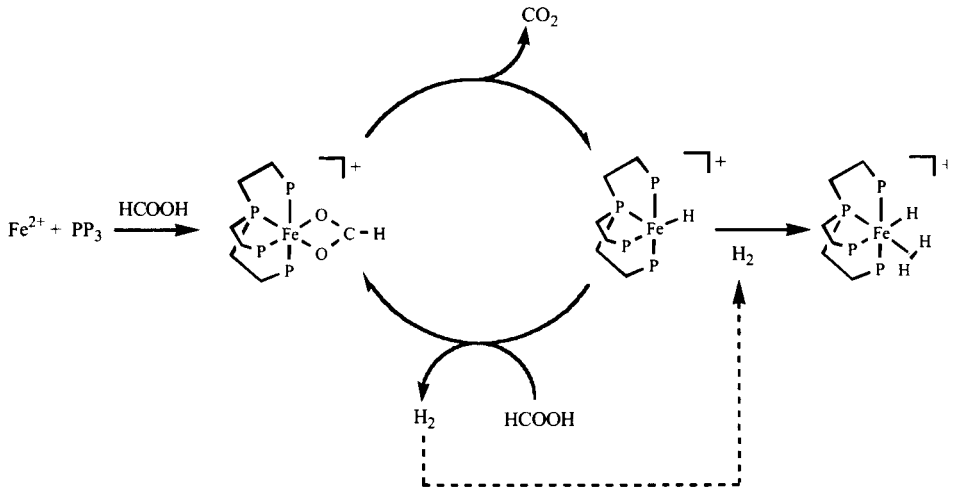

Scheme 16

The catalytic decomposition of HCOOH by $[(PP_3)FeH(H_2)]BPh_4$ and by the ruthenium derivative $[(PP_3)RuH(H_2)]BPh_4$ has successfully been exploited to hydrogenate 1-alkynes to alkenes using either catalyst precursor [74, 75].

The capability of molecular hydrogen complexes to hydrogenate catalytically CO_2 to formic acid has been demonstrated by Lau and co-workers for the reaction of $[\{\eta^5{:}\eta^1\text{-}C_5H_4(CH_2)_nNMe_2\}Ru(dppm)]BF_4$ (n = 2, 3) with H_2/CO_2 mixtures [dppm = 1,2-bis(diphenylphosphino)methane] [76]. Heating THF solutions of these ruthenium complexes under a 1:1 mixture of H_2/CO_2 (40 bar/40 bar) at 80 °C produced formic acid, although in low yields (highest turnover frequency 8). Monitoring the reaction by *in situ* $^{31}P\{^1H\}$ HPNMR spectroscopy showed that key species in the hydrogenation processes are the monohydrido complexes $[\{\eta^5\text{-}C_5H_4(CH_2)_nNMe_2H\}RuH(dppm)]^+$ (n = 2, 3) in which a pendant protonated amine group, formed upon base-assisted heterolytic splitting of H_2, interacts intramolecularly with the ruthenium hydride via an N-H···H-Ru hydrogen bond (Scheme 17) [77].

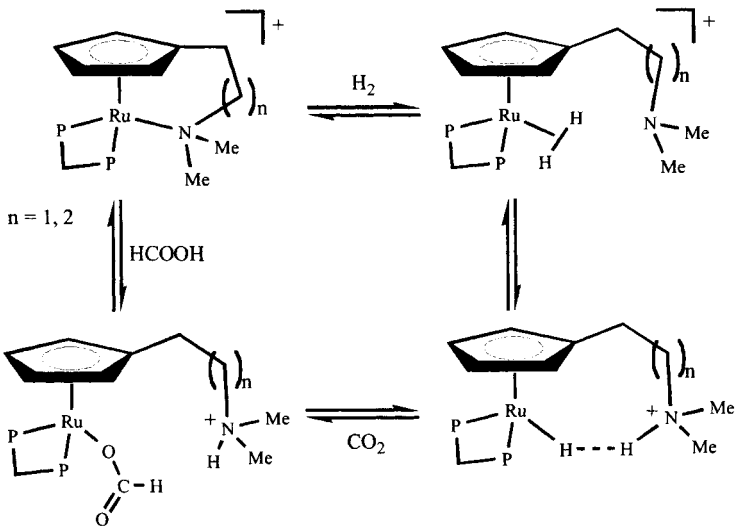

Scheme 17

The reaction of $[\{\eta^5{:}\eta^1\text{-}C_5H_4(CH_2)_nNMe_2\}Ru(dppm)]BF_4$ with formic acid yields free CO_2 and the hydrogen-bonded hydride complex. An intermediate formate complex was proposed to form during this process but it was not detected by NMR spectroscopy. However, $[\{\eta^5{:}\eta^1\text{-}C_5H_4(CH_2)_nNMe_2\}Ru(dppm)]BF_4$ was found to react with HCOONa to give $[\{(\eta^5\text{-}C_5H_4(CH_2)_nNMe_2\}RuH(dppm)]$ (n = 2, 3), while the use of CS_2 in the place of CO_2 allowed the isolation of a stable dithioformate complex [76].

9.5 HYDROGENOLYSIS OF SI-O BONDS IN SILYL ENOL ETHERS

The η^2-H_2 complex $[RuCl(H_2)(dppe)_2]OTf$, prepared by reaction of $[RuCl(dppe)_2]OTf$ with H_2, was found by Hidai to be an active catalyst for the hydrogenolysis of trimethylsilyl enol ethers (Scheme 18) [78]. A mechanistic clue on this reaction was obtained from the observation that the related complex $[RuH(H_2)(dppe)_2]OTf$ (pK_a =15.0) [79], which is less acidic than $[RuCl(H_2)(dppe)_2]OTf$ (pK_a 6.0) [80], does not catalyse the hydrogenolysis reaction. This finding suggested that the acidic η^2-H_2 ligand protonates the oxygen atom of the enol ether while the remaining hydride at ruthenium is scavenged by the trimethylsilyl group as $SiMe_3H$. In keeping with this hypothesis, when the reaction was carried out under D_2, the incorporation of deuterium (D% *ca.* 95%) occurred selectively in α-position (Scheme 18).

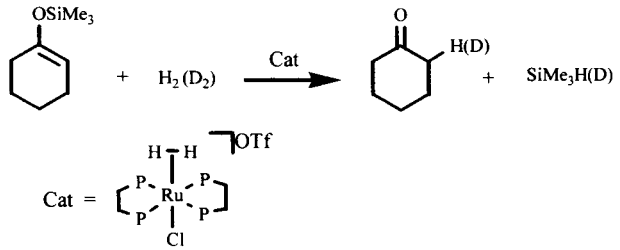

Scheme 18

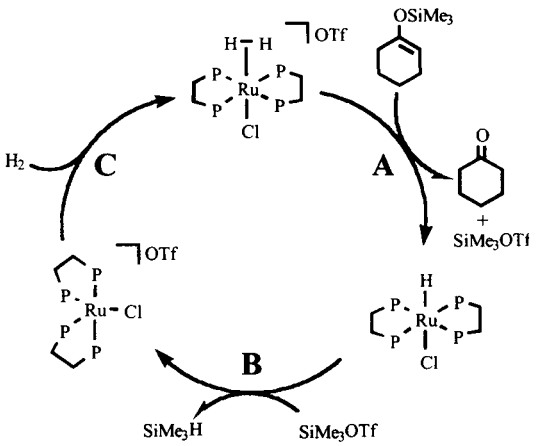

Scheme 19

In the proposed mechanism (Scheme 19), the highly acidic H_2 ligand protonates the enol ether at the oxygen atom yielding, after tautomerisation of the intermediate enol, the final ketone and $SiMe_3OTf$ (**A**). Once formed, the silyl triflate reacts with the residual hydride ligand of $[RuCl(H)(dppe)_2]$ yielding the silane and the

coordinatively unsaturated complex $[RuCl(dppe)_2]OTf$ (**B**), which regenerates the η^2-H_2 complex (**C**). Model reactions on isolated intermediates proved the occurrence of steps **B** and **C**. Under similar reaction conditions, conventional hydrogenation catalysts, like the Wilkinson complex, did not promote the hydrogenolysis reaction, and exclusively gave the saturated trimethylsilyl ethers via hydrogenation of the C-C double bond [78].

9.6 HYDROSILYLATION OF ALKYNES AND DEHYDROGENATIVE SILYLATION OF ALKENES

The intermediacy of the η^2-H_2 complex $[Os(SiEt_3)Cl(H_2)(CO)(P^iPr_3)_2]$ in the catalytic hydrosilylation of phenylacetylene was first observed by Oro and co-workers when the neutral hydride $[OsHCl(CO)(P^iPr_3)_2]$ was reacted with triethylsilane and the alkyne [81]. A theoretical study of silane addition across the C-C triple bond has also been reported [82] and the general scope of this reaction has been amply reviewed [17].

The hydrosilylation of ethylene by $[RuH_2(H_2)_2(PCy_3)_2]$ was studied by Sabo-Etienne and co-workers, who surprisingly discovered the occurrence of competitive dehydrogenative silylation of the alkene (Scheme 20), i. e. the reaction of ethylene and triethylsilane in the presence of the ruthenium catalyst gave preferentially vinylsilane CH_2=$CHSiEt_3$ [83]. In particular, depending on the reaction conditions, the vinylsilane may become the largely predominant product (up to 99%) [18, 83].

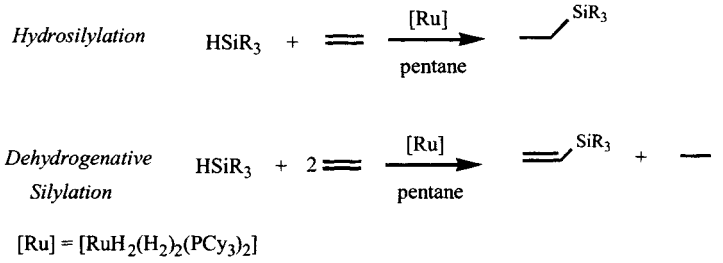

Scheme 20

Isolation of $[RuH(C_2H_4)\{(\eta^3\text{-}C_6H_8)PCy_2\}(PCy_3)]$ from the reaction with C_2H_4 and of the (silyl)dihydride Ru(IV) complex $[RuH_2(SiEt_3)\{(\eta^3\text{-}C_6H_8)PCy_2\}(PCy_3)]$ by treatment of the ethylene adduct with triethylsilane provided valuable mechanistic information to account for the dehydrogenative silylation of the alkene. In the proposed reaction mechanism, $[RuH_2(H_2)_2(PCy_3)_2]$ is the catalyst

precursor while the ethylene adduct behaves as the catalyst resting state [83]. A sketch illustrating these transformations is given in Scheme 21.

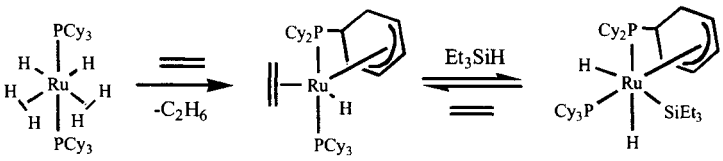

Scheme 21

9.7 CARBON-CARBON BOND FORMING REACTIONS

9.7.1 Alkylation of aromatic hydrocarbons via Murai-type reaction

Chaudret and co-workers have demonstrated that some ruthenium complexes containing dihydrogen ligands catalyse the Murai reaction [84], *i. e.* the coupling of monosubstituted alkenes to aromatic ketones at the *ortho* position (Scheme 22) [85-87]. In particular, $[RuH_2(H_2)_2(PCy_3)_2]$ was found to catalyse the insertion of ethylene into C-H bonds of acetophenone and benzophenone with high *ortho*-selectivity. In the benzophenone case, a mixture of mono- and double insertion products was obtained with high selectivity (96 %) in the bis-insertion derivative 2,2'-diethylbenzophenone (Scheme 23). Remarkably, the coupling reaction with the aromatic ketone catalysed by $[RuH_2(H_2)_2(PCy_3)_2]$ occurs at room temperature under 20 bar of C_2H_4, whereas the original Murai's catalyst $[RuH_2(CO)(PPh_3)_3]$ is active only in refluxing toluene [85-87].

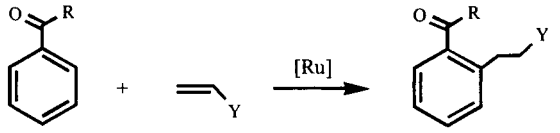

[Ru] = $[RuH_2(H_2)_2(PCy_3)_2]$

Scheme 22

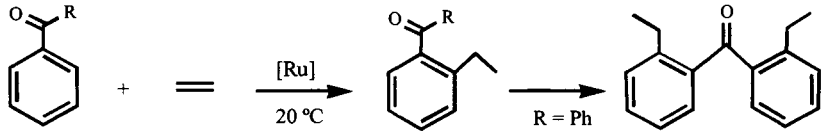

[Ru] = $[RuH_2(H_2)_2(PCy_3)_2]$ R = Me, Ph

Scheme 23

A similar catalytic activity in the Murai-type reaction was displayed by the trihydride $[RuH(H_2)(PCy_3)_2\{o\text{-}C_6H_4C(O)R)\}]$ (R = Me, Ph) prepared by treatment of $[RuH_2(H_2)_2(PCy_3)_2]$ with acetophenone or benzophenone (Scheme 24). The ability of the *o*-metalated complex to catalyse the coupling of ethylene to functional arenes provides experimental support to the generally accepted mechanism of the Murai reaction [88-89] where the origin of the high ortho-selectivity in the coupling product is ascribed to the coordination of the carbonyl oxygen of the aromatic ketone, followed by breakage of the proximal ortho C-H bond. The orthometalated species which was formed from this sequence has been proved to be the catalytic resting state [84].

The great potential of $[RuH_2(H_2)_2(PCy_3)_2]$ and of the related dimer $[\{(dcpp)RuH\}(\mu\text{-}H)_3\{(dcpp)Ru(H_2)\}]$ (dcpp = $Cy_2PCH_2CH_2CH_2PCy_2$) as catalyst precursors for Murai-type couplings involving a variety of aromatic ketones as well other activated arenes such as 2-α-styrylpyridine has also been shown by Busch and Leitner [90].

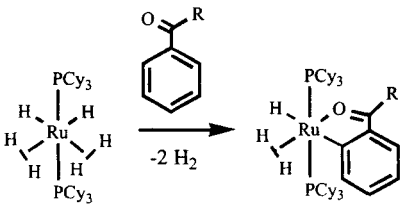

Scheme 24

9.7.2 Stereoselective dimerization of 1-alkynes to 1,4-disubstituted butenynes

In Section 9.2.1, it has been mentioned that the complex $[(PP_3)RuH(\eta^2\text{-}H_2)]BPh_4$ behaves as catalyst precursor for the selective hydrogenation of 1-alkynes to alkenes [25, 26]. When this ruthenium complex was treated with an excess of 1-alkyne *in the absence of* H_2, a catalytic reaction occurred to give (*Z*)-1,4-disubstituted butenynes via regio- and steroselective coupling of two 1-alkyne molecules [26, 91, 92]. Like the ruthenium complex, also the cognate osmium derivative $[(PP_3)OsH(\eta^2\text{-}H_2)]BPh_4$ is capable of promoting the head-to-tail coupling of terminal alkynes [92, 93]. The catalysis cycle for the Ru- or Os-assisted stereoselective dimerization of 1-alkynes to 1,4-disubstituted butenynes has been elucidated by *in situ* NMR spectroscopy combined with the isolation and characterization of important intermediates (Scheme 25).

In these C-C bond forming reactions, the molecular hydrogen precursors lose the H_2 ligand under mild conditions. As a consequence, a free coordination site is generated where the 1-alkyne tautomerises to vinylidene (**A**). It has been

shown that the active catalyst is the coordinatively unsaturated σ-alkynyl species (**B**) which forms via a reaction sequence encompassing the formation of the isolable *cis*-hydrido(vinylidene) intermediate (**A**). Reaction of **B** with further alkyne results in the C-C bond forming step which occurs with the intermediacy of a σ-alkynyl(vinylidene) complex and ultimately yields an η^3-bonded enynyl complex (*E*)-[$(PP_3)M(\eta^3$-$RC_3CHR)]BPh_4$ [94]. σ-Bond metathesis with a fourth molecule of 1-alkyne releases the butenyne and regenerates the active species **B**.

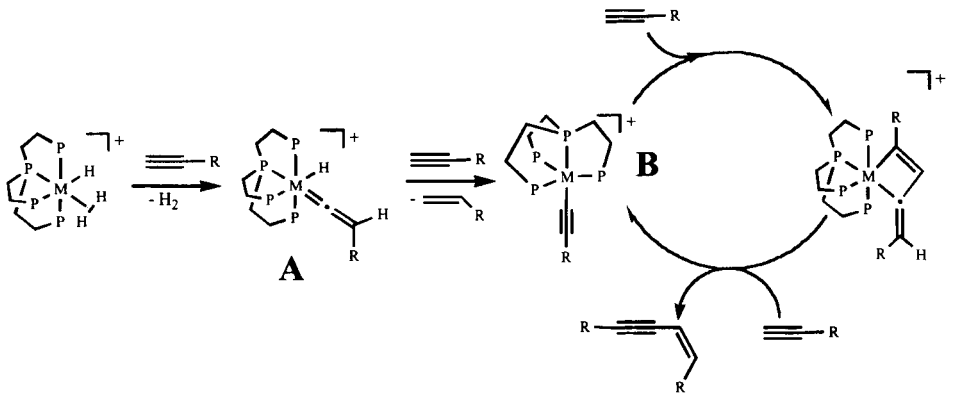

Scheme 25

9.7.3 Polymerization of propene

The polymerisation of propene with isospecific C_2-symmetric zirconocene catalysts has recently been proposed by Resconi to involve η^2-H_2(allyl) intermediates whose formation accounts for a number of experimental observables indeed [95]. The reversible formation of zirconocene dihydrogen(allyl) species in the course of the propene polymerisation involves a sequence of β and γ hydrogen shifts (Scheme 26) Theoretical support to the formation of a Group IV dihydrogen(allyl) complex from metal-alkyl has been provided by Ziegler [96-97] while a transient titanium η^2-H_2 derivative has been provided by Bergman and Anderson to be a plausible intermediate in the hydrogenation of $Cp^*_2TiS(py)$ to $Cp^*_2TiH(SH)$ [98].

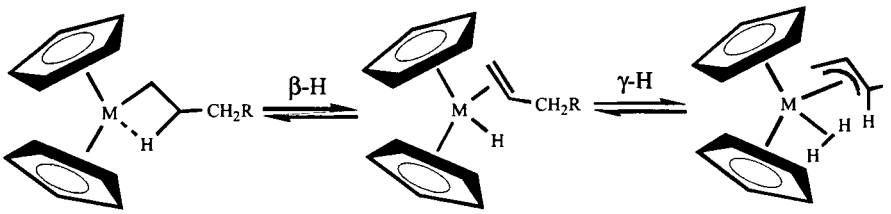

Scheme 26

9.7.4 Tandem ROMP-hydrogenation catalysis

Ring-opening metathesis polymerization (ROMP) of cyclic olefins, followed by hydrogenation, in the presence of a unique metal catalyst is an innovative technique for the synthesis of polyolefins that can not be obtained by Ziegler-Natta or metallocene catalysis [99]. An efficient catalyst for tandem ROMP-hydrogenation is the ruthenium(II)-carbene complex $[RuCl_2(CHPh)(PCy_3)_2]$ described by Grubbs [100]. The η^2-H_2 complex $[RuCl_2(H_2)(PCy_3)_2]$, recently isolated by hydrogenation of the Grubbs catalysts [101], has been proposed to be an intermediate species in the tandem reaction due to its unsaturated nature and the facile tautomerism to the classical ruthenium(IV) derivative $[Ru(H)_2Cl_2(PCy_3)_2]$.

9.8 CONCLUSIONS

As is shown in this book, the activation of dihydrogen by single metal sites encompasses a broad spectrum of research fields, from biochemistry to chemistry and spectroscopy, hence to catalysis, industrial processes, and theoretical analyses. The studies outlined in this chapter are indicative of the range of ongoing applications and challenges of η^2-H_2 metal complexes in homogeneous and heterogeneous catalysis.

Like dioxygen [102], dihydrogen behaves as both a ligand in coordination chemistry and a transferable reagent in catalysis. In catalytic processes, dihydrogen can play three different roles, the third of which represents a unique chemical characteristic:

- Weakly bound ligand
- Stabilizing agent for catalytically active species
- Source of H^+ and H^- species via heterolytic splitting

ACKNOWLEDGMENTS

We thank the European Community for financial support through the COST Working Group D17/0003/00 *"C-C bond formation mediated by transition metal complexes: fundamental studies and mechanistic aspects"* within the COST D17 Chemistry Action. C. B. thanks MURST (legge 95/95) for financial support. Our heartiest thanks go to all our co-workers at ISSECC-CNR, whose names are listed in the references, for their contribution to the chemistry herein described.

REFERENCES

[1] G. J. Kubas, R. R. Ryan, B. I. Swanson, P. J. Vergamini, H. J. Wasserman, J. Am. Chem. Soc. 106 (1984) 451.
[2] P. G. Jessop, R. H. Morris, Coord. Chem. Rev. 121 (1992) 155.
[3] D. M. Heinekey, W. J. Jr. Oldham, Chem. Rev. 93 (1993) 913.
[4] R. H. Morris, Can. J. Chem. 74 (1996) 1907.
[5] S. Sabo-Etienne, B. Chaudret, Chem. Rev. 98 (1998) 2077.
[6] R. H. Crabtree, Acc. Chem. Res. 23 (1990) 95.
[7] G. J. Kubas, Acc. Chem. Res. 21 (1988) 120.
[8] R. H. Crabtree, Angew. Chem., Int. Ed. Engl. 32 (1993) 789.
[9] G. J. Kubas, Comm. Inorg. Chem. 7 (1988) 17.
[10] G. Jia, C.-P. Lau, Coord. Chem. Rev. 190/192 (1999) 83.
[11] Z. Lin, M. B. Hall, Coord. Chem. Rev. 135/136 (1994) 845.
[12] See for example: C. Hall, W. D. Jones, R. J. Mawby, R. Osman, R. N. Perutz, M. K. Whittlesey, J. Am. Chem. Soc. 114 (1994), 7425.
[13] C. J. Sleigh, S. B. Duckett, Prog. Nucl. Magn. Reson. Spectrosc. 34 (1999) 71 and references therein.
[14] I. Horvath, J. M. Millar, Chem. Rev. 91 (1991) 1339.
[15] I. S. Butler, C. Edwards, Book of Abstracts of the XXXIII ICCC, Florence (Italy), August 1998, Abstract 450.
[16] Reversible protonation of *cis*-[$FeH_2(Ph_2PCH_2CH_2PPh_2)_2$] by alcohols to yield *trans*-[$FeH(H_2)(Ph_2PCH_2CH_2PPh_2)_2$] was first reported by Field and co-workers. See: M. V. Baker, L. D. Field, D. J. Young, J. Chem. Soc. Chem. Commun. (1988) 546.
[17] M. A. Esteruelas, L. A. Oro, Chem. Rev. 98 (1998) 577.
[18] S. Sabo-Etienne, B. Chaudret, Coord. Chem. Rev. 178/180 (1998) 381.
[19] R. H. Henderson, Chapter 18 in this book.
[20] C. Chin, A. J. Lough, R. H. Morris, C. T. Scheweitzer, C. D'Agostino, Inorg. Chem. 33 (1994) 6278.
[21] E. Rocchini, A. Mezzetti, H. Rüegger, U. Burckhardt, V. Gramlich, A. Del Zotto, P. Martinuzzi, P. Rigo, Inorg. Chem. 36 (1997) 711.
[22] Z. Xu, I. Bytheway, G. Jia, Z. Lin, Organometallics 18 (1999) 1761.
[23] K. Abdur-Rashid, T. P. Fong, B. Greaves, D. G. Gusev, J. G. Hinman, S. E. Landau, A. J. Lough, R. H. Morris, J. Am. Chem. Soc. 122 (2000) 9155.
[24] R. H. Morris, Chapter 1 in this book.
[25] C. Bianchini, A. Meli, M. Peruzzini, F. Vizza, F. Zanobini, P. Frediani, Organometallics 8 (1989) 2080. C. Bianchini, A. Meli, M. Peruzzini, P. Frediani, C. Bohanna, M. A. Esteruelas, L. A. Oro, Organometallics 11 (1992) 138.
[26] C. Bianchini, C. Bohanna, M.A. Esteruelas, P. Frediani, A. Meli, L. A. Oro, M. Peruzzini, Organometallics 11 (1992) 3837.
[27] J. Eckert, A. Albinati, R. P. White, C. Bianchini, M. Peruzzini, Inorg. Chem. 31 (1992) 4244.
[28] C. Bianchini, D. Masi, M. Peruzzini, M. Casarin, C. Maccato, G. A. Rizzi, Inorg. Chem. 36 (1997) 1061].
[29] W.-C. Chan, C.-P. Lau, Y.-Z. Chen, Y.-Q. Fang, S.-M. Ng, G. Jia, Organometallics 16 (1997) 34.
[30] C. S. Yi, D. W. Lee, Z. He, A. L. Rheingold, K.-C. Lam, T. E. Concolino,

Organometallics 19 (2000) 2909.
[31] H.M. Budzelaar, N. N. P. Moonen, R. de Gelder, J. M. M. Smits, A. W. Gal, Eur. J. Inorg. Chem. (2000) 753.
[32] M. J. Burk, M. P. Mc Grath, R. Wheeler, R. H. Crabtree, J. Am. Chem. Soc. 110 (1988) 5034.
[33] C. R. Landis, P. Hilfenhaus, S. Feldgus, J. Am. Chem. Soc. 121 (2000) 8741.
[34] T. LO, Z. Xu, T. B. Wen, W. S. Ng, S. H. Liu, Z. Y. Zhou, Z. Lin, C. P. Lau, G. Jia, Organometallics 19 (2000) 4523.
[35] A. M. Joshi, B. R. James, J. Chem. Soc. Chem. Commun. (1989) 1785.
[36] D. E. K. Y. Chau, B. R. James, Inorg. Chim. Acta 240 (1995) 419.
[37] A. M. Joshi, K. S. Macfarlane, B. R. James, J. Organomet. Chem. 488 (1995) 161.
[38] E. Sola, V. I. Bakhmutov, F. Torres, A. Eldunque, J. A. López, F. J. Lahoz, H. Werner, L. A. Oro, Organometallics 17 (1998) 683.
[39] F. Torres, E. Sola, A. Elduque, A. P. Martinez, F. J. Lahoz, L. A. Oro, Chem. Eur. J. 6 (2000) 2120.
[40] L. A. Oro, E. Sola, F. Torres, A. Eldunque, Book of Abstracts of the ISHC-12, Stockholm (Sweden), August 2000, Abstract C6, p.36.
[41] C. Bianchini, A. Meli, J. Chem. Soc., Dalton Trans. (1996) 801.
[42] C. Bianchini, A. Meli, F. Vizza, Eur. J. Inorg. Chem. (2000) 000.
[43] H. Topsøe, B. S. Clausen, F. E. Massoth, Hydrotreating Catalysis, Springer, New York, 1996.
[44] A. F. Borowski, S. Sabo-Etienne, B. Chaudret, Book of Abstracts of the ISHC-12, Stockholm (Sweden), August 2000, Abstract P36, p.76.
[45] C. Bianchini, A. Meli, M. Peruzzini, F. Vizza, S. Moneti, V. Herrera, R. A. Sánchez-Delgado, J. Am. Chem. Soc. 116 (1994) 4370.
[46] For this reaction see also C. Bianchini, S. Moneti, M. Peruzzini, F. Vizza, Inorg. Chem. 36 (1997) 5818.
[47] M. Neurock, R. A. van Santen, J. Am. Chem. Soc. 116 (1994) 4427.
[48] R. L. Augustine, Catalysis Today 37 (1997) 419.
[49] R. L. Sweany, J. Am. Chem. Soc. 107 (1985) 2374.
[50] (a) J. A. Ozin, J. Garcia-Prieto, J. Am. Chem. Soc. 108 (1986) 3099; (b) L. Andrews, L. Manceron, M. E. Alikhani, X. Wang, J. Am. Chem. Soc. 122 (2000) 11011.
[51] M. A. Aubart, B. D. Chandler, R. A. T. Gould, D. A. Krogstad, M. F. J. Schoondergang, L. H. Pignolet, Inorg. Chem. 33 (1994) 3724.
[52] C. Bianchini, E. Farnetti, M. Graziani, J. Kaspar, F. Vizza, J. Am. Chem. Soc. 115 (1993) 1753.
[53] P. Barbaro, C. Bianchini, A. Meli, M. Peruzzini, A. Vacca, F. Vizza, Organometallics 10 (1991) 2227.
[54] V. I. Bakhmutov, C. Bianchini, M. Peruzzini, F. Vizza, E. V. Vorontsov, Inorg. Chem. 38 (2000) 1655.
[55] C. Bianchini, D. G. Burnaby, J. Evans, P. Frediani, A. Meli, W. Oberhauser, R. Psaro, L. Sordelli, F. Vizza, J. Am. Chem. Soc. 121 (1999) 5961.
[56] C. Bianchini, V. Del Santo, A. Meli, W. Oberhauser, R. Psaro, F. Vizza, Organometallics, 19 (2000) 2433.
[57] B. Chaudret, P. Dagnac, D. Labroue, S. Sabo-Etienne, New. J. Chem. 20 (1996) 1137.

[58] C. Bianchini, M. Peruzzini, E. Farnetti, J. Kaspar, M. Graziani, J. Organomet. Chem. 488 (1995) 91.
[59] C. Bianchini, E. Farnetti, M. Graziani, M. Peruzzini, A. Polo, Organometallics 12 (1993) 3753.
[60] R. M. Bullock, J. S. Song, J. Am. Chem. Soc. 116 (1994) 8602.
[61] Q. Jiang, Y. Jiang, D. Xiao, P. Cao, X. Zhang, Angew. Chem. Int. Ed. Engl. 37 (1998) 1100.
[62] V. I. Bakhmutov, E. V. Vorontsov, D. Yu. Antonov, Inorg. Chim. Acta 278 (1998) 122.
[63] K. Abdur-Rashid, A. J. Lough, R. H. Morris, Organometallics 19 (2000) 2655.
[64] M. Yamakawa, H. Itro, R. Noyori, J. Am. Chem. Soc. 122 (2000) 1466.
[65] K. J. Haack, S. Hashiguci, A. Fuji, T. Ikarya, R. Noyori, Angew. Chem., Int. Ed. Engl. 36 (1997) 285.
[66] P. Brothers, Progr. Inorg. Chem. 28 (1981) 1.
[67] A. Mezzetti, A. Tschumper, G. Consiglio, J. Chem. Soc., Dalton Trans. (1995) 49.
[68] C. Bianchini, P. Barbaro, G. Scapacci, F. Zanobini, Organometallics 19 (2000) 2450.
[69] M. M. Taqui Khan, S. B. Halligudi, S. Shukla, J. Mol. Catal. 57 (1989) 47.
[70] P. G. Jessop, T. Ikariya, R. Noyori, Nature 368 (1994) 231.
[71] P. G. Jessop, T. Ikariya, R. Noyori, Chem. Rev. 95 (1995) 259.
[72] F. Hutschka, A. Dedieu, M. Eicherger, R. Fornika, W. Leitner, J. Am. Chem. Soc. 119 (1997) 4432.
[73] B. R. James, Adv. Organomet. Chem. 17 (1979), 319.
[74] C. Bianchini, M. Peruzzini, A. Polo, A. Vacca, F. Zanobini, Gazz. Chim. It. 121 (1991) 543.
[75] C. Bianchini, M. Peruzzini, unpublished results.
[76] H. S. Chu, C. P. Lau, K. Y. Wong, W. T. Wong, Organometallics 17 (1998) 2768.
[77] A variety of hydrogen-bonded complexes featuring weak intra- or intermolecular H···H interactions are known. For comprehensive reviews on this subject see the Chapters by Morris (Ch. 1), Clot/Eisenstein/Lee/Crabtree (Ch. 3) and Epstein/ Belkova/Shubina (Ch. 14) in this book.
[78] Y. Nishibayashi, I. Takei, M. Hidai, Angew. Chem., Int. Ed. 38 (1999) 3047.
[79] E. P. Cappellani, S. D. Drouin, G. Jia, P. A. Maltby, R. H. Morris, C. T. Schweitzer, J. Am. Chem. Soc. 116 (1994) 3375.
[80] B. Chin, A. J. Lough, R. H. Morris, C. T. Schweitzer, C. D'Agostino, Inorg. Chem. 33 (1994) 6278.
[81] M. A. Esteruelas, L. A. Oro, Organometallics 10 (1991) 462.
[82] F. Maseras, A. Lledós, Organometallics 15 (1996) 1218.
[83] M. L. Christ, S. Sabo-Etienne, B. Chaudret, Organometallics 14 (1995) 1082.
[84] Y. Guari, S. Sabo-Etienne, B. Chaudret, J. Am. Chem. Soc. 120 (1998) 4228.
[85] S. Murai, F. Kaciuchi, S. Sekine, Y. Tanaka, A. Kamatani, M. Sonoda, N. Chatani, Nature 366 (1993) 529.
[86] M. Sonoda, F. Kaciuchi, N. Chatani, S. Murai, Chem. Lett. (1996) 113.
[87] S. Murai, N. Chatani, F. Kaciuchi Pure Appl. Chem. 69 (1997) 589.
[88] F. Kaciuchi, S. Sekine, Y. Tanaka, A. Kamatani, M. Sonoda, N. Chatani, S. Murai, Bull. Soc. Chim. Jpn. 68 (1995) 62.

[89] T. Matsubara, N. Koga, D. G. Musaev, K. Morokuma, Organometallics 19 (2000) 2318.
[90] S. Busch, W. Leitner, J. Chem. Soc., Chem. Commun. (1999) 2305.
[91] C. Bianchini, P. Frediani, D. Masi, M. Peruzzini, F. Zanobini, Organometallics 4616 (1994) 13.
[92] C. Bianchini, M. Peruzzini, Phosphorus Res. Bull. 6 (1996) 151.
[93] P. Barbaro, C. Bianchini, M. Peruzzini, A. Polo, F. Zanobini, P. Frediani, Inorg. Chim. Acta 220 (1994) 5.
[94] C. Bianchini, M. Peruzzini, F. Zanobini, P. Frediani, A. Albinati, J. Am. Chem. Soc. 110 (1991) 5454.
[95] L. Resconi, J. Mol. Catal. A: Chemical 146 (1999) 167.
[96] P. M. Margl, T. K. Woo, P. E. Blöchl, T. Ziegler, J. Am. Chem. Soc. 120 (1998) 2174.
[97] P. M. Margl, T. K. Woo, T. Ziegler, Organometallics 17 (1998) 4997.
[98] H. Sweeney, J. L. Polse, R. G. Bergman, R. A. Andersen, Organometallics 18 (1999) 5502.
[99] E. L. Dias, R. H. Grubbs, Organometallics 17 (1998) 2758.
[100] P. Schwab, M. B. France, J. W. Ziller, R. H. Grubbs, Angew. Chem., Int. Ed. Engl. 34 (1995) 2039.
[101] S. D. Drouin, G. P. A. Yap, D. E. Fogg, Inorg. Chem. 39 (2000) 5412.
[102] C. Bianchini, R. A. Zoellner, Adv. Inorg. Chem. 44 (1996) 263.

This Page Intentionally Left Blank

Chapter 10

Mechanistic Aspects of Dihydrogen Activation and Catalysis by Dinuclear Complexes

Luis A. Oro and Eduardo Sola

Departamento de Química de la Coordinación y Catálisis Homogénea, Instituto de Ciencia de Materiales de Aragón, Universidad de Zaragoza-CSIC, E-50009 Zaragoza, Spain

CONTENTS

10.1 INTRODUCTION

Transition metal hydrides and dihydrogen are important molecules which are involved in most homogeneous catalytic reactions. Due to their relative simplicity and their accessibility using ^1H NMR spectroscopy, these molecules have been the basis of numerous relevant experimental observations, which have significantly increased our understanding of reaction mechanisms in solution. Examples of this are the activation of σ-bonds and the dynamic behavior of unsaturated complexes in solution.

Bearing in mind this demonstrated ability of dihydrogen and hydrides to provide useful mechanistic information, this chapter analyzes some selected recent results in the chemistry of dinuclear hydrides, intending to extract from them those mechanistic features characteristic of dinuclear environments that could be relevant to homogeneous catalysis. This analysis has not been conceived as an exhaustive review of the chemistry and catalytic applications of dinuclear hydrides, although most relevant work in this field has been either discussed or referenced. The selected examples discussed along the following pages concentrate on dinuclear complexes containing robust bridging ligands which allow short metal-to-metal separations, even though labile dinuclear compounds and species having rather distant metal centers may also participate in genuine dinuclear reactivity patterns.[1]

10.2 ACTIVATION OF DIHYDROGEN BY DINUCLEAR COMPLEXES

The oxidative addition of dihydrogen to mononuclear metal complexes is a well-understood fundamental reaction.[2] It involves the concerted addition of the substrate to a metal species that must be both coordinatively unsaturated and electron-rich. These conditions are fulfilled by many late transition metal complexes, specially those having a d^8 electronic configuration.[3] In the case of dinuclear complexes, such general conditions seem to be subjected to some restrictions since, among the large number of electron-rich and unsaturated d^8d^8 dinuclear compounds described so far, only certain structures appear to be suitable for the oxidative addition of dihydrogen.

10.2.1 Homovalent d^8 dinuclear complexes

Theoretical studies have shown that the concerted addition of H_2 across a metal-metal bond is forbidden by orbital symmetry considerations,[4] and also have predicted high activation barriers for such two-metal concerted additions in non-bonded dinuclear d^8d^8 compounds.[5] These calculations also indicate that the more realistic mechanistic alternative for the addition of dihydrogen to a homovalent d^8 complex would be that initiated by a single-metal oxidative addition. In agreement with this proposal, the addition of H_2 to the *A-frame* complex $[Ir_2(\mu\text{-}S)(CO)_2(dppm)_2]$ (**1**, dppm = $Ph_2PCH_2PPh_2$) has been shown to involve single-metal oxidative additions steps followed by hydride migration processes (Scheme 1).

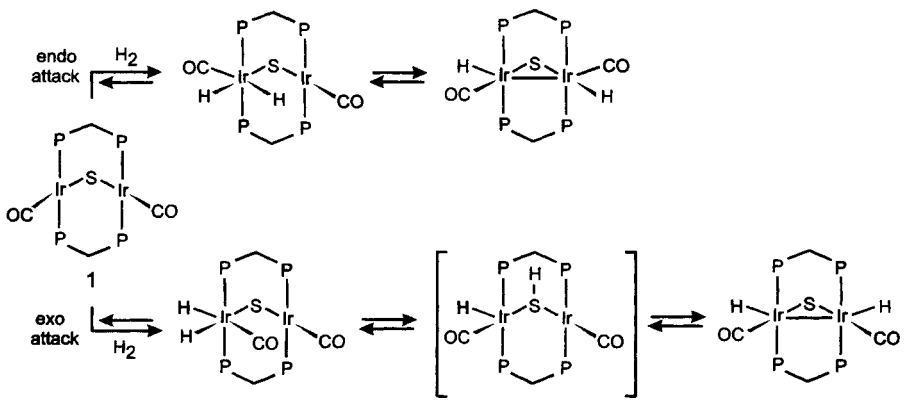

Scheme 1

The mechanism of Scheme 1 is the result of a detailed study including the observation of most reaction intermediates by parahydrogen-induced polarization NMR spectroscopy.[6] This study has concluded that dihydrogen can attack either inside (endo) or outside (exo) the pocket of the dinuclear frame, and has suggested that the hydride migrations can occur either directly, through the formation of hydride bridges, or indirectly, through the protonation of the bridging sulfide.[7]

Other bis-dppm-bridged d^8d^8 complexes having *A-frame* and *face-to-face* structures have been reported to react with dihydrogen, with the nature of the reaction products being strongly dependent on the metals and the ancillary ligands present in the complex. Thus, the reaction of H_2 with the dirhodium analogue of **1** has been shown to stop at the initial single-metal oxidative addition, which has been found to be reversible.[6] In turn, such single-metal additions were found to be irreversible, at the iridium atom, in heterodinuclear RhIr *A-frame* derivatives with sulfide, chloride,[8] and phenylacetylide [9] bridges. Dihydrogen has been found to add to the *A-frame* cation $[Ir_2(\mu\text{-}Cl)(CO)_2(dppm)_2]^+$ (**2**) along an (endo) addition-hydride migration pathway similar to that of Scheme 1. Under dihydrogen excess, this initial addition can be followed by a reversible second addition affording tetrahydride complexes.[8, 10] A double dihydrogen addition has also been reported for the iodide-bridged analogue of **2**, although, in this case, the second addition was not preceded by a hydride migration step and was irreversible, since the tetrahydride eliminated HI instead of H_2.[8]

The neutral *face-to-face* complexes $[Ir_2X_2(CO)_2(dppm)_2]$ (X = Cl, I), have been found to be in equilibrium with their related cationic *A-frame* species through the dissociation of one halide ligand.[8, 11] Not surprisingly, the addition of dihydrogen to both types of compounds has been found to involve common intermediates, although the final reaction products are different.[8,10]

The reactivity of the bis-dppm-bridged complexes described above, although diverse, suggests a common mechanism of dihydrogen activation initiated by a single-metal addition. After this common activation step, the feasibility of subsequent reactions such as hydride migrations, further dihydrogen additions, or reductive eliminations is determined by the specific features of each compound, which also define the nature of the final reaction product.

The facility with which dihydrogen activation occurs in these *A-frame* and *face-to-face* bis-dppm-bridged rhodium and iridium complexes is striking when considering the scarcity of reported examples for such activations with d^8d^8 compounds of different structure. [12]

The diruthenium(0) complexes $[Ru_2(CO)_4\{\mu\text{-}(RO)_2PN(Et)P(OR)_2\}_2]$ (**3**, R = Me, ^{i}Pr) (Scheme 2) have been reported to react with dihydrogen affording 1,2-dihydrides.[13] Despite the formal similarity between these compounds and the previously described iridium and rhodium dppm derivatives, they display different coordination environments around the metal atoms. This could be related to the fact that, unlike the typical planar structure of most mononuclear d^8 species, the unsaturated zerovalent ruthenium fragments adopt a structure which resembles a trigonal bipyramid with an empty equatorial site.[14]

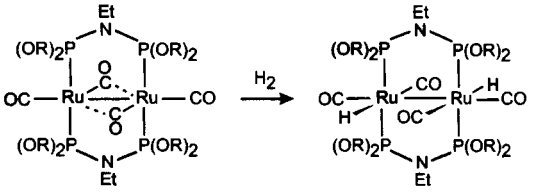

3

Scheme 2

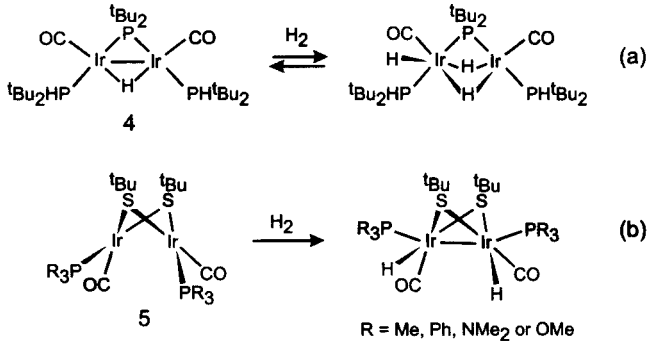

4

5

Scheme 3

The two diiridium(I) complexes of Scheme 3, which show *planar* and *open-book* structures, respectively, constitute further examples of d^8d^8 H_2-activating species. The reaction of the *planar* complex $[Ir_2(\mu\text{-}H)(\mu\text{-}P^tBu_2)(CO)_2(PH^tBu_2)_2]$ (**4**) is consistent with a reversible single-metal addition,[15] while the mechanism proposed in the case of the *open-book* thiolate complexes $[Ir(\mu\text{-}S^tBu)(CO)(PR_3)]_2$ (**5**) is similar to that depicted in Scheme 1, consisting of a (endo) single-metal addition followed by a hydride migration step.[16] The migration step has been found to be hindered by bulky PR_3 ligands, which direct the reaction towards the product of a double single-metal addition.[17]

Interestingly, the reaction of Scheme 3(b) constitutes an exceptional example for the dihydrogen addition to a d^8d^8 compound of *open-book* structure. This singularity can be considered very remarkable, since complexes with this structure are very abundant and their reactivity toward small molecules has been profusely investigated. In our own experience, which comprises several rhodium and iridium dinuclear complexes with *open-book* structures and different N-donor bridging ligands, we have observed that the H_2 addition to homovalent d^8 compounds does not take place, even under harsh reaction conditions. This is in contrast to the affinity of such dinuclear compounds for other oxidative addition reactants such as halogens or alkyl halides.[18] A significant example for such arrested reactivity towards H_2 is provided by the 32 e^- pyrazolate-bridged complexes $[M(\mu\text{-}Pz)(CN^tBu)_2]_2$ (M = Rh, Ir), highly nucleophilic species capable of activating a wide range of halocarbons, but inert towards dihydrogen.[19]

Such substrate selectivity can be rationalized in mechanistic terms, since it is well-established that hydrogen and halocarbons undergo oxidative addition through different mechanisms. Thus, the S_N2 addition of halocarbons requires a filled orbital in the complex in order to allow the starting nucleophilic attack, whereas the addition of hydrogen demands, first of all, an accessible empty orbital for dihydrogen coordination. In addition, it has been shown that the H_2 coordination requires some distortion of the square planar geometry typical of 16 e^- d^8 complexes, in order to minimize the four-electron repulsion between the filled metal d_z^2 orbital and the $\sigma(H_2)$.[2, 3] The theoretical analysis of d^8d^8 complexes with *open-book* structures has provided a molecular orbital description of these species which is only slightly different from that corresponding to independent mononuclear fragments, since the two metals are essentially non-bonded.[20-22] Nevertheless, these calculations predict a weak metal-metal interaction resulting from the combined effect of the repulsion between the electrons in the d_z^2 orbitals of the mononuclear fragments (interaction 1, in Scheme 4) and the donor-acceptor interactions between the d_z^2 electrons and the empty p_z orbitals (interaction 2, in Scheme 4). This interaction has been proposed to contribute significantly to the stabilization of the bent structures of these compounds (within a range of 10 Kcal/mol).[20]

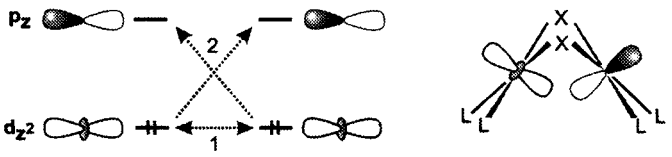

Scheme 4

From this molecular orbital description, it is expected that these dinuclear complexes maintain a reactivity in S_N2 oxidative additions comparable to that of mononuclear analogues, since they are still electron rich at the axis of the dinuclear framework. On the other hand, it is likely that the weak metal-metal interaction could contribute to hinder the dihydrogen coordination to the empty p_z orbitals, by increasing the activation energy necessary to rehybridize the metal fragment orbitals from the ground state square-planar geometry towards the distorted transition state. Given that the geometric constraints in dinuclear complexes are frequently larger than those in mononuclear species, the steric or conformational contribution to the energy required for this distortion could be also significant in some cases.

The aforementioned arguments may account for a generic decrease in the dihydrogen activation capabilities on going from mononuclear d^8 complexes to dinuclear species adopting *open-book* structures. *Planar* complexes such as **4** and those having distorted structures like **3** are not expected to suffer from such deactivation, since the orbital overlap shown in Scheme 4 seems unlikely in these structures. Moreover, this generic effect can turn out to be irrelevant for complexes in which the specific features of the ligand system allow the use of empty orbitals other than p_z for dihydrogen coordination. Most likely, this is the case of the *A-frame* compounds described above, since it has been shown that the halide or pseudohalide ligand at the bridgehead position can easily turn its bridging coordination mode into terminal, creating an "incipient unsaturation" in one of the metal centers.[8-10] This would generate a new empty orbital for dihydrogen coordination at a 14 e^- metal center, favoring oxidative addition. The situation would be parallel to that recognized for the Wilkinson catalyst, in which the oxidative addition of H_2 to 14 e^- intermediates was found to be the only kinetically relevant one, since it occurs at least 10^4 times faster than the corresponding addition to the 16 e^- precursor.[23] The singular reactivity found for the *open-book* thiolate complexes **5** could be also tentatively attributed to the lability of the bridges or, alternatively, to the presence of sulfur atoms, since it has been shown that S-donor bridges can participate in the activation of small molecules by dinuclear compounds.[24] This active role can properly be illustrated by the reactions of Scheme 5, which depicts a reversible double H_2 addition on a bis(μ-

sulfido)-dirhodium(III) core,[25] and one step of the mechanism proposed for the hydrogenolysis of carbon-halogen bonds catalyzed by dimolybdenum complexes.[26] In this proposal, the dihydrogen is deprotonated by an external base after its activation at the Mo-S moiety.

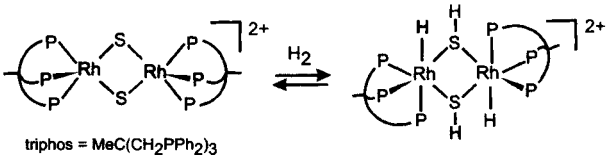

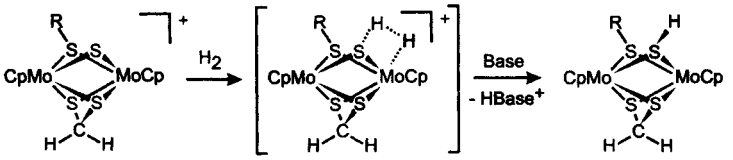

Scheme 5

10.2.2 Dinuclear complexes of other electronic configurations

In the previous section we have tentatively attributed the relative inertness towards H_2 of certain d^8d^8 structures to their inability to pre-coordinate dihydrogen, since the empty orbitals of such dinuclear species appear to be relatively more hidden than those of mononuclear analogues. It turns out from this proposal that the modification of the orbital or electronic features of these species in order to attain more accessible empty orbitals would bring H_2-activating compounds.

The reaction of Scheme 6 reveals that disproportionation of the d^8d^8 *open-book* structure into a d^9d^7 configuration can afford H_2-activating species. In this mixed-valence configuration, which has been found to be stabilized in diiridium complexes containing diphosphazane ligands, the d^7 metal center can offer a neat empty orbital for dihydrogen coordination, thus favoring dihydrogen activation.[27]

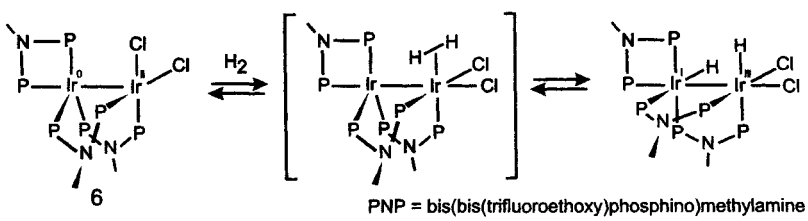

Scheme 6

The reversible reaction of H_2 with complex **6** has been proposed to involve dihydrogen coordination to an equatorial position of the Ir(II) center, followed by single-metal addition and hydride migration steps. The axial-to-equatorial movement of the coordination vacancy required by this mechanism has been shown to be a facile process.

Another feasible modification of non-reactive homovalent d^8 compounds, leading to active species, has been shown to involve the oxidation of these complexes to give d^6d^8 or d^7d^7 compounds (Scheme 7).[28] The facility with which the Ir(III)Ir(I) derivative **8** and the diiridium(II) species **9** react with dihydrogen strongly contrasts with the inertness of their *open-book* precursor **7** under the same reaction conditions. This behavior is consistent with the aforementioned arguments attributing the lack of reactivity of d^8d^8 species to their orbital architecture since, otherwise, an enhancement of the oxidative addition affinity, after oxidation, would be very surprising.

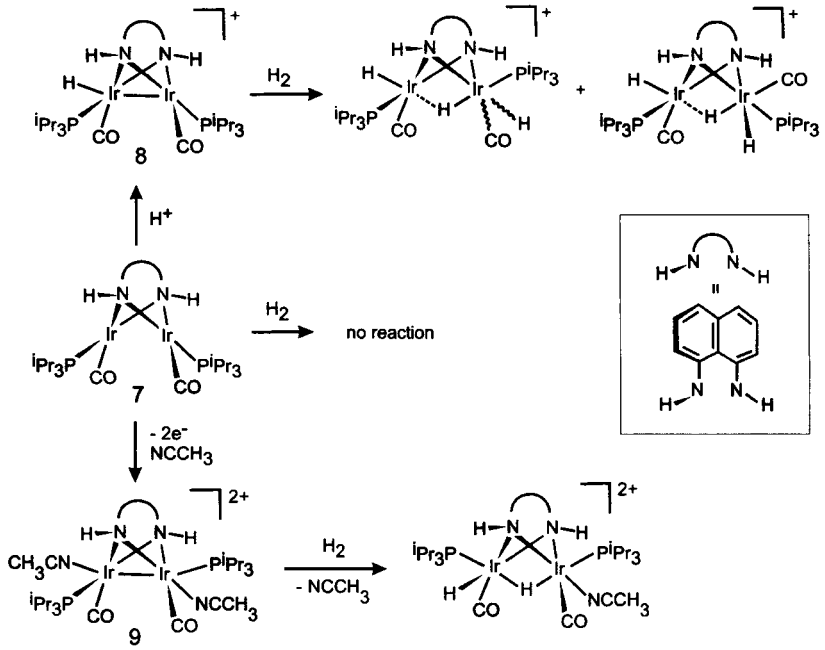

Scheme 7

The stereochemistry of the reaction products of Scheme 7 again suggests that these reactions involve single-metal additions preceded by dihydrogen coordination to equatorial positions. In this respect, it has been shown that complex **9** can readily dissociate its acetonitrile ligands, and exchange them from axial to equatorial positions with low kinetic barriers.[28] Such vacancy rearrangements

are also likely for complex **8** since, assuming the presence of a dative Ir(I)-Ir(III) bond,[29] this complex only differs from **9** as a result of the electron counting formalism.

The requirement for H_2 coordination at an equatorial position (endo attack) is a likely consequence of the fact that the electron density necessary to cleave the H-H bond accumulates at the intermetallic region of these complexes. In agreement with this, other unsaturated metal-metal bonded complexes have been shown to undergo facile oxidative addition of dihydrogen, suggesting that metal-metal bonds are convenient sources of electron density for such additions. The reported examples involve dinuclear complexes of electron-rich metal centers such as Ir(II) [30-32] and Re(I), [33] but also compounds of early transition metals such as W(III), [34] Ta(III) [35] and Zr(III).[36]

The structure found in the product of H_2 addition to the early-late complex **10** (Scheme 8) is again that expected for an endo attack of dihydrogen followed by a single-metal addition.[36] The preference of dihydrogen for the early transition metal, in the presence of an unsaturated electron-rich Ir(II), would result from the favored coordination of the reactant to the acidic Zr center.

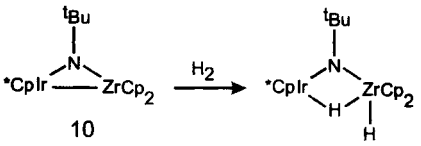

10

Scheme 8

The reactions of Schemes 6-8 can be regarded as accumulative evidences suggesting a general pathway for the activation of dihydrogen by metal-metal bonded complexes. This pathway would involve the dihydrogen coordination to a vacancy *cis* to the metal-metal bond followed by a single-metal addition step. Since the electron density at the metal-metal bond is removed in the process (only partially in multiply bonded compounds), a likely result of this mechanism would be the replacement of the former metal-metal bond by a bridging hydride, in agreement with the reactions of Schemes 7 and 8. Nevertheless, due to the high mobility of the hydride ligands in the dinuclear framework (see next section), the structures of the thermodynamic products of these additions are expected to be those better satisfying the specific electronic and steric features of the compound, independently on the addition mechanism. Therefore, any mechanistic interpretation based on the structure of the final reaction products should be considered with caution. In this respect, it should be mentioned that most of the above referenced additions involving symmetric metal-metal bonded species have been shown to afford symmetric bis-μ-hydrido species. Such structures, although compatible with the above mechanism in the view of the hydride mobility, may suggest alternative mechanistic proposals.

In order to illustrate that the mechanisms of H_2 addition to dinuclear complexes are not restricted to the pathway suggested by most of the aforementioned reactions, it can be useful to comment on the reaction shown in Scheme 9, which represents a singular example in many respects. The reaction has been shown to produce a hydrido bridged complex, while the second hydrogen atom has been transferred to the bridging system, a μ-η^2-dinitrogen ligand in this case. A possible intermediate along this addition, which has been isolated and characterized by X-ray diffraction methods, contains the dihydrogen moiety coordinated to both metal atoms in a μ-η^2 fashion. The evolution of this intermediate to the final reaction product has been proposed to involve the heterolytic cleavage of the dihydrogen moiety through a four center transition state.[37] This unusual coordination of the dihydrogen has also been found in metallodiporphyrin ruthenium complexes, and has claimed to be relevant to the dinuclear reductive elimination of dihydrogen.[38]

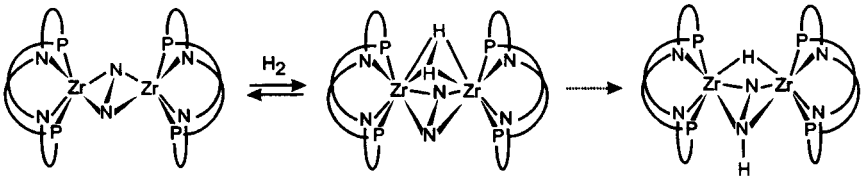

Scheme 9

Decreasing further the electron counting to non-metal-metal-bonded d^6d^6 species has been shown to afford H_2-activating compounds in the presence of basic ligand environments, much as observed in mononuclear analogues. This is the case of the diruthenium(II) complex **11** (Scheme 10), which reacts with dihydrogen under mild conditions to give a 1,2-addition product.[39] A mechanisms involving a single-metal oxidative addition step has also been proposed in this case.

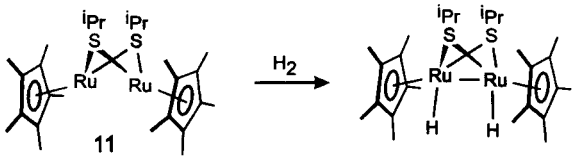

Scheme 10

The treatment of the diiridium(III) complex **12** (Scheme 11) with D_2 has been shown to afford deuterated isotopomers of **12**, indicating that this d^6d^6 species also activates dihydrogen. [40] In this case, instead of oxidative addition prod-

ucts, the η^2-dihydrogen complex **13** has been observed during the activation reaction. This species has been shown to undergo fast exchange between the H atoms of the η^2-H_2 and the hydride ligands, on the NMR time scale. With regard to the mechanistic proposals concerning related mononuclear species, this exchange involves, most likely, single-metal oxidative addition and reductive elimination reactions, though possible Ir(V) intermediates.[41]

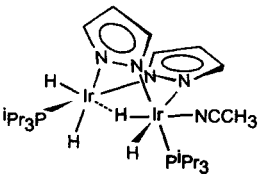

12

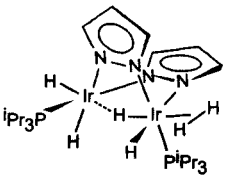

13

Scheme 11

Other dinuclear η^2-dihydrogen complexes involved in similar activation processes are the ruthenium compounds of formulas $[(P_2)(\eta^2\text{-}H_2)Ru(\mu\text{-}Cl)_3RuCl(P_2)]$,[42] $[(P_2)(\eta^2\text{-}H_2)ClRu(\mu\text{-}H)_2RuCl(\eta^2\text{-}H_2)(P_2)]$[43] ($P_2$ = diphosphine), $[(PR_3)_2(\eta^2\text{-}H_2)Ru(\mu\text{-}H)(\mu\text{-}Cl)_2RuH(PR_3)_2]$,[44] and $[(PPh_3)_2(\eta^2\text{-}H_2)Ru(\mu\text{-}H)(\mu\text{-}X)_2Re(CO)(PPh_3)_2]BF_4$ (X = H, Cl).[45] Interestingly, all these η^2-dihydrogen compounds have been identified in the course of mechanistic investigations of hydrogenation reactions catalyzed by dinuclear species.[46]

Electron-richer d^8d^{10} compounds can also be considered as H_2-activating alternatives to compounds with the unfavorable d^8d^8 configuration. In the case of the bis-dppm bridged Rh(I)Ir(-I) complex **14**, the d^8d^{10} configuration has been found to result in a metal-metal bonded species in which the coordination around the rhodium center is similar to that in *planar* homovalent d^8 compounds.[47] The kinetic product of dihydrogen addition to **14** is consistent with the occurrence of a single-metal oxidative addition to the Rh(I) (Scheme 12). This kinetic product is thermally unstable and reductively eliminates methane from the iridium center. The overall reaction constitutes a clear example of bimetallic cooperation, since the oxidative addition to one center provokes a reductive elimination in the other metal.

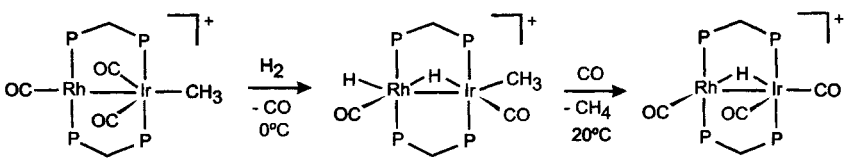

14

Scheme 12

Other d^8d^{10} complexes containing Ir(I)-Ag(I) and Ir(I)-Cu(I) metal cores have been reported to react with dihydrogen.[48] The structures deduced for the products of these reactions are also those expected from single-metal oxidative additions to the Ir(I) centers.

Some of the H_2-activating dinuclear species mentioned along this section have been found to undergo the oxidative addition of other substrates containing single bonds such as C-H, O-H, N-H, S-H, etc. Scheme 13 shows some representative examples of C-H activation reactions [9, 32, 36, 49] in which the similarity of the reaction products to those resulting from the H_2 oxidative addition suggests common mechanisms. It follows from this observation that the peculiarities of the dinuclear compounds analyzed along this section are also likely to affect the concerted activation of other substrates.

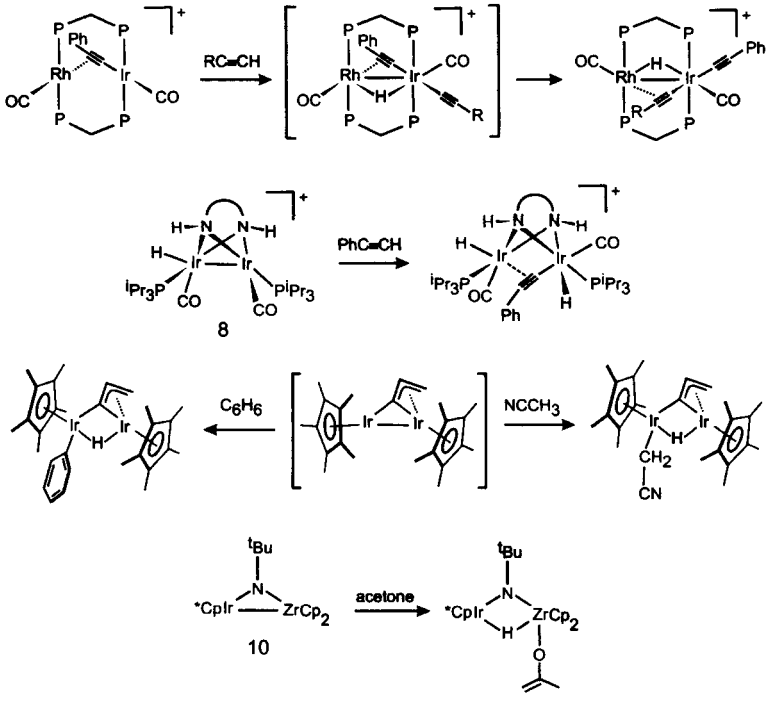

Scheme 13

10.2.3 Acidic dinuclear hydrides: heterolysis of dihydrogen

The Brønsted acidity of transition metal hydrides is a well known phenomenon which has been extensively studied in both mononuclear and polynuclear compounds. [50] The Brønsted acidity is a likely property of the dinuclear products resulting from H_2 additions, especially for cationic species, since they often contain metal centers in relatively high formal oxidation states. In this respect, it

has been shown that the course of some dihydrogen additions to cationic complexes in polar solvents can be altered by the occurrence of deprotonation reactions, which can lead to the formation of unexpected reaction products. A simple case is depicted in Scheme 14, where the kinetic product of dihydrogen addition to complex **9** readily isomerizes to a new species with mutually *trans* hydride ligands.[28] In agreement with the participation of deprotonated intermediates during such isomerizations, it has been observed that the reactions are accelerated by the presence of small amounts of triethylamine. Moreover, when the isomerizations were carried out in acetone-d_6, deuterated isotopomers were obtained, due to the H/D scrambling between the proton and the solvent.[51, 52]

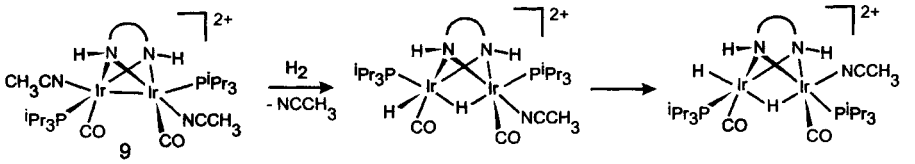

Scheme 14

These deuterations have been found to be very diagnostic, allowing the identification of those positions of the dinuclear framework which are kinetically more acidic. Thus, upon treatment of complex **15** (Scheme 15) with acetone-d_6, fast deuteration of the terminal hydride ligand was observed, whereas the replacement of the bridging hydride by deuterium occurred only after extended reaction times (up to 2 h). In contrast, deprotonation of **15** with triethylamine afforded complex **8**, after the formal abstraction of the bridging hydride. This implies that the thermodynamic acidity of the bridging hydride is greater than that of the terminal hydride, the latter being kinetically more acidic. Similar conclusions have been obtained from the behavior of other polynuclear hydrides.[50]

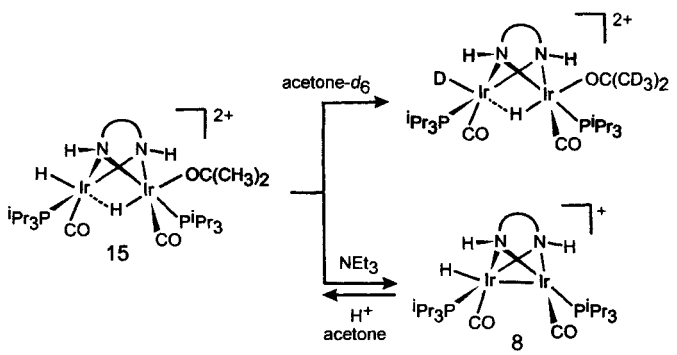

Scheme 15

The acidic properties of the H_2 oxidative addition products may also have interesting consequences when complexes capable of generating various coordination vacancies are used, since the deprotonation of the products leads to reduced species which can undergo a new addition of dihydrogen. Thus, after the stepwise reaction of the labile complex **16** with two equivalents of dihydrogen, trihydride complexes together with one equivalent of acid were obtained, providing a clear example of dihydrogen heterolysis (Scheme 16).[28] Reaction sequences similar to this are likely involved in the dihydrogen additions to the neutral complex $[Ir(\mu\text{-}O_2CCF_3)(dfepe)]_2$ (dfepe = $(C_2F_5)_2PCH_2CH_2P(C_2F_5)_2$)[53] and to the cationic species $[Rh_2(\mu\text{-}CO)(CO)_2(dppm)_2](CF_3SO_3)_2$. [51]

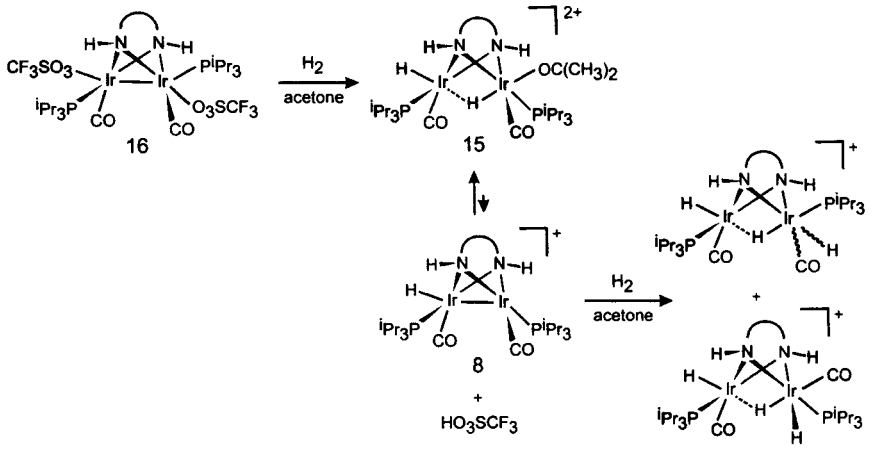

Scheme 16

Again, the features observed for H_2 addition can be extrapolated to other substrates susceptible to oxidative addition, as illustrated by the double heterolysis of the phenylacetylene C-H bonds depicted in Scheme 17.[49]

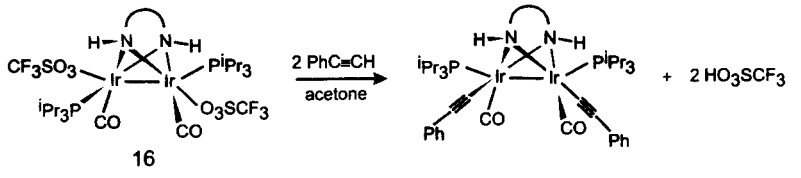

Scheme 17

10.3 HYDRIDE MIGRATIONS IN DINUCLEAR COMPLEXES

The vast majority of known polynuclear metal hydride complexes contains bridging hydride ligands. Obviously, the possibility of this bonding mode constitutes the main peculiarity of polynuclear compounds in comparison to mononuclear hydrides. Some representative examples of dinuclear complexes containing up to four hydride bridges are shown in Scheme 18.[54-56]

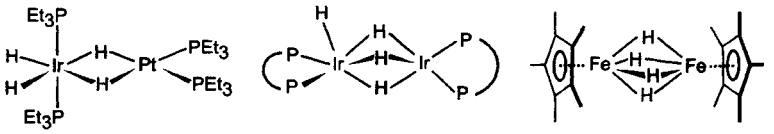

Scheme 18

As for the main group elements, the bridging transition metals hydrides form three center–two electron bonds, so that the bridges are bent, and the resulting dinuclear hydrides are electron deficient compounds.[57, 58] Because of the latter traits, these compounds can readily generate coordination vacancies by turning the bridging mode of the hydride into a terminal mode, a facile process which has been studied in some detail.[59] The opposite effect has also been observed, since polynuclear species containing bridging hydrides often constitute the resting states of reactive unsaturated mononuclear fragments containing hydrides. This was found to be the case with the complex $[Ir_2H_2(\mu\text{-}H)_3(PPh_3)_4]PF_6$, which was formed during hydrogenation reactions catalyzed by the cationic precursor $[Ir(cod)(PPh_3)_2]PF_6$, and which was found to be catalytically inactive.[60] This condensation of unsaturated or labile mononuclear hydrides now constitutes a powerful method for the synthesis of dinuclear or polynuclear hydrides.[58, 61, 62]

As illustrated by some of the reactions mentioned along the previous section, the interconversion between bridging and terminal hydrides constitutes a key step that potentially leads to the migration of hydrides from one metal to the other.[3, 58, 63] In general, such migrations are facile processes, as can be concluded from the fast hydride exchange in the NMR time scale shown by some dinuclear polyhydrides.[12, 42-45, 55-58, 64] As also pointed out in the previous section, in some particular cases the hydride transfer between the metal centers may involve the protonation of the bridging system rather than the formation of bridging hydrides.[7, 24]

Taking into account the usual dynamic behavior in solution of mononuclear polyhydrides, the occurrence of these intermetallic hydride exchanges is not surprising, although its importance can not be underestimated. In fact, hydride transfer among metals has been found to be crucial in order to observe intermetallic cooperation in polynuclear catalysts. This subject will be analyzed in the

following section of this chapter, although it may be useful to provide here some examples of elementary reactions in which hydride mobility within dinuclear frameworks is important.

The two reactions depicted in Scheme 19 show alkyne insertions into a metal-H bond of a dinuclear complex. In Scheme 19a,[65] the insertion of the alkyne takes place even though the vacancy for alkyne coordination and the hydride ligand are situated on different metal centers of the starting complex **8**.[28] In the second example (Scheme 19b), it was proposed that the incoming substrate initially coordinates to the complex as a bridging m-η^2:η^2 ligand, and then undergoes subsequent insertion.[66]

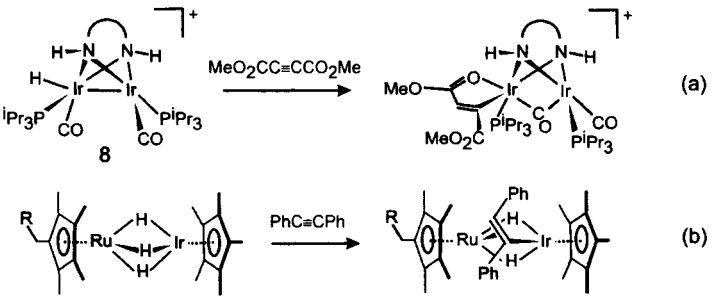

Scheme 19

Noteworthy, the stereochemistry of the vinyl moiety in both products was found to be that resulting from a *trans* addition to the triple bond, in contrast to the *cis* addition products expected from a concerted single-metal insertion.[67] This suggests that insertion reactions leading to *trans* addition products are entirely feasible in dinuclear species, probably as a consequence of the concerted action of both metal centers. This observation may be relevant in the context of some catalytic processes, such as alkyne hydrosilylations, which rather frequently afford *trans* addition products.[68] This unusual selectivity might result from intermolecular hydride transfer steps, similar to those recognized during catalytic hydroformylations,[69] or from the formation of dinuclear active species under catalytic conditions.[70]

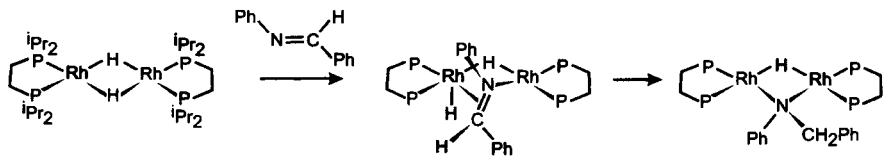

Scheme 20

Dinuclear hydride cores have been shown to be advantageous also for the insertion of imines into metal-hydride bonds. The catalytic hydrogenation of sub-

strates containing C=N bonds is frequently found to be more difficult than alkene hydrogenation. Several factors have been recognized as potentially responsible for this difficulty, one of them being the stronger donating ability of the nitrogen lone pair compared with that of the double bond. This is thought to prevent the η^2-coordination of the substrate to the metal center, which is almost certainly a requirement within a catalytic cycle.[71] In systems which hydrogenate imines under mild conditions, it has been proposed that the nitrogen lone pair is occupied in some manner other than bonding to the metal, as for example in forming hydrogen-bonds with a coordinating solvent molecule.[72] Binding sites at the pocket of dinuclear complexes meet adequate features to favor the required η^2-coordination of the C=N moiety, since after the σ coordination of the substrate to one of the metals, the additional center nearby could coordinate it in a π fashion. This coordination and the subsequent fast insertion of the imine into a Rh-H bond has been characterized in the dirhodium complex shown in Scheme 20.[73] Similar insertion pathways have been suggested for related rhodium mononuclear complexes which hydrogenate imines through dinuclear active species formed under catalytic conditions.[74]

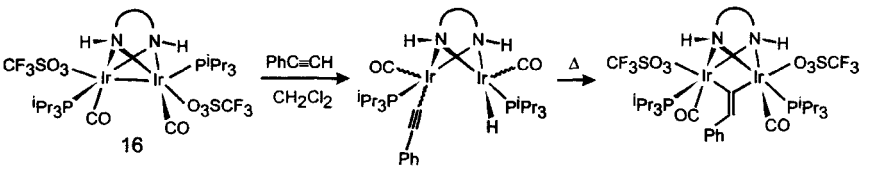

Scheme 21

Scheme 21 shows another example for a transformation involving a hydride migration within a dinuclear complex: a terminal alkyne to vinylidene tautomerization.[49] The observed hydride-alkynyl intermediate of this reaction was though to be formed after an activation process similar to that shown in Scheme 13 for the related complex **8**, followed by the rearrangement of the bridging alkynyl into a terminal ligand. Subsequent hydrogen shift from one metal to the alkynyl β-carbon would lead to the formation of the bridging vinylidene. This latter reaction constitutes an intramolecular version of the bimolecular hydrogen shift mechanism proposed for alkyne to vinylidene transformations, which, on the basis of theoretical calculations, has been found to be energetically favored over mononuclear pathways even for bulky mononuclear compounds.[75] A similar tautomerization reaction, involving also similar observed intermediates, has been found to occur in the diiridium(I) *A-frame* complex $[Ir_2I_2(CO)(\mu\text{-}CO)(dppm)_2]$.[76]

*10.3.1 Dinuclear **trans** effect*

Figure 1 shows the structures, as determined by X-ray diffraction, of two complexes containing a bridging hydride: the cationic 1,8-diamidonaphtalene-bridged complex **15**, [28] and the bis-pyrazolate-bridged complex $[Ir_2(\mu\text{-}H)(\mu\text{-}Pz)_2\{\eta^1\text{-}C_6H_4\text{-}2\text{-}[\eta^1\text{-}(Z)\text{-}C{=}CHPh]\}\{(Z)\text{-}C(Ph){=}CHPh\}(NCCH_3)(P^iPr_3)_2]$(**17**).[77] In both structures, a hydride has been located in the difference Fourier maps bridging the iridium atoms with different distances: 1.87 and 1.74 Å in the case of **15**, and 1.99 and 1.52 Å for complex **17**. Even though the hydride positions obtained from X-ray must be interpreted with some caution, the asymmetric locations of these hydrides agree well with the observed NMR spectra of the complexes. Thus, the ^{1}H NMR signal corresponding to the bridging hydride of **15** displays two very different J_{HP} couplings of 13.2 and 2.1 Hz, and the bridging hydride of **17** is coupled with only one phosphine ligand (J_{HP} = 9.3 Hz). These data also suggest that the asymmetric bridging position of the hydride is maintained in solution.

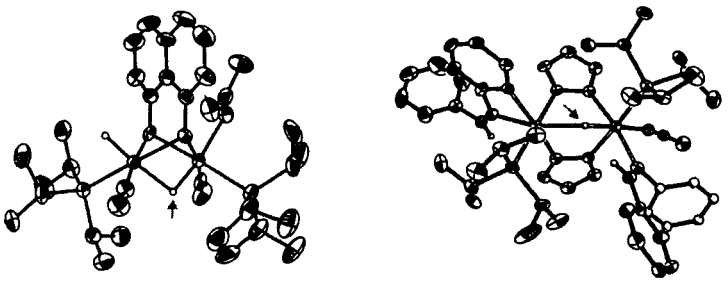

Figure 1. Molecular structures of the cation of complex **15** (left) and the complex **17** (right).

Similar asymmetric M(μ-H)M bridges have been found by X-ray diffraction in complexes such as $[Et_4N][Mo_2(\mu\text{-}H)(CO)_9PPh_3]$ [78] and $[Ru_2(\mu\text{-}H)(\mu\text{-}Pz)_2(cod)_2]$ [79], and by neutron diffraction analysis in compound $[Pt_2(\mu\text{-}H)H(dppe)_2]$ (dppe = $Ph_2PCH_2CH_2PPh_2$). [80]

In the above-mentioned examples, the bridging hydride coordinates *trans* to ligands having very different *trans* influences, hence, the asymmetric position of the hydride was attributed to this fact. In agreement with this explanation, the neutron diffraction analysis of the complex $[Pt_2(\mu\text{-}H)(Ph)_2(PMe_3)_4][BPh_4]$, in which the hydride coordinates *trans* to two phenyl ligands, revealed two equal Pt-H distances. [81] Furthermore, in compound $[Pt_2(\mu\text{-}H)(H)(Ph)_2(PMe_3)_2][BPh_4]$ having two good *trans* labilizing ligands (H and Ph) *trans* to the bridging hydride, two nearly equal Pt-H distances were observed by neutron diffraction.[82]

The two compounds of Figure 2 represent another example for the sensitivity of the bridging hydride position to the *trans* influence of the ligands, and also illustrate how this small structural detail can dramatically affect the reactivity of the compounds.

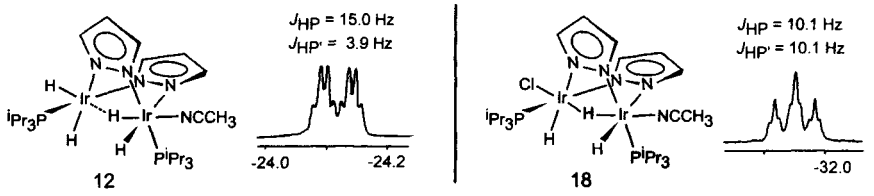

Figure 2. Complexes **12** and **18** and their respective ^{1}H NMR signals corresponding to the bridging hydride.

Thus, whereas the chloro-trihydride complex **18** contains a symmetric hydride bridge, and is inert towards the substitution of the acetonitrile ligand, the tetrahydride **12**, which contains an asymmetric bridge, readily dissociates acetonitrile ($\Delta H^{\ddagger}$= 21 kcal mol^{-1}), favoring substitution processes, small molecule activation reactions, and catalytic hydrogenation. [40] This difference in reactivity results from the ability of the bridging hydride to transmit the *trans* influence of a ligand bonded to one metal center to the other metal center, by tuning its relative position between the metals. In kinetic terms, this result shows that there is a transmission of *trans* effects from one side of the dinuclear framework to the other, via the bridging hydride.

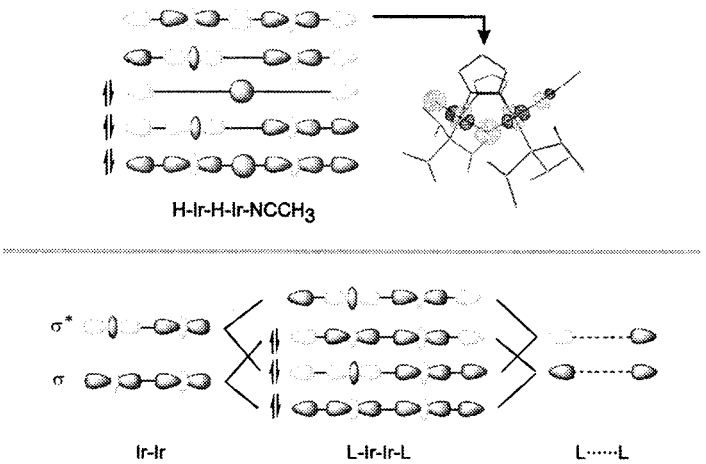

Figure 3. Above: Schematic representation of the molecular orbitals calculated for the hydride bridged complex **12**. Below: Schematic representation of the molecular orbitals calculated for a generic diiridium(II) complex.

The occurrence of this *trans* effect transmission is consistent with the molecular orbital scheme calculated for **12**, which shows a strong mixing of the σ orbitals of the H-Ir-H-Ir-$NCCH_3$ backbone (Figure 3). [40] This could permit the transmission of a *trans* effect due to a σ-bonding ligand from one extreme of the molecule to the other.

The set of σ molecular orbitals calculated for the complexes containing a bridging hydride is essentially similar to the orbital situation predicted for a diiridium(II) complex containing a metal-metal bond,[83] which is schematically shown also in Figure 3. From this Scheme, and taking into account the behavior of the hydrido bridged compounds, it seems very likely that *trans* influences and *trans* effects could also be transmitted from one metal to another in complexes containing metal-metal bonds, which constitute a very abundant class of complexes.

Indeed, the transmission of *trans* influences through Au(II)-Au(II) bonds has been suggested to rationalize the structural features found in bis(ylide) complexes containing L-Au-Au-L' backbones, since the Au-L bond distances seem to be controlled by the L' *trans* ligand influences, while the Au-Au bond lengths remain unaffected.[84] Moreover, the behavior towards CO of the two Ir(III)Ir(I) isomers of Scheme 22 indicates that ligand *trans* effects are also transmitted through the Ir-Ir dative bond of these compounds.[18,29] Thus, the coordination of CO to the isomer having a strong *trans* labilizing methyl group in the axial position has been found to be weak (reversible), whereas upon the same treatment the other isomer afforded a stable adduct.[85]

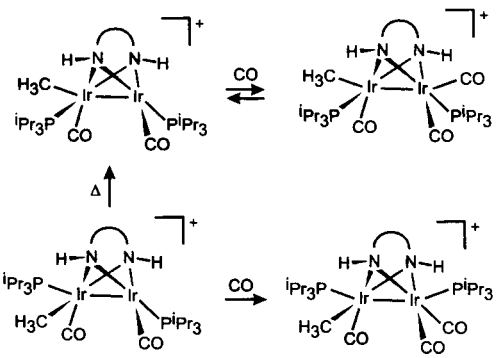

Scheme 22

This latter observation, together with the reactivity differences outlined for the complexes of Figure 2, are clear examples showing how the reactivity of a metal center in a dinuclear complex can be altered by modification of the other metal center. In these examples, electronic information was transmitted between the metal centers in the form of dinuclear *trans* effects, but this is probably just one of the various possible ways for intermetallic relationships within dinuclear compounds.[86, 87]

10.4 DINUCLEAR HYDRIDES IN CATALYSIS

The preceding pages contain several representative examples for stoichiometric reactions occurring with dinuclear compounds, including activations of small molecules, insertions, and isomerizations. Even though the intimate mechanistic details of these reactions are, in most cases, still unknown, it is apparent that the processes display features that are different from those typically found with mononuclear complexes. Thus, most of the reactions mentioned involve either the combination of fragments initially bonded to different metals, or the breaking of molecules to give fragments that end in different metals. Therefore, it appears likely that the participation of such steps in catalytic transformations could result in peculiar selectivities or distinct kinetics. Because of the latter, elementary steps similar to those aforementioned have been commonly employed to work out mechanistic proposals which attempt to explain why in some cases dinuclear catalyst precursors perform differently, and occasionally more efficiently, than closely related mononuclear catalysts.[88, 89, 90] The involvement of dinuclear active hydrides, or the occurrence of key dinuclear steps involving hydride migrations, has been reported for catalytic processes such as hydrogenations,[12, 42-44, 74,75, 91, 92, 93] hydrosilylations,[70] carbonylations,[94] and hydroformylations.[69, 95, 96, 97] Nevertheless, some of these mechanistic proposals are still controversial.[95, 98, 99]

An exceptional case of catalytic performance, likely involving dinuclear elementary steps, is provided by the cationic dirhodium complex of formula $[Rh_2(nbd)_2L]^{2+}$, where L is the racemic diastereomer of the tetraphosphine $(Et_2PCH_2CH_2)(Ph)PCH_2P(Ph)(CH_2CH_2PEt_2)$.[100] This compound was found to be an excellent hydroformylation catalyst for olefins such as propylene, 1-hexene and 1-octene, combining high regioselectivity with high activity. The latter was more than two orders of magnitude higher than the activity shown under the same conditions by related $[Rh(nbd)(P_2)]^+$ mononuclear complexes. On the basis of spectroscopic (IR and NMR) observations of the catalytic reactions, a mechanism containing dinuclear steps such as hydride migrations and dinuclear reductive eliminations, has been proposed. A simplified form of the proposed cycle is depicted Scheme 23. In favor of this dinuclear mechanism, it was observed that the introduction of spacers in the L ligand, in order to disfavor the intermetallic interactions, resulted in poor and non-selective catalysts.

The possible pathways for intermetallic cooperation during catalysis are not restricted to dinuclear elementary steps such as those already mentioned. It has been shown that genuine dinuclear mechanisms can operate in unsaturated species where the metals are capable of sharing coordination vacancies. This is possible through processes of vacancy migrations between metals, which are the consequence of the high mobility of hydrides combined with the transmission of *trans* effects within the dinuclear frames. This phenomenon can be illustrated

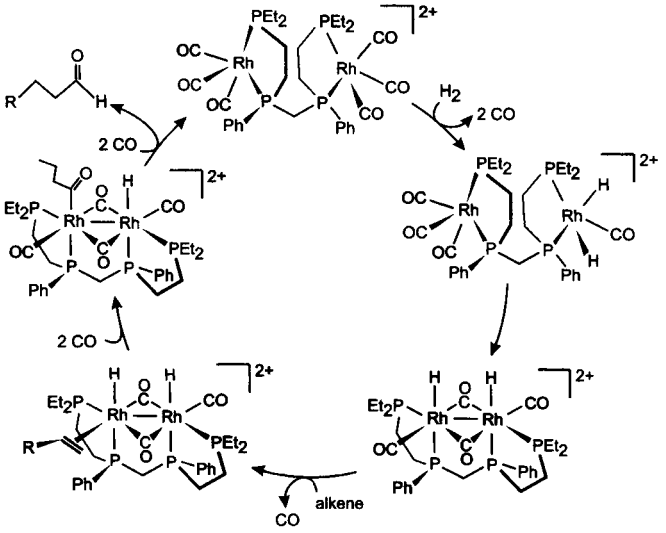

Scheme 23

by the insertion reaction shown in Scheme 24.[40] The reaction of pyrazole with the dinuclear ethylene complex attempted to trap the ethyl complex formed after insertion of ethylene into an Ir-H bond. Indeed, the ethyl compound was trapped but its structure differed from that expected, since the alkyl moiety and the incoming ligand were found to be coordinated to different metal centers.

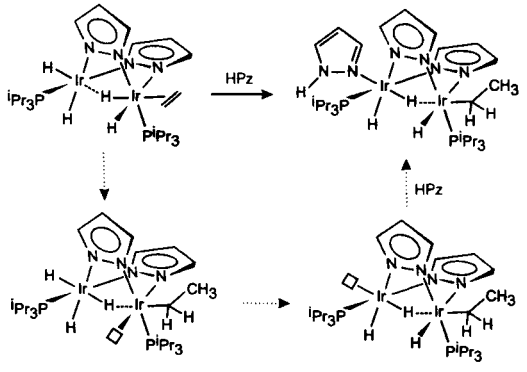

Scheme 24

The formation of this ethyl complex can be rationalized assuming that the vacancy generated by the insertion step migrates to the position labilized by the large *trans* effect of the alkyl group. Actually, this position lies at the other extreme of the molecule, as a result of the transmission of the *trans* effect through the bridging hydride.

The coordination vacancy migrations permit the concerted use of the two potentially labile positions of these complexes, those *trans* to the bridging hydride, for substrate coordination and product release. This brings along catalytic hydrogenation cycles which are dinuclear, since both metals participate in each turnover, even though all the elementary steps involved are single-metal transformations. The Scheme 25 shows the cycle deduced for the hydrogenation of diphenylacetylene to *cis*-stilbene, catalyzed by complex **12**.[77]

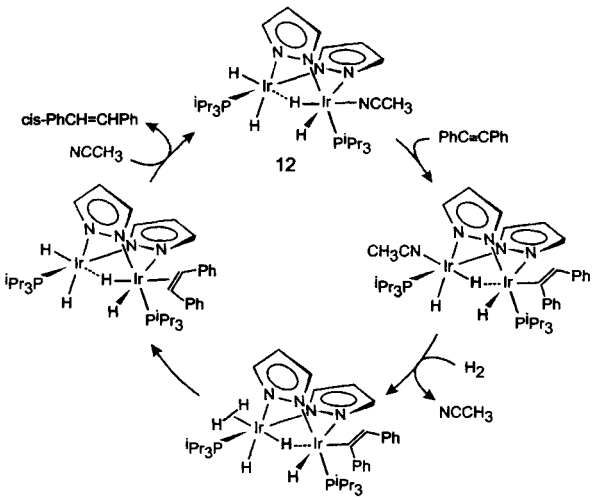

Scheme 25

In a way similar to that previously shown for ethylene, the reaction of **12** with the alkyne leads to a compound in which the vinyl moiety and the labile acetonitrile ligand are situated on different metal centers. Dissociation of the acetonitrile from this intermediate would provide a reaction site for hydrogen, leading to the formation of *cis*-stilbene. Since the olefin is formed at a labile coordination position of the complex, it can be easily released to restart the catalytic cycle. In favor of this mechanism, when the vinyl intermediate species was reacted with D_2, non-deuterated *cis*-stilbene together with deuterated isotopomers of **12** were formed.

Further support of this dinuclear mechanism has been provided by the observation of an alternative mononuclear route, which leads to a different selectivity in the reaction products, and which operates in compounds closely related to **12** where one of the labilized positions is blocked.[77] This is the case for complex **17**, in which one of the positions *trans* to the bridging hydride is not available due to the orthometallation of a vinyl ligand (Scheme 26). Under such conditions, alkyne hydrogenation using the only available labile position is still pos-

sible, but the alkene is now formed at a non-labile position *trans* to pyrazolate. The consequence is that the release of alkene is hindered, and reaction product is now the alkane.

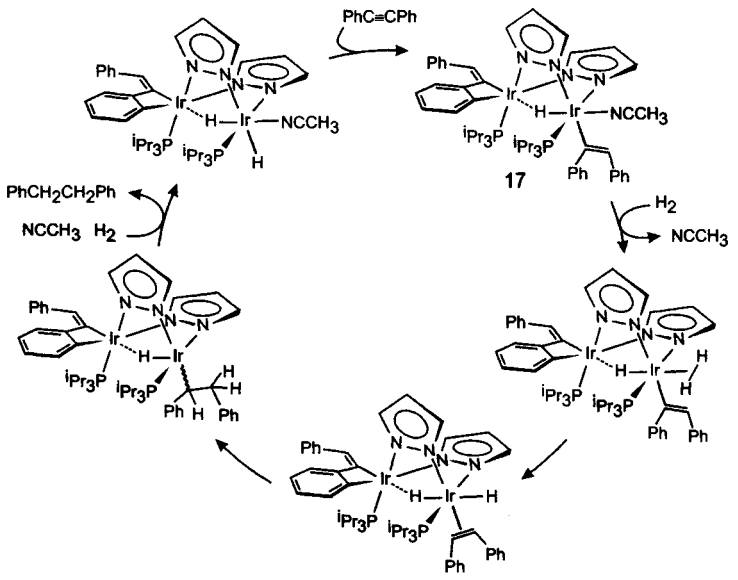

Scheme 26

The dinuclear mechanism of Scheme 25 allows the hydrogenation of alkenes and alkynes under very mild conditions, and has been shown to be favored over the mononuclear pathway of Scheme 26.[77] This is in contrast to the situation found for the dirhodium catalysts precursor $[Rh(\mu\text{-}H)(P^iPr_2(CH_2)_n{}^iPr_2P)]_2$, in which the hydrogenation of styrene catalyzed by mononuclear fragments was shown to be favored over a possible dinuclear mechanism.[12d]

10.5 CONCLUDING REMARKS

The existence of bridging coordination sites, and the possibility of metal-metal bonds or interactions typify the chemistry of dinuclear compounds. Not surprisingly, the chemistry analyzed along the preceding pages points to these characteristics as the ultimate causes for the distinctive reactivity and catalytic performance displayed by dinuclear hydrides. The bridging coordination sites allow the migration of hydrides along the dinuclear frameworks, a process which causes unusual reactivity patterns, unexpected selectivities, and dinuclear cata-

lytic cycles. In addition, dinuclear coordination sites offer adequate environments for the activation of substrates such as imines, dihydrogen, and even dinitrogen. Weak metal-metal interactions could cause a relative decrease in the affinity for dihydrogen of d^8 compounds. In turn, metal-metal bonds seem to be adequate sources of electron density to effect dihydrogen activation. Both bridging hydrides and metal-metal bonds constitute channels for the transmission of electronic information between metals, in the form of *trans* effects. Such electronic effects can also drive intermetallic cooperation during catalysis.

ACKNOWLEDGEMENTS

The authors' own work described in this chapter has received financial support from the Spanish Dirección de Investigación Científica y Técnica (DGICYT), under the projects: PB94-1186, PB95-0318 and BQU2000-1170. We gratefully acknowledge the efforts of the co-workers involved in these studies: M. Victoria Jiménez, Francisco Torres, José A. López, Anabel Elduque, Ana P. Martínez and Fernando J. Lahoz. Our special gratitude goes to Prof. Helmut Werner and Prof. Vladimir I. Bakhmutov for their stimulating discussions and collaborations.

REFERENCES

1 See for example: (a) M. A. Esteruelas, M. P. García, A. M. López and L. A. Oro, Organometallics, 10 (1991) 127. (b) X.-X. Zhang and B. Wayland, J. Am. Chem. Soc., 116 (1994) 7897.
2 P. J. Hay, in A. Dedieu (ed.), Transition Metal Hydrides, VCH, New York 1992, p. 309.
3 P. P. Deutsch and R. Eisenberg, Chem. Rev., 88 (1988) 1147.
4 G. Trinquier and R. Hoffmann, Organometallics, 3 (1984) 370.
5 A. Sevin, Y. Hengtai and P. Chaquin, J. Organometal. Chem., 262 (1984) 391.
6 S. M. Oldham, J. F. Houlis, C. J. Sleigh, S. B. Duckett and R. Eisenberg, Organometallics, 19 (2000) 2985.
7 R. McDonald and M. Cowie, Inorg. Chem., 32 (1993) 1671.
8 B. A. Vaartstra and M. Cowie, Inorg. Chem., 28 (1989) 3138.
9 D. S. A. George, R. McDonald and M. Cowie, Organometallics, 17 (1998) 2553.
10 B. R. Sutherland and M. Cowie, Organometallics, 4 (1985) 1801.
11 B. R. Sutherland and M. Cowie, Organometallics, 4 (1985) 1637.
12 The reported examples include the single-metal additions to the catalyst precur-

sors $[Rh(\mu\text{-}Cl)(PPh_3)_2]_2$, $[Rh(\mu\text{-}H)(P(OR)_3)_2]_2$ and $[Rh(\mu\text{-}H)(P^iPr_2(CH_2)_n{}^iPr_2P)]_2$, as well as a similar reversible addition to the complex $[Ir_2(COD)(PNNP)]BF_4$ (PNNP = 2,4-diphenylphosphinomethyl-pyrazolate). Since these complexes have either (presumably) labile chloride or hydride bridges, or rather distant metal centers, they have not be considered for this discussion. See: (a) J. Halpern, Inorg. Chim. Acta, 62 (1982) 31. (b) E. L. Muetterties, Inorg. Chim. Acta, 50 (1981) 1. (c) E. B. Meier, R. R. Burch and E. L. Muetterties, J. Am. Chem. Soc., 104 (1982) 2661. (d) M. D. Fryzuk, W. E. Piers, F. W. B. Einstein and T. Jones, Can. J. Chem. 67 (1989) 883. (e) T.G. Shenck, J. M. Downes, C. R. C. Milne, P. B. Mackenzie, H. Boucher, J. Whelan and B. Bosnich, Inorg. Chem., 24 (1985) 2334.

13 J. S. Field, R. J. Haynes, M. W. Stewart, J. Sundermeyer and S. F. Woollam, J. Chem. Soc., Dalton Trans., (1993) 947.

14 T. Gottschalk-Gaudig, J. C. Huffman, H. Gérard, O. Eisenstein and K. G. Caulton, Inorg. Chem., 39 (2000) 3957.

15 A. M. Arif, D. E. Heaton, R. A. Jones, K. B. Kidd, T. C. Wright, B. C. Whittlesey, J. L. Atwood, W. E. Hunter and H. Zhang, Inorg. Chem., 26 (1987) 4065.

16 (a) J. J. Bonnet, A. Thorez, A. Maisonnat, J. Galy and R. Poilblanc, J. Am. Chem. Soc., 101 (1979) 5940. (b) R. Poilblanc, Inorg. Chim. Acta, 62 (1982) 75.

17 E. Guilmet, A. Maisonnat and R. Poilblanc, Organometallics, 2 (1983) 1123.

18 For some representative examples see: M. V. Jiménez, E. Sola, M. A. Egea, A. Huet, A. C. Francisco, F. J. Lahoz and L. A. Oro, Inorg. Chem., 39 (2000) 4868 and references therein.

19 (a) L. A. Oro, M. A. Ciriano and C. Tejel, Pure Appl. Chem., 70 (1998) 779. (b) C. Tejel, M. A. Ciriano, A. J. Edwards, F. J. Lahoz and L. A. Oro, Organometallics, 16 (1997) 45.

20 G. Aullón, G. Ujaque, A. Lledós, S. Alvarez and P. Alemany, Inorg. Chem., 37 (1998) 804.

21 G. Aullón, G. Ujaque, A. Lledós and S. Alvarez, Chem. Eur. J., 5 (1999) 1391.

22 D. L. Lichtenberger, A. S. Copenhaver, H. B. Gray, J. L. Marshall and M. D. Hopkins, Inorg. Chem., 27 (1988) 4488.

23 J. Halpern and S. Wong, J. Chem. Soc. Chem. Commun., (1973) 629.

24 M. Rakowski DuBois, Chem. Rev., 89 (1989) 1.

25 C. Bianchini, C. Mealli, A. Meli and M. Sabat, Inorg. Chem., 25 (1986) 4618.

26 M. Rakowski Dubois, in R. A. Adams and F. A. Cotton (Eds.), Catalysis by Di- and Polynuclear Metal Cluster Complexes, Wiley-VCH, New York 1998, p. 127.

27 A. F. Heyduk and D. Nocera, J. Am. Chem. Soc., 122 (2000) 9415.

28 M. V. Jiménez, E. Sola, J. A. López, F. J. Lahoz and L. A. Oro, Chem. Eur. J., 4 (1998) 1398.

29 L. A. Oro, E. Sola, J. A. López, F. Torres, A. Elduque and F. J. Lahoz, Inorg. Chem. Commun., 1 (1998) 64.

30 M. Nishio, Y. Mizobe, H. Matsuzaka and M. Hidai, Inorg. Chim. Acta, 265 (1997) 59.

31 D. M. Heinekey, D. A. Fine and D. Barnhart, Organometallics, 16 (1997) 2530.

32 W. D. McGhee and R. G. Bergman, J. Am. Chem. Soc., 108 (1986) 5621.

33 C. P. Casey, H. Sakaba, P. N. Hazin and D. R. Powell, J. Am. Chem. Soc., 113 (1991) 8165.

34 M. L. H. Green and P. Mountford, J. Chem. Soc., Chem. Commun., (1989) 732.
35 (a) A. P. Sattelberger, R. B. Wilson, Jr. and J. C. Huffman, J. Am. Chem. Soc., 102 (1980) 7111. (b) C. Ting, N, Baenziger and L. Messerle, J. Chem. Soc., Chem. Commun., (1988) 1133.
36 A. M. Baranger and R. G. Bergman, J. Am. Chem. Soc., 116 (1994) 3822.
37 M. D. Fryzuk, J. B. Love, S. J. Rettig and V. G. Young, Science, 275 (1997) 1445.
38 J. P. Collman, J. E. Hutchison, P. S. Wagenknecht, N. S. Lewis, M. A. Lopez and R. Guilard, J. Am. Chem. Soc., 112 (1990) 8206.
39 (a) A. Takahashi, Y. Mizobe, H. Matsuzaka, S. Dev and M. Hidai, J. Organomet. Chem., 456 (1993) 243. (b) M. Hidai, Y. Mizobe and H. Matsuzaka, J. Organomet. Chem. 473 (1994) 1.
40 E. Sola, V. I. Bakhmutov, F. Torres, A. Elduque, J. A. López, F. J. Lahoz, H. Werner and L. A. Oro, Organometallics, 17 (1998) 683.
41 (a) P. J. Alaimo and R. G. Bergman, Organometallics, 18 (1999) 2707. (b) S. R. Klei, T. D. Tilley and R. G. Bergman, J. Am. Chem. Soc., 122 (2000) 1816.
42 (a) A. M. Joshi and B. R. James, J. Chem. Soc., Chem. Commun., (1989) 1785. (b) C. R. S. M. Hampton, I. R. Butler, W. R. Cullen, B. R. James, J. P. Charland, and J. Simpson, Inorg. Chem., 31 (1992) 5509. (c) D. E. K-Y. Chau and B. R. James, Inorg. Chim. Acta, 240 (1995) 419. (d) A. M. Joshi, K. S. MacFarlane and B. R. James, J. Organometal. Chem., 408 (1995) 161. (e) A. Mezzetti, A. Tschumper and G. Consiglio, J. Chem. Soc., Dalton Trans., (1995) 49.
43 C. Bianchini, P. Barbaro, G. Scapacci and F. Zanobini, Organometallics, 19 (2000) 2450.
44 C. Hampton, W. R. Cullen and B. R. James, J. Am. Chem. Soc., 110 (1988) 6918.
45 Z. He, S. Nefedov, N. Lugan, D. Neibecker and R. Mathieu, Organometallics, 12 (1993) 3837.
46 M. A. Esteruelas and L. A. Oro, Chem Rev., 98 (1998) 577.
47 F. H. Antwi-Nsiah, O. Oke and M. Cowie, Organometallics, 15 (1996) 1042.
48 A. T. Hutton, P. G. Pringle and B. L. Shaw, Organometallics, 2 (1983) 1889.
49 M. V. Jiménez, E. Sola, A. P. Martínez, F. J. Lahoz and L. A. Oro, Organometallics, 18 (1999) 1125.
50 (a) S. S. Kristjándsdóttir and J. R. Norton, in A. Dedieu (ed.), Transition Metal Hydrides, VCH, New York 1992, p. 309. (b) K. W. Kramarz and J. R. Norton, Prog. Inorg. Chem., 42 (1994) 1.
51 F. Safiq and R. Eisenberg, J. Organomet. Chem., 472 (1994) 337.
52 C. Bianchini, K. Linn, D. Masi, M. Peruzzini, A. Polo, A. Vacca and F. Zanobini, Inorg. Chem., 32 (1993) 2366.
53 R. C. Schnabel and D. M. Roddick, Organometallics, 15 (1996) 3550.
54 A. Albinati, T. J. Emge, T. F. Koetzle, S. V. Meille, A. Musco and L. M. Venanzi, Inorg. Chem., 25 (1986) 4812.
55 R. C. Schnabel, P. S. Carroll and D. Roddick, Organometallics, 15 (1996) 655.
56 Y. Ohki and H. Suzuki, Angew. Chem., Int. Ed., 39 (2000) 3120.
57 T. Albright, J. K. Burdett and M.-H. Whangbo, Orbital Interactions in Chemistry, Wiley, New York, 1980.
58 L. M. Venanzi, Coord. Chem. Rev., 43 (1982) 251, and references therein.
59 (a) J. Powell, M. R. Gregg and J. F. Sawyer, J. Chem. Soc., Chem. Commun.,

(1987) 1029. (b) T. M. Gilbert and R. G. Bergman, J. Am. Chem. Soc., 107 (1985) 3502. (c) H. Suzuki, T. Takao, M. Tanaka and Y. Moro-oka, J. Chem. Soc., Chem. Commun., (1984) 1398. (d) M. Jahncke, G. Meister, G. Rheinwald, H. Stoekli-Evans and G. Süss-Fink, Organometallics, 16 (1997) 1137.

60 R. H. Crabtree, Acc. Chem. Res., 12 (1979) 126.

61 T. M. Gomes Carneiro, D. Matt and P. Braunstein, Coord. Chem. Rev. 96 (1989) 49.

62 (a) K. G. Anderson, Adv. Organometal. Chem. 35 (1993) 1. (b) A. Albinati and L. M. Venanzi, Coord. Chem. Rev., 200-202 (2000) 687.

63 V. Branchadell and A. Dedieu, New. J. Chem., 12 (1988) 443.

64 (a) H. Werner, M. Treiber, A. Nessel, F. Lippert, P. Betz and C. Kruger, Chem. Ber., 125 (1992) 337. (b) D. M. Heinekey, D. A. Fine, G. P. Harper and S. T. Michel, Can. J. Chem., 73 (1995) 1116.

65 M. V. Jiménez, E. Sola, A. P. Martínez, F. J. Lahoz and L. A. Oro, manuscript in preparation.

66 T. Shima and H. Suzuki, Organometallics, 19 (2000) 2420.

67 R. H. Crabtree, The Organometallic Chemistry of the Transition Metals, John Wiley and Sons, New York 1988, p. 148.

68 (a) M. A. Esteruelas, J. Herrero and L. A. Oro, Organometallics, 12 (1993) 2377. (b) I. Ojima, N. Clos, R. J. Donovan and P. Ingallina, Organometallics, 9 (1990) 3127. (c) R. S. Tanke and R. H. Crabtree, J. Chem. Soc., Chem. Commun., (1990) 1056. (d) A. Mori, E. Takahisa, H. Kajiro, Y. Nishihara and T. Hiyama, Polyhedron, 19 (2000) 567.

69 (a) B. D. Martin, K. E. Warner and J. R. Norton, J. Am. Chem. Soc., 108 (1986) 33. (b) M. J. Nappa, R. Santi and J. Halpern, Organometallics, 4 (1985) 34. (c) Y. Koyasu, A. Fukukoa, Y. Uchida and M. Hidai, Chem. Lett., (1985) 1083. (d) J. P. Collman, J. A. Belmont and J. I. Brauman, J. Am. Chem. Soc., 105 (1983) 7288. (e) F. Ungváry and L. Markó, Organometallics, 2 (1983) 1608. (f) W. D. Jones, J. M. Huggins and R. G. Bergman, J. Am. Chem. Soc., 103 (1981) 4415.

70 (a) K. Osakada, J. Organomet. Chem., 611 (2000) 323. (b) K. Osakada, T. Koizumi and T. Yamamoto, Organometallics, 16 (1997) 2063. (c) M. Fryzuk, L. Rosenberg and S. J. Rettig, Organometallics, 15 (1996) 2871.

71 B. R. James, in B. Marciniec and J. J. Ziolkowski (eds.), Education in Advanced Chemistry, Vol 2., Poznan-Wroclaw, 1996 p. 83.

72 (a) C. J. Longley, T. Goodwin and G. Wilkinson, Polyhedron, 5 (1986) 1625. (b) A. G. Becalski, W. R. Cullen, M. D. Fryzuk, B. R. James, G-J. Kang and S. J. Rettig, Inorg. Chem., 30 (1991) 5002.

73 M. D. Fryzuk and W. E. Piers, Organometallics, 9 (1990) 986.

74 G. E. Ball, W. R. Cullen, M. D. Fryzuk, W. J. Henderson, B. R. James and K. S. MacFarlane, Inorg. Chem., 33 (1994) 1464.

75 Y. Wakatsuki, N. Yoga, H. Werner and K. Morokuma, J. Am. Chem. Soc., 119 (1997) 360.

76 J. Xiao and M. Cowie, Organometallics, 12 (1993) 463.

77 F. Torres, E. Sola, A. Elduque, A. P. Martínez, F. J. Lahoz and L. A. Oro, Chem. Eur. J., 6 (2000) 2120.

78 M. Y. Darensbourg, J. L. Atwood, R. R. Burch, jr., W. E. Hunter and N. Walker, J. Am. Chem. Soc., 101 (1979) 2632.

79 (a) T. V. Ashworth, D. C. Liles and E. Singleton, J. Chem. Soc., Chem. Commun, (1984) 1317. (b) M. O. Albers, S. F. A. Crosby, D. C. Liles, D. J. Robinson, A. Shaver and E. Singleton, Organometallics, 6 (1987) 2014.
80 M. Y. Chiang, R. Bau, G. Minghetti, A. L. Bandini, G. Banditelli and T. F. Koetzle, Inorg. Chem., 23 (1984) 124.
81 A. Albinati, S. Chaloupka, J. Eckert, L. M. Venanzi and M. K. Wolfer, Inorg. Chim. Acta, 259 (1997) 305.
82 A. Albinati, G. Bracher, D. Carmona, J. H. P. Jans, W. T. Klooster, T. F. Koetzle, A. Macchioni, J. S. Ricci, R. Thouvenot and L. M. Venanzi, Inorg. Chim. Acta, 265 (1997) 255.
83 C. Tejel, M. A. Ciriano, J. A. López, F. J. Lahoz, and L. A. Oro, Organometallics, 17 (1998) 1449.
84 (a) H. H. Murray, J. P. Fackler, jr., and B. Trzcinska-Bancroft, Organometallics, 4 (1985) 1633. (b) A. Laguna, M. Laguna, J. Jiménez, F. J. Lahoz and E. Olmos, J. Organomet. Chem., 435 (1992) 235.
85 E. Sola, S. E. Ruiz, J. A. López, M. V. Jiménez, F. Torres, A. Elduque, F. J. Lahoz and L. A. Oro, manuscript in preparation.
86 B. Bosnich, Inorg. Chem., 38 (1999) 2554.
87 G. Aullón, P. Alemany and S. Alvarez, J. Organomet. Chem., 478 (1994) 75.
88 R. A. Adams and F. A. Cotton (Eds.), Catalysis by Di- and Polynuclear Metal Cluster Complexes, Wiley-VCH, New York 1998.
89 E. K. van der Beuken and B. L. Feringa, Tetrahedron, 54 (1998) 12985.
90 P. A. Chaloner, M. A. Esteruelas, F. Joó and L. A. Oro, Homogeneous Hydrogenation, Kluwer, Dordrecht 1993, p. 56.
91 C. Bianchini, A. Meli, F. Laschi, J. A. Ramirez, P. Zanello and A. Vacca, Inorg. Chem., 27 (1988) 4429.
92 S. Ogo, N. Makihara and Y. Watanabe, Organometallics, 18 (1999) 5470.
93 (a) M. Cowie and T. G. Southern, Inorg. Chem., 21 (1982) 246. (b) C. P. Kubiak, C. Woodcock and R. Eisenberg, Inorg. Chem., 21 (1982) 2119.
94 P. Kalck, C. Serra, C. Machet, R. Broussier, B. Gautheron, G. Delmas, G. Trouvé and M. Kubicki, Organometallics, 12 (1993) 1021.
95 J. C. Bayón, C. Claver and A. M. Masdeu-Bultó, Coord. Chem. Rev., 193-195 (1999) 73.
96 P. Kalck, Polyhedron, 7 (1988) 2441.
97 L. Gelmini and D. W. Stephan, Organometallics, 7 (1988) 849.
98 R. Davis, J. W. Epton and T. G. Southern, J. Mol. Catal., 77 (1992) 159.
99 M. Garland, Organometallics, 12 (1993) 535.
100 (a) M. E. Broussard, B. Juma, S. G. Train, W.-J. Peng, S. A. Laneman and G. G. Stanley, Science, 260 (1993) 1784. (b) G. Süss-Fink, Angew. Chem. Int. Ed. Engl., 33 (1994) 67. (c) R. C. Matthews, D. K. Howell, W.-J. Peng, S. G. Train, W. D. Treleaven and G. G. Stanley, Angew. Chem. Int. Ed. Engl., 35 (1996) 2253. (d) G. G. Stanley in reference 88, p. 345.

This Page Intentionally Left Blank

Chapter 11

Mechanistic Aspects of Inorganic Chemistry Probed via the Parahydrogen Phenomenon

S. B. Duckett

Department of Chemistry, University of York, Heslington, York, YO10 5DD, UK

CONTENTS

11.1 INTRODUCTION

The study of reaction mechanisms associated with the activation of simple substrates such as H_2 by co-ordination compounds has produced many interesting observations. Over the last decade these studies have utilised techniques involving fast laser spectroscopy which enable the detection of unsaturated intermediates and the rationalisation of their subsequent reactivity. Indeed, the addition of H_2 to unsaturated metal centres has been shown to proceed through a discrete η^2-H_2 interaction, followed by relaxation to the normally stable metal

dihydride. Remarkably, in certain situations Kubas and others showed the η^2-H_2 form to be stable [1]. More recently similar co-ordination modes have been observed for C-H and Si-H bonds, with the extent of bonding interaction between the incoming centres being controlled by the ligand sphere of the metal.

From a synthetic perspective, one of the easiest routes to prepare a metal dihydride complex remains the direct reaction of a suitable precursor with H_2. Such reactions can be readily monitored by NMR spectroscopy since the associated hydride resonance normally occurs with a characteristically high field shift. It might therefore seem sensible to assume that we also know a great deal about the role of metal hydride complexes in catalytic transformations. Unfortunately, however, the inherent low sensitivity of the NMR approach results in the fact that the most reliably studied reactions correspond to those where the addition step is favourable and high concentrations of metal dihydride are available. Such species might therefore correspond to resting states that lie outside the catalytic cycle. Catalytic action then takes these species through to the final product via many sequential steps of which each features an intermediate that has the opportunity to exist in a variety of isomeric forms, each with its own unique reactivity. Clearly while kinetic evidence, in conjunction with chemical intuition based on detected species, plays a valuable role in the construction of a reaction mechanism, the detection of reaction intermediates themselves remains essential. Halpern and Brown most elegantly illustrated the importance of the detection of minor species in equilibria by their studies on asymmetric hydrogenation. These studies involved the hydrogenation of prochiral enamides by cationic rhodium complexes containing a chiral diphosphine such as DIPAMP. Brown demonstrated through careful NMR studies that the less stable enamide isomer reacted substantially faster with H_2 and was responsible for the observed enatiomeric selectivity in the hydrogenation product [2].

This chapter discusses some of the advancements in awareness that have been facilitated by utilisation of parahydrogen enhanced NMR studies. This effect makes use of the fact that H_2 exists in two forms that differ in the arrangements of their nuclear spins to generate products which contain non-Boltzmann spin populations and are thus easier to detect in the NMR experiment. Bowers and Weitekamp demonstrated this result in 1986 when they monitored the hydrogenation of styrene by Wilkinson's complex using para enriched hydrogen as the substrate [3]. The associated increase in NMR signal strength has since be used to facilitate the study of transition metal dihydride complexes by enabling both the detection of previously unseen intermediates and the exploration of their catalytic role. Several detailed reviews have already been published in this area [4,5,6].

11.2 GENERAL PRINCIPLES OF THE PARAHYDROGEN EFFECT

The *para*-isomer of H_2 has an anti-symmetric spin configuration ($\alpha\beta$–$\beta\alpha$) and the triply degenerate *ortho*-isomers have symmetric spin configurations ($\alpha\alpha$, $\beta\beta$, $\alpha\beta$+$\beta\alpha$). Since the *para* isomer is restricted to symmetric rotational states (J = 0, 2, 4...), and the ortho forms to anti-symmetric states, their population is temperature dependent. However, interconversion between *ortho-* and *para-*forms is forbidden with conversion times approaching one year under normal conditions. Fortunately, interaction with a paramagnetic material enables the rapid interconversion of spin states, and on removal of the catalyst the H_2 is therefore slow to re-establish spin state thermodynamic equilibrium. *Para-*hydrogen enrichment can therefore be achieved in the laboratory by simply cooling H_2 to 77 K in a glass bulb that contains a small amount of iron oxide [7]. After one hour the resulting *para*-enriched H_2 can be transferred to a sample tube on a high vacuum line prior to *in-situ* NMR monitoring.

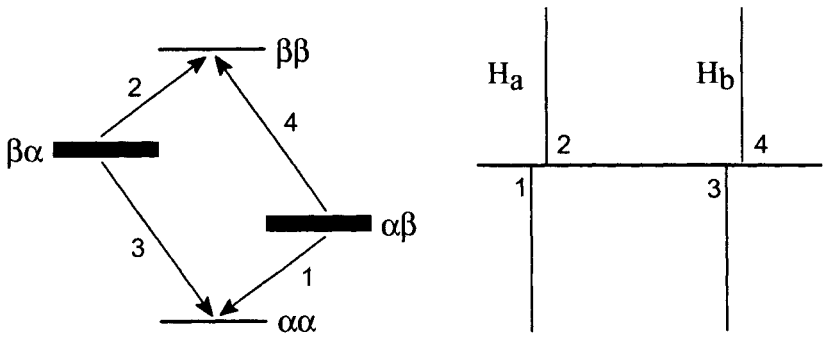

Figure 1. Energy level diagram and ^1H spectral features for a metal dihydride with magnetically distinct protons H_a and H_b. Population differences are indicated for the situation that arises when the product is formed from p-H_2.

The resulting spectral effect can be easily understood by reference to the situation where the metal dihydride product contains two inequivalent hydride ligands, H_a and H_b, that are spin-spin-coupled. Since the nuclear spins of H_a and H_b can be arranged in the orientations $\alpha\alpha$, $\alpha\beta$, $\beta\alpha$, $\beta\beta$ the associated ^1H NMR spectrum consists of two distinct resonances for protons H_a and H_b which are split by the action of the magnetic moment (α or β) of the partner (H_b or H_a). When protons H_a and H_b originate from a single *para*-hydrogen molecule, and the addition process is spin correlated, the starting spin state selectively populates the $\alpha\beta$ and $\beta\alpha$ product states. Consequently, the population differences, and hence signal intensities, for the resonances due to the metal

hydride ligands which show 'emission' and 'absorption' character are enhanced over their normal levels. The 'emission' line comes to higher frequency when J_{HH} is negative, as illustrated in Fig. 1. The results of this process have been referred to by the terms PASADENA (parahydrogen and synthesis allow dramatically enhanced nuclear alignment) [9] and PHIP (parahydrogen induced polarisation) [10] and are rigorously treated elsewhere [5].

11.3 OXIDATIVE ADDITION REACTIONS STUDIED VIA PARAHYDROGEN

The activation of dihydrogen by a metal centre is a key step in homogeneous hydrogenation. Since the process of oxidative addition of hydrogen proceeds to increase the electron count of a metal centre by two units, 16 electron square planar d^8 complexes feature extensively as systems that readily add H_2. Not surprisingly, such systems have also featured in the development of the parahydrogen effect. The first example of p-H_2 addition to form a metal dihydride involved $RhCl(PPh_3)_3$ and was reported by Bowers and Weitekamp. However, since the product $RhH_2Cl(PPh_3)_3$ contains a very labile phosphine ligand the associated signals were rather broad (Fig. 2); we later showed that the corresponding resonances in $RhH_2Cl(PMe_3)_3$ showed much larger enhancements [11]. Eisenschmid *et al* closely followed this report with a description of how the addition of p-H_2 to the related complex IrX(CO)(dppe), where X = CN and Br led to the observation of enhanced hydride resonances for the H_2 addition products $Ir(H)_2X(CO)(dppe)$ [10]. In their later reports, they monitored the addition of p-H_2 to the iridium complexes $Ir(CO)P_2X$ (where X = Br, Cl and P = PPh_3, P_2 = dppe, dppv, dppb) [12] at temperatures where the addition is reversible. For the dppb system, the corresponding hydride resonances were well resolved and their signal enhancement was estimated to be 12 fold at 321 K, with cross relaxation enhancing the corresponding ^{31}P resonances by a factor of 7 [13]. It was later demonstrated that when 0.3 mg of IrBr(CO)(dppe) was reacted with p-H_2 at 342 K in benzene-d_6 the hydride resonances due to $IrH_2Br(CO)(dppe)$ showed a 95 fold increase in signal intensity over their normal level [14]. The hydride resonances of Vaska's dihydride, $IrH_2Cl(CO)(PPh_3)_2$, were found to be 40 fold enhanced under similar conditions. If the degree of signal enhancement is similar for both species, it is possible to conclude that the ratio of H_2 reductive elimination from the dppe system is roughly twice that of the PPh_3 complex. Methods employing direct population transfer in conjunction with p-H_2 have been reported to enable the detection of ^{31}P and ^{13}C signals in these complexes [14]. Impressively, the ^{13}C signal for the carbonyl ligand of $IrH_2Br(CO)(dppe)$ was detected in only 32 scans while using

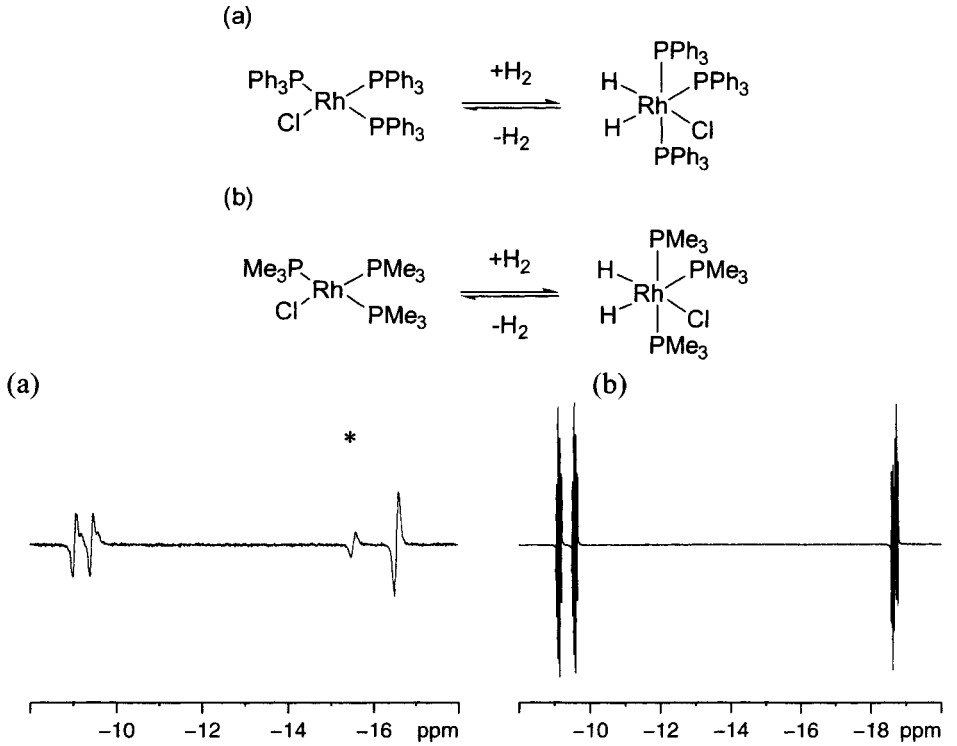

Figure 2. (a) Typical ^{1}H NMR spectrum obtained when $RhCl(PPh_3)_3$ is warmed with p-H_2 to 295 K in the presence of styrene. (* = $Rh(H_2)Cl(PPh_3)_2$(styrene)). (b) ^{1}H NMR spectrum obtained when $RhCl(PMe_3)_3$ is warmed with p-H_2 to 333 K.

0.3 mg of a sample containing ^{13}C at its normal level. Under the same conditions, but using normal H_2, 28 days of acquisition would have been required to achieve the same result.

It is worth noting at this stage that modified COSY, HSQC, HMQC and NOESY sequences can be used in conjunction with the parahydrogen phenomenon. In addition, several other NMR approaches have been developed by reference to parahydrogen incorporation into organic hydrogenation products. The net result of these reports has been to place sufficient information in the literature as to make the utilisation of the p-H_2 effect to characterise reaction intermediates an attractive proposition.

For the d^8 complexes $IrCl(CO)(PPh_3)_2$ and IrCl(CO)(dppe) there is a wide body of evidence to suggest that H_2 addition occurs in a concerted, pairwise manner, and places the hydrides in a mutually *cis* orientation. In the case of Vaska's complex this had been accepted to correspond to addition over the OC-Ir-Cl axis (Fig. 3). However, in the case of IrCl(CO)(dppe), H_2 addition over

the P-Ir-CO axis led to a kinetic product, which subsequently equilibrated with a second isomer that is produced by H_2 addition over the P-Ir-Cl axis. In order to examine what happened when the addition to Vaska's complex was completed under kinetic rather than thermodynamic control we studied the reaction with p-H_2 at 295 K where the addition is irreversible. In the corresponding ^{1}H NMR spectrum polarised hydride resonances were detected for the expected product *cis-trans*-$IrH_2(CO)(PPh_3)_2Cl$ and the new product *cis-cis*-$IrH_2(CO)(PPh_3)_2Cl$. The enhanced hydride resonance associated with this minor species were only visible when $IrCl(CO)(PPh_3)_2$ was available to react with *p*-H_2. Nevertheless, this observation indicated that H_2 addition over the P-Ir-P axis of $IrCl(CO)(PPh_3)_2$ is possible and serves to illustrate the complexity of what was thought to be a simple reaction (Fig. 3). This result is consistent with calculations by Sargent and Hall that revealed that H_2 addition over the OC-Ir-Cl axis rather than the P-Ir-P axis is favoured by 9.5 kJmol^{-1} in the case of $Ir(CO)(PMe_3)_2Cl$ [15]. When the less well known complex, $Ir(CO)(PMe_3)_2Cl$, was examined with p-H_2 both addition products were again detected.

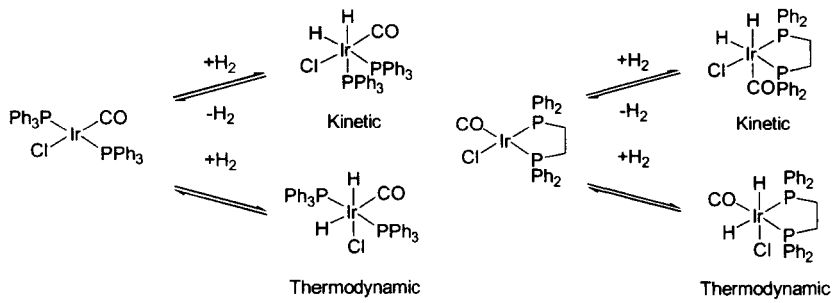

Figure 3. Kinetic and thermodynamic products of H_2 addition to $IrCl(CO)(PPh_3)_2$ and IrCl(CO)(dppe).

The utilisation of parahydrogen induced polarisation to detect minor isomers of metal dihydrides marks one of the most widespread successes of the parahydrogen approach. When the related d^8 complex $Ir(CO)(PPh_3)(Et_2dtc)$ was examined with normal H_2 three dihydride complexes were rapidly formed and their concentrations shown to equilibrate rapidly (Fig. 4). As expected, it proved a simple matter to assign product structures based on the coupling patterns of the hydride resonances [16]. Thus the dihydride isomer producing the hydride resonances at δ -6.11 and δ -15.70 has a *fac* arrangement of the phosphine and hydride ligands (**1**), while the isomer with resonances at δ -7.74 and –16.52 has hydrides *trans* to phosphine and sulfur (**2**). The third species, a minor product, had two equivalent hydrides and a *fac* arrangement for the phosphine and hydrides. With p-H_2 it proved possible to demonstrate that the kinetic selectivity

for **1** over **2** was 170:1. Interestingly, the dominant reaction pathway again corresponds to addition of H_2 over the axis of the starting square planar complex containing the CO ligand. It has been proposed that the CO ligand, and that which is *trans* to it, move into positions corresponding to the equatorial sites in the trigonal bipyramid intermediate. In this position, CO can through back bonding, reduce the repulsive interaction between the filled Ir d_z^2 orbital and the filled σ orbital of the H_2 molecule (see Fig. 5). This interaction has been suggested to contribute significantly to the activation barrier for H_2 addition in such complexes.

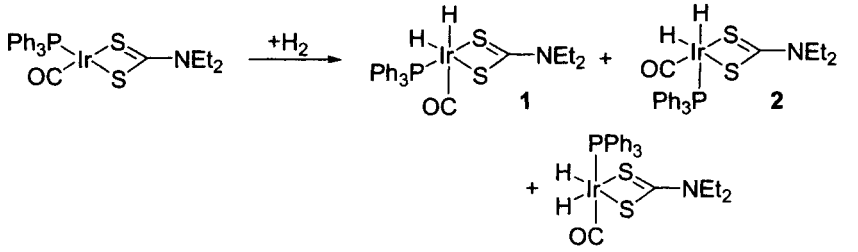

Figure 4. H_2 addition products of $Ir(CO)(PPh_3)(S_2CNEt_2)$.

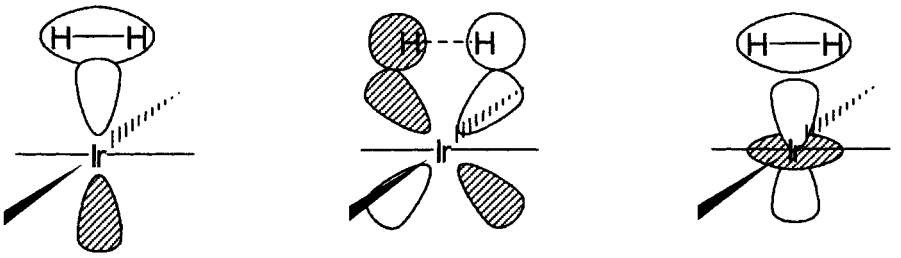

Figure 5. Important orbital interactions during H_2 addition to a square planar Ir(I) complex: σ-$H_2 \leftrightarrow p_z$, σ^*-$H_2 \leftrightarrow d_{xz}$ or d_{yz} and σ-$H_2 \leftrightarrow d_z^2$.

For d^{10} complexes of Pt(0), the addition of H_2 was also presumed to take place in a concerted manner although the evidence in this regard was less compelling. With p-H_2 definitive evidence for the pairwise addition of dihydrogen was however readily obtained. In order to achieve this it was necessary to first prepare a product in which the transferred protons are magnetically distinct. The unsymmetrical bidentate ligand $Ph_2PCH_2CH(Me)OPPh_2$ ((dpp)$_2$mop) was selected for this task and the corresponding dihydride complex $Pt(H)_2$((dpp)$_2$mop) synthesised [17]. When this complex was monitored with p-H_2, the signals corresponding to the two hydride ligands at δ -0.282 and -0.014 were estimated to be enhanced by a factor of 1600. Interestingly, the phase of the hydride

signals polarisation (A/E) indicated that the sign of the J_{HH} coupling constant was positive. These results severed to establish unequivocally that addition of H_2 to Pt((dpp)$_2$mop) proceeded via a pairwise mechanism.

The reactions of stable 18 electron complexes such as $RuH_2(CO)_2L_2$ (L = $AsMe_2Ph$, PMe_2Ph and PMe_3) have also been monitored with p-H_2. In this case, the detection and conclusive identification of minor isomers of these complexes was facilitated by rapid free H_2 - RuH_2 exchange. For L = $AsMe_2Ph$, the *trans-cis-cis* (*tcc*) and all-*cis* (*ccc*) dihydrides are observable under normal conditions (Fig. 6). This fact enabled the hydride resonances of the all-*cis* isomer to be shown to be 1035 fold enhanced at 343 K [18]. However, when a C_6D_6 solution containing <1 mg of $[Ru(PMe_3)_2(CO)_2(H)_2]$ was monitored under normal-H_2 only the *tcc* isomer was observed after 10,000 scans. It was only with p-H_2 that evidence for the elusive *ccc* isomer was obtained. Equilibria have now been shown to exist between *ccc* and *tcc* forms of $RuH_2(CO)_2L_2$ for L = $AsMe_2Ph$, PMe_3, PPh_3 and PMe_2Ph. In the case of L = $AsMe_2Ph$ $k_{tcc\text{-}ccc}$ = 0.21 s^{-1}, $k_{ccc\text{-}tcc}$ = 0.21 s^{-1} and K = 1. In addition, it was reported that the introduction of a ^{13}CO label made the major *tcc* isomer p-H_2 active by virtue of the second order spin system that it created (Fig. 6). This represented the first report of p-H_2 activity in a system containing a square planar $MH_2(CO)(^{13}CO)$ core and served to illustrate that the need for magnetically distinct hydrides could be satisfied synthetically.

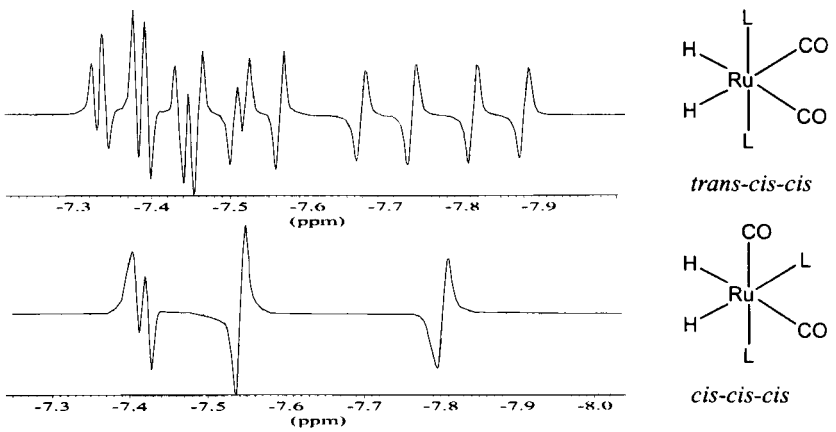

Figure 6. NMR spectra obtained by warming $Ru(H)_2(^{13}CO)_2(PMe_3)_2$ with p-H_2 to 343 K. (a) ^1H NMR spectrum (b) $^1H\{^{31}P\}$ NMR spectrum.

A substantial amount of data can also be found in the literature relating to the reactions of the d^8-rhodium complexes $RhX(CO)(PR_3)_2$ where X = Cl, Br, I and R = Ph, Me with p-H_2. The parent member of this series, $RhCl(CO)(PPh_3)_2$, was

first synthesised in 1957 and is one of the best known complexes of rhodium(I) [19]. This complex is readily formed from $RhCl(PPh_3)_3$ by CO addition or aldehyde decarbonylation [20], undergoes facile photodissociation of CO and functions as a photo-catalyst for benzene carbonylation [21,22]. However, unlike $IrCl(CO)(PPh_3)_2$, $RhCl(CO)(PPh_3)_2$ had not previously been seen to react with dihydrogen. Surprisingly however, rather than detecting the expected mononuclear complex $RhH_2X(CO)(PR_3)_2$ a series of binuclear complexes were observed. With $RhX(CO)(PPh_3)_2$ these were shown to correspond to $H_2Rh(PPh_3)_2(\mu\text{-}X)_2Rh(PPh_3)(CO)$ with hydrides *trans* to chloride bridges that were rendered inequivalent by ligands *trans* to the chlorides on the Rh(I) centre. A mechanism was proposed to account for the formation of $H_2Rh(PPh_3)_2(\mu\text{-}X)_2Rh(PPh_3)(CO)$ that began with the oxidative addition of H_2 to $RhX(CO)(PPh_3)_2$ (Fig. 7). However, in view of the fact that even with the signal enhancement of PHIP, the initial dihydrogen activation product $RhH_2X(CO)(PPh_3)_2$ was not detected it was suggested that facile CO loss led to the generation of the unsaturated species $RhH_2X(PPh_3)_2$. After generation of the co-ordinatively unsaturated species $RhH_2X(PPh_3)_2$, the next step in binuclear product formation was suggested to involve attack on the unsaturated Rh(III) centre by an electron pair of the halide ligand of unreacted $RhX(CO)(PPh_3)_2$. The resultant binuclear intermediate then forms $H_2Rh(PPh_3)_2(\mu\text{-}X)_2Rh(PPh_3)(CO)$ by generation of a second halide bridge from the Rh(III) ion to the Rh(I) centre and subsequent PPh_3 loss.

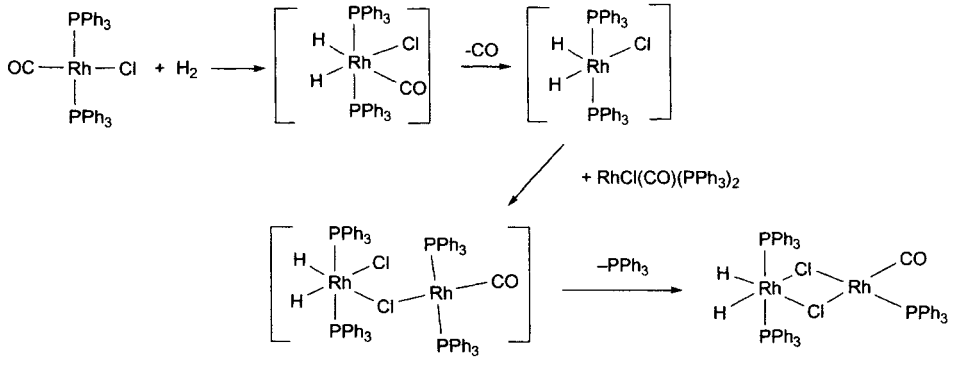

Figure 7. Suggested route to $H_2Rh(PPh_3)_2(\mu\text{-}Cl)_2Rh(PPh_3)(CO)$ as detected in the reaction of $RhCl(CO)(PPh_3)_2$ with p-H_2.

When the reaction of $RhCl(CO)(PMe_3)_2$ was monitored at 342 K under 3 atm of p-H_2, the major product corresponded to $H(Cl)Rh(PMe_3)_2(\mu\text{-}H)(\mu\text{-}Cl)Rh(PMe_3)(CO)$, with bridging and terminal hydrides (Fig. 8). In keeping

with the previously proposed mechanism for the formation of $H_2Rh(PPh_3)_2(\mu\text{-}X)_2Rh(PPh_3)(CO)$, it was suggested that a hydride of the Rh(III) centre competed with the halide to form the second bridge. This was supported by the observation that when $RhI(CO)(PMe_3)_2$ was monitored in a similar way five new species were detected (Fig. 9). At 348 K the most intense signals were shown to originate from the analogous complex $(H)(I)Rh(PMe_3)_2(\mu\text{-}H)(\mu\text{-}I)Rh(CO)(PMe_3)$ **1** in which the hydrido-bridge is *trans* to phosphine. A minor reaction product corresponding to the isomer of $(H)(I)Rh(PMe_3)_2(\mu\text{-}H)(\mu\text{-}I)Rh(CO)(PMe_3)$ **2** with the hydrido-bridge *trans* to carbonyl was also characterised at this temperature.

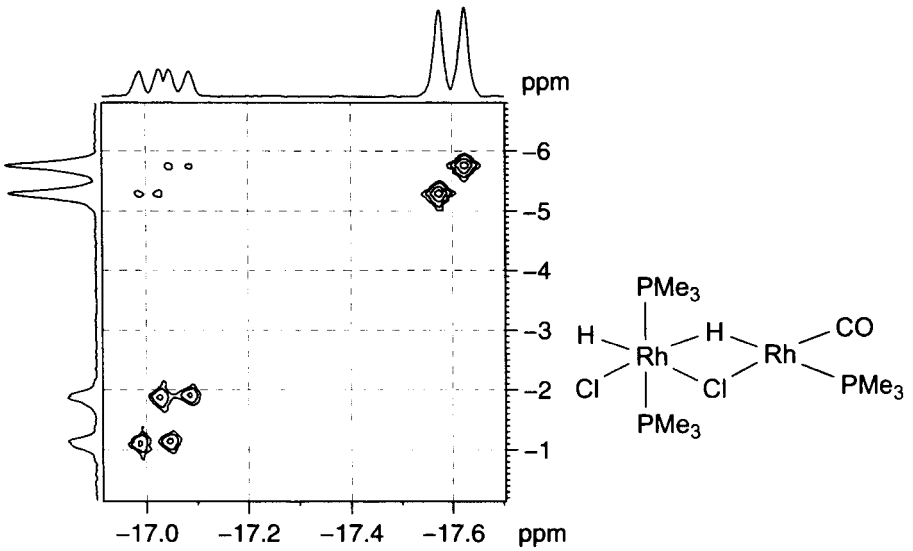

Figure 8. ^1H-^{31}P 2D HMQC correlation spectrum of $H(Cl)Rh(PMe_3)_2(\mu\text{-}H)(\mu\text{-}Cl)Rh(PMe_3)(CO)$ illustrating bridging and terminal hydride connections to both types of PMe_3 ligand.

The remaining products were characterised at 313 K where the associated hydride resonances became sharper and hence easier to monitor. These products were reported to be $(H)_2Rh(PMe_3)_2(\mu\text{-}I)_2Rh(CO)(PMe_3)$ **3**, $Rh(H)_2I(PMe_3)_3$ and the triply-bridged species $HRh(PMe_3)_2(\mu\text{-}H)(\mu\text{-}I)_2Rh(PMe_3)(CO)$ **4** (Fig. 9). The diverse range of products observed in these reactions prompted the authors to analyse the structures and stabilities of the bimetallic products by approximate density functional theory. For each of the three halides, distinct minima were located on the potential energy surface, corresponding to each of the four structural types identified in the parahydrogen enhanced NMR studies (Fig. 10). Interestingly, for the iodide complexes, all four structures were found to lie less

than 12 kJmol^{-1} above the most stable diiodide bridged isomer, a result that was consistent with the mixture of products observed in solution. Of the two mixed iodide/hydride-bridged species, the form with the hydride *trans* to the PH_3 group was found to lie 6 kJmol^{-1} lower in energy than the alternative with H *trans*

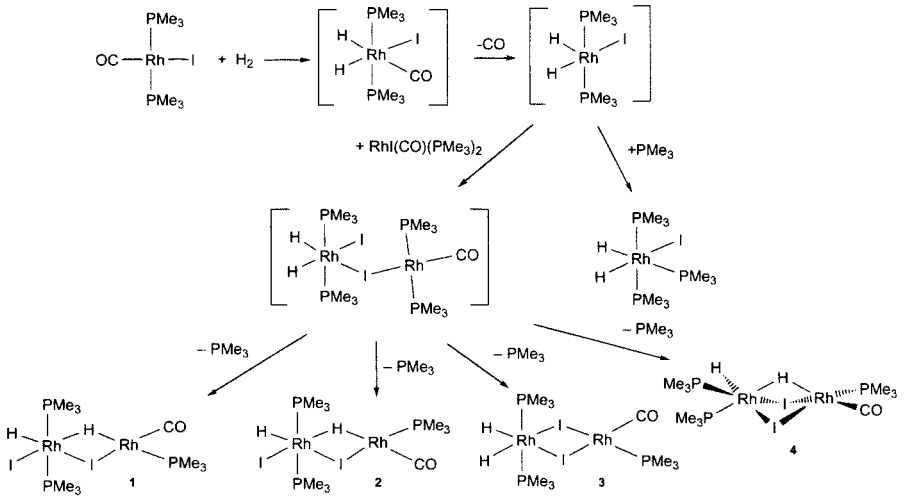

Figure 9. Suggested routes to the binuclear products that are observed in the reaction of $RhI(CO)(PMe_3)_2$ with H_2.

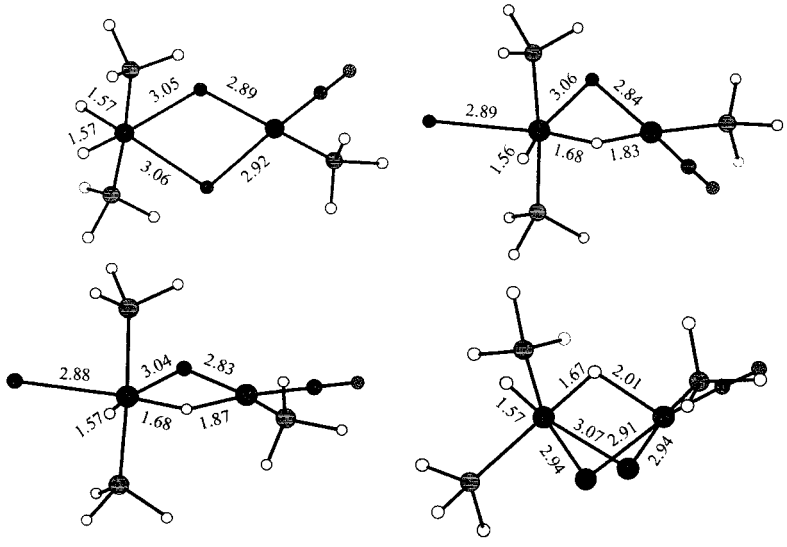

Figure 10. Reaction product geometries as determined via DFT calculations for the reaction of H_2 with $RhX(CO)(PH_3)_2$.

to CO, a result that was again consistent with the observed signal strengths in solution. Interestingly, the Rh-H-Rh bridges were revealed to be significantly asymmetric. This report served to illustrate the benefit of coupling experimental and theoretical observations.

11.4 OBSERVATIONS ON POLYHYDRIDE COMPLEXES

We have demonstrated that the trihydrides $IrH_3(CO)_x(PR_3)_y$ [x =2 and y= 1; x=1 and y = 2; PR_3 = PPh_3, PMe_3 and $AsMe_2Ph$] can be examined with p-H_2. These studies have provided a number of interesting observations. Firstly, the ^1H NMR spectra of the isomers of $IrH_3(CO)(PPh_3)_2$, with *trans* phosphines and *mer*-hydrides and with *cis* phosphines and *fac*-hydrides, yield enhanced hydride resonances. The two polarised hydride resonances at δ -9.29 and -10.02 were assigned to the isomer with *mer*-hydrides [4]. In a regular $^1H\{^{31}P\}$ spectrum these signals would appear as doublets and triplets respectively with peak separations J_{HH}. However, with p-H_2, although the observed signals have relative intensities of 2:1 their anti-phase line separation is 4.4 and 8.8 Hz respectively (Fig. 11). This indicates that the central feature of the triplet is no longer visible [23].

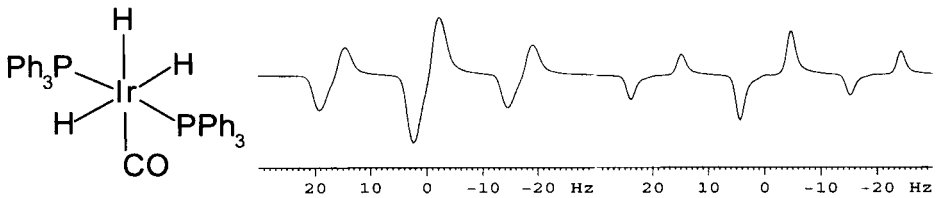

Figure 11. ^1H NMR spectra for the inset complex obtained with p-H_2. The larger H-H splitting in the right trace is due to the hydride ligand that is *trans* to CO. It is twice the size of corresponding splitting for the left trace.

The origin of this effect can be understood by examining the p-H_2 controlled populations of the eight spin wave-functions of the trihydride (AX_2). While four wave-functions are simple products of the form ααα, $\underline{\alpha\beta\beta}$, $\underline{\beta\alpha\alpha}$ and βββ, four belong to combinations of the form $\underline{\alpha(\alpha\beta-\beta\alpha)}$, $\underline{\alpha(\alpha\beta+\beta\alpha)}$, $\underline{\beta(\alpha\beta-\beta\alpha)}$ and $\underline{\beta(\alpha\beta+\beta\alpha)}$. Exchange with p-$H_2$ (αβ-βα spin state) involves the A and one X nucleus, with the result that the underlined states become equally populated while the ααα and βββ states are unpopulated. Consequently, visible transitions for nucleus A, correspond to spin flips ααα ↔ $\underline{\beta\alpha\alpha}$ and $\underline{\alpha\beta\beta}$ ↔ $\underline{\beta\beta\beta}$, and the outer lines of the triplet, separated by $2J_{AX}$, and are seen in emission

and absorption. The central line, corresponding to the transitions $\alpha(\alpha\beta\text{-}\beta\alpha) \leftrightarrow \beta(\alpha\beta\text{-}\beta\alpha)$ and $\alpha(\alpha\beta\text{+}\beta\alpha) \leftrightarrow \beta(\alpha\beta\text{+}\beta\alpha)$, vanishes because the associated levels have identical populations. Examination of the four symmetry allowed transitions for X_2 reveals that observable spin flips connect $\alpha\alpha\alpha \leftrightarrow \underline{\alpha(\alpha\beta+\beta\alpha)}$ and $\underline{\beta(\alpha\beta+\beta\alpha)} \leftrightarrow \beta\beta\beta$. These transitions, separated by J_{AX} (J_{HH}), are also visible as emission and absorption signals, with twice the overall intensity seen for the signal due to H_A, the hydride that is *trans* to CO.

When a benzene-d_6 solution of $IrH(CO)_2(PPh_3)_2$ was examined under an atmosphere of p-H_2 at 333 K, in addition to the two previously mentioned complexes, $IrH_3(CO)_2(PPh_3)$ with *fac*-hydrides was detected. Furthermore when $IrH_3(CO)(PPh_3)_2$ was irradiated with UV light for 5 minutes prior to being monitored several new species including the remaining isomer of the *bis*-phosphine trihydride and a second isomer of $IrH_3(CO)_2(PPh_3)$ were detected. This result demonstrates that UV irradiation prior to sample monitoring is a valuable route to expanding the number of structural isomers that are visible through the p-H_2 technique.

Eisenberg *et al* have reported studies on the reaction of the benzyne-hydride complex ($Cp^*_2Ta(C_6H_4)H$) with p-H_2 [24]. At 273 K, the complex reacted to form a new phenyl dihydride complex, $Cp^*_2Ta(C_6H_5)H_2$, which yielded enhanced hydride resonances with p-H_2. This complex went on to eliminate benzene and react with H_2 to form the trihydride complex $Cp^*_2TaH_3$. The central component of the proton resonance due to the central hydride ligand was again absent under PHIP conditions. This report is especially noteworthy because it represented the first example of PHIP at an early transition metal centre.

We have also examined the reaction of $WH_4(dppe)_2$ with p-H_2. This work is still proceeding, but we can state the hydride resonances for this species are parahydrogen enhanced.

These reports serve to illustrate the fact that the majority of systems that have been studied with parahydrogen involve the formation of metal dihydride complexes. In view of the numerous examples of polyhydride complexes this situation is somewhat surprising and illustrates an area of potential study.

11.5 LIGAND EXCHANGE PATHWAYS

The methods available to determine reaction rates by NMR spectroscopy include line broadening, spin saturation transfer and exchange spectroscopy (EXSY). The latter approach can be completed by both 1 and 2 D procedures. Several studies in the literature have served to illustrate that the dynamic behaviour of complexes detected through the parahydrogen effect can be examined. A general feature of this approach has involved the refocusing of the initial antiphase magnetisation.

This approach has been used to examine the dynamic behaviour of the hydride ligands in $IrH_2(CO)Cl(PPh_3)_2$ and $IrH_2Cl(PPh_3)_3$ [25]. In the reported experiments peaks due to chemical exchange and nOe effects were visible. At 343 K, nOe peaks were observed to connect the hydride resonances of $IrH_2Cl(CO)(PPh_3)_2$, to themselves and the ortho-phenyl protons of the phosphine. The lack of an exchange peak to free H_2 was taken to indicate that the reductive elimination of H_2 from $IrH_2Cl(CO)(PPh_3)_2$ was slower than the NMR timescale. NOe peaks were also reported to connect signals due to the hydride protons and the *ortho*-phenyl protons of the inequivalent phosphines in $IrH_2Cl(PPh_3)_3$. However, exchange cross-peaks were observed to connect the hydride resonances of this complex to that of molecular hydrogen. This information was taken to suggest that exchange with free hydrogen is much faster for $IrH_2Cl(PPh_3)_3$ than $IrH_2Cl(CO)(PPh_3)_2$. Interestingly, increasing the concentration of free phosphine led to the observation of hydride-hydride exchange peaks and a reduction in the size of the exchange peak to free hydrogen. At even higher concentrations of free phosphine the rate of the hydride self exchange were reported to diminish. This data was interpreted to mean that H_2 elimination proceeded via the 16 electron complex $IrH_2Cl(PPh_3)_2$, formed from $IrH_2Cl(PPh_3)_3$ by loss of the PPh_3 ligand *trans* to hydride (Fig. 12). The observation that the hydride interconversion rate was reduced at higher PPh_3 concentrations suggested that $IrH_2Cl(PPh_3)_2$ must contain chemically distinct hydrides requiring it to adopt a square-pyramidal geometry. This paper therefore demonstrated the potential of the parahydrogen technique to directly provide qualitative information about the configuration, reactivity and lability of reaction intermediates.

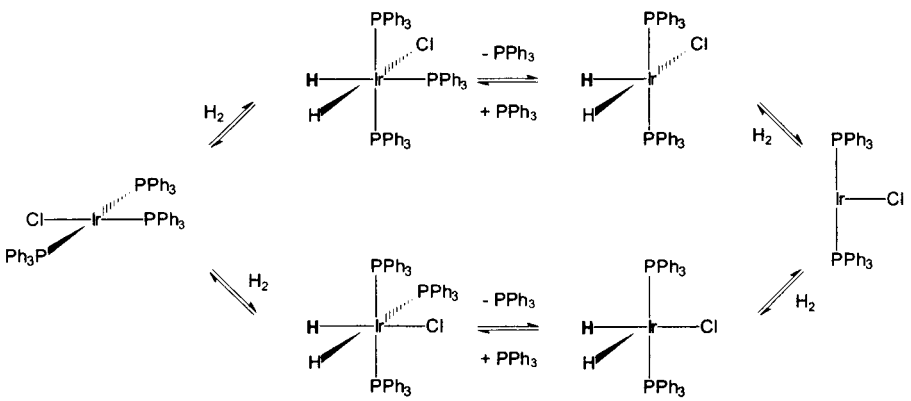

Figure 12. Kinetic studies with p-H_2 have demonstrated that hydrogen exchange at $IrH_2Cl(PPh_3)_3$ involves 16-electron $IrH_2(PPh_3)_2Cl$ with chemically and magnetically distinct hydrides.

Several papers have since demonstrated that quantitative information can be obtained in a similar way. The first of these involved the examination of the

hydrogen addition chemistry of $[IrI_2(CO)_2]NBu_4$ and $[RhI_2(CO)_2]NBu_4$. Initially, both these d^8 complexes were shown to add p-H_2 and form all-*cis* isomer of $[M(H)_2(CO)_2I_2]NBu_4$. While such complexes were previously known to react with MeI to form $[MI_3Me(CO)_2]NBu_4$, and play a substantial role in acetic acid generation, their reactivity towards hydrogen was far less well understood [26]. Interestingly, H_2 loss was now shown to involve the 18 electron complex $[Ir(H)_2(CO)_2I_2]NBu_4$. The rate of H_2 elimination at 325 K was reported to be 0.17 s^{-1}, with the activation parameters $\Delta H^{\neq}$ 106 ± 10 kJ mol^{-1} and $\Delta S^{\neq}$ 60 ± 6 J $K^{-1}mol^{-1}$ being determined. Exchange between all-*cis* isomer $[Ir(H)_2(CO)_2I_2]NBu_4$ and the *trans(CO)-cis-cis* isomer occurs via iodide loss and the formation of square pyramidal $[Ir(H)_2(CO)_2I]$ (Fig. 13). Trapping of the resultant intermediate with PPh_3 led to the detection of 4 neutral and 3 charged dihydrides containing one phosphine ligand.

We have also used the EXSY approach to examine hydride interchange in the *tcc* and *ccc* isomers of $RuH_2(CO)_2L_2$ (L = $AsMe_2Ph$, PMe_2Ph and PMe_3) described earlier. The rate for hydride interchange in the *ccc* isomer of $RuH_2(CO)_2(PMe_3)_2$ is 0.95 s^{-1} while that for *ccc* to *tcc* interconversion is 0.32 s^{-1} at 350 K (Fig. 14). Activation parameters of $\Delta H^{\neq}$ 59 ± 6 kJ mol^{-1} and $\Delta S^{\neq}$ -80 ± 16 J $K^{-1}mol^{-1}$, and $\Delta H^{\neq}$ 107 ± 17 kJ mol^{-1} and $\Delta S^{\neq}$ 56 ± 48 J $K^{-1}mol^{-1}$ were determined for these two processes respectively when L = PMe_3. We have interpreted this data to signify that hydride interchange, and isomer interconversion, occur via an η^2-H_2 complex..

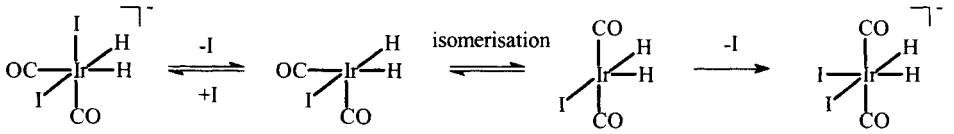

Figure 13. Isomerisation of the all-cis isomer of $[Ir(H)_2(CO)_2I_2]NBu_4$ into the trans-cis-cis form occurs via square pyramidal $Ir(H)_2(CO)_2I$.

11.6 ENHANCEMENTS AT SITES WHERE THE P-H_2 NUCLEI ARE MAGNETICALLY EQUIVALENT.

Up to this point this chapter has referred to a number of straightforward examples in which the nuclei originating in parahydrogen are transported into magnetically distinct environments. This situation often results in strongly enhanced NMR signals, as indicated in section 11.3. One potential drawback of the parahydrogen technique is therefore the need to create a product with magnetically inequivalent hydrides. Surprisingly, a number of instances have been described in the literature where enhanced signals are observed for pairs of magnetically equivalent protons [18,27]. Aime and Canet elegantly illustrated the origin of

this effect by reference to the addition of parahydrogen to $Os_3(CO)_{10}(NCCH_3)_2$ [28]. This reaction first yields two isomers of $H(\mu\text{-}H)Os_3(CO)_{10}(NCCH_3)$ which react further to form $H_2Os_3(CO)_{10}$ a species in which the two hydrogen nuclei are magnetically equivalent. They demonstrated that the observation of an enhanced hydride signal for $H_2Os_3(CO)_{10}$ necessitated the involvement of an intermediate with inequivalent hydrides, and subsequent cross-correlation between the relaxation mechanisms dipolar interaction and chemical shift anisotropy. These workers have also examined the reaction of $Ru_3(CO)_{11}(NCCH_3)$ with parahydrogen [29].

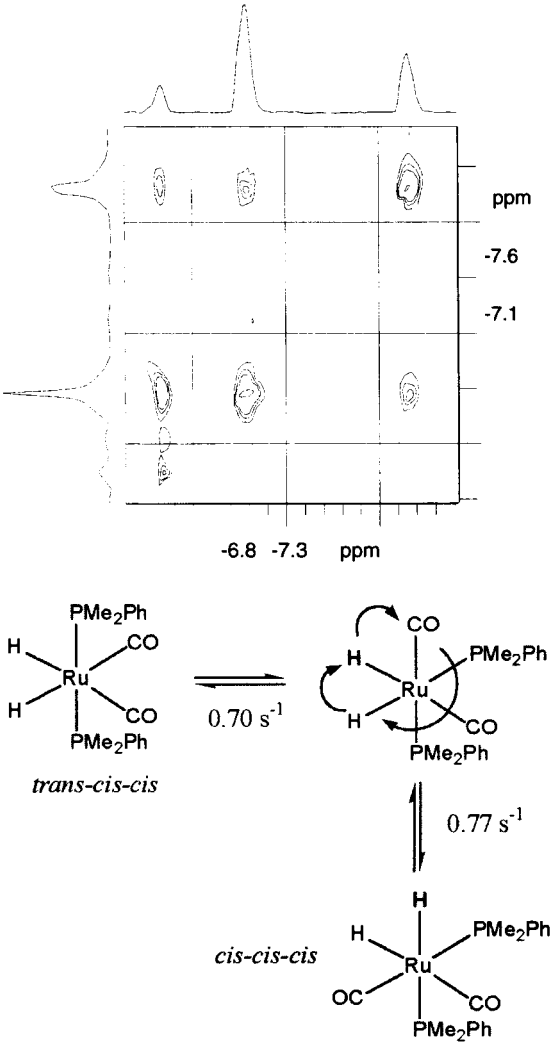

Figure 14. Hydride region of $^1H\text{-}^1H\{^{31}P\}$ EXSY spectrum of $Ru(H)_2(CO)_2(PMe_3)_2$ at 350 K with hydride connections illustrating *cis-cis-cis* intramolecular exchange, and *trans-cis-cis* – *cis-cis-cis* isomer interchange.

The observation of an enhanced emission signal for molecular hydrogen was interpreted to indicate the reversible interaction of p-H_2 via the formation of a Ru_3 cluster with inequivalent hydrides. This suggestion was consistent with the fact that H_2 addition to $Ru_3(CO)_{11}(NCCH_3)$ is known to form $H(\mu\text{-}H)Ru_3(\mu\text{-}CO)(CO)_{10}$ initially and then $[Ru_3(CO)_{11}]$ and H_2. We have examined the reactions of the cluster series $Ru_3(CO)_9(PR_3)_3$, $Ru_3(CO)_{10}(PR_3)_2$ and $Ru_3(CO)_{11}(PR_3)$ [PR_3 = PPh_3, PMe_2Ph and PCy_3] with p-H_2 [30]. These studies have revealed that related products such as $H(\mu\text{-}H)Ru_3(CO)_8(PPh_3)_3$ are formed, and that in the case of PR_3 = PPh_3, cluster fragmentation yields signals for the meridional isomer of $Ru(CO)_3(H)_2(PPh_3)$ (Fig. 15). This observation was especially noteworthy since $Ru_3(CO)_{12}$ and PPh_3, as well as $Ru(CO)_3(H)_2(PPh_3)$ have been implicated in hydroformylation catalysis. Fig. 16 illustrates some of dynamic data obtained for these systems.

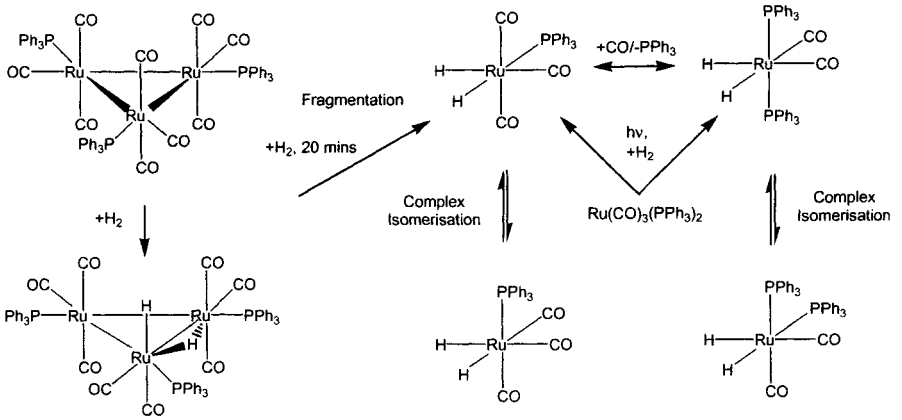

Figure 15. Reaction products that are detected when $Ru_3(CO)_9(PPh_3)_3$ is warmed with p-H_2.

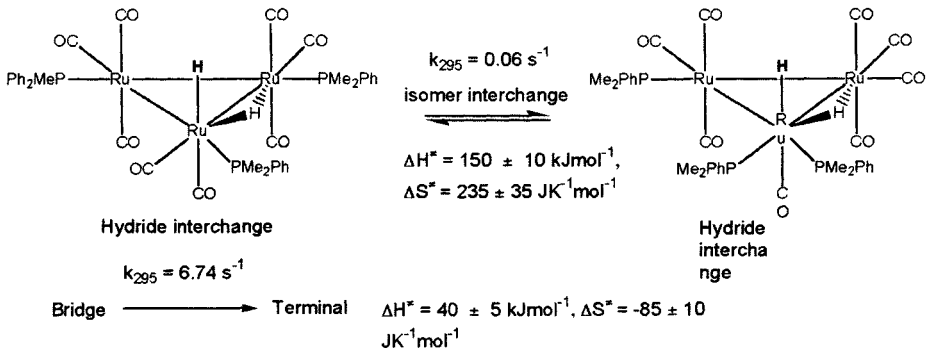

Figure 16. Summary of kinetic and thermodynamic information provided by studies on the dynamics of hydride interchange in $H(\mu\text{-}H)Ru_3(CO)_8(PMe_2Ph)_3$.

11.7 MECHANISTIC INFORMATION FROM CATALYTIC STUDIES

Hydrogenation by Wilkinson's complex, $RhCh(PPh_3)_3$ is one of the most studied reactions and has been examined many times with p-H_2. These studied comprise of two distinct types, those that involve the direct detection of metal based intermediates, and those where the dynamics of NMR spin physics are used to indirectly probe the reaction. Thus in hydrogenation reactions catalysed by Wilkinson's catalyst, the binuclear dihydride species $H_2Rh(PPh_3)_2(\mu\text{-}Cl)_2Rh(PPh_3)$(alkene) was shown to be present [31]. The experimental results indicate that this product contains two inequivalent *trans* phosphines that are attached to a Rh(III) centre [32]. This suggestion is consistent with calculations that have shown it is energetically more favourable for an alkene to bind to a ML_3 fragment with the C=C bond arranged perpendicular to the plane containing the framework atoms [33]. For styrene the alkene substituents are therefore unsymmetrically displaced about the plane containing the Rh atoms while for *cis*-stilbene the presence of a mirror plane make the phosphines equivalent.

Not surprisingly, the signals for these binuclear complexes decay rapidly as the hydrogen present in solution is consumed. The dynamic behaviour of the associated hydride ligands has been probed by 1D-nOe methods involving selective excitation at either δ -18.8 or -19.6. The data provided by this work indicated that the two hydrides interchange positions in a process that is independent the concentration of styrene and catalyst. This was taken to suggest that the exchange process was intramolecular. The activation parameters for hydride interchange in $(H)_2Rh(PPh_3)_2(\mu\text{-}Cl)_2Rh(PPh_3)$(styrene) were reported to be $\Delta H = 43 \pm 14$ kJ mol^{-1} and $\Delta S = -98 \pm 45$ J K^{-1} mol^{-1}. Interestingly, the hydride ligands were shown to become free H_2 in a process that increased in significance as the alkene concentration decreased. Surprisingly, at relatively low alkene concentrations magnetisation transfer from the hydrides of $(H)_2Rh(PPh_3)_2(\mu\text{-}Cl)_2Rh(PPh_3)$(styrene) to the alkyl protons of the hydrogenation product ethylbenzene was observed (Fig. 17). This demonstrated that these hydride ligands are transferred directly to an alkene and provided direct evidence for the metal dihydride complex being involved in alkene hydrogenation.

Further evidence for the involvement of binuclear species in hydrogenation was obtained via reactions involving $RhCl(CO)(PMe_3)_2$ as the catalyst. When the reaction of $RhCl(CO)(PMe_3)_2$ with p-H_2 at 295K was compared to that when styrene was also present a dramatic increase in hydride signal enhancements was observed. This facilitated the detection of the previously unseen species $(H)_2Rh(PMe_3)_2(\mu\text{-}Cl)_2Rh(CO)(PMe_3)$ in addition to $HRh(PMe_3)_2(\mu\text{-}H)(\mu\text{-}Cl)_2Rh(CO)(PMe_3)$ [34]. The dramatic promotion of hydrogen cycling by hydrogenation demonstrated conclusively that these species are actively involved in the alkene hydrogenation. In addition this result demonstrated that a sacrificial alkene can dramatically extend the ability of the parahydrogen methods by promoting H_2 cycling. This information is summarised in Fig. 18.

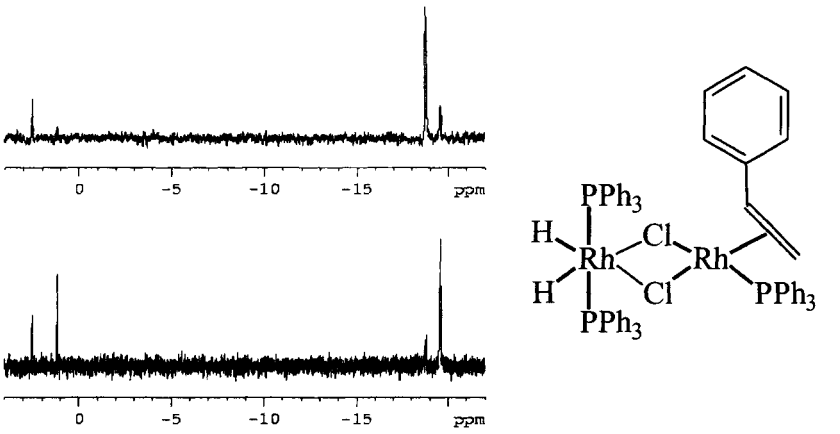

Figure 17. $^1H\{^{31}P\}$ 1D-nOe spectra of p-H_2 enhanced $(H)_2Rh(PPh_3)_2(\mu\text{-}Cl)_2Rh(PPh_3)$ (styrene) (structure inset) at 295 K showing intramolecular hydride interchange and conversion to ethylbenzene during the 200 ms exchange time. The largest peaks in each trace correspond to the excitation or spin labelling point while the three smaller peaks are due to chemical exchange.

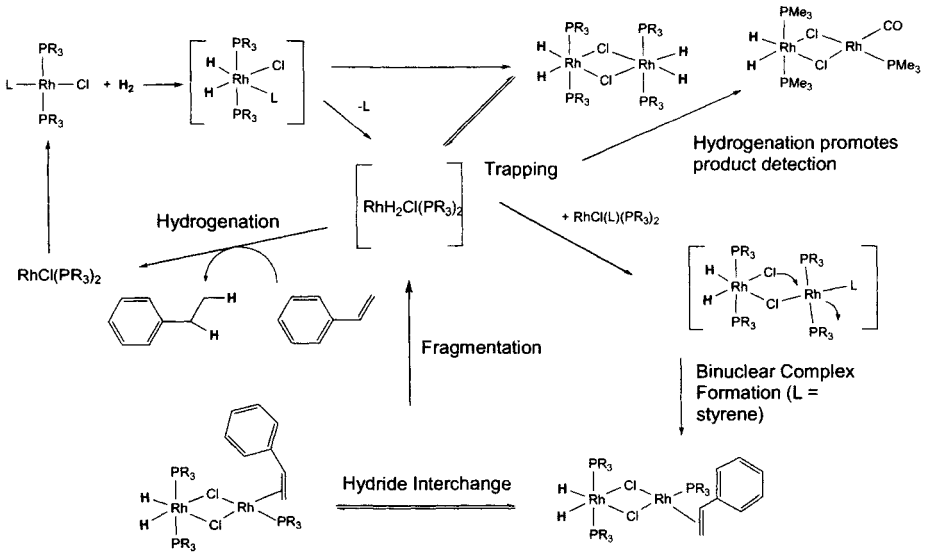

Figure 18. Schematic diagram illustrating the fate of H_2 during hydrogenation by $RhCl(PR_3)_3$.

In an earlier report, polarised resonances were observed that could be attributed to a true mononuclear intermediate in the catalytic process [31]. These resonances were assigned to a dihydride species that contained an alkene ligand and *cis* phosphines. Hydrogenation of itaconic acid by the rhodium catalysts

Rh(NBD)(bisphosphinite)BF_4 has also been observed to yield p-H_2 enhanced hydride resonances for a potential intermediate in the hydrogenation cycle [35]. Bargon has studied the mechanism of alkyne hydrogenation by [$(PR_3)_2$PtHX]/ SnX_2 (PR_3 = PPh_3, $PMePh_2$; X = Cl and Br) with p-H_2. A Pt(IV) dihydride of the form *cis*-[Pt$(H)_2(PR_3)(SnX_3)$(σ-alkenyl)(acetone)] was detected in these studies [36,37].

Chinn and Eisenberg used PHIP to measure the rate of the catalytic hydrogenation of ethyl (Z)-acetamidocinnamate by [Rh(NBD)(chiraphos)]BF_4 [39]. The decay of polarisation intensity in the hydrogenation product resonances was modelled to determine the rate of hydrogenation. Data obtained in this way matched that collected using standard methods and confirmed that the PHIP approach can be used to measure hydrogenation rate constants. This approach has been refined by Bargon [39] and can be used to provide indirect evidence about the role of catalytic intermediates [40]. Bargon *et al* have also demonstrated that the modelling of the spectral features of hydrogenation products can be used to produce an indirect route to examining the role of reaction intermediates involved in product generation. This involves examination of the extent of nuclear singlet/triplet mixing that occurs during hydrogenation with p-H_2. They first demonstrated the quantitative nature of the data provided by this approach in a study of the $RhCl(PPh_3)_3$ and [Rh(COD)(Ph-β-glup-OH)]BF_4 catalysed hydrogenation of 1,4-dihydro-1,4-expoxynaphthalene to 1,4-epoxytetralin. Computer calculations were used to simulate the experimentally observed polarisation profiles of the hydrogenation products as a function of the time the hydrides spend in magnetically inequivalent positions on the catalyst. In the case of the $RhCl(PPh_3)_3$ catalysed reaction, the p-H_2 protons were shown to transfer as a mixture of S/T_0 nuclear spin state. The spectral profile required that hydrogenation by Wilkinson's catalyst proceeded through an intermediate with inequivalent hydrides and a lifetime of >1.7 ms at 313 K. The [Rh(COD)(Ph-β-glup-OH)]BF_4 catalysed reaction was shown to involve an intermediate with chemically and magnetically equivalent hydrides [41]. In these reactions, the polarisation profiles of the product have been shown to depend critically on the substrate, which indicates that catalyst action is substrate dependent [42]. A dynamic model that simulates these effects has now been reported [43].

11.8 SUMMARY

This chapter has illustrated how the field of parahydrogen assisted NMR studies has worked to expand our understanding of metal hydride chemistry since the first observations were made in 1987. The utility of this technique

rapidly expanded in the last decade, with many transition metal complexes being detected solely because of the signal gains associate with p-H_2. It will be interesting to see how this technique develops over the next decade.

ACKNOWLEDGEMENTS

I would like to thank the EPSRC, the SCI, the Royal Society, the University of York, Bruker UK, BP Chemicals, and NATO for their financial support for our research involving parahydrogen. I am also grateful to Prof. R. Eisenberg, Dr. P. Morran, Dr. B. Messerle, Dr. M. Partridge, Dr. D. Taylor, Dr. J. Lohman, Dr. M. Taylor, Dr. G. Barlow, Dr C. Sleigh, Dr. P. J. Dyson, Dr. D. Law, Dr. J. McGrady, Prof. B. C. Johnson, Dr. R. Mawby, Prof. R.Perutz, Dr. S. Hasnip, Mr D. Blazina and Mr S. Colebrooke for their valuable contributions to our work in this area. Special thanks go to Johnson Matthey for the loan of precious metal salts.

REFERENCES

[1] G. J. Kubas. Account. Chem. Res. 1988 (21) 120.
[2] J. M. Brown. Chem. Soc. Rev. 22 (1993) 25.
[3] C. R. Bowers, D. P. Weitekamp, Phys. Rev. Lett. 57 (1986) 2645.
[4] C. R. Bowers, D. H. Jones, N. D. Kurur, J. A. Labinger, M. G. Pravica, D. P. Weitekamp, Advances in Mag. Res. 14 (1990) 269.
[5] J. Natterer, J. Bargon, Prog. Nucl. Magn. Reson. Spectrsc. 31 (1997) 293.
[6] S. B. Duckett, C. J. Sleigh. Prog. Nucl. Magn. Reson. Spectrsc. 31 (1999) 71.
[7] S. B. Duckett, C. L. Newell, R. Eisenberg, J. Am. Chem. Soc. 116 (1994) 10548.
[8] When the reaction occurs outside the spectrometer a different effect, termed ALTADENA (Adiabatic Longitudinal Transport After Dissociation Engenders Nuclear Alignment), is observed. Under these conditions the spectra are much simpler as only one of the ab or ba becomes populated. M. G. Pravica, D. P. Weitekamp. Chem. Phys. Lett. 145 (1988) 255.
[9] C. R. Bowers, D. P. Weitekamp, J. Am. Chem. Soc. 109 (1987) 5541.
[10] T. C. Eisenschmid, R. U. Kirss, P. P. Deutsch, S. I. Hommeltoft, R. Eisenberg, J. Bargon, D. G. Lawler, A. L. Balch, J. Am. Chem. Soc. 109 (1987) 8089.
[11] S. B. Duckett, G. K. Barlow, M. G. Partridge, B. A. Messerle, J. Chem. Soc. Dalton. Trans. (1995) 3427.
[12] dppe - $Ph_2CH_2CH_2Ph_2$; dppv - *cis*-$Ph_2PCHCHPH_2$; dppb - o-$(Ph_2P)_2C_6H_4$.
[13] T. C. Eisenschmid, J. McDonald, R. Eisenberg, R. G. Lawler, J. Am. Chem. Soc. 111 (1989) 7267.
[14] S. B. Duckett, C. L. Newell, R. Eisenberg, J. Am. Chem. Soc. 115 (1993) 1156.
[15] A. L. Sargent and M. B. Hall. Inorg. Chem. 31 (1992) 317.
[16] G. Suardi, B. P. Cleary, S. B. Duckett, C. Sleigh, M. Rau, W. E. Reed, J. A. B. Lohman and R. Eisenberg. J. Am. Chem. Soc, 119 (1997) 7716.
[17] M. Jang, S. B. Duckett and R. Eisenberg. Organometallics 15 (1996) 2863. S. P.

Millar, M. Jang, R. J. Lachicotte and R. Eisenberg. Inorganica Chimica Acta. 270 (1998) 363.
[18] S. B. Duckett, R. J. Mawby, M. G. Partridge, J. Chem. Soc. Chem. Commun. (1996) 383.
[19] L. Vallarino, J. Chem. Soc. (1957) 2287.
[20] J. A. Osborn, F. H. Jardine, J. F. Young and G. Wilkinson. J. Chem. Soc. A (1966) 1711.
[21] P.C. Ford, T. L. Netzel, C. T. Spillert, and D. B. Poureau, P. App. Chem. 62 (1990) 1091. C. T. Spillett, and P. C. Ford, J. Am. Chem. Soc. 111 (1989) 1932. D. A. Wink. And P. C. Ford, J. Am. Chem. Soc. 109 (1987) 436.
[22] A. J. Kunin and R. Eisenberg, Organomet. 7 (1988) 2124.
[23] S. Hasnip, S. B. Duckett, D. R. Taylor, M. J. Taylor, J. Chem. Soc. Chem. Commun. (1998) 923.
[24] S. P. Millar, D. L. Zubris, J. E. Bercaw and R. Eisenberg. J. Am. Chem. Soc. 120 (1998) 5329.
[25] B. A . Messerle, C. J. Sleigh, M. G. Partridge and S. B. Duckett. Dalton. Trans. (1999) 1429.
[26] P. M. Maitlis, A. Haynes, G. J. Sunley, and M. J. Howard, J. Chem. Soc., Dalton Trans. (1996) 2187.
[27] M. Haake, J. Barkemeyer and J. Bargon. J. J. Phys. Chem. 99 (1995) 17539.
[28] S. Aime, R. Gobetto and D. Canet. J. Am. Chem. Soc. 120 (1998) 6770.
[29] S. Aime, W. Dastru, R. Gobetto, A. Russo, A. Viale and D. Canet. J. Phys. Chem. (A). 103 (1999) 9702.
[30] C. J. Sleigh, S. B. Duckett, R. J. Mawby and J. P. Lowe, Chem. Commun. (1999) 1223.
[31] S. B. Duckett, C. L. Newell, R. Eisenberg, J. Am. Chem. Soc. 116 (1994) 10548, ibid 119 (1997) 2048.
[32] S. A. Colebrooke, S. B. Duckett and J. A. B. Lohman. Chem. Comm. (2000) 685
[33] T. A. Albright, R. Hoffmann, J. C. Thibeault and D. L. Thorn. J. Am. Chem. Soc. 107 (1979) 3801.
[34] P. D. Morran, P. D., S. B. Duckett, P. R. Howe, J E. McGrady, S. A. Colebrooke, R. Eisenberg, M G. Partridge and J. A. B. Lohman. J. Chem. Soc., Dalton Trans. (1999) 3949
[35] A. Harthun, J. Bargon. Angew. Chem. Int. Ed. Engl. 109 (1997) 1103.
[36] C. Ulrich A. Permin, V. Petrosyan and J. Bargon. Eur. J. Inorg. Chem. 5 (2000) 898.
[37] C. Deibele, A. B. Permin, V. S. Petrosyan and J. Bargon. Eur. J. Inorg. Chem. (1998) 1915.
[38] M. S. Chinn, R. Eisenberg. J. Am. Chem. Soc. 114 (1992) 1908.
[39] P. Hubler, R. Geirnoth, G. Kummerle and J. Bargon. J. Am. Chem. Soc. 121 (1999) 5311.
[40] P. Hubler, Natterer, J. Bargon. J. Ber. Bunsen-Ges. Phys. Chem. 1998 (1998) 364.
[41] P. Katting, A. Wandelt, R.Selke, J. Bargon. J. Phys. Chem. 97 (1993) 13313.
[42] M. Haake, J. Barkemeyer, J. Bargon. J. Phys. Chem. 99 (1995) 17539.
[43] G. Buntkowsky, J. Bargon, H-H Limbach, J. Am. Chem. Soc. 118 (1996) 8677.

Chapter 12

NMR Relaxation Studies of Polynuclear Hydrides Derivatives

S. Aime, W. Dastrù, R. Gobetto, A. Viale

Dipartimento di Chimica I.F.M., Università di Torino, V. P. Giuria 7; 10125 Torino, Italy

CONTENTS

12.1 INTRODUCTION.

Recent developments in NMR spectroscopy have resulted in it becoming one of the most successful analytical techniques for the study of transition-metal hydrides. Normally the ^{1}H resonances of these ligands fall in the characteristic region -5/-20 ppm upfield of TMS,[1] allowing their rapid and unambiguous characterization. Few exceptions to this general rule have been reported until

now, and their observation is consistent with an early theoretical treatment of δ_H forwarded by Buckingam and Stephens.[2] This suggestion has gained further support from recent work by T. Ziegler *et al.*,[3] who presented a theoretical study of the ^1H NMR chemical shifts based on density functional theory and gauge-including atomic orbitals. Their calculations clearly show that the paramagnetic current localized in the adjacent metal fragment is responsible for the negative "hydridic" shift observed in low valent transition metal hydrides.

Scalar couplings, both with nuclei on other ligands, and with magnetically active metals, are also very useful in enabling the absolute assignment of hydride position in such complexes. [4-10]

This chapter is aimed at showing how the understanding of relaxation processes can be exploited to gain insight into the structural, dynamic and electronic properties of polynuclear hydride derivatives.

Actually, although both direct and indirect localization of hydrides may be performed in the X-ray structural determination, there is still the need for a spectroscopic approach, in order to obtain a better understanding of the bonding scheme involving hydrides while avoiding the annoying problems often associated with neutron diffraction analysis.[11]

On the other hand, results obtained by solution based NMR spectroscopy refer to the liquid state, which could be different from the situation occurring at the solid state, where packing forces may be responsible for the observed spatial arrangements.

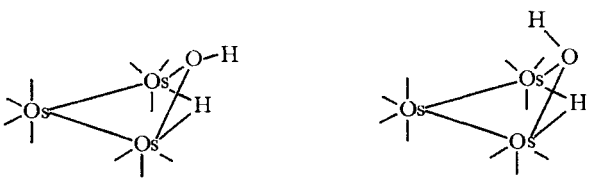

Ia **Ib**

Scheme 1

Normally, most hydride resonances have relatively long relaxation times[12] with only non-classical hydrides displaying short relaxation times due to the close proximity of the two H-nuclei in the coordinated H_2 molecule.[13] However no example of this class of η^2-H_2 coordination has yet been reported for cluster compounds, and this possibility will not be further considered here.

In general, the longitudinal relaxation rate of a hydride resonance is dominated by dipolar and chemical shift anisotropy contributions, the former being by far the most important in determining the observed relaxation time.[14] Thus a first look to the T_1 value may provide a useful tool for structural assignments, since it immediately reports on the distances with respect to other magnetically active

nuclei (mainly protons) in proximity to the observed one.[14] For instance, $(\mu\text{-H})(\mu\text{-OH})Os_3(CO)_{10}$ is present in solution as two non-exchanging isomers (**Ia** and **Ib,** see scheme 1), which afford slightly different ^1H resonances for the hydride ligands at –12.88 and –12.91 ppm respectively.[15] The two hydride resonances differ markedly in their T_1, being 28.8 and 56.1 s respectively. Clearly, the observed behaviour has to be related to the differences in H---H distances in $(\mu\text{-H})(\mu\text{-OH})Os_3(CO)_{10}$, resulting in a shorter T_1 for the **Ia** isomer.

12.2 DETERMINATION OF H---H DISTANCES *VIA* THE ASSESSMENT OF THE DIPOLAR (DD) CONTRIBUTION TO RELAXATION.

A good evaluation of the H---H distance can be pursued only with a proper knowledge of the dipole-dipole contribution ($1/T_1^{DD}$) from the proton of interest to the overall relaxation rate of the hydride resonance.

Commonly $1/T_1^{DD}$ is easily evaluated through the measurement of the nuclear Overhauser enhancement when the two ^1H nuclei resonate at different frequencies.[16]

Alternatively, we suggested another approach based on comparisons between the relaxation rates of (H,H) and (H,D) isotopomers.[14] For instance, the $1/T_1^{DD}$ contribution to the relaxation of the hydride resonance in $(\mu\text{-H})_2Os_3(CO)_{10}$ (**II**, scheme 2) has been determined through the measurement of T_1 in $(\mu\text{-H})_2Os_3(CO)_{10}$ (**IIa**) (T_1 = 6.5 s at 293 K, 270 MHz) and in $(\mu\text{-H})(\mu\text{-D})Os_3(CO)_{10}$ (**IIb**) (T_1 = 30.2 s at 293 K, 270 MHz). [14]

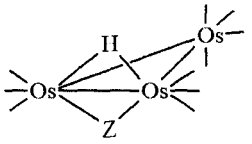

IIa : Z = H
IIb : Z = D

Scheme 2

It follows that:

$$R_1^{DD} = \frac{1}{T_1^{DD}} = \left(\frac{1}{T_1^{\mathbf{IIa}}} - \frac{1}{T_1^{\mathbf{IIb}}} \right) \frac{1}{0.96} \quad [s^{-1}] \qquad (1)$$

where the term 1/0.96 has been introduced to compensate for the residual dipolar contribution from the ^2H nucleus. Now, applying the usual equation for $1/T_1^{DD}$ for the intramolecular H-H interaction in the fast correlation time (τ_c) limit,[17] we get:

$$r_{H-H} = \sqrt[6]{\frac{3}{2}\gamma_H^4 \eta^2 \tau_c T_1^{DD}} \qquad (2)$$

where γ_H is the gyromagnetic ratio for the proton, and by using a τ_c value of 25 ps (which proved to be satisfactory in the study of ^{13}C and ^{17}O relaxation behaviour in the same molecule), we have calculated an r_{H-H} distance of 2.35 ± 0.03 Å. This distance is very similar to that found in the solid state from a neutron diffraction study (2.37 Å).[18]

An analogous approach could be used to calculate the M-H distance if different metal isotopes are available. This is the case of the $[Pt(PEt_3)_3H]BF_4$ complex (**III**),[19] for which the hydride T_1 measurement for the ^{195}Pt isotopomer (I = ½) is slightly shorter (2.03 s) than the corresponding T_1 in the isotopomer having I = 0 platinum nuclei (2.38 s). The dipolar contribution to the hydride relaxation due to the magnetically active ^{195}Pt is then equal to 0.0724 s^{-1}; assuming τ_c = 60 ps (reasonable value for ionic mononuclear complexes), a Pt-H distance of 1.67 Å has been obtained.

One may note that the evaluation of equation (2) implies that the condition $\omega_0\tau_c << 1$ is satisfied (ω_0 is the operating frequency expressed in rad s^{-1}), as it is usually the case for systems of such size dissolved in non viscous solvents, at ambient temperature.

A route to a good estimation of τ_c deals with the measurement of T_1^{DD} over an extended range of temperatures and with the fitting of the obtained data to the complete expression for the modulation of the dipolar interaction:[17]

$$\frac{1}{T_1^{DD}} = \frac{3}{10}\left(\frac{\mu_0}{4\pi}\right)^2 \frac{\hbar^2\gamma_H^4\tau_c}{r_{H-H}^6}\left(\frac{1}{1+\omega_o^2\tau_c^2} + \frac{4}{1+4\omega_o^2\tau_c^2}\right) \qquad (3)$$

(where μ_0 is the magnetic susceptibility in the vacuum). The molecular reorientational time τ_c depends on the temperature according to:

$$\tau_c = \tau_0 e^{\frac{E_a}{RT}} \qquad (4)$$

where R is the Boltzmann constant in $Jmol^{-1}K^{-1}$ and E_a is the activation energy for the reorientational motion. T_1 is expected to decrease as the temperature decreases to reach a minimum where the τ_c value is simply given by:

$$\tau_c = \frac{0.6158}{\omega_0} \quad (5)$$

This procedure has been applied to determine the distance between the bridging and the terminal hydride in $(H)(\mu\text{-}H)Os_3(CO)_{11}$ (**IV**, scheme 3),[20] whose T_1(minimum) is reached at 207 K (in toluene-d_8) on an instrument operating at 90 MHz (2.1 T). Thus, with a τ_c value of 977 ps, the inter-hydrides distance $r_{H\text{-}H}$ results to be equal to 2.46 Å. These $r_{H\text{-}H}$ and τ_c values could subsequently be used as the starting parameters to fit, by successive iterative runs, the $1/T_1$ *vs* 1/T curves of the terminal and bridging hydrides to the theoretical values determined by equations (3) and (4).

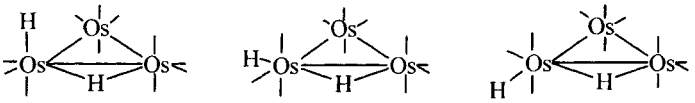

IVa **IV b** **IV c**

$r_{H\text{-}H}$ = 2.46 ± 0.07 Å $r_{H\text{-}H}$ = 3.34 ± 0.07 Å $r_{H\text{-}H}$ = 2.12 ± 0.06 Å

Scheme 3

We think that the H,D replacement method is the method of choice to get an accurate determination of the dipolar term in the hydride moiety, as the overall T_1 of the hydride resonances may receive relevant contributions also from other relaxation sources. For instance, Beringhelli et al. showed that in $(\mu\text{-}H)_2Re_2(CO)_8$ the dipolar H---H relaxation accounts for only the 9.5 % of the total relaxation rate.[21] In this derivative the importance of the dipolar interactions with the metal itself is remarkable. In the case of Re (^{185}Re: I = 5/2, natural abundance = 37.07 %; ^{187}Re: I = 5/2, natural abundance = 62.93 %) the small γ of rhenium isotopes is partially counterbalanced by the factor I(I+1) = 8.75 which makes the "effective γ" *ca.* 18 10^7 rad $T^{-1}s^{-1}$ (to be compared with 26.7223 10^7 rad $T^{-1}s^{-1}$ for ^{1}H). In the extreme narrowing condition, for a hydride bound to it ($r_{H,Re}$ = 1.68 Å) a rhenium atom is as effective as an hydrogen atom at 1.95 Å, as far as the dipolar interactions are concerned (provided that the correlation times for the two interactions are the same).

12.3 THE CHEMICAL SHIFT ANISOTROPY OF HYDRIDES.

Interestingly, when the hydride relaxation times of **IV** are measured at higher magnetic field strenghts (6.34 and 9.4 T), the Chemical Shift Anisotropy (CSA) contribution to the relaxation rate is no longer negligeable. The hydrides CSA

can then be extracted by fitting the experimental data to the equation which takes into account both dipolar and CSA contributions to relaxation:[17]

$$\frac{1}{T_1}=\frac{1}{T_1^{DD}}+\frac{1}{T_1^{CSA}}= \\ =\frac{3}{10}\left(\frac{\mu_0}{4\pi}\right)^2\frac{\gamma_H^4\hbar^2\tau_c}{r_{H,H}^6}\left(\frac{1}{1+\varpi^2\tau_c^2}+\frac{4}{1+4\varpi^2\tau_c^2}\right)+\frac{2}{15}\gamma_H^2B_0^2\Delta\sigma^2\tau_c\left(\frac{1}{1+\varpi^2\tau_c^2}\right) \quad (6)$$

where B_0 is the operating magnetic field and $\Delta\sigma$ is the CSA. This allowed us to determine the CSA values for the bridging and the terminal hydrides in **IV**, which are 22.6 ± 2.0 and 20.0 ± 1.9 ppm respectively. Such values are very similar to those obtained by Nicol and Vaugham for bridging hydride ligands in **II** and $(\mu\text{-H})_4Ru_4(CO)_{12}$ from solid state ^{1}H NMR experiments.[22] The relative insensitivity to structural change of the CSA parameters for terminal and bridging hydride ligands is rather unexpected in the light of previous observations reporting variations of *ca.* 10 ppm upon hydrogen bonds formation in organic compounds in the solid state.[23]

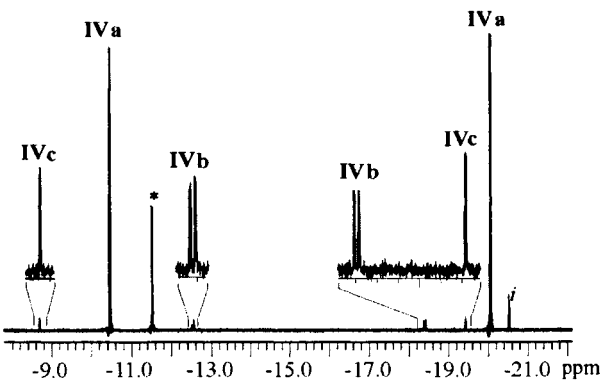

Figure 1: ^{1}H NMR spectrum of **IV** (toluene-d_8, 183 K, 9.4 T), showing the presence of the two minor isomers' resonances.

The assessment of τ_c for the main isomer of **IV** (**IVa**) has been exploited to yield the H---H interatomic distances in the two minor isomeric forms of this compound (**IVb** and **IVc**, see scheme 3). In fact, a careful examination of the hydride region in the ^{1}H NMR spectrum of **IV** at 183 K (fig. 1) reveals the presence of low intensity resonances (*ca* 1:100 with respect to the main signals) ascribed to the occurrence of two novel structural isomers of the cluster. Since

the three isomers have the same molecular weight and the same overall molecular shape, the τ_c values measured for the main isomer (**IVa**) can be safely transferred to the minor isomers as well. The relaxation times of the hydrides resonances of the minor isomers has then been measured at 217 K (9.4 T) and, through eq. (3), the H---H distances reported in scheme 3 have been determined.

It is worth noting that the short H---H distance in isomer **IVc** may suggest the occurrence of some interaction between the two hydride ligands. Indeed, in several organometallic systems the occurrence of such short H---H distances have been associated with the presence of unconventional hydrogen bonds.[24-29] In **IVc**, one may suggest that a difference in the polarisation of the bridging and terminal hydride-metal bonds causes the upsurge of different polarities at the hydride ligands, which in turn yield to the set-up of an H---H interaction. Such an interaction can be envisaged as an intermediate state in the pathway of molecular hydrogen elimination from **IV**.[30]

What is the error in the determination of H---H distances when the CSA contribution to the observed relaxation rate of an hydride is neglected? In order to answer this question we have re-investigated the relaxation processes in **II**. In fig. 2 the temperature dependence of T_1 at 6.34 T is reported.

By using r_{H-H} equal to 2.38 Å and the reported value for the CSA (18.89 ppm),[22] we were able to fit the experimental data to equations (3)-(6), obtaining τ_0 = 5.7 10^{-13} s and E_a = 9.3 kJ/mol. By repeating the same measurements at 9.4 T we found a good agreement between the experimental data and those calculated by using the parameters previously derived at 6.34 T. At 9.4 T the omission of the CSA contribution should produce an overestimation of about 10% of the dipolar term, with an error of only 2% in the evaluation of the r_{H-H} distance (2.39 Å instead of 2.35 Å).

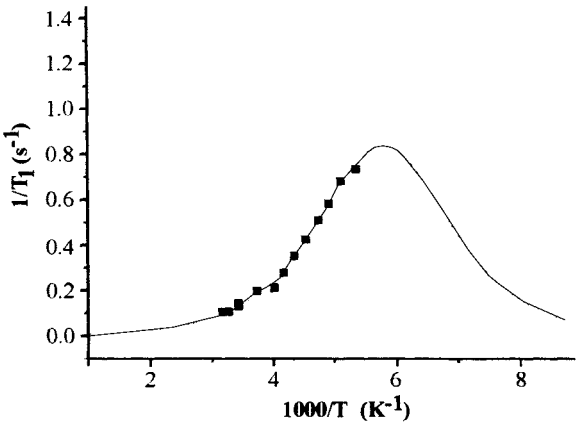

Figure 2: Temperature dependence of the hydrides resonance relaxation rate for **II** ($CDCl_3$, 6.34 T).

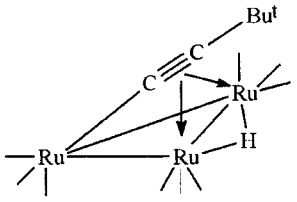

Scheme 4

Of course, the CSA term may play a more relevant role when the dipolar mechanism is less efficient. This is, for instance, the case of $(\mu\text{-H})Ru_3(CO)_9(C_2Bu^t)$ (**V**, scheme 4), a compound which is formed by oxidative addition of H-C≡C-Bu^t on the tri-ruthenium surface.[31]

The organic ligand acts as a five-electron donor through the formation of one σ- and two π-bonds. From the results of a neutron diffraction study[32] it is possible to estimate a distance of *ca.* 4.0 Å between the hydride ligand and the protons of the freely rotating t-Bu group. Thus, the long H---H distance reduces the relevancy of the dipolar term with a consequent increase in the overall T_1 of the hydride resonance, which results to be equal to 28.5 s at 298 K in toluene-d_8 at 9.4 T.[33] Measurements of T_1 as a function of the applied magnetic field are reported in fig. 3.

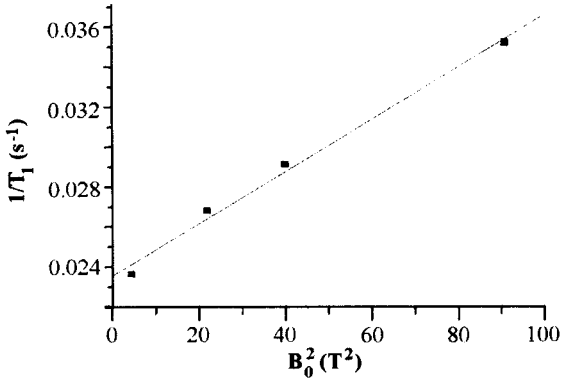

Figure 3: Dependence of the hydride T_1 upon the applied magnetic field strenght for **V** (toluene-d_8, 298 K).

From the slope of the line, on the assumption that τ_c is 30 ps, a value of 21.7 ppm has been obtained for the CSA of the hydride resonance. The measurement

of the hydride signal's T_1 over an extended range of temperatures (fig. 4) discloses an interesting property of this compound, that possibly can be general in the class of cluster derivatives. In fact, whereas the behaviour of T_1 from low to room temperature corresponds nicely to the behaviour shown by other hydrides, above 308 K the hydride relaxation rate suddenly increases. The observed behaviour (well reversible) can be accounted for in terms of the occurrence of an additional relaxation contribution which increases with increase in temperature. We believe that the increased temperature allows the promotion of unpaired electron density into metal-metal antibonding molecular orbitals. Such a termally activated process preceeds the homolytic fission of the metal-metal bond in metal clusters and its detection in **V** has been possible because of the role of the capping acetylide moiety in keeping the cluster integrity.

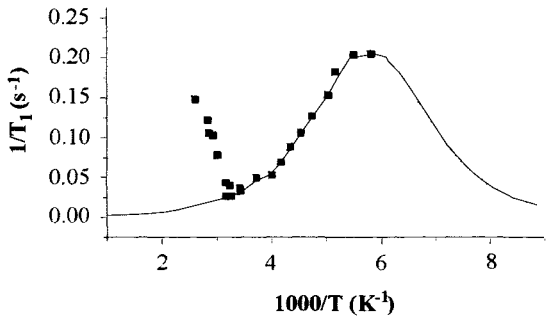

Figure 4: Temperature dependence of the hydride resonance relaxation rate for **V** (toluene-d_8, 6.34 T).

12.4 THE DD-CSA INTERFERENCE TERM.

As shown above (fig. 1) the ^1H NMR spectrum of **IVa** at 400 MHz consists of two doublets ($J_{H,H}$ = 2.3 Hz) for the terminal and bridging hydrides. A careful inspection of the spectrum shows that the linewidths within each of the doublets differ by about 0.3 Hz. This difference is almost completely removed at 270 MHz. The reason for this differential broadening is related to the presence of a cross-relaxation contribution to the transverse relaxation time, due to interference between CSA and dipolar interaction.[34]

Errors in the measurement of the small differential broadening in the doublets restrict its utility for the direct evaluation of the interference term. An alternative approach is represented by the use of the longitudinal relaxation times.

It has been shown that the interference term cannot be directly obtained from an inversion recovery experiment which uses the usual 180°-τ-90° pulse

sequence. Dalvit and Bodenhausen showed[35] that by using the pulse sequence 180°-τ-β, with β = 20° the difference of the longitudinal relaxation times for the doublets components of an AX spin system can be related to the interference term by the equation (for nucleus A):

$$\frac{1}{T_1^{DD-CSA}} = \frac{1}{10}\left(\frac{\mu_0}{4\pi}\right)\gamma_A^2\gamma_X\hbar < r_{AX}^{-3} > B_0\Delta\sigma_A \frac{\tau_C}{1+\omega_A^2\tau_C^2}\frac{1}{2}\left(3cos^2\varphi - 1\right) \qquad (7)$$

From the data on the terminal hydride doublet of **IVa** we found two possible values for φ, respectively of 47.2° and 132.8°. If it's assumed that the principal component of the CSA vector lies along the direction of the M-H bond, the value of 132.8° seems to be the most plausible.

By repeating the same measurements on **IVb**, we found a φ value of 2.1° or 177.6°. This appears in good agreement with the trans arrangement of the two hydride ligands in this isomer.

It will be shown later that the interference term, whose contribution to the overall relaxation rate of hydride ligands is very small, becomes of paramount importance in some experiments with para-H_2 (*vide infra*).

12.5 ^{2}H QUADRUPOLAR COUPLING CONSTANTS (^{2}H-QCC) OF HYDRIDES.

Another parameter which can provide useful insights into the minor electronic differences of hydride typologies deal with the evaluation of the ^{2}H Quadrupolar Coupling Constants (^{2}H-QCC)[17] in suitably deuterated derivatives. As a prototype example for the evaluation of this parameter and its application we considered **IVa**.[20] The ^{2}H-NMR spectrum (fig. 5) shows that the terminal hydride signal is significatively broader than that of the bridging hydride (unfortunately the larger linewidth and the lower frequency separation of the ^{2}H resonances prevented the observation of the minor isomers **IVb** and **IVc**).

In the presence of isotropic molecular motion, the difference in the linewidths of the two hydride resonances is an unambiguous reporter of the difference in their ^{2}H-QCC values. ^{2}H nuclei (I = 1) are quadrupolar and have a non-spherical charge distribution characterized by the electric quadrupole moment eQ; *i.e.* the ^{2}H nuclei behave as prolate ellipsoids. This affords the possibility of a relaxation mechanism which does not depend upon a fluctuating magnetic field at the nucleus, but upon the interaction of the non-spherical nuclear charge with fluctuating electric field gradients at the nuclei. These electric field gradients

are produced by a non-spherical electron distribution about the nuclei. Thus the QCC represents such interaction and its measurement reports about the distribution of electronic charge along the metal-hydrogen bond.

The accurate determination of the latter parameter is possible by measuring the longitudinal relaxation time T_1 of the two ^2H resonances and by applying equation (8). [36]

$$\frac{1}{T_1} = \frac{3}{50}\pi^2 \frac{2I+3}{I^2(2I+1)}(QCC(^2H))^2\left(1+\frac{\eta^2}{3}\right)\left(\frac{\tau_c}{1+\omega_o^2\tau_c^2}+\frac{4\tau_c}{1+4\omega_o^2\tau_c^2}\right) \quad (8)$$

where:

$$QCC(^2H) = \frac{e^2 q_{zz} Q}{h} \quad (9)$$

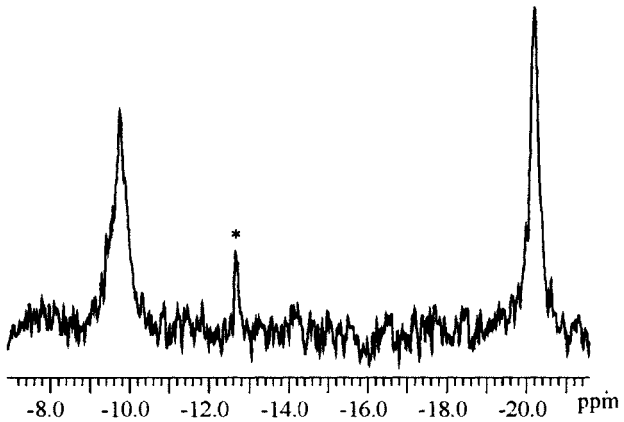

Figure 5: ^2H NMR spectrum of **IV** (toluene-d_8, 183 K, 9.4 T). * indicates $(\mu\text{-}^2H)Os_3(CO)_{10}$.

By assuming that the asymmetry factor, η, is equal to zero, and by using the τ_c value obtained from the ^1H T_1 measurements, the ^2H-QCC values of 86.4 ± 1.5 kHz and 60.1 ± 2.0 kHz for H_T and H_B respectively were obtained by fitting the experimental T_1 *vs* 1/T data against equation 8.

Deuterium QCC's have been reported for several metallic hydrides.[36-38] The smallest value (33 kHz) has been found for LiD getting close to the ionic limit of a M-D bond with a zero QCC(^2H).[36] The pure covalent end of the scale is reported for the HD molecule, whose ^2H-QCC is 227 kHz. In the field of metal carbonyl hydrides, the QCC(^2H) values have been measured for a

terminal hydride in $^2HMn(CO)_5$[38] (68.1 kHz) and for bridging hydrides in six binuclear derivatives of formula $[(\mu\text{-}^2H)M_2(CO)_{10}]^-X^+$ (M = Cr, Mo) (with values ranging from 54.8 to 90.4 kHz, depending on the metal ion and on the counterion X^+).[37] Thus, although the values found for **IVa** fall in the range of the literature data, it appears difficult to draw an overall rationalisation of the relationship between the ^2H-QCC values and the hydride bonding scheme in metal complexes. However, it seems reasonable to compare the deuterium QCC's for related classes of compounds, and even more for different hydrides in the same molecule, as in **IVa**. Of course, the assumption of the same η (equal to zero) for both the terminal and the bridging hydrides in the latter compound may introduce an error in the determination of their ^2H-QCC's. Anyway, it is clear that the asymmetry should be larger for the bridging than for the terminally bound hydride: thus the difference between the deuterium QCC's of the two hydrides calculated in this work represents a low-limit value.

Some further considerations can be made on the basis of the suggestion that the ionicity of the M-D bonds in metal hydrides can be estimated by applying the following equation [36]:

$$i = 1 - \frac{QCC(^2H)}{227} \qquad (10)$$

Upon introducing the ^2H-QCC values calculated for **IVa**, *i* values of 0.736 and 0.620 have been obtained for H_B and H_T respectively. This finding supports the occurrence of a different "hydridicity" for bridging and terminal hydrides in the title molecule, being H_T less negatively charged than H_B. One may further speculate that H_T in isomer **IVc** might have an even reduced "hydridicity" (as it is trans to an Os-Os bond) to make more acceptable the idea of some H---H interaction as their distance would suggest.

12.6 EXCHANGE PROCESSES INVESTIGATED BY T_1 AND T_2 OF HYDRIDE LIGANDS.

In principle, the time dependence of the magnetic interactions responsible for the relaxation processes can be exploited to investigate dynamic processes as the chemical exchange of ligands in coordination complexes.

A thorough example of this kind of application is provided by the study of the hydride exchange in $[(H)(\mu\text{-}H)_2Pt_2(dppe)_2][BF_4]$[39] (dppe = bis(diphenylphosphino)-ethane, **VI**, see scheme 5)). Variable temperature ^1H

NMR studies of this compound are consistent with a rapid exchange of the terminal and the bridging hydride ligands, which cannot be "frozen out" down to the lowest accessible temperature.

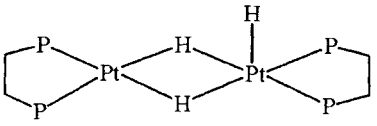

VI

Scheme 5

The hydride region of **VI** (fig. 6) shows a pattern of quintets arising from the coupling of the hydride resonance with four equivalent phosphorous (^{31}P, I = ½, natural abundance 100%) and two equivalent Pt nuclei (^{195}Pt, I = ½, natural abundance 33.8%).

From this spectral pattern one may only obtain the averaged value for proton-phosphorous ($J_{P,H}$ = 37.0 Hz) and proton-platinum ($J_{Pt,H}$ = 500.4 Hz) coupling constants.

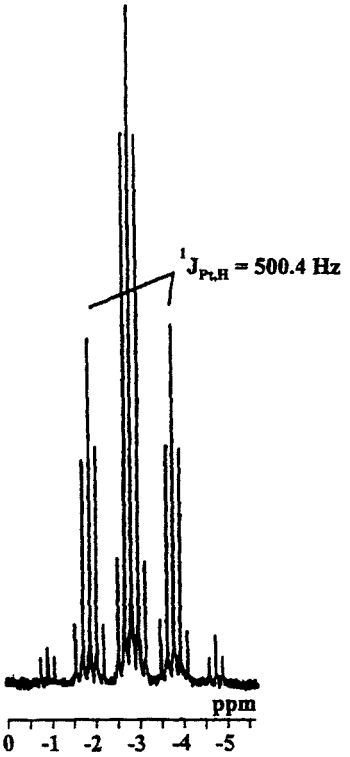

Figure 6: Hydride region of the ^1H NMR spectrum of **VI** (CD_2Cl_2, 297 K, 6.34 T).

The occurrence of different isotopomers and the fast chemical exchange cause significant differences in the longitudinal and transverse relaxation rates of the satellite peaks with respect to the central ones. The T_1 of the central peaks is dominated by H---H and P---H dipolar interactions, modulated by the molecular tumbling. The T_2 of this set of resonances is shorter because, in addition to the dipolar interaction, it experiences a contribution arising from the fast exchange between bridging and terminal sites:

$$\frac{1}{T_2^{obs}} = \frac{1}{T_2^0} + \frac{1}{T_2^{ex}} \tag{11}$$

where T_2^0, the transverse relaxation time in the absence of exchange, is set equal to T_1. Furthermore, it may be shown that:

$$\frac{1}{T_2^{ex}} = 0.22(\delta_\omega)^2 \tau_M \tag{12}$$

where δ_ω is the chemical shift separation between bridging and terminal hydride resonances, and τ_M is their exchange lifetime.

On the other hand, the transverse relaxation rate of the satellite peaks is significantly higher than that of the central peaks because it receives contributions from the dipolar and scalar coupling to the magnetically active ^{195}Pt nuclei:

$$\frac{1}{T_2^{sat}} = \frac{1}{T_2^{central}} + \frac{1}{T_2^{DD(Pt-H)}} + \frac{1}{T_2^{sc}} \tag{13}$$

$1/T_2^{DD(Pt\text{-}H)}$ corresponds to the increment measured for T_1 of the satellite peaks in respect to the central ones.

The scalar coupling contribution ($1/T_2^{sc}$) is determined by:

$$\frac{1}{T_2^{sc}} = \frac{{}^1J_{Pt,H}^2 S(S+1)}{3}\left[\tau_M + \frac{\tau_M}{1+(\omega_H - \omega_{Pt})^2 \tau_M^2}\right] \tag{14}$$

Since the averaged $^1J_{Pt,H}$ values are known, evaluation of equation (14) allows the determination of τ_M. This has been done at different temperatures, and an Arrhenius plot of the log of the exchange rates ($K = 1/\tau_M$) *vs* 1/T provides the activation energy associated to the exchange (17.2 kJ/mol). Now the knowledge of τ_M allows to get an estimation of δ_ω according to equation (12); from the body of these calculations, the chemical shift separation between bridging and terminal hydrides results to be equal to 2.0 ± 0.1 ppm.

Figure 7 shows the behaviour of $\log T_1$ and $\log T_2$ *vs* 1/T (K^{-1}).

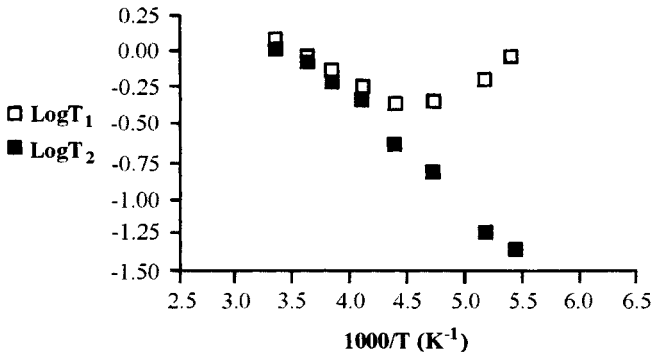

Figure 7: Temperature dependence of $logT_1$ and $logT_2$ for **VI** (CD_2Cl_2, 6.34 T).

The compound shows a T_1 minimum close to 223 K: at this temperature then $\omega_0\tau_c = 0.623$. It follows that we can estimate the magnitude of the magnetic interaction C, whose modulation *via* τ_c determines the T_1 of the central peaks:

$$\frac{1}{T_1^{central}} = C\tau_c \tag{15}$$

By assuming that C does not vary in the range of temperatures considered in this study, we can compute the τ_c values at each temperature at which T_1's have been measured. An Arrhenius plot of these values *vs* 1/T affords the activation energy associated with the molecular tumbling (8.6 kJ/mol).

For the central peaks, C results from several H---H and H---P magnetic interactions, but to a first approximation it may be roughly regarded as the result of the interactions inside the set of the three hydride resonances:

$$C = \frac{2\gamma_H^4\eta^2 I(I+1)}{r_{H-H}^6} \tag{16}$$

If we consider that each hydride interacts with both the other two, an averaged $r_{H\text{-}H}$ distance of 2.53 ± 0.03 Å is found, in good agreement with the 2.399, 2.401 and 2.561 Å obtained for the $r_{H\text{-}H}$ distances from the neutron diffraction study.[40]

12.7 DETECTION OF UNCONVENTIONAL HYDROGEN BONDS INVOLVING HYDRIDE LIGANDS.

A conventional hydrogen bond is the interaction between a proton donor, such as an OH group, and a proton acceptor, such as an oxygen or nitrogen lone pair. Few years ago a new type of interaction, the H---H or dihydrogen bond, between a typical proton donor such as an N-H or O-H group and an hydride ligand as acceptor was described [41]. Such an interaction has been classified as unconventional hydrogen bond. Both inter-[24-26] and intramolecular[27-29] examples of this new type of interaction have been reported and it was anticipated that it might be capable of stabilizing reaction intermediates[42] and, in turn, of providing novel routes for investigating the reactivity and catalytic activity of metal-hydride containing species. The M-H---H-X systems resulting from this kind of interaction have close H---H contacts and therefore can be determined by ^{1}H NMR relaxation measurements.

The close proximity of ligands bound to the surface of metallic clusters may strongly prompt the formation of analogous interactions, thus directing the regiospecificity of a suitable entering ligand. This concept has been proved by considering the reactions between the electronically unsaturated cluster **II** and Lewis base ligands L (L = NH_2Et, $NHEt_2$, NEt_3).[43] On the basis of a number of related reactions involving isonitriles and nitrogen bases as added ligands, we expected the products of these reactions to be the coordinatively saturated $(H)(\mu\text{-}H)Os_3(CO)_{10}(L)$ (**VII**) species, containing L in either the syn (**VIIa**) or anti (**VIIb**) position with respect to the terminal hydride H_T (scheme 6).

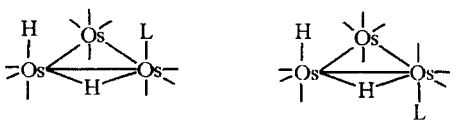

VIIa **VIIb**

Scheme 6

By carrying out the reactions in $CDCl_3$, it was found that, whereas no reaction takes place in the case of L = NEt_3, only the syn-isomers are formed when L = NH_2Et or $NHEt_2$. The distance H_T---H-N has been determined through the evaluation of the dipolar contribution from the amine to the relaxation rate of the terminal hydride resonance. This term has been accurately determined by comparing the hydride relaxation rates for the H-N and ^{2}H-N containing isotopomers and then applying equation (1), using a τ_c value of 245 ps (as obtained from the determination of minimum T_1). An $r_{H\text{-}H}$ value of 2.1 ± 0.05 Å has been found for both complexes (scheme 7). Such a short contact

strongly suggests the occurrence of an unconventional hydrogen bond in which the Os-H_T bond acts as proton acceptor from the N-H bond. This strong interaction is then responsible for the stabilisation of isomer **VIIa** and the lack of formation of isomer **VIIb** for both (H)(μ-H)$Os_3(CO)_{10}(NH_2Et)$ and (H)(μ-H)$Os_3(CO)_{10}(NHEt_2)$ in chloroform. Furthermore, in the absence of such an "anchoring" link, as in the case of NEt_3, no product is formed.

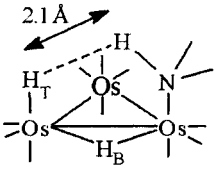

Scheme 7

Moreover, the occurrence of such a Os-H_T---H-N interaction on the surface of a metallic cluster has prompted us to pursue the synthesis of a novel class of terminally bound imine derivatives.[44] In fact it has been shown that the reactions of (H)(μ-H)$Os_3(CO)_{10}(NH_3)$ with several aldehydes in chloroform or methylene chloride readily afford the (H)(μ-H)$Os_3(CO)_{10}$(HN=CHR) (R = Me, Ph, CH_2Ph, i-Bu) derivatives, where the stabilization of the coordinated imine is promoted by the occurrence of the unconventional hydrogen bond described above (scheme 8).

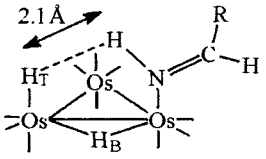

Scheme 8

However, when these (H)(μ-H)$Os_3(CO)_{10}$(imine) derivatives are dissolved in polar solvents such as methanol or acetone, both syn- and anti-isomers are present.[45] Thus it is clear that the overall stereochemistry of the resulting complexes is dependent upon the competition between intra- and intermolecular hydrogen-bonding interactions. It is worth to note that ^1H relaxation measurements show that in the syn-isomers the distance between the imine proton and the terminal hydride is significantly longer when the compounds are dissolved in the polar solvents rather than when they are dissolved in non-polar solvents (*i.e.* ca 4.0 Å against 2.1 Å). This finding has been accounted for on the basis of differences in the orientation of the imine

ligand in the syn-isomers in the two kinds of solvents. In solvents such as chloroform or methylene chloride the presence of an hydrogen bond minimizes the distance between the imine proton and the terminal hydride, thus forcing the imine ligand to be aligned with the Os-Os bond containing the bridging hydride. Conversely, when a polar solvent such as acetone is used, the weak intramolecular hydrogen bond interaction is no longer operative, allowing the imine ligand to rotate into a different, low-energy, orientation with a longer H_T—H-N distance, thus maximising the binding energy with the solvent molecules.

It is worth to note that the solid state X-ray structure determination of $(H)(\mu\text{-}H)Os_3(CO)_{10}(HN{=}CPh_2)$ (syn-isomer) yields an Os-H_T---H-N distance of only 1.79(6) Å.[46] This finding provides support to the view that the corresponding distances determined in solution by the relaxometric method represent averaged values, as the imine ligand appears to be involved in large oscillations over the metallic cluster. Clearly the competition for the formation of intermolecular hydrogen bonds with the dipolar solvent molecules further increases the space swept by the imine ligand as testified by the increased value of the Os-H_T—H-N distance measured in acetone.

12.8 RELAXATION PROCESSES AND PARA-H_2 EFFECTS IN ^{1}H NMR SPECTRA.

Since its discovery in 1986, para-H_2 effects in NMR spectra have been exploited in several applications, mainly dealing with the characterisation of solution structures of species which are present in solution in very low concentration and with the elucidation of hydrogenation reactions mechanisms.[47-53] This phenomenon comes from the tremendous enhancement of proton NMR transitions in the para-hydrogenated derivatives, which in theory may reach values as high as 10^5 times the signal intensity of the corresponding species produced with normal H_2[49] (which is a mixture of 25 % of para-H_2 and 75 % of ortho-H_2). In fact the addition of one molecule of para-H_2 to a substrate S leads to the formation of an SH_2 species, whose two hydrogen atoms maintain the polarization order of the parent para-H_2 molecule. So, in the case they give raise to an AX spin system, only the $\alpha\beta$ and/or $\beta\alpha$ eigenstates will be populated, whereas the $\alpha\alpha$ and $\beta\beta$ will not. It follows that the intensities of the four transitions of the AX spectrum will be markedly affected by such an unbalance in the spin populations; *i.e.* the $\alpha\beta\rightarrow\beta\beta$ and $\beta\alpha\rightarrow\beta\beta$ transitions will result in strongly enhanced absorption signals, whereas the $\alpha\beta\rightarrow\alpha\alpha$ and $\beta\alpha\rightarrow\alpha\alpha$ transitions will give raise to enhanced emission signals in the ^{1}H NMR spectrum of the product (fig. 8).[49]

The para-H_2 effects in the NMR spectra last for the time associated with the re-establishment of the Boltzmann populations defined by the strength of the applied magnetic field and the experimental temperature. Thus, the kinetics associated to the return of the NMR signals to their normal intensities provides information on the relaxation rates of the hydrogenated product as well as of the eventual intermediate(s) formed along the hydrogenation pathway.

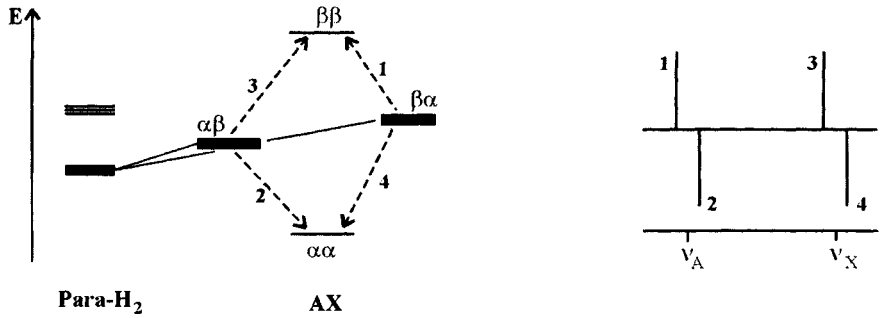

Figure 8: (a) Diagram of the energy levels in the AX spin system of an hydrogenated product showing the overpopulation of the αβ and βα states due to para-H_2 and (b) schematic representation of the resulting ^{1}H NMR spectrum.

Upon investigating the hydrogenation reaction of $Os_3(CO)_{10}(NCCH_3)_2$ (**VIII**), which leads to the formation of **II**, we found that the relaxation paths occurring at the intermediate $(H)(\mu\text{-}H)Os_3(CO)_{10}(NCCH_3)$ (**IX**) are responsible for the strong emission observed for the hydride resonance of the product.[54] At a first glance this result was rather surprising as the two protons in **II** are strictly magnetically equivalent and should not lead to any kind of enhancement. The negative signal observed for the two equivalent protons can be accounted for only on the ground of the mechanism of its formation (scheme 9).

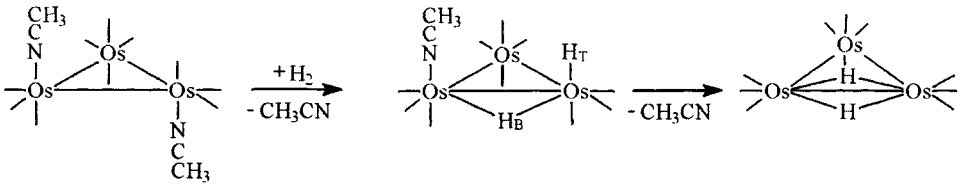

Scheme 9

According to this mechanism, the added H_2 molecule is first transformed into the AX spin system of the intermediate **IX** and then back again to an A_2 spin system in **II**. The critical points represented by the lifetime of the intermediate

containing the two magnetically non-equivalent hydrogen atoms. In this case, the bridging and the terminal hydrides in **IX** relax through dipolar, CSA and DD-CSA interactions. Whereas the first two processes contribute to the same extent to the relaxation of the terminal and bridging hydrides, the latter term does not. Such a difference between the relaxation rates of the two types of hydride ligands leaves a memory in the relative populations of the A_2 spin system in **II**, resulting in an excess of spin population in the ββ state (fig. 9). Such an unbalance is, in turn, responsible for the observed emission signal.

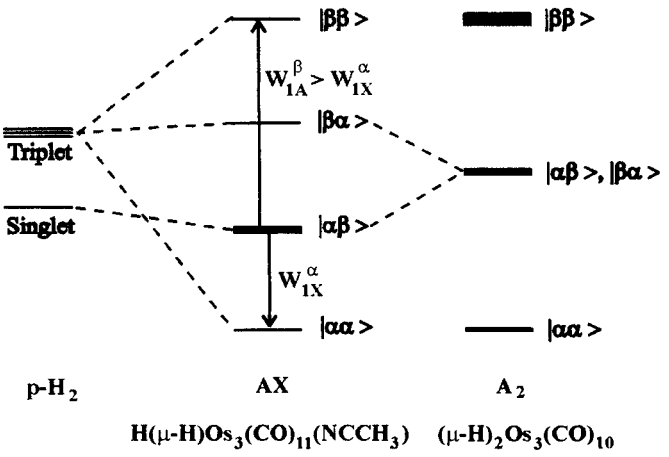

Figure 9: Schematic representation of the relative populations of the energy levels of para-H_2, **IX** (AX spin system) and **II** (A_2 spin system) upon hydrogenation of **VIII**.

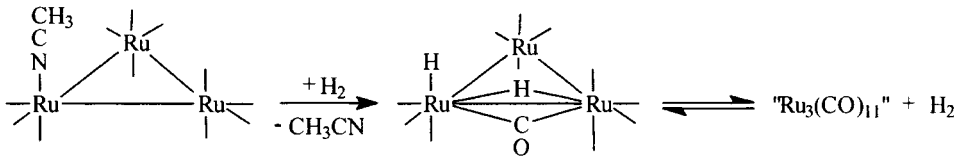

Scheme 10

A related experiment deals with the reaction of $Ru_3(CO)_{11}(NCCH_3)$ (**X**) with H_2 to give $(H)(\mu\text{-}H)Ru_3(\mu\text{-}CO)(CO)_{10}$ (**XI**), which, unlike its Os analogous derivative, contains a bridging carbonyl. This minor structural change appears to be responsible for the noticeable difference in reactivity with respect to the Os case: in fact at room temperature **XI** is in equilibrium with the coordinatively unsaturated "$Ru_3(CO)_{11}$" species and H_2 (scheme 10).[55]

When para-H_2 is used, the free hydrogen resonance results in a strong emission signal. The observed behaviour can be accounted for by a polarization transfer from para-H_2 to the AX spin system of **XI** and then to the ortho-H_2, which is formed from **XI** by the dissociative pathway depicted in scheme 10. The otherwise forbidden singlet (para-H_2) to triplet (ortho-H_2) transition is then made possible through the intermediacy of the bis-hydride derivative.[56]

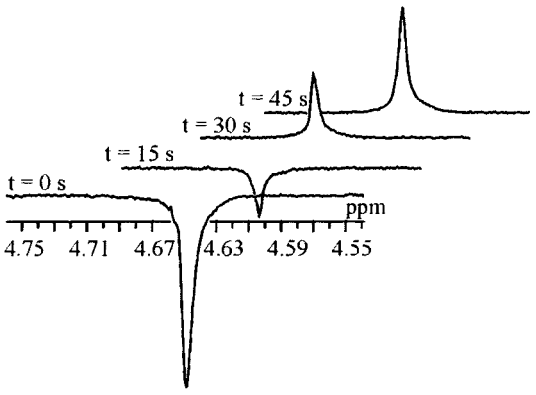

Figure 10: Recovery of the molecular hydrogen signal intensity obtained by introducing different delays (t) before the acquisition of the ^{1}H-NMR spectrum (see scheme 10).

On comparing ^{1}H NMR spectra obtained for the reaction of para-H_2 with **X** at different reaction times (fig. 10), it can be seen that the H_2 signal starts as an enhanced negative value (due to the initial transfer from para-H_2), and then reaches its thermal equilibrium value by a complex mechanism basically determined by the relaxation rates of the protons in the ruthenium complex. Clearly, the exchange rate of H_2 over the triruthenium cluster should be faster than the relaxation rate of the hydride ligands, otherwise no memory of the intermediate state could have been revealed in the molecular hydrogen resonance.[56]

12.9 CONCLUDING REMARKS.

The results summarized in this chapter show that a detailed knowledge of the relaxation processes of hydride ligands can provide a number of structural, electronic and dynamic informations, which may result to be very useful for an in-depth elucidation of this important class of organometallic derivatives. In fact the assessment of the set of parameters involved in the relaxation mechanisms of hydride ligands provides the organometallic chemist with powerful tools,

nicely complementary with the information available from the analysis of their chemical shifts and coupling patterns.

Fields associated to the use of ^{2}H-QCC and ^{1}H-CSA of hydride ligands have been largely neglected in the past and certainly will deserve a strong impact in the future developments of this chemistry.

Particularly valuable appears the possibility of determining hydrogen-bonding interactions involving hydride ligands as they may represent key-steps in the molecular recognition processes which are at the basis of their further reactivity. Likely such unconventional hydrogen-bonding interactions may have a relevant role in addressing the chemical transformation on the surfaces of metallic clusters.

Finally, it has been shown how para-H_2 effects in the NMR spectra of hydrogenated products are largely affected by the relaxation processes occurring at intermediate steps represented by hydride derivatives. It is reasonable to foresee that a better control of the hydride relaxation processes occurring at these intermediate steps will allow the detection of even more impressive effects and, as a consequence, novel applications of the PHIP (Para Hydrogen Induced Polarization) experiments.[49]

REFERENCES.

[1] a) H.D. Kaesz; P.B. Saillant, Chem. Rev. 1972, 7, 231; b) C.J. Jameson; J. Mason in "Multinuclear NMR", J. Mason Ed. Plenum Press New York, p. 51; c) C. Eischenbroich; A. Salzer, "Organometallics: a Concise Introduction", Znd Ed. Verlag Chemie: Weinheim, Germany, 1992.

[2] a) A.D. Buckingham; P.J. Stephens, J. Chem. Soc. 1964, 2747; b) A.D. Buckingham; P.J. Stephens, J. Chem. Soc. 1964, 4563.

[3] Y. Ruiz-Morales; G. Schreckenbach; T. Ziegler, Organometallics 1996, 15, 3920.

[4] B.E. Mann; C. Masters; B.L. Shaw, Chem. Commun. 1970, 1041.

[5] D.G. Vander Velde; H.S. Holmgren; J.R. Shapley, Inorg. Chem. 1987, 26, 3077.

[6] A.A. Koridze; O.A. Kizas; N.E. Kolobova; P.V. Petroskii; E.I. Fedin, J. Organomet. Chem. 1984, 265, C33.

[7] J.S. Holmgren; J.R. Shapley; P.A. Belmonte, J. Organomet. Chem. 1985, 284, C5.

[8] E.C. Constable; B.F.G. Johnson; J. Lewis; G.N. Paine; H.J. Taylor, J. Chem. Soc., Chem. Comm. 1982, 754.

[9] J.A Cabeza; B.E. Mann; C. Brevard; P.M. Maitlis, J. Chem. Soc., Chem. Comm. 1985, 65.

[10] J.A. Cabeza; B.E. Mann; C. Brevard; P.M. Maitlis; C.J. Brevard, J. Chem. Soc., Dalton Trans. 1988, 629.

[11] R.G. Teller; R. Bau, Struct. Bonding (Berlin), 1981, 44, 1.

[12] C. Ammann; F. Isaia; P.S. Pregosin, Magn. Res. Chem. 1988, 26, 236.

[13] See for example: D.G. Hamilton; R.H. Crabtree, J. Am. Chem. Soc. 1989, 111, 8823.

[14] S. Aime; M. Botta; R. Gobetto; D. Osella, Inorg. Chem. 1987, 26, 2531.
[15] S. Aime; M. Cisero; R. Gobetto; D. Osella; A.J. Arce, Inorg. Chem. 1991, 30, 1614.
[16] J.H. Noggle; R.E. Schirmer, "The nuclear Overhauser effect, Chemical Applications", Academic Press, 1971.
[17] R.K. Harris in "Nuclear Magnetic Resonance Spectroscopy", Pitman Ed.: London, 1983.
[18] R.W. Broach; J.M. Williams, Inorg. Chem. 1979, 18, 314.
[19] R.H. Cratbree; B.E. Segmuller; R.J. Uriarte, Inorg. Chem. 1985, 24, 1949.
[20] S. Aime; W. Dastrù; R. Gobetto; A. Viale, Inorg. Chem. 2000, 39, 2422.
[21] T. Beringhelli; G. D'Alfonso; M. Freni; A.P. Minoja, Inorg. Chem. 1992, 31, 848.
[22] A.T. Nicol; R.W. Vaugham, Adv. Chem. Ser. 1978, 167, 248.
[23] E. Brunner; U. Sternberg, Progr. Nucl. Magn. Reson. Spectrosc. 1998, 32, 21.
[24] E. Peris; J.C. Lee; R.H. Crabtree, J. Chem. Soc., Chem. Comm. 1994, 2573.
[25] J.C. Lee; A.L. Rheingold; B. Muller; P.S. Pregosin; R.H. Crabtree, J. Chem. Soc., Chem. Comm. 1994, 1021.
[26] J. Wessel; J.C. Lee; E. Peris; G.P.A. Yap; J.B. Fortin; J.S. Ricci; G. Sini; A. Albinati; T.F. Koetzle; O. Eisenstein; A.L. Rheingold; R.H. Crabtree, Angew. Chem. Int. Ed. Engl. 1995, 34, 2507.
[27] E.S. Shubina; N.V. Belkova; L.M. Epstein, J. Organomet. Chem. 1997, 536-537, 17.
[28] L.M. Epstein; E.S. Shubina, Berichte der Bunsen-Gesllaschft Phys. Chem. Chem. Phys., 1998, 102, 359.
[29] E.S. Shubina; N.V. Beilkova; A.N. Krylov; E.V. Vorontsov; L.M. Epstein; D.G. Gusev; M. Niedermann; H. Berke, J. Am. Chem. Soc. 1996, 118, 1105.
[30] A.J. Pöe; C.N. Simpson; R.T. Smith, J. Am. Chem. Soc. 1993, 115, 3174.
[31] E. Sappa; O. Gambino; L. Milone; G. Cetini, J. Organomet. Chem. 1972, 39, 169.
[32] M. Catti; G. Gervasio; S.A. Mason, J. Chem. Soc. Dalton Trans. 1977, 2260.
[33] S. Aime, R. Gobetto; unpublished results.
[34] M. Goldman, J. Magn. Res. 1984, 60, 437.
[35] C. Dalvit; G. Bodenhausen, Chem. Phys. Lett. 1989, 161, 554.
[36] D. Nietlispach; V.I. Backmutov; H. Berke, J. Am.Chem. Soc. 1993, 115, 9191.
[37] A.J. Kim; F.R. Fronczen; L.G. Butler; S. Chen; E.A. Keiter, J. Am. Chem. Soc. 1991, 113, 9090.
[38] P.S. Ireland; L.W. Olson; T.L. Brown, J. Am. Chem. Soc. 1975, 97, 3548.
[39] S. Aime; R. Gobetto; A.L. Bandini; G. Banditelli; G. Minghetti, Inorg. Chem. 1991, 30, 316.
[40] M.Y. Chiang; R. Bau; R. Minghetti; A.L. Bandini; G. Banditelli; T.F. Koetzle, Inorg. Chem. 1984, 23, 122.
[41] R.H. Crabtree; P.E.M. Siegbahn; O. Eisenstein; A.L. Rheingold; T.F. Koetzle, Acc. Chem. Res. 1996, 29, 348.
[42] V.I. Bakhmutov; E.V. Bakhmutova; N.V. Belkova; C. Bianchini; L.M. Epstein: M. Peruzzini; E.S. Shubina; E.V. Vorontsov; F. Zanobini, "Euro-Hydride 2000", Dijon, France, September 2000, book of abstracts, p. 35.
[43] S. Aime; R. Gobetto; E. Valls, Organometallics 1997, 16, 5140.

[44] S. Aime; M. Ferriz; R. Gobetto; E. Valls, Organometallics 1999, 18, 2030.
[45] S. Aime; M. Ferriz; R. Gobetto; E. Valls, Organometallics 2000, 19, 707.
[46] S. Aime; R. Gobetto; M. Milanesio; E. Valls, D. Viterbo, manuscript in preparation.
[47] C.R. Bowers; D.P. Weitekamp, Phys. Rev. Lett. 1986, 57, 2645.
[48] C.R. Bowers; D.H. Jones; N.D. Kurur; J.A. Labinger; M.G. Pravica; D.P. Weitekamp, Adv. Magn. Res. 1990, 14, 269 and references therein
[49] R. Eisenberg, Acc. Chem. Res. 1991, 24, 110 and references therein
[50] S.B. Duckett; C.L. Newell; R. Eisenberg, J. Am. Chem. Soc. 1994, 116, 10548.
[51] S.B. Duckett; G.K. Barlow; M.G. Partridge; B.A. Messerie, J. Chem. Soc. Dalton Trans. 1995, 3427.
[52] J. Bargon; J. Kandels; P. Kating, J. Chem. Phys. 1993, 98, 6150.
[53] J. Bargon; J. Kandels; P. Kating; A. Thomas; K. Woelk, Tetrahedron Lett. 1990, 31, 5721.
[54] S. Aime; D. Canet; R. Gobetto, J. Am. Chem. Soc. 1998, 120, 6770.
[55] S. Aime; W. Dastrù; R. Gobetto; A. Viale, Organometallics 1998, 17, 3182.
[56] S. Aime; D. Canet; W. Dastrù; R. Gobetto; A. Russo; A. Viale, J. Phys. Chem. A, 1999, 103, 9702.

Chapter 13

Deuterium NMR Relaxation as a Method for the Characterization and Study of Transition Metal Hydride Systems in Solution

Vladimir I. Bakhmutov

INEOS-Russian Academy of Sciences, Vavilov Str. 28, 117813 - Moscow (Russia). Departamento de Quimica, Centro de Investigacion y de Estudios Avanzados del I.P.N., A. P. 14-740. Mexico, D. F. 07000 Mexico.

CONTENTS

13.1 INTRODUCTION

The spectroscopy of multinuclear magnetic resonance in solution is one of the most important analytical methods in structural studies of transition metal hydride complexes. Among different nuclei, the proton plays the main role because ^1H NMR provides a direct information about spectral properties of the hydride ligands. In addition the proton, being a non-quadrupolar and long-relaxing nucleus, gives rise to well-resolved NMR spectra which are very

conveniently analyzed. The NMR signals of quadrupole nuclei are usually broadened due to rapid relaxation and sometimes they even become unobservable. This situation relates to the well-known difficulties in the realization of the NMR experiments of such nuclei. In contrast, ^2H nuclei relax relatively slowly due to their small quadrupole moment and their solution NMR spectra are as well resolved as in the case of ^1H. This circumstance explains why the ^2H NMR spectroscopy has been applied in the chemistry of transition metal hydrides mainly in the traditional manner exploiting only the magnetic properties of such nuclei having a quadrupole moment (Q).

The energy of interaction of the nuclear quadrupole moment, Q, with the molecular electric field gradient, EFG, can be experimentally measured as the nuclear quadrupole coupling constant, NQCC [1]. EFG and NQCC are very sensitive to changes of the electronic distribution in the molecule, intermolecular association and solid-state effects [2]. Among different nuclei, the deuterium quadrupole coupling constant (DQCC) is of special interest, because there are many hydrogen atoms in organic and inorganic molecules, which may serve as probes for the studies of local EFGs. At the same time, the deuterium quadrupolar coupling constants are difficult to access among other reasons due to the low quadrupole moment of ^2H in comparison with other quadrupole nuclei. As a kind of substitute for this deficiency the deuterium became in recent years subject of quantum chemical calculations, which predict the DQCC value as a function of the electronic structure of organic and inorganic molecules [2-5].

It is well known that the nature of the metal - hydride bonds in transition metal hydride complexes is different in classical hydrides from those showing a quantum - mechanical behavior and finally in dihydrogen complexes [6-10] with H_2 binding to a metal atom in the η^2-fashion. It is obvious that these various metal - hydride bonding modes could be very interesting subjects for theoretical and experimental studies of the EFGs and DQCCs of deuterium ligands. In this paper we show how the DQCC values in transition metal hydride systems can be determined from deuterium spin – lattice (T_1) relaxation experiments in solution. In addition we would like to discuss the DQCC dependence on the changes of the metal-hydride bonding mode.

13.2 DEFINITIONS:THE ELECTRIC FIELD GRADIENT, THE ASYMMETRY PARAMETER OF THE ELECTRIC FIELD GRADIENT AND THE DEUTERIUM QUADRUPOLE COUPLING CONSTANT.

A covalent metal – deuterium bond creates a strong non - homogeneous electric field along the M - D direction (the Z axis). One of the important parameters, describing the electric field, is the magnitude of the EFG at the D

nucleus [11]. The quadrupole moment, Q, of the deuterium nucleus, created by a non-spherical distribution of the nuclear charge, can be characterized by the quantized energy levels. These levels correspond to different orientations of Q with respect to the EFG.

The EFG represents a tensor with the diagonal elements eq_{ZZ}, eq_{YY} and eq_{XX} where, by convention, the largest element of the tensor, eq_{ZZ}, is lying along the M-D bond. The energy of interactions of Q with the EFG (eq_{ZZ}) is expressed through DQCC as: $DQCC = e^2q_{zz}Q/h$. Thus, measurements of the DQCC values in transition metal hydrides lead to experimental characterizations of *a size* of EFG at D binding to the metal centre.

The spatial extension of an EFG is defined through the asymmetry parameter, $\eta = q_{XX} - q_{YY}/q_{ZZ}$. Thus this parameter represents the ratio between the diagonal elements of the EFG tensor. When η equals 0, the EFG tensor is axially symmetric. According to quantum chemical calculations, this situation is realised, for example, in C-D bonds of organic molecules, such as CD_3X (X=F. Cl, Br, I) [3], CD_3CN, D_2CO, CD_2F_2 [4] and etc. The EFG tensor is also practically axially - symmetric in the M-D bonds of terminal transition metal hydrides (see below).

It follows from the above definitions that the size and the shape of EFG are controlled by the charge distribution, surrounding D in the M-D bond. Obviously EFG and DQCC must be close to 0 when the charge distribution is spherical, for example in the case of the D^- anion. The zero DQCC value was also found experimentally in solid PdD where the environment of D has an octahedral symmetry [11].

13.3 THE ^2H SPIN - LATTICE (T_1) RELAXATION IN SOLUTION AS A METHOD TO DETERMINE DQCC IN TRANSITION METAL HYDRIDE SYSTEMS.

The DQCC values can be experimentally determined from ^2H solid - state NMR spectra [12], in NMR experiments with liquid crystal solvents [13] and also by microwave spectroscopy and nuclear double resonance [14]. However, the application of these techniques for transition metal hydrides seems to be problematic for different practical reasons. We show here that the DQCC values can also be determined by ^2H T_1 relaxation experiments on the D - derivatives of transition metal hydrides in solution. It is remarkable that T_1 relaxation studies on ^1H nuclei played a great role for the development of the transition metal hydride chemistry and led to the development of excellent methods providing reasonable geometric descriptions of the MH or $M(H_2)$ moieties in solution [15, 16].

In contrast to ^1H, the spin - lattice relaxation of ^2H is completely dominated by quadrupole interactions in eq. (1):

$$1/T_1 = (3/50)\pi^2(2I+3)(I^2(2I-1))^{-1}(e^2q_{zz}Q/h)^2(1+\eta^2/3)$$
$$(\tau_c/(1+\omega_D^2\tau_c^2)+4\tau_c/(1+4\omega_D^2\tau_c^2)) \quad (1)$$
$$\tau_c = \tau_0 \exp(E_{act}/RT)$$

where DQCC (kHz) = $(e^2q_{zz}Q/h)$, I is the spin of ^2H, η is the asymmetry parameter of EFG at ^2H and τ_c is the correlation time for molecular re - orientations with the activation energy E_{act} [17]. It is important that dipole –dipole interactions with the participation of D are negligible due to the small deuterium gyromagnetic ratio [17] and hence the DQCC value can be calculated directly from the T_1 time if the values of τ_c and η are known.

As in the case of ^1H, the T_1 time of deuterium can be obtained with the inversion - recovery (180^0 - τ - 90^0) experiments. The standard treatment of the collected data [16] as *monoexponential* NMR decays provides a quite good accuracy in the T_1 determination with errors < 5% [16]. Note that a non - exponential or biexponential deuterium relaxation in solution is rather a rare phenomenon [18].

A DQCC value for a transition metal hydride complex can be principally obtained from a single ^2H T_1 relaxation experiment, for example, at room temperature. Under these conditions molecular re-orientations are very fast ($1 >> \omega_D^2\tau_c^2$) and eq. (1) is simplified:

$$1/T_1 = 0.3\pi^2(2I+3)(I^2(2I-1))^{-1}(e^2q_{zz}Q/h)^2(1+\eta^2/3)\tau_c \quad (2)$$

The application of this approach can be demonstrated with the complex $(PPh_3)_3Ru(H_2)H_2$. This complex shows in the variable - temperature ^1H NMR spectra one averaged hydride resonance due to a fast hydride/dihydrogen positional exchange. Under a D_2 atmosphere in toluene the complex undergoes an isotopic H/D exchange to yield the product, containing D in the hydride positions and the *ortho* positions of the aromatic rings [19]. Both resonances are well detected in the ^2H room - temperature spectrum. The DQCC value in the C-D bonds of the aromatic ring is known (see, for example, [12]) and hence the measurements of the T_1 times for both ^2H nuclei provide to exclude the τ_c time from eq. (2). Finally it gives the DQCC value of 68.7 kHz for the hydride positions in the proposition $\eta = 0$ (see below). However it should be noted that the simple relaxation approach provides rather an estimation of DQCC. Actually such treatment is valid when the C-D and Ru-D vectors (corresponding to the orientations of the major components of EFG) move with the same τ_c time. This situation is usually realised for rather spherical molecules when molecular re - orientations are isotropic. However, molecular motions in solutions of transition

metal hydride complexes are anisotropic in most cases [16] and therefore the above DQCC determinations can produce some errors.

The correlation time in eq. (2) can be measured independently, for example, from the variable–temperature ^1H T_1 studies of H-derivatives of hydride complexes. Then, DQCC can be calculated using the found τ_c value and the ^2H T_1 time, measured for D- derivatives of the hydrides. This approach was recently applied to determine the DQCC values of 86.4 and 60.1 kHz for the terminal and bridging ligand in the complex $D(\mu\text{-}D)Os_3(CO)_{11}$ [20].

An analysis of the influence of anisotropic molecular motions on the measured T_1 times of the hydride resonances has been carried out for the ^1H frequency [16]. It was shown that these effects are minimized when the relaxation times reach minimums (T_{1min}). It is theoretically clear that in such cases the task of the DQCC determination is significantly simplified. Actually when the ^2H T_1 time reaches a minimum ($\tau_c = 0.62/\omega$), eq. (1) transforms to eq. (3) [21, 22]:

$$DQCC\ (kHz) = 1.220\ (1+ \eta^2/3)^{-1/2}(\nu\ (MHz) / T_{1min}\ (s))^{1/2} \qquad (3)$$

where ν is Larmor frequency of D. Thus the ^2H T_{1min} measurement gives directly the DQCC value in kHz.

From the experimental point of view the measurements of T_{1min} times in solutions of transition metal hydride complexes are not problematic at the ^1H frequency. In fact these minimal values are easily reached with modern spectrometers at low temperatures between - 60 and - 90^0 C. Moreover the ^1H T_{1min} time measurements are widely used in the structural analysis of hydride systems. In contrast to ^1H, deuterium has a low gyromagnetic ratio and therefore a low Larmor frequency. Hence the appearance of ^2H T_{1min} has to be expected at significantly lower temperatures with respect to ^1H. In addition, activation energies of molecular motions of transition metal hydride complexes are quite small and have values between 1.5 and 3.6 Kcal/mol [16]. For this reason the approach to a ^2H T_1 minimum is a challenging VT - NMR experiment [22]. Nevertheless it has been found that the use of concentrated solutions, increasing significantly the molecular correlation time [21, 22], provides to reach ^2H T_{1min} of transition metal hydrides. Add that toluene–H_8 and CH_2Cl_2 are the most convenient solvents for such experiments, because they provide a great temperature diapason and show a relatively large viscosity at low temperatures.

It is obvious that the DQCC value is directly calculated from the measured minimal T_1 time (see eq. (3)). However, the more accurate DQCC determinations can be carried out by the use of fitting procedures of the experimental points to eq. (1). These procedures give usually good agreements between the theoretical and experimental data, correct T_{1min} values and reasonable activation energies (2.5 - 4.0 kcal/mol) for molecular motions in solution [21, 23].

The solution relaxation experiments on the terminal transition metal hydride

complexes assuming $\eta = 0$ have revealed good agreements with solid - state ^2H NMR data. For example, complexes $MnD(CO)_3(PEt_3)_2$ (solution) and $MnD(CO)_5$ (solid state) show similar DQCC values of 66.7 ± 1.0 [21] and 68.1 [24] kHz, respectively. Similar DQCC values have also been determined for the terminal D ligand of complex $[RuD(D_2)(dppe)_2]^+$ in solution (79.0 kHz, [25]) and from the solid state ^2H NMR spectra (~ 75 kHz, [22]). The solution relaxation experiments on the CD_2 groups of the *dppm* ligands in complex Cp*(dppm)RuDMe led to a DQCC value of 164 kHz [26]. According to the ^2H solid state spectra, the methylene groups show DQCC values around 167 kHz [12].

From the methodical point of view, it should be emphasized that the collected relaxation data must be undistorted by possible D/D exchanges. This is especially important for hydride complexes obtained by protonation with an acid *in situ*. For example, it was shown that complex PP_3RuD_2 is easily protonated with an excess of CF_3COOD to yield dihydrogen compound $[PP_3Ru(D_2)D]^+$, $[PP_3=P(CH_2CH_2PPh_2)_3]$(eq. (4)) [25]. It is obvious that a slow $CF_3COOD/Ru(D_2)$ exchange [27], operating on the T_1 time scale, can distort the relaxation data. In such case it is useful to measure the relaxation times for both D-resonances. For example, the simple comparison of the variable-temperature T_1 data in Table 1 rules out the possible exchange effects. Similar data have been reported for complex $[(triphos)Rh(D_2)D_2]^+$, [tripos=$MeC(CH_2PPH_2)_3$] [28].

$$PP_3RuD_2 + D^+ \rightleftharpoons [PP_3Ru(D_2)D]^+ \qquad (4)$$

Table 1. Variable-temperature ^2H-T_1 times (ms, 61.402 MHz) for the OD and (D_2) resonances in solution of $[PP_3Ru(D_2)D]^+$ and CF_3COOD in CH_2Cl_2 [25].

CF_3COOD	(D_2)
5,7	58.8 (180 K)
6.5	43.4 (190 K)
11.4	78.3 (200 K)
15.1	79.4 (210 K)

13.4 THE ^2H T_1 RELAXATION AND THE DQCC VALUES IN TERMINAL TRANSITION METAL HYDRIDES IN SOLUTION.

The relaxation approach to the DQCC determination is based on the assumption that the asymmetry parameter of EFG is equal to zero in the terminal M-D bonds. Unfortunately this important parameter, characterizing the EFG shape, cannot be obtained from the relaxation data. Nevertheless the approximation

$\eta = 0$ seems to be realistic and is supported by MO calculations [25], Table 2. Actually η is calculated to be close to 0 in four transition metal hydride complexes and takes low values between 0.053 and 0.085. Thus, the EFG tensor is practically axial - symmetric in the terminal M-D bond. As mentioned above, the standard ^2H relaxation T_1 experiments give errors < 5%. Thus, for terminal hydrides the DQCC values can be determined with errors of 2-3% in spite of the ambiguity in the η parameter.

Table 2. Major components of EFG (eq_{ZZ}) and asymmetry parameters η, obtained for the terminal hydride ligands from the molecular orbital calculations (B3LYP).

Complex	eq_{ZZ} (au)	η
$WD(NO)(CO)_2(PH_3)_2$	- 0.1044	0.078
$OsD(D_2)(CO)Cl(PH_3)_2$	-0.1830	0.085
$[PP_3Ru(D_2)D]^+$	-0.1314	0.056
$[PP_3Os(D_2)D]^+$	-0.1490	0.053

Remarkable deviations of EFG from the axial symmetry should be expected for systems where one hydride ligand is connecting two metal centers. For example, the solid – state ^2H NMR spectra of complexes $[R_4N][DM_2(CO)_{10}]$, containing bridging hydride ligands, have shown a η value as large as 0.31 [29]. However, a simple inspection of eq. (1) reveals that even in this case the magnitude $(1+\eta^2/3)^{1/2}$ changes just insignificantly.

The nuclear quadrupole coupling constant is dictated by the size of EFG (eq_{ZZ}) depending on the charge distribution at a quadrupole nucleus. The eq_{ZZ} magnitude is quantitatively described as the sum of nuclear and electronic terms in equation (5):

$$eq_{zz} = +\sum_n K_n(3z_n^2 - r_n^2)/r_n^5 - e\ \psi^* \sum_i (3z_i^2 - r_i^2)/r_i^2\ \psi \qquad (5)$$

where n is the index of the other nuclei with charge K_n, i is the index of the electrons of the molecule, and r_n and r_i are corresponding distances [11]. In the context of M-D bonds this expression predicts that the DQCC value of terminal transition metal hydrides is sensitive to the nature of the metal and its ligand environment. According to the experimental data in Tables 3 and 4, these dependencies are actually pronounced and thus the variations in DQCC can be used for characterization of the metal – hydride bonding mode.

Table 3. The DQCC values in terminal Os hydride complexes.

Complex	DQCC (kHz)
PP_3OsD_2	79.7 [25]
$[OsD(D_2)(dppe)_2]^+$	81.0 [22]
$OsD(D_2)(CO)Cl(PPr^i_3)_2$	87.3 [23]
$OsD_4(PTol_3)_3$	91.0 [21]
$D(\mu\text{-}D)Os_3(CO)_{11}$	86.4 [20]

Eq. (5), having a common character, is valid for any quadrupole nuclei (N) and shows how eq_{ZZ} (or NQCC) strongly depends on the charge of neighbouring nuclei (X) in the X-N bond and the X-N bond length. Nevertheless the chemical meaning of this equation is not clear. The variations of the ^{35}Cl quadrupole constants in numerous organic and organometallic compounds were interpreted in terms of the ionic character of the element-chlorine bond [33]. A similar interpretation has been suggested for DQCC in terminal metal hydrides [21]. Then the ionic character of the M-D bond (**i**) can be expressed through the simple relation (6):

$$\mathbf{i} = 1 - DQCC/227 \qquad (6)$$

Table 4. The influence of the metal on the DQCC value (the ^2H T_1 relaxation, error $\leq \pm$ 1 kHz) in terminal transition metal hydride complexes

Complex	DQCC (kHz)
Cp_2ZrD_2	46.7 [31] Solid-state NMR
Cp_2MoD_2	52 [32] Solid-state NMR
Cp_2WD_2	54 [32] Solid-state NMR
PP_3RhD	73.9 [30]
PP_3RuD_2	73.3
	76.1 [25]
PP_3CoD	76.5 [30]
PP_3OsD_2	79.7 [25]
$(triphos)RhD_3$	83.2 [28]
$(triphos)IrD_3$	95.0 [28]

where DQCC is a measured magnitude and the factor of 227 (kHz) represents the DQCC value in the purely – covalent HD molecule. It is obvious that in the case of a purely - ionic M^+ D^- bond, the distribution of the negative charge around D is spherical and therefore DQCC is zero. In fact the alkali metal hydrides RbD and LiD, having the highest ionic character of all metal – hydride

bonds, show minimal DQCC values (Table 5). At the same time the C-D bonds in the methylene groups give, according to eq. (6), a reasonable low ionicity: DQCC = 167 kHZ and i = 0. 26.

Table 5. The DQCC values in transition metal hydride complexes and the ionic character (**i**) of the M-D bonds.

Compound	**DQCC (kHz)**	**i**
RbD	19.7 [11]	0.91
LiD	33 [11]	0.85
Cp_2ZrD_2	46.7 [31]	0.79
Cp_2MoD_2	52 [32]	0.77
$WD(CO)_2(NO)(PMe_3)_2$	55 [21]	0.76
$MnD(CO)_3(PEt_3)_2$	66.7 [21]	0.71
$OsD(D_2)(CO)Cl(PPr^i_3)_2$	87.3 [23]	0.61
$OsD_4(PTol_3)_3$	91.0 [21]	0.60
$RhDCl_2(PPr^i_3)_2$	136 [21]	0.40
HD	227 [11]	0

In spite of the simplicity of this DQCC interpretation, it provides a general conclusion: the M-H bonds in transition metal hydride complexes are quite polarized in the ground state. In the case of hydride complexes such as Cp_2ZrH_2 or Cp_2MoH_2 the conclusion agrees well with their chemical behaviour demonstrating the high hydridic character of the H-ligands [34-36]. In addition it was shown that the protonation of Cp_2MoD_2 and Cp_2WD_2 with HCl to yield the dihydrogen complexes follows an initial proton attack at the hydride ligand [37].

The DQCC measurement in complex $WD(CO)_2(NO)(PPh_3)_2$ reveals its high ionic character (Table 5). This pronounced hydridicity in the ground state correlates well with the behavior of the complex in the presence of proton donors: even less acidic alcohols interact with the hydride ligand to yield intermolecular $W\text{-}H^{\delta+}\ldots{}^{\delta-}HO$ hydrogen bonds [38]. Now the formation of dihydrogen $M\text{-}H^{\delta+}\ldots{}^{\delta-}HO$ bonds is well established for numerous transition metals [39, 40] and thus this phenomenon has a common character. Finally, the Os-D bonds show ionic character even in a complex such as $OsD_4(PTol_3)_3$. It is remarkable that this result agrees with a theoretical analysis of topological properties of the electron density on the osmium - hydride bonds in the complexes $OsH_4(PH_3)_3$ and $OsH_3\{k\text{-}N,k\text{-}S\text{-}(2\text{-}Spy)\}(PH_3)_2$ [41, 42]. It has been found that the Laplacian of the charge density takes positive values reflecting well an ionic character of the Os-H bonding.

13.5 DIHYDROGEN COMPLEXES: ^2H T_1 RELAXATION AND DQCC VALUES.

The unusual H-H bonding mode in dihydrogen complexes is of the greatest interest, also from the point of view of DQCC measurements. MO calculations of a simple $[Rb\text{-}D_2]^+$ model have shown that a transformation of classical dihydride structures to dihydrogen complexes leads to a dramatic increase of DQCC from 50 up to 155 kHz [11]. In addition, the asymmetry parameter η grows from 0.025 to 0.62 and the orientation of the major axis of EFG (eq_{ZZ}) is remarkably deviated from the D-D vector in the dihydrogen complex (Scheme 1). Similar data have also been obtained in MO calculations of transition metal hydrides (Table 6).

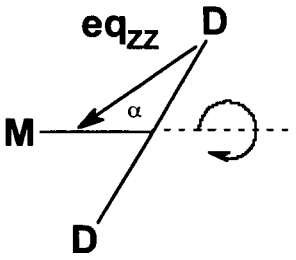

Scheme 1

Table 6. EFG (eq_{ZZ}) parameters, η, the DQCC and α values (see Scheme 1) calculated for transition metal dyhydrogen complexes (B3LYP level) [25].

Complex	eq_{ZZ} (au)	η	DQCC (kHz)	α
$W(D_2)(CO)_3(PH_3)_2$	-0.1767	0.64	119	84
$OsD(D_2)(CO)(Cl)(PH_3)_2$	-0.1830	0.085	123	-
$OsD(D_2)(CO)(Cl)(PH_3)_2$	-0.1919	0.481	129	84
$PP_3RuD(D_2)^+$	-0.1314	0.056	88	-
$PP_3RuD(D_2)^+$	-0.2231	0.45	150	84
	-0.2141	0.49	144	83
$PP_3OsD(D_2)^+$	-0.1490	0.053	100	-
$PP_3OsD(D_2)^+$	-0.1601	0.83	108	74
	-0.1530	0.87	103	72

It is seen that the classical hydride ligand in complex $PP_3RuD(D_2)^+$ shows a moderate DQCC value of 88 kHz while 150 kHz are calculated for the dihydrogen ligand. However, this tendency is probably not common because, for

example, the DQCC values of the hydride and dihydrogen ligands in Os complexes are quite similar. Nevertheless the η values and the orientations of eq_{ZZ} in the dihydrogen ligands of these complexes are close to those in the $[Rb\text{-}(D_2)]+$ model.

MO studies reveal that for the dihydrogen bonding mode one can expect DQCC values between 103 and 155 kHz. However, the theoretical DQCC values can be remarkably overestimated. This overestimation is directly observed for the terminal hydride ligands. According to MO calculations [25], the DQCC values in the W-D and Os-D bonds of complexes $WD(NO)(CO)_2(PH_3)_2$ and $OsD(D_2)(CO)Cl(PH_3)_2$ are equal to 70.2 and 123 kHz, respectively [25] versus 55.2 [21] and 87.3 [25] kHz measured experimentally. It should be noted that the MO – calculated eq_{ZZ} values can be converted into DQCC through the relation: DQCC = q_{ZZ}(au) 672 (kHz au^{-1}) [11]. It is quite probable that the coefficient of 672 requires some correction (see, for example, [5] for the deuterium constants and [44] for the coupling constants of other quadrupole nuclei). This circumstance complicates the DQCC studies of dihydrogen compounds.

Solution and solid state studies of non-classical transition metal hydride systems have revealed fast intramolecular motions of the dihydrogen ligands [7, 8]. These motions represent a rotational diffusion around the axis perpendicular to the H-H (or D-D) vector (Scheme 1), a libration (Scheme 2) or 180° - jumps (Scheme 3) around the same axis [43]. It has been shown that the type of motion, its frequency and the orientation of eq_{ZZ} (angle α in Scheme 1) affect strongly on the ^2H NMR parameters, causing an elongation of the ^2H T_1 time in solution [25] or a decrease of the quadrupole splitting in the solid -state ^2H NMR spectra [22]. This influence creates additional problems for DQCC determinations from experimental relaxation measurements or solid state NMR data, particularly when the orientation of the eq_{ZZ} vector is unknown.

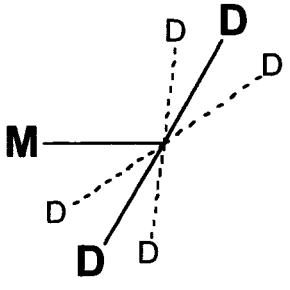

Scheme 2

The theoretical analysis of the relaxation [25] in the presence of a fast motion has shown that, for example, the ^2H T_{1min} value of 43 ms (61.402 MHz), measured for the dihydrogen ligand in a solution of $PP_3RuD(D_2)^+$, can give a DQCC value of 43.2 (fixed D_2 ligand), 86.4 (fast – spinning D_2 ligand at $\alpha = 90^0$), 102 (fast rotation at $\alpha = 77^0$) or 47 kHz (fast libration). Without additional independent data, this situation can result in ambiguous conclusions.

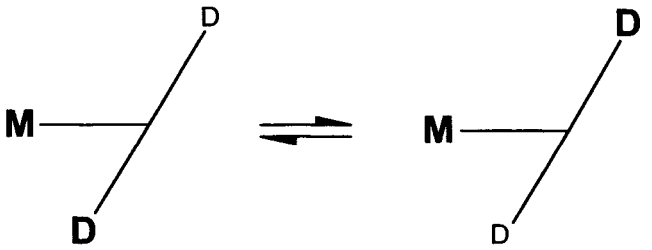

Scheme 3

Table 7 lists the DQCC values calculated directly from the T_{1min} relaxation times measured for the (D_2) ligands of transition metal dihydrogen complexes in solution. These values have been calculated by eq. (3) with the assumption of η being zero or varying between 0 and 1. All these DQCC values are remarkably smaller than those of classical hydride systems (see Table 3 and 4). They also differ significantly from the values predicted by MO calculations (Table 6). Probably the DQCC values in Table 7 are reduced due to the presence of fast (D_2) motions. According to ^2H solid state NMR, the motions are present even at lowest temperatures in the solid state [22].

Theoretical considerations show that a fast – spinning dihydrogen ligand can cause significant effects on the measured ^2H T_{1min} time. In the fast rotation regime, eq. (3) transforms to eq. (7) [25, 22],

$$DQCC = 2.440\ (1+ \eta^2/3)^{-1/2}[\nu / (T_{1min}\ (3\cos^2\alpha - 1)^2)]^{1/2} \qquad (7)$$

predicting *a maximal T_{1min} elongation* (for any DQCC value) when α is close to the magic angle ($\approx 54^0$). From a formalistic point of view, this situation corresponds to $T_{1min}(D_2) \rightarrow \infty$. It should be noted that this unusual feature could be a good test for the structural formulation of dihydrogen compounds.

The ^1H relaxation experiments on the hydride ligands led to the formulation of the T_1 criterion [15], providing the identification of transition metal dihydrogen complexes in solution. In practice, the ^1H T_1 time undergoes a strong *shortening* on going from the classical hydride ligands to dihydrogen ones. This effect is based on dipolar proton – proton interactions in the dihydrogen ligands and is due to the short hydride - hydride distances. An opposite effect, connected

with the other property of dihydrogen ligands (their fast intramolecular motions) should be expected for the ^2H T_{1min} time. Accordingly, it has recently been found that the minimum T_1 value of the (D_2) ligand in $RuD(D_2)(dppe)_2^+$ is 12 times *greater* than that of the terminal deuteride ligand [22]. A more pronounced elongation of T_{1min} has been reported for such complexes as $(triphos)RhD_2(D_2)^+$ or $(triphos)IrD_2(D_2)^+$ [28]. Here the T_{1min} time increases approximately 80-fold, going from the classical deuteride ligand to the (D_2) ligand. In these Rh and Ir complexes the fast – spinning dihydrogen ligands have an eq_{ZZ} with α being close to the magic angle.

Table 7. DQCC values of transition metal dihydrogen complexes directly determined from ^2H T_{1min} times in solution.

Complex	DQCC (kHz)
$OsD(D_2)(CO)Cl(PPr^i_3)_2$	74 [23]
$PP_3OsD(D_2)^+$	43 [25]
$OsD(D_2)(dppe)_2^+$	27-31 [22]
trans-$OsCl(D_2)(dppe)_2^+$	59-68 [22]
$Os(D_2)(CO)Cl_2(PPr^i_3)_2$	120-167 (solid state NMR) [22]
$PP_3RuD(D_2)^+$	43 [25]
$RuD_2(D_2)(PPh_3)_3$	58 [25]
$RuD(D_2)(dppe)_2^+$	19-22 [22]
trans-$RuCl(D_2)(dppe)_2^+$	38-44 [22]
$Cp^*Ru(D_2)(dppm)_2^+$	57-66 [22], 65 [25]
$ReD(D_2)(CO)(NO)(PMe_3)_2$	70 [21]
$Re(D_2)(CO)(PMe_3)_4^+$	57 [21]

Table 8 shows DQCC values for two relative osmium dihydrogen complexes, obtained experimentally in solution (^2H T_{1min} measurements), solid - state (line - shape analysis of the ^2H NMR resonances) and by the quantum – chemistry calculations. The solution relaxation data for $OsD(D_2)(CO)Cl(PPr^i_3)_2$, analyzed in terms of a fast – librating dihydrogen ligand [43] (α and η were taken from the MO calculations [25]), lead to 86 kHz. This value is similar to 87.3 kHz, determined for the classical D ligand in this complex (see Table 3), but can increase to 101 kHz when α is close to the magic angle (~54°) in the librating dihydrogen ligand.

The MO calculations of DQCC in the (D_2) ligand of $OsD(D_2)(CO)Cl(PH_3)_2$ resulted in a remarkably larger value of 129 kHz. However, as mentioned above, this value can be overestimated. Thus on the basis of the relaxation and MO studies one can deduce a semi-quantitative conclusion: the DQCC value in the dihydrogen ligand of complex $OsD(D_2)(CO)Cl(PPr^i_3)_2$) is lying between 86 and 129 kHz and the direction of the eq_{ZZ} vector is remarkably deviated from the D-D bond.

According to the variable - temperature solid -state ^2H NMR studies, the (D_2) ligand in the relative dihydroden complex $Os(D_2)(CO)Cl_2(PPr^i_3)_2$ undergoes fast 180^0 jumps [22]. The line – shape analysis gives two possible sets of the parameters: DQCC = 120 kHz at $\eta = 0$ and $\alpha = 52.5^o$ or DQCC = 167 kHz when $\alpha = 49.7^o$ and $\eta = 0.28$. Note that both DQCC values are significantly larger than those measured for the classical hydride ligands of the Os complexes in Table 3.

Table 8. DQCC values in the dihydrogen ligands of Os complexes obtained from ^2H T_{1min} measurements in solution [25], by the line-shape analysis of the ^2H NMR signals in solid state [22] and molecular orbital calculations (MO) [25]

Complex	Solution	Solid states	MO
$OsD(D_2)(CO)Cl(PPr^i_3)_2$	86 kHz ($\alpha = 84^0$) 101 kHz ($\alpha = 54^0$) T_{1min} = 14. 7 ms (61.402 MHz)		129 kHz; (η =0.481, $\alpha = 84^0$)
$Os(D_2)(CO)Cl_2(PPr^i_3)_2$		120 kHz ($\eta = 0$, $\alpha = 52.5^0$) 166.7 ($\eta = 0.28$, $\alpha = 49.7^0$) T_{1min} = 40 ms (61.402 MHz)	

The presented data demonstrate the ambiguity in the interpretation connected with the (D_2) motions. Nevertheless they show that in terms of the deuterium behaviour, the properties of these (D_2) ligands can significantly differ even in similar dihydrogen complexes. The direct comparison of the T_{1min} data obtained for $OsD(D_2)(CO)Cl(PPr^i_3)_2$ in solution and $Os(D_2)(CO)Cl_2(PPr^i_3)_2$ in the solid state supports this conclusion.

13.7 CONCLUSIONS AND PERSPECTIVES

The DQCC values, characterizing the hydride ligands in transition metal complexes, can be determined by solution ^2H T_1 relaxation experiments. These experiments are relatively simple and provide good agreements with solid state ^2H NMR studies which require a special equipment. The DQCC values in terminal transition metal hydrides are sensitive to the nature of the central metal and ligand environments.

The range of DQCC values between 19.7 (RbD) and 136 kHz ($RhDCl_2(PPr^i_3)_2$) in terminal hydrides is interpreted in terms of the change of the ionic character of the metal – D bonds. This interpretation is, however, simplified. In spite of its simplicity, it provides an estimation of the ionicity of the M-D bonds in the ground state in accord with the chemical properties of the complexes. One should believe that DQCC can be used as an important parameter for the characterization of the metal – hydride bonding mode. In contrast to ^1H, this

parameter reflects quadrupole interactions and therefore it gives independent and additional information about the M-D bonding mode.

DQCC values of dihydrogen ligands are of most interest and their measurements seem to be intriguing and promising. The first studies of D-derivatives of non-classical hydride complexes by ^{2}H NMR have shown the great sensitivity of the DQCC values towards intramolecular motions of the dihydrogen ligands. The fast motions cause *an effect of the pronounced* $^2H\ T_{1min}$ *elongation* in solution as well as in solid state. This important relaxation feature can be used for structural formulation of the dihydrogen complexes. A correct determination of DQCC values and eq_{ZZ} orientations, with independent methods, can provide a better understanding of the motions of the dihydrogen ligand as its important and fundamental property.

The effects of the fast (D_2) motions on the measured DQCC values complicate the interpretation of the experimental data. Nevertheless on the basis of the ^{2}H NMR studies and molecular orbital calculations, one can formulate the common conclusion. The transformation of classical transition metal dihydrides to dihydrogen complexes is accompanied by the following changes: the asymmetry parameter of EFG at D increases to 0.87, the DQCC value can increase from 47 – 91 kHz up to 167 kHz and the eq_{ZZ} vector (the major axis of the electric field gradient) moves from the M-D bond to the direction of the D-D bond. These effects depend strongly on the nature of the transition metal and can thus give a new description of the bonding mode in the dihydrogen complexes.

REFERENCES

[1] J. A. S. Smith, Chem. Soc. Rev. 15 (1986) 225.
[2] G. B. Bacskay, J. E. Gready. J. Chem. Phys. 88 (1988) 2526.
[3] J. Vaara, Y. Hiltunen, J. Chem. Phys. 107 (1997) 1744.
[4] H. Huber, J. Chem. Phys. 83 (1985) 4591.
[5] W. C. Bailey, J. Mol. Spectr. 190 (1998) 318.
[6] G. J. Kubas, R. R. Ryan, B. I. Swanson, P. J. Vergamini, H. Wasserman, J. Am. Chem. Soc. 106 (1984) 451.
[7] D. M. Heinekey, W. J. Oldham, Chem. Rev. 93 (1993) 913.
[8] P. G. Jessop, R. H. Morris, Coord. Chem. Rev. 121 (1992) 155.
[9] D. H. Jones, J. A. Labinger, D. P. Weitekamp, J. Am. Chem. Soc. 111 (1989) 3087.
[10] K. W. Zilm, D. M. Heinekey, J. M. Millar, N. G. Payne, P. Demou, J. Am. Chem. Soc. 111 (1989) 3088.
[11] L. G. Butler, E. A. Keiter, J. Coord. Chem. 32 (1994) 121.
[12] J. B. Lambert, F. G. Riddel, The Multinuclear Approach to NMR Spectroscopy, D. Reidel Publishing Company. Boston. 1982, pp. 151-167.
[13] C. P. Slichter. Nuclear Magnetic Resonance in Liquid Crystals, ed., by J. W. Emsley, Riedel, Dordrecht, 1985.
[14] L. S. Snyder. J. Chem. Phys. 68 (1978) 291.

[15] D. G. Hamilton, R. H. Crabtree, J. Am. Chem. Soc. 110 (1988) 4126.
[16] V. I. Bakhmutov, E. V. Vorontsov, Rev. Inorg. Chem. 18 (1998) 183.
[17] A. Abragam, The Principles of Nuclear Magnetism, Oxford University; New York, 1971.
[18] H. Gilboa, B. E. Chapman, P. W. Kuchel, J. Magn. Reson. 119 (1996) 1.
[19]. D. G. Gusev, A. B. Vimenits, V. I. Bakhmutov, Inorg. Chim. Acta 179 (1991) 195.
[20] S. Aime, W. Dastrú, R. Gobetto, A. Viale, Inorg. Chem. 39 (2000) 2422.
[21] D. Nietlispach, V. I. Bakhmutov, H. Berke, J. Am. Chem. Soc., 115 (1993) 9191.
[22] G. A. Facey, T. P. Fong, D. Gusev, P. M. Macdonalds, R. H. Morris, M. Schlaf, W. Xu. Can. J. Chem. 77 (1999) 1911.
[23] V. I. Bakhmutov, J. Bertran, M. Esteruelas, A. Lledos, F. Maseras, J. Modrego, L. A. Oro, E. Sola, Chem. Eur. J. 2 (1996) 815.
[24] P. S. Ireland, L. W. Olson, T. L. Brown, J. Am. Chem. Soc., 97 (1975) 3548.
[25] V. I. Bakhmutov, C. Bianchini, F. Maseras, A. Lledos, M. Peruzzini, E. V. Vorontsov, Chem. Eur. J. 5 (1999) 3318.
[26] V. I. Bakhmutov, C. Bianchini, M. Peruzzini, E. V. Vorontsov, (unpublished data).
[27] S. Feracin, T. Burgi, V. I. Bakhmutov, I. L. Eremenko, E. V. Vorontsov, A. B. Vimenits, H. Berke, Organometallics 13 (1994) 4194.
[28] V. I. Bakhmutov, C. Bianchini, M. Peruzzini, F. Vizza, E. V. Vorontsov. Inorg. Chem. 39 (2000) 1655.
[29] A. J. Kim, F. R. Fronczek, L. G. Butler, S. Chen, E. A. Keitler, J. Am. Chem. Soc. 113 (1991) 9090.
[30] V. I. Bakhmutov, C. Bianchini, F. Maseras, A. Lledos, M. Peruzzini, E. V. Vorontsov, (manuscript in preparation).
[31] W. L. Jarrett, R. D. Farlee, L. G. Butler, Inorg. Chem. 26 (1987) 1381.
[32] I. Y.Wei, B. M. Fung, J. Chem. Phys., 55 (1971) 1486.
[33] L. Ramakrishan, S. Soundararajan, V. S. S. Sastry, J. Ramakishna. Coord. Chem. Rev. 22 (1977) 123.
[34] J. A. Labinger, in Transition Metal Hydrides; Dedieu, A. Ed.; VCH, NY, 1992, Chapter 10.
[35] N. Sarker, J. W. Bruno, J. Am. Chem. Soc. 121 (1999) 2174.
[36] T.-Y.Cheng, B. S. Brunschwig, R. M. Bullock, J. Am. Chem. Soc. 120 (1998) 13121.
[37] R. A. Henderson, K. E. Oglieve, J. Chem. Soc., Dalton Trans. (1993) 3431.
[38] E. S. Shubina, N. V. Belkova, A. N. Krylov, E. V. Vorontsov, L. M. Epstein, D. G. Gusev, M. Niedermann, H. Berke, J. Am. Chem. Soc. 118 (1996) 1105.
[39] E. S. Shubina, N. V. Belkova, E. V. Bakhmutova, E. V. Vorontsov, V. I. Bakhmutov, A. V. Ionidis, C. Bianchini, L. Marvelli, M. Peruzzini, L. M. Epstein, Inorg. Chim. Acta. 280 (1998) 302.
[40] J. A. Ayllon, C. Gervaux, S. Sabo-Etienne, B. Chaudret, Organometallics 16 (1997) 2000.
[41] F. Maseras, A. Lledos, M. Costas, J. M. Poblet Orgamometallics 15 (1996) 2947.
[42] A. Castillo, G. Barea, M. A. Esteruelas, F. J. Lahoz, A. Lledos, F. Maseras, J. Modrego, E. Onate, L. A. Oro, N. Ruiz, E. Sola, Inorg. Chem. 38 (1999) 1814.
[43] R. H. Morris, R. Witterbort, J. Magn. Reson. Chem. 35 (1997) 243.
[44] G. Luca, N. Russo, A. M. Koster, P. Calaminici, K. Jug, Mol. Phys. 97 (1999) 347.

Chapter 14

Dihydrogen Bonded Complexes and Proton Transfer to Hydride Ligands by Spectral (IR, NMR) Studies

Lina M. Epstein, Natalia V. Belkova, Elena S. Shubina

A.N. Nesmeyanov Institute of Organoelement Compounds, Russian Academy of Sciences, Vavilov str. 28, V-334, 117813 Moscow, Russia

CONTENTS

14.1 INTRODUCTION

One of the most fundamental reactions in chemistry and biochemistry is proton transfer, and this proceeds through hydrogen bonded intermediates. This chapter is devoted to an analysis of the spectral and thermodynamic features of hydrogen bonding to hydride ligands, their role as intermediates in proton transfer reactions (Eq. 1) and the place of this novel type of H-bonding in the general hydrogen bond concept.

$$MH + HX \rightleftharpoons MH\cdots HX \rightleftharpoons M(H_2)^+\cdots X^- \rightleftharpoons M(\eta^2\text{-}H_2)^+ + X^- \qquad (1)$$

The term "hydrogen bond" was introduced by Linus Pauling [1] and numerous experimental and theoretical investigations of hydrogen bonding in organic systems [2-5] have subsequently broadened the scope of hydrogen bonding partners and further developed the hydrogen bond concept. Not only the electronegative elements X of the first period but also those of periods II-IV and their conjugate XH acids are now well known to engage as partners in hydrogen bonding. The hydrogen bonding energy varies in a very broad range from 1 to 40 kcal/mol from the weak H-bonds of CH-groups as proton donors [6,7] and π-electrons of multiple bonds or even noble gases as proton acceptors [8] to the strongest low barrier H-bonded complexes [9-11]. The spectral and structural parameters and even the nature of the hydrogen bond (from mostly electrostatic to almost purely covalent bond) vary depending on the hydrogen bonding strength. The development of modern physico-chemical approaches and computational techniques create new perspectives and provide significant success in organic, supramolecular and biochemistry [3,4,9-13]. Consequently, the outburst of discoveries and investigations of several novel types of hydrogen bonding that are specific for inorganic or organometallic complexes in the 90s benefitted from the wealth of background knowledge gathered from organic systems and also from studies of inorganic and organometallic systems with classical hydrogen bonding [14-15]. Recent reviews on these subjects are available [16,17].

Intermolecular hydrogen-bonding of proton donors to transition metal d electrons, M···HX, was first discovered (1990) on the basis of the general rules developed for intramolecular M···HX interaction [17a,18]. Several systems with M···HX bonding which were studied by IR spectroscopy in common solvents by our group [19,20] or in supercritical media by Kazarian and Poliakoff [21] appeared to obey the regularities established for classical hydrogen bonded systems. Ionic H-bonds ($M^{-}\cdots{}^{+}HN$) were characterized in the crystalline state [17b,22] and more recently in solution [23]. It has been shown that hydrogen bonding precedes proton transfer leading to intermediate ion pairs that are stabilized by hydrogen bonding ($MH^+\cdots X^-$, Eq. 2) [19c,20a,24a].

$$M + HX \rightleftharpoons M\cdots HX \rightleftharpoons MH^+\cdots X^- \rightleftharpoons MH^+ + X^- \quad (2)$$

The discovery of these ionic H-bonds stimulated the search for ion-molecular hydrogen bonding to neutral organic bases. Suitable conditions for the formation of $(MH)^+\cdots B$ hydrogen bonds were found and the participation of these bonds in deprotonation reactions was demonstrated (Eq. 3) [20b,24b].

$$MH^+ + B \rightleftharpoons MH^+\cdots B \rightleftharpoons M + HB^+ \quad (3)$$

These ion-molecular H-bonded complexes were also observed in the solid state [25], though attempts to detect molecular MH···B hydrogen bonding were unsuccessfull [26].

As was shown in previous chapters the unusual MH···HX bonding was first observed simultaneously by the Morris and Crabtree groups in 1994 as an *intra*molecular interaction [27, 28]. Very soon thereafter, an *inter*molecular H···H hydrogen bond in the solid state was reported by the Crabtree group [29]. We provided the first spectral, thermodynamic and structural data for MH···HX bonding in solution [30, 31]. The term "dihydrogen bond" was proposed by Crabtree in contrast to the term "hydridic-protonic" bond introduced by Morris. In this chapter we adopt the first term to distinguish this type of interaction from the hydrogen bonds to other bases. It will be shown, however, that the H···H hydrogen bond is characterized by the same properties as the classical hydrogen bonds. So, one should not treat the dihydrogen bond any differently from other types of hydrogen bonding.

The chapter describes the spectral (IR, NMR) criteria for the identification of dihydrogen bond formation and competition with H-bonding to other ligands. The spectral and thermodynamic features of these unconventional H-bonds will be compared with those of the classical H-bonds. A discussion of some peculiarities of the proton transfer process and the first examples of full energy profile determination for protonation reactions leading to dihydrogen complexes will be also presented.

14.2 DIHYDROGEN BOND FEATURES

14.2.1 Spectral (IR, NMR) criteria of MH···HX hydrogen bond formation

14.2.1.1 Criteria of hydrogen bonding.

The most typical IR spectral characteristics of classical hydrogen bond formation are the changes of XH-stretching vibration bands of the proton donors in the presence of bases: decrease in intensity of the free XH band, $\nu_{XH(free)}$, and appearance of a low frequency broad and intense $\nu_{XH(bonded)}$ band. These changes become

more pronounced with an increase of the proton-donating ability (acidity). The same changes and dependence have been found in the presence of transition metal hydrides. IR measurements have typically been performed in non-polar or low polar media at low XH-acid concentrations to avoid self-association (005-0.01 mol/l) in the presence of an excess of the hydride compound. All spectral characteristics of the $\nu_{XH(bonded)}$ bands, namely the frequency shift $\Delta\nu = \nu_{(free)} - \nu_{(bonded)}$, the half-width $\Delta\nu_{1/2}$, and the integral intensity enhancement $\Delta A^{1/2}$, increase with the proton donors strength (MeOH < i-PrOH < CF_3CH_2OH (TFE) < $(CF_3)_2CHOH$ (HFIP) < $(CF_3)_3COH$ (PFTB). ^1H NMR spectra of XH-acids in the presence of excess hydride reveal downfield chemical shifts of the HX proton signal similar to what is observed in the presence of organic bases. These criteria characterise hydrogen bond formation but do not provide structural information.

14.2.1.2 Coordination site determination

14.2.1.2.1 IR spectra.

To determine the site of coordination in a hydride possessing different potential proton accepting sites (M-H, CO, NO, M-Hal), all pertinent ligand stretching vibrations should be investigated.

The direct evidence for the hydride ligand being the proton-accepting site (MH···HX) is the appearance of a new low-frequency ν_{M-H} band (or shoulder) in addition to new high-frequency bands (or shoulders) for the other ligands vibrations.

For example, upon hydrogen bonding of HFIP to $WH(CO)_2(NO)(PEt_3)_2$ the intensity of ν_{W-H} at 1670 cm^{-1} in hexane decreases and a broad low-frequency shoulder (at about 1640 cm^{-1}) appears (Fig. 1a) [30a]. One can also observe the appearance of a new ν_{CO} high-frequency band and a high frequency shoulder for the ν_{NO} band. The ν_{CO} band high frequency shift increases with the proton-donating ability of the alcohol: PhOH (11 cm^{-1}) < HFIP (14 cm^{-1}) < PFTB (17 cm^{-1}). This band is very sensitive not only to the proton donor strength but also to temperature changes. Its intensity increases on cooling while that of the $\nu_{CO(free)}$ band decreases (Fig. 1b).

A more complicated picture is observed in the case of di- or polyhydrides, where the low-frequency $\nu_{M-H(bonded)}$ band is accompanied by the appearance of new high-frequency bands due to the vibration of non-bonded terminal M-H groups. In many cases a broad unresolved envelope of $\nu_{M-H(bonded)}$, $\nu_{M-H(free)}$ and $\nu_{M-H(term.)}$ occurs. An example is provided by the interaction between $H_2Re(CO)(NO)_2(PR_3)_2$ and fluorinated alcohols [30b, 31c]. The increase of the integral intensity of the unresolved $\nu_{(Re-H)}$ band in comparison with that of $\nu_{Re-H(free)}$ was observed when R = Me. Substitution by R = Et induced a better resolution with the observation of a clear low frequency shoulder for the $\nu_{Re-H(bonded)}$ band. The important information which is based on the analysis of the ν_{NO} changes in parallel to those of ν_{Re-H}, will

be discussed below. Unfortunately, the ν_{M-H} bands are broad as a rule, weak and in some cases even unobservable. The role of the NMR information in these situations increases.

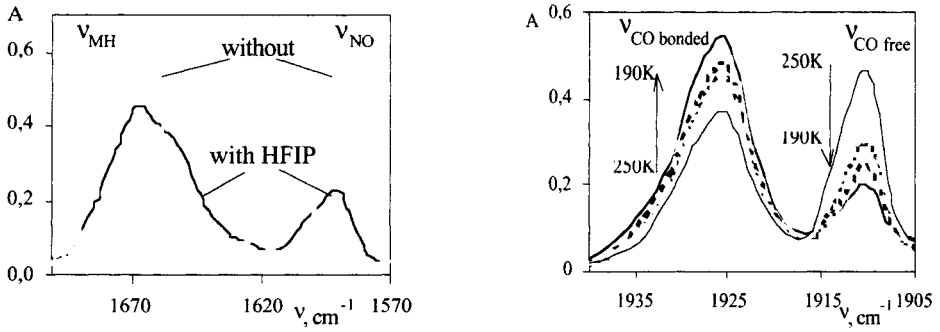

Figure 1. a) IR spectra in the ν_{MH} and ν_{NO} range of $WH(CO)_2(NO)(PEt_3)_2$/HFIP (0.004/0.012 mol/L) at 200K; b) Variable-temperature IR spectra in the ν_{CO} range of $WH(CO)_2(NO)(PEt_3)_2$/HFIP (0.001/0.008mol/L) in hexane [30a].

14.2.1.2.2 NMR spectra.

The NMR spectral criteria for MH···HX bonding are a rather small upfield shift *of* the hydride atom signal and a decrease of the relaxation time (T_{1min}).Unfortunately, the H-bond formation process is fast on the NMR time scale resulting in the coalescence of the free and bonded M-H signals, even at 190 K. An upfield drift of the broad average signal is temperature and concentration dependent and consists usually of -0.2÷-0.8 ppm at 200 K in the presence of an excess of proton donors. The MH···HX studies in liquid freons allowing to rich very low temperatures (down to 90K) hold considerable promise [30c]. This approach was developed by Golubev and Denisov [11a] and its effectiveness in the study of organic hydrogen bonded complexes has been demonstrated (for example [11b]). The study of the interaction between Cp*ReH(CO)(NO) and R^FOH in a CDF_3/CDF_2Cl mixture at 96K has allowed, for the first time, decoalescence of the hydride resonance into two signals (at δ = -7.54 and -8.87), corresponding to the free Re-H and the ReH···HO complex, respectively [30c]. For polyhydrides, a linear correlation was established by Chaudret and Limbach between the hydride signal upfield shift and the quantum exchange coupling, indicating that the latter parameter could be used as an additional sensor of dihydrogen bond formation, strength and geometry [32a]. The first application of this method involves the interaction of proton donors with $Cp^*RuH_3(PCy_3)$ in d_8–toluene or in a freon mixture [32]. The value of the hydride signal J_{ab} constant is of the order of 80 Hz for the free hydride and increases in the presence of excess R^FOH to about 220 Hz in both solvents.

Another very sensitive criterion for dihydrogen bonding is a decrease of the spin-lattice longitudinal relaxation time (T_{1min}) of the hydride signal. In the presence of XH the magnitude of T_{1min} decreases by a factor of 1.5 to 3 [30,31]. Moreover, the T_1 measurement is a reliable approach to determine H···H distances: a proton donor closer to H-M induces a faster relaxation (shorter T_1) for the hydride signal. The r(H···H) distance (in Å) can be calculated from the known equation 4 (by analogy to the situation of a η^2–H_2 ligand) [33].

$$r(H\cdots H) = 5.817(\nu\, \Delta R_{1,\,min})^{-1/6} \qquad (4)$$

In equation 4, ν is the frequency of the NMR signal in MHz and $\Delta R_{1,min}$ is the difference between the $1/T_{1min}$ values for the H-complex and for the initial hydride in s^{-1}. Short H···H distances, less than the sum of the van der Waals radii, were determined for intermolecular dihydrogen bonding in solution for $WH(CO)_2(NO)(PMe_3)_2$/HFIP (1.77 Å) [30a], $H_2Re(CO)_2(NO)(PMe_3)_2$/PFTB (1.85 Å) [30b], $[MeC(CH_2PPh_2)_3]Re(CO)_2H$/PFTB (1.83 Å) [31a], and $[MeC(CH_2PPh_2)_3]Ru(CO)H_2$/HFIP (1.81 Å) [31b].

14.2.2 Comparative analysis of MH···HX and classical hydrogen bond properties.

The unconventional character of the novel MH···HX hydrogen bonds warrants a comparative analysis of their spectral features with those of the classical (XH···B) hydrogen bonds. The hydride hydrogen as the proton-accepting site has neither a lone pair of electrons nor π-electrons. That is beyond the scope of traditional H-bonding concepts. Such an expansion of proton acceptor types demands a verification of whether a significant resemblance of the spectral (and thermodynamic) properties characterising the unconventional and the classical H-bonds exists. In our studies, the approaches developed for H-bonded organic complexes have been used. The similarity between the IR spectral manifestations of the unconventional and the classical hydrogen bonding in the ν_{XH} range has already been mentioned (section 14.3.1.1). The quantitative or semi-quantitative features will now be presented.

14.2.2.1 Spectral properties.

A first check is provided by the *isotopic ratio of frequencies*, ν_{XH}/ν_{XD}. The measurements of $\nu_{OH(bonded)}$ and $\nu_{OD(bonded)}$ for OH-acids and OD–analogues in the presence of hydride complexes yields $\nu_{OH\cdots HM}/\nu_{OD\cdots HM} \approx 1.35$, *i.e.* the same as for conventional hydrogen bonds of medium strength. This value was determined for a series of H-complexes between $(CF_3)_2CHOH(D)$ and $WH(CO)_2(NO)(PEt_3)_2$ [30a], $H_2Re(CO)(NO)(PMe_3)_2$ [31c] and Cp*ReH(CO)(NO) [30c].

The *linear dependence between* $\Delta\nu$ *and* $\Delta\nu_{1/2}$ was found to be similar to that for conventional hydrogen bonds. For example, the shift and half-width values for transition metal hydrides interacting with HFIP are related by the equation $\Delta\nu_{1/2} = 1.09\Delta\nu - 73$ [30e].

The *temperature dependence demonstrates a reversible equilibrium* (Eq. 5) for the dihydrogen bonded complex formation.

$$XH + HM \rightleftharpoons XH\cdots HM \qquad (5)$$

As in the case of classical H-bonds, the number of hydrogen bonded groups and therefore the intensity of the absorption increase reversibly upon cooling. We have observed several reversible cycles of intensity increase/decrease as the temperature changes in the 200 to 260 K range for the systems $WH(CO)(NO)(PR_3)_2$/HFIP (Fig. 1b) [30a] and $[MeC(CH_2PPh_2)_3]ReH(CO)_2$/PFTB [31a]. The intensity changes of the new $\nu_{CO(XH\ldots HM)}$ and $\nu_{MH(bonded)}$ bands and the NMR data for $[MeC(CH_2PPh_2)_3]RuH_2(CO)$/HFIP system confirmed the reversibility of the H-bonding process [31b].

14.2.2.2 Thermodynamic properties.

Different attempts to use spectral features as a measure of hydrogen bonding strength have always been popular throughout the development of this field of science. The simple Badger-Bauer rule (Eq. 6) continued to be considered valid even after the non-linearity of the function $-\Delta H = f(\Delta\nu)$ was demonstrated [2,34].

$$-\Delta H^{\circ}(\text{kcal/mol}) \approx 0.024\Delta\nu \qquad (6)$$

Many other relations between $-\Delta H$ and $\Delta\nu$ (many of which are valid for separate classes of organic acids and bases) and a relation between $-\Delta H$ and the ν_{XH} band intensity enhancement ($\Delta A^{1/2}$) have been proposed [34]. A more detailed and thorough analysis of the experimental spectral characteristics and enthalpies for various organic acid/base H-complexes was provided by Iogansen on the basis of several methods (chromatography, calorimetry and so on). The author suggested an universal proportionality relationship which was named "the intensity rule" [34] (equation 7), where $\Delta A^{1/2} = A^{1/2}_{bonded} - A^{1/2}_{free}$.

$$-\Delta H^{\circ}(\text{kcal/mol}) = 2.9\Delta A^{1/2} \qquad (7)$$

Eq. 7 proved to be valid for different types of H-complexes from homo- and heteroassociates in solution or in the gas phase to polymer chains (or cycles) of hydrogen bonds in crystals and associated liquids. The mean square root deviation of $-\Delta H$(Eq. 7) vs $-\Delta H$(measured) for 180 systems is 7.3% of the mean $-\Delta H$

value, which does not exceed the probable errors on the measured -ΔH values in the range of energies from 0.1 kcal/mol to 15 kcal/mol [34d].

The correlation between ΔH and Δν in equation (8) has a lower accuracy. However, since the measurements of shift values are usually simpler, this proportionality is widely used for organic compounds.

$$-\Delta H^\circ = \frac{18\Delta\nu}{\Delta\nu + 720} \tag{8}$$

The unconventional character of MH···HX hydrogen bonding demands the validity of equations (7) and (8) to be tested. Therefore, we calculated -ΔH° values by van't Hoff's method, from H-bonds formation constants (K_f of Eq. 5) determined from the characteristic band intensity changes at different temperatures. The linear correlation equation between the logarithm of the formation constants and 1/T allows the calculation of the enthalpy (Eq. 9) and entropy values.

$$-\Delta H^\circ = \frac{d \ln K_f}{dT} RT^2 \tag{9}$$

The similarity between the enthalpy values calculated from (7), and (8) and those from (9) proves that the correlation equations (7) and (8) hold true for the unconventional dihydrogen bonds (Table 1).

Table 1. Enthalpies of dihydrogen bond formation, -ΔH° (kcal/mol), and basicity factors from Eq. (7)-(9).

[MH]	HX	-ΔH° (8)	-ΔH° (7)	-ΔH° (9)	E_j	mean E_j	Ref.
	PhOH	5.0	4.9		0.87		
$WH(CO)_2(NO)(PEt_3)_2$	HFIP	5.3	5.1	4.9	0.87	0.86±0.01	[30a]
	PFTB	6.5	6.4		0.85		
	PhOH	4.5	4.4		0.78		
$ReH_2(CO)(NO)(PMe_3)_2$	HFIP	5.0	4.7		0.82	0.80±0.02	[31c]
	PFTB	6.1	6.1	5.8	0.80		
	PhOH	4.4			0.95		
$[MeC(CH_2PPh_2)_3]Re(CO)_2H$	HFIP	4.8			0.98	0.97±0.02	[31a]
	PFTB	6.0			0.99		
	MFE	4.7			1.38		
$[MeC(CH_2PPh_2)_3]Ru(CO)H_2$	TFE	5.8			1.40	1.39±0.02	[31b]
	HFIP	6.6		6.7	1.37		

For example, the -ΔH° values found from Eqs.(7)-(9) for the $WH(CO)_2(NO)(PR_3)_2$/ HFIP hydrogen bond are equal to 5.3, 5.1, and 4.9 kcal/mol, respec-

tively [30a]. In the case of $ReH_2(CO)(NO)(PMe_3)_2$/PFTB, the -ΔH° value is 5.8 kcal/mol from the van't Hoff method and 6.1 kcal/mol from Eqs. (8) and (9) [31c]. Finally, for the $[MeC(CH_2PPh_2)_3]Ru(CO)H_2$ /HFIP system the van't Hoff method yields -ΔH° = 6.7 kcal/mol and -ΔS° = 19.6 e.u.; the -ΔH° value is similar to the 6.6 kcal/mol value calculated by the use of Eq. (8) [31b]. It is noteworthy that the thermodynamic parameters obtained from van't Hoff plots by using NMR experiments are in good agreement with those obtained from IR data (-ΔH° = 7.1 kcal/mol, -ΔS° = 19.0 e.u.). Note that the validity of Eqs.(7) and (8) was also shown by us for other new types of hydrogen bonds:, namely M···HX [17a] and BH···HX (see Section 14.3.2.5 below). All the enthalpies of dihydrogen bonded MH···HX complexes are typical of medium strength H-bonds (4-7.5 kcal/mol) and increase with the proton donating ability of the XH acid. The calculated entropy values (-ΔS° = 9.8-17.6 e.u.) are in the same range known for H-bonds in organic systems (5-20 e.u.).

14.2.2.3 Scale of basicity factors for hydride ligands.

Another important empirical correlation proposed by Iogansen on the basis of a large array of spectral and calorimetric data, the so-called "rule of factors " [34a,b], appears to be also applicable to dihydrogen bonding. The general equation for a proton donor *i* and a proton acceptor *j* is $\Delta X_{ij} = \Delta X_{11} P_i E_j$, where ΔX_{ij} stands for either spectral (Δν, ΔA) or thermodynamic (-ΔH°) characteristic in a specific solvent. ΔX_{11} refers to the phenol - diethyl ether pair taken as a "standard", for which the basicity and acidity factors are taken as unity: $P_i=E_j=1$. This rule demonstrates the invariability of proton donating (P_i) and proton accepting (E_j) properties of organic acids and bases in hydrogen bonding. Basicity factors E_j for hydride ligands were calculated using eq. 10 from experimental enthalpy data ($-\Delta H_{ij}$) and from the known [34a,b] P_i values.

$$E_j = \frac{\Delta H_{ij}}{\Delta H_{11} P_i} \qquad (10)$$

The enthalpy of the standard complex (ΔH_{11}) is solvent dependent, *i.e.* –4.6 kcal/mol for CH_2Cl_2 and -5.7 kcal/mol for hexane, so the enthalpy values to be used in Eq. (10) should be measured in the corresponding solvent [34a,b]. The E_j factor obtained in this manner should be independent not only on the nature of proton donors but also on the medium. As one can see from Table 1, the basicity factor for a given hydride is really independent on the acidity (proton donating ability) of the proton donor. Comparison of the E_j values in Table 1 shows that the proton accepting properties increase from rhenium to tungsten and to ruthenium complexes. These E_j values enable us to define a scale of basicity factors for the

hydride hydrogen of different hydrides and to compare the proton accepting properties of hydride complexes with those of organic compounds and metal atoms in organometallic complexes (Fig. 2). As one can see, E_j factors of hydride ligands vary over the wide range from 0.6 to 1.6, comparable with the values of M atoms in organometallic complexes [17a]. All E_j factor values are considerably larger than those of the π-density in aromatic compounds ($E_j < 0.4$). The most basic hydrides have E_j values greater than DMSO ($E_j = 1.27$) and comparable with pyridine ($E_j = 1.67$) [34].

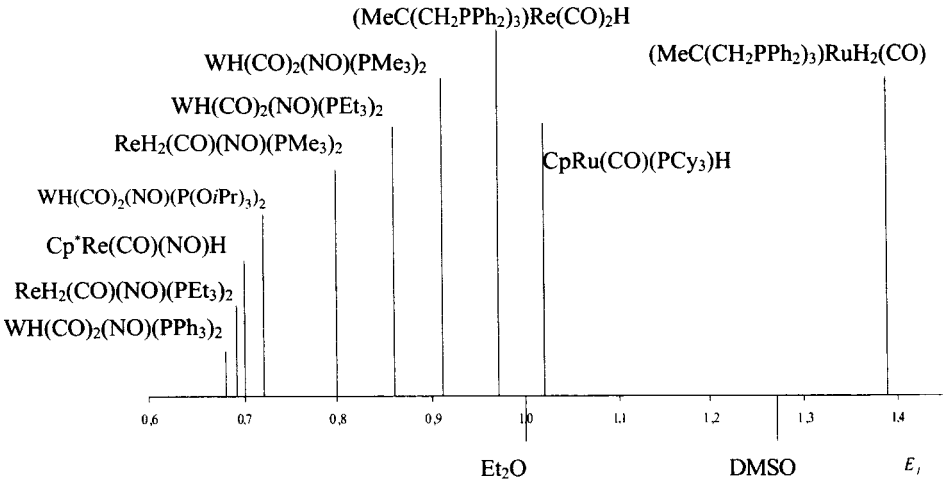

Figure 2. Scale of basicity factors (*Ej*) for some transition metals hydrides and organic bases.

It would be very interesting to analyse the relationships between the basicity factor or the -ΔH of the hydrogen bond formation and the parameters associated to the full proton transfer (pK_a or -ΔH of the protonation reaction). The first one is a very good sensor of the electron density distribution in the ground state of the proton acceptor due to the small changes induced by H-bonding (see below). Full proton transfer, on the other hand, demands covalent bond formation and a significant electronic and geometric reorganisation, so its parameters depend on the differences between the starting base and the protonation product. Relations of this kind between H-bonding and protonation parameters were obtained for organic systems and showed a linear character, but only within a given class of organic bases [5c].

14.2.2.4 Structure of dihydrogen bonded complexes

The applicability of the empirical correlations (7), (8) and (10), obtained for linear hydrogen bonding with organic bases, to the dihydrogen bond suggests

linearity of the H···HX fragment. The results of *ab initio* and density functional theory (DFT) calculations confirmed this assumption [30b, 35, 36]. The atom arrangement in FH···H(Li) and FH···H(Mn) fragments was shown to be linear by *ab initio* calculations [35]. The F-H and H-Mn bonds in the latter H-complex are lengthened by the H-bonding interaction. A linear two-center hydrogen bond is energetically preferable relative to a non-linear three-center H-bond, as shown by DFT calculations [30b]. The dihydrogen bond energy for the linear $(PH_3)_2(NO)(CO)ReH_2\cdots H_2O$ model is 2.3 times greater than for the non-linear disposition. Rather small deviations from 180° (174-164° depending on the calculation method) were shown for the $(PH_3)_2(NO)(CO)_2MH\cdots HX$ model where M = Mo or W and HX = H_2O or HF [36].

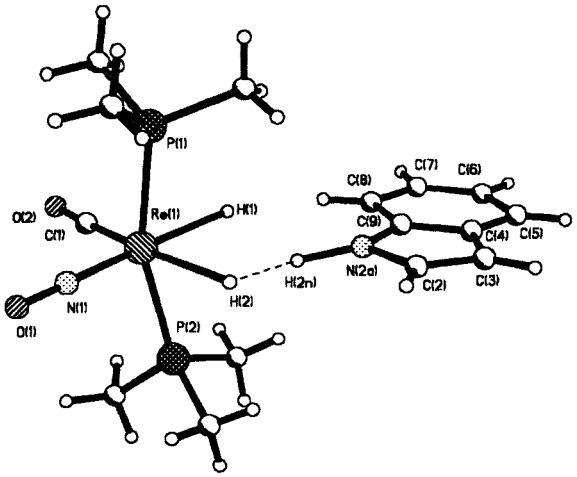

Figure 3. X-Ray structure of hydrogen bonded complex $[(PMe_3)_2(NO)(CO)ReH_2$ •indole].

Only few crystal structures are reported for MH···HX adducts [29, 37]. The most precise one was obtained by neutron diffraction for the $[ReH_5(PMePh_2)_3$•indole] adduct [37a-c]. The structures of $[ReH_5(PMePh_2)_3$•imidazole] [37b,c] and $[(PMe_3)_2(NO)(CO)ReH_2$•indole] [31c] have been obtained by X-Ray diffraction methods. An asymmetric three-centre hydrogen bonding with H···H distances of 1.73 and 2.21 Å was reported for the first adduct (a theoretical analysis by DFT methods gives 1.92 and 2.48 Å for these distances, respectively). Note that the corresponding N-H···H angles at these two H-atoms are 163.1° and 130.9°. Therefore, only the first value corresponds to a close to linear NH···H arrangement. The distances and the angles are similar to those of the adduct of the same hydride complex with imidazole [37]. The X-ray structure of $[(PMe_3)_2(NO)(CO)ReH_2$•indole] (Fig. 3) exhibits coplanarity of the indole molecule with the Re(CO)(NO) frag-

ment [31c]. The ReH_2 moiety contains two non-equivalent Re-H bonds (Re-H(1) 1.63(3) and Re-H(2) 2.36(3) Å), the second "long" bond being positioned in front of the elongated N-H bond of indole (r = 1.28(3) Å). The H···H distances, 1.79(5) and 2.21(3) Å, are similar to those mentioned above. In all cases, the longer distances are close to the sum of the van der Waals radii (2.40 Å) and the corresponding NH···H angles are far from 180°. Therefore, it could be suggested that the additional interaction has no hydrogen-bonding character and its existence could be caused by a simple crystal packing effect [4]. Notably, the strength of the dihydrogen bond in solution, as obtained from the IR data, is smaller than that in the solid state confirming the effect of crystal packing forces. For example the H-bond formation enthalpy for $[(PMe_3)_2(NO)(CO)ReH_2$•indole] increases by a factor of two on going from solution to the crystal [31c].

It is interesting that the hydrogen bond with transition metal atoms as well as that with hydride ligands of boron hydrides (see below) also displays a linear arrangement for the X-H···M and X-H···H(B) fragments. The linearity of the ionic hydrogen bonds $N\text{-}H^+\cdots[Co]^-$ and $N\text{-}H^+\cdots[Pt]^-$ was proven by neutron diffraction studies of the corresponding salts [22a,b].

14.2.2.5 Nature of the dihydrogen bonding

The interaction between proton donors and hydride ligands is generally supposed to lead to the formation of a dihydrogen bond. However, electron rich transition metals may also possess lone pairs of d electrons which, as was mentioned above, could form hydrogen bonds of the M···HX type. Therefore, the metal and the hydride ligands could compete for the proton donor but the IR and NMR spectral criteria described in section 14.3.1.2 allow to distinguish these two situations. On the other hand, the interaction with a hydride ligand could be complemented by the participation of d electrons in dihydrogen bonding. The first data showing a minimal effect of d orbitals were obtained in comparative IR investigations of films of hydrogen-bonded complexes of d^2 and d^0 rhenium hydrides, namely $[ReH_5(PPh_3)_3]$ and $[ReH_7(dppe)]$ [37a]. The dihydrogen bond is also formed by the d^0 compound, although this is weaker than that formed by the d^2 complex. This conclusion was confirmed by theoretical studies [37].

Another way to prove the minimal effect of occupied d orbitals is the investigation of hydrides of the main group element as models. Using the Cambridge Structural Database of aminoboranes, Crabtree discussed the possibility of an interaction between an NH group and a hydride ligand of borohydrides as a bent hydrogen bond from the NH donor to the B-H σ–bond acceptor [37b, 38a], namely featuring bent N-H···H(B) and linear B-H···H(N) fragments. As also shown in Chapter 3 (Crabtree et al.), this incorrect conclusion resulted from the misassignment of the B and N atoms from the X-Ray study of the clue hydride dimer $(BH_3NH_3)_2$. A recent [38b] neutron diffraction study has allowed the correct

assignment to be made, resulting in a linear N-H···H(B) dihydrogen bond with a short r(H···H) distance (2.03 Å) and, as expected, a bent B-H···H(N) moiety.

Our spectroscopic studies of XH···HB dihydrogen bonding of ionic (BH_4^-) and neutral (BH_3NEt_3, $BH_3P(OEt_3)$) boron hydrides with different proton donors in solution showed a close similarity between the spectral and thermodynamic characteristics of this and XH···HM dihydrogen bonds [39]. These are the linear correlations between the enthalpies of these two types of dihydrogen bonding and the acidity factors of XH acids (Fig.4). As one can see the ionic H_3BH···HX bonds are stronger than the MH···HX bonds, whereas H-bonds involving neutral borohydrides are weaker. The E_j factors are indeed independent on the partners and the BH_4^- anion has a very large proton accepting ability (E_j = 1.28), while neutral borohydrides have minimal basicity factors (E_j = 0.53÷0.41), *i.e.* comparable to that of the oxygen atom in diphenyl ether [39a].

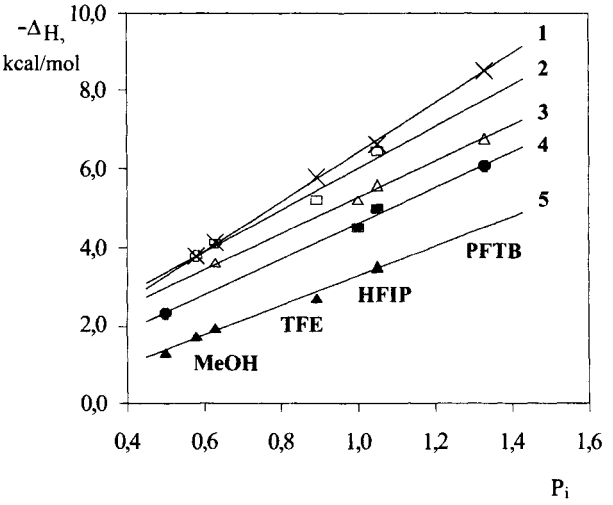

Figure 4. Correlation between enthalpies (-ΔH°) of MH···HX and BH···HX complexes and acidity factors of proton donors (P_i). 1 – BH_4Bu_4N; 2 - $[MeC(CH_2PPh_2)_3]MRuH_2CO$; 3 – $WH(CO)_2(NO)(PMe_3)_2$; 4 - $ReH_2(CO)(NO)(PMe_3)_2$; 5 – BH_3NEt_3.

Theoretical studies (HF 6-31G) of dihydrogen bonded complexes of BH_4^- and BH_3NH_3 with H_2O or MeOH and of BH_4^- with HCN as well as of the $(H_3NBH_3)_2$ dimer revealed the local minima on the potential energy surface corresponding to monodentate coordination of one hydride atom to the H-atom of the proton donor and a linear arrangement of the X-H···H moiety [39a]. The X-H···H angles are equal to 179-172°. There appears to be only one exception with a greater deviation from linearity for the complex $[H_3B]H$···HOH, the angle being 154°. This fact was explained by the additional interaction between the free hydrogen atoms

of BH_4^- and the second hydrogen atom of H_2O. Note, that this interaction should not be considered as a hydrogen bond because the H···H distance is 2.691 Å, that is, longer than the sum of the van der Waals radii (2.40 Å). As was written in the theoretical report [39c], the energetically most preferable structure for the $[H_3B]H$-···HCN complex is non-linear. However, the less favourable (by only 2.5 kcal/mol) linear structure, rather than this non-linear one, exhibits characteristics typical of the dihydrogen bond. The linear H-complex has a shorter H···H distance (1.7 rather than 2.2 Å), a positive H···H overlap population (0.079), and a stronger polarisation of the partners [39a]. Although the experiments were conducted in solution while the calculations refer to the gas phase, the resemblance in properties of MH···HX and BH···HX confirms the conclusion that the lone pairs of d electrons have no evident effect on the interaction with hydride ligands of transition metal hydrides

In conclusion, it is correct to use BH···HX dihydrogen complexes as appropriate models to elucidate the nature of dihydrogen bonds, including MH···HX interactions. The calculations on the above mentioned borohydride complexes with proton donors revealed that the driving force of dihydrogen bond formation is the electrostatic interaction between the partly positive hydrogen atom of the proton donor (q = 0.43 – 0.47) and the partly negative hydride atom (q = -0.27 – -0.15) in the $B\text{-}H^{\delta-}\cdots{}^{\delta+}H\text{-}X$ moiety. These charges increase by the same amount (*ca.* 0.01 – 0.07 a.u.) upon dihydrogen bond formation. The XH and BH bonds stretch out and a very small but positive overlap population (0.005 – 0.021) appears between the H atoms. The H···H distances vary in the same range as the MH···HX bonds (1.8 – 2.1Å). The electron density changes are not restricted to this fragment and affect both hydrogen bonding partners. The increase of O-H/N-H bond polarity and the electronic redistribution of the other atoms of the proton donor molecule are similar to those observed during the formation of H-complexes with organic bases. The increase of the negative charge on the hydride atom in the hydride molecule is accompanied by electron density changes of other atoms and by changes of overlap population. Thus, the mutual polarisation of the electron clouds of the two partners contributes to increase the mutual electrostatic attraction in the $B\text{-}H^{\delta-}\cdots{}^{\delta+}H\text{-}X$ fragment.

Ab initio calculations (MP2/6-311+6(2d,2f)) were performed recently for the complex of the novel rare gas dihydride XeH_2 with water, HXeH···HOH [40]. This dihydrogen bonded complex has a planar geometry with an elongated O-H bonded group and a short H···H distance (1.711 Å), typical for a dihydrogen bond. In this case, however, the bonded group charges (O-H and Xe-H) decrease upon interaction. The calculated energy of this H-bond is probably overestimated, the result ranging from 16.5 to 9 kcal/mol (strong to middle-strength complex) depending on the chosen basis set.

Orlova and Sheiner have carried out DFT calculations on PH_3 models of MH···HX complexes experimentally studied by us, namely $MH(NO)(CO)_2(PH_3)_2$

(M = W, Mo), as well as $CpRu(CO)(PH_3)H$ and $Cp^*Re(H)(NO)(CO)$, with proton donors such as HF, H_2O, and $HOCF_3$ [36, 41]. The results show a similar electronic and geometrical structure for these MH···HX systems and the above described BH···HX dihydrogen bonded systems. The linearity of the H···H-X fragment (the (M)H···H-X angles lie in the 165 – 178° range depending on the calculation method) and a lengthening of both X-H and M-H bonds were demonstrated. The $M\text{-}H^{\delta-}\cdots^{\delta+}H\text{-}X$ electrostatic interaction was found to be the driving force of the bond formation as for the $B\text{-}H^{\delta-}\cdots^{\delta+}H\text{-}X$ systems. The Kitaura - Morokuma decomposition analysis of the bond energy contributions for the simple HNO···HX and LiH···HX models allows a comparison of the various energetic components in classical and dihydrogen bonds to be made. The electrostatic energy (ES) makes the largest contribution to the total energy of the MH···HX bond, like in classical H-bonds. The conventional (O···HX) hydrogen bond is classified as "ES > CT" since the electrostatic component is more important than the charge transfer (CT) component, while the contribution of the polarisation energy (PL) is considerably smaller. It is of interest that the contribution of the polarisation energy is considerably larger for the dihydrogen bonds with respect to the classical cases. Therefore, the dihydrogen bond energy might be termed as "ES > PL ≈ CT". Note that the ES component as well as the total energy for the LiH···HX interaction is somewhat larger than for HNO···HX. This difference is in agreement with our experimental data on the smaller proton accepting ability of the NO ligand relative to the hydride ligand in rhenium dihydride complexes.

In conclusion, the nature of hydrogen bonding to a hydride ligand in transition metal complexes and in boron hydrides is common and does not indicate any d electron effect in the former case. Both types of H···H interaction are similar to conventional hydrogen bonding, the only difference being an increase of the polarisation component of the interaction energy for the dihydrogen bond.

14.3 FACTORS AFFECTING THE HYDRIDE LIGAND BASICITY

14.3.1 Dependence of basicity factors on the nature of the metal atom.

One can find out the effect of the metal nature by analysing the basicity factors of complexes with isostructural ligand surroundings. Unfortunately, there is still very little information on hydride complexes involving metals of the same group. Only for the $[P(CH_2CH_2PPh_2)_3]MH_2$ hydrides of the iron subgroup have such studies been carried out. The basicity factor E_j increases down the group: 1.0 [H(Fe)] < 1.33 [H(Ru)] < 1.6 [H(Os)] [42]. The same trend was established earlier for the basicity of the transition metal atom in the XH···M type of hydrogen bond. The transition metal basicity increases down the group, in contrast to the basicity of main group atoms which shows the opposite trend [17a,19]. There are

still insufficient data to analyse the influence of the metal position in a Period on the E_j factors of the hydride ligand. By analogy with the E_j factors in M···HX bonds, we could suggest that the E_j value of the hydride ligand should increase upon moving to the right of the Periodic Table [17a].

14.3.2 Dependence of basicity factors on the electronic and steric effects of ligands.

The proton accepting ability of the hydridic hydrogen significantly depends on the electronic and steric effects of phosphine ligands. The E_j factor for $WH(CO)_2(NO)(PR_3)_2$ increases in the order $PPh_3 < P(O^iPr)_3 < PEt_3 < PMe_3$ as a result of changes of the phosphine ligand cone angle and basicity [30a]. A stronger donation is expected to increase the proton accepting properties of the hydride ligand. Note that the first two phosphines give very similar E_j values (0.70 and 0.72), whereas the E_j of complexes with PEt_3 and PMe_3 is much greater (0.87 and 0.91). However, the situation for Re hydrides with similar ligand surroundings, $H_2Re(CO)(NO)(PR_3)_2$, unexpectedly appears more complicated [30b, 31c]. The type and amount of hydrogen bonded species depend on the phosphine. An analysis of all the available spectral data shows the dominant role of PR_3 ligands steric effects in the competition between two different hydrogen bonding sites: ReH and ReNO. The dihydrogen bond is not observed at all when $PR_3 = P^iPr_3$, *i.e.* the ligand with maximum steric hindrance (cone angle $\theta = 160°$ [43]), in spite of the maximal electron donating power of this ligand. The IR spectra show the exclusive formation of the NO···HOR bond: only a broad low frequency $\nu_{NO\cdots HO}$ band appears, whose position depends on the proton donor strength ($\Delta\nu$ = -45 cm^{-1} with HFIP and -53 cm^{-1} with PFTB) [31c]. From the data, a low basicity factor of the nitroso group (E_j = 0.60), a low enthalpy ($-\Delta H°$ = 4.5 kcal/mol) and a high entropy ($-\Delta S°$ = 13.8 e.u.) for the interaction with PFTB have been derived. In the case of $PR_3 = PEt_3$ the E_j increases to 0.69. At the same time, the decrease of the phosphine steric hindrance ($\theta = 132°$) leads to the coexistence of two types of H-bonded complexes with ReH···HOR and NO···HOR interactions. A new high-frequency ν_{NO} band and a low frequency shoulder on the ν_{ReH} band correspond to the former complex and low frequency ν_{NO} is assigned to the latter one (Fig. 5).

It is clear that the basicity factor for this hydride relates to the proton accepting properties averaged over the two centres, while the E_j factor for the hydride ligand should be slightly higher. A further decrease of steric hindrance ($PR_3 = PMe_3$) continues to tilt the balance in favour of the hydride ligand (in spite of the basicity order $PEt_3 > PMe_3$). Here the dihydrogen complex predominates, the low frequency $\nu_{NO...HOR}$ band being almost unobservable. The low intensity of this band yields a fraction of less than 6% (Fig. 6) for the NO···HOR complex. Thus, for the $H_2Re(CO)(NO)(PR_3)_2$ series of compounds, that containing PMe_3 has the highest proton accepting ability (E_j = 0.8), the maximum strength of the interaction

with PFTB ($-\Delta H° = 5.8$ kcal/mol), as well as the minimum entropy change ($-\Delta S° = 6.8$e.u.).

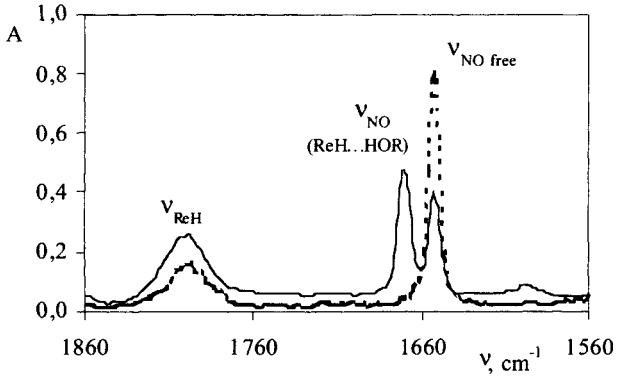

Figure 5. IR spectra in the ν_{NO} and ν_{MH} range of free hydride $H_2Re(CO)(NO)(PEt_3)_2$ (0.008 mol/L) (- - -) and in the presence of PFTB (0.080 mol/L) (—) in hexane at 200K [31c].

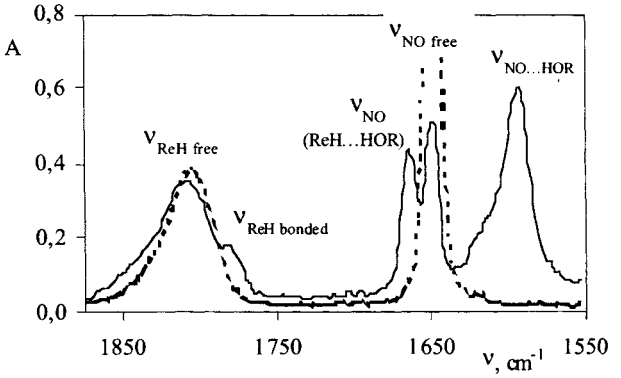

Figure 6. IR spectra in the ν_{NO} and ν_{MH} range of free hydride $H_2Re(CO)(NO)(PMe_3)_2$ (0.004 mol/L) (- - -) and in the presence of PFTB (0.008 mol/L) (—) in hexane at 200K [31c].

Interestingly, the monohydride $(Cl)HRe(CO)(NO)(PMe_3)_2$ forms only one type of hydrogen bonding to the chloride ligand, ReCl···HOR, as proven by the appearance of a new low frequency band for the ν_{ReCl} vibration in the presence of alcohol. The intensity of this band grows upon increasing the excess of proton donor and upon cooling (Fig.7). The characteristic bands of the other non-bonded ligands, on the other hand, are shifted as expected to higher frequencies.

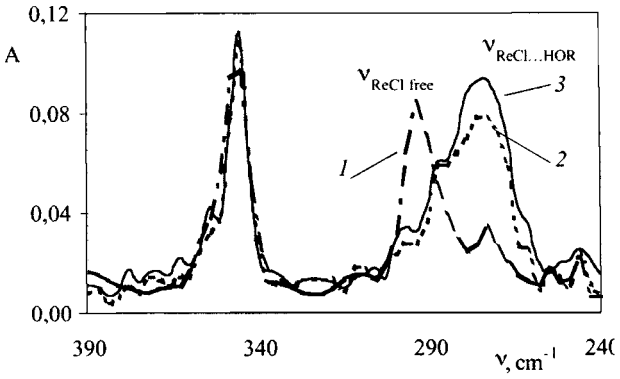

Figure 7. IR spectra in the ν_{ReCl} range of the hydride H(Cl)Re(CO)(NO)$(PMe_3)_2$ (0.006 mol/L, 1) in the presence of 0.015 (2) and 0.030 (3) mol/L PFTB in hexane at 200K [31c].

Note that the same IR spectral changes were observed in the ν_{OsCl} region for the formation of OsH(Cl)(CO)$(P^tBuMe_2)_2$•HFIP, proving Os···Cl hydrogen bonding [44]. It appears that the proton accepting ability (E_j = 0.68) of the Cl-ligand in (Cl)HRe(CO)(NO)$(PMe_3)_2$ is less than that of the hydride ligand in corresponding dihydride H_2Re(CO)(NO)$(PMe_3)_2$ (E_j = 0.8). Therefore, the chlorine electron-withdrawing effect decreases the proton accepting ability of the hydride and NO ligands, deactivating these potential binding sites.

14.3.3 Basicity factors and proton transfer.

To foresee whether the interaction of a hydride with a weak XH acids will lead to proton transfer one should know the spectral manifestations of dihydrogen complexes and their dependence on the proton accepting ability of the hydride ligand. Our investigations during the last few years have allowed us to determine the E_j factors of several hydrides and to observe the appearance of IR bands and NMR signals assigned to cationic nonclassical hydrides as a result of the interaction with several proton donors of different strength (see below).

Our results have shown that proton transfer by weak acids (fluorinated alcohols) to hydrides having an *E_j value of less than 0.8* never occurs, even in the presence of a large excess of the acid. Only rather strong proton donors such as trifluoroacetic acid induce low temperature proton transfer, as was shown for H_2Re(CO)(NO)$(PR_3)_2$ and (Cl)HRe(CO)(NO)$(PMe_3)_2$ [30b, 31c]. It is interesting that under conditions favouring the proton transfer (high concentration of the strongest alcohol, PFTB, and low temperature, 200-220K) a second proton donor molecule binds these rhenium complexes. Furthermore, in spite of the diversity of

the 1:1 adduct structures (possessing ReH···H, NO···H, ReCl···H hydrogen bonds) the hydride ligand is always the second hydrogen bonding site in each 2:1 complex. This means that the hydrogen-bonded complexes certainly have a hydride atom as one of the accepting sites under conditions approaching the proton transfer.

If the E_j *value is greater than 0.8*, proton transfer takes place also in the presence of rather weak XH acids. The higher the proton accepting ability of the hydride ligand, the weaker the proton donor which can lead to proton transfer. For example, PFTB was needed to investigate the quantitative proton transfer to $[MeC(CH_2PPh_2)_3]ReH(CO)_2$ (E_j = 0.97) [31a], while the weaker alcohol, HFIP, was sufficient to carry out the same investigation for $[MeC(CH_2PPh_2)_3]RuH_2(CO)$ (E_j = 1.39) [31b].

14.4 DIHYDROGEN BOND AND PROTON TRANSFER.

The complete proton transfer process from an acid to a hydride complex resulting in the loss of a dihydrogen molecule is a well established phenomenon. The discovery of dihydrogen complexes by Kubas [45a] and the subsequent intensive studies of transition metal hydride protonations have shown that these complexes are intermediates of the proton transfer processes [45b,c]. The existence of stable adducts displaying dihydrogen bonding in solution has allowed the proposal that the proton transfer reactions leading to dihydrogen complexes involve the intermediacy of these adducts (Eq. 11).

$$\underset{\mathbf{1}}{[MH]} + HX \rightleftharpoons \underset{\mathbf{2}}{[MH]\cdots HX} \rightleftharpoons \underset{\mathbf{3}}{[M(\eta^2\text{-}H_2)]^+ X^-} \longrightarrow \underset{\mathbf{4}}{[MX]} + H_2 \qquad (11)$$

It is possible to observe intermediates in the proton transfer reactions by using low-polar or non-polar media and by varying the concentration and strength of proton donors with the combination of variable temperature IR and NMR spectroscopies. Under suitable conditions, this approach further enables the determination of the thermodynamic parameters associated to each step from the temperature dependence of the corresponding formation constants. It is now experimentally confirmed that the first step of the interaction indeed consists of the dihydrogen bond formation.

As shown above (Section 14.3.3) the proton accepting ability of the hydride ligand (expressed as the E_j factor) determines the thermodynamic drive toward proton transfer from different acids. For weak basicity hydrides (E_j < 0.8), proton transfer is possible only from strong acids like HBF_4 or CF_3COOH, while those

hydrides with E_j factors greater than 0.8 can also be protonated by weaker acids such as alcohols.

The IR and NMR spectral manifestations of dihydrogen bonding adducts, **2**, were described in detail in the preceding parts. The NMR spectral manifestations of dihydrogen complexes, **3**, are well known (see for example [31, 32, 45a,b]). The formation of cationic dihydrogen complexes leads to significant high frequency shifts of the stretching vibrations of all ligands in the IR spectra [30,31,46]. For instance, the protonation of $ReH_2(CO)(NO)(PMe_3)_2$ (Ej = 0.80) to $[ReH(H_2)(CO)(NO)(PMe_3)_2]^+$ by trifluoroacetic acid leads to high frequency shifts of ν_{CO} (+98 cm^{-1}), ν_{MH} (+60 cm^{-1}) and ν_{NO} (+93 cm^{-1}) [31c].

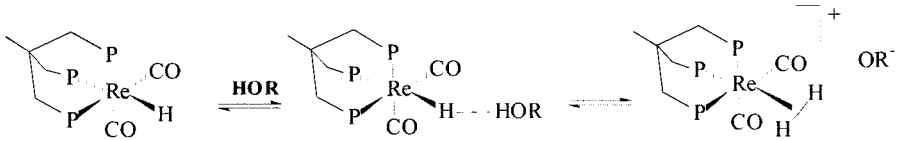

1 **2** **3**

Scheme 1

The study of the interaction between $[MeC(CH_2PPh_2)_3]Re(CO)_2H$ and proton donors (PFTB and $ClCH_2COOH$) in CH_2Cl_2 by IR and NMR at low temperature (190 – 260 K) showed the reversibility of this process (Scheme 1, Fig. 8) [31a, 46]. New high frequency bands ($\Delta\nu$ = +84 cm^{-1}) of the ν^s_{CO} and ν^{as}_{CO} of $\{[MeC(CH_2PPh_2)_3]Re(CO)_2(\eta^2\text{-}H_2)\}^+$ appear in the presence of excess proton donor at 200 K. The intensity of these bands decreases as the temperature increases to 260 K with the simultaneous growth of the bands of the initial hydride, **1**, and the high frequency shoulders (shifted by 9–11cm^{-1}) of the dihydrogen bonded adduct, **2** (Fig.8). These changes can be reversed upon cooling again to 200 K. This equilibrium can also be observed in the ^1H NMR spectra by the intensities redistribution of the averaged hydride resonance of **1** and **2** in the -5.83 to -6.28 ppm range and the broad resonance of **3** at –4.8 ppm. It is noteworthy that the very short T_{1min} time of the dihydrogen ligand in **3** (0.012 s at 200 MHz at 200 K) greatly differs from the T_{1min} of the hydride ligand of **2** (0.073 s at 200 K) [31a].

The same equilibrium was found for the interaction of $[MeC(CH_2PPh_2)_3]RuH_2(CO)$ with alcohols by IR and NMR studies [31b]. This hydride has a higher E_j factor (1.4) relative to the above mentioned Re analogue, leading to more pronounced spectral changes for the interaction with a weaker alcohol (HFIP instead of PFTB). The ν_{CO} band of the dihydrogen bonded intermediate, **2**, is shifted to higher frequencies by 29 cm^{-1} relative to the starting hydride **1** (Fig.9). A new distinct ν_{CO} band also appears for the dihydrogen complex, **3**, ($\Delta\nu$ = +103 cm^{-1})

whose intensity reversibly increases upon cooling to 190 K. The observed temperature dependence indicates that the cationic complex **3** is thermodynamically more stable than the hydrogen bonded intermediate **2**. However, an irreversible H_2 elimination occurs at temperatures higher than 260 K, with formation of the neutral organyloxo complexes **4** (Eq. 11), which can be easily detected by IR spectroscopy [30a, 31a].

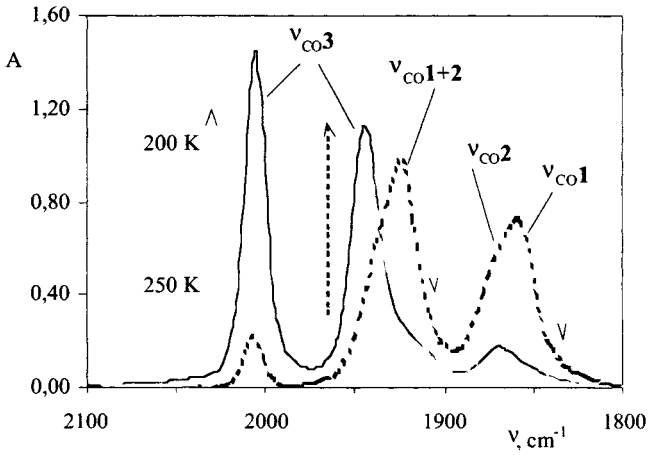

Figure 8. Variable-temperature IR spectra in the ν_{CO} region of $[MeC(CH_2PPh_2)_3]ReH(CO)_2$ (0.005 mol/L) in CH_2Cl_2 in the presence of PFTB (0.050 mol/L) at 200 – 250 K [46].

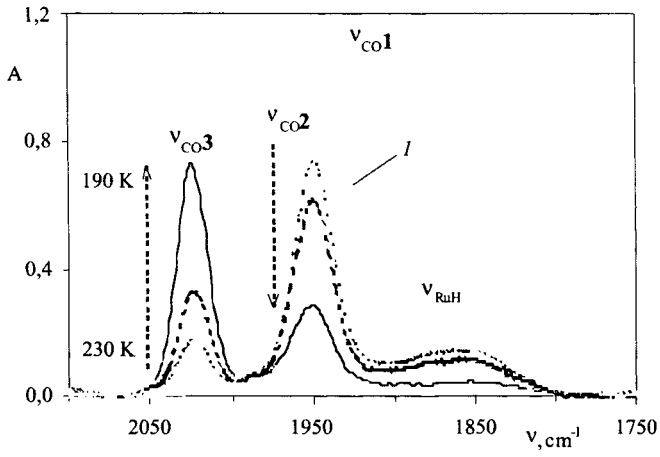

Figure 9. Variable-temperature IR spectra in the ν_{CO} region of $[MeC(CH_2PPh_2)_3]RuH_2(CO)$ (0.006 mol/L) in CH_2Cl_2 at 190 K (curve *1*) and in the presence of HFIP (0.060M) at 190 – 230 K [31b].

More recently, another new intermediate of the proton transfer reaction has been detected for the protonation study of CpRuH(CO)(PCy_3) (Scheme 2). This has been identified as the ion pair [CpRu(CO)(PCy_3)(η^2-H_2)]$^+$···OR^-, which is stabilised by a hydrogen bond between the dihydrogen ligand and the counter-ion [30d,e, 50]. This study presents the first evidence of the dihydrogen ligand participation in hydrogen bonding as a proton donor. The replacement of BF_4^- by coordinating anions leads to the considerable shifts of ν_{CO} from 2020 cm^{-1} to the low-frequency region (1996-1966 cm^{-1}), in accordance with the increasing H-bonding ability of the anion: $\Delta\nu$ = -24 cm^{-1} (CF_3COO^-) < -54 cm^{-1} (($CF_3)_3CO^-$) [50].

The observation of this intermediate, which is in the equilibrium with the dihydrogen bonded complex **2** and the free cation **3** (Scheme 2), greatly contributes to the knowledge of the detailed mechanism of the proton transfer process to transition metal hydrides and is in accordance with the concept of proton transfer to metal atoms in organometallic complexes [19c, 21a, 24a].

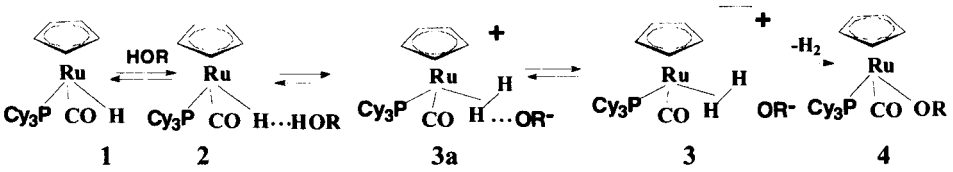

Scheme 2

14.4.1 Thermodynamics of proton transfer reactions.

Few attempts to determine the thermodynamic characteristics of proton transfer from alcohols to hydrides can be found in the literature. [32a ,47] However, the NMR technique used in those studies has obvious limitations in that it does not allow the determination of the equilibrium concentrations for each intermediate in Eq. 11 and the calculation of their formation constants. These limitations originate from the averaging of the hydride signal in the ^1H NMR spectrum due to a fast interconversion between **1** and **2**. Similar technical difficulties also occasionally arise in the IR investigations, resulting for instance from the overlap of the ν_{CO} bands of the initial hydride **1** and the H-bonded adduct **2**.

Combined IR/NMR experiments were recently used to overcome these difficulties and to allow the determination of the equilibrium concentrations of every intermediate of the proton transfer reaction (Eq. 11) at different temperatures. This made it possible to obtain the thermodynamic parameters not only for the dihydrogen bond formation (as was shown above) but also for the proton transfer stage. For instance, the enthalpy and entropy values of dihydrogen bonding calculated from the NMR investigations for the [$MeC(CH_2PPh_2)_3$]$Ru(CO)H_2$/HFIP and [$MeC(CH_2PPh_2)_3$]$Re(CO)_2H$/PFTB systems are in good agreement with those obtained from the IR spectral results [31b, 46]. The equilibrium constants were

calculated in the temperature range 200 - 260 K where H_2 evolution does not take place. Subsequently, the thermodynamic parameters of the second stage, **2** ↔ **3** and the total energy gain in the reaction **1** ↔ **3** were determined from the plots of $\ln K_{2\text{-}3}$ and $\ln K_{1\text{-}3}$ vs 1/T, respectively.

In this way, enthalpy and entropy values for the interaction of $[MeC(CH_2PPh_2)_3]$-$ReH(CO)_2$ with PFTB were obtained for the **2** to **3** conversion as well as for the overall reaction ($-\Delta H°_{2\text{-}3}$ = 2.3 kcal mol^{-1}, $-\Delta S°_{2\text{-}3}$ = 8.4 e.u.; $-\Delta H°_{1\text{-}3}$ = 8.3 kcal mol^{-1}, $-\Delta S°_{1\text{-}3}$ = 31 e.u.). The corresponding values obtained for the $[MeC(CH_2PPh_2)_3]Ru(CO)H_2$ /HFIP system are: $-\Delta H°_{2\text{-}3}$ = 8.6 kcal/mol, $-\Delta S°_{2\text{-}3}$ = 42 e.u.; $-\Delta H°_{1\text{-}3}$ = 16.1 kcal/mol, and $-\Delta S°_{1\text{-}3}$ = 65 e.u. [31b]. Note that the increase of the proton accepting ability for the hydride ligand in the latter case facilitates the proton transfer permitting the determination of the thermodynamic parameters for the reaction with a weaker XH acid (HFIP instead of PFTB).

These experimental data are summarized in the energy profile of Fig. 10, where the abscissa represents the H-H distance obtained from NMR relaxation data. The potential energy surface has two minima. The first one corresponds to the dihydrogen bonded adduct **2** with an H···H bond length of 1.81 Å, while the second one corresponds to the thermodynamically more stable cationic nonclassical hydride complex **3**, with an H-H distance of 0.93 Å. The significant impact of the hydrogen bonding energy into the total energy gain confirms its role as a driving force for proton transfer reactions.

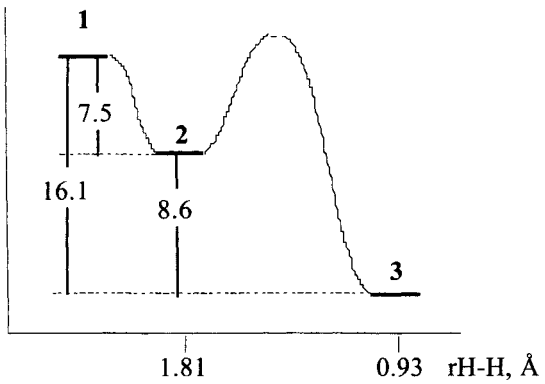

Figure 10. Energy profile for the transformation of $[MeC(CH_2PPh_2)_3]Ru(CO)H_2$ (**1**) into $\{[MeC(CH_2PPh_2)_3]Ru(CO)H(\eta^2\text{-}H_2)\}^+$ (**3**) via $[MeC(CH_2PPh_2)_3]Ru(CO)(H)$ H···$HOCH(CF_3)_2$ (**2**) in CH_2Cl_2 [31b].

14.4.2 Kinetics of proton transfer reactions

Obviously the barriers heights in the energy profile of Fig. 10 are determined by the rates of the corresponding transformations. The H-bonded adduct formation is always a diffusion-controlled process, therefore there is no barrier for this step [3].

The transition state energy for the conversion of **2** to **3** is shown only qualitatively in Fig. 10, but there are some indications that this step is slow, and upper and lower limits for the rate constants and for the barrier value can be estimated.

The observation of separated ^{1}H NMR signals for the hydride ligands in **2** and **3** with no broadening of the resonances is consistent with a lifetime longer than 10 s for these species [48]. Accordingly, an upper limit of 10^{-1} s^{-1} can be envisaged for the corresponding rate constant. A lower limit may roughly be estimated by considering that the conventional IR technique does not allow to monitor band intensity changes for processes faster than a few minutes. Since no time evolution of the intensity was observed, it may be assumed that the half-life of the proton transfer reaction is shorter than 1-2 min, providing a lower limit of 10^{-2} s^{-1} for the rate constant. It may thus be concluded that the transformation of **2** into **3** has an activation barrier $\Delta G^{\ddagger}$ (200 K) of ca. 12 - 13 kcal/mol, in agreement with the literature data [41, 49]. According to theoretical studies of proton transfer to Re and Ru hydrides, the proton-transfer barriers depend on both the metal complex basicity and the strength of the acid and were predicted to lie in a range from 10 to 0.7 kcal/mol [41b]. On the other hand, rather low rates of proton transfer and dihydrogen complex generation (varying from 10^6 to $10^{-1}s^{-1}$ with activation barriers $\Delta G^{\ddagger}$ (290 K) of ca. 6.5-12 kcal/mol) have been reported for the reactions of Fe and Ru hydrido complexes with strong acids [49].

Taking into account that the hydrogen bond formation is a diffusion controlled process, one can safely assume that the rate-limiting step in this proton transfer reaction is the conversion of the dihydrogen bonded complex into the cationic dihydrogen complex. So far, only one system, namely $CpRuH(CO)(PCy_3)$/PFTB, has been found where this slow conversion can be followed by conventional IR spectroscopy [50]. The rate constants obtained at 200 K in CH_2Cl_2 and at 200 – 250 K in hexane fall in the range 10^{-4} s^{-1} – 10^{-3} s^{-1}, providing barrier heights $\Delta G^{\ddagger}$ (200 K) of 13.7 kcal mol^{-1} in CH_2Cl_2 and 15.0 kcal mol^{-1} in hexane [52]. The temperature-dependent study in hexane has allowed for the first time the determination of the activation enthalpy ($\Delta H^{\ddagger}$ = 7.4 kcal/mol) and entropy ($\Delta S^{\ddagger}$ = -36 e.u.) for the transformation of a dihydrogen bonded complex into a cationic nonclassical complex.

Finally, we would like to remark that the energetic profile describing the formation of the dihydrogen complex via the dihydrogen-bonded adduct was achieved on the basis of the thermodynamic parameters determined by an effective combination of two spectral methods. It is important that the formation of the dihydrogen bonded intermediate contributes considerably to the total energy of the proton transfer leading to the dihydrogen complex and it is tempting to suggest a generalisation of this type of potential energy surface.

14.5 CONCLUSIONS

The studies described in this chapter show the intensive and continuing activity in this new field of knowledge. A wealth of experimental and theoretical information has contributed to elucidate the nature of the novel unconventional dihydrogen bonding. The strength and structure of this type of interaction have been determined for several systems. The formation of MH···HX bonds as the first step of the proton transfer process has been demonstrated but the thermodynamic data on each reaction step are still rather limited. Evidence for the ion pair formation between a dihydrogen cation and an anion, as well as the kinetics of the conversion of a dihydrogen bonded complex into a cationic dihydrogen complex have only been obtained once. There are still many open questions in this area of chemistry, demanding further active investigations. For instance, studies of ionic pairs stabilised by hydrogen bonding between the dihydrogen ligand in the cation and the anion, the effects of metal, ligands and solvent on the hydride basicity factor and on the potential energy surface of proton transfer, especially on the height of the proton transfer barrier. Much work still needs to be done before general rules governing proton transfer processes of importance in inorganic, bio-organic and supramolecular chemistry may be formulated.

ACKNOWLEDGEMENT

The authors are very grateful to Professors V.I. Bakhmutov, H. Berke, H.-H. Limbach and M. Peruzzini for useful discussions. The authors extremely appreciate the work of their co-workers and collaborators and financial support from INTAS and RFBR.

REFERENCES

[1] (a) L. Pauling, J. Am. Chem. Soc. 53 (1931) 1637; (b) L. Pauling, The Nature of the Chemical Bond, Ithaca, N.Y.. Cornell University Press, 1939

[2] (a) G.C. Pimentel, A.L. McClellan, The Hydrogen Bond, San Francisco, Freeman,1960. (b) The Hydrogen Bond, (Eds. P.Shuster, G.Zundel, C.Sandorfy), North-Holland, Amsterdam, 1976.

[3] St. Scheiner, Hydrogen Bonding. Theoretical Perspectives, N.Y.,Oxford University Press, 1997.

[4] (a) G.A. Jeffrey, W Saenger, Hydrogen Bonding in Biological Structures, Springer–Verlag, Berlin, 1991, (b) G.A.Jeffrey, An Introduction to Hydrogen Bonding, N.Y., Oxford University Press, 1997.

[5] (a) L. Legon, J. Millen, Acc. Chem. Res. 20 (1987) 39; (b) L.M. Epstein, A.V. Iogansen, Usp. Khim. 59 (1990) 22; (c) L.M. Epstein, Usp. Khim. 53 (1979) 1602.

[6] N.D. Sokolov, V.A. Savel'ev, Chem. Phys. 252 (2000) 406.

[7] (a) G. R. Desiraju, Acc. Chem. Res. 24 (1991) 290, and 29 (1996) 441; (b) Th. Steiner, G.R.Desiraju, J. Chem. Soc. Chem. Commun. (1998) 891.
[8] (a) J. L. Atwood, F. Hamada, K.D. Robinson, G.W. Orr, P.L. Vincent, Nature, 349 (1991) 683. (b) G.T. Fraser, A.S. Pine, J. Chem. Phys. 85 (1986) 2502; (c) H. Kleeberg, C.Eisenberg, T. Zinn, J. Mol. Struct. 240 (1990) 1271.
[9] Stu Borman, Chem.and Engineering News, Science/technology, 77 (1999) 36.
[10] W.W. Cleeland, M.M. Kreevoy, Science, 264 (1994) 1887, Science, 269 (1995) 104.
[11] (a) N.S. Golubev, G.S. Denisov, J. Mol. Structure, 270 (1992) 263; (b) N.S. Golubev, I.G. Shenderovich, S.N. Smirnov, G.S. Denisov, H.H.Limbach, Chem. Eur. J., 5 (1999) 491.
[12] (a) S. Subramanian, M.J. Zawarotko, Coord. Chem. Rev. 137 (1994) 357, (b) C.B. Aakeroy, Acta Crystallogr., B53 (1997) 569.
[13] (a) I. Ebata, A.M. Fujii, N.Mukami, Int. Rev. Phys. Chem., 17 (1998) 331; (b) F. Huisken, Adv.Chem. Phys. 81 (1992) 63.
[14] (a) M.J. Darensbourg, Prog. Inorg. Chem. 33 (1985) 221; (b) B.V. Lokshin, S.G. Kazaryan, A.G. Ginsburg, J. Mol. Struct., 174 (1988) 29; (c) P.A. Hamley, S.G. Kazarian, M. Poliakoff, Organometallics 13 (1994) 1767.
[15] (a) L.M.. Epstein, L.D. Ashkinadze, S.O. Rabicheva, L.A.Kazitsyna, Dokl. Acad. Nauk SSSR, 190 (1970) 128. (b) L.A. Leites, L.E. Vinogradova, N.A. Ogorodnikova, L.I. Zacharkin, Zh. Prikl. Spectrosk. 16 (1972) 357; (c) G. Cerichelli, G. Illuminati, G. Ortaggi, A.M. Guiliani, J. Organomet. Chem., 127 (1977) 357; (d) M. Nishio, Y. Umeeezawa, M. Hirota, Y. Takeuchi, Tetrahedron, 51 (1995) 8665.
[16] (a) D. Braga, F. Grepioni, Acc. Chem. Res. 30 (1997) 81. (b) D. Braga, F. Grepioni, M.J. Calhorda, P.E.M. Lopes, New J. Chem., 1999, 219.
[17] (a) E.S. Shubina, N.V. Belkova, L.M. Epstein, J. Organomet. Chem., 536-537 (1997) 17; (b) J.C.M. Rivas, L. Brammer, Coord. Chem. Rev., 183 (1999) 43.
[18] (a) L.E. Vinogradova, L.A. Leites, I.T. Chizevskii, N.V. Rastova, N.E. Kolobova, A.I. Yanovsky, Yu.T. Struchkov, Metalloorg. Khim., 4 (1989) 769 (English Translation in Organomet. Chem. In USSR, 1991); (b) E.S. Shubina, L.M. Epstein, J. Mol. Struct., 265 (1992) 367.
[19] (a) L.E. Vinogradova, A.Z. Kreindlin, L.A. Leites, I.T. Chizevskii, E.S. Shubina, L.M. Epstein, Metalloorg. Khim., 3 (1990) 1192 (English Translation in Organomet. Chem. In USSR, 3 (1990) 618); (b)E.S. Shubina, A.N. Krylov, A.Z. Kreindlin, M.I. Rybinskaya, L.M. Epstein, J. Mol. Struct., 301 (1993) 1. (c) L.M. Epstein, A.N. Krylov, E.S. Shubina, J. Mol. Struct., 322 (1994) 345.
[20] (a) E.S. Shubina, A.N. Krylov, D.V. Muratov, A.A. Fil'chikov, L.M. Epstein, Izv. Akad. Nauk, Ser. Khim., 11 (1993) 2002 (Russ. Chem. Bull. 42 (1993) 1919); (b). E.S. Shubina, A.N. Krylov, N.V. Belkova, L.M. Epstein, A.P. Borisov, V.D. Mahaev, J. Organomet. Chem., 493 (1995) 275.
[21] (a) S.G. Kazarian, P.A. Hamley, M. Poliakoff, J. Am. Chem. Soc., 115 (1993) 9069; (b) S.G. Kazarian, M. Jobling, M. Poliakoff, Mendeleev Commun., (1993) 148; (c) M. Poliakoff, S.M. Howdle, S.G. Kazarian, Angew. Chem. Int. Ed. Engl., 34 (1995) 1275.
[22] (a) L. Brammer, M.C. McCann, R.M. Bullock, R.K. McMullan, P. Sherwood, Organometallics, 11 (1992) 2339. (b) L. Brammer, J.M. Charnock, P.L. Goggin, R.J. Goodfellow, A.G. Orpen and T.F. Koetzle, J. Chem. Soc., Dalton Trans., (1991)

1789; (c) I.C.M. Wehman-Ooyeevaar, D.M. Grove, H. Kooijman, P. van der Sluis, A.L. Spek, G. van Koten, J. Am. Chem. Soc. 115 (1992) 9916.

[23] L. Brammer, D.Zhao, F.T. Ladipo, J. Braddok-Wilking, P. Sherwood, Organometallics 15 (1996) 1154.

[24] (a) E.S. Shubina, A.N. Krylov, A.Z. Kreindlin, M.I. Rybinskaya, L.M. Epstein, J. Organomet. Chem., 465 (1994) 259. (b) L.M. Epstein, E.S. Shubina, A.N. Krylov, A.Z. Kreindlin, M.I. Rybinskaya, J. Organomet. Chem., 447 (1993) 277.

[25] (a) E.Peris, R.H. Crabtree, J. Chem. Soc., Chem. Commun. (1995) 2179. (b) S.A. Fairshurst, R.A. Anderson, D.L. Hughes, S.K. Ibrahim, C.J. Pickett, J. Chem. Soc., Chem. Commun. (1995) 1569, (c) D. Braga, F. Grepioni, E. Tedesco, K.Birradha, G.R. Desiraju, Organometallics, 15 (1996) 2692.

[26] S.S. Kristjansdottir, J.R. Norton, A. Moroz, R.L. Sweany, S.L Whittenburg, Organometallics, 10 (1991) 2357.

[27] (a) A.J. Lough, S. Park, R. Ramachandran, R.H. Morris, J. Am. Chem. Soc., 116 (1994) 8356; (b) S. Park, R. Ramachandran, A.J. Lough, R.H. Morris, J. Chem. Soc., Chem. Commun., (1994) 2201.

[28] (a) J.C. Lee, E. Peris, A. Rheingold, R.H. Crabtree, J. Am. Chem. Soc., 116 (1994) 11014; (b) J.C. Lee, A. Rheingold, B. Muller, P.S. Pregosin, R.H. Crabtree, J. Chem. Soc., Chem. Commun., (1994) 1021. (c) E. Peris, J.C. Lee, J.R. Rambo, O. Eisenstein, R.H. Crabtree, J. Am. Chem. Soc., 117 (1995) 3485.

[29] (a) E. Peris, J. Wessel, B.P. Patel, R.H. Crabtree, J. Chem Soc., Chem. Commun., (1995) 2175; (b) J. Wessel, J.C. Lee, E. Peris, G.P.A. Yap, J.B. Fortin, J.S. Ricci, G. Sini, A. Albinati, T.F. Koetzle, O. Eisenstein, A.L. Rheingold, R.H. Crabtree, Angew. Chem., Int. Ed. Eng., 34 (1995) 2507.

[30] (a) E.S. Shubina, N.V. Belkova, A.N. Krylov, E.V. Vorontsov, L.M. Epstein, D.G. Gusev, M. Niedermann, H. Berke, J. Am. Chem. Soc., 118 (1996) 1105; (b) N.V. Belkova, E.S. Shubina, A.V. Ionidis, L.M. Epstein, H. Jacobsen, A.Messmer, H. Berke, Inorg. Chem., 36 (1997) 1522; (c) E.S. Shubina, N.V. Belkova, A.V. Ionidis, N.S. Golubev, L.M. Epstein, Izv. Akad. Nauk, Ser. Khim., (1997) 1405 (Russ. Chem. Bull., 44 (1997) 1349); (d) L.M. Epstein, E.S. Shubina, Ber. Bunsenges. Phys. Chem., 102 (1998) 359; (e) E.S. Shubina, N.V. Belkova, E.V. Bakhmutova, L.N. Saitkulova, A.V. Ionidis, L.M. Epstein, Izv. Akad. Nauk, Ser. Khim., (1999) 846 (Russ. Chem. Bull., 47 (1999) 817).

[31] (a) E.S. Shubina, N.V. Belkova, E.V. Bakhmutova, E.V. Vorontsov, V.I. Bakhmutov, A.V. Ionidis, C. Bianchini, L. Marvelli, M. Peruzzini, L. M. Epstein, Inorg. Chim. Acta, 280 (1998) 302; (b) V.I. Bakhmutov, E.V. Bakhmutova, N.V. Belkova, C. Bianchini, L.M. Epstein, M. Peruzzini, E.S. Shubina, E.V. Vorontsov, F. Zanobini, Can. J. Chem. 79 (2001) 475; (c) N.V. Belkova, E.S. Shubina, E.I. Gutsul, L.M. Epstein, S.E. Nefedov, I.L. Eremenko, J. Organomet. Chem., 610 (2000) 58.

[32] (a) J.A. Ayllon, C. Gervaux, S. Sabo-Etienne, B. Chaudret, Organometallics, 16 (1997) 2000; (b) S. Gruendemann, S. Ulrich, H.-H. Limbach, N.S. Golubev, G.S. Denisov, L.M. Epstein, S. Sabo-Etienne, B. Chaudret, Inorg. Chem., 38 (1999) 2550.

[33] L.H Desrosiers,. Z.R. Cai, R. Lin., R Richards., J Halpern., J. Am. Chem. Soc., 113 (1991) 4173.

[34] (a) A.V. Iogansen, Theor. Experim. Khim., 7 (1971) 314. (b) A.V. Iogansen, Theor.

Experim. Khim., 7 (1971) 302; (c) A.V. Iogansen, The Hydrogen Bond, Moscow: Nauka, 1981, p. 134. (d) A.V. Iogansen, Spectrochim. Acta A, 55 (1999) 1585.
[35] Q. Liu, R. Hoffmann, J. Am. Chem. Soc., 117 (1995) 10108.
[36] (a) G. Orlova, S. Sheiner. J. Phys. Chem. A, 102 (1998) 260
[37] (a) E. Peris, J. Wessel, B.P. Patel, R.H. Crabtree, J. Chem Soc., Chem. Commun., (1995) 2175; (b) R.H. Crabtree, P.E.M. Siegbahn, O. Eisenstein, A.L. Rheingold, T.F. Koetzle, Acc. Chem. Res., 29 (1996) 348; (c) B.P. Patel, J. Wessel, W. Yao, J.C. Lee, Jr., E. Peris, T.F. Koetzle, G.P.A. Yap, J.B. Fortin, J.S. Ricci; G. Sini, A. Albinati, O. Eisenstein, A.L. Rheingold, R.H. Crabtree, New J. Chem. 21 (1997) 413.
[38] (a) T.B.Richardson, S. De Gala, R.H. Crabtree, P.E.M. Siegbahn, J Am. Chem. Soc., 117 (1995) 12875, (b) W.T. Klooster, T.F. Koetzle, P.E.M. Siegbahn, T.B.Richardson, R.H. Crabtree, J. Am. Chem. Soc 121 (1999) 6337
[39] ((a) L.M. Epstein, E.S. Shubina, E.V. Bakhmutova, L.N. Saitkulova, V.I. Bakhmutov, A.L.Chistyakov, I.V. Stankevich, Inorg. Chem., 37 (1998) 3013; (b) E.S. Shubina, E.V. Bakhmutova, L.N. Saitkulova, L.M. Epstein, Mendeleev Commun., (1997) 83; (c) I. Alkorta, J. Elguero, C. Foces-Foces, J. Chem. Soc., Chem. Commun. (1996) 1633.
[40] J.Lundell, M.Petterson, Phys.Chem. Chem. Phys. 1 (1999) 1691.
[41] (a) G.Orlova, S.Sheiner, J. Phys. Chem. A, 102 (1998) 4813; (b) G. Orlova, S. Sheiner, T. Kar, J. Phys. Chem. A, 103 (1999) 514.
[42] E.I. Gutsul, N.V. Belkova, E.S. Shubina, L.M. Epstein, C. Bianchini, M. Peruzzini, F. Zanobini, preliminary data.
[43] C. Tolman, Chem. Rev., 77 (1977) 313.
[44] D.V.Yandulov, K.G. Caulton, N.V. Belkova, E.S. Shubina, L.M. Epstein, D.V. Khoroshun, D.G.Musaev, K. Morokuma, J. Am. Chem. Soc., 120 (1998) 12553.
[45] (a) G.J. Kubas, Acc. Chem. Res., 21 (1988) 120; (b) P.J. Jessop, R.H. Morris, Coord. Chem. Rev. 121 (1992) 155; (c) F. Maseras, A. Lledos, E. Clot, O. Eisenstein, Chem. Rev. 100 (2000) 601.
[46] N.V. Belkova, E.V. Bakhmutova, E.S. Shubina, C. Bianchini, M. Peruzzini, V.I. Bakhmutov, L.M. Epstein, Eur. J. Inorg. Chem. (2000) 2163.
[47] C.D. Field, T.W. Hambley, B.C.K. Yam, Inorg. Chem., 33 (1994) 2009.
[48] H.Gunter, NMR Spectroscopy. J.Wiley and Sons Ltd, Chichester, N.Y., 1980.
[49] (a) M.G. Basallote, J. Duran, M.J. Fernandez-Trujillo, M.A. Manez, J.R.de la Torre, J.Chem. Soc., Dalton Trans., (1998) 745; (b) M.G. Basallote, J. Duran, M.J. Fernandez-Trujillo, M.A. Manez, J. Chem. Soc., Dalton Trans., (1998) 2205; (c) M.G. Basallote, J. Duran, M.J. Fernandez-Trujillo, M.A. Manez, Inorg. Chem., 38 (1999) 5067.
[50] N.V. Belkova, A.V. Ionidis, L.M. Epstein, E.S. Shubina, S.Gründemann, N.S. Golubev, H.-H. Limbach, Eur. J. Inorg. Chem. (2000) ,submitted.

Chapter 15

Quantum mechanical phenomena in dihydrogen and polyhydride transition metal systems: a unified view

Agustí Lledós, José Maria Lluch, Feliu Maseras and Miquel Moreno

Departament de Química, Edifici Cn, Universitat Autònoma de Barcelona, 08193 Bellaterra (Barcelona), Catalonia, Spain

CONTENTS

15.1 UNUSUAL PHENOMENA IN POLYHYDRIDE COMPLEXES

Transition metal polyhydride complexes are remarkable for a number of reasons. Most of them are related to the peculiar chemical properties of the metal-hydride combination. There are, however, some specific phenomena in

the behaviour of these chemical compounds which cannot be explained through "conventional" chemistry concepts, and must be explained in view of the particular quantum phenomena associated to the small size of the hydrogen nucleus. This chapter will summarise these phenomena and show how the methods of theoretical chemistry prove their common origin.

15.1.1 Unusual but normal behaviours of polyhydride complexes

Before entering the discussion of quantum mechanical phenomena, we will briefly review other peculiar behaviours observed in transition metal hydrides, and emphasise how they can be explained with "conventional" chemistry concepts. The first original behaviour that can be mentioned is the existence of both "classical" hydrides and dihydrogen complexes [1]. In "classical" hydrides there is no strong interaction between the hydrogen atoms attached to the metal, whereas in dihydrogen complexes the H-H bond remains as such in the transition metal coordination sphere. Although the first reports of dihydrogen complexes were presented in 1984 by Kubas [2], the nature of these compounds as different from traditional hydrides has been clearly stated since that time by a variety of methods, including neutron diffraction, NMR analysis and theoretical calculations. The more clear-cut characterisation comes certainly from neutron diffraction, where values of H-H below 0.9 Å clearly indicate the presence of a dihydrogen bond. Theoretical calculations [3] have also had a significant contribution in proving that the existence of these compounds is the result of a subtle balance between the donation of the σ orbital of H_2 to an empty orbital of the metal atom and the back-donation from an occupied orbital of the metal to the σ^* orbital of H_2. Although first identified in dihydrogen complexes, this type of bonding is not exclusive of these species. Metal centres have been found to coordinate also other σ bonds such as Si-H and B-H [4]. Even the intramolecular coordination of C-H bonds leading to agostic distortions has been shown to be related to a similar chemical interaction in a number of cases [5].

Another characteristic aspect of transition metal polyhydride chemistry is the high fluxionality of these compounds. Apart from the just mentioned dihydrogen/dihydride equilibrium, hydrogen atoms in the coordination sphere of transition metal complexes have been shown to change position easily. This is for example the case in $[Os(P^iPr_3)_2H_3(BH_4)]$, where the four non-equivalent types of hydrogen atoms attached to osmium and boron can exchange position at given temperatures [6]. Again, the ability of the hydrogen atom to move from one centre to another is of a purely chemical nature, likely related to the combination of the lack of steric effects, the intermediate electronegativity and the existence of only one non-directional valence orbital.

The experimental location of hydrogen in transition metal complexes presents some significant challenges and difficulties. The commonly used X-ray diffraction

method does not properly locate hydrogen atoms, especially in the vicinity of metal atoms. Neutron diffraction is optimal [7], but the difficulty of growing large monocrystals associated with the limited availability of the international neutron diffraction facilities makes its application troublesome. This complicates significantly the experimental characterisation of transition metal polyhydrides, and has led in fact to a number of structural reassignments. The difficult location of hydrogen atoms by X-ray diffraction can be easily explained by realizing that what the experiment measures is the electron density, and that the electron density at the hydrogen centre is usually much smaller than that of surrounding atoms. It is certainly a phenomenon specific of hydrogen, but it has no quantum origin whatsoever.

There are finally a number of properties related to the nuclear spin of hydrogen that have been innovatively applied in the NMR spectroscopy of transition metal complexes. One must mention in this context the use of the ^{1}H-T_1 relaxation time [8]. This parameter allows an estimation of the H-H distance from its value, and has been indeed applied successfully to the identification as such of a number of dihydrogen complexes. A typical value of T_1 for a dihydrogen complex is 0.03 s, while a usual value for a dihydride is 0.3 s [8]. Another experimental parameter which is currently receiving increasing attention is the deuterium quadrupole coupling constant (DQCC) [9]. This parameter seems related to the ionicity of the metal-deuterium bond, and it has been shown recently that it can be evaluated from ^{2}H-T_1 relaxation times. The utility of these NMR magnitudes is certainly quite peculiar of the hydrogen isotopes involved, and also associated to the proximity between the nuclei that can be only observed when hydrogen is involved. However, it is again a phenomenon that can be explained without need to refer to the quantum nature of these nuclei.

15.1.2 Unusual and abnormal behaviours of polyhydride complexes

The phenomena described above have all one characteristic in common: they can be properly described with a sufficiently accurate ab initio calculation with a standard package. These calculations, based in the Born-Oppenheimer approximation, consider explicitly only the quantum mechanical nature of electrons, while dealing with the nuclei in a classical formalism. In contrast, there are a number of phenomena in transition metal polyhydrides that cannot be described with this scheme. We are going to present them briefly in the remaining of this section. The rest of the chapter will present a detailed explanation of their origin.

The first phenomenon involving the quantum mechanical properties of hydrogen nuclei that was recognised as such involved dihydrogen complexes and was characterised in 1988 by Eckert and Kubas, shortly after the discovery of these compounds [10]. A level splitting of the librational ground state of activated

molecular dihydrogen bound in a tungsten complex was measured by inelastic neutron scattering (INS). Its origin was readily identified as associated to a rotational tunnelling effect. This immediate identification was simple because of the good knowledge of rotational tunnelling in other unrelated chemical systems [11]. Later on, rotational tunnelling has been observed with this same INS technique in other transition metal dihydrogen complexes. The rotational tunnelling transition has an approximately exponential dependence on the barrier height and it is therefore extremely sensitive to its magnitude. Indeed taking a simple model for the rotation, the rotational tunnelling spectrum has been used to derive the barrier height for dihydrogen rotation in several complexes [12,13]. Some selected data are gathered in Table 1. Ground state librational splittings between 20 and 0.6 cm^{-1} have been observed [14,15]. The associated barriers to rotation that were derived by use of a simple model range from 0.5 to 2.5 kcal/mol. Tunnel splittings below 0.01 cm^{-1} are unobservable by INS experiments. In this case the rotational barrier must be above 3 kcal/mol.

TABLE 1. Rotational tunnel splitting (ω_t, cm^{-1}) and derived rotational barriers (E, kcal/mol) for dihydrogen complexes.

Compound	ω_t	E	Ref.
$M(CO)_3(PCy_3)_2(\eta^2\text{-}H_2)$			
M = Cr	4.33	1.30	14
M = Mo	2.82	1.70	16
M = W	0.89	2.20	16
$[MH(\eta^2\text{-}H_2)PP_3]^+$			
M = Fe	1.15	1.82	17
M = Ru	2.58	1.36	17
$IrClH_2(\eta^2\text{-}H_2)(P^iP_3)_2$	19.9	0.46	18
$Mo(CO)(\eta^2\text{-}H_2)(dppe)_2$	16.9	0.50	15
$Tp^{Me2}RhH_2(\eta^2\text{-}H_2)$	6.7	0.56	19
trans-$[FeH(\eta^2\text{-}H_2)(dppe)_2]^+$	2.1	2.3	20

Dihydrogen complexes with high activation barriers for the rotation present a surprising behaviour. Rotational barriers of ca.10 kcal/mol have been estimated for tantalocene and niobocene dihydrogen complexes [21]. As a consequence of the high barrier, rotation of the dihydrogen molecule seems to be blocked at the NMR time scale. For these complexes a single resonance is obtained for the NMR spectrum at high temperatures. When the temperature is lowered, decoalescence is not observed for the non-isotopically substituted dihydrogen species, but it is observed in the partially deuterated HD species.

A second abnormal behaviour of transition metal polyhydrides originating from quantum mechanical effects of the hydrogen nucleus concerns the ^{1}H NMR spectra of some particular compounds. The understanding of this behaviour was not immediate, and in fact a number of tentative hypothesis had been proposed throughout the years. A nice review on this particular subject has been published recently by Sabo-Etienne and Chaudret [22]. Tebbe and Parshall [23] had already observed in 1971 that the addition of the Lewis acid $AlEt_3$ to Cp_2NbH_3 led to the observation of large H-H coupling constants (>100 Hz) which were not explained at that time. The ^{1}H NMR spectrum of this niobium complex, even without additional Lewis acid, was already puzzling, with two broad peaks in a 2:1 ratio in the hydride region. This was in contrast with the behaviour of the analogous tantalum species Cp_2TaH_3, which was characterised by the expected AB_2 pattern with a J_{A-B} coupling constant of ca.10 Hz. One hypothesis given in the early 80's to explain this strange behaviour was the existence of a large quadrupolar moment on niobium [24], an explanation which was disproved later on in 1985 [25]. Another interesting result reported at the time was the awkward temperature dependence of the H-H coupling constant, varying from 11.2 Hz at 301 K to 0.0 Hz at 232 K [25].

The behaviour of these niobium complexes remained as an oddity until the discovery of dihydrogen complexes brought renewed interest to the analysis of the properties of transition metal polyhydrides. Chaudret and co-workers [26] extended in 1988 the study of early-transition metal sandwich complexes to the behaviour of a series of niobium and tantalum trihydrides L_2MH_3 (L = C_5Me_5, Cp; L = $C_5H_4SiMe_3$, Cp'; L = $C_5H_3(SiMe_3)_2$, Cp"; M = Nb, Ta) containing cyclopentadienyl ligands substituted by methyl or trimethylsilyl groups, the latter possessing a strong electron-withdrawing character. The H-H coupling constant was found to respond in an opposite way for niobium and tantalum upon a decrease in the electron density on the metal. In the case of tantalum, the coupling constant diminished slightly with the presence of silyl substituents (from 13 Hz in $Cp^*_2TaH_3$ to 7.3 Hz in Cp"TaH_3). In the case of niobium, the coupling constant was increased substantially by the silyl substituents, the values being 4 Hz in Cp_2NbH_3, 36.5 Hz in Cp'_2NbH_3, and 70.0 Hz in $Cp"_2NbH_3$. This was at the time interpreted as a sign of the presence of a dihydrogen unit, a hypothesis which was supported by measurements of the T_1 relaxation time. The coupling constant presented also significant temperature dependence for some of the niobium complexes. The eventual existence of a trihydrogen ligand was suggested at the time [26].

Other experimental studies in the same years showed that this strange behaviour of the ^{1}H NMR coupling constants was not exclusive of early-transition metal sandwich complexes. In 1987, Chaudret and co-workers [27] reported a similar behaviour for $Cp^*RuH_3(PR_3)$ (R = Cy, ^{i}Pr) complexes. The H-H coupling constant was also temperature-dependent, and reached a value as

large as 181 Hz at 237 K. Heinekey and co-workers reported a similar behaviour for $[CpIrH_3L]^+$ ($L = PMe_3$, PPh_3, $AsPh_3$) [28]. In this case, the coupling constants reached values of 100, 287 and 410 Hz for the different compounds at 178 K. This result, coupled with the predictions of qualitative calculations with the extended Hückel method [29], led to the proposal of an unprecedented trihydrogen ligand in these complexes [28]. This trihydrogen ligand would be a structural unit with three hydrogen atoms bound to each other. This appealing suggestion was however proven false by the neutron diffraction structure of $[CpIrH_3(PMe_3)]^+$ published by the same group shortly thereafter in 1990 [28]. In this structure, the shortest H-H distance between the hydride ligands is 1.67 Å, which rules out any significant H-H interaction.

The attainment of this neutron diffraction structure led to the acceptance of the quantum mechanical origin for this strange NMR phenomena that had been proposed in 1989 by two different groups [30,31]. This theory has been later refined, and its current form will be detailed in the following sections of this chapter. A definite proof of the involvement of the quantum mechanical nature of the hydrogen nucleus in these phenomena is their disappearance upon the replacement of one or a sufficient number of the involved atoms by deuterium.

Abnormal phenomena have been observed afterwards in a number of transition metal polyhydrides, and most of them are collected in the review by Sabo-Etienne and Chaudret [22]. Extensive experimental work on transition metal hydride complexes showing the so-called quantum exchange coupling led to the systematisation of several trends. The magnitude of the coupling was found to be a sensitive function of the ligands attached to the metal, the nature of the metal and the charge of the complex.

In the series of complexes $[CpIrH_3(PR_3)]^+$ the magnitude of the exchange coupling was found to decrease with an increase of ligand basicity. Extremely large couplings (up to 1565 Hz) were observed for phosphite ligands [28]. In the series of metallocene trihydrides $[Cp_2MH_3]^{n+}$(M = Mo, W; n = 1; M = Nb, Ta; n = 0), no exchange coupling was detected for W and Ta, a modest temperature-dependent quantum exchange coupling was measured for the Nb complex, and an important exchange coupling was exhibited by the Mo complex [32]. Whereas the neutral $Cp^*Os(CO)H_3$ complex shows no exchange coupling, large couplings were measured for the cationic $[(C_6H_6)Os(L)H_3]^+$ [33]. As a conclusion, it seems that a decreased electron density of the metal centre leads to larger couplings.

The sensibility of the quantum exchange coupling to the chemical environment has been also proven in a series of osmium trihydride compounds containing an asymmetrical OsH_3 unit. Depending on the nature of the co-ligands, these systems undergo zero, one or two quantum exchange coupling processes [34]. Moreover, the exchange coupling can be modified without variation of the ligands directly attached to the metal. The addition of Lewis acids which can

form adducts with a trihydride changes the exchange coupling constants [35]. The magnitude of exchange coupling has been found to be also solvent [22,36] and pressure [37] dependent. The addition of proton donors which can form H···H hydrogen bonds with the hydride ligands increase the quantum exchange in $Cp^*RuH_3(PCy_3)$ [38]. The quantum exchange coupling has proven to be a hypersensitive indicator of weak interactions [36].

A third area of polyhydride transition metal chemistry where quantum mechanical effects of hydrogen nuclei have also an influence, although more subtle, is that of the so-called elongated dihydrogen complexes. These are species that fall in between the usual H-H ranges of distance of dihydrogen (< 1.0 Å) and dihydride (> 1.4 Å). Detailed characterisation of these complexes is extremely complicated because they present usually a very high fluxionality between the dihydrogen and the dihydride structures, which in these cases happen to be very close in energy. In any case, quite a few of them have been conclusively identified by neutron diffraction [7]. A characteristic of these complexes is that their structures are unexpectedly elusive to the calculation with high level ab initio based methods. It is certainly true that nowadays computational chemistry is still not capable of accurately reproducing every single experimental structure. However, it is also true that a similar quality of reproduction must be expected for similar species. In particular, the Hartree-Fock based MP2 level, or the DFT based Becke3LYP level are usually sufficient to describe the structure of most experimentally known dihydrogen or dihydride complexes with a margin error in the H-H distance in the few hundredths of one Å [3,39]. This is conspicuously not the case for elongated dihydrogen complexes. A good example of this behaviour can be found in the comparative study at the DFT-based Becke3LYP of the four different complexes $W(H_2)(CO)_3(PH_3)_2$, $OsH_4(PH_3)_3$, IrH"H···H"$Cl_2(PH_3)_2$ and $[Os"H\cdots H"(NH_2(CH_2)_2NH_2)_2(HCO_2)]^+$ [40]. The four species correspond to simplified forms of experimental species where neutron-diffraction data are available. The simplification is in all the cases similar, corresponding to the replacement of bulky substituents in the ligands by hydrogen atoms. The theoretically computed value for the H-H distance is in very good agreement with the experimental value for the first compound (0.818 vs. 0.82 Å), which is a dihydrogen complex; and for the second one (1.861 vs. 1.84 Å), which is a classical polyhydride. Agreement is significantly worse for the other two species, with discrepancies of 0.12 Å (0.984 vs. 1.11) and 0.09 Å (1.428 vs. 1.34). These two latter species are elongated dihydrogen complexes. This difficult theoretical reproduction of experimental values of H-H distances in elongated dihydrogen complexes has also been shown to be related to the quantum mechanical behaviour of hydrogen nuclei. Additionally, some unusual temperature dependence of J(H, D) coupling constants has been discovered for the few elongated dihydrogen complexes that have been subject of detailed NMR studies. In $[Ru(H\cdots D)(Cp^*)(dppm)]^+$ J(H,D) decreases as the

temperature increases [41]. An opposite behaviour has been observed in *trans*-$[Os(H\cdots H)H(depe)_2]^+$ and *trans*-$[Os(H\cdots H)Cl(depe)_2]^+$ [42]. Although the variation of J(H,D) with the temperature is weak (less than 1 Hz in a range of 50 K), it has been considered as significant.

After this presentation of unexpected phenomena in transition metal polyhydrides, this chapter is composed of two more sections. In the following one, a brief review on the nature and the chemical manifestations of the quantum phenomena of nuclei will be presented. The third section will show how the concepts exposed in the second section provide a unified explanation of the behaviours that have been just presented in this first section.

15.2 QUANTUM MECHANICAL EFFECTS IN CHEMISTRY.

15.2.1 The Schrödinger equation.

Quantum mechanics is based on the resolution of the Schrödinger equation (Eq 1). This equation includes the coordinates of all the participating particles. In a molecule, and from the point of view of a chemist, this means the electrons and the nuclei. Because of their quite different mass, the Schrödinger equation is customarily divided in two parts by assuming that the total wavefunction can be expressed as in Eq 2. Ψ_e and Ψ_n, the electronic and nuclear wavefunctions, are the solutions of Eqs 3 and 4.

The electronic hamiltonian includes all the terms of the total hamiltonian but the nuclear kinetic term. Equation (3) is called the electronic Schrödinger equation as it only includes the motion of electrons as variables. The coordinates of the nuclei are only parameters in this equation so that the obtained electronic energy is a function of the nuclear coordinates. This is the potential energy surface (PES). Equation (4) is the nuclear Schrödinger equation. As it contains the PES, it can only be treated once the electronic equation (3) has been solved. This split of the Schrödinger equation in two is known as the Born-Oppenheimer separation.

$$\hat{H}\Psi = E\Psi \tag{1}$$

$$\Psi = \Psi_e \cdot \Psi_n \tag{2}$$

$$\hat{H}_{el}\Psi_e = E_{el}\Psi_e \tag{3}$$

$$(\hat{T}_n + E_{el})\Psi_n = E\Psi_n \tag{4}$$

Traditionally the applications of quantum mechanics in chemistry have been restricted to the electronic motion, that is, to the solution of Equation (3). The nuclear motion is usually not considered at all or, at best, is treated within a classical mechanics framework. This is usually a good enough approximation for the heavy nuclei but it is now well established that motion of hydrogen atoms, the lightest element in the periodic table, can easily show quantum effects. Among them the so called tunnelling effect is the most studied one [43] though there is more in the picture as will be shown in the following subsections.

15.2.2. The tunnelling effect.

15.2.2.1 The symmetric double well.

Let us consider the hypothetical one-dimensional potential energy profile depicted in Figure 1. It features two equivalent minima (reactants and products) separated by an energy barrier (a transition state). This is a very well known problem in quantum physics as a huge number of systems falls in the category of the so called "symmetric double well" profile.

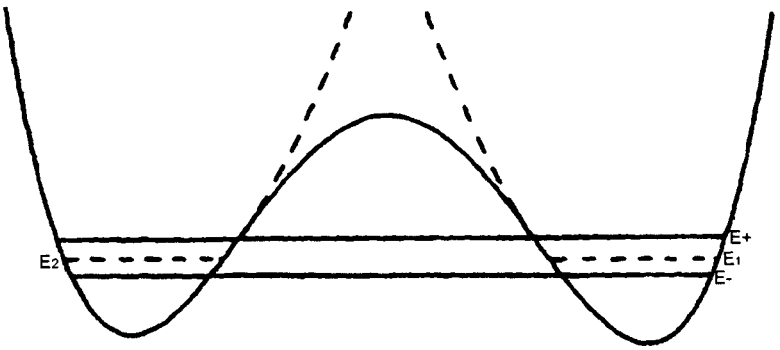

Figure 1. Symmetric double well profile in one dimension with the lowest two vibrational energy levels. The dashed line indicates the degenerate levels in the case of an infinite barrier. The energy (Y-axis) and the distance (X-axis) are in arbitrary units

If the barrier separating the two wells were of infinite height (as indicated by dashed lines in Figure 1) or else the two wells were separated by an infinite distance then there would be two uncoupled stationary states Ψ_1 and Ψ_2 located in each side of the double well with energies $E_1 = E_2$. In this case there would

be no tunnelling connecting both wells. However, if the energy barrier and the distance between minima are not infinite, a coupling W_{12} takes place between both wells so that Ψ_1 and Ψ_2 are no longer stationary states of the system. It can be easily demonstrated [44] that in this case the new stationary states Ψ_+ and Ψ_- have associated energies E_+ and E_- so that a tunnelling splitting ω_t (Eq 5) appears.

$$\omega_t = E_+ - E_- = 2|W_{12}| \tag{5}$$

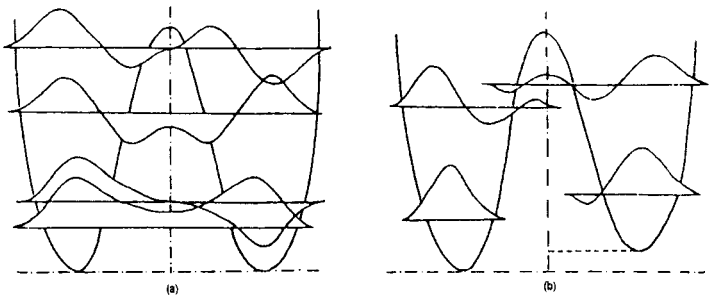

Figure 2. Wavefunctions corresponding to the lowest vibrational levels in a double well. (a) Symmetric case. (b) Asymmetric case. The energy (Y-axis) and the distance (X-axis) are in arbitrary units. The amplitude of the wave function superposed on the potential energy profile is also arbitrary

This situation is also shown in Figure 1. Ψ_+ and Ψ_- are now fully delocalised between the two wells as seen in Figure 2(a).

It may not be apparent what is the relationship between this energy splitting and the motion of a particle going through a potential energy barrier, as tunnelling is customarily envisaged. To clarify this point let us consider that initially the system is described by the non-stationary Ψ_2 wavefunction so that the system is localised on the left well and it has not enough energy to (classically) surpass the energy barrier. By making use of the time-dependent Schrödinger equation it can be easily shown that in this case the system will evolve in time and after a period of time of $h/2(E_+ - E_-)$, the system is described by Ψ_1 so that it becomes totally localised in the right well. As the double well is symmetric, this localisation of the wavefunction in either side of the barrier will take place periodically. Thus, the tunnelling rate or frequency is given by Eq 6.

$$k = 2(E_+ - E_-)/h \tag{6}$$

The magnitude of the coupling, and so of the splitting, depends on the energy barrier and the distance between both minima so that the splitting is greater when the energy barrier is lower and/or the distance is shorter. It is to be

noted that the distance is measured in mass-weighted coordinates so that the length depends on the mass of the system. In this way if displacements along the coordinate imply the motion of a heavy particle, the two wells are greatly separated and the tunnelling effect becomes negligible.

Up to now it has been assumed that there is only one tunnelling doublet and the system is found there so that it has a well defined energy. Usually a double well profile will support more than one of such pairs with energy below the barrier. As the pair of states lies closer to the top of the barrier, the interaction between both wells grows so that tunnelling splittings increase as shown in Figure 2(a). Usually the experimental data are not obtained at a fixed energy but at a given temperature so that a thermal average over all the significantly populated levels must be carried out. Assuming that the Maxwell-Boltzmann statistics holds the averaged tunnelling splitting at a given temperature can be obtained by Eq 7, where the sum extends over all the significantly populated pairs of levels, each one with a given tunnelling splitting ω_i. As at higher temperatures the higher pairs of levels are more populated, the tunnelling splitting will increase with temperature. Eq 7 implicitly assumes that the levels above the energy barrier are not significantly populated. When this is the case (at high enough temperatures) the transfer between both wells is not a pure tunnelling event and equation 7 is no longer valid.

$$\omega_t(T) = \sum_i \omega_i \exp(-E_i / k_B T) \tag{7}$$

15.2.2.2 The asymmetric double well.

In the preceding subsection we considered that the two minima of the double well were identical. If this is the case, it is not formally possible to distinguish between the system located in the right well (described by Ψ_1) and the system located in the left well described by Ψ_2. However, if the two minima are not identical, the double well is not symmetric and localisation of the wavefunction in the right or left well gives rise to two different situations that can be sorted out.

Application of quantum mechanics to the asymmetric double well is also quite straightforward though the final formulas are somewhat more complicated [44]. In short, for the asymmetric double well, wavefunctions are not fully delocalised between the two wells. In fact, slight departures from symmetry always produce a large decrease in the tunnelling rate. Only when the asymmetry and/or the energy barrier are very small there is some degree of interaction between the two wells. Figure 2(b) shows, for the generic asymmetric double well, the more common situation of two states with different energies $E_1 \neq E_2$ and correspondingly fully localised wavefunctions.

In the asymmetric double well the tunnelling rate constant can be expressed according to Eq 8, where the angle ϑ is defined by Eq 9.

$$k = \frac{2(E_+ - E_-)}{h} sin^2(\vartheta) \tag{8}$$

$$tan(\vartheta) = \frac{2W_{12}}{E_1 - E_2} \tag{9}$$

As the asymmetry increases, $\vartheta \rightarrow 0°$ and $k \rightarrow 0$. If $E_1 = E_2$, $\vartheta = 90°$ and Eq 8 reverts to Eq 6, the tunnelling frequency of a symmetric double well. The decrease in the tunnelling rate can be qualitatively attributed to the fact that asymmetry destroys the exact state of resonance between the energy levels of both wells so that tunnelling is no longer a first order interaction but a second order one.

15.2.2.3. Experimental manifestations of tunnelling.

In the preceding subsections we have presented the tunnelling effect for a double well system. In chemistry, any given reaction can usually be represented as a double well system with reactants and products as the two minima and the transition state located in the barrier separating both wells. Sure, chemical reactions are not one-dimensional systems as it was assumed in the preceding Figures but the formulas presented up to now remain valid irrespective of the dimensionality of the double well.

To be more precise let us restrict ourselves to an internal rearrangement of a molecule. This is an unimolecular process with precisely defined reactants and products (the two isomers). If the rearrangement involves two identical molecular configurations the system is a prototype of a symmetric double well. Obviously in this case it is not possible to distinguish reactants from products but this does not mean that tunnelling cannot be detected. As explained above, for a symmetric double well the vibrational levels of the system, which are found below the energy barrier, will appear as quasi-degenerated pairs with an energy splitting separating the two states of the pair. The energy splitting is usually a small quantity as compared with the magnitude of the vibrational energy of the molecule. Still the difference exists and, if a radiation of the correct frequency is used, an induced transition between both states of the pair may occur. The energy splitting can thus be experimentally measured from the spectrum. Usually, vibrational spectra are recorded in the infrared zone of the electromagnetic field. However, the splitting is usually such a smaller quantity that it falls in a lower energy zone of the electromagnetic spectrum. The inversion of ammonia and the proton transfer in malonaldehyde are well known cases of systems where such a tunnelling splitting has been measured by recording their spectra in the microwave region of the electromagnetic field (Figure 3). The measured values of the ground state (v = 0) splittings are 21 and 0.8 cm^{-1} for malonadehyde

[45] and ammonia [46], respectively. The higher splitting in malonaldehyde may be due to a lower energy barrier as compared with the ammonia inversion process or, more likely, to the fact that only one hydrogen atom is moving in the malonaldehyde tautomerization so that the two wells are less separated in that case. In the ammonia inversion spectrum, the first vibrational excited state (v = 1) has been observed to possess a splitting of 36 cm^{-1}, a higher value to be expected on the grounds that excited vibrational states are closer to the top of the energy barrier (Figure 3).

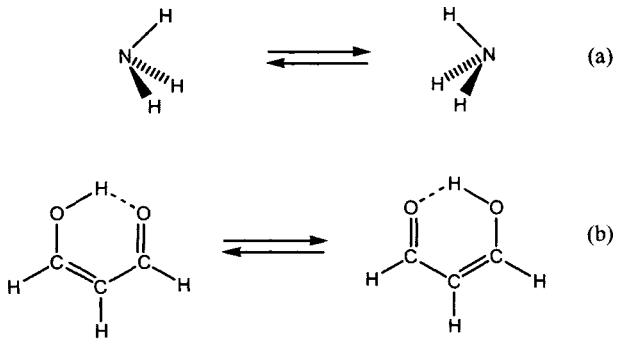

Figure 3. Hydrogen inversion of ammonia(a) and proton transfer in malonaldehyde (b)

Another clear manifestation of tunnelling is the magnitude of the isotopic effect when the moving hydrogen atoms are substituted by deuterium atoms (or tritium atoms). As the mass of deuterium is twice the mass of "normal" hydrogen, tunnelling is almost quenched upon deuteration. For instance it has been measured that the tunnelling splitting of the ground vibrational state in the ND_3 inversion is just 0.05 cm^{-1} [46]. On the theoretical grounds given in the preceding subsection, the larger mass of the deuterium produces a larger separation between the two minima and tunnelling is, consequently, smaller. Obviously, isotopic substitution of hydrogen by tritium (three times the mass of hydrogen) will produce a larger diminution of the tunnelling splitting. These changes in the double well profiles upon isotopic substitution are schematically depicted in Figure 4.

More kinetically relevant data for reactions that proceed via tunnelling can be obtained in some cases from the analysis of NMR spectra. In an NMR spectrum the position of the band corresponding to a particular nucleus is affected by its environment (the so-called chemical shift). If a system contains magnetic nuclei of a particular kind, let us say protons, in two different environments,

the observed spectrum will depend on whether, and how rapidly, the nuclei can change places between the two sites, either by direct exchange or by exchange from each site with other species. If exchange is absent or very slow, two separate sharp lines will appear for the two sites, while if exchange is very fast, a single sharp line will appear at a position corresponding to a weighted mean of the two resonances. Intermediate rates of exchange will produce broader spectra, which may or may not have two peaks. These changes in the NMR spectrum upon modification of the exchange rate are graphically depicted in Figure 5. Obviously the concept of slow or fast is relative and depends on the resolution of the spectrometer. In NMR the rates at which the two signals coalesce into one are in the range $1\text{-}10^5\ s^{-1}$. If a given reaction lies within this range, analysis of the intermediate range can be used to determine the rate of the process. Spectroscopic techniques other than NMR can be used in an analogous manner though the range of reaction rates suitable for the quantitative study will be quite different.

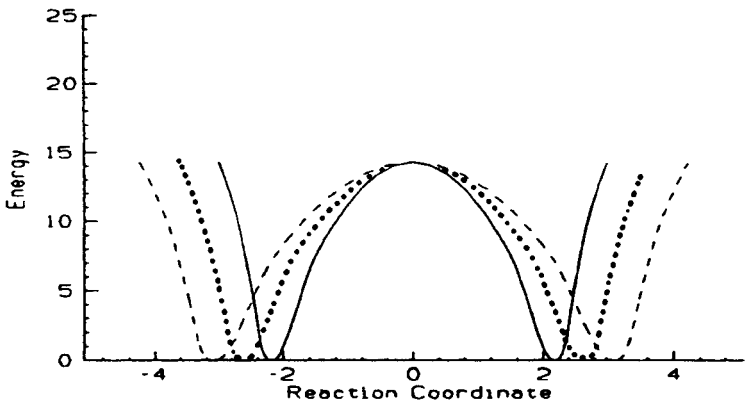

Figure 4. Effect of the isotopic substitution on the total path length of a given H-atom transfer reaction. Solid line: the exchanging particle is a hydrogen. Dotted line: the exchanging particle is a deuterium. Dashed line: The exchanging particle is a tritium.

Now let us consider a reaction that may take place through a tunnelling mechanism. To be more precise, consider the *meso*-tetraphenylporphine shown in Figure 6. *Meso*-tetraphenylporphine has two degenerated tautomeric forms depicted in the figure. The rate of the process can be followed by observing the chemical shifts, not of the transferring hydrogen atoms, but of the hydrogen atoms bonded to the pyrrolic rings. In each one of the two frozen structures of

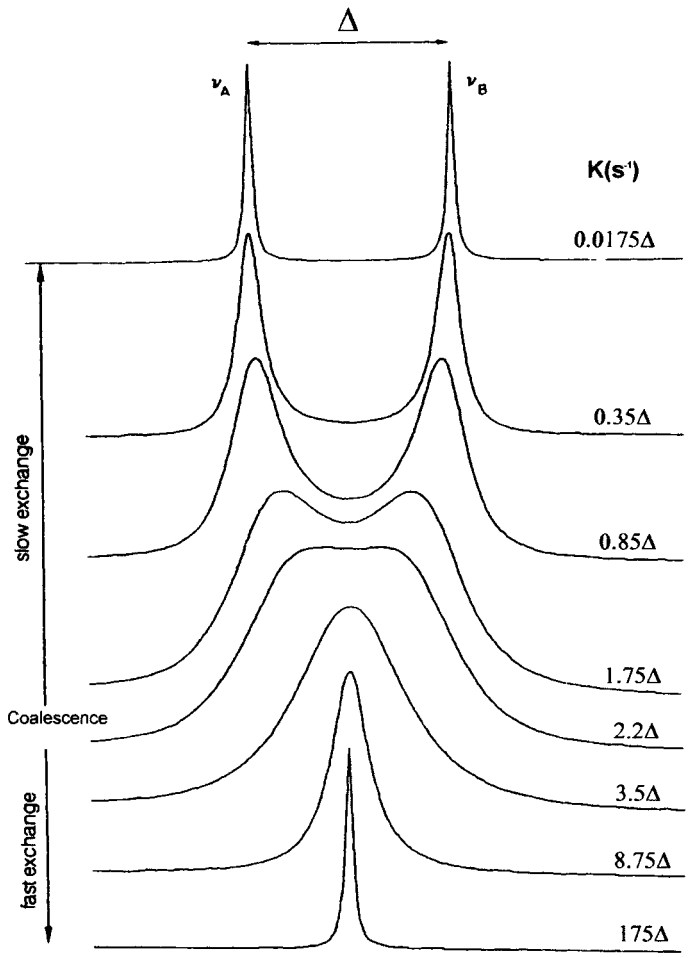

Figure 5. Evolution of two signals in a NMR spectrum as a function of the interconversion rate

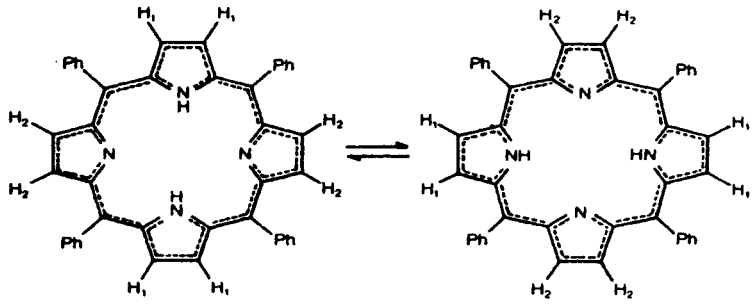

Figure 6. Double H-atom transfer in *meso*-tetraphenylporphine

the porphine shown in Figure 6 there are two different kinds of hydrogen atoms (indicated H_1 and H_2). If the tautomerism is fast enough, H_1 and H_2 will show a single NMR signal but if the hydrogen transfer is slow in comparison with the NMR time scale, two separate signals will be seen for the two chemically different protons. This reaction has been studied in a wide range of temperatures and the rate constant has been measured upon analysis of the resulting NMR spectrum [47]. Arrhenius plots of the obtained results are shown in Figure 7 for *meso*-tetraphenylporphine and its isotopomer where the two transferring hydrogen atoms have been substituted by deuterium atoms. If tautomerization were only a classical (over the barrier) process, the Arrhenius plot will be a straight line that will tend to zero at low enough temperature.

To say it in other words, at low enough temperatures the system would be confined in one of the two sides of the double well and the transfer would stop. However, if tunnelling is present at low enough temperatures the transfer will not be totally quenched as the tunnelling frequency of the lowest vibrational level will always operate. If this tunnelling frequency is high enough to be detected, the rate constant will not tend to zero but to a constant (albeit small) value. This is what has been observed for the meso-tetraphenylporphine as depicted in Figure 7 [47].

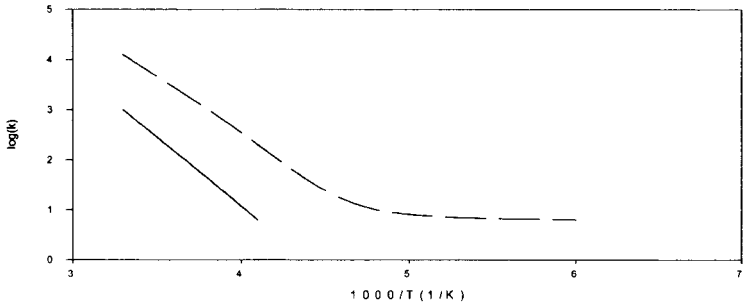

Figure 7. Arrhenius plots for the H-exchange in meso-tetraphenylporphine. Dashed line: normal (H) isotopomer. Solid line: bideuterated molecule. The Y-axis represents the decimal logarithm of the rate constant in s^{-1}

Conversely, the deuterated molecule does not show the appearance of a lower limit for the rate constant. This does not mean that there is not a tunnelling process in this case but it indicates that the tunnelling frequency for the deuterated porphine is below the range available at the NMR time scale.

15.2.3 Delocalisation of the nuclear wavefunction.

In the preceding section the theory and manifestations of tunnelling in chemistry have been described. In this section we will deal with another manifestation of the quantum nature of the nuclear motion which is, in fact, simpler than the tunnelling effect though it is usually ignored when analysing experimental data.

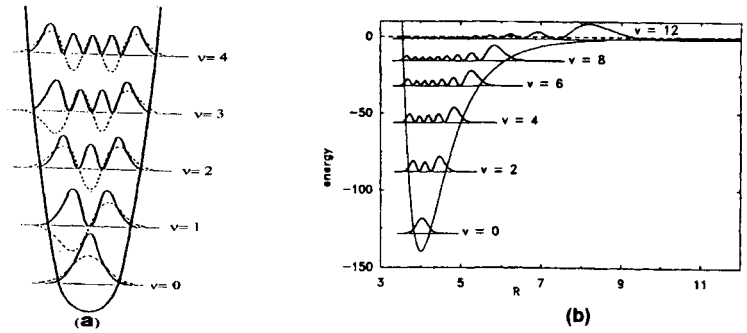

Figure 8. Vibrational wavefunctions for the harmonic (a) and the anharmonic wells (b). In the harmonic case the wavefunction is indicated by a dashed line and its square by a solid line. In (b) only the square of the wavefunction is depicted. The energy (Y-axis) and the distance (X-axis) are in arbitrary units. The amplitude of the wavefunctions superposed on the potential energy surface is also arbitrary

To begin with, let us consider the harmonic potential depicted in Figure 8(a). This is one of the few systems for which the Schrödinger equation can be exactly solved. The energies and wavefunctions are well known and they have been indicated in a pictorial way in Figure 8(a). The harmonic potential is also the simplest model for the vibration of molecules so that the wavefunctions depicted in Figure 8(a) can be thought as the ones corresponding to a given normal vibrational mode. It is also well known that vibrational modes are not truly harmonic as there is (usually) a dissociation limit. That is, at high enough deformation the molecule breaks down and the energy is no longer quantized. This *anharmonic* (more real) situation is depicted in Figure 8(b). When anharmonicity is taken into account the energy levels are no longer found at a constant energy interval but the separation between two consecutive levels diminishes at energies closer to the dissociation limit. Also, the corresponding anharmonic wavefunctions are no longer symmetric but displaced towards larger values of the normal mode.

What is the effect of the anharmonicity in "real world" chemistry? The closing of the energy separation between consecutive vibrational levels is fairly well known as it is directly reflected in the vibrational spectra (IR or Raman). Conversely, the asymmetry of the wavefunction is not usually taken into consideration. However, this asymmetry may have important implications when measuring molecular geometrical parameters. To make the point, let us consider a stretching between two bonded atoms A-B. If this stretching mode is harmonic, the nuclear wavefunction of the ground vibrational level as well as the ones of all the excited levels will be symmetric and centred at the value of the minimum potential energy x_0 (see Figure 8(a)). However, in the anharmonic case, the wavefunctions are not symmetric but shifted towards higher values of the normal coordinate. For the ground state this effect is usually moderate or even negligible if the well is deep enough so that the harmonic approximation holds. However, for the higher vibrational levels the asymmetry is important and the wavefunction is no longer centred in x_0. In this case a measurement that obtains the average value of the A-B distance x will not produce x_0 but a higher value. If anharmonicity is important, this effect can persist down to the ground vibrational state.

If this delocalisation of the wavefunction is important the averaged value of the A-B distance may differ significantly from the value of the minimum x_0. Moreover, the value of the averaged A-B distance will depend on the temperature tending to higher values as temperature increases. The formula relating the A-B measured distance with the temperature is analogous to equation (7) for the thermal averaged tunnelling splitting at a given temperature.

15.3. THEORETICAL BASIS AND CALCULATION OF THE QUANTUM MECHANICAL PHENOMENA IN POLYHYDRIDE COMPLEXES

As mentioned in section 1.2, both polyhydride and η^2-dihydrogen transition-metal complexes exhibit very interesting spectroscopic properties that can be observed in the proton NMR spectra or in the inelastic neutron scattering spectra, respectively. At first glance the two types of phenomena have nothing in common, but they actually both come from the same origin: in short, the quantum mechanical exchange of a pair of hydrogen nuclei through an energy barrier in a double well potential.

On this basis, in what follows we intend to shed light on the special spectroscopic properties of those complexes. To this aim, we will focus fundamentally on some of the complexes theoretically studied by our group in the last years. Other authors have dealt with this topic [37,48,49]. Special mention must be done to the work of Clot and co-workers [13,36,50].

15.3.1 Quantum exchange coupling in transition-metal polyhydride complexes.

Let us first consider the case of a dihydride transition metal complex whose two hydrides, H_1 and H_2, lie at two chemically inequivalent binding sites, A and B, respectively (an AB nuclear spin system). A magnetic scalar proton-proton coupling J_m between the corresponding nuclear spin angular momenta, I_1 and I_2, appears, mainly due to the Fermi contact term. As a consequence, the signal corresponding to the frequency of the proton NMR transition, in the radiofrequency region of the electromagnetic spectrum, associated with I_1 splits into two lines separated by just J_m. Likewise, the line associated with I_2 is split. Then the known AB pattern consisting of two doublets is obtained. However, an additional quantum mechanical effect can alter this simple picture. Although the binding sites A and B are inequivalent, H_1 and H_2 are indistinguishable particles (fermions). Thus, two possible distinct configurations (positions of the nuclei) can be envisaged for the minimum energy structure of the dihydride complex: H_1 and H_2 are at binding sites A and B, respectively, or, conversely, H_2 and H_1 are at binding sites A and B, respectively. Evidently, both configurations have exactly the same energy and are related by means of the permutation of the two hydrides. Therefore, the potential energy surface of the dihydride complex contains two degenerate wells separated by an energy barrier in such a way that the exchange process corresponds to a double well system. Under the influence of an external static magnetic field, the Hamiltonian operator of the two spin-1/2 hydrides involves two clearly different parts, the magnetic one and the part accounting for the hydride exchange. The magnetic part of the Hamiltonian (the unique contribution usually present in the normal NMR problems) includes the terms that depend on the shielding constants and cause the chemical shifts of both nuclei, along with the term representing the coupling between the nuclear spin angular momenta, I_1 and I_2, which depend on the magnetic scalar coupling J_m.

The portion of the Hamiltonian related with the motion of the two nuclei contains the kinetic energy operators plus the potential energy term corresponding to a symmetric double well problem. The nuclear Schrödinger equation with that complete Hamiltonian provides the energy levels and wavefunctions of the problem. The energy levels turn out to be a non-trivial combination of the magnitudes that determine the nuclear spin energy levels in a normal NMR problem (shielding constants and the magnetic scalar coupling) and the energies corresponding to the symmetric and antisymmetric stationary states of the symmetric double well system (see above). Applying the appropriate NMR selection rules the allowed transitions give rise to an apparently normal AB pattern but with the lines forming each doublet being separated by $J_m + \omega_J$, where w_J is the tunnelling splitting in a symmetric double well. As a consequence, the proton NMR spectrum of a dihydride transition-metal complex provides a total observed coupling $J_T = J_m + \omega_J$. Since ω_J appears as a result of the quantum motion on a double well corresponding to a nuclear exchange process, it is called

quantum mechanical hydrogen exchange coupling. Note that the origin of w_J is not magnetic at all, but if its value is such that the allowed transitions between the energy levels fall inside the radiofrequency region of the electromagnetic spectrum, it can be measured from the NMR spectra.

For the sake of simplicity we have explained the physical basis of the quantum exchange coupling using the example of a dihydride. However it is in principle present in any polyhydride, most of the experimental observations having been performed concretely in trihydrides. The fact that this phenomenon is essentially the same, even though more than two hydrides are present, shows that it is related with the exchange of a single pair of nuclei, at least in a first approximation. As we will see below, the nature of the quantum exchange coupling allows us to understand the unusual features of the proton NMR spectrum of polyhydrides transition-metal complexes: large (or even very large) observed couplings, large temperature dependence and striking isotope effects. Weitekamp *et al.* [30] and Zilm *et al.* [31] were simultaneously the first who proposed a similar explanation of the physical origin of those NMR effects in terms of quantum exchange coupling.

15.3.1.1. The Landesmann's model

Once the cause of the large observed J_T couplings has been identified, we focus on the theoretical quantitative determination of the w_J values. The first attempt was due to Zilm *et al.* [51] who adapted a previous model developed by Landesmann [52] to treat the quantum mechanical exchange couplings involving ^{3}He atoms in solid ^{3}He. In this case the ^{3}He wavefunction turns out to be rather delocalised as demonstrated by the large zero-point vibrational amplitude of the ^{3}He atoms around their lattice sites. This delocalisation permits pairs of ^{3}He atoms to exchange positions via the quantum mechanical exchange interaction as a result of a small but significant overlap in their respective vibrational wavefunctions.

To outline the particular application of the Landesmann's model to get w_J let us first consider two nuclei (H_1 and H_2) strongly localised in two distinct potential energy wells. For the polyhydrides these would be the binding sites A and B. If these hydrides are far enough so they do not interact with each other, their vibrational motion can be treated independently. Assuming that each potential energy well corresponds to an isotropic three-dimensional harmonic oscillator, the single-hydride ground-state wavefunction is a gaussian function (Eq 10), where m is the mass of the hydride and k_i is the vibrational force constant of the binding site i. However, if there is at least a little interaction between both nuclei, the small but finite overlap of their vibrational wavefunctions gives rise to quantum mechanical exchange (as a consequence of the corresponding delocalisation along the double well).

$$\Psi(\vec{r}_i) = (\alpha/\pi)^{3/4} \cdot \exp(-\alpha r_i^2/2) \quad , \qquad \alpha = \left(\frac{mk_i}{\eta^2}\right)^{1/2} \tag{10}$$

Using a basis set of gaussian functions given in equation (10) and assuming a hard-sphere inter-particle potential, an analytical expression for ω_J (Eq 11) can be obtained, where a is the internuclear distance between both hydrides and λ is the hard-sphere diameter of each nucleus. Eq 11 is valid as long as $\alpha\lambda^2 \gg 1$, which in practice is easily fulfilled. The hard-sphere approximation means that no configurations in which the nuclei are within λ of each other will be allowed. If the nuclei are separated by more than their hard-sphere diameter, the potential energy is just the sum of the two single-nucleus energies.

$$\omega_J = \frac{\eta\alpha}{m}\sqrt{\frac{2\alpha a^2}{\pi}} \cdot \exp\left[-\frac{\alpha}{2}(a^2+\lambda^2)\right] \tag{11}$$

A more useful equation for calculations (Eq 12) is obtained substituting α by $3/2\delta^2$ and converting the units to Hertz. δ^2 is the root mean square displacement of the ground-state isotropic three-dimensional harmonic oscillator and is found to obey Eq 13, where ν is the harmonic oscillator fundamental frequency. δ is a measure of the delocalisation of each individual nucleus. According to equation (12), δ is a fundamental factor in determining the size of the quantum exchange coupling. When either the nuclear mass or the vibrational frequency is decreased, δ increases and the nuclei become more delocalised, then augmenting the magnitude of ω_J. A small internuclear distance also favours a large quantum exchange coupling. On the other hand, it can be seen that Eqs 12 and 13 introduce a temperature dependence of ω_J.

$$\omega_J = \frac{3\eta a}{4\pi m\delta^3}\sqrt{\frac{3}{\pi}} \cdot \exp\left[-\frac{3}{4}\frac{a^2+\lambda^2}{\delta^2}\right] \tag{12}$$

$$\delta^2(T) = \frac{3h}{8\pi^2 m\nu}\coth\left(\frac{h\nu}{2k_B T}\right) \tag{13}$$

The advantage of the Landesmann's model is that it provides an analytical solution from which some trends of the quantum exchange coupling process can be analysed. However, the model is much too simple to describe correctly many related subtle effects like, for instance, the nature of the transition metal, the ligands or the isotopic effects. Moreover, the values of the parameters involved in Eqs 12 and 13 have to be assumed or fitted a posteriori to the experimental

data of the measured couplings. Then the Landesmann's model is unable to provide an a priori quantitative estimation of the quantum exchange coupling in a given polyhydride transition metal complex. On the other hand, a two-dimensional Landesmann's model has been proposed in some cases where the one-dimensional model considered up to now cannot fit the available experimental results. In this case the corresponding expressions are slightly different from the results given in Eqs 12 and 13 [53].

15.3.1.2. Calculation of the quantum mechanical exchange coupling from first principles

The most accurate way to calculate the quantum exchange coupling is from first principles as a tunnelling splitting of a double well potential. For a polyhydride transition metal complex containing n nuclei that double well belongs to a potential energy surface of $3n$-6 dimensions (excluding the 3 translations and the 3 rotations). Even assuming that the unique relevant coordinates are those corresponding to the two exchanging hydrides, the motion of both nuclei under the field of the rest of the complex gives rise to a six-dimensional double well. This high number of degrees of freedom makes the rigorous calculation impossible to carry out for two reasons: from the electronic point of view, it is not possible, in practice, to build up a six-dimensional potential energy surface. From the nuclear point of view, to obtain the tunnelling splitting one should diagonalize the matrix representation of the exact Hamiltonian of the system on a given set of basis functions. This is clearly out of reach for such a high number of dimensions. The most logical simplification consists of reducing the dimensionality of the system. In this case one has to ensure that the resulting reduced potential energy surface actually contains the minimum-energy path (or, at least, a good approach to it) that connects the two single wells. This implies some knowledge of the mechanism of the hydrogen exchange. In this sense some feasible reaction paths have been proposed. For example, Limbach *et al.* considered three possible mechanisms [54]. Mechanism I involves a reaction path corresponding to the motion of the two exchanging hydrogen nuclei along their internuclear distance vector. The reaction path of mechanism II corresponds to a rotation of the internuclear distance vector leading to the permutation of both hydrogen atoms. Mechanism III takes place in two steps: firstly, an intermediate dihydrogen complex is formed (in thermal equilibrium with the more stable dihydride structure); then, the rotation of the dihydrogen ligand occurs, what properly produces the exchange. So, mechanism III would consist of a pre-equilibrium + rotational tunnelling. Limbach *et al.* concluded that mechanism III is the simplest model that can be fitted with the experimental observations.

We performed the first combined ab initio/tunnelling dynamics study of the quantum mechanical hydrogen exchange for a polyhydride transition-metal complex using $[CpIr(PH_3)H_3]^+$ as a model of the d^4 iridium trihydride complex $[CpIr(PMe_3)H_3]^+$ [55]. The optimized geometry of the model complex is shown in Figure 9. The electronic Schrödinger equation was solved at the restricted Hartree-Fock (RHF) level using a suitable basis set. In some cases, correlation energy was introduced by using the Møller-Plesset perturbation theory up to second order (MP2) [56]. An effective core potential operator was used for the core electrons of iridium and phosphorus atoms. Firstly, we built up a tridimensional reduced potential energy surface for the $[CpIr(PH_3)H_3]^+$ complex by taking as grid parameters the distance (R_{HH}) between the two exchanging hydrogen atoms (H_1 and H_2), the distance (R_{MX}) between the Ir and the midpoint (X) of the H_1-H_2 segment, and the rotational angle (q) of the H_1-H_2 bond in the plane orthogonal to the MX direction. The remaining geometrical parameters were fixed at the RHF fully optimised values of the trihydride. Using such a geometrical definition, the RHF minimum energy structure corresponds to R_{HH} = 1.57 Å, R_{MX} = 1.37 Å, and q = 0°.

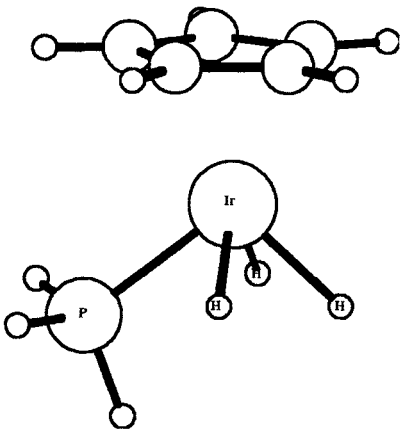

Figure 9. Optimized geometry of $[CpIr(PH_3)H_3]^+$

About 400 RHF energy calculations were carried out in order to construct that tridimensional surface, and the energies of more than 50 points belonging to the most significant regions of the potential energy surface were recalculated at the MP2 level (all the relevant energy values were taken from the calculations at this level). Within the tridimensional surface, the transition state of the hydrogen exchange appears at θ = 90°, R_{MX} = 1.72 Å and R_{HH} = 0.88Å, and it has a geometry corresponding to a 90° rotated η^2-H_2 entity. It imposes an energy barrier of 14.4 kcal/mol with respect to the minimum energy structure.

A comparison between the minimum energy structure and the transition state of the tridimensional surface with the corresponding stationary points located at the full potential energy surface at the MP2 level (with full optimisation but the forced planarity of the cyclopentadienyl group) shows just very slight differences in geometries, this validates the reduced surface used (the true MP2 energy barrier turns out to be 14.1 kcal/mol).

On this tridimensional surface the reaction path for the exchange was built up. Given that the direction of the eigenvector, which has an imaginary frequency in the MP2 transition state, clearly indicates a rotation of the two permuting hydrogen atoms, the chosen reaction path was the one beginning at the transition state by rotating both hydrogen atoms from $\theta = 90°$ up to the planar ($\theta = 0°$) conformation. Going down in this direction, a η^2-H_2 structure with R_{MX} = 1.67 Å, R_{HH} = 0.88 Å and $\theta = 0°$, was first reached 8.7 kcal/mol above the minimum energy structure. This structure, however, does not correspond to an actual minimum of the whole MP2 potential energy surface (a full MP2 optimisation of this structure leads to the trihydride minimum). In short, starting from the minimum energy structure (a trihydride) the reaction path consists of a simultaneous lengthening of the Ir-X distance and shortening of the H_1-H_2 distance, eventually reaching that hydride η^2-H_2 structure. Then, the H_1-H_2 rotation from $\theta = 0°$ to 90° takes place to reach the η^2-H_2 transition state. Due to the symmetry of the problem, the motions are reversed to arrive to the final structure. The reaction path so constructed is expected to be the shortest one (in mass-weighted Cartesian coordinates) that joins both single wells passing through the transition state. The mechanism we proposed differs from the Limbach's mechanism III in that no real intermediate dihydrogen complex is required. Our mechanism for the hydrogen exchanging does not involve a pre-equilibrium + rotation tunnelling, but just a vibrational tunnelling process.

Once the reaction path was defined, the quantum exchange was treated in terms of a one-dimensional tunnelling model. The energy profiles corresponding to the symmetric double wells were built by means of cubic splines functions fitted in such a way that the energy barrier of the exchange was that obtained for the transition state located in the full-dimensional MP2 potential energy surface. The path length (a very important and decisive magnitude in tunnelling problems) was evaluated by geometrical analysis of the reaction path obtained in the tridimensional reduced potential energy surface. In order to obtain the vibrational states of the double well, the nuclear Schrödinger equation has to be solved. To this aim, a basis set method was used by taking a set of localised gaussian functions with the form [57]:

$$\chi_i(s) = (\alpha/\pi)^{1/4} \exp\left[-\frac{\alpha}{2}\cdot(s - s_i)^2\right] \tag{14}$$

where α is an optimizable parameter, s is the arc length and the s_i values are equally spaced points along the reaction path. Then, a variational calculation by using n gaussian functions provides the lowest n vibrational eigenvalues and eigenfunctions of the one-dimensional system. In this particular case 81 gaussian functions were used. The tunnelling splitting corresponding to the ground pair of vibrational states provides the theoretical quantum exchange coupling for the $[CpIr(PH_3)H_3]^+$ trihydride model complex: 112.3 Hz. This result compares very well with the total observed coupling measured at the lower temperature (T = 176 K) for the $[CpIr(PMe_3)H_3]^+$ complex (96 Hz) [28]. The good agreement between the theoretical and the experimental results confirms the quantum mechanical hydrogen exchange coupling as the physical origin of the large couplings observed in the proton NMR spectra of polyhydrides transition-metal complexes.

Another combined ab initio/tunnelling dynamics approach has been derived by Clot *et al.* for the complex $OsH_3X(PH_3)_2$ (X = Cl, I), a model system for $OsH_3X(P^iPr_3)_2$ (X = Cl, I) [50]. They also found good theoretical values for the quantum exchange coupling, but in contrast to our previous work, the reaction path for the hydrogen exchanging in their complex does not involve a significant decrease of the H_1-H_2 distance prior to rotation. Thus, in these Os complexes, the site exchange between hydrides seems to occur without the formation of an H-H bond at the transition state which retains instead the trihydride structure (from the minimum energy structure to the transition sate the exchanging hydrides approach each other less than 0.2 Å).

At this point several considerations should be made. First of all, although quite successful, the theoretical process to determine the quantum exchange coupling is quite elaborated (both the electronic and the nuclear Schrödinger equations need to be solved) and computer time consuming. Second, the quantum exchange coupling is very sensitive (an exponential dependence) to the precision with which the energy barrier and the path length are calculated. As a consequence, we can only expect agreement with the measured coupling in the order of magnitude. Third, it has to be remembered that the total observed coupling includes a contribution of 0 - 40 Hz (that can even be negative) coming from the magnetic scalar coupling.

In what follows we will analyse the effect of different factors on the size of the quantum exchange coupling: ligand substitution, temperature, isotopic substitution, change of the transition metal and the addition of a Lewis acid.

15.3.1.2.1. Effect of the ligand substitution

Experimental results of Heinekey *et al.* show that the exchange coupling of $[CpIr(L)H_3]^+$ trihydride complexes increases when the π-acceptor character of the ligand L is enhanced [28]. To study this effect we applied the combined

ab initio/tunnelling dynamics treatment described above to the $[CpIr(CO)H_3]^+$ complex [55]. It is well-known that CO is a good π-acceptor group so that it tends to diminish the electronic density at the iridium atom and, as a consequence, the π-back donation to the s^* orbital of H_2. Then, it should be expected that the presence of the CO group instead of PH_3 group would favour the appearance of η^2-H_2 configurations, so that the exchange coupling will increase. Theoretical results show that the minimum energy structure has again a trihydride coordination mode and the transition state contains a 90° rotated dihydrogen unit, imposing an energy barrier of only 10.7 kcal/mol. Rotation of the dihydrogen in the transition state leads to a η^2-H_2 structure with an energy 6.1 kcal/mol above the trihydride minimum (again this point is not a minimum at the MP2 level as a full geometry optimisation leads to the trihydride minimum). So the reaction path for the hydrogen exchange parallels the one found for the $[CpIr(PH)_3H_3]^+$ but the energy requirements are now clearly lower, in agreement with the above mentioned expectations. Then the theoretical quantum exchange coupling of the $[CpIr(CO)H_3]^+$ complex turns out to be clearly higher (1279.5 Hz). Analysis of the NMR spectrum for this complex also indicates an important increment of the exchange coupling (the total observed coupling could be larger than 20000 Hz) [58].

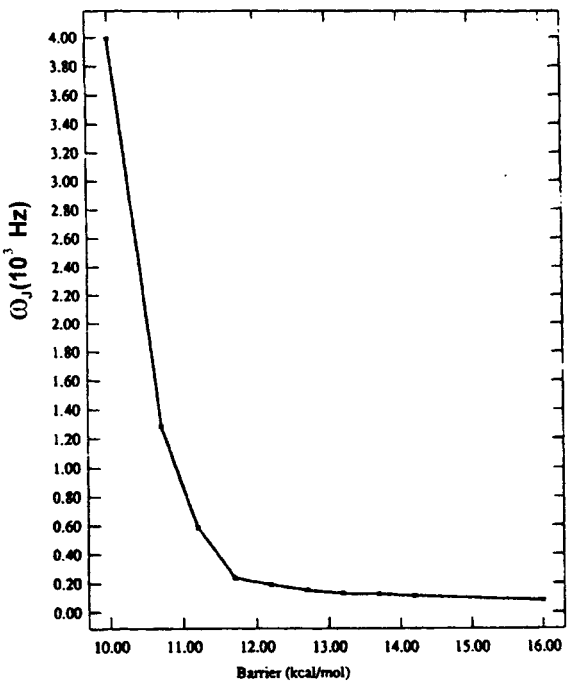

Figure 10. Dependence of the quantum exchange coupling on the barrier height

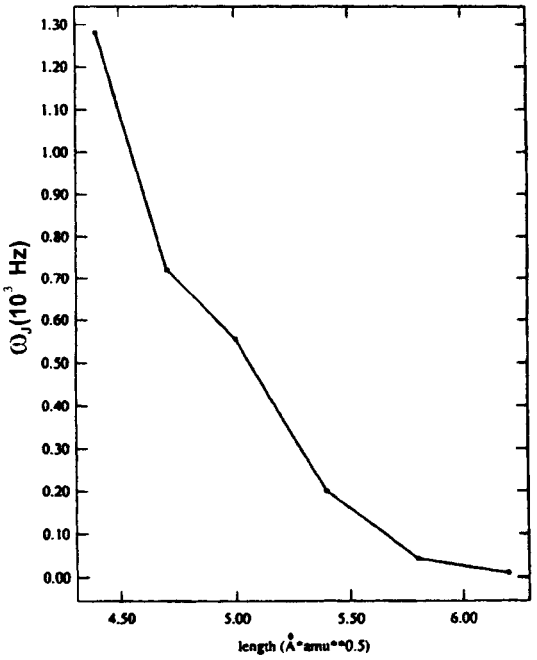

Figure 11. Dependence of the quantum exchange coupling on the total path length (in mass-weighted Cartesian coordinates).

At this point, it is clear that the magnitude of the exchange coupling is extremely sensitive to the energy barrier height. This can be seen in Figure 10 where we have applied our one-dimensional tunnelling model to compute the quantum exchange within a range of energy barrier values, the path lengths used being the one corresponding to the $[CpIr(PH_3)H_3]^+$ complex (roughly the same value as that associated with the $[CpIr(CO)H_3]^+$ complex). Below 11-12 kcal/mol the exchange coupling increases very sharply. This explains why a slight change of the electronic properties of the ligands noticeably modifies the experimentally observed couplings. Conversely, when the energy barrier increases the exchange coupling slowly decreases, so that at the limit of infinite barrier the exchange coupling will vanish. The size of the exchange coupling also greatly depends on the reaction path length (in mass-weighted Cartesian coordinates). In Figure 11 we have used our one-dimensional tunnelling model to calculate the exchange coupling within a range of path length values. We have taken the energy barrier corresponding to the $[CpIr(CO)H_3]^+$ complex [55]. It is evident that exchange coupling rapidly decreases as the path length increases. Note that the electronic calculations (i.e. from the electronic Schrödinger equation) do not depend on the path length, but this magnitude is fundamental in the nuclear calculation. On the other hand, this dependence permits to understand why, at least in all the

cases studied by our group, the formation of a η^2-H_2 structure prior to the rotation that exchange both hydrogen atoms favours the exchange coupling: the major contribution to the reaction path length comes from the rotation which implies a long travel of both nuclei, unless that the H_1-H_2 internuclear distance is very short. So, before rotation, if the H_1-H_2 distance is reduced as much as possible (forming a H_2 unit) the reaction path becomes shorter. In short, the lower the energy barrier for the exchange and the shorter the corresponding tunnelling path, the greater the exchange coupling.

15.3.1.2.2. Dependence on the temperature

Up to this point we have only dealt with quantum exchange in the ground pair of vibrational states. To take into account the temperature effect, higher lying pairs of vibrational states have to be considered as well. The vibrational levels of the double well are obtained by solving the nuclear Schrödinger equation. They appear in near-degenerate pairs. Since vibrational pairs are widely spaced, it may be assumed that the exchange process occurs independently in each pair.

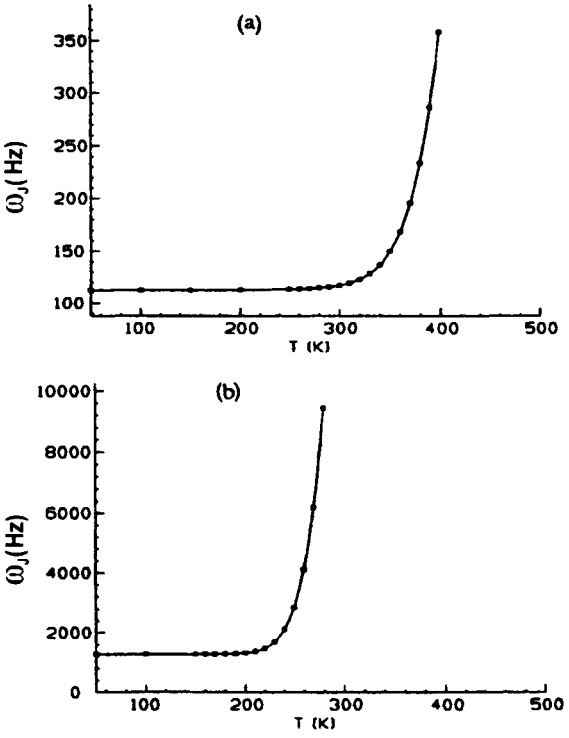

Figure 12. Temperature dependence of the quantum exchange coupling for the $[CpIr(CO)H_3]^+$ complexes: (a) L = PH_3. (b) L = CO

The energy difference between the lowest pair is a direct measure of the exchange coupling at zero Kelvin. At sufficiently low temperatures only this ground-state pair will be significantly occupied. As the temperature increases, the higher pairs become more populated. On the other hand, the tunnelling splitting quickly increases at higher energies.

Because the transition rate from one vibrational state to another is expected to be very fast, the exchange coupling at a given temperature can be obtained by a population-weighted average following a Boltzmann distribution over the thermally accessible pairs of vibrational states (equation (7)). Our calculations for the $[CpIr(PH_3)H_3]^+$ and $[CpIr(CO)H_3]^+$ complexes show that in these cases the influence of the second vibrational pair begins at 200 K, while the sharp increase of the averaged exchange coupling is essentially due to the contributions of the third and higher lying vibrational states (see Figure 12) [55].

15.3.1.2.3. Isotope effects

The quantum mechanical exchange coupling is partially, or even totally, quenched by the excess of mass derived from the isotopic substitution. For this reason we have studied the primary isotope effect that appears when one or both exchanging hydrogen atoms are replaced by deuterium atoms in the $[CpIr(PH_3)H_3]^+$ and $[CpIr(CO)H_3]^+$ complexes [55]. According to the Born-Oppenheimer approach the electronic energy and, as a consequence, the classical energy barriers (i.e., without zero-point correction) are not dependent on the isotopic substitution. Conversely, in mass-weighted Cartesian coordinates, the path length of the exchange is increased as the number of $^1H/^2H$ substitutions increases. For instance, the reaction path lengths corresponding to the exchange in the $[CpIr(CO)H_3]^+$ and $[CpIr(CO)D_2H]^+$ complexes turn out to be 4.40 $amu^{1/2}$Å and 6.75 $amu^{1/2}$Å, respectively. Due to its high dependence on the path length, the quantum exchange coupling for the complexes with two exchanging deuterium atoms diminishes very drastically. So, the theoretical exchange couplings for the $[CpIr(PH_3)D_2H]^+$ and $[CpIr(CO)D_2H]^+$ complexes turn out to be 6.04 Hz and 9.48 Hz, respectively.

Due to the double substitution of both exchanging ^1H by deuterium atoms, the case just described above preserves the symmetry of the double well. However, when only one of the ^1H is substituted, the symmetry of the double well is broken. In this case the increase of the path length is not the important factor as the particles which are interchanging between inequivalent sites A and B are now not identical (a hydrogen and a deuterium). As a result of the change in vibrational frequencies due to the change in mass, the double well will no longer be energetically degenerate when the zero-point energy is introduced. Numerical evaluation of this slightly asymmetric double well confirms the total quenching of the quantum exchange coupling as now the vibrational levels become fully

located at each side of the double well. This result explains the inability to observe the exchange coupling in the NMR spectra of these asymmetrically substituted isotopes.

Finally, it has to be mentioned that a secondary isotope effect has been detected in some cases [28], although no definitive explanation of it has been given yet.

15.3.1.2.4. Effect of the change of the transition metal

We have just seen that the substitution of the ligands modifies the electronic density of the transition metal, in this way varying the size of the exchange coupling. Indeed, the same effect should be expected if the transition metal itself is changed. We proved theoretically this fact [59] by reproducing the experimental results obtained by Heinekey for the metallocene d^0 transition-metal trihydride complexes $[Cp_2MH_3]^{n+}$ (M = Mo, W, n = 1; M = Nb, Ta, n = 0) [32(a)]. In this case the Density Functional Theory (DFT) was used to solve the electronic Schrödinger equation. The particular functional used was the Becke's three-parameter hybrid method using the LYP correlation functional (Becke3LYP) [60]. An effective core potential was used to replace core electrons of transition metal atoms. The nuclear part was solved by means of a one-dimensional tunnelling model using a basis set method similar to the one explained for the iridium complexes.

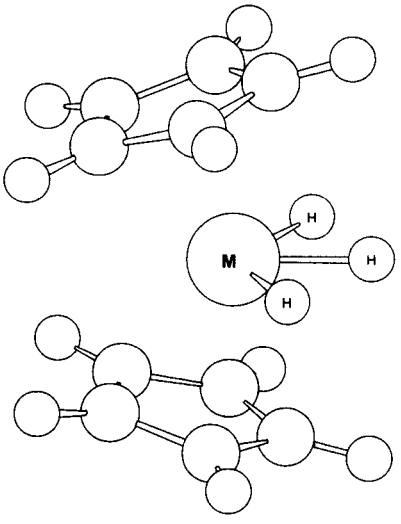

Figure 13. Minimum energy structure of $[Cp_2MH_3]^{n+}$ (M = Mo, W, n = 1; M = Nb, Ta, n = 0) complexes

The reaction path for the hydrogen exchange turns out to be consistent with the mechanism already described for the d^4 iridium complexes. For each d^0 transition metal complex, from the trihydride corresponding to the minimum energy structure (Figure 13), an lengthening of the two M-H distances and a shortening of the H_1-H_2 distance takes place in order to ease the exchange. This motion corresponds to the evolution towards the formation of a dihydrogen unit bound to the transition metal which is able to rotate in such a way that the tunnelling path is relatively short and takes place through a relatively low energy barrier.

As for the case of the iridium complexes, the nonclassical dihydrogen structures preceding the exchanging rotation are not actual minima on the potential energy surface. The difference in energy between these η^2-H_2 structures and the corresponding trihydride minima increases along the series Mo<Nb<W<Ta. This result is in agreement with previous calculations by Lin and Hall on the relative stabilities of classical and nonclassical isomers of 18-electron polyhydride transition-metal complexes [61]. They found that the classical hydrides are preferred for transition metal with more diffuse d orbitals. It is well known that the diffuse nature of transition metal d orbitals increases from right to left and from top to bottom in the Periodic Table [61]. On the other hand, the ordering of the energy barriers for the hydrogen exchange follows the same trend as the η^2-H_2 structures.

TABLE 2. Calculated values of the exchange coupling (in Hz) at different temperatures for $[Cp_2MH_3]$ complexes.

Metal	150 K	200 K	300 K
Nb	$6.1 \cdot 10^{-2}$	$8.0 \cdot 10^{-2}$	$3.5 \cdot 10^{-1}$
Ta	$4.9 \cdot 10^{-3}$	$4.9 \cdot 10^{-3}$	$5.0 \cdot 10^{-3}$
Mo	$6.9 \cdot 10^{2}$	$9.0 \cdot 10^{2}$	$2.0 \cdot 10^{3}$
W	$1.5 \cdot 10^{-2}$	$1.5 \cdot 10^{-2}$	$1.8 \cdot 10^{-2}$

Theoretical exchange couplings at different temperatures for the four metallocenes are given in Table 2. Taking into account the difficulty for obtaining very accurate theoretical values for the exchange coupling, the agreement with the experimental results is very good. The values obtained allow a classification of the four complexes in three categories. Firstly, the Ta and W complexes show a negligible exchange coupling that is also quite temperature independent. Second, the Nb complex also has an almost zero exchange coupling at low temperature. This coupling, however, becomes higher as temperature increases. Finally, the exchange coupling values for the Mo complex are orders of magnitude higher than for the other three transition metals. It has to be remarked that the stability

of the η^2-H_2 structures relative to the corresponding minimum energy trihydrides is the main factor that governs the magnitude of the exchange coupling, so that the coupling is lower when the η^2-H_2 structures are less stable with respect to the corresponding trihydride complexes. That stability depends on the transition metal and the ligands attached to it that affect the subtle balance between donation and back-donation that rules the relative energies of dihydride and dihydrogen species. Within these terms it is easy to understand the effect of the change of the central transition metal in a family of isoelectronic species.

15.3.1.2.5. Effect of the addition of a Lewis Acid

The formation of an adduct between some substituted niobocene trihydrides and a Lewis acid stabilises the dihydrogen species by decreasing the electron density on niobium, so favouring the elimination of molecular hydrogen [62]. Since exchange coupling greatly depends on the electronic density around the transition metal, it is to be expected that a Lewis acid can augment it. Although this is not true in some special cases, this effect has been found in the proton NMR spectrum of the adduct $Cp_2NbH_3 \cdot AlEt_3$ [24]. To analyse this fact we carried out the first theoretical study of the effect of a Lewis acid on the exchange coupling for a polyhydride transition-metal complex. Concretely, the different adducts that can be formed when the metallocene transition-metal trihydride complex Cp_2NbH_3 interacts with AlH_3 were studied [63]. Both the electronic and the nuclear problems were solved by using similar methodologies to the ones previously cited in the study of metallocene trihydride complexes.

The DFT calculations show that the Lewis acid can interact with the hydride ligands of the Cp_2NbH_3 complex leading to two different adducts depending on whether the interaction of the aluminium atom is with the inner hydride or with one of the outer hydrides [63]. The adduct with the inner hydride is the absolute minimum and has a negligible quantum exchange coupling, even at room temperature, as the interchange of the inner hydride with one of the outer hydrides would imply a very high energy barrier, because the interaction of the Lewis acid with the inner hydride would disappear during the exchange process. Conversely, the adducts with one of the outer hydrides are 1.71 kcal/mol higher than the absolute minimum (close enough to the absolute minimum to be significantly populated at the range of temperatures corresponding to the NMR measures). The other two hydrogen ligands are still hydrides, although their internuclear distance clearly diminishes showing an incipient evolution toward the formation of a dihydrogen ligand. The latter is expected to be favoured due to the reduction of the niobium electron density induced by the Lewis acid. These outer adducts are responsible for the quantum exchange being higher in $Cp_2NbH_3 \cdot AlH_3$ than in Cp_2NbH_3. The measured quantum coupling at a given temperature is the result of a Boltzmann average over all the possible adducts. So

the measured effect of the Lewis acid becomes more prominent as temperature increases, *i.e.* as the outer adduct is populated enough to appreciably contribute to the average.

15.3.2. Rotational tunnelling in η^2-dihydrogen transition-metal complexes

Many η^2-dihydrogen transition metal complexes exhibit the phenomenon of rotational tunnelling splitting, which is observed by inelastic neutron scattering (INS) in the microwave region of the electromagnetic spectrum [11]. The origin of the phenomenon is also the quantum mechanical exchange of a pair of hydrogen nuclei through a potential energy barrier, that produces a tunnelling splitting of the vibrational levels of a double well. In a dihydrogen complex just an internal rotation is required to achieve the hydrogen exchange. The differences with the case corresponding to a polyhydride is that for a η^2-dihydrogen the length of the reaction path is shorter (the previous shortening of the H_1-H_2 distance is not required now because the minimum energy structure has already a dihydrogen unit) and the energy barrier of the exchange is lower: normal values turn out to be less than 3.5 kcal/mol for the dihydrogen rotational process but more than 10 kcal/mol for the hydride exchange. Both factors combined make the tunnelling splitting of a dihydrogen rotation huge in comparison with the one corresponding to a exchange of a pair of hydrides. As a consequence, the separation between the vibrational levels arising from the splitting is very far away from the radiofrequency region and cannot be detected in Hz by NMR, but falls in the microwave region and is measured in cm^{-1} by INS. Note that 1 cm^{-1} corresponds to a frequency of $3 \cdot 10^{10}$ Hz.

The rotational tunnelling splitting can also be obtained from first principles using the same kind of electronic and nuclear methods already described for the polyhydrides. We did it for the $TpRhH_2(\eta^2\text{-}H_2)$ complex [64]. Its optimized structure (Figure 14) corresponds to a dihydrogen complex, with a H-H dihydrogen distance of 0.836 Å, only 0.1 Å longer than in the isolated dihydrogen. The transition state for the exchanging rotation has a slightly shorter H-H distance (0.828 Å) and imposes an energy barrier of only 0.45 kcal/mol. This very low barrier is probably due to the fact that in this d^6-transition-metal complex the π-back-donation to the σ^*orbital of the dihydrogen does not vary significantly along the rotation of the dihydrogen unit. Finally, the theoretical rotational tunnelling splitting turns out to be 9.2 cm^{-1}, in excellent accord with the value spectroscopically found by means of INS and reported by Eckert *et al* [19]. When the dideuterated complex $TpRhH_2(\eta^2\text{-}D_2)$ was theoretically studied, the longer reaction path (in mass-weighted Cartesian coordinates), due to the augment of the masses of the exchanging nuclei, reduced the rotational tunnelling splitting to 1.5 cm^{-1}, as expected.

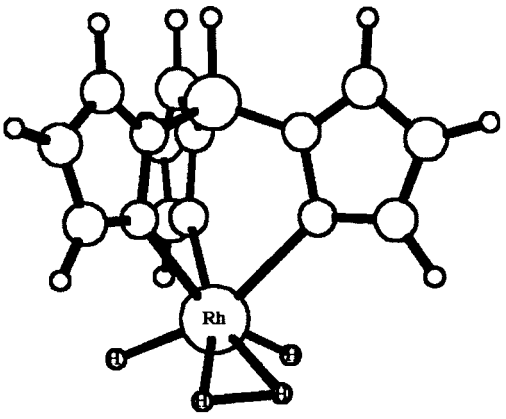

Figure 14. Minimum energy structure of $TpRhH_2(h^2\text{-}H_2)$

The similarity, although falling in different scales, of quantum exchange in polyhydrides and the rotational tunnelling in dihydrogen complexes suggests that there should exist intermediate situations between both cases. This is what has been found in the η^2-dihydrogen isocyanide niobocene complexes $[Nb(\eta^5\text{-}C_5H_4SiMe_3)_2(\eta^2\text{-}H_2)(CNR)]^+$ [21(c)]. These H-H complexes and their monodeuterated H-D isotopomers show very interesting spectroscopic properties. Their NMR spectra present a single high-field resonance at room temperature. By lowering the temperature to 178 K, decoalescence of the signal was observed for the H-D complexes but not for the H-H ones. The temperature of decoalescence has allowed the estimation of the activation free energy of the dihydrogen internal rotation, which ranges between 8.4 and 9.1 kcal/mol [21(c)].

TABLE 3. Calculated exchange coupling at various temperatures for isotopomers of complexes $[Nb(\eta^5\text{-}C_5H_5)_2(\eta^2\text{-}H_2)(CNCH_3)]^+$

T(K)	$J_{H\text{-}H}$(Hz)	$J_{D\text{-}D}$(Hz)	$J_{T\text{-}T}$(Hz)
0	$9.9 \cdot 10^5$	$2.7 \cdot 10^2$	$2.3 \cdot 10^0$
50	$9.9 \cdot 10^5$	$2.7 \cdot 10^2$	$2.3 \cdot 10^0$
100	$9.9 \cdot 10^5$	$2.8 \cdot 10^2$	$2.3 \cdot 10^0$
150	$1.0 \cdot 10^6$	$4.3 \cdot 10^2$	$3.9 \cdot 10^0$
200	$1.2 \cdot 10^6$	$2.1 \cdot 10^3$	$1.4 \cdot 10^2$

We theoretically demonstrated the existence of exchange coupling in the complex $[Nb(\eta^5\text{-}C_5H_5)_2(\eta^2\text{-}H_2)(CNCH_3)]^+$ taken as a realistic model of the experimental cases [21(c)]. Since this species is a dihydrogen complex, the hydrogen exchange takes place by just an internal rotation, as in the $TpRhH_2(\eta^2\text{-}H_2)$ complex, the theoretical treatment being analogous. However,

in this case the energy barrier for the rotation turns out to be 10.85 kcal/mol at the DFT Becke3LYP level of calculation. This abnormally high rotational barrier can be attributed to the complete loss of π-back-donation in the transition state for the rotation. Therefore, the rotational tunnelling splitting does not fall in the microwave region yet, but in the radiofrequency region, its consequences being detected in the NMR spectra.

The calculated tunnelling splittings are given in Table 3. We obtained exchange couplings of ca. 10^6 Hz for the H-H case at 200 K, so that the decoalescence cannot occur. Even at 0 K the quantum hydrogen exchange (not the classical H-H rotation) would still be too fast to be observed by NMR experiments. Conversely, for the H-D isotopomer, the difference in zero-point energy corresponding to the non-equivalent (H-D and D-H positions) leads to a slight asymmetry which dramatically reduces the coupling, allowing decoalescence to be observed. Therefore, for this complex, the H-D classical rotation and the quantum exchange processes will not be practically observed, whereas for the H-H isomer, only the classical process is quenched out on the NMR time scale when temperature is going down. According to our results, the D-D isotopomer would not show decoalescence as it is a symmetric case, but the exchange coupling values, even at low temperatures, are still very large compared with the NMR chemical shifts of the deuterium. Conversely, for the T-T isotopomer, decoalescence would be seen so, at very low temperature, the classical rotation as well the quantum exchange of the T-T species would be blocked at the NMR time scale.

In conclusion, the complex $[Nb(\eta^5\text{-}C_5H_5)_2(\eta^2\text{-}H_2)(CNCH_3)]^+$ is an intermediate case between the hydrogen rotation of dihydrogen complexes and the exchange of a pair of hydrides in polyhydride complexes. In short, the former implies the exchange of hydrogen atoms through a low energy barrier and a relatively short reaction path, leading to a splitting of the vibrational energy levels for the double well potential which can be found by INS in the microwave region (frequencies on the order of ca. 10^{10} Hz). On the other hand, for polyhydrides, the exchange implies a high energy barrier and a very long reaction path. Both factors diminish the tunnelling splitting, so that these processes can be observed in the radiofrequency region of the electromagnetic spectrum, around 10^3 Hz. For the complex $[Nb(\eta^5\text{-}C_5H_5)_2(\eta^2\text{-}H_2)(CNCH_3)]^+$ the energy barrier is high but the reaction path is short, so that exchange couplings are on the order of 10^6 Hz. These couplings are to be detected in the NMR spectra, preventing the decoalescence of the H_2 signal. A similar effect would occur if a case of low energy barrier but long reaction path for the H-H exchange could be found.

15.3.3 Elongated dihydrogen complexes

Up to now we have dealt with quantum phenomena in polyhydride and dihydrogen complexes. In both cases the tunnelling effect is used to explain

apparently different striking phenomena (extremely large and temperature dependent NMR couplings in polyhydrides and rotational tunnelling in dihydrogen complexes). The difference between both types of complexes is the H-H distance. A value larger than 1.4 Å is expected for a dihydride and values below 1.0 Å are typical for a dihydrogen complex. Recently, this difference has faded out as complexes with intermediate H-H distances have been identified. These complexes are known as elongated dihydrogen complexes (they could be termed stretched dihydride complexes as well) [1]. These complexes show also some intriguing features hard to fit on a classical mechanics basis. To begin with the H-H stretching for the $[Ru(H\cdots H)(C_5Me_5)(dppm)]^+$ complex was assigned a value of 2082 cm^{-1} while the value corresponding to free H_2 is near 4300 cm^{-1} [65].

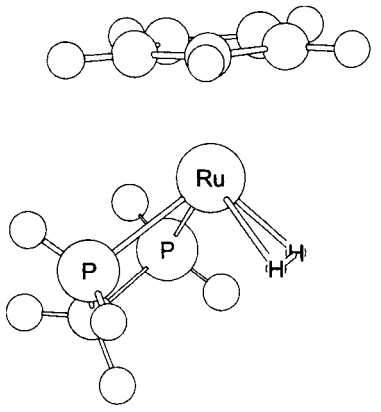

Figure 15. Optimized geometry of $[Ru(H\cdots H)(C_5H_5)(H_2PCH_2PH_2)]^+$.

Maltby *et al.* [42] and Heinekey and Luther [66] found a linear correlation between the hydrogen-deuterium magnetic coupling constant J(H,D) and the H-H distance, namely $r_{HH} = 1.42 - 0.0167J(H,D)$ (assuming that isotopic substitution does not modify the H-H distance), by studying a series of dihydrogen complexes whose structures were known from diffraction studies. For the elongated dihydrogen complexes, the J(H,D) coupling has been seen to depend on the temperature [41,42,67]. Different explanations have been suggested to explain this fact. The first one invoked a fast equilibrium between a dihydrogen and a dihydride structure [67]. This mechanism was quickly ruled out as at very low temperature the neutron diffraction techniques still detected an elongated dihydrogen structure. At those temperatures the equilibrium would be totally displaced towards the more stable species. A subsequent explanation attributed the temperature dependence of the J(H,D) coupling constant to differences in the

population of the vibrational states of the H_2 unit [41]. At higher temperatures the population of the excited states would increase leading to a longer mean H-D distance and, consequently, a lower J(H,D) value. While this explains the behaviour of the complex $[Ru(H\cdots H)(C_5Me_5)(dppm)]^+$, it fails to explain that of the osmium complexes *trans*-$[Os(H\cdots H)Cl(dppe)_2]^+$ and $[Os(H\cdots H)(en)_2(OAc)]^+$ where coupling constants actually increase with temperature [42,68]. Finally, while studying the complex *trans*-$[Os(H\cdots H)Cl(dppe)_2]^+$, Maltby *et al.* [42] suggested an explanation based on the rapid motion of two hydrogen atoms in a flat potential energy surface with a shallow minimum at the crystallographically determined H-H distance.

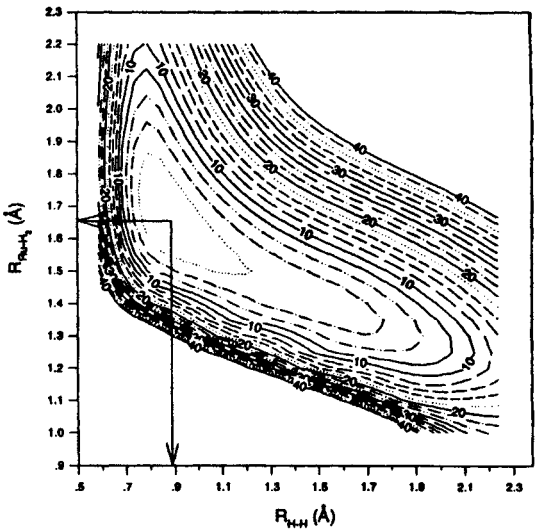

Figure 16. Contour plot of the bidimensional potential energy surface for the complex $[Ru(H\cdots H)(C_5H_5)(H_2PCH_2PH_2)]^+$. Energy contours are given in kcal/mol. The arrows indicate the position of the minimum in potential energy.

From a theoretical point of view, electronic calculations have also systematically failed to provide correct H-H distances for the elongated dihydrogen complexes. We performed theoretical calculations in the $[Ru(H\cdots H)(C_5H_5)(H_2PCH_2PH_2)]^+$ complex, taken as a model of the permethylated dppm compound [69]. Its optimised geometry is depicted in Figure 15.

We have also noted that the current state-of-the-art methods (DFT based Becke3LYP method with an extended basis set) correctly reproduce the geometries of the $[Ru(H\cdots H)(C_5Me_5)(dppm)]^+$ complex except for the H-H distance where the experimental data (1.10 Å) was far from the value at

the localised minimum (0.89 Å) so that DFT calculations would classify this complex as a regular (not elongated) dihydrogen complex. A careful analysis of the potential energy surface was then carried out taking the H-H and the Ru-H_2 distances as geometrical parameters [69]. The obtained surface is shown in Figure 16. A high anharmonicity in the neighbourhood of the minimum was discovered for these two modes. This anharmonicity is the key factor to understand the odd properties of this elongated complex. First of all, calculation of the vibrational levels for these two degrees of freedom shows that in this case it is not possible to separate the H-H and the Ru-H_2 motions as the normal modes show an extended coupling (that can be envisaged just looking at Figure 16).

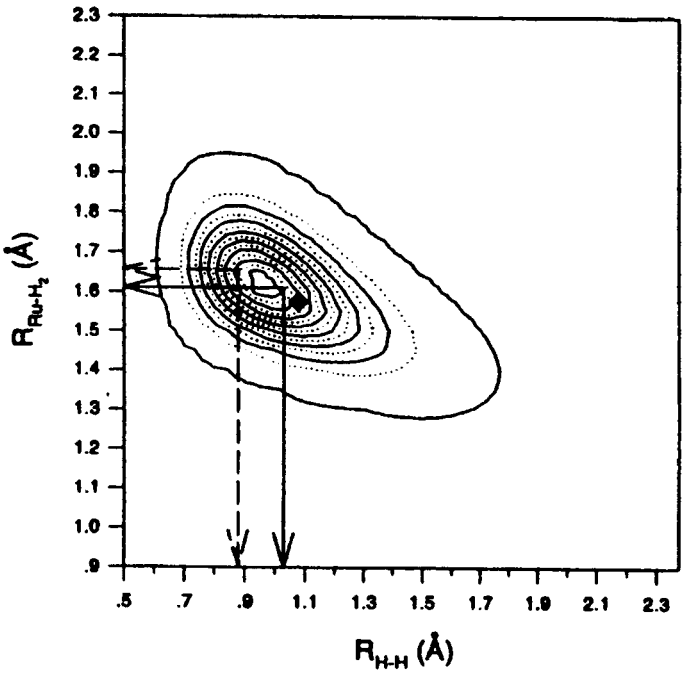

Figure 17. Probability density plot of the vibrational ground-state wavefunction of complex $[Ru(H\cdots H)(C_5H_5)(dppm)]^+$. The dashed arrows indicate the position of the minimum in the potential energy surface, the solid arrows indicate that of the expectation values for this vibrational state, and the square mark indicates that of the experimentally reported data from neutron diffraction.

The calculation of the normal modes on the bidimensional potential energy surface depicted in Figure 16 showed a remarkable agreement with the experimental values coming from the analysis of the Raman spectra for both (η^2-H_2) and (η^2-D_2) isotopomers [65]. By calculating the wavefunctions of

the corresponding vibrational levels and averaging over the temperature, the dependence of J(H,D) on the temperature was also satisfactorily explained as higher vibrational levels have larger mean H-H distances. The discrepancy between the measured H-H distance and this value at the calculated minimum comes also from the high anharmonicity of the surface that is quite flat at high H-H distances. Figure 17 depicts the shape of the ground-state wavefunction where the position of the minimum and that of the expectation value are depicted and shown to be notoriously different: 0.89 and 1.02 Å respectively, the latter quite close to the 1.10 Å value that comes from neutron diffraction experiments. Though less remarkable, the Ru-H_2 averaged distance is also different (and closer to the diffraction data) from the value at the minimum.

Later on we extended the study to the *trans*-$[Os(H\cdots H)Cl(dppe)_2]^+$ complex [70]. In this case the J(H,D) coupling constant increases on increasing temperature. Through the same methodology used previously we found again a very flat surface in the H-H stretching distance so that this behaviour seems common to the elongated dihydrogen complexes. To account for the decrease in H-H distance at high temperatures it was necessary, in this case, to add up an additional dimension to the potential energy surface: the spinning of the H-H unit around the Os-H_2 axis. It was observed that the value of the librational potential energy barrier depends on the elongation of the H-H distance, becoming higher for longer H-H distances. The effects of this behaviour are that the potential energy valley becomes wider in the areas of the surface in which the H-H distance is small and narrower in those zones of the surface where the H-H distance is longer. Accordingly, there are certain low-energy vibrational states whose nuclear wavefunction is able to spread out toward these wide potential energy valleys, which are found in short H-H distance zones of the surface, in this way leading to short expectation values for the H-H distances.

For both elongated complexes our results also predict a dependence of the measured H-H distance on the isotopic substitution. That is, given the high anharmonicity of the calculated surfaces in the H-H direction, the H-H distance is predicted to become noticeably shorter when heavier isotopes (deuterium or, even better, tritium) are used in the dihydrogen ligand. Recent experimental results have verified this prediction for the $[Cp^*Ru(dppm)(H_2)]^+$ elongated dihydrogen complex [71].

15.4 CONCLUDING REMARKS

Usually one tries to interpret the properties of a molecule focusing only on its electronic features. As a result of the different time scales of the electronic and nuclear motions, the Born-Oppenheimer approach is generally applied,

leading to the nuclear Schrödinger equation. Within this frame, the electronic Schrödinger equation is just an intermediate and an auxiliary step to provide the potential energy term of the nuclear equation, which is the equation that really contains the relevant chemical information of the molecule. However, the most extended treatment consists of solving the electronic equation in order to get the electronic wavefunctions and energy levels, from which, by adding the corresponding internuclear repulsion, the potential energy surfaces are obtained. Then a classical behaviour for the nuclei is assumed and the nuclear Schrödinger equation is ignored. The well-known transition-state theory and the classical concept of a static, well-defined equilibrium structure corresponding to a minimum energy point of the potential energy surface are clear examples of this way of reasoning. Nevertheless, when light nuclei like hydrogen atoms are relevant to the chemical problem, the quantum effects on their motions cannot be neglected at all. In these cases, some phenomena occur that can only be understood on going beyond the electronic problem and taking into account the quantum mechanical behaviour of the nuclei. This is especially true for the polyhydride and η^2-dihydrogen transition-metal complexes in which the hydrogen nuclei are bonded to the transition metal quite less rigidly than, for instance, in a normal organic molecule. This implies a high fluxionality of the hydrogen nuclei within the transition-metal complexes that has to be treated quantum mechanically in order to have some insight of its behaviour. Quantum exchange coupling, rotational tunnelling and the existence of elongated dihydrogen complexes are clear examples of these processes. In these cases, restricting the study to only electronic calculations may lead to severe misinterpretations of the previously obtained experimental data.

REFERENCES

1. (a) G. J. Kubas, *Acc. Chem. Res.*, *21* (1988) 120. (b) R. H. Crabtree, *Acc. Chem. Res.*, *23* (1990) 95. (c) P. G. Jessop and R. H. Morris, *Coord. Chem. Rev.*, *121* (1992) 155. (d) D. M. Heinekey and W. J. Oldham Jr., *Chem. Rev.*, *93* (1993) 91.
2. G. J. Kubas, R. R. Ryan, B. I. Swanson, P. J. Vergamini and H. J. Wasserman, *J. Am. Chem. Soc.*, *106* (1984) 451.
3. F. Maseras, A. Lledós, E. Clot and O. Eisenstein, *Chem. Rev.*, *100* (2000) 601.
4. (a) V. Schubert, *Adv. Organomet. Chem.*, *30* (1990) 151. (b) J. F. Hartwig, C. N. Muhoro, X. He, O. Eisenstein, R. Bosque and F. Maseras, F, *J. Am. Chem. Soc.* , *118* (1996) 10936.
5. M. Brookhart, M. L. H. Green and L.-L. Wong, *Prog. Inorg. Chem.*, *36* (1988) 1.
6. I. Demachy, M. A. Esteruelas, Y. Jean, A. Lledós, F. Maseras, L. A. Oro, C. Valero and F. Volatron, *J. Am. Chem. Soc.*, *118* (1996) 8388.
7. R. Bau and M. H. Drabnis, *Inorg. Chim. Acta*, *259* (1997) 27.

8. D. G. Hamilton and R. H. Crabtree, *J. Am. Chem. Soc.*, *110* (1989) 4126.
9. V. I. Bakhmutov, C. Bianchini, F. Maseras, A. Lledós, M. Peruzzini and E. V. Vorontsov, *Chem. Eur. J.*, *5* (1999) 3318. See also Chapter 13 of this monograph.
10. J. Eckert, G. J. Kubas and A. J. Dianoux, *J. Chem. Phys.*, *88* (1988) 466.
11. M. Prager and A. Heidemann *Chem. Rev.*, *97* (1997) 2933.
12. J. Eckert and G. J. Kubas, *J. Phys. Chem.*, *97* (1993) 2378.
13. E. Clot and J. Eckert, *J. Am. Chem. Soc.*, *21* (1999) 8855.
14. J. Eckert, G. J. Kubas and R. P. White, *Inorg. Chem.*, *31* (1992) 1550.
15. G. J. Kubas, C. J. Burns, J. Eckert, S. W. Johnson, A. C. Larson, P. J. Vergamini, C. J. Unkefer, G. R. K. Khalsa, S. A. Jackson and O. Eisenstein, *J. Am. Chem. Soc. 115* (1993) 569.
16. J. Eckert, G. J. Kubas, J. H. Hall, P. J. Hay and C. M. Boyle, *J. Am. Chem. Soc.*, *112* (1990) 2324.
17. J. Eckert, A. Albinati, R. P. White, C. Bianchini and M. Peruzzini, *Inorg. Chem.*, *31* (1992) 4241.
18. J. Eckert, C. M. Jensen, G. Jones, E. Clot, and O. Eisenstein, *J. Am. Chem. Soc.* , *115* (1993) 11056.
19. J. Eckert, A. Albinati, U. E. Bucher and L. M. Venanzi, *Inorg. Chem.*, *35* (1996) 1292.
20. J. Eckert, H. Blank, M. T. Bautista and R. H. Morris, *Inorg. Chem., 29* (1990) 747.
21. (a) S. Sabo-Etienne, B. Chaudret, B.; H. Abou El Makarim, J. C. Barthelat, J. P. Daudey, S. Ulrich, H. Limbach and C. Moïse, *J. Am. Chem. Soc.*, *117* (1995) 11602. (b) F. A. Jalon, A. Otero, B. Manzano, E. Villaseñor and B. Chaudret, *J. Am. Chem. Soc.*, *117* (1995) 10123. (c) A. Antiñolo, F. Carrillo-Hermosilla, M. Fajardo, S. García-Yuste, A. Otero, S. Camanyes, F. Maseras, M. Moreno, A. Lledós and J. M. Lluch, *J. Am. Chem. Soc.*, *119* (1997) 6107.
22. S. Sabo-Etienne and B. Chaudret, *Chem. Rev. 98* (1998) 2077.
23. F. N. Tebbe and G. W. Parshall, *J. Am. Chem. Soc.*, *93* (1971) 3793.
24. J. A. Labinger, *Compr. Organomet. Chem.*, *3* (1982) 707.
25. M. D. Curtis, L. G. Bell and W. M. Butler, *Organometallics*, *4* (1985) 701.
26. A. Antiñolo, B. Chaudret, G. Commenges, M. Fajardo, F. Jalón, R. H. Morris, A. Otero and C. J. Schweltzer, *J. Chem. Soc. Chem. Commun.*, (1988) 1210.
27. T. Arliguie, B. Chaudret, J. Devillers and R. Poilblanc, *C. R. Acad. Sci. Ser. 2, 305-II* (1987) 1523.
28. D. M. Heinekey, J. M. Millar, T. F. Koetzle, N. G. Payne and K. W. Zilm, *J. Am. Chem. Soc.*, *112* (1990) 909.
29. J. K. Burdett, J. R. Phillips, M. R. Pourian, M. Poliakoff, J. J.Turner and R. Upmacis, *Inorg. Chem.*, *26* (1987) 3054.
30. D. H. Jones, J. A. Labinger and D. P. Weitekamp, *J. Am. Chem. Soc.*, *111* (1989) 3087.
31. K. W. Zilm, D. M. Heinekey, J. M. Millar, N. G. Payne and P. Demou, *J. Am. Chem. Soc.*, *111* (1989) 3088.
32. (a) D. M. Heinekey, *J. Am. Chem. Soc.*, *113* (1991) 6074. (b) J. C. Barthelat, B. Chaudret, J. P. Daudey, P. Deloth and R. Poilblanc, R. *J. Am. Chem. Soc.*, *113* (1991) 9896.
33. D. M. Heinekey and G. P. Harper, G. P. *Organometallics*, *10* (1991) 2891.

34. A. Castillo, G. Barea, M. A. Esteruelas, F. J. Lahoz, A. Lledós, F. Maseras, J. Modrego, E. Oñate, L. A. Oro, N. Ruiz and E. Sola, *Inorg. Chem.*, *38* (1999) 1814.
35. (a) A. Antiñolo, F. Carrillo, J. Fernández-Baeza, A. Otero, M. Fajardo and B. Chaudret, *Inorg. Chem.*, *31* (1992) 5156. (b) A. Antiñolo, F. Carrillo, B. Chaudret, M. Fajardo, J. Fernández-Baeza, M. Lanfranchi, H. Limbach, M. Maurer, A. Otero, and M. A. Pellinghelli, *Inorg. Chem.*, *33* (1994) 5163. (c) A. Antiñolo, F. Carrillo, B. Chaudret, M. Fajardo, J. Fernández-Baeza, M. Lanfranchi, H. Limbach, M. Maurer, A. Otero and M. A. Pellinghelli, *Inorg. Chem.*, *35* (1996) 7873.
36. R. Kuhlman, E. Clot, C. Leforestier, W. E. Streib, O. Eisenstein and K. G. Caulton, *J. Am. Chem. Soc.*, *119* (1997) 10153.
37. R. Wiedenbruch, M. Schick, A. Pampel, B. H. Meier, R. Meyer, R. R. Ernst, S. Chaloupka and L. M. Venanzi, *J. Phys. Chem.*, *99* (1995) 13088.
38. J. A. Ayllon, S. Sabo-Etienne, B. Chaudret, S. Ulrich and H. Limbach, *Inorg. Chim. Acta*, *259* (1997) 1.
39. H. Basch, D. G. Musaev, K. Morokuma, M. D. Fryzuk, J. B. Love, W. W. Seidel, A. Albinati, T. F. Koetzle, W. Klooster, S. A. Mason, S. A. and J. Eckert, *J. Am. Chem. Soc.*, *121* (1999) 523.
40. F. Maseras, A. Lledós, M. Costas and J. M. Poblet, *Organometallics*, *15* (1996) 2947.
41. W. T. Klooster, T. F. Koetzle, G. Jia, T. P. Fong, R. H. Morris and A. Albinati, *J. Am. Chem. Soc., 116* (1994) 7677.
42. P. A. Maltby, M. Schlaf, M. Steinbeck, A. J. Lough, R. H. Morris, W. T. Klooster, T. F. Koetzle and R. C. Srivastava, *J. Am. Chem. Soc.*, *118* (1996) 5396.
43. R. P. Bell, *The Tunnel Effect in Chemistry*, Chapman and Hall, London, 1990.
44. C. Cohen-Tannoudji, B. Diu and F. Laloë, *Quantum Mechanics*, Hermann and J. Wiley & Sons, Paris, 1977.
45. (a) S. L. Baughcum, R. W.; Duerst, W. F.; Rowe, Z. Smith and E. B. Wilson, *J. Am. Chem. Soc.*, *103* (1981) 6296. (b) S. L. Baughcum, R. W. Duerst, W. F. Rowe, Z. Smith and E. B. Wilson, *J. Am. Chem. Soc.*, *106*, (1984) 2260.
46. T. M. Sugden and C. N. Kenney, *Microwave Spectroscopy of Gases*, Van Nostrand, London, 1965.
47. (a) J. Hennig and H. Limbach, *J. Chem. Soc. Faraday II*, *75* (1979) 752. (b) J. Hennig, J. and H. Limbach, *J. Chem. Phys.*, *71* (1979) 320.
48. (a) E. M. Hiller and R. A. Harris, *J. Chem. Phys.*, *98* (1993) 2077. (b) E. M. Hiller and R. A. Harris, *J. Chem. Phys.*, *99* (1993) 7652. (c) E. M. Hiller and R. A. Harris, *J. Chem. Phys.*, *100* (1994) 2522.
49. (a) S. Szymanski, *J. Chem. Phys.* 1996, *104* (1996) 8216. (b) Ch. Scheurer, R. Wiedenbruch, R. Meyer, R. R. Ernst and D. M. Heinekey, *J. Chem. Phys.*, *106* (1997)1.
50. E. Clot, C. Leforestier, O. Eisenstein and M. Pellisier, *J. Am. Chem. Soc., 117* (1995) 1797.
51. K. W. Zilm, D. M. Heinekey, J. M. Millar, N. G. Payne, S. P. Neshyba, J. C. Duchamp and J. Szczyra, *J. Am. Chem. Soc.*, *112* (1990) 920.
52. A. Landesmann, *Ann. Phys. (Fr.), 8* (1973) 53.
53. (a) D. M. Heinekey, N. G. Payne and G. K. Schulte, *J. Am. Chem. Soc.*, 110 (1988)

2303. (b) D. M. Heinekey, A. S. Hinkle and J. D. Close, *J. Am. Chem. Soc., 118* (1996) 5353. (b)
54. H. Limbach, G. Scherer, M. Maurer and B. Chaudret, *Angew. Chem. Int. Ed. Engl., 31* (1992) 1369.
55. (a) A. Jarid, M. Moreno, A. Lledós, J. M. Lluch and J. Bertrán, *J. Am. Chem. Soc., 115* (1993) 5861. (b) A. Jarid, M. Moreno, A. Lledós, J. M. Lluch and J. Bertrán, *J. Am. Chem. Soc., 117* (1995) 1069.
56. (a) C. Møller, and M. S. Plesset, *Phys. Rev., 46* (1936) 618. (b) J. A. Pople, J. A.; J. S. Binkley and R. Seeger, *Int. J. Quantum Chem., S10* (1976) 1.
57. (a) I. P. Hamilton and J. Light, *J. Chem. Phys., 84* (1986) 306. (b) N. Makri and W. H. Miller, *J. Chem. Phys., 86* (1987) 1451.
58. D. M. Heinekey, Personal communication.
59. S. Camanyes, F. Maseras, M. Moreno, A. Lledós, J. M. Lluch and J. Bertrán, *J. Am. Chem. Soc., 118* (1996) 4617.
60. C. Lee, W. Yang and R. G. Parr, *Phys. Rev., B 37* (1988) 785.
61. (a) Z. Lin and M. B. Hall, *J. Am. Chem. Soc., 114* (1992) 6102. (b) Z. Lin and M. B. Hall, *Coord. Chem. Rev., 135* (1994) 845.
62. (a) S. Camanyes, F. Maseras, M. Moreno, A. Lledós, J. M. Lluch and J. Bertrán, *Angew. Chem. Int. Ed. Engl.* , *36* (1997) 265. (b) S. Camanyes, F. Maseras, M. Moreno, A. Lledós, J. M. Lluch and J. Bertrán, *Chem. Eur. J., 5* (1999) 1166.
63. S. Camanyes, F. Maseras, M. Moreno, A. Lledós, J. M. Lluch and J. Bertrán, *Inorg. Chem., 37* (1998) 2334.
64. R. Gelabert, M. Moreno, J. M. Lluch and A. Lledós, *Organometallics, 16* (1997) 3805.
65. M. Chopra, K. F. Wong, G. Jia and N.-T. Yu, *J. Mol. Struct., 379* (1996) 93.
66. (a) D. M. Heinekey and T. A. Luther, *Inorg. Chem., 35* (1996) 4396. (b) T. A. Luther and D. M. Heinekey, *J. Am. Chem. Soc., 119* (1997) 6688.
67. K. A. Earl, G. Jia, P. A. Maltby, and R. H. Morris, *J. Am. Chem. Soc., 113* (1991) 3027.
68. T. Hasegawa, Z. Li, S. Parkin, H. Hope, R. K. McMullan, T. F. Koetzle and H. Taube, *J. Am. Chem. Soc., 116* (1994) 4352.
69. (a) R. Gelabert, M. Moreno, J. M. Lluch and A. Lledós, *J. Am. Chem. Soc., 119* (1997) 9840. (b) R. Gelabert, M. Moreno, J. M. Lluch and A. Lledós, *Chem. Phys., 241* (1999) 155.
70. R. Gelabert, M. Moreno, J. M. Lluch and A. Lledós, *J. Am. Chem. Soc., 120* (1998) 8168.
71. J. K. Law, H. Mellows and D. M. Heinekey, *J. Am. Chem. Soc., 123* (2001) 2085.

This Page Intentionally Left Blank

Chapter 16

Metal Hydride Intermediates in Hydrogenases and Nitrogenases: Enzymological and Model Studies.

Richard A Henderson

Department of Chemistry, Bedson Building, University of Newcastle, Newcastle-upon-Tyne, NE1 7RU, UK

CONTENTS

16.1 INTRODUCTION

This chapter deals with the involvement of metal hydrides in certain metalloenzymes, namely hydrogenases and nitrogenases. The proposition that metal hydrides are naturally associated with the action of biological compounds

is something that many might find bizarre. However, nothing more vividly illustrates the futility of compartmentalising inorganic chemistry than the discovery of the Co-CH_3 bond in Vitamin B_{12} coenzyme [1,2]. Here an unarguably biological molecule contains one of the defining characteristics of organometallic chemistry: a metal-carbon bond. More recently the boundaries between bioinorganic and organometallic chemistry have been further blurred with the discovery that the active sites of hydrogenases have been shown to include Fe-CO ligands.

If we consider the reactions of metalloenzymes, it is not difficult to identify organometallic-type chemistry. Many of these reactions have been known for some time. For example, the well-known deleterious effect that carbon monoxide has on the reactivity of a variety of metalloproteins. The effect is a consequence of carbon monoxide binding to a metal site in the enzyme.

Metal hydrides, and more recently metal dihydrogen species have been implicated in the action of the hydrogenases and nitrogenases. The role of metal-hydrides in these two enzymes is the main theme of this chapter. In the course of the presentation we will see how metal hydrides can in principle play a variety of diverse roles in nitrogenases and hydrogenases most notably as intermediates in dihydrogen production or uptake but also in the binding and transformation of substrates. Although an undoubted oversimplification, hydrogenases are rather simple enzymes whose chemistry involves only the uptake and production of dihydrogen, and metal hydrides have long been proposed as intermediates in their action. In contrast the action of nitrogenases is appreciably more complicated. Thus, whilst the physiological role of the nitrogenases is to transform dinitrogen into ammonia, in the laboratory the enzyme will transform a variety of other small, mostly unsaturated molecules and ions (*eg* H^+, CN^-, RNC, N_3^-, N_2O, C_2H_2, cyclopropane). Metal hydrides have also been implicated in the action of this enzyme, both in the reduction of H^+ to H_2 and also in the binding and transformation of substrates.

It is important to emphasise from the start that the evidence for metal hydride involvement in biological systems is entirely circumstantial. The spectroscopic problems of detecting metal hydrides are well documented, and include inherently weak IR spectral bands, and the location of a single peak in the ^1H NMR spectrum, or detection by coupling in EPR spectrum for paramagnetic states. All of these problems are compounded in enzymes by the transient nature of hydrides in catalytic reactions.

The chemistry and biochemistry outlined in this chapter, not only addresses the as yet unsolved problems of the mechanisms of hydrogenase and nitrogenase action, but also how chemists trying to mimic this behaviour using simple chemical models have opened up new areas of chemical research related to metal hydrides. These new research areas have little or no biological relevance, but are just as intriguing and intellectually demanding as the direct solution to

the biological problem. The synergism of tackling the biological problem and developing related new chemistry will be a further recurring theme throughout this chapter. It is important to emphasise, from the outset, that many of the simple chemical model systems aim to mimic the *reactivity* of the active site and not necessarily its structure.

16.2 HYDROGENASES

The hydrogenases [3-6] are a group of enzymes which accomplish the reaction shown in Equation (1). Most hydrogenases can perform this reaction in either direction but some are more uni-directional than others. In general, NiFe-based hydrogenases involve the reduction of protons, whereas Fe-only hydrogenases oxidise H_2.

$$2H^+ + 2e \rightleftharpoons H_2 \qquad (1)$$

16.2.1 Classification of the Hydrogenases.

The hydrogenases are classified according to their composition. Three distinct classes of metal-containing hydrogenases have been identified [3]: Fe-only hydrogenases; NiFe-hydrogenases and NiFeSe-hydrogenases.

16.2.1.1 Fe-only Hydrogenases.

Fe-only hydrogenases from *Desulfovibrio vulgaris* and *Clostridium pasteuranium* have molecular weights *ca* 60kDa and contain 11-22 Fe and a similar amount of "inorganic" S (S^{2-}).

The Fe-only hydrogenases contain only Fe-S clusters, with the active site being a special Fe-S cluster called the H-cluster. The structure of this cluster has over many years been the topic of much speculation. At last this speculation has been resolved by crystallography.

The X-ray structure of the Fe-only hydrogenase from *Clostridium pasteuranium* has been determined at 1.8Å resolution [4-6]. It is a highly complex protein consisting of twenty iron atoms arranged into five individual metal cluster assemblies. The protein is mushroom shaped and is divided into four domains with the top one containing the active site. The smaller domains contain three $\{Fe_4S_4\}$ clusters and a single $\{Fe_2S_2\}$ cluster, which presumably make up the

electron transfer pathway to and from the active site. The active site cluster (H cluster) is structurally unique and is shown in Figure 1. Basically, it comprises a $\{Fe_4S_4\}$ cluster bridged by a cysteinate sulfur to a dimeric Fe_2 unit, in which each iron atom has an octahedral geometry: in addition to two bridging cysteinate sulfurs and a bridging water molecule, both iron atoms are coordinated by five diatomic ligands (CO and CN^-), while one iron is bonded to the $\{Fe_4S_4\}$ cluster *via* a cysteinate ligand.

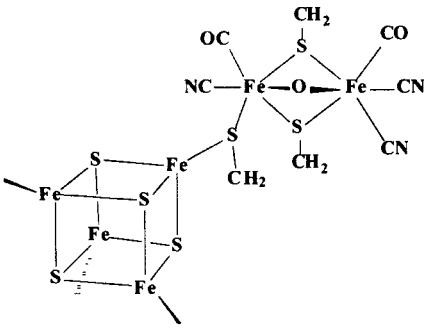

Figure 1. The H-cluster of the Fe-only hydrogenase.

16.2.1.2 The NiFe-Hydrogenases.

A major problem in the purification and crystallization of the NiFe-hydrogenases has been that they are often membrane-bound enzymes and hence it has been difficult to solubilise and hence crystallise these proteins. Thus, it is only recently that the structures of Ni-containing hydrogenases have been determined [7-14].

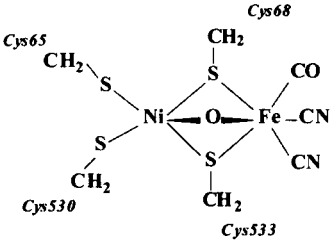

Figure 2. The NiFe cluster of the NiFe-hydrogenase in *D. gigas*.

All NiFe hydrogenases comprise at least two subunits of molecular weights *ca* 60 and 30kDa respectively. The metal content comprises: a NiFe centre and at least two Fe_4S_4 clusters. The NAD (nicotinamide diphosphate) reducing

hydrogenases of hydrogen bacteria (such as *A. eutrophus*) also contain additional subunits with a Fe_2S_2 cluster and flavin mononucleotide (FMN). The methanogenic F-420 reducing hydrogenases such as *Methanobacterium thermoautotrophicum* contain a third subunit. The structure of the oxidised NiFe binuclear active site from *Desulfovibrio gigas* has the arrangement of clusters shown in Figure 2.

The catalytic site is buried deep in the larger subunit, whilst the Fe-S clusters are contained within the small subunit and form an approximate linear arrangement. This arrangement supports the proposal that these clusters form an electron transfer pathway between the external reductant and the active site. It is surprising that the Fe_3S_4 (E = -70mV) cluster is between the two Fe_4S_4 clusters (E = -291 and –340mV) whose potentials are close to that for dihydrogen activation (-310mV). The close separation of the clusters (*ca* 10Å) means that the high midpoint potential for Fe_3S_4 cluster does not make electron transfer rate-limiting. The arrangement of clusters is shown diagrammatically in Figure 3.

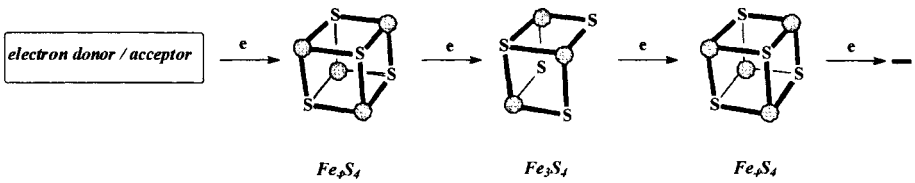

Figure 3. The electron-transfer pathway of the NiFe-hydrogenase in *D. gigas*.

The binuclear active site comprises a nickel atom which is predominantly coordinated by cysteinate (thiolate) ligands and a hydroxide in a distorted square-based pyramidal arrangement. Two of the cysteinate ligands and the hydroxide act as bridges to an adjacent iron atom. The iron atom has a distorted octahedral geometry. In addition, from at least one source [15] a 1,3-dithiopropane ligand bridges the nickel and iron. The coordination sphere of the iron atom is analogous to that found in the Fe-only hydrogenase binuclear active site. It comprises three diatomic non-protein ligands: CO and CN^-. Recent FTIR spectroscopic studies [16] have shown three unique bands in the region 1910-2100cm^{-1} for a range of Fe-only and NiFe-hydrogenases, attributable to the Fe-CO and Fe-CN ligands. Since it is difficult to distinguish between N and O atoms by X-ray crystallography, the number of CO and CN ligands cannot be determined directly by crystallography. However, IR spectroscopic studies on ^{15}N and ^{13}C labelled enzymes shows shifted bands indicating one CO and two CN ligands on the Fe

atoms [17]. Presumably CO and CN are beneficial for the chemistry that the site performs, nonetheless they seem rather bizarre choices of ligands.

It has been proposed that the role of the nickel in the NiFe-hydrogenases facilitate substrate binding. Thus, although the Fe-only hydrogenases have a higher hydrogenase activity (V_V = 9000-50000 μmol min^{-1} mg^{-1}) they have lower dihydrogen affinity (K_M = 7μmol dm^{-3}) than the NiFe hydrogenase (V_V = 700 μmol min^{-1} mg^{-1}; K_M = 0.07μmol dm^{-3}).

A sub-class of the NiFe-hydrogenases are the NiFeSe-hydrogenases which also contain Se in the form selenocysteinate as a ligand to nickel.

16.2.1.3 Metal-Free Hydrogenases.

Finally, it is worth noting that there is a hydrogenase which apparently does not contain any metal [6]. N5,N10-methylenetetrahydromethanopterin dehydrogenase, isolated from methanogenic bacteria is capable of producing and consuming dihydrogen with coenzyme F-420 (deazaflavin) as acceptor.

16.2.2 Mechanistic Studies

16.2.2.1 Studies on the Hydrogenases During Turnover.

There have been many mechanisms suggested for the action of metal-based hydrogenases. Herein are presented only those mechanisms proposed since the determination of the active sites X-ray crystal structures. Before going through the salient features of these mechanisms it is pertinent to briefly outline the experimental facts which these mechanisms must accommodate.

Enzymological studies on the NiFe-hydrogenase indicate that at least six states of the binuclear NiFe site are detectable, with three states characterised by EPR spectroscopy [3,18-21]. The EPR detectable states have been labelled Ni-SR (EPR silent); Ni-C (only paramagnetic state; formed from reduction of Ni-SR) and Ni-R (EPR silent; formed by reduction of Ni-C). The EPR signals have been attributed to the nickel atom in the binuclear active site, indicating that the iron is low spin Fe^{II} throughout the catalysis. The evidence that the signals are attributable to the nickel centre are: (i) ^{61}Ni hyperfine is observed [22,23] and (ii) nuclear interaction of ^{57}Fe with paramagnetic nickel has been observed [24]. The oxidation state of the nickel is unknown but Ni^{I} or Ni^{III} have been proposed.

Comparison of EPR [25] and ESEEM [26] spectra of the NiFe-hydrogenases in H_2O and D_2O indicates the presence of exchangable protons in the vicinity of the nickel in the Ni-C state. Q-band ENDOR spectroscopy [27] indicates two types of exchangable protons. These exchangable protons only interact weakly with nickel and so it is concluded that they are outside the first coordination

sphere and probably represent water or acidic amino acid side chains. It is unlikely that the protons correspond to Ni-H or Ni-H_2 species because the weak coupling constants (4.4 and 16.6MHz) observed are inconsistent with such species. Ni-H or Ni-H_2 species would be expected to have coupling constants of 100's MHz. In addition, flushing the system with argon did not remove these signals (*ie* H_2 was not flushed away).

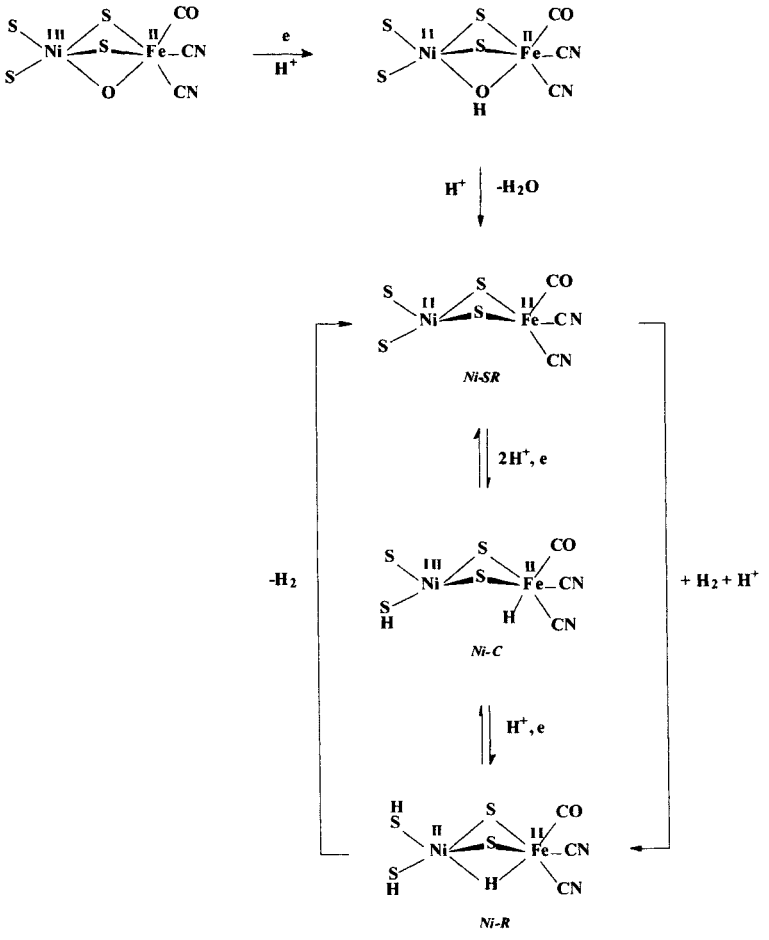

Figure 4. Proposed mechanism for the action of NiFe-hydrogenase, indicating the identity of the experimentally-detected states of the enzyme.

Recent studies using 2D ESEEM spectroscopy [28] has provided evidence that a conserved histidine amino acid residue (His-371) is close to the active site and is thus a good candidate for a base that may be required in the heterolytic cleavage of dihydrogen.

16.2.2.2 Model Studies

Most of the mechanistic studies have focussed on NiFe-hydrogenases. A common approach has been to develop mechanisms using theoretical quantum mechanical calculations. Much attention has been paid to attempting to assign structures to the EPR spectroscopically-characterised states using these theoretical models. To date this approach has paid little or no attention to the role of the surrounding polypeptide, and potential roles for conserved amino acid residues such as His-371.

One mechanism consistent with many of the experimental observations [3] is shown in Figure 4. The initial "activation" of the binuclear site by reduction, protonation and consequent dissociation of water primes the site for binding dihydrogen. The activation of dihydrogen involves the formation of a hydride (proposed to bridge between the iron and nickel) and a coordinated thiol. In this manner dihydrogen is formally cleaved heterolytically into H^- and H^+.

Figure 5 shows a similar mechanism proposed [29] by Dole et al, in which dihydrogen binds to the active site and is heterolytically cleaved to produce a bridging hydride and protonated cysteinate ligand.

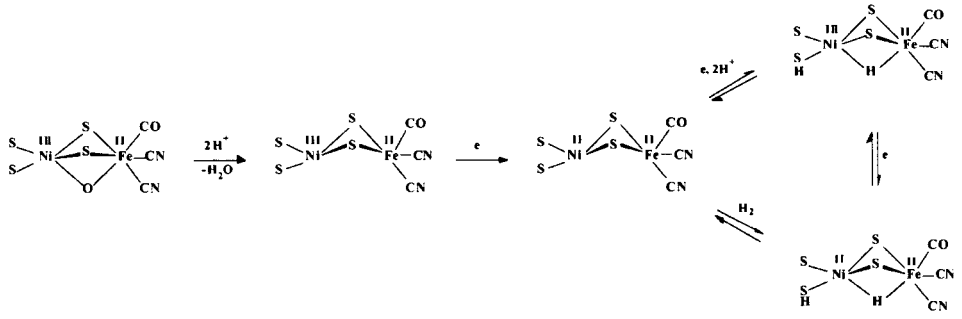

Figure 5. Proposed mechanism [29] for the action of the NiFe-hydrogenase.

The possible intermediates in this mechanism have been investigated by calculations [30] and the results show that: (i) despite valence state changes of the nickel, the electron density remains remarkably unchanged; (ii) in paramagnetic states, the spin density is mainly localised on the nickel and its sulfur ligands, which confirms the diamagnetic nature of the iron throughout the catalysis and (iii) a hydrogen atom can bridge the two metals without any major structural reorganisation except a shortening of the Ni-Fe distance.

In a further study using DFT calculations, Pavlov et al [31] have probed the mechanism of the NiFe hydrogenase by probing all possible oxidation states

and spin states. The proposed mechanism for dihydrogen oxidation involves initial binding of the substrate to iron to form a η^2-H_2 species (Figure 6), which then undergoes heterolytic splitting. In the key step, hydride transfer to iron and proton transfer to an adjacent cysteinate sulfur is accompanied by ligand dissociation of the thiol cysteine from nickel while remaining bound to iron. Simultaneously, the cyanide ligand on iron binds to nickel in a bridging mode. After dihydrogen dissociation, the hydride bound to iron can be transferred to nickel.

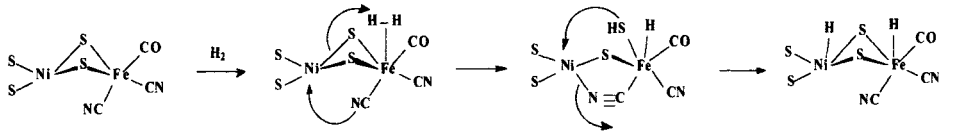

Figure 6. Proposed mechanism [31] for the action of the NiFe-hydrogenase.

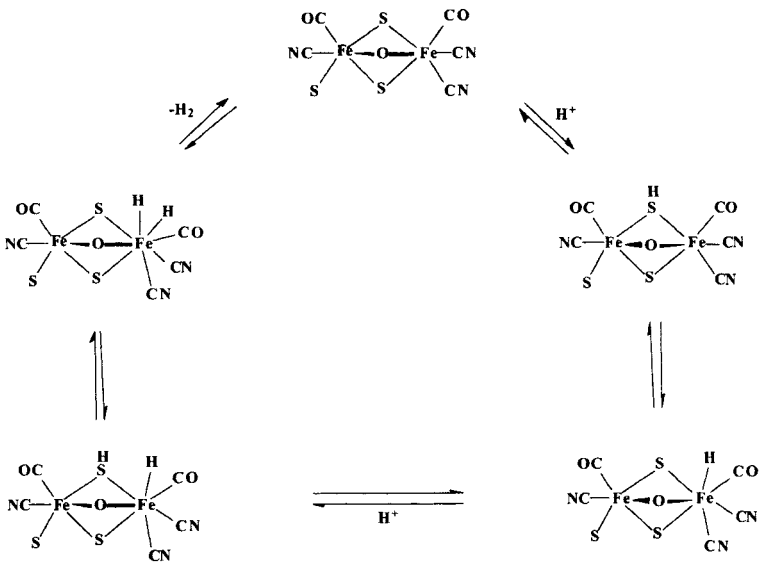

Figure 7. Proposed mechanism [32] for the action of the Fe-only hydrogenase.

DFT calculations have also been applied to the active site of the Fe-only hydrogenase [32]. In the mechanism shown in Figure 7 the stereochemical flexibility of the terminal cyano- and bridging cysteinate ligands aids the reaction.

This is also a feature of the mechanism in Figure 6, whereas in the mechanisms of Figures 4 and 5 cysteinate and cyano ligands are merely spectators. The DFT calculations on the Fe-only hydrogenase show that dihydrogen binds weakly to the iron remote from the $\{Fe_4S_4\}$ cluster. When two electron reduced, a mechanistically significant barrierless transfer of one H atom from Fe-H_2 to form S-H occurs.

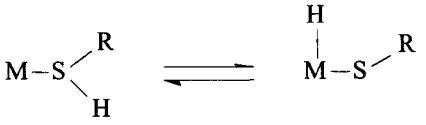

(2)

Irrespective of the mechanism, it is pertinent to ask why nature has chosen to use the exceptionally toxic CO and CN ligands for hydrogenases. The definitive answer is yet to be forthcoming but studies on simple dihydrogen complexes offer one suggestion. The position of the tautomeric equilibrium between a dihydride and dihydrogen species is influenced by the ancillary ligands. Strongly electron-withdrawing CO ligands on the dihydrogen binding site could favour the dihydrogen species (*ie* disfavour intramolecular H-H cleavage to make the corresponding dihydride). Effectively holding the substrate as dihydrogen gives the system the opportunity to cleave dihydrogen heterolytically. With less electron-withdrawing co-ligands the dihydride form would be favoured (*ie* homolytic H-H cleavage).

One elementary reaction which features in all of the mechanisms outlined above, is the migration of protons between sulfur and metal atoms as shown in Equation (2).

The movement of protons between metal and sulfur ligands has been proposed in the action of other metalloenzymes. Thus, both the nitrogenases [33,34] and hydrogenases [3] catalyse the reduction of protons to dihydrogen. The structures of the active sites of both these enzymes have been determined. The binuclear sites of hydrogenases have been discussed above. For the Mo-based nitrogenase, the active site is a cluster whose core comprises $MoFe_7S_9$ (*vide infra*). The structures of the active sites of these enzymes give little indication of how protons are reduced to dihydrogen but the predominant sulfur ligation in both sites has led to the reasonable conclusion that sulfur plays a key role in the process.

Although thiol and hydride/thiolate complexes are known, there are few studies which show that the hydrogen can move between metal and sulfur [35-38]. The transfer of a proton from sulfur to metal has been proposed before. For example, the so-called oxidative-addition of RSH to $[IrCl(CO)(PPh_3)_2]$ has been suggested to involve a three-centre, Ir-H-SR transition state in which the lengthening of the S-H bond is synchronous with the binding of these two atoms to the iridium centre [39]. More recently [40] an agostic Os---H-S interaction has

been proposed in the substitution reaction of thiols with $[Os_3(CO)_{11}(NCMe)]$. This is considered an intermediate state in the proton transfer reaction. Finally, proton transfer has been observed between sulfur and hydride [41] ligands in $[Os(\eta^2\text{-}H_2)(CO)(quS)(PPh_3)_2]^+$ (quS = quinoline-8-thiolate). In studies where there is evidence for metal-to-sulfur proton transfer, no kinetic studies have been performed. Consequently we have only a poor understanding of the electronic factors which facilitate this transfer, and no direct evidence that the reaction is truly *intramolecular*. Whilst the intramolecular migration of protons between metal and ligand is a reaction which is widespread with carbon-based ligands as shown in Equation (3) [42], migration pathways are less evident with more electronegative donor atoms, where acid-base-catalysed mechanisms can be energetically more favourable (*vide infra*) [43].

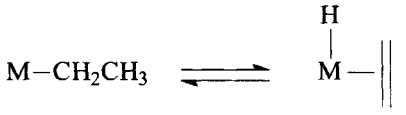

(3)

The kinetics of the protonation of $[Ni(SEt)(triphos)]^+$ (triphos = $\{Ph_2PCH_2CH_2\}_2PPh$) by $[lutH]^+$ (lut = 2,6-dimethylpyridine) is consistent with a mechanism comprising two coupled equilibria [44], as shown in Equation (4). Initial protonation occurs at the sulfur. This is followed by the intramolecular equilibration of the proton between the sulfur and nickel sites.

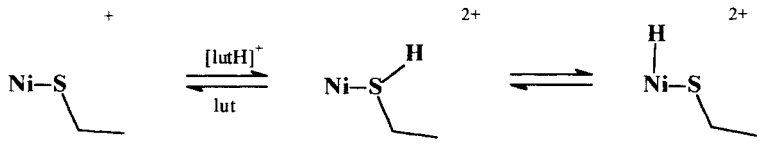

(4)

In these studies the use of the relatively weak acid, $[lutH]^+$ (pK_a = 15.4) [45] has ensured that only single protonation of $[Ni(SEt)(triphos)]^+$ occurs. However, when $[Ni(SEt)(triphos)]^+$ reacts with an excess of anhydrous HCl, EtSH is released according to Equation (5).

$$[Ni(SEt)(triphos)]^+ + HCl \longrightarrow [NiCl(triphos)]^+ + EtSH \qquad (5)$$

This reaction is complete within the dead time of the stopped-flow apparatus (2ms) even at the lowest concentration of HCl. In the reaction with $[lutH]^+$ there is no evidence of the dissociation of the thiol over more than 100 seconds. In

MeCN, HCl is 10^6 times stronger acid than $[lutH]^+$ and it seems likely that HCl can protonate *both* the sulfur and nickel, resulting in the rapid dissociation of the thiol.

That diprotonation leads to labilisation of the thiol whilst monoprotonation does not has been observed in other systems, most notably in the reactivity of iron-sulfur-based clusters [46]. It has been argued that the reason for the marked labilising effect of two protons is a consequence of the nature of the bonding between thiols and transition metal sites [46, 47]. Thiolates are good σ-donors. Protonation of the thiolate will decrease the σ-donation and the resulting thiol is a good π-acceptor. The σ-donating and π-accepting bonding of thiol oppose one another. What electron density is lost by thiolate in σ-donation, upon protonation is gained in π-acceptance and the result is that the Ni-S bond strength is little changed between thiolate and thiol, with consequently little change in lability. It is only on the addition of a further proton (this time on the nickel) that the system becomes labile. It seems likely that protonation of the nickel diminishes the Ni-to-S π-backbonding, thus facilitating dissociation of the thiol.

Studies on simple nickel-thiolate complexes are pertinent to discussions on the mechanisms of action of hydrogenases. Consider the pathway for reduction of protons. Initial protonation of metal-thiolate species will always occur at the lone pair of electrons on sulfur (most basic site). Protonation at the metal is thermodynamically less favourable, and usually kinetically slower than protonation of a stereochemical lone pair of electrons [48-50].

If it is essential during the enzyme's action that proton transfer to the metal occur, then a pathway involving diprotonation of the complex would be unfavourable since protonation of *both* metal and sulfur leads to rapid dissociation of the thiol. The studies on simple nickel complexes show that single protonation of the sulfur can be followed by intramolecular transfer of the proton to nickel.

16.3.2.3 Heterolytic H_2 Activation: Isotopomer Scrambling

More than any other single feature the involvement of metal hydrides in the action of hydrogenases is indicated by the ability of these enzymes to catalyse the hydrogen isotope exchange shown in Equation (6) and the equilibration of *ortho-* and *para*-hydrogen shown in Equation (7).

$$D_2O + H_2 \rightleftharpoons xHD + (1 - x)D_2 + H_2O \quad (6)$$

$$ortho\text{-}H_2 \rightleftharpoons para\text{-}H_2 \quad (7)$$

These reactions are well known in simple polyhydrido-complexes, and are merely a consequence of rapid proton/hydride exchange at the metal site [51] as shown in Figure 8.

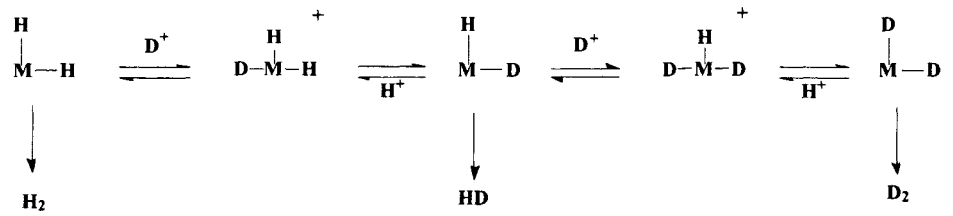

Figure 8. Proton exchange at polyhydridic metal sites leading to the release of mixtures of H_2, HD and D_2.

In principle, the equilibrations shown in Figure 8 can result in the selective formation of H_2, HD or D_2, but the reactions are difficult to control. The problem is further exacerbated by hydrogen exchange with suitable ligands. As shown in Equation (8) phenyl groups on (*eg* phosphine) ligands can undergo *ortho*-metallation with coordinatively-unsaturated metal sites. The evidence that such pathways operate is the incorporation of deuterium into the *ortho*-positions of the phenyl residue.

The main point is that forming mixtures of dihydrogen isotopomers is a trivial aspect of the protonation (deuteration) chemistry of metal deuterides (hydrides) and is an expected feature of the reactions of hydridic sites. The chemical challenge is not to mimic such scrambling but rather to control it, and selectively produce the various dihydrogen isotopomers. The limited number of studies reported which realise this selectivity will now be briefly presented.

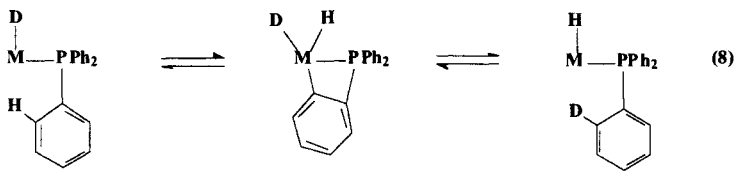

(8)

16.2.2.3.1 Formation of HD.

The selective formation of HD has been accomplished [47,52] using [RhH(CO)(buS_4)] (buS_4 = $SC_6H_2(^tBu)_2SCH_2CH_2SC_6H_2(^tBu)_2S$) shown in Figure 9.

This system catalyses the D_2/H^+ exchange by a pathway involving heterolytic cleavage of D_2 on the metal site with transfer of D^+ to the thiolate sulfur. Rapid exchange of S-D with free H^+ in solution produces S-H. In a subsequent re-coupling reaction HD is produced selectively, at least in the presence of a large excess of dihydrogen. The selective formation of HD is obtained because,

in general, the rate of proton exchange at metal-hydrides is much slower than at sulfur donor atoms.

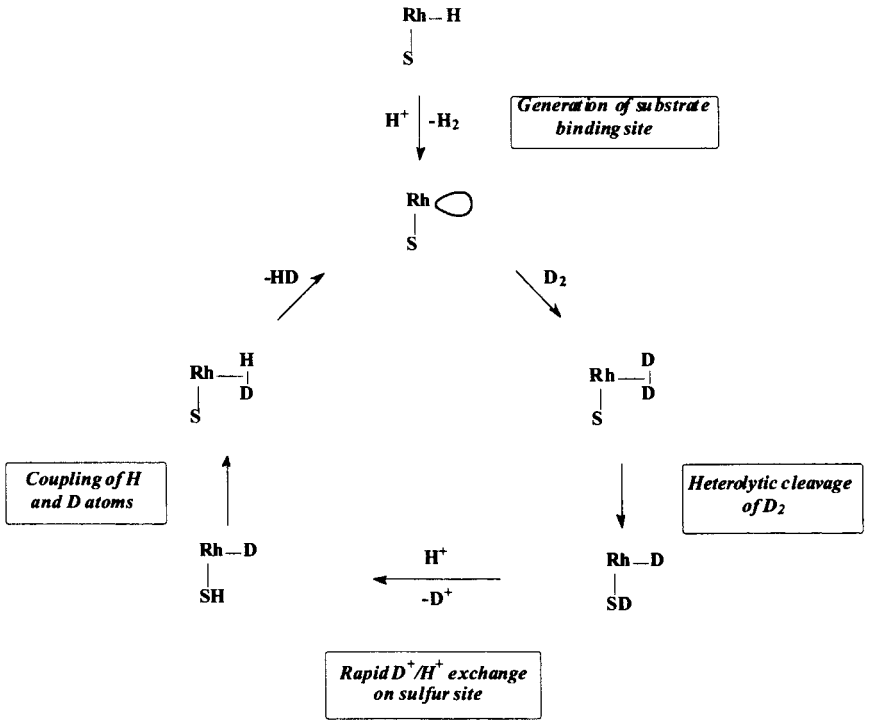

Figure 9. Catalytic cycle for the selective formation of HD in [RhH(CO)(buS_4)]. For simplicity only the Rh and one S atom are shown.

16.2.2.3.2 Formation of D_2.

The selective formation of HD or D_2 has been achieved in the reaction of [Ni($Ph_2PCH_2CH_2PPh_2$)$_2$] with DCl: HD being the exclusive product at low acid concentrations and D_2 at high acid concentrations. Both pathways involve the formation of the detected intermediate, [NiD($Ph_2PCH_2CH_2PPh_2$)$_2$]$^+$ as shown in Figure 10. The formation of HD occurs by the pathway [53] shown at the top of the Figure.

Deuteration of the metal labilises the Ni-P bond to dissociation and at low concentration of DCl this reaction is faster than D^+ attack at the Ni-D bond. Thus, at low concentrations of acid *ortho*-metallation occurs. Subsequent release of HD and further attack of D^+ results in deuteration of the *ortho*-site on the phenyl group. At high concentrations of DCl the rate of D^+ attack at Ni-D is faster than ortho-metallation resulting in the selective release of D_2.

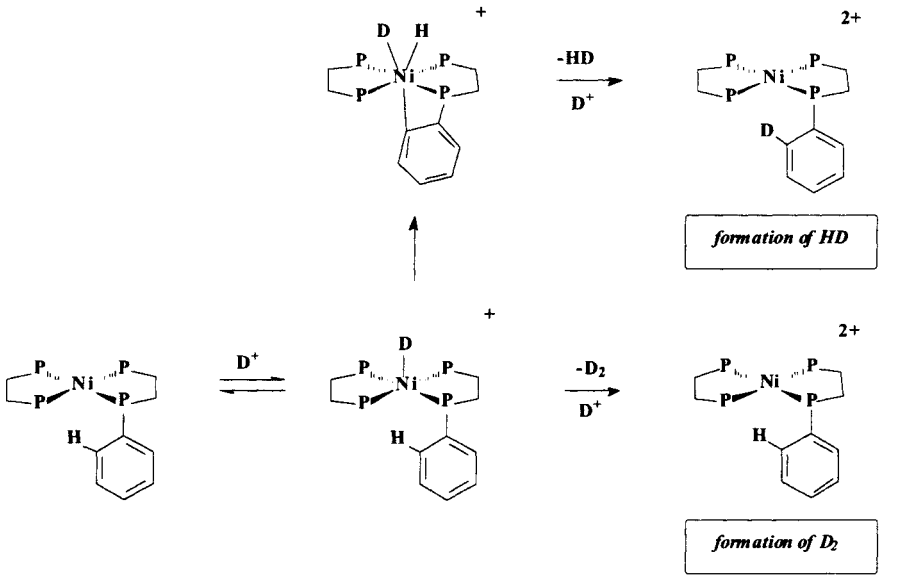

Figure 10. Pathways for the formation of HD (top) and D_2 (bottom) in the reaction of anhydrous DCl with $[Ni(Ph_2PCH_2CH_2PPh_2)_2]$.

16.2.2.3.3 Formation of H_2.

Although a somewhat academic question, it is intriguing to consider if treatment of a polyhydride with D^+ can ever produce H_2. This selectivity has been observed in the reaction [54] of DCl with $[WH_3(OCMeO)(Ph_2PCH_2CH_2PPh_2)_2]$ which produces H_2 and $[WHD(O_2CMe)(Ph_2PCH_2CH_2PPh_2)_2]^+$, but no HD or D_2. This selectivity is a consequence of the novel two site character of the trihydride: the pendant acetate ligand is the kinetically favoured site of deuteration. Deuteration labilises the metal site towards H_2 evolution, as shown in Figure 11. Chelate ring-closure and deuteration of the tungsten completes the reaction.

In hydrogenases, the involvement of metal hydrides is restricted to the pathways for the release and/or uptake of dihydrogen. We will see in the following sections that the nitrogenases also reduce protons to dihydrogen, but using a very different active site. In addition, there are other potential roles for hydrides in the action of this more complicated enzyme. Most notably roles for hydrides in the binding of dinitrogen to the active site and in the transformation of some of the substrates.

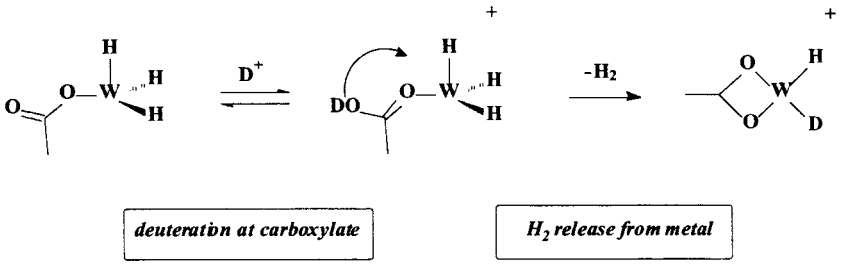

Figure 11. The formation of H_2 in the reaction of DCl with $[WH_3(OCMeO)(Ph_2PCH_2CH_2PPh_2)_2]$.

16.3 NITROGENASES

16.3.1 Classification of the Nitrogenases

The nitrogenases are a class of metalloenzymes whose physiological role is to catalyse the conversion of dinitrogen to ammonia. This it accomplishes by sequences of coupled electron and proton transfer reactions [33]. Like the hydrogenases, the nitrogenases have been classified according to their metal content [55]. The most long established, and consequently best studied, nitrogenase is that containing molybdenum. The Mo-based nitrogenase contains Fe, Mo and "inorganic" S. More recently a V-based nitrogenase has been identified which comprises Fe, V and S. It is reasonably assumed that vanadium occupies the position (both structurally and functionally) occupied by molybdenum. Finally, there is an Fe-only nitrogenase which apparently contains no heterometal, and in which iron has presumably replaced the vanadium or molybdenum.

16.3.2 Structure and Composition of Nitrogenases

The make up of all the nitrogenases are essentially the same [55,56]. The most studied is the Mo-based enzyme which consists of two metalloproteins: the smaller Fe-protein (mol wt = *ca* 65,000) and the larger MoFe-protein (mol wt = *ca* 220,000). The Fe-protein contains a single cubane $\{Fe_4S_4\}$ cluster, which mediates electron transfer from the external reductant (a ferredoxin or flavodoxin) to the MoFe-protein.

The MoFe-protein contains two structurally unique Fe-S clusters. First, there are the so-called P-clusters which comprise a $\{Fe_8S_7\}$ cluster core. The role of these clusters is still poorly defined but they are probably a storage place for electrons (transferred from the Fe-protein), until those electrons are required by the active site when substrates are transformed. The active site is the so-called

FeMo-cofactor (in the Mo-enzyme), FeV-cofactor (in the V-enzyme) or FeFe-cofactor (in the Fe-only-enzyme).

The cofactor is a structurally unique cluster which has been characterised in the Mo-based nitrogenase from *Azotobacter vinelandii*. The cluster core has the composition, Fe_7S_9Mo, and is bound to the polypeptide at only two positions: through a cysteinate sulfur to the unique tetrahedral iron site (the other six irons are all three coordinate), and through an imidazole group of a histidine amino acid residue. The molybdenum is six coordinate, with part of the coordination sphere comprising a R-homocitrate ligand, chelating *via* an alkoxy and carboxylate linkage. The electron transfer pathway [57,58], together with the structures of the P- and FeMo-cofactor clusters, is shown in Figure 12.

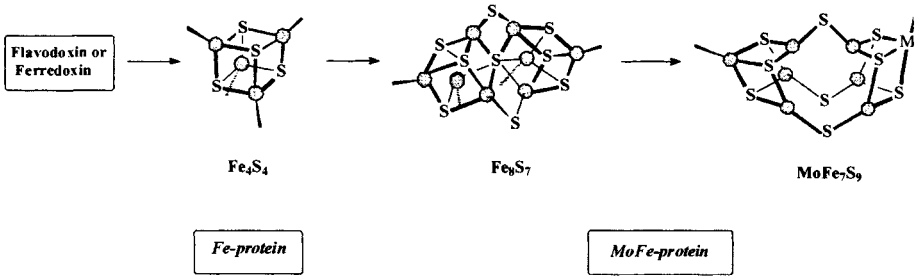

Figure 12. The electron-transfer pathway for the action of the nitrogenases.

The idealised stoichiometry for nitrogen fixation is shown in Equation (9). However, this is never attained in practice. In the absence of a substrate the enzyme reduces protons to dihydrogen according to the stoichiometry shown in Equation (10).

$$N_2 + 6H^+ + 6e \longrightarrow 2NH_3 \quad (9)$$

$$2H^+ + 2e \longrightarrow H_2 \quad (10)$$

Thus, in the presence of dinitrogen there is a decrease in the amount of dihydrogen produced by nitrogenase, as more of the electrons are routed preferentially into the reduction of dinitrogen. However, even at extreme pressures of dinitrogen the reduction of protons can never be entirely suppressed. The generally accepted limiting stoichiometry of the Mo-based nitrogenase is shown in Equation (11), in which one molecule of dihydrogen is produced for every molecule of dinitrogen converted into ammonia. This production of dihydrogen is commonly referred to as obligatory dihydrogen evolution.

$$N_2 + 8H^+ + 8e \longrightarrow 2NH_3 + H_2 \quad (11)$$

A few years ago this limiting stoichiometry was assumed to have a mechanistic significance for the binding of dinitrogen, which we will now discuss.

16.3.3 Dinitrogen Binding to a Metal-Hydride Site

It has been well known for many years that coordinatively-saturated polyhydrido-complexes can bind molecules and ions by displacement of dihydrogen. The mechanism of this reaction is shown in its simplest form in Equation (12), in which the coupling of two hydride ligands and reductive-elimination of dihydrogen generates a transient coordinatively-unsaturated intermediate which is subsequently attacked by molecules or ions.

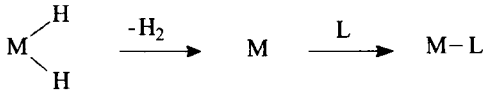

(12)

Whilst this reaction is a fundamental feature of traditional organometallic chemistry and one of the elementary reactions of many homogeneous catalyses [59], the coupling of hydride ligands and release of dihydrogen to produce a substrate binding site was not invoked in biology until the characteristic reactivity of nitrogenase was considered [60].

The limiting stoichiometry of the Mo-based enzyme {Equation (11)} is identical to that of Equation (12), implicating the obligatory evolution of one molecule of dihydrogen arising from generation of a vacant site on the enzyme at which dinitrogen can bind [61]. This has been elaborated upon in: (i) the mechanism of action of the enzyme and (ii) model systems.

16.3.3.1The Enzyme Mechanism.

The most complete proposal [62] for the mechanism of the action of the enzyme is that shown in the Figure 13. This mechanism has been derived from studies and simulations of the pre-steady state time-courses of ammonia production, dihydrogen release and ethylene release from acetylene reduction. A particularly crucial factor in analysing the system has been understanding the lag phases observed with each substrate. These lags correspond to the enzyme in its resting state (E_0) preparing itself for the binding of the substrate. The mechanism shown in Figure 13 was established for the Mo-based nitrogenase. It is assumed that the V-based and Fe-only nitrogenases operate by an analogous mechanism.

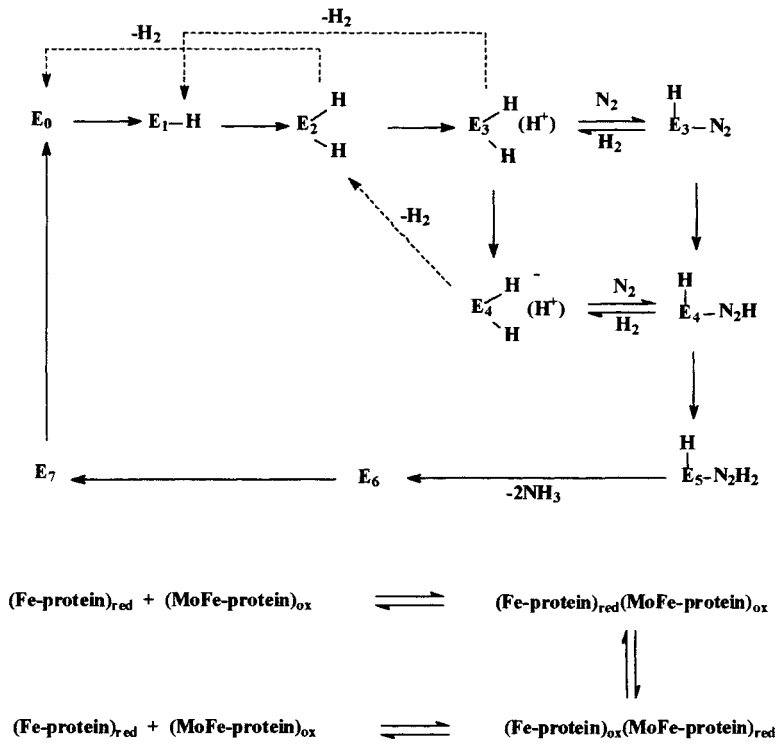

Figure 13. Scheme showing the eight states of the MoFe-protein during the catalytic cycle of nitrogenase. States which evolve H_2, bind N_2 and NH_3 are indicated. The elementary steps involved in the reduction of MoFe-protein by the Fe-protein are shown at the foot of the Figure.

In Figure 13 the symbol, E_n represent various states of the enzyme, with the subscript n corresponding to the total number of electrons transferred to the MoFe-protein. The arrows which interconnect E_n and E_{n+1} actually comprise three elementary reactions shown at the foot of the Figure: (i) the binding of the reduced Fe-protein to the oxidised MoFe-protein to form an adduct; (ii) transfer of an electron from Fe-protein to MoFe-protein within the adduct and (iii) dissociation of the adduct. This same sequence of elementary reactions is performed at each step around the cycle with (it is assumed) unchanged rate constants. The rate-limiting step of nitrogenase is the dissociation of the component proteins ($k = 6.4\ s^{-1}$).

Having been oxidised within the adduct, the dissociated Fe-protein is reduced again by the external reductant (Flavodoxin or Ferredoxin, or $S_2O_4^{2-}$ *in vitro*), in a MgATP-dependent process (ATP = adenosine triphosphate). That the Fe-protein must dissociate before it can be reduced is contentious. Although it is true

in vitro, where $S_2O_4^{2-}$ is used as the external reductant, when flavodoxin or ferredoxins are employed (*in vivo*), dissociation does not seem to be necessary.

The obligatory evolution of dihydrogen is implicitly built into the mechanism of Figure 13. The eight steps which comprise the main cycle correspond to the eight electrons consumed in the limiting stoichiometry of the Mo-based enzyme's action shown in Equation (11).

Metal hydrides are proposed to be involved in several parts of this mechanism as follows. (i) Formation of hydrides are implicated in the early stages of the cycle since dinitrogen does not bind until after three electrons (and implied three protons, for charge neutralisation) have been added to E_0. (ii) Dihydrogen evolution can occur from states E_2, E_3 and E_4, producing E_0, E_1 and E_2 respectively. (iii) Dinitrogen binds by displacing H_2 at E_3.

Parenthetically, it is worth noting that it is not surprising dihydrogen formation is an unwanted side product in the reaction of this enzyme. In order to activate dinitrogen towards protonation it is necessary to bind dinitrogen to an electron-rich site. The combination of electrons and protons will favour dihydrogen formation. This is particularly evident in the early stages of the cycle. Once dinitrogen is bound, protonation of the dinitrogen is favoured and this suppresses dihydrogen production. Effectively the electron-flux is being routed away from dihydrogen production and into dinitrogen fixation.

There are three observations which have been instrumental in suggesting a metal hydride binding site in nitrogenase: (i) obligatory evolution of dihydrogen as implicated in the limiting stoichiometry of the Mo-based enzyme discussed above; (ii) that dihydrogen is a competitive inhibitor of dinitrogen reduction and (iii) dinitrogen accelerates the formation of HD in the reactions of the enzyme under an atmosphere of D_2.

The simplest proposal, which rationalises all the above observations, is that the three electrons needed to convert E_0 to E_3 are also associated with three protons to produce a metal trihydride. It is this trihydride which eliminates dihydrogen and binds dinitrogen, as shown in Equation (13).

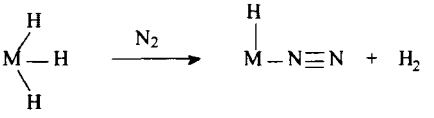

(13)

The identity of the hydridic binding species can be probed by experiments [63] in the presence of D_2 (or T_2). These experiments demonstrate unambiguously that the active site cannot be a trihydride. The following key features need to be rationalised in any proposition concerning the nature of E_3. (i) During turnover under D_2 (or T_2), no HD (or HT) is formed and (ii) In experiments under T_2,

no T^+ is incorporated into the solution. Points (i) and (ii) are inconsistent with a trihydride because the necessary release of H_2 would, (for instance) in the presence of D_2 generate MHD_2 species as shown in Equation (14).

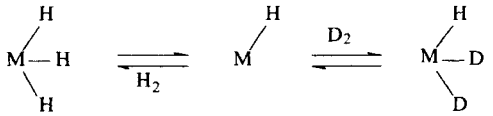

(14)

MHD_2 would, in its turn produce HD. The only way in which HD formation from MHD_2 could be avoided would be if the trihydride were in a sense asymmetric, with one M-H bond chemically distinct from the other two and hence unable to reductively-eliminate H_2 with either of the other M-H bonds. It is not difficult to envisage such a situation brought about by stereochemical restrictions. However, such a species is without precedent in simple chemical systems. It seems more likely that the observations with the various dihydrogen isotopomers dictate that only a dihydridic state is produced. Point (ii) demonstrates that any metal hydride is not involved in a protolytic equilibrium as shown in Equation (15), or at least that this exchange process is slow.

(15)

It has been proposed that E_3 is a metal dihydride which is activated by protonation from an adjacent protic amino acid side chain as shown in Figure 14. There are two features of this mechanism that need special attention. First, this mechanism implies that protonation of a hydride site facilitates the release of dihydrogen from the site. Secondly, proton attack does not occur at the metal since this would produce a trihydride which is untenable for the reasons outlined above. Rather, protonation affects the reactivity without becoming associated with the metal. This implicates direct protonation of the hydride ligand.

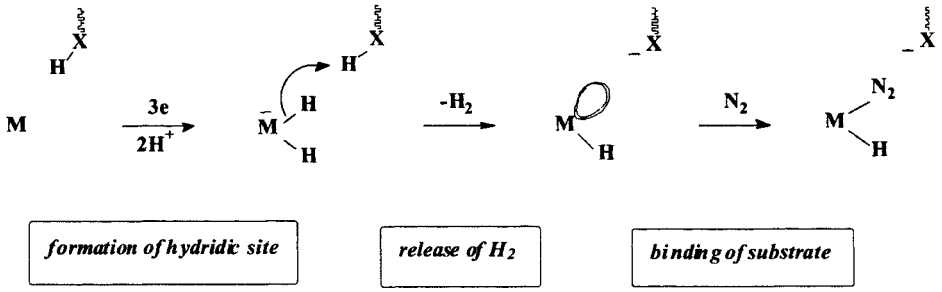

Figure 14. Proposed intimate mechanism for N_2 binding by nitrogenase.

16.3.3.2 Model Systems.

The ability of protonation to facilitate release of dihydrogen from simple polyhydrido-complexes was not unknown before the mechanism of nitrogenase was proposed, but it was only in work inspired by these proposals that it was appreciated how versatile this mode of activation can be. A particularly versatile system which shows a variety of different reactivities (depending on the substrate) is now presented.

16.3.3.2.1 Binding and Activation of Small Molecules at Metal Hydrides.

When $[MoH_4(Ph_2PCH_2CH_2PPh_2)_2]$ reacts with an excess of anhydrous HX (X = Cl or Br) the reaction shown in Equation (16) is observed [64].

$$[MoH_4(Ph_2PCH_2CH_2PPh_2)_2] + 2HX \longrightarrow [MoH_2X_2(Ph_2PCH_2CH_2PPh_2)_2] + 2H_2 \quad (16)$$

The release of dihydrogen is rapid and reaction (16) is complete within a few seconds, under ambient conditions. In contrast, in the absence of acid, dissociation of dihydrogen from the parent $[MoH_4(Ph_2PCH_2CH_2PPh_2)_2]$ has a half-life of *ca* 2 hours.

If the reaction of $[MoH_4(Ph_2PCH_2CH_2PPh_2)_2]$ with anhydrous HCl is performed in the presence of a variety of potential ligands (*eg* RCCH, N_2, CN^-, N_3^- *etc*) the product is always $[MoH_2Cl_2(Ph_2PCH_2CH_2PPh_2)_2]$. It seems that Cl^- is a better nucleophile than these other molecules and so binds to the molybdenum preferentially. By using an acid, such as HBF_4, with a poorly coordinating anion, other molecules can bind to the molybdenum. Selected reactions of this system are illustrated in Figure 15.

The products can be categorised into three headings according to how they are formed. (i) Those where the substrate has replaced dihydrogen with no transformation of the coordinated substrate (*eg* PhCCH). (ii) Reactions in which the site formally abstracts atoms from molecules and ions (*eg* O from H_2O; S from H_2S or N from N_3^-). (iii) Upon binding to the molybdenum, some substrates (*eg* N_3^- and N_2) become protonated. When bound dinitrogen, is protonated to form the hydrazido(2-)-species, *trans*-$[Mo(NNH_2)F(Ph_2PCH_2CH_2PPh_2)_2]^+$ which was originally prepared by protonation of *trans*-$[Mo(N_2)_2(Ph_2PCH_2CH_2PPh_2)_2]$. Indeed it was essential that *trans*-$[Mo(NNH_2)F(Ph_2PCH_2CH_2PPh_2)_2]^+$ was already known since the hydrazide is formed in relatively low yield in the reaction of acid with $[MoH_4(Ph_2PCH_2CH_2PPh_2)_2]$, and is contaminated with $[MoF_2(Ph_2PCH_2CH_2PPh_2)_2]BF_4$ from which it is difficult to separate. However, ^{31}P NMR spectroscopy was able to unambiguously identify *trans*-$[Mo(NNH_2)F(Ph_2PCH_2CH_2PPh_2)_2]^+$ in the mixture. The important point is that the reaction involving *trans*-$[MoH_4(Ph_2PCH_2CH_2PPh_2)_2]$ was the first

demonstration that dinitrogen could bind to a hydride site which is activated by protonation. Finally, it is important to note that BF_4^- is not entirely innocent, and in some of these reactions acts as a source of F^- which can coordinate to the molybdenum site.

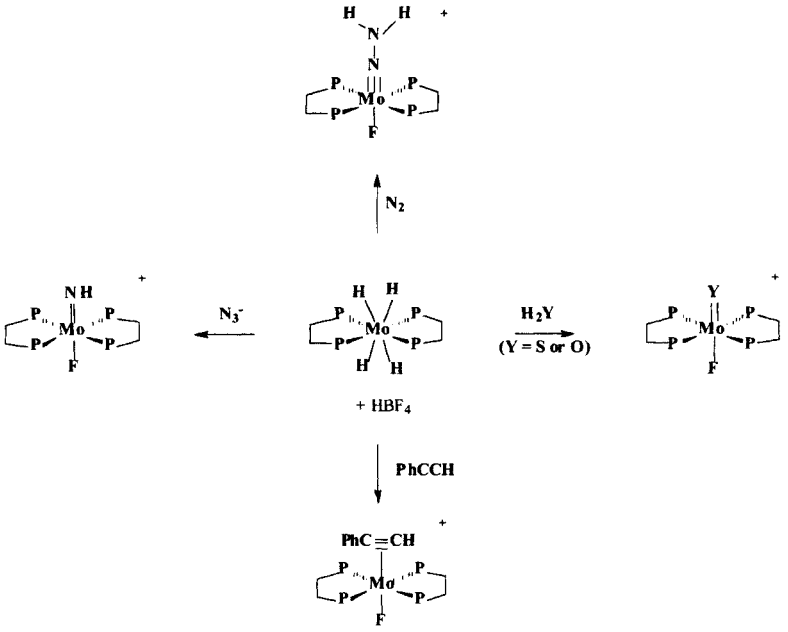

Figure 15. Reactions of $[MoH_4(Ph_2PCH_2CH_2PPh_2)_2]$ with HBF_4 in the presence of selected small molecules and ions.

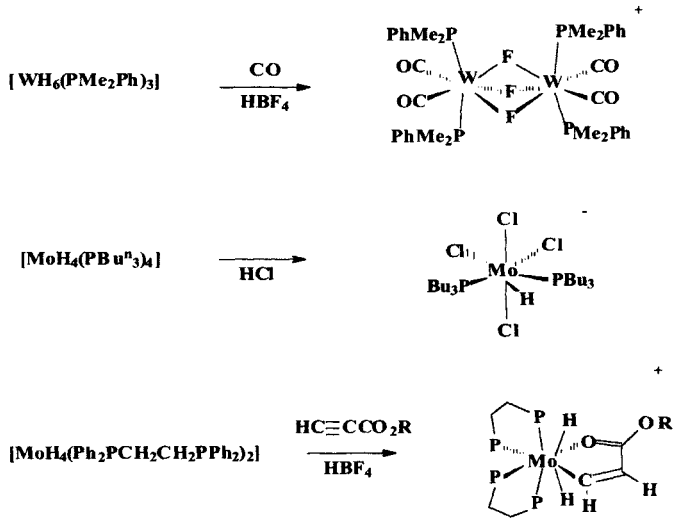

Figure 16. Examples of the protonation of polyhydrido-complexes

In a further development of this work, the reactions of acid with other polyhydrides [65-68] has been used as a synthetic strategy to produce new compounds, unattainable by other routes, as shown in Figure 16. However, a major limitation of developing this approach as a general synthetic strategy is that it is difficult to predict the outcome of the reactions.

Studies on the mechanism of the reaction between $[MoH_4(Ph_2PCH_2CH_2PPh_2)_2]$ and acid reveal an unexpected complication. Kinetic analysis shows [69] that two protons bind to $[MoH_4(Ph_2PCH_2CH_2PPh_2)_2]$ prior to the dissociation of dihydrogen. This leads to a conceptual problem since $[MoH_6(dppe)_2]^{2+}$ would be Mo^{VIII}; a clear impossibility! A mechanistic rationalisation is shown in Figure 17.

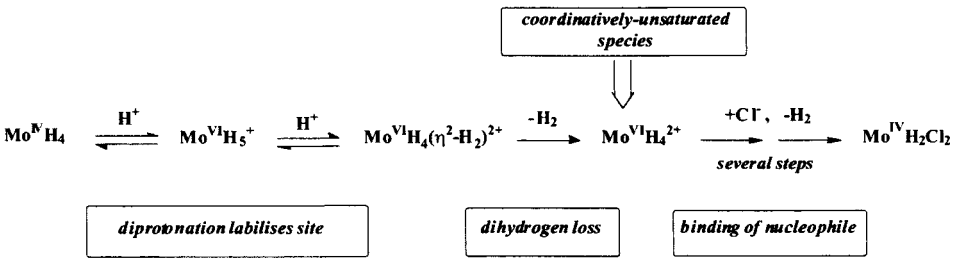

Figure 17. The mechanism of H_2 release following diprotonation of $[MoH_4(Ph_2PCH_2CH_2PPh_2)_2]$.

Initial protonation of molybdenum, produces $[MoH_5(Ph_2PCH_2CH_2PPh_2)_2]^+$ (the W analogue of this compound can be isolated and NMR spectroscopy shows it to be a classical, fluxional pentahydride). Further protonation of $[MoH_5(Ph_2PCH_2CH_2PPh_2)_2]^+$ at molybdenum is not possible since the metal is already in its maximum oxidation state (+VI). Further protonation can only occur under two circumstances. (i) After intramolecular coupling of hydride ligands to generate $[MoH_3(\eta^2\text{-}H_2)(Ph_2PCH_2CH_2PPh_2)_2]^+$. Hydride-hydride coupling effectively releases two electrons to molybdenum to produce a formally Mo^{IV} species which can be further protonated at the metal. (ii) Alternatively, protonation can occur directly at one of the hydride ligands. In either case the species formed after the addition of two protons is $[MoH_4(\eta^2\text{-}H_2)(Ph_2PCH_2CH_2PPh_2)_2]^{2+}$ which is a Mo^{VI} species, labile to dissociation of dihydrogen. It is interesting to note that the dihydrogen molecule that is going to dissociate has been preformed on the metal centre.

$[MoH_4(Ph_2PCH_2CH_2PPh_2)_2]$ is a coordinatively-saturated, eighteen-electron complex. Clearly binding protons to the molybdenum cannot alter the

formal electron count of the complex, and so it is only upon dissociation of dihydrogen that a coordinatively-unsaturated species is formed at which small molecules and ions can bind. A crucial aspect of this system is the availability of the hydride ligands *and* protons in solution. It is conceptually useful to consider that in the protonation reactions of metal hydrides, H^- and H^+ are available for transforming substrates. The availability of both H^- and H^+ means that the system is capable of reacting with a wide range of molecules in a variety of different ways.

16.3.3.2.2 Direct Protonation of Hydride Ligand.

The intimate mechanism of protonation of hydrido-complexes will now be addressed. One aspect of the proposed mechanism of nitrogenase shown in Figure 14 is the direct protonation of the hydride ligand. Even before detailed kinetic investigations on protonation of polyhydrido-complexes had been undertaken, there were indications in the literature that direct proton attack at transition metal hydride ligands could occur. For example, it was known that $[WH_6(PMe_2Ph)_3]$ rapidly evolves dihydrogen on reaction with acid [70]. Yet the tungsten is in its maximum oxidation state and so cannot be protonated directly. Two limiting mechanisms can be envisaged, directly analogous to those described above for $[MoH_5(Ph_2PCH_2CH_2PPh_2)_2]^+$: either initial intramolecular H-H coupling, followed by protonation at the metal or direct protonation of a hydride ligand. Both pathways result in $[WH_5(\eta^2\text{-}H_2)(PMe_2Ph)_3]^+$, which could lose dihydrogen to generate the coordinatively-unsaturated $[WH_5(PMe_2Ph)_3]^+$, at which nucleophiles can bind. Studies on the reaction shown in Equation (17) have demonstrated that direct protonation of a hydride ligand can occur [71].

$$[WH_4(PMe_2Ph)_4] + HCl \longrightarrow [WH_5(PMe_2Ph)_4]^+ + Cl^- \qquad (17)$$

Stoichiometrically Equation (17) is a very simple reaction. However, the kinetics are complicated, and show that this reaction does not involve the direct, single step protonation of the metal, but rather involves initial protonation at a hydride ligand to produce a transient dihydrogen species which subsequently undergoes intramolecular H-H cleavage to form the classical pentahydride product $[WH_5(PMe_2Ph)_4]^+$, as shown in Figure 18.

Recently, further details about protonation of hydride ligands have been obtained. In particular, it has been shown that the protonation of $[MH_2(Ph_2PCH_2CH_2PPh_2)_2]$ (M = Fe, Ru or Os) to form *trans*-$[MH(\eta^2\text{-}H_2)(Ph_2PCH_2CH_2PPh_2)_2]^+$ are associated with an inverse kinetic isotope effect ($k_H/k_D < 1$) [72]. This suggests that the protonation occurs through a late transition state involving hydrogen bonding between the acid and hydride ligand prior to the transfer of the proton to the hydride.

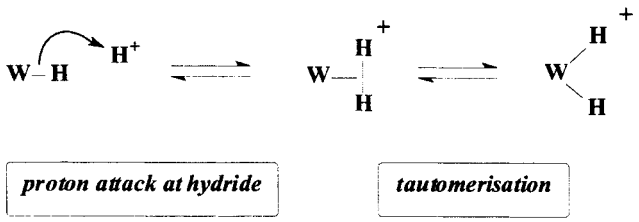

Figure 18. The mechanism of formation of classical hydride by initial protonation of hydride ligand and formation of η^2-H_2

16.3.3.2.3 Binding Dinitrogen and Dihydrogen Evolution

The reactions discussed above, whilst aiming to model the proposed mechanism of nitrogenase, involve dinitrogen (or another substrate) displacing dihydrogen. An alternative, fundamentally different model, has been proposed in which dinitrogen binding involves displacement of a carboxylate ligand with dihydrogen evolution occurring subsequently. This model rationalises both obligatory and non-obligatory dihydrogen production.

$[MoH_2(\eta^2\text{-}O_2CMe)(Ph_2PCH_2CH_2PPh_2)_2]^+$ catalyses the reduction of protons to dihydrogen by the mechanism [73] shown in Figure 19. In the enzyme mechanism it was proposed that dinitrogen binding occurs before dihydrogen evolution since it was known that dinitrogen accelerates the formation of HD from D_2 [74]. Figure 19 shows a mechanism in which dinitrogen binding precedes dihydrogen evolution.

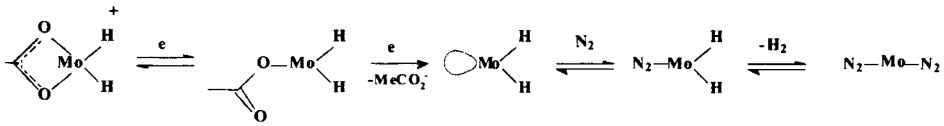

Figure 19. Pathway showing N_2 binding by displacement of carboxylate ligand, and subsequent evolution of H_2.

Two electron reduction [75] of $[MoH_2(\eta^2\text{-}O_2CMe)(Ph_2PCH_2CH_2PPh_2)_2]^+$, under an atmosphere of dinitrogen, results in the expulsion of the carboxylate ligand and the exposure of a site on the molybdenum at which dinitrogen can bind. Transient formation of the detected $[MoH_2(N_2)(Ph_2PCH_2CH_2PPh_2)_2]$ is followed by dissociation of dihydrogen, and ultimate production of *trans*-$[Mo(N_2)_2(Ph_2PCH_2CH_2PPh_2)_2]$.

In the absence of dinitrogen (or any other substrate) only dihydrogen is formed. If $[MoH_2(\eta^2\text{-}O_2CMe)(Ph_2PCH_2CH_2PPh_2)_2]^+$ is only one-electron reduced $[MoH_2(OCMeO)(Ph_2PCH_2CH_2PPh_2)_2]$ is formed, in which the acetate is a monodentate ligand. Protonation can now occur at the more open molybdenum site and subsequent attack of the carboxylate releases dihydrogen. Support for this mechanism comes from isolation of the analogous $[WH_3(OCMeO)(Ph_2PCH_2CH_2PPh_2)_2]$ (*vide supra*), and characterisation by X-ray crystallography [76].

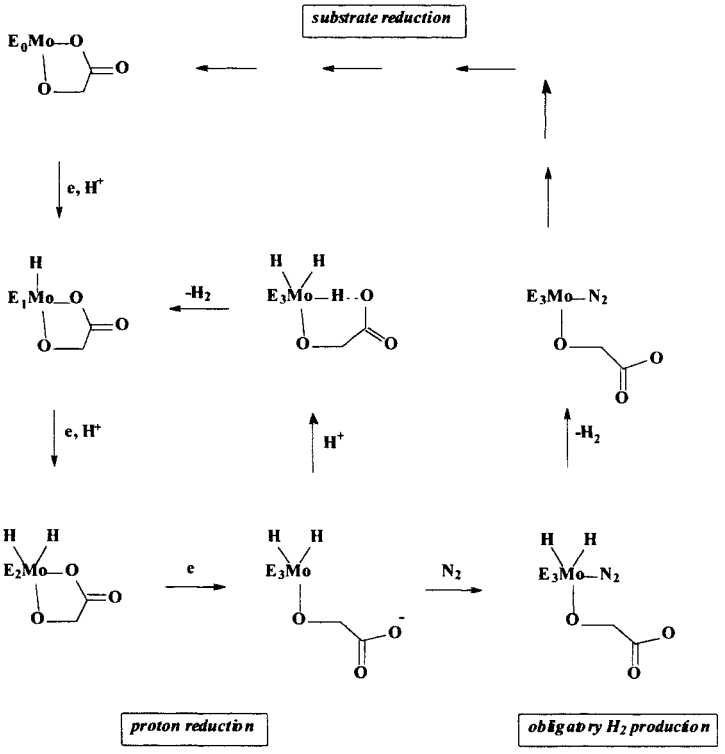

Figure 20. Proposed pathways for H_2 evolution and N_2 binding in nitrogenases, involving carboxylate dissociation (from R-homocitrate).

It has been proposed [75] that an analogous pathway operates in the enzyme as shown in Figure 20, which indicates pathways for dihydrogen production in the absence of other substrates and the obligatory evolution of dihydrogen as a consequence of dinitrogen binding. In this mechanism the obligatory evolution of dihydrogen is not a prerequisite to dinitrogen binding, but is a consequence

of dinitrogen binding to a hydridic site. It is proposed that the site is naturally hydridic because protonation of molybdenum facilitates reduction of the site and labilises carboxylate at a higher potential than could otherwise be achieved.

The mechanism also proposes that the R-homocitrate bound to the FeMo-cofactor provides a carboxylate leaving group [73, 75] to allow dinitrogen to bind. It is known that R-homocitrate is specifically required for the enzyme to be a good nitrogen fixer [76]. Replacing R-homocitrate by citrate effectively switches off nitrogen fixation. It has been proposed that the specificity for R-homocitrate is a consequence of hydrogen bonding of the long $-CH_2CH_2CO_2^-$ arm with the imidazole of His-442 which is ligated to molybdenum. The hydrogen bond only "switches on" when the R-homocitrate becomes monodentate, and this primes the electron-richness of FeMo-cofactor, facilitating dinitrogen binding and/or protonation of the bound substrate [77].

The question of how FeMo-cofactor evolves dihydrogen remains. There have been several theoretical studies exploring the way in which dinitrogen is bound and transformed at FeMo-cofactor. However, only one report, using DFT calculations, describes how dihydrogen may be evolved at cofactor [34], as illustrated in Figure 21.

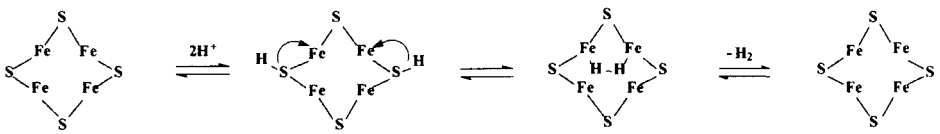

Figure 21. Proposed pathway [34], based on DFT calculations, for the reduction of H^+ to H_2 on FeMo-cofactor. Only the central Fe_4S_4 face of FeMo-cofactor is shown.

The protons bind initially to the μ_2-S atoms. Calculations indicate that protonation weakens the μ_2-S-Fe bonds, lengthening the Fe-S bonds and shortening Fe-Fe distances. The hydrogens then move together *via* the mediation of the Fe-H bonds, and form dihydrogen which separates from the cluster. When H is bound to Fe it lengthens the Fe-Fe distance.

16.3.3.5 Why Bind Dinitrogen by Displacing Dihydrogen?

The modelling studies discussed above lend credence to the proposal that metal hydrides are involved in the binding of dinitrogen to nitrogenase. But further considerations reveal some concerns about the enzyme mechanism.

As noted above, in order to get to a state of the enzyme which will bind dinitrogen (E_3, Figure 13) the enzyme "resting state" (E_0) has to bind three electrons. For each electron transferred it is generally accepted that a minimum

of two ATP molecules have to be hydrolysed. Having consumed these three electrons (and hence six ATP molecules) it seems surprising that the enzyme now wastes two electrons (and four ATP molecules), by evolving dihydrogen. Why would the enzyme want (or be prepared) to waste these electrons and energy? The reason is not at all clear but one possibility could be that employing a hydridic site allows the enzyme more control on when substrates can bind [69]. Certainly it would be unproductive to bind dinitrogen if the enzyme was in a state unprepared to transform the substrate. To illustrate this principle more clearly consider the simple description of binding of a substrate, shown in Figure 22.

If a metal site binds substrates by simple dissociation of the leaving group then the system has little control when the substrate can bind; it just has to await the dissociation of the M-X bond, and hence is a hostage to the inherent lability of the site. One way around this is to control both the formation and dissociation of the leaving group. This is just such the situation in protonation of polyhydride species: the formation of the leaving group requires the protonation of the metal and coupling of two hydrides to form a dihydrogen ligand. Further protonation of the metal labilises the dihydrogen ligand. Thus, the system has at least three controllable elementary reactions, prior to dinitrogen binding.

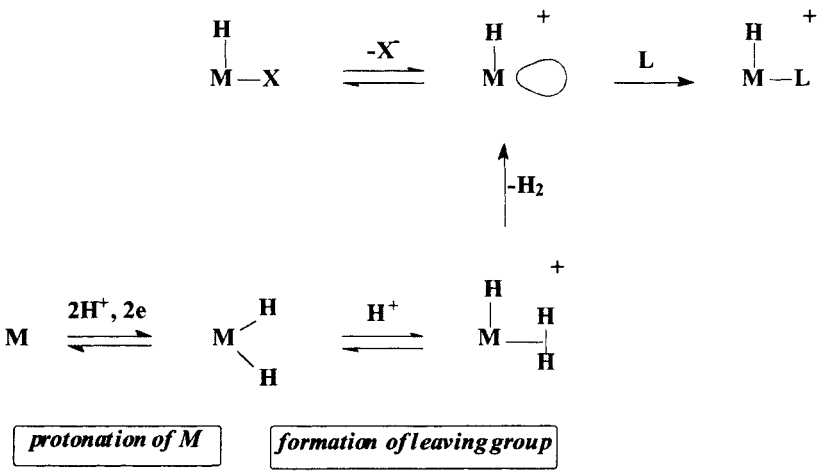

Figure 22. Controlling the binding of substrate L at a metal site. Top line shows binding at a site generated by simple displacement of X^-. Bottom line shows the binding by acid-catalysed displacement of H_2 from metal-hydride site, itself formed by protonation reactions.

16.3.3.6 Is the Limiting Stoichiometry Mechanistically Significant?

For many years the limiting stoichiometry and the inhibitory effect of dihydrogen on the fixation of dinitrogen was taken as evidence for the involvement of a hydridic site for dinitrogen binding. The discovery and purification of the V-based and Fe-only nitrogenases, and the measurement of the limiting stoichiometry of these enzymes must cast doubt on this interpretation. The V- based and Fe-only nitrogenases have been shown to have a limiting stoichiometry, in which more than one molecule of dihydrogen is produced for every molecule of dinitrogen transformed as shown in Equations (18) and (19) respectively [55,58].

$$N_2 + 12H^+ + 12e \longrightarrow 2NH_3 + 3H_2 \quad (18)$$

$$N_2 + 21H^+ + 21e \longrightarrow 2NH_3 + 7.5H_2 \quad (19)$$

It is unacceptable that more than one dihydrogen has to be released to bind one dinitrogen. Clearly there are problems in measuring the ratio of dihydrogen released to dinitrogen reduced in an enzyme accurately. There can be little doubt that for the Mo-based enzyme this number is about 1, but it cannot be claimed with any certainty that it is exactly 1.0. If this ratio could be measured with high precision and it was found that the value was exactly 0.9 or 1.1, our interpretation of the mechanistic significance of this value would be quite different. Indeed, as early as 1975 the value of this ratio was quoted as being in the range 0.6-0.9!

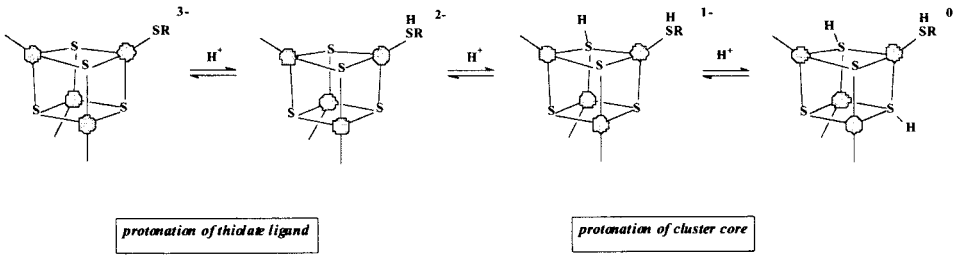

Figure 23. The protonation states and sites of $[Fe_4S_4(SPh)_4]^{3-}$.

A recent study on the reactions of $[Fe_4S_4(SPh)_4]^{3-}$ shows a behaviour which may be more pertinent to what happens in nitrogenases [78]. Studies on the protonation of $[Fe_4S_4(SPh)_4]^{3-}$ in MeCN have shown that at high concentrations of $[lutH]^+$ (lut = 2,6-dimethylpyridine) the cluster binds three protons, as shown in Figure 23, with one of the thiolate ligands protonated and two of the μ_3-S.

It is only this triprotonated cluster which is capable of evolving dihydrogen or converting acetylene into ethylene (*vide infra*). In the absence of any substrate the triprotonated cluster evolves stoichiometric amounts of dihydrogen, according to Equation (20), the limiting reactant being the cluster which supplies the electrons to accomplish the reaction, being oxidised to $[Fe_4S_4(SPh)_4]^{2-}$ in the process. The detailed pathway for dihydrogen formation is unknown but could well involve migration of hydrogen from sulfur to metal.

$$[Fe_4S_2(SH)_2(SPh)_3(SHPh)] \longrightarrow [Fe_4S_3(SH)(SPh)_3(SHPh)] + 0.5H_2 \qquad (20)$$

In the presence of acetylene the triprotonated cluster produces ethylene and evolves less dihydrogen. An important point is that there is a balance of electrons: if the electrons are not going into the formation of dihydrogen they are going into the formation of ethylene, as shown in Figure 24. As the concentration of acetylene is increased, progressively more ethylene, and less dihydrogen, is produced. However, the production of dihydrogen can never be entirely suppressed, and a limiting product distribution comprising *ca*70% ethylene and *ca*30% dihydrogen is obtained. This can be described by the limiting stoichiometry in Equation (21).

$$2C_2H_2 + 6H^+ + 6e \longrightarrow 2C_2H_4 + H_2 \qquad (21)$$

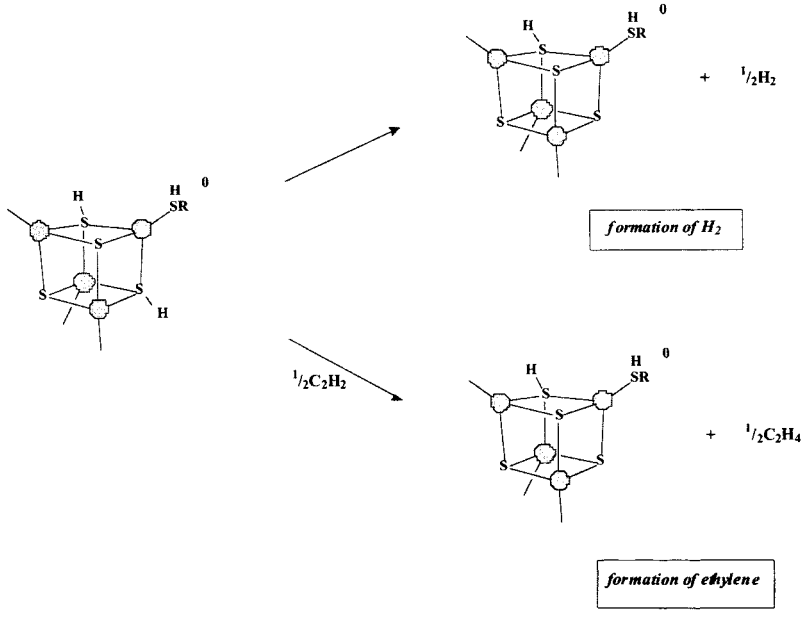

Figure 24. Parallel pathways for the conversions of H^+ into H_2 and C_2H_2 into C_2H_4 at $[Fe_4S_4(SPh)_4]^{3-}$.

Clearly, this limiting stoichiometry is an approximation, but the most important feature is that the only mechanistic significance of this stoichiometry is that bound acetylene is an insufficiently good electron sink to route all the electrons towards its reduction, and the pathway resulting in dihydrogen can never be entirely suppressed.

Perhaps this study on $[Fe_4S_4(SPh)_4]^{3-}$ is closer to what happens during the reduction of dinitrogen at FeMo-cofactor in the enzyme. It is conceivable that the limiting stoichiometries of the various nitrogenases {Equations (11), (18) and (19)} merely reflect the ability of dinitrogen in each enzyme to divert the electron-flux away from dihydrogen production.

Certainly, FeMo-cofactor, even removed from the polypeptide, is capable of reducing protons to dihydrogen. The electrochemical behaviour of FeMo-cofactor has been investigated [79,80] and two redox waves have been observed at –0.32V and *ca* –1.0V (relative to NHE). These potentials are modified slightly by binding of thiol. If a relatively acidic thiol such as C_6F_5SH is used then electrochemical studies reveal a catalytic process in which dihydrogen is being produced, and this occurs at the relatively high potential of –0.28V.

16.3.4 Role of Hydrides in the Transformation of Substrates

At its most basic level, nitrogenase operates by binding dinitrogen to an electron-rich site and subsequently transforms the dinitrogen by a sequence of coupled electron- and proton-transfer reactions. Thus, it is to be expected that metal-hydrides would be formed either because the electron-rich metal is the preferred site of protonation, or because initial protonation of the substrate is followed by proton transfer to the metal. Two limiting situations can be envisaged. Either protonation of the metal is a side reaction which is unnecessary for the transformation of the substrate, or is an essential pre-requisite to the action of the enzyme. Studies on model complexes indicate that both can occur depending on the substrate. Herein we will discuss the chemistry of those substrates where hydrides are involved either directly or indirectly. Although hydrides may be important to all substrates, there is only information on a few; we will discuss only those where evidence is available.

16.3.4.1 Transformation of Dinitrogen.

The most well defined chemical system for the conversion of dinitrogen into ammonia at a metal site is that developed [81,82] with complexes of the type $[M(N_2)_2(PR_3)_4]$ {M = Mo or W; PR_3 = monodentate tertiary phosphine or 0.5(bidentate tertiary diphosphine)}. The cycle by which dinitrogen is transformed into ammonia by protonation and electron transfer reactions is illustrated in Figure 25.

While exploring the protonation chemistry of mononuclear dinitrogen complexes, metal-hydride species were observed. This is because the $\{M(PR_3)_4\}$ sites are electron-rich and thus protonation under the right circumstances can occur at the metal rather than the ligand. Hydride formation is particularly evident in the early stages of the cycle (ie M-N_2, M-NNH and M-NNH_2). However, protonation at the metal centre is not beneficial to the activation of the dinitrogen as illustrated by the study illustrated in Figure 26. The reaction of *trans*-$[Mo(N_2)_2(Et_2PCH_2CH_2PEt_2)_2]$ with an excess of anhydrous HCl in tetrahydrofuran produces $[MoH(N_2)_2(Et_2PCH_2CH_2PEt_2)_2]^+$ which has been isolated and characterised [83]. At low concentrations of HCl, dinitrogen dissociates from $[MoH(N_2)_2(Et_2PCH_2CH_2PEt_2)_2]^+$ and $[MoH_2Cl_2(Et_2PCH_2CH_2PEt_2)_2]$ is ultimately produced. Thus, initial protonation of the metal to produce a hydride, labilises dinitrogen towards dissociation. This type of reaction has also been observed [84] in the analogous reactions of anhydrous HCl with *trans*-$[M(N_2)_2(Ph_2PCH_2CH_2PPh_2)_2]$ (M = Mo or W). However, with the more electron-releasing $Et_2PCH_2CH_2PEt_2$ ligand, increasing the concentration of HCl produces progressively less $[MoH_2Cl_2(Et_2PCH_2CH_2PEt_2)_2]$ and more *trans*-$[Mo(NNH_2)Cl(Et_2PCH_2CH_2PEt_2)_2]^+$. At high concentrations of acid, the hydrazide complex is the exclusive product. The two pathways are summarised in Figure 26.

A detailed discussion of the factors controlling protonation at the metal or ligand is pertinent at this point. Studies have shown that protonation of end-on coordinated dinitrogen ligands, when bound to electron-rich sites occurs at, or close to, the diffusion-controlled limit (protonation of a stereochemical lone pair of electrons on nitrogen atom). In contrast, protonation of the metal is several orders of magnitude slower (severe electronic and structural reorganisations necessary upon protonation). Now, formation of the hydrazide requires not only protonation of one of the dinitrogen ligands, but also, dissociation of the other *trans*-dinitrogen. With the electron-releasing $Et_2PCH_2CH_2PEt_2$ co-ligand dissociation of the dinitrogen is slow. Thus, although protonation of one dinitrogen is faster than protonation of the molybdenum, the poor lability of the *trans*-dinitrogen allows the complex time to protonate at the molybdenum (a kinetically slower but thermodynamically more irreversible process). Protonation of the metal deactivates the dinitrogen by making them less basic and more labile resulting in $[MoH_2Cl_2(Et_2PCH_2CH_2PEt_2)_2]$. With the analogous $[MoH(N_2)_2(Ph_2PCH_2CH_2PPh_2)_2]^+$ this is the only pathway observed under all conditions. With the more electron-releasing $Et_2PCH_2CH_2PEt_2$ ligand the dinitrogen ligands are sufficiently basic that at high concentrations of HCl protonation can still occur. Generation of $[MoH(NNH)(N_2)(Et_2PCH_2CH_2PEt_2)_2]^{2+}$ labilises the complex to dissociation of the dinitrogen. Subsequent binding of chloride and loss of the hydride ligand (as a proton) result in the hydrazide product.

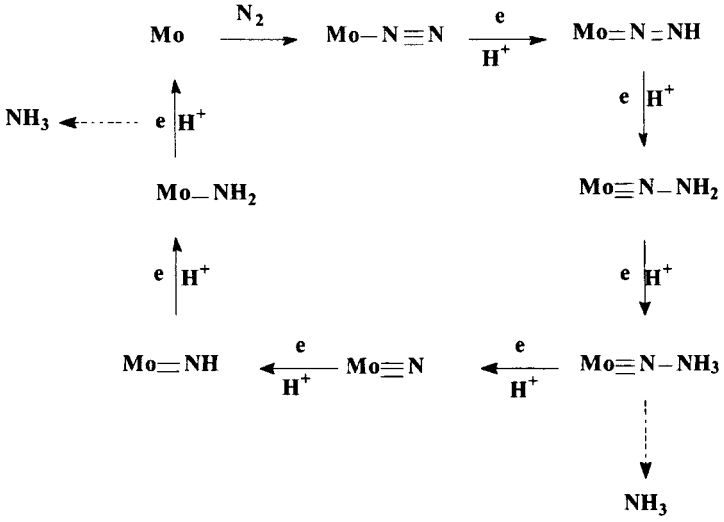

Figure 25. The conversion of coordinated N_2 into NH_3 at a mononuclear metal site, as defined by the chemistry at $[M(N_2)_2(PR_3)_4]$ (M = Mo or W; PR_3 = monodentate tertiary phosphine or 0.5(bidentate ditertiary phosphine).

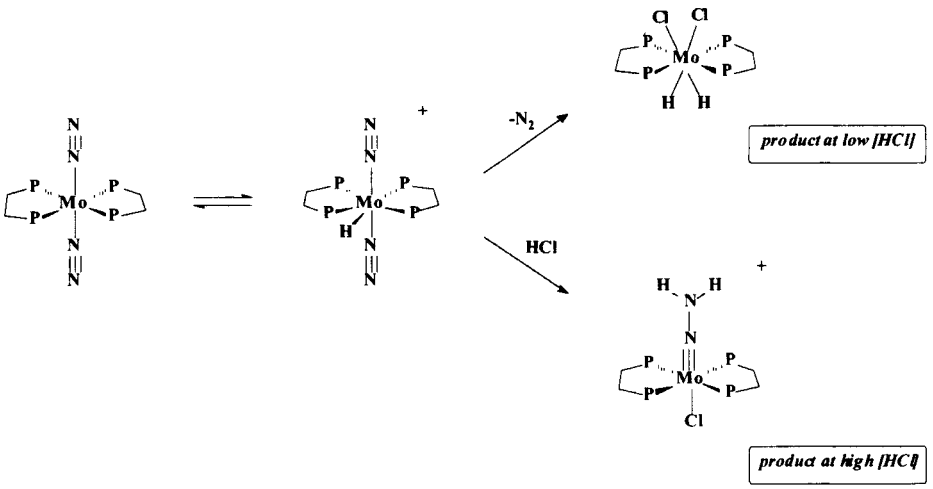

Figure 26. Reactions of anhydrous HCl with *trans*-$[Mo(N_2)_2(Et_2PCH_2CH_2PEt_2)_2]$ involving the enforced intermediacy of $[MoH(N_2)_2(Et_2PCH_2CH_2PEt_2)_2]^+$. Substituents on diphosphine ligands omitted for clarity.

There is no evidence for the intramolecular migration of the hydride in the reaction of *trans*-$[Mo(N_2)_2(Et_2PCH_2CH_2PEt_2)_2]$. In fact the transfer of a proton from metal to dinitrogen ligand is accomplished by a sequence of acid-base catalysed reactions. Indeed, there are very few reactions of nitrogenous ligands

where true intramolecular proton migration between metal and ligand has been demonstrated. This is exemplified in the so-called insertion of diazonium cations into metal-hydride bonds [85]. Kinetic studies [86,87] on the reaction of diazonium cations (ArN_2^+) with $[RhHCl_2(PEtPh_2)_3]$ and $[PtHCl(PEt_3)_2]$ to form aryldiazene complexes indicate that the reaction is neither an insertion, nor an intramolecular migration. Rather the mechanism involves initial binding of the diazonium cation to the metal. This facilitates the release of the hydride as a proton, then recapture of H^+ by the nitrogen atom adjacent to the metal, to give the aryldiazene complex as shown in Figure 27.

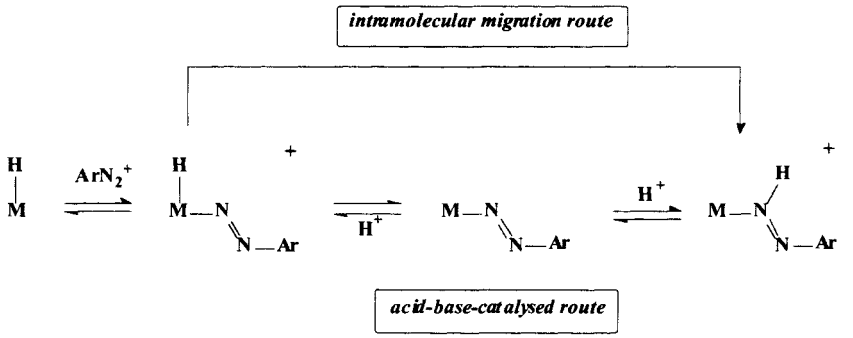

Figure 27. Possible mechanisms for the "insertion" of ArN_2^+ into M-H bonds involving either acid-base catalysis or intramolecular migration routes.

It is likely that many of the so-called insertion of diazonium salts into metal hydride bonds (as typified by those of Pt [85], Ru [88], Rh [88], Os [88] and Ir [89]) are accomplished by mechanisms other than intramolecular migration. However, intramolecular proton transfer between metal and ligand has been observed [90]. As shown in Equation (22), $[W(\eta^5\text{-}C_5Me_5)_2H(NNHAr)]^+$ contains a bent hydrazide ligand. Upon warming, the rearrangement to form a side-on coordinated hydrazide(1-) ligand occurs, which involves the movement of a hydrogen from tungsten to nitrogen.

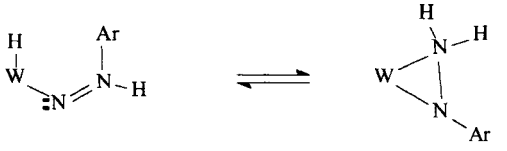

(22)

16.3.4.2 Transformation of other Nitrogen-Containing Substrates.

The reactions at the $\{M(PR_3)_4\}$ (M = Mo or W) site, typified by those of *trans*-$[Mo(N_2)_2(Et_2PCH_2CH_2PEt_2)_2]$ discussed above, involve the formation of hydrides despite protonation at ligand sites being more rapid. Although protonation of the metal is the wrong site the system can subsequently "correct" itself by a series of acid-base reactions. In other systems it is known that the ligand is protonated initially and subsequently the proton moves on to the metal. This is most noted in the reactions of nitriles [91] (in $[ReCl(NCR)(Ph_2PCH_2CH_2PPh_2)_2]$) and isonitriles [92] (in $[Mo(CNR)_2(Ph_2PCH_2CH_2PPh_2)_2]$), as shown in Figures 28 and 29.

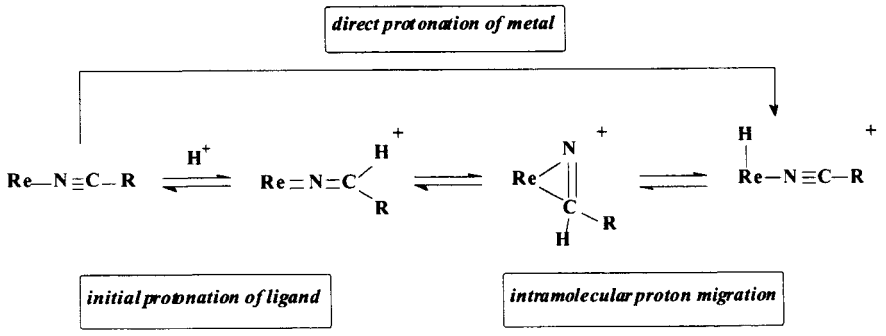

Figure 28. Proposed pathway for the intramolecular transfer of a proton from carbon to metal in $[ReCl(NCR)(Ph_2PCH_2CH_2PPh_2)_2]$.

In both the nitrile and isonitrile complexes rapid reaction techniques indicate that protonation occurs at the ligand initially, but subsequent rearrangement yields a metal-hydride product. However, in both cases protonation is at the atom remote from the metal and so the transfer from ligand to metal must involve the proton either: (i) "sliding" down the ligand or (ii) sequentially "hoping" from one atom to another as shown in the Figures 28 and 29.

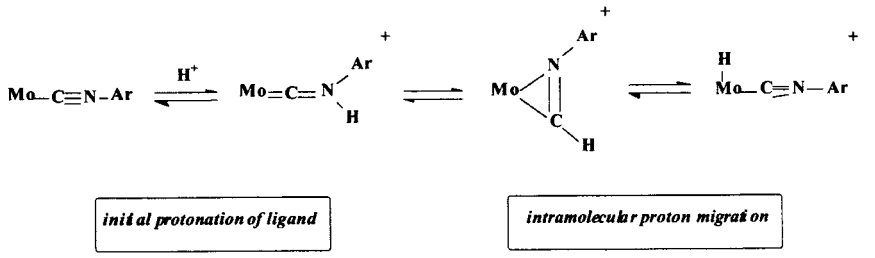

Figure 29. Proposed pathway for the intramolecular transfer of a proton from nitrogen to metal in $[Mo(CNR)(Ph_2PCH_2CH_2PPh_2)_2]$.

16.3.4.3 Transformation of Alkynes.

In the laboratory nitrogenase will transform a wide range of substrates it is unlikely to meet in its natural environment. Arguably the most important of these is acetylene, since it is used as a convenient test for nitrogenase content of soils.

The various nitrogenases differ slightly in their reaction with acetylene [55]. All nitrogenases produce predominantly ethylene and in all cases the reaction is stereospecific, with C_2D_2 transformed [93] into *cis*-CHD=CHD. For the Mo-based nitrogenase this is the exclusive product, but with the V-based and Fe-only nitrogenases some ethane is also produced.

Pre-steady state kinetic studies [94,95] on the conversion of acetylene to ethylene by the Mo-based enzyme have shown that: (i) acetylene will bind at states E_1 or E_2 (*ie* states of the enzyme more oxidised than those necessary to bind dinitrogen) and (ii) ethylene is not produced until three electrons (and implied protons) have been added. These features are shown in Figure 30

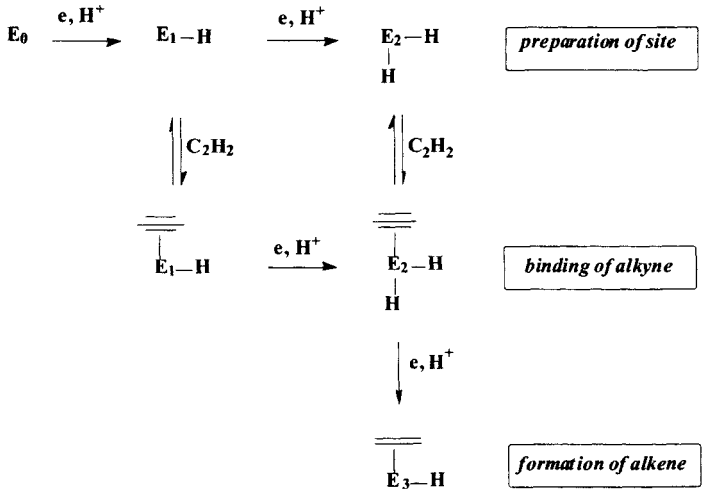

Figure 30. Summary of the states of the MoFe-protein of nitrogenase which interact with C_2H_2 and C_2H_4. Compare with Figure 13.

It has been proposed that (i) and (ii) could be rationalised if the mechanism involved the transient formation of an ethyl intermediate [95]. It was argued that the three electrons and protons added to the coordinated acetylene would result in a coordinated ethyl species. If the active site is coordinatively-unsaturated, β-elimination of the ethyl ligand can occur to produce ethylene and a metal hydride. Such behaviour is well-established in organometallic chemistry and specifically has been demonstrated [96] at the $\{M(R_2PCH_2CH_2PR_2)_2\}$ site (M = Mo or W; R = Ph or Et) as shown in Figure 31.

The problem with this proposal is that it is difficult to rationalise the stereospecificity of the reaction. Consider the reaction with C_2D_2. Formation of the C-C single bond in the M-$CHDCH_2D$ species, followed by β-elimination, would result in a mixture of *cis*- and *trans*-CHDCHD because of free rotation about the C-C single bond. It was argued that steric constraints in the active site of the enzyme enforced the observed formation of *cis*-alkene [95] by restricting rotation about the C-C axis of the ethyl ligand. The proposal that the geometry of the active site can restrict C-C rotation is pushing credibility too far.

Studies on chemical models show that the stereospecific formation of *cis*-CHD=CHD is not a consequence of any constraints imposed by the enzyme. It has been shown that $[Fe_4S_4(SPh)_4]^{3-}$ reduces acetylene to ethylene in the presence of a proton source (*vide supra*), and when the reaction is performed in the presence of deutero-acid stereoselective formation of *cis*-CHD=CHD [97] is observed. Indeed, even simpler systems show that even in structurally very symmetrical complexes, such as $[V(\eta^5\text{-}C_5H_5)_2(\eta^2\text{-}RCCR')]$, alkynes are converted to *cis*-alkenes upon protonation [98,99]. In some cases this transformation has been shown to operate through the intermediate formation of a hydride.

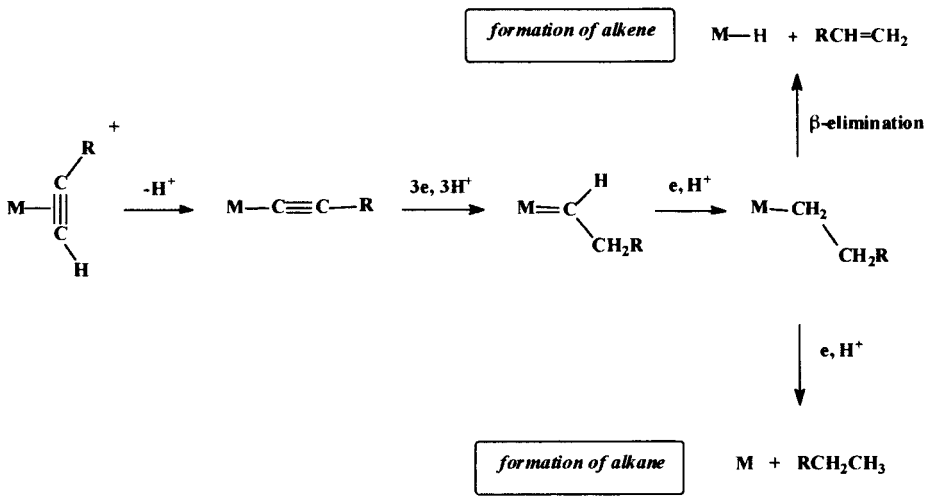

Figure 31. Protonation reactions and transformations of alkynes when bound to electron-rich {M(diphosphine)$_2$} (M = Mo or W; diphosphine = $Ph_2PCH_2CH_2PPh_2$ or $Et_2PCH_2CH_2PEt_2$) sites.

Clearly the stereoselectivity observed both in the simple chemical systems and in the enzyme must be a consequence of the intimate mechanism of coordinated acetylene being transformed into ethylene. Consideration of the η^2-alkyne ligand shows that *cis*-alkenes are exclusively formed as a consequence

of initial protonation at the metal to form a hydride as shown in Figure 32. Migration of the hydride to the alkyne ligand naturally produces the *cis*-vinyl ligand, and subsequent protonation of the vinyl ligand at the metal-carbon bond produces the *cis*-alkene.

If initial protonation occurs directly at the alkyne then a *trans*-vinyl ligand is produced, and subsequent further protonation produces the *trans*-alkene. The key features of this reaction are: (i) that no C-C single bond is formed, and thus the initial site of protonation defines the stereochemistry of the alkene and (ii) hydrido-species are an essential requirement for the preferential formation of *cis*-alkenes, since this is the pathway by which protonation generates *cis*-vinyl species.

In this mechanism the destruction of the stereospecificity can only come about if the second protonation occurs at the carbon atom remote from the metal. This will result in the formation of an alkylidene and even if deprotonation can occur, the rapid rotation about the C-C single bond would result in the loss of stereospecificity.

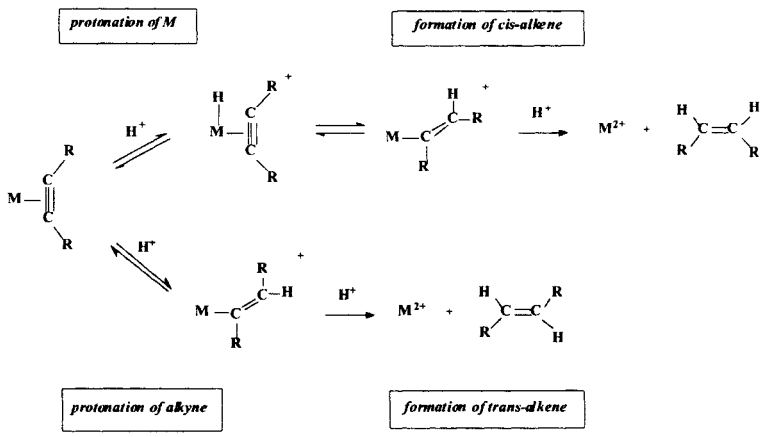

Figure 32. The regioselective protonation of alkyne complexes, leading to stereoselective formation of *cis* or *trans*-alkenes.

16.4 SUMMARY

This review has focused on the possible roles for metal hydrides on two metalloenzymes which are currently still the focus of active research: hydrogenaes and nitrogenases. Besides the obvious role of hydrides being crucial intermediates in the uptake and production of dihydrogen in both these enzymes,

participation of hydrides in the binding and transformation of dinitrogen (and other substrates) in nitrogenases has also been included.

Understanding how these enzymes operate has been helped by complementary studies on the enzyme and simple inorganic complexes. The reactivity of the complexes aim to model the putative elementary reactions of the enzymes. The interplay between enzymological and bio-mimetic study has been a recurring theme throughout this chapter. Whilst the involvement of metal hydrides in enzyme action is of interest in its own right, just as intriguing is the chemistry of the model systems. Of course not all the chemistry that has developed from these model complexes has biological significance. Nonetheless all the studies have led to exciting new chemistry which would perhaps not have been found if it were not for the intellectual driving force of the search to understand the action of the hydrogenases and nitrogenases.

REFERENCES

1. D Dolphin (ed), B_{12}, Wiley, New York, 1982.
2. L G Marzilli, *Bioinorganic Catalysis* (ed J Reedijk and E Bouwman), Marcel Dekker, New York, 1999, ch 13.
3. R Cammack and P van Vliet, *Bioinorganic Catalysis* (ed J Reedijk and E Bouwman), Marcel Dekker, New York, 1999, ch 9.
4. J C Fontecilla-Camps, *J Biol Inorg Chem*, 1996, ***1***, 91.
5. M Frey, *Structure*, 1998, ***90***, 98.
6. R K Thauer, A R Klein and G C Hartmann, *Chem Rev*, 1996, ***96***, 3031.
7. A Volbeda, M –H Charon, C Piras, E C Hatchikian, M Frey and J C Fontecilla-Camps, *Nature*, 1995, ***373***, 580.
8. A Volbeda, E Garcin, C Piras, A L deLacey, V M Fernandez, E C Hatchikian, M Frey and J C Fontecilla-Camps, *J Am Chem Soc*, 1996, ***118***, 12989.
9. J C Fontecilla-Camps, M Frey, E Garcin, C Hatchikian, Y Montet, C Piras, X Vernede and A Volbeda, *Biochimie*, 1997, ***79***, 661.
10. Y Higuchi, H Ogata, K Miki, N Yasuo and T Yagi, *Structure*, 1997, ***5***, 1671.
11. J W Peters, W N Lanzilotta, B J Lemon and L C Seefeldt, *Science*, 1998, ***282***, 1853.
12. E Garcin, X Vernede, E C Hatchikian, A Volbeda, M Frey and J C Fontecilla-Camps, *Structure*, 1999, *7*, 557.
13. Y Higuchi, H Otaga, K Miki, N Yasuo and T Yagi, *Structure*, 1999, *7*, 549.
14. Y Nicolet, C Piras, P Legrand, C E Hatchikian and J C Fontecilla-Camps, *Structure*, 1999, *7*, 13.
15. A Le Cloirec, S P Best, S Borg, S C Davies, D J Evans, D L Hughes and C J Pickett, *J Chem Soc, Chem Comm*, 1999, 2285.
16. T M van der Spek, A F Arendsen, R P Happe, S Yum, K Bagley, D J Stufkens, W R Hagen and S P J Albracht, *Eur J Biochem*, 1996, ***237***, 629.

17. A J Pierek, M Hulstein, W Hagen and S P J Albracht, *Eur J Biochem*, 1998, ***258***, 572.
18. V M Fernandez, E C Hatchikian, D S Patil and R Cammack, *Biochim Biophys Acta*, 1986, ***883***, 145.
19. L M Roberts and P A Lindahl, *Biochem*, 1994, ***33***, 14339.
20. L M Roberts and P A Lindahl, *J Am Chem Soc*, 1995, ***117***, 2565.
21. S P J Albracht, *Biochim Biophys Acta*, 1994, ***1188***, 167.
22. S P J Albracht, E G Graft and R K Thauer, *FEBS Letts*, 1982, ***140***, 311.
23. J R Lancaster, *Science*, 1982, ***216***, 1324.
24. M Teixevira, I Moura, A V Xavier, J J G Moura, J Legall, D V DerVartanian, H D Peck Jnr and B Huynh, *J Biol Chem*, 1989, ***264***, 16435.
25. J W van der Zwaan, S P J Albracht, R D Fontiju and E C Slater, FEBS Letts, 1985, ***179***, 271.
26. A Chapman, R Cammack, E Chatchikian, J McCracken and J Peisach, *FEBS Letts*, 1988, ***242***, 134.
27. C L Fan, M Teeixeira, J Moura, I Moura, B M Huynh, J Legall, H D Peck and B M Hoffman, *J Am Chem Soc*, 1991, ***113***, 20.
28. A Chapman, R Cammack, E Chatchikian, J McCracken and J Peisach, *FEBS Letts*, 1988, ***242***, 134.
29. F Dole, A Fournel, V Magro, E C Hatchikian, P Bertrand and B Guiliarelli, *Biochemistry*, 1997, ***36***, 7847.
30. L De Gloia, P Fantucci, B Guigliarelli and P Bertrand, *Inorg Chem*, 1999, ***38***, 2658.
31. M Pavlov, P E M Siegbahn, M R A Bolmberg and R H Crabtree, *J Am Chem Soc*, 1998, ***120***, 548.
32. I Dance, *J Chem Soc, Chem Comm*, 1999, 1655.
33. D J Evans, R A Henderson and B E Smith, *Bioinorganic Catalysis* (ed J Reedijk and E Bouwman), Marcel Dekker, New York, 1999, ch 7.
34. I G Dance, *J Chem Soc, Chem Comm,* 1998, 523.
35. T E Burrows, A Hills, D L Hughes, J D Lane, R H Morris and R L Richards, *J Chem Soc, Dalton Trans*, 1991, 1813.
36. R Fandos, M Lanfranchi, A Otero, M A Pellinghelli, M J Ruiz and P Terreros, *Organometallics*, 1996, ***15***, 4725.
37. P B Hitchcock, D L Hughes, M J Maguire, K Marjani and R L Richards, *J Chem Soc, Dalton*, 1997, 4747.
38. M Y Darensbourg, W –F Liaw and C G Riordan, *J Am Chem Soc*, 1989, ***111***, 8051.
39. J R Gaylor and C V Senoff, *Can J Chem*, 1972, ***50***, 1868.
40. K Kiriakidou, M R Plutino, F Prestopino, M Monari, M Johansson, L I Elding, E Valls, R Gobetto, S Aime and E Nordlander, *J Chem Soc, Chem Comm*, 1998, 2721.
41. M Schlaff and R H Morris, *J Chem Soc, Chem Comm*, 1995, 625.
42. R H Crabtree, *"The Organometallic Chemistry of Transition Metals"* (2nd edition), Wiley, New York, 1994, p161.
43. R A Henderson, *J Chem Soc, Dalton Trans*, 1995, 503.
44. W Clegg and R A Henderson, submitted for publication.

45. K Izutsu, *"Acid-Base Dissociation Constants in Dipolar Aprotic Solvents"* Blackwell Scientific, Oxford, 1990.
46. V R Almeida, C A Gormal, K L C Gronberg, R A Henderson, K E Oglieve and B E Smith, *Inorg Chim Acta*, 1999, ***291***, 212.
47. D Sellmann and J Sutter, *Acc Chem Res*, 1997, ***30***, 460.
48. R A Henderson, *Angew Chemie*, 1996, ***35***, 946.
49. K W Kramarz and J R Norton, *Prog Inorg Chem*, 1994, ***42***, 1.
50. S S Kristjansdottir and J R Norton, *Transition Metal Hydrides: Recent Advances in Theory and Experiment*, (ed A Dedieu), 1992, ch9.
51. D S Moore and S D Robinson, *Chem Soc Rev*, 1983, 415.
52. D Sellmann, J Kappler and M Moll, *J Am Chem Soc*, 1993, ***115***, 1830.
53. S C Davies, R A Henderson, D L Hughes and K E Oglieve, *J Chem Soc, Dalton Trans*, 1998, 425.
54. R A Henderson, S K Ibrahim, K E Oglieve and C J Pickett, *J Chem Soc, Chem Comm*, 1995, 1571.
55. R R Eady, *Chem Rev*, 1996, ***96***, 3013.
56. J B Howard and D C Rees, *Chem Rev*, 1996, ***96***, 2965.
57. B K Burgess and D J Lowe, *Chem Rev*, 1996, ***96***, 2983.
58. B E Smith and R R Eady, *Eur J Biochem*, 1992, ***205***, 1.
59. M L Tobe and J Burgess, *Inorganic Reaction Mechanisms,* Addison Wesley, Longman, Harlow, 1999, ch10.
60. R H Crabtree, *Inorg Chim Acta*, 1986, ***125***, L7.
61. E K Jackson, G W Parshall and R W F Hardy, *J Biol Chem*, 1968, ***243***, 4952.
62. R N F Thorneley and D J Lowe, *Molybdenum Enzymes* (ed T G Spiro), Wiley Interscience, New York, 1985, p221.
63. B K Burgess, S Wherland, W E Newton and E I Stiefel, *Biochem*, 1981, ***20***, 5140.
64. R Ellis, R A Henderson, A Hills and D L Hughes, *J Organomet Chem*, 1987, ***333***, C6.
65. D Dawson, R A Henderson, A Hills and D L Hughes, *Polyhedron*, 1989, ***8***, 1870.
66. D M Dawson, R A Henderson, A Hills and D L Hughes, *J Chem Soc, Dalton Trans*, 1992, 969.
67. D M Dawson, R A Henderson, A Hills and D L Hughes, *J Chem Soc, Dalton Trans*, 1992, 973.
68. N Kashef and R L Richards, *J Organomet Chem*, 1989, ***365***, 309.
69. R A Henderson, *J Chem Soc, Chem Comm*, 1987, 1670.
70. G G Hlatky and R H Crabtree, *Coord Chem Rev*, 1985, ***65***, 1.
71. K E Oglieve and R A Henderson, *J Chem Soc, Chem Comm*, 1992, 441.
72. M G Basallote, J Durain, J Fernandez-Trujillo and A Manez, *J Organomet Chem*, 2000, ***609***, 29.
73. D L Hughes, S K Ibrahim, G Querne, A Laouenan, J Talarmin, A Querios, A Fouseca and C J Pickett, *Polyhedron*, 1994, ***13***, 3341.
74. B K Burgess, S Wherland, W E Newton and E I Stiefel, *Biochemistry*, 1981, ***20***, 5140.
75. C J Pickett, *J Biol Inorg Chem*, 1996, ***1***, 601.
76. S A Fairhurst, R A Henderson, D L Hughes, S K Ibrahim and C J Pickett, *J Chem Soc, Chem Comm*, 1995, 1569.

77. K L C Gronberg, C A Gormal, M C Durrant, B E Smith and R A Henderson, *J Am Chem Soc*, 1998, ***120***, 10613.
78. K L C Gronberg, R A Henderson and K E Oglieve, *J Chem Soc, Dalton Trans*, 1998, 3093.
79. P A Schultz, S F Gheller, B K Burgess, S Lough and W E Newton, *J Am Chem Soc*, 1985, ***107***, 5364.
80. B E Smith, M C Durrant, S A Fairhurst, C A Gormal, K L C Gronberg, R A Henderson, S K Ibrahim, T LeGall and C J Pickett, *Coord Chem Rev*, 1999, ***185***, 669.
81. J Chatt, J R Dilworth and R L Richards, *Chem Rev*, 1977,***78***, 589.
82. R A Henderson, G J Leigh and C J Pickett, *Adv Inorg Chem and Radiochem*, 1983, ***27***, 198.
83. R A Henderson, *J Chem Soc, Dalton Trans*, 1984, 2259.
84. J Chatt, G A Heath and R L Richards, *J Chem Soc, Dalton Trans*, 1974, 2074.
85. G W Parshall, *J Am Chem Soc*, 1965, ***87***, 2133.
86. R A Henderson, *J Chem Soc, Dalton Trans*, 1985, 2067.
87. V L Frost and R A Henderson, *J Chem Soc, Dalton Trans*, 1985, 2059.
88. K R Laing, S D Robinson and M F Uttley, *J Chem Soc, Dalton Trans*, 1973, 2713.
89. L Toniolo and R Eisenberg, *J Chem Soc, Chem Comm*, 1971, 445.
90. J A Carroll and D Sutton, *Inorg Chem*, 1980, ***19***, 3137.
91. J J R Frausto da Silva, M F C Guedes da Silva, R A Henderson, A J L Pombeiro and R L Richards, *J Organomet Chem*, 1993, ***461***, 141.
92. R A Henderson, A J L Pombeiro, R L Richards, J J R Frausto da Silva and Y Wang, *J Chem Soc, Dalton Trans*, 1995, 1193.
93. M J Dilworth, *Biochim Biophys Acta*, 1966, ***127***, 283.
94. G A Ashby, M J Dilworth and R N F Thorneley, *Biochem J*, 1987, ***247***, 547.
95. D J Lowe, K Fisher and R N F Thorneley, *Biochem J*, 1990, ***272***, 621.
96. A Hills, D L Hughes, N Kashef, M A N D A Lemos, A J L Pombeiro and R L Richards, *J Chem Soc, Dalton Trans*, 1992, 1775.
97. R S McMillan, J Renauld, J G Reynolds and R H Holm, *J Inorg Biochem*, 1979, ***11***, 213.
98. R A Henderson, D J Lowe and P Salisbury, *J Organomet Chem*, 1995, ***489***, C22.
99. J A Labinger and J Schwartz, *J Am Chem Soc*, 1975, ***97***, 1596.

This Page Intentionally Left Blank

Chapter 17

Proton Wave Functions in Palladium Studied by Ab Initio Calculations and Inelastic Neutron Scattering Methods

D.K. Ross[a], J.E. Totolici[a], M. Kemali[a], I. Morrison[a], A. Ivanov[b], M.R. Johnson[b] and C. Elsässer[c]

[a]*Institute of Materials Research, University of Salford, Salford, M5 4WT, U.K.*
[b]*Institut Laue-Langevin, Grenoble, France*
[c]*Max Planck Institut für Metallsforschung, D-70174, Stuttgart, Germany*

CONTENTS

17.1 INTRODUCTION

This chapter is concerned with a major class of hydrides, namely compounds, whether stoichiometric or non-stoichiometric, that are produced by the direct solution of hydrogen in metals. The major interest has been in the metallic hydrides rather than the saline hydrides, that is to say, in the electrically conducting compounds [1]. Here, we can distinguish between those systems that are formed exothermically and the remainder that are produced endothermically. The latter can only form hydrides at high hydrogen pressures (e.g. NiH [2]). At normal pressures and ambient temperatures, these will only form solid solutions of hydrogen in the metal lattice. For free energy reasons, in these systems the hydrogen solubility increases with temperature. In contrast, exothermic systems will form stable hydrides at ambient temperatures and pressures. For binary systems, stable hydrides are formed with a number of transition metals including the classic case of palladium as discovered by Graham in 1866 [3], the rare earths and the actinides. There are also a wide variety of intermetallic hydrides [4].

Probably the major feature that distinguishes metallic hydrides from the organic hydrides that form the major topic of this volume is that they are electrical conductors. This is simply because the electron from the hydrogen atom is donated to the delocalised electronic structure of the metal. In general, some of the extra electrons appear as low-lying s-like states while some go to the conduction band of the metal. Electrons at the Fermi Surface are scattered by the positive charge of the proton and thus screen it to a greater or lesser extent, depending on the metal.

Where the hydrogen is more electronegative than the metal, the resulting electron density in an atomic sphere around the hydrogen will exceed that of the proton and the binding will thus have an ionic character. In these systems, the hydrogen atoms tend to locate themselves remote from the electron density of the metal, e.g. in the tetrahedral sites in an f.c.c. lattice (ZrH_2). On the other hand, where the screening is weaker (longer-ranged) e.g. palladium, the atomic sphere around the proton will have a net positive charge and it will seek a site where the metallic electron density is high, as at the octahedral site in f.c.c structures (e.g. palladium)[5].

Metallic hydrides are of considerable scientific interest for a variety of reasons. They are, for instance, excellent examples of lattice gases because they form wide solid solution ranges at sufficiently high temperatures and also often form a number of different super-lattices at lower temperature. By equilibrating the system with hydrogen gas at a given temperature and pressure, we can define the chemical potential of the system and this quantity can then be modelled using the methods of statistical thermodynamics. The mobility of hydrogen in solution in metals is also remarkable and so these systems are convenient for studying solid state diffusion. They are also of interest because of the importance of

the quantum properties of the proton and because of the ready availability of other isotopes with considerably different quantum properties (D, T and μ^+). And finally, of particular relevance to the present chapter, hydrogen is particularly easily measured using neutron scattering techniques due to the large incoherent cross section of the proton [6].

Metal-hydrogen systems are also of considerable interest as a result of their technical applications. A major reason for this stems from the high mobility of the H^+ ion through the lattice. Of late, the main activity here has been concerned with the development of rechargeable metal hydride battery electrodes, where now increasingly high power levels and cycle life times are being achieved, with the expectation that the Ni-Cd rechargeable market will be completely superseded in a few years. The highest power to weight ratio, however, will always be achieved by Li-ion batteries and these will probably in future be the battery of choice in premium markets. Increasingly now, however, global warming is driving interest in replacing hydrocarbons with hydrogen for vehicle propulsion. Prototype vehicles have been propelled using hydrogen stored in intermetallic hydrides with appropriate reversible charging characteristics. However, it is generally recognised that a practical fuel cell system will only emerge if we can achieve at least 7% by mass of hydrogen in the storage system and it seems impossible to achieve this target with metal hydride systems. Thus, for instance, carbon nanotubes or other porous carbon structures currently seem much more likely to achieve this target. However, any general move to a hydrogen economy will undoubtedly involve extensive use of hydrogen permeable membranes and these are likely to be based on a metal in which hydrogen is notably mobile such as Pd. Moreover, there is still a considerable need to fully understand hydrogen embitterment in structural alloys. In the regular lattice of an endothermic absorber such as iron, hydrogen will always exist in small quantities. At lattice defects, however, there will be sites at which the hydrogen is trapped exothermically. Local stress, for instance at crack tips, will reduce the energy of hydrogen atoms on some sites and the mobility of hydrogen will ensure that hydrogen will diffuse to these sites until, locally, a brittle hydride is formed which will then propagate through the material. Also, hydrogen trapped in the vicinity of dislocations actually increases the mobility of the dislocations by always moving to relieve the local stress distribution. The mechanisms involved are thus very complex and difficult to model and have great importance to the design of metallic components under stress, particularly when these are for use in the presence of hydrogen gas.

Given the need in materials development to survey a wide range of possible compositions, there is a clear requirement to be able to simulate on a computer the properties of real systems as part of the optimisation process. Being able to predict and hence survey the properties of "virtual materials" will thus considerably shorten the development times for new applications. Where these appli-

cations involve hydrogen-metal systems, the simulation process will inevitably involve being able to model the quantum properties of hydrogen in the metallic environment. This is the long term motivation of our recent work in testing ab initio modelling methods for the prediction of proton wave functions and the use of neutron scattering to verify these models. In particular, inelastic neutron scattering measures the probability that the neutron will change the quantum state of the proton and this process is a very sensitive test of the ab initio calculations.

17.2 NEUTRON SCATTERING STUDIES OF METAL HYDROGEN SYSTEMS

The traditional physicist's approach to the dynamics of a stoichiometric metal hydride with a periodic lattice is to describe them in terms of phonons, of frequency ω and wave vector, $\mathbf{q}$. There will be 3n dispersion curves, $\omega(\mathbf{q})$, where n is the number of atoms/Bravais lattice point. Of these, there will be three/H in the unit cell that will constitute the "optical" vibrations where the hydrogen atoms are in anti-phase with the metal lattice and therefore the hydrogen atom amplitude will exceed the average metal amplitude in the mass ratio, M_H/M_M. For the same reason, the frequencies will be significantly higher than the acoustic (and optical where there is more than one metal atom/unit cell) modes in the pure metal. In the other dispersion curves, the H atoms will move more or less in phase with at least one of the metal atoms, thus having comparable amplitudes and frequencies to the pure metal modes. As the inelastic neutron scattering cross section is proportional to the vibration amplitude of the scattering nucleus squared and because of the large cross section of hydrogen, the inelastic neutron scattering will be dominated by the optical vibrations of the hydrogen. We should stress here that the phonon theory of lattice vibrations is built entirely on the assumption of harmonic theory, i.e. that the restoring force is always proportional to the displacement of the atoms. When this is translated into quantum theory, the quantum states are uniformly spaced at energy intervals of $\hbar\omega$, whether the excitation considered is localised on one site or delocalised as for a phonon. It is interesting to note that the localised picture, originally due to Fermi [7] and the delocalised phonon picture become equivalent if the dispersion curve is flat because this makes the group velocity zero. In this case, if all the phonon energy is initially on one atom, it stays there indefinitely. If the metal atom is heavy enough, it will show negligible movement in anti-phase to the adjacent hydrogen and so coupling between hydrogen atoms, and hence dispersion, will only arise due to direct H-H interactions.

At this point, we should introduce the difference between coherent and incoherent scattering. The neutron wave is scattered by the nucleus (in the

absence of atomic magnetism) and the amplitude of the scattered wave is proportional to the "scattering length", a, of the nucleus which results from the nature of the specific neutron-nucleus interaction. Because the neutron scattering length is both isotope and neutron spin dependent, it fluctuates from nucleus to nucleus for a given chemical species. Now, the scattering cross section is proportional to the modulus-squared of the sum of the neutron waves scattered from the set of nuclei involved. The details of the mathematics of this process can be found in the standard textbooks on the method [8,9]. Suffice it to say here that the cross section breaks up into two parts. The first, proportional to the square of the average scattering length, $\langle a \rangle^2$, is determined by interference between the scattering from all the atoms in the system, taken in pairs, including the pair involving the nucleus itself (the diagonal of the matrix). This would be the total scattering if all the atoms had the same scattering length, as in the case of X-ray diffraction, and is called coherent scattering. The remaining scattering, which is proportional to $(\langle a^2 \rangle - \langle a \rangle^2)$, is known as the incoherent scattering and is essentially the independent scattering from each atom due to the self-terms. Because there is no interference involved, it is isotropic. Now it happens that the scattering from hydrogen is unique, in that, not only is it some twenty times stronger than from any other nucleus, it is almost entirely incoherent ($\sigma^{inc} = 80$ barns, $\sigma^{coh} = 1.8$ barns, where 1 barn, the traditional unit of cross section, σ, is 10^{-28} m^2). On the other hand, for deuterium, the scattering is similar in magnitude to other elements and is mainly coherent. This distinction is important in using neutron scattering to study the dynamics of hydrogen because the incoherent scattering is just the sum of the scattering from all the hydrogen atoms taken individually and hence is proportional to the frequency distribution of all the phonons in the Brillouin Zone. On the other hand, the coherent scattering has to satisfy the momentum conservation condition

$$\hbar\mathbf{Q} = \hbar\mathbf{q} + \hbar\tau$$

Here $\hbar\mathbf{Q}$ is the momentum transferred from the neutron and τ is one of the reciprocal lattice vectors of the palladium lattice. Thus, the incoherent scattering sees all the vibration modes but the coherent scattering selects one particular phonon for a particular experimental value of $\mathbf{Q}$. It is now clear that both the incoherent and coherent one-phonon scattering will depend on the shape of the optical dispersion curves and hence will be influenced by hydrogen-hydrogen interactions. Indeed, one of the first observations of inelastic scattering from a hydride [10] interpreted the shape of the "optical peak" in terms of a frequency distribution broadened by H-H interactions.

As mentioned above, the localised model used to describe the quantum states of light atoms in a heavy atom matrix is the Simple Harmonic Oscillator [7].

For a site of cubic symmetry, the wave function of the n^{th} excited state in each Cartesian direction is given in terms of the n^{th} Hermite Polynomials and has an energy $(n + 1/2)\hbar\omega$. These states can be labelled (n_i, n_j, n_k). Thus, the general expression for the energy of a state is $(3/2 + n_i + n_j + n_k)\ \hbar\omega$, where i, j and k are the number of quantum states in the x, y and z directions respectively. Thus the ground state (a singlet state) has energy $3/2\ \hbar\omega$; the first excited state (1, 0, 0) is three fold degenerate with an energy $5/2\ \hbar\omega$ while the second excited state, (2,0,0) or (1,1,0) with an energy $7/2\ \hbar\omega$, is six-fold degenerate and so on for higher levels. As mentioned above, the equivalence to the phonon picture is complete if the interactions between adjacent hydrogen atoms can be neglected and the dispersion is therefore negligible. Full accounts of neutron scattering investigations of metal hydride systems can be found in recent reviews [6]. There are also reviews on results for intermetallic hydrides [4].

17.3 THE PALLADIUM HYDROGEN SYSTEM

The results reported in this chapter refer to the palladium-hydrogen system, which, for a number of reasons, is often seen as the prototype metal-hydrogen system. Thus, as mentioned above, palladium was the first known case of a metal that dissolved hydrogen [3]. Moreover, the crystal lattice is very simple (NaCl) and the metal lattice in the hydride case is the same as in the metal (f.c.c.). This is particularly important in that it provides the opportunity to produce single crystals of the stoichiometric hydride, which makes it possible to study the individual excited states of the proton.

As for a number of simple hydrides, the phase diagram resembles a gas/liquid/solid system At room temperature, there is a solid solution phase at low concentrations, the α-phase, while, at H/M ratios greater than 0.6, a non-stoichiometric β-phase, also f.c.c. but with a slightly larger lattice parameter, appears. At low temperatures, the hydrogen atoms become ordered into superlattices, due to their mutual repulsions[6]. At megabar hydrogen pressures, the stoichiometric concentration can be achieved [11,12]. In all phases, the hydrogen atoms are in the octahedral sites; i.e. the stoichiometric composition has the NaCl structure. The α-phase has a lattice parameter of 3.96Å while, in the β-phase, the lattice parameter increases linearly from 4.03Å at $PdH_{0.6}$ to 4.08Å at $PdH_{1.0}$. As the temperature is raised, the two-phase region progressively narrows until the system shows a critical temperature, at which point the two phases become indistinguishable. It is thus possible to form a β-phase hydride without passing through a disruptive phase transition. The Pd-D phase diagram is similar, but with a rather lower critical temperature and pressure. The hydrogen pressure isotherms and the corresponding phase diagram are very similar to

systems like CO_2 - on the basis of this analogy, the α-phase is a lattice gas while the β-phase is a lattice liquid. The general form of the phase diagram is clearly understood in terms of a long-range attraction and a short-range repulsion (the Lacher Model [3]) but is complicated by the nature of the short range repulsions between the H (D) which give rise to a series of superlattices at low temperatures[13].

The incoherent scattering from β-PdH_x shows a peak at 57 meV with a broad shoulder extending up to 100 meV [14]. The optical dispersion curves for PdD_x were first measured by Rowe et al [15] using a triple axis spectrometer. The phonon peaks were rather broad as might be expected due to the non-stoichiometry but the dispersion curves were well-defined and the longitudinal phonons were easily distinguished from the transverse phonons using the polarisation condition, namely that the phonon intensity is proportional to $|\mathbf{u}.\mathbf{Q}|^2$ where **u** is the displacement vector for the phonon in question (u is parallel to **q** for longitudinal phonons and is perpendicular to **q** for transverse phonons). Not surprisingly, there was little dispersion in the transverse modes but the dispersion in the longitudinal modes was substantial, implying an interaction between nearest neighbour hydrogen atoms when their separation is changed. Rahman et al [16] performed dispersion curve calculations for a large superlattice cell, assuming the experimental D/Pd ratio to mimic the non-stoichiometry and using the experimentally defined force constants for PdD_x. They then calculated the corresponding phonon density-of-states and hence the corresponding incoherent scattering for PdH_x. They concluded that the shoulder at high energy was indeed due to the dispersion of the longitudinal optic modes and that the peak at 57 meV corresponded to the flat transverse modes. They also found that it was necessary to make a correction to the mean frequency beyond that expected for hydrogen isotope mass, in going from H to D, which they attributed to anharmonicity in the potential well. Subsequent measurements of the higher excited states of H confirmed the conclusion that the H potential well in Pd/H was far from harmonic but calculations on this effect based on a Taylor's Expansion of the potential energy surface around the centre of the site were not entirely satisfactory [17]. The most accurate measurements of the higher excited states in PdH, for a stoichiometric polycrystalline sample produced under megabar hydrogen pressure [18] showed strong anharmonicity in the higher excited states. Because the sample had strong preferred orientation, it was possible to sample the scattering in different crystallographic directions. It was found that, while the scattering to the first excited state was isotropic, there was clear evidence of directional modulation in the intensity of the second and higher excited states, as predicted by Simple Harmonic Theory [9]. This allowed an identification of the energy levels that could therefore be confidently compared with the predictions of ab initio calculations, which will now be described.

17.4 AB INITIO CALCULATIONS OF METAL-HYDROGEN SYSTEMS

Recent advances in our understanding of the nature of metal-hydrogen systems have come from developments in the ab initio calculations on these systems. These depend on the development of the Local Density Approximation for dealing with the effect of electron-electron correlation on the electronic charge density in the lattice. Computational methods have been developed to minimise the total energy of a lattice by relaxing the nuclear positions and repeating the proper quantum mechanical calculation of the electronic energy [19, 20]. This approach depends on the use of the Born-Oppenheimer Approximation in that one is separating the electronic and nuclear movements because they take place on very different time scales. When one uses this approach for hydrogen metal systems, the assumption is made that one can use the same approximation again to separate the metal and hydrogen movements. Thus, the metal lattice is relaxed with the hydrogen nucleus in the centre of its site. The hydrogen sub-lattice is then moved around in a rigid way and the total energy is calculated at each position of the hydrogen sub-lattice. This predicts the shape of the potential energy surface in which the proton is located. The proton wave functions can now be determined by direct solution of the proton Schrödinger Equation. This technique was developed by Ho et al [21] and by Tao et al [22] for the case of NbH. They were able to predict the higher energy levels in this system with considerable accuracy. The method was extended to the PdH system by Elsässer et al. [23,24], Ho et al [25] and Krimmel et al [26]. The major advance introduced by Elsässer et al arose from the observation that the H potential energy surface on the octahedral site had a very flat bottom but with an approximately parabolic shape for larger displacements. (Fig 1). This meant that the Taylor's Expansion method was quite inappropriate and these authors developed the use of a Fourier Series method for determining the proton wave functions. The resulting energy levels showed excellent agreement with the neutron data [17,18]. It should be noted that, because the potential energy surface can no longer be described in terms of three separable Cartesian parabolic functions, one cannot describe the perturbed energy levels in terms of the Cartesian quantum numbers, (n_i, n_j, n_k). Perturbation Theory predicts a mixing of the Cartesian wave functions and this notation can be carried over to the Fourier Series representation. Thus, the six-fold degenerate second excited state of Simple Harmonic Theory is split into three degenerate (1,1,0) levels, a two-fold degenerate (2,|A>), (2,|B>) level and a 1-fold degenerate (2,|C>) level.

The beauty of this method is that it yields the actual proton wave function for each excited state. We can thus directly use Fermi's Golden Rule to predict the inelastic neutron scattering cross-section for comparison with experiment.

This result can be stated:

$$S_{inc}(\boldsymbol{Q},\omega) = \sum_f \left| \int \phi_i(r)\, exp(-i\,\boldsymbol{Q}.\boldsymbol{r})\, \phi_f(\boldsymbol{r})\, d\boldsymbol{r} \right|^2 . \delta(\varepsilon_f - \varepsilon_i + \hbar\omega) \qquad (1)$$

Here $S_{inc}(\boldsymbol{Q},\omega)$ is the neutron scattering function which can be directly extracted from the measured cross sections, $\phi_i(\boldsymbol{r})$ and $\phi_f(\boldsymbol{r})$ are the initial and final wave functions of the proton, ε_i and ε_f are the initial and final energies and the summation is over all possible final states where the delta function ensured energy conservation. We thus have a framework for testing the ab initio calculations against experiment in a very direct way, and, having established its accuracy, we have a theory that can be extended to predict a number of other important properties of the system. In the following sections, we describe the current state of our work in this direction.

17.5 EXPERIMENTAL MEASUREMENTS OF THE INELASTIC NEUTRON SCATTERING FORM FACTORS FOR SCATTERING TO EXCITED STATES IN Pd-H

We have recently completed a series of inelastic neutron scattering experiments on a single crystal of $PdH_{0.85}$ using the Beryllium Filter INS spectrometer at the Institute Laue-Langevin at Grenoble. A preliminary report on this work has already been published [27]. Two crystals were used, 3 mm diameter x 10 mm long, with axes respectively along the [100] and the [110] directions. The hydrogenation took place well above the critical temperature, 623 K, to avoid damage to the lattice, using a high pressure Sievert's apparatus. Final equilibration took place at ambient temperatures at P = 10^7 Pa. The final concentrations were obtained by weighing. The surfaces were poisoned using Na_2S solution and the crystals were stored at 80 K to avoid loss of hydrogen. They were then mounted in the instrumental cryostat with crystal axes normal to the scattering plane and cooled to 20 K. On the Be Filter Triple Axis Spectrometer, the final energy is fixed at 0.35 meV by the filter. The incident energy was selected using the (220) plane of Cu. Measurements were made in the range 30-400 meV energy transfer, with a resolution of $\Delta\omega/\omega \approx 4\%$. The crystals could be rotated about their axes, which were normal to the scattering plane. Thus, although the magnitude of Q was determined by the energy transfer being observed, the modulation of scattering intensity with direction could be scanned in two relevant scattering planes (one for each crystal). This method is ideal for measuring the incoherent inelastic form factors for scattering from the ground state to the accessible excited states.

17.6 CALCULATIONS OF THE PROTON WAVE FUNCTIONS AND THE INELASTIC SCATTERING CROSS SECTIONS

The adiabatic energy surface obtained by Elsässer et al [23] is shown in Fig 1 and can be understood by reference to the unit cell shown in Fig 2. The origin of the potential energy surface is taken to be at the octahedral site, (1/2,1/2,1/2), and separate curves show the profile in the [001], [110] and [111] directions. The last of these directions goes through a triangular aperture to the tetrahedral site at (1/4,1/4,1/4). The barrier height is 0.28 eV and the energy at the tetrahedral site is 0.08 eV above that of the octahedral site. As the T site will clearly have a higher zero point energy than the O site, this confirms the experimentally observed O site occupancy. The other important point to note is the flatness of the potential around the O site, which is clearly far from harmonic.

Elsässer et al [23] then fitted proton wave functions into this potential energy surface using a Fourier Series representation of the potential energy surface and obtaining a Fourier representation of the corresponding proton wave functions. The resulting energies of the wave functions and of the corresponding measured values are given in Table I. Here, the energy states are described with the following notation:

$$e_{M.|\mu>} = E_{M.|\mu>} - E_{0.|000>}$$

i.e. e represents the energy difference between the zero point energy and the $M.|\mu>$ state where M is the number of quanta of energy (M = l + m + n) and .| $\mu>$ represents the particular eigen-function.

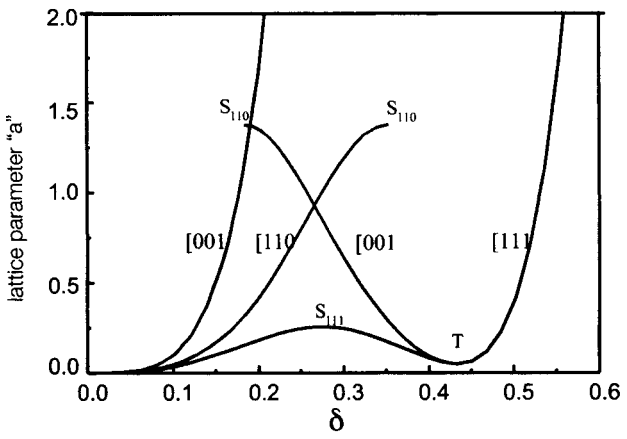

Figure 1. Calculated adiabatic potential energy surface of H in $PdH_{1.0}$ plotted against the displacement of the whole H sublattice in one of the three symmetry directions, [001], [110] and [111], where δ is the distance displaced and a is the lattice parameter.

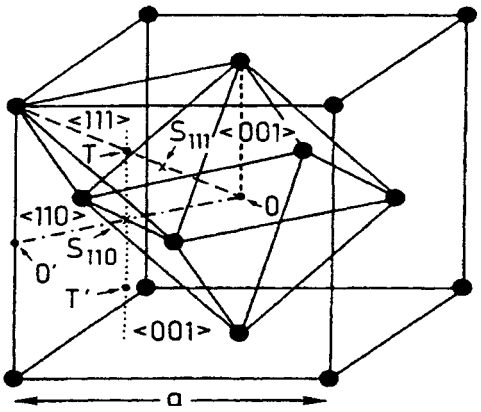

Figure 2. Diagram of the f.c.c. lattice showing the octahedral sites, O, the tetrahedral sites, T, and the directions <100>, <110> and <111> from the O site. S_{110} and S_{111} mark the points at which the H potential passes through a maximum.

Table 1. Energy levels for Hydrogen in palladium.
The Table records the observed and calculated excitation energies $e_{M,|n,m,l>}$ of a hydrogen atom centred on the octahedral site in the PdH system (M represents the energy level and n, m, l represent quantum numbers of the corresponding harmonic-oscillator states). Note that A, B, C refer to linear combinations of the harmonic wave functions [23]. The column headed $PdH_{0.85}$ refers to our recent measurements on single crystal samples on the Be Filter TAS in Grenoble [27] while the column headed $PdH_{1.00}$ refers to our earlier measurements on a stoichiometric polycrystalline sample [18].

ENERGY STATE	*THEORY (meV)*	*$PdH_{0.85}$ (meV)*	*$PdH_{1.0}$ (meV)*
$e_{1,\|001>} = e_{1,\|010>} = e_{1,\|100>}$	62	57	55.8
$e_{2,\|011>} = e_{2,\|101>} = e_{2,\|110>}$	117	115.5	110.4
$e_{2,\|C>}$	132	139 ± 2	135
$e_{2,\|A>} = e_{2,\|B>}$	147	155 ± 3	148
$= e_{3,\|111>}$	164	~170	-

It has already been established that the lattice parameter of PdH_x increases with x according to the relation valid at low temperature:

$$a(x) = a_{\beta min}\,[1 + 0.044(x - \beta_{min})] \qquad (2)$$

where $a_{\beta min}$ = 4.025 Å and β_{min} (= 0.607) is the value of x at its minimum value in the beta phase[28]. In consequence, as would be expected, the energy of the peak in the inelastic scattering cross section decreases as x is increased through the β phase [29]. This accounts for the reduction in the peak energy as recorded in the table, going from x = 0.85 to x = 1.00. It will be seen that the calculation is excellent for the higher energy levels but is significantly higher than the observed energies in the (100) and (110) levels. It should also be noted that the calculation actually predicts a lattice parameter of 4.07 Å compared with an experimental value of 4.04 Å. This suggests that the calculation is not able to accurately reproduce the form of the potential energy surface in its flat-bottomed part.

The most stringent comparison of theory and experiment is, however, through the shape of the wave functions and the corresponding shape of the inelastic scattering function, as calculated using Equation 1. A full description of the wave functions will be given elsewhere [30]. The ground-state wave function is nearly spherically symmetric and has a radial dependence that is nearly Gaussian. The three states corresponding to the first excited level each have a single node in one Cartesian direction and roughly Gaussian profiles in the other two directions. As an illustration, the wave function for the (110) level is shown in Figure 3.

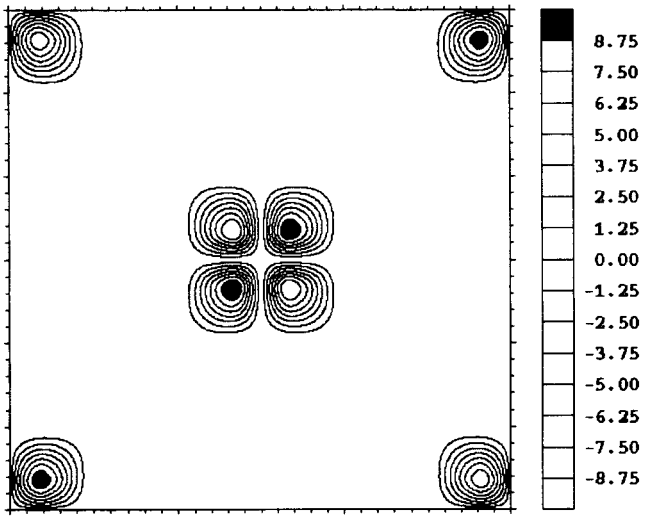

Figure 3. The ab initio second excited state wave function of the proton ((110) level) centred on the octahedral site.

The figure shows a contour plot in the x,y plane through the centre of the octahedral site. Each of the four features in each of the four quadrants has a cigar shape, intersecting this plane at its mid point. It will also be noted that the sign of the wave function alternates from quadrant to quadrant.

The (2,0,0) levels are more complex. In the harmonic approximation, for each of the three degenerate states, one Cartesian direction would show two nodes and the other two directions would have Gaussian profiles. However, because of the anharmonicity, these levels become mixed. The resulting wave functions are shown in Figures 4 (the C level) and 5 (the A level). As can be seen, the C wave function is on average closer to the centre of the site and hence has a lower energy.

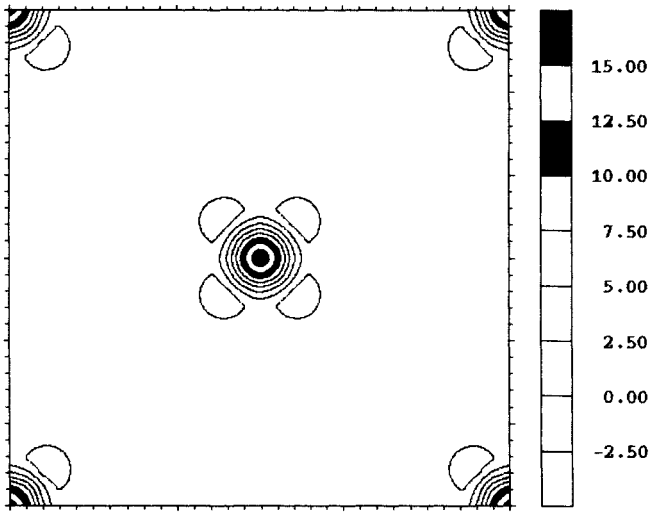

Figure 4. The ab initio second excited state wave function of the proton (C level) centred on the octahedral site.

The highest energy level of current interest is the (111) level. As expected from harmonic theory, this wave function shows equivalent features centred on the octahedral sites with alternating signs in each of the octants, (+/-x, +/-y, +/-z). It is interesting to note that these features extend into the tetrahedral site although the amplitude is only a few % of its value near the octahedral site. Nevertheless, this implies that the third level would be entirely delocalised because the tetrahedral site has the same geometrical relationship to the next octahedral site.

As mentioned above, the inelastic scattering function can be directly calculated from these wave functions using Fermi's Golden Rule, equation (1) above. The

symmetry of the scattering function follows from the symmetry of the wave function. Thus if **Q** lies in the (x,z) or the (y,z) planes, integration over the plane normal to **Q** will pass through equal regions of positive and negative amplitude, ensuring that S(**Q**,ω) is zero. The resulting scattering function is shown in Figure 6.

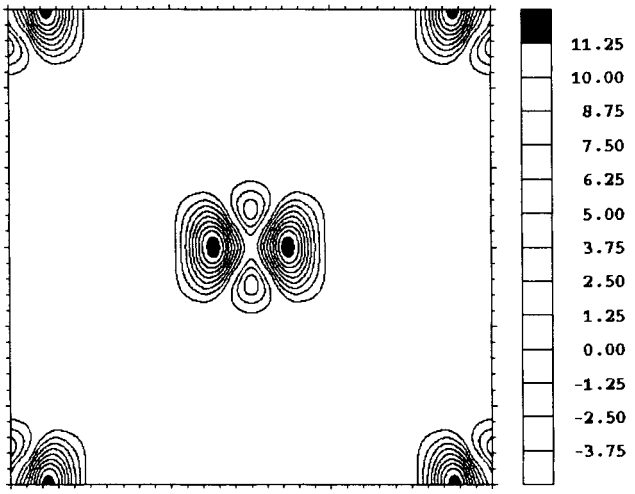

Figure 5. The ab initio second excited state wave function of the proton (A level) centred on the octahedral site.

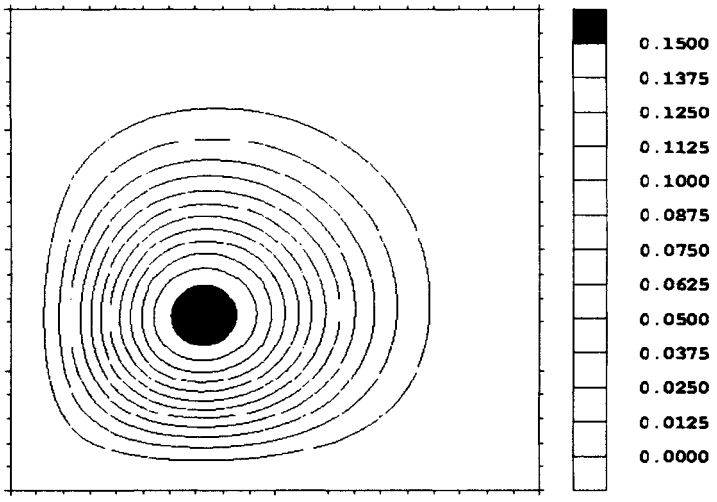

Figure 6. Calculated S(Q,ω) for scattering from the ground state to the (110) level. Contour plot in (Q_x,Q_y) plane for Q_z=0. The lower left hand corner is the Q=0 point.

The scattering function has 4-fold symmetry about this origin, consisting of four cigar shaped features (positive intensity) normal to the (x,y) plane. In contrast, the two (002) states (Figures 7 and 8) have their maximum intensity along the x and y axes. As expected from the shape of the wave functions, the C state shows much less angular modulation around the z axis than do the A, B states. All these features have their maxima in the z=0 plane with gradually decreasing intensities in the +/- z directions. As would be expected, the scattering function for the (111) level has no intensity in any of the (x,y), (y,z) or (z,x) planes but shows lobes into all eight octants.

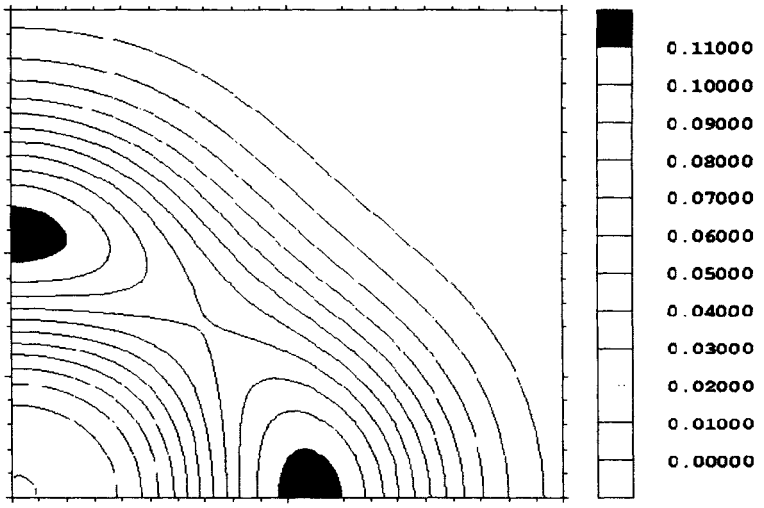

Figure 7. Calculated $S(Q,\omega)$ for scattering from the ground state to the C level. Contour plot in (Q_x,Q_y) plane for $Q_z=0$.

It is now clear why the Be Filter TAS is particularly appropriate for measuring these features as it enables us to rotate the direction of Q relative to the crystal axes. The inability to vary the magnitude of Q for a given energy transfer is less important because the variation with the magnitude of Q is much less interesting. The variation of $S(Q,\omega)$ with angle about the (001) and (110) axes are given in Figures 9 and 10. It is clear that the observation of the modulation in the scattering function enables us to identify a particular energy unequivocally.

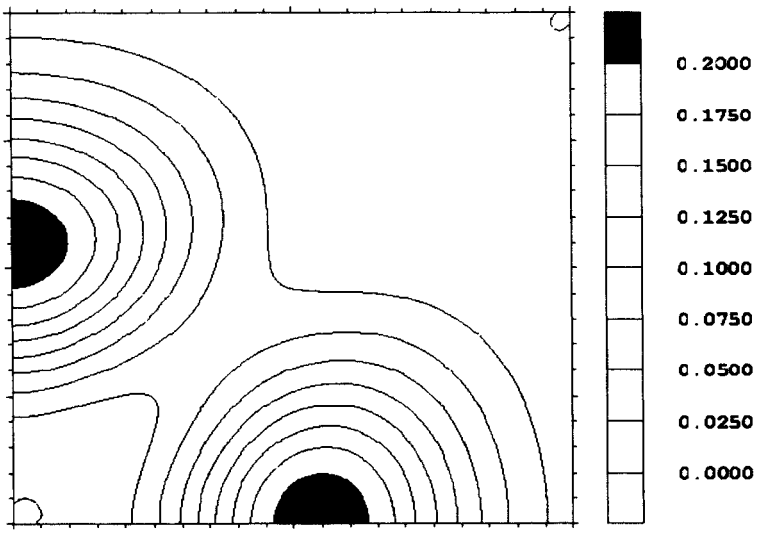

Figure 8. Calculated S(Q,ω) for scattering from the ground state to the A, B levels. Contour plot in (Q_x,Q_y) plane for Q_z=0.

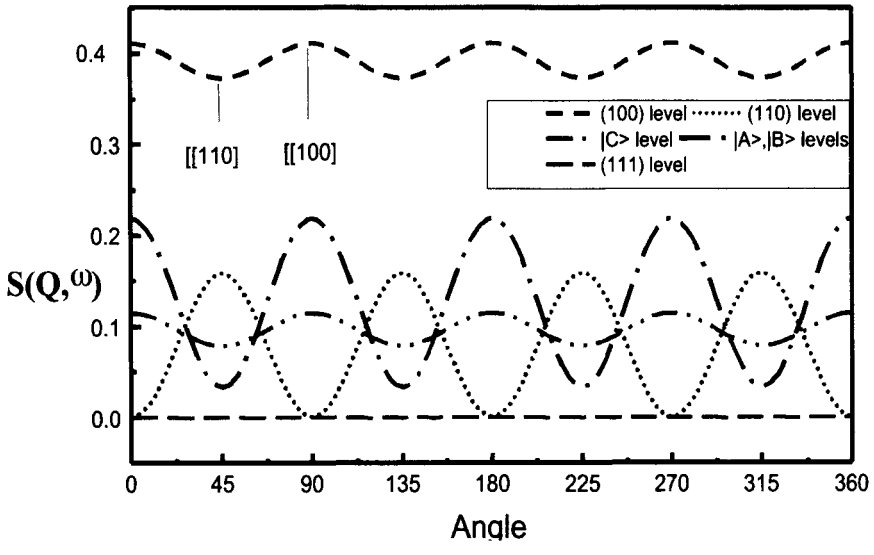

Figure 9. The dynamical structure factor as a function of the Q direction for the first three excited states. The z-axis of the crystal is along the [001] direction.

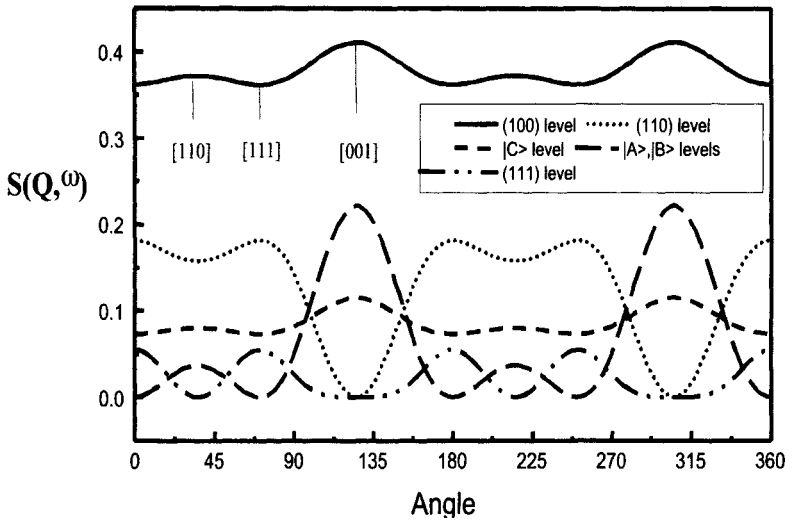

Figure 10. The dynamical structure factor as a function of the Q direction for the first three excited states. The z-axis of the crystal is along the [110] direction.

17.7 COMPARISON WITH EXPERIMENT

These calculations can now be compared with experiment. The first measurements were made as a function of energy transfer with the direction of the Q vector respectively parallel to the (001), (110) and (111) directions (Figure 11). Theoretical scattering functions were obtained by broadening delta functions in ω with the calculated resolution function of the instrument. The first excited level at about 60 meV is more or less isotropic as expected. The second, at about 120 meV is only present in the (111) and (110) directions, as expected for the (110) level. The third level shows a shoulder at about 140 meV in all three directions which would indicate the C state while the next peak at about 160 meV is much stronger in the (001) direction, thus indicating the A,B levels. There is also a suggestion of a peak in the (111) direction at about 170 meV, suggestive of the (111) level.

In Figures 11 and 12, the data taken for fixed energy transfers as a function of crystal orientation is presented. In Figure 11, we show data collected for the crystal grown along the [001] axis for energy transfers centred on 115.5 and 155 meV. The theoretical curve is based on the assumption that the former curve corresponds to the (110) level and the latter to the A and B levels. It should be noted that a constant intensity has been added to the theoretical curves to allow them to fit the data. It is clear that this extra intensity is due to multiple scattering in the sample due to the large probability that a neutron will have two or more scat-

ters in the crystal, in particular, due to a first inelastic scatter down to 3.5 meV followed by an isotropic elastic scatter. Approximate estimates of its magnitude agree with the observed angular independent scattering. In Figure 12, data collected with the crystal grown along the [110] direction is presented for the (110) level (115.5 meV). Again, a contribution to represent isotropic multiple scattering has been added to the theoretical curve.

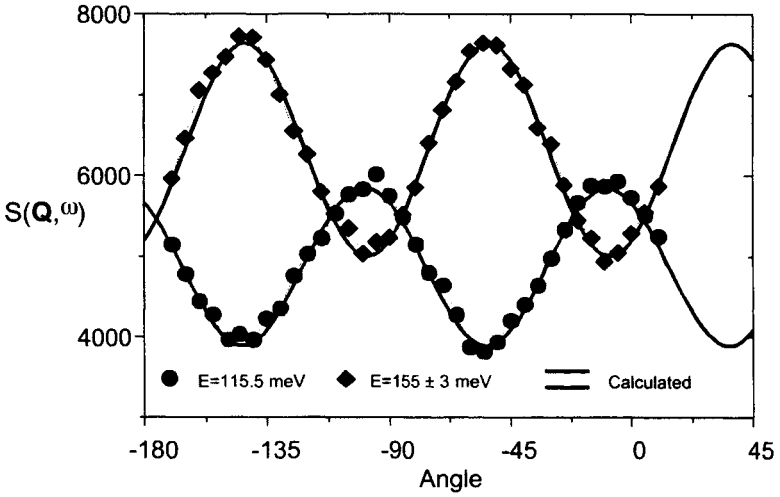

Figure 11. The dynamical structure factor as a function of the Q direction corresponding to the (110), A and B levels, for the [001] crystal. The full lines represent the theory and the dotted lines represent the experiment.

It should be emphasised here that the basic modulation seen in the data is very close to that predicted by the SHO model. SHO theory predicts that the (110) level summed over the three degenerate states should vary as $Q^4(\cos^2\theta_x\cos^2\theta_y + \cos^2\theta_y\cos^2\theta_z + \cos^2\theta_z\cos^2\theta_x)$ while the (200) peak, again summed over the three degenerate states varies as $(1/2)Q^4(\cos^4\theta_x + \cos^4\theta_y + \cos^4\theta_z)$ [9]. The calculated modulation differs slightly from these forms but shows the same symmetry. It should be noted that the sum of the intensities of all the SHO intensities corresponding to scattering to the second level should vary isotropically as Q^4 exp(-2W) where exp(-2W) is the Debye Waller factor. Thus, in the absence of anharmonicity to split the states within a given level, no modulation would be observed. It is thus the anharmonicity that makes this an interesting system for which to investigate the proton wave functions.

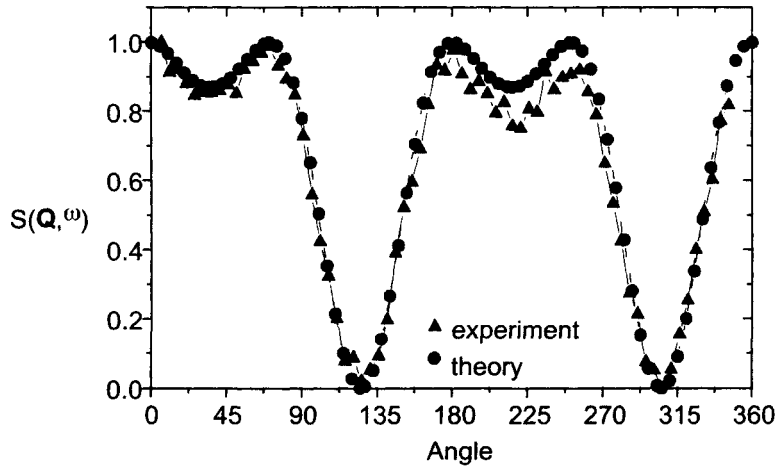

Figure 12. The dynamical structure factor (normalised) as a function of the Q direction corresponding to the (110) level for the [110] crystal. The red curve represents the theory and the blue one represents the measured data.

17.8 FURTHER CONSEQUENCES OF THE QUANTUM NATURE OF THE HYDROGEN NUCLEUS

17.8.1 Isotope Effects in the Lattice Parameter

Having demonstrated the considerable success of the ab initio calculations for the Pd-H system [23-26], we have extended the quantum treatment of the system to include the quantum properties more completely. Our initial objective was to include the ground state energy of the proton in the relaxation process, i.e. to calculate the total energy of the system including the zero point energy of the hydrogen and to minimise this quantity as a function of the lattice parameter. To do this, we first set up a completely independent calculation of the hydrogen wave functions following the approach adopted by Elsässer et al but with a different software package (CASTEP) along with a rather different set of approximations in the process of applying the Local Density Approximation. The full details of this calculation will be given elsewhere [30].

The new calculation scheme was first applied to the Pd lattice itself. With an energy cut-off for the plane wave representation of the electron states of 700 eV and the core corrections being taken into account via the non-linear core-valence exchange-correlation energy functional, the total energy was minimised yielding a lattice parameter of 3.90 Å which is identical with the experimental value. This approach was therefore adopted for the PdH system, with a local norm-conserving pseudopotential derived from the coulomb potential for the hydrogen

nucleus. By again calculating the total energy as a function of the lattice parameter, the minimum value was found to be 4.091 Å compared with the experimental value of 4.090 Å [28].

The method of fitting the wave functions into the resulting potential energy surface has also been performed in a rather more detailed way, making use of the greater computational power now available to us. We used a regular grid of points in real space rather than points restricted to symmetry directions, allowing for the resultant loss of symmetry. It is believed that this process produces a more unique fit to the Fourier components. Again, details can be found elsewhere [30]. The resulting proton energies are 5-10% higher than found by Elsässer et al [23-26] when the 4.091 Å lattice parameter was used. The calculation was then repeated for a range of lattice parameters and the zero point energy for the proton was calculated at each value. The total energy, including the proton zero point energy, is now a minimum at a lattice parameter of 4.10 Å and the energy levels for this lattice parameter are rather lower than for the unrelaxed lattice (Table II). Comparison with Table I shows that the calculated values are still somewhat too high.

Table 2. The excitatiton energies of proton for $PdH_{1.0}$ calculated for two different lattice constants:

ENERGY STATE	*$PdH_{1.0}$* **a = 4.091 Å**	*$PdH_{1.0}$* **a = 4.100 Å**
$E_{1,\|001\rangle} = e_{1,\|010\rangle} = e_{1,\|100\rangle}$	**64**	**63**
$E_{2,\|011\rangle} = e_{2,\|101\rangle} = e_{2,\|110\rangle}$	**125**	**122**
$E_{2,\|C\rangle}$	**144**	**141**
$E_{2,\|A\rangle} = e_{2,\|B\rangle}$	**153**	**150**
$E_{3,\|111\rangle}$	**180**	**176**

17.9 QUANTUM EFFECTS ON OPTICAL PHONONDISPERSION

These new calculations have also been used to predict the notable dispersion effects observed experimentally in the longitudinal optic dispersion curve. Thus, the original calculation effectively moves the whole Hydrogen sublattice in phase relative to the Pd lattice. The calculation therefore corresponds to the Γ

point ($\mathbf{q} = 0$) on the dispersion curves. Now, we can, for instance, displace the phonons in the pattern corresponding to the Zone Edge phonon, with alternate planes of atoms in anti-phase and recalculate the energy surface as a function of H displacement. If we then fit the corresponding wave function in both the ground state and the first excited state, then the difference should be the correct energy for the corresponding phonon. The measured dispersion curves for $PdD_{0.82}$ are shown in Figure 12 [32]. We have performed this calculation for the Σ point in the (110) direction, where the dispersion curve measured for D passes through a maximum of 5.5 THz (23 meV) above the Γ point. The method used employs a 1-D Schrödinger Equation in each Cartesian direction and so is not precise. The results are shown in Table III. for both H and D and for ground state and first excited state. This gives a change in the energy difference between the two levels for D of 25.3 meV and so the agreement with experiment is very encouraging.

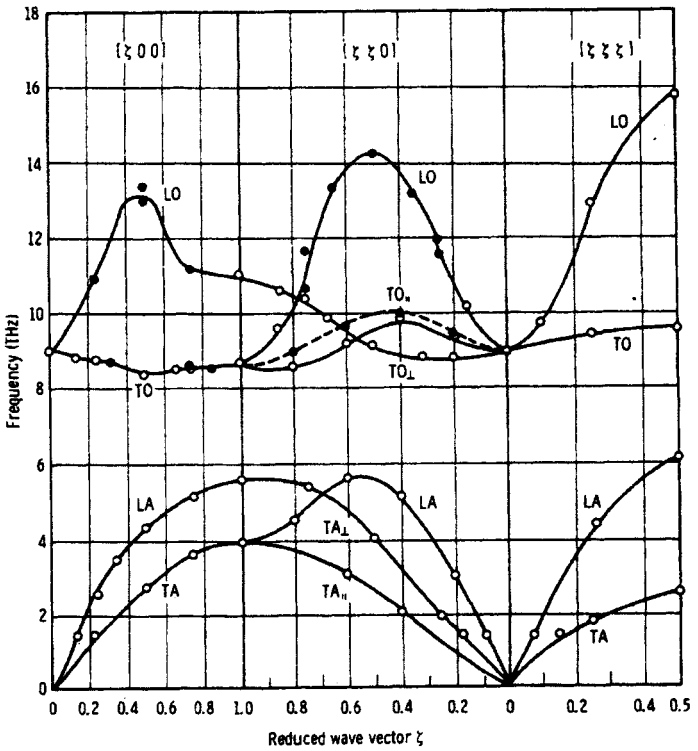

Figure 12. Experimental dispersion curves for $PdD_{0.82}$ [31]

Table 3. Ground state and first excited state energies for both proton and deuteron for Γ and Σ points.

PROTON		DEUTERON	
1-dim (Γ point)	1-dim (Σ point)	1-dim (Γ point)	1-dim (Σ point)
$E_0^{<110>}$ = 22.3709	$E_0^{<110>}$ = 41.0507	$E_0^{<110>}$ = 14.7935	$E_0^{<110>}$ = 28.4147
$E_1^{<110>}$ = 75.2883	$E_1^{<110>}$ = 128.4282	$E_1^{<110>}$ = 49.4226	$E_1^{<110>}$ = 88.3819

17.10 IS THE FIRST EXCITED STATE A FRANCK-CONDON LEVEL?

Elsässer et al [23] raised the question as to whether the hydrogen would be excited to a Franck-Condon level, by analogy with the behaviour of trapped electrons as described by Stoneham [32]. The Franck-Condon State describes the situation where the lattice has relaxed adiabatically to minimise the total energy when the hydrogen is in its excited state. This implies that the Pd atoms relax away from the octahedral site so as to minimise the energy of the first excited state plus the additional elastic energy due to the displacement of the palladium atoms. The criterion for this to happen in place of the normal excited state in the unrelaxed lattice (the so-called zero phonon state) is that there should be acoustic phonons available to absorb this relaxation energy and hence that the Franck-Condon shift is sufficient to match the peak in the acoustic phonon spectrum (about 20 meV). It is clear that the Franck-Condon level, if it exists, will be localised, whereas the "Zero Phonon" level will couple with the other hydrogen atoms and will therefore show dispersion, as is measured for PdD.

This calculation is, in principle, possible but is quite difficult. Either one has to go to a non-periodic model or one has to use a sufficiently large super-cell to accommodate the displacement field. We are currently looking at this problem. The alternative approach is to examine the experimental data for evidence of a Franck-Condon level. The idea is in fact very attractive as it explains the sharpness of the peak for the first excited state in PdH [18]. The accumulated measurements on this peak show that it gets narrower as the hydrogen concentration approaches stoichiometry and the sample temperature

is reduced. In [18], the scattering to the first excited state is fitted with three gaussians, the sharp one at 55.8 meV having a width of 4.8 meV, compared with an instrumental resolution of 1.4 meV, giving an actual width of 4.6 meV. Now, the traditional explanation of this peak is that it is due to the density of states in the transverse dispersion curves. These peaks are indeed quite clearly observed in the measurements on $PdD_{0.85}$ (Figure 12) by measuring with $\mathbf{Q} \perp \mathbf{q}$. They vary in the range 36-42 meV and thus would be expected to give a much wider density of states peak than is observed. We have recently re-measured the optical dispersion curves in a single crystal of $PdD_{0.85}$ to see if we can distinguish between the transverse phonons and a Franck-Condon Peak. A number of the scans do clearly show two peaks, one of which is at a constant energy of 38 meV while the other, which satisfies the $\mathbf{Q} \perp \mathbf{q}$ condition for a transverse phonon, is at a variable and somewhat higher energy, agreeing with the published transverse dispersion curves [31]. However, to be certain that this is a Franck-Condon level, we need to establish that it is not a density of states peak derived from the incoherent part of the D scattering cross-section. We are currently testing this possibility by measuring the spin polarisation in this peak. Incoherent scattering would give rise to a proportion of spin flip events while a Franck-Condon level, consisting of both coherent and incoherent parts (indistinguishable, being a localised site) would have much less spin flip.

17.11 CONCLUSIONS

We have demonstrated that the ab initio calculations are capable of describing the energy levels and related modulations of the inelastic neutron scattering from H in Pd with remarkable accuracy. Having demonstrated that the theory provides an excellent match to the experimental data, we are applying the same model to predict other experimentally accessible data for this system, such as the isotope dependence of the lattice parameter and assessing the possibility of observing Franck-Condon transitions.

REFERENCES

[1] Hydrogen in Metals Vol I, II (Eds G. Alefeld and J. Volkl) Topics in Applied Physics: Springer, Berlin (1978); Hydrogen in Metals III (Ed H. Wipf) Topics in Applied Physics: Springer, Berlin (1997)

[2] B. Dorner, I.T. Belash, E.L. Bokhenkov, E.G. Ponyatovski, V.E.Antonov, L.N. Pronina, Solid State Commun. 69 121(1989)

[3] T. Graham, Phil. Trans. Roy. Soc. (London) 165 399 (1866)

[4] Hydrogen in Intermetallic Compounds Vol I and II (Ed L. Schlapbach) Topics in Applied Physics: Springer, Berlin (1992)

[5] J. Hauch and H.J. Schenk, J. Less-Comm. Metals 51, 251(1977)
[6] D.K. Ross in Hydrogen in Metal III (Ed H.Wipf) Topics in Applied Physics: Springer, Berlin (1997) Chapter 5.
[7] E. Fermi, Ric. Sci. 1 13 (1936)
[8] G.L. Squires, Introduction to the Theory of Thermal Neutron Scattering, (Cambridge University Press, Cambridge 1978)
[9] V.F. Turchin, Slow Neutrons (IPTS, Jerusalem,1965)
[10] J.G. Couch, O.K. Harling, L.C. Clune, Phys. Rev. B 4 2675 (1971)
[11] E. Wicke and H. Brodowsky in Hydrogen in Metals II (Eds G. Alefeld and J. Volkl) Springer, Berlin (1978)
[12] Y. Fukai: The Hydrogen-Metal System - Basic Bulk Properties Springer Series: Materials Science 21 Springer, Berlin (1992)
[13] R.A. Bond and D.K. Ross, J. Phys. F 12 597 (1982)
[14] D.G. Hunt and D.K. Ross, J. Less-Comm. Met. 49 169 (1976)
[15] J.M. Rowe, J.J. Rush, H.G. Smith, M. Mosteller, H.E. Flotow, Phys. Rev. Letts. 33 1297 (1974)
[16] A. Rahman, K. Skold, C. Pelizzari, S.K. Sinha, K. Flotow, Phys. Rev. B 14 3630 (1976)
[17] J.J. Rush, J.M. Rowe, D. Richter, Z. Phys. B 55 283 (1984)
[18] D.K. Ross, V.E. Antonov, E.L. Bokhenkov, A.I. Kolesnikov, E.G. Ponyatovsky, J. Tomkinson, Phys. Rev. B. 58 2591 (1998)
[19] P.Hohenberg and W. Kohn, Phys. Rev. 136 864 (1964)
[20] W. Kohn and L.J. Sham, Phys. Rev. 140 1133 (1965)
[21] K.M. Ho, H.J. Tao, X.Y. Zhu, Phys. Rev. Lett. 53 1586 (1984)
[22] H.J. Tao, K.M.Ho, Z.Y. Zhu, Phys Rev. B 34 8394 (1986)
[23] C. Elsässer, K.M. Ho, C.T. Chan, M. Fähne, Phys Rev B 44 10377 (1991)
[24] K.M. Ho, C. Elsässer, C.T. Chan, M. Fähne, J. Phys. Condensed Matter 4 5189 (1992)
[25] C. Elsässer, K.M. Ho C.T. Chan, M. Fähne, J. Phys Condensed Matter 4 5207 (1992)
[26] H. Krimmel, L. Schimmele, C. Elsässer M. Fähne, J. Phys. Condensed Matter 6 7679 (1994)
[27] M. Kemali, J.E.Totolici, D.K. Ross, I. Morrison, Phys. Rev. Lett. 84 1531 (2000)
[28] J.E. Schriber and B.Morosin, Phys. Rev. B 12 117 (1975)
[29] D.K. Ross, P.F. Martin, W.A. Oates and R. Khoda-Bakhsh, Z. Phys. Chem. Neue Folge 114 221 (1979)
[30] J.E. Totolici, I. Morrison, M. Kemali and D.K Ross, to be published.
[31] M.W. McKergow, P.W. Gilberd, D.J. Picton, D.K. Ross, P. Fratzl, O. Blaschko, I.S. Anderson, and M. Hagen, Z. Phys. Chem. N.F. 146 159 (1985)
[32] A.M. Stoneham "Theory of Defects in Solids" Clarendon Press, Oxford, 1975, Chapter 10.

Chapter 18

Hydrides for Hydrogen Storage

Arnulf J. Maeland

Institute for Energy Technology, Kjeller, Norway

CONTENTS

18.1 INTRODUCTION

Dihydrogen, H_2, as an energy carrier? The well known science fiction writer Jules Verne in one of his novels, The Mysterious Island published in 1874, posed the question of what happens when the supply of coal runs out. What can be used as fuel? The answer: "I believe that water will one day be employed as fuel, that hydrogen and oxygen which constitute it, used singly or together, will furnish an inexhaustible source of heat and light". Pure science fiction or did Jules

Verne have a visionary view of a real possibility? It is evident from research activities around the world that hydrogen is given serious consideration as an energy carrier and the concept of a hydrogen economy has evolved and gained in credibility in the past 25 - 30 years. [1] The motivation and the driving force for these activities are the alarming increase of air pollution. Large amounts of carbon mono- and di-oxide, nitrogen and sulfur oxides, hydrocarbons and particulates produced in energy generating combustion processes, particularly in automotive vehicles, continue to pollute the atmospheres, at times resulting in dangerous levels of these contaminants in metropolitan areas. Devices to reduce the level of pollutants, such as the catalytic converter used in the automobile and scrubbers used in electric power generation, have to some degree eased, but not eliminated the problem and while further improvements may be forthcoming, complete removal is an unrealistic expectation. There is, however, another solution: employ a fuel which does not produce pollutants. The proponents of the hydrogen economy emphasize the fact that the primary combustion product of dihydrogen with air is water and hydrogen is therefore a clean fuel. Variable amounts of nitrogen oxide, depending on the combustion temperature, are formed, but the amounts are by comparison miniscule and devices to remove nitrogen oxide are available. It is also emphasized that hydrogen can be used with very high efficiency in fuel cells to generate electrical energy, the estimated efficiency is twice that of the present day automobile engine. The automobile industry is under pressure to reduce emissions substantially and most car makers are engaged in research programs which include fuel cell technology and there has been a number of successful vehicular demonstration projects in which hydrogen fuel cells have provided the power.[2] However, the extensive use of dihydrogen as energy carrier in the transportation sector depends on satisfactory methods for onboard storage or processes for onboard production of dihydrogen. Both approaches are being pursued, but we will in this review be concerned with the onboard hydrogen storage issue.

It is interesting to observe that the historical development of fuel sources, which was driven by the need for greater efficiency, has by chance, more than methodologically, also moved towards cleaner energy through the process of decarbonisation. Despite this shift to cleaner energy sources, from wood to coal, to oil and gas, however, the gains have been more than offset by large increases in energy consumption. Decarbonisation, the progressive reduction of carbon in relation to hydrogen content in fossil fuel energy sources required to produce a given amount of energy,[3] is illustrated by the following: Burning wood to produce energy uses about 10 carbon atoms for each hydrogen atom, burning coal 1 - 2 carbon atoms per hydrogen; in the combustion of oil the ratio is 1 carbon per 2 hydrogen and with gas (methane) the ratio is 1 carbon for each 4 hydrogen atoms. In the combustion process carbon ends up as soot, carbon monoxide and carbon dioxide, depending on the dioxygen/carbon molar

ratio, while hydrogen ends up as water. Carbon is thus the dirty element which produces pollution while hydrogen is the clean one since it does not produce any pollutants. Decarbonisation is, therefore, a desirable process, and, in order to reduce environmental pollution, the ultimately clean fuel is dihydrogen. Dihydrogen is in this respect an ideal energy carrier. It is also widely available being the most abundant element in the universe on a molar basis. Hydrogen is generally combined with other elements, while molecular hydrogen, H_2, is only found in trace amounts in the atmosphere. Technologies for H_2 production, such as electrolysis, hydrocarbon cracking, photoconversion of water, biological production from waste, high temperatures decomposition of water, etc., are well known. Furthermore, hydrogen has a high specific energy content of 33.3 kWh/kg which is nearly three times that of gasoline or diesel. Despite these desirable properties, dihydrogen has not yet become a major energy carrier except in special cases, e. g. in the launching of space vehicles where high specific energy content of the propulsion fuel is of outmost importance. Liquid dihydrogen is in this case the fuel of choice to maximize the payload capacity.

One of the major factors negatively contributing to the introduction of dihydrogen as a major energy carrier is its cost. Dihydrogen is not available as such and must be generated from other compounds with energy expenditure and as a result it is relatively expensive. This is not, however, the complete story. Fossil fuels cause pollution and damage to the environment while dihydrogen does not. The cost of cleaning up the environment and repairing the damage is not easily assessed, but should clearly be part of the comparative evaluation. Only when this is done can an accurate cost comparison be made and dihydrogen given a fair evaluation.

A second major factor is due to the difficulty of storing dihydrogen in an energy dense form. Dihydrogen, being the molecular form of the lightest element hydrogen (atomic weight 1.0079), is a gas under ambient conditions. The density at STP is 0.08988 kg/m^3 [4] which is by way of comparison only one seventh that of methane. Therefore, despite the high specific energy content, densification is required for most applications. Densification can be achieved by compression and even more efficiently by liquefaction and solidification. These processes are energy intensive. Liquefaction, for example, consumes nearly 30 % of the total energy contained in dihydrogen and in addition requires expensive equipment and energy to retain dihydrogen in the liquid state. Solidification requires even more energy, and compression of dihydrogen up to say 35 MPa requires nearly 20 % of its total energy content. Chemical conversion of dihydrogen into a reversible metal hydride represents an alternative, attractive and safe method of hydrogen storage. This form of storage has received a lot of attention in the past 30 years or so and has been the subject of a number of reviews; which are to be mentioned here. The two volume set, *Hydrogen in Metals I and II*, published in 1978 [5] is an excellent review of the science of metal-hydrogen systems.

Volume I treats basic properties and volume II is devoted to application-oriented properties. *Hydrogen in Intermetallic Compounds I*, published in 1988, and *Hydrogen in Intermetallic Compounds II*, published in 1992, contain perhaps the most comprehensive information on the reversible hydrides of intermetallic compounds and on their applications.[6] Another good review is by Buschow et al.[7] Sandrock has written several fine reviews,[8-10] the comprehensive and highly application-oriented one, published as a Report to the US Office of Naval Research, is especially recommended.[9] A guide to the metal hydride literature is also available.[11]

In this review dihydrogen as a possible energy carrier will be considered and metal hydrides as potential hydrogen densification and storage media will be reviewed. The classification and some of the basic properties of metal hydrides and their relation to hydrogen storage are surveyed; advantages and disadvantages are identified and new and creative approaches to improving storage capacities are considered.

18.2 FORMATION AND CLASSIFICATION OF METAL HYDRIDES

Many metals and alloys react with hydrogen gas to form metal hydrides according to equation (1):

$$M + s/2\, H_2 \rightarrow MH_s \qquad (1)$$

Here M is a metal, a solid solution alloy or an intermetallic compound, MH_s is the hydride and s the molar ratio of hydrogen to metal, H/M. The hydrides frequently show large deviations from stoichiometry. The reaction is in most cases exothermic and reversible, i.e. dihydrogen is recovered by application of heat. The elements which form solid binary metal hydrides are shown in Figure 1.

The nature of the metal-hydrogen bond and the resulting properties are in general related to the position of the metal in the periodic table. On this basis, it is convenient to classify the hydrides as ionic (or salt like), covalent and metallic without implying rigid boundaries between the classes. In ionic hydrides the metals exist as positive cations, M^+, and hydrogen as anions, H^-. The alkali metals form ionic monohydrides and the alkaline earth metals form ionic dihydrides similar to the corresponding halides. Europium and ytterbium also form ionic hydrides due to the stability of the 4*f* shell in these metals and the availability of the two 6s electrons for bonding. The metals to the right of Group 10 in the periodic table form hydrides in which the bonding is predominantly covalent; most of them are unstable and are generally difficult to prepare directly and reversibly by reaction (1) and are therefore of no interest as storage media.

Be and Mg in Group 2 form relatively stable covalent hydrides, BeH_2 and MgH_2 (MgH_2 may also be classified as an ionic hydride). The covalent hydrides are typically colourless solids, polymeric in nature (e.g. AlH_3). MgH_2 is unique among the covalent hydrides in that it does form reversibly according to (1) and is not polymeric. Most of the transition metals and the rare earths, and all the actinides form metallic hydrides which retain certain metallic properties, e. g. metallic luster and conductivity. This was at one time looked upon as being due to the hydrogen atom donating its electron to the unfilled metal d-band. In this model hydrogen existed as a proton, screened by the electron sea. However, most metallic hydrides lack the characteristic metallic property of ductility and are quite brittle. Some degree of ionic bonding was therefore assumed and the anion model of metallic hydrides, in which hydrogen existed as H^-, evolved. The current view [12] is that in the metallic hydrides the 1s electron on the hydrogen atom participates in the conduction band of the metal to generate new M-H bonding states. The new bonding states contain both protonic and anionic components and this model thus contains elements of the earlier two models. The metal-hydrogen bonds are not purely of one type, e.g. the bonding in MgH_2 presents some degree of covalent character. The degree of ionicity is related to the position in the periodic table; e.g. LiH has more covalent character than CsH.

1	2												
Li	Be											13	14
Na	Mg *Mg*	3	4	5	6	7	8	9	10	11	12	Al	
K	*Ca*	**Sc**	**Ti**	**V**	**Cr***	**Mn***	**Fe***	**Co***	**Ni***	Cu	Zn	Ga	
Rb	*Sr*	**Y**	**Zr**	**Nb**	**Mo***	**Tc***		**Rh***	**Pd**		Cd	In	Sn
Cs	*Ba*	**La**	**Hf**	**Ta**								Tl	Pb
		Ac											

Ce	**Pr**	**Nd**		**Sm**	*Eu*	**Gd**	**Tb**	**Dy**	**Ho**	**Er**	**Tm**	Yb *Yb*	**Lu**
Th	**Pa**	**U**	**Np**	**Pu**	**Am**	**Cm**	**Bk**						

Ionic hydrides, Covalent hydrides, **Metallic hydrides**

* Non hydride forming requires high pressures to be formed

Figure 1. Metallic elements from Group 1 to Group 14, which form solid metal hydrides.

Table 1. Examples of intermetallic hydrides

Compositional	Structural Type	Representative examples
AB_5	hexagonal $CaNi_5$	$LaNi_5H_7$, $CaNi_5H_6$, $LaNi_4MnH_6$
AB_3	hexagonal $PuNi_3$	$CeNi_3H_3$, YFe_3H_3
AB_2	hexagonal AlB_2	$ZrBe_2H_2$, $ThNi_2H_{2.6}$
AB_2	hexagonal $MgZn_2$	$ZrMn_2H_3$, $Ti_{1.2}Mn_{1.8}H_{3.1}$
AB_2	cubic $MgCu_2$	$ErFe_2H_{4.1}$, $ZrV_2H_{5.3}$
AB	cubic CsCl	TiFeH, $TiFeH_2$
AB	orthorhombic CrB	$ZrNiH_3$, $ZrCoH_3$, $LaNiH_{3.7}$
A_2B_7	Hexagonal Ce_2Ni_7	$Ce_2Co_7H_{6.7}$, $La_2Ni_7H_{10}$
A_6B_{23}	cubic Th_6Mn_{23}	$Y_6Fe_{23}H_{23}$, $Th_6Mn_{23}H_{30}$
A_2B	cubic Ti_2Ni	Ti_2NiH, $Hf_2CoH_{3.8}$
A_2B	hexagonal Mg_2Ni	Mg_2NiH_4, $CaMgNiH_4$
A_2B	tetragonal $MoSi_2$	Zr_2PdH_2, $Zr_2PdH_{5.5}$
A_2B	tetragonal Al_2Cu	Th_2AlH_2 ,Th_2AlH_4, $Zr_2NiH_{4.9}$

The binary metal hydrides have very limited use as storage materials because of their stability (see discussion below). Their use have generally been that of laboratory sources of pure dihydrogen. The stability of each metal hydride is a fixed property. Alloying to form solid solutions allows for some change of hydride stability. From a practical point of view, however, there are only a few systems for which this technique has proven useful, e.g. the modification of the stability of body centered cubic (bcc) solid solutions of Ti and V with other elements. A dramatic breakthrough came in 1958 when the first hydride formation with an intermetallic compound was reported. Libowitz et al. discovered that the intermetallic compound ZrNi reacts reversibly with dihydrogen to form the ternary hydride $ZrNiH_3$.[13] The stability of this *ternary* hydride was determined to be intermediate between the stable ZrH_2 and the unstable NiH. The discovery opened the way to a new class of hydrides, the intermetallic hydrides, which could be regarded as "pseudo binary" with properties which could, at least to some extent, be controlled by alloying and substitution. The 1958 discovery went unnoticed for several years, but that changed around 1970, following the discovery of hydrides of the Mg_2Ni,[14] $LaNi_5$ [15] and FeTi [16] alloys. A flurry of activities was directed to discovering

new intermetallic hydrides which in turn were modified by further alloying, aimed at "tailor-made" stable hydrides. Methods to maximize other properties desirable in a storage material (see below) were also developed.

Most of the intermetallic hydrides of interest as storage materials have properties which are similar to those of metallic hydrides. Several hundred intermetallic hydrides have been reported and studied to date and a number of interesting compositional types identified. The more important ones include the AB_5 type intermetallic hydrides, the AB type, the AB_2, the AB_3 type, and the A_2B_7 type where A represents a hydride forming element and B represents in general a non hydride forming element, but can also be a hydride forming element. Examples from each group are shown in Table I. The metal atom arrangements in intermetallic hydrides are in general similar to the corresponding hydrogen-free compounds except for the usual lattice expansion and distortion accompanying hydride formation (between 0.002 and 0.003 nm^3 per hydrogen atom) and can therefore be conveniently identified according to the structure type of the hydrogen free compounds as noted in Table I. Extensive reviews of the intermetallic hydrides have been published [6, 7, 9] and a database of hydride alloy listings is available at http://hydpark.ca.sandia.gov. The database contains nearly 2000 entries (as of February 2000) and is periodically updated. The database covers binary metal hydrides, hydrides as solid solutions, intermetallic hydrides, transition metal hydrides, non-transition metal hydrides (discussed below), and miscellaneous hydrides.

18.3 PROPERTIES OF REVERSIBLE METAL HYDRIDES

The hydrogen density in metal hydrides is very high; higher in fact in some hydrides than in liquid or even solid dihydrogen, see Table II. The number of hydrogen atoms/cm^3 in VH_2, for example, is 11.4×10^{22}. This is more than twice that in solid dihydrogen at 4.2 K.

For typical storage materials such as $FeTiH_2$ and $LaNi_5H_7$ the corresponding numbers are 6.0×10^{22} and 7.6×10^{22} atoms/cm^3, respectively. Other compounds also have high volumetric densities of hydrogen; H_2O, for example, has a volumetric hydrogen density larger than solid hydrogen, 6.7×10^{22} atoms/cm^3 *vs* 5.3×10^{22} atoms/cm^3. However, temperatures in excess of 2000 K are needed to thermally initiate decomposition of H_2O and temperatures around 3300 K are needed to achieve substantial decomposition and recovery of hydrogen! The relatively high density of hydrogen in the metal hydrides combined with the relative ease of dihydrogen recovery form the basis for their potential

use as hydrogen storage materials. The ease of hydrogen recovery is reflected in the dissociation pressure of the hydride and can be best understood by considering the pressure-composition isotherm shown in Figure 2. Dihydrogen first dissociates on the metal surface to form H atoms which generally diffuse rapidly through the bulk metal even at room temperature to form a M-H solid solution commonly referred to as the α-phase, see eq (2).

$$M + y/2\ H_2 \rightarrow MH_y \quad \text{solid solution } \alpha\text{-phase} \tag{2}$$

Table 2. Volumetric and gravimetric hydrogen densities in various media

Medium	Vol. hydrogen density, 10^{22}atoms/cm^3	Gravimetric densities, wt%
H_2 gas, 10 MPa	0.5	100
H_2 liq., 20 K	4.2	100
H_2 Sol., 4.2 K	5.3	100
H_2O liq. r.t.	6.7	11.2
LiH	5.9	12.6
$PdH_{0.6}$	4.3	0.6
MgH_2	6.7	7.6
TiH_2	9.2	4.0
VH_2	11.4	3.8
$FeTiH_2$	6.0	1.9
$LaNi_5H_7$	7.6	1.6
Mg_2NiH_4	5.9	3.6
$LiAlH_4$	5.7	10.6

The hydrogen concentration in the α-phase (C_H) is pressure dependent and frequently follows Sieverts' law, i.e. $C_H=kP^{1/2}$ where k is a temperature-dependent constant and P is the dihydrogen pressure. As the dihydrogen pressure is increased, saturation occurs and the metal hydride MH_x starts to form. Conversion of the saturated solution phase to hydride continues as hydrogen is added. The pressure remains constant while this conversion takes place in accordance with the Phase Rule:

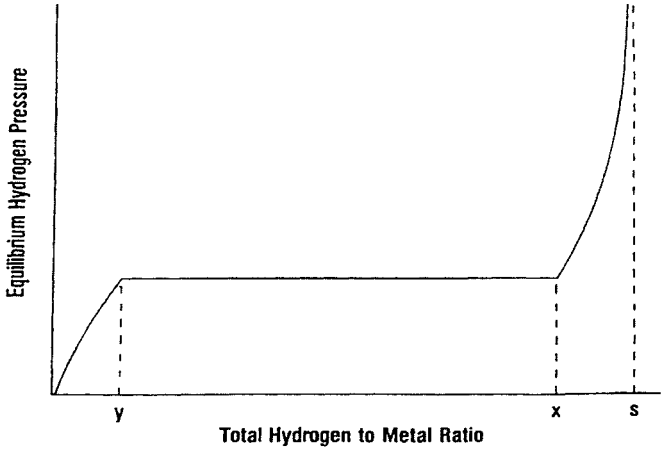

Figure 2. Pressure/Composition Isotherm (schematic)

$$MH_y + (x-y)/2\ H_2 \rightarrow MH_x \text{ nonstoichiometric hydride phase} \quad (3)$$

The invariant plateau pressure is the equilibrium dissociation pressure of the hydride at the temperature of the isotherm and is a measure of the stability of the hydride. After complete conversion to the hydride phase, further dissolution of dihydrogen in the non-stoichiometric hydride takes place as the pressure increases, see eq. (4).

$$MH_x + (s - x)/2\ H_2 \rightarrow MH_s \text{ hydride solution phase} \quad (4)$$

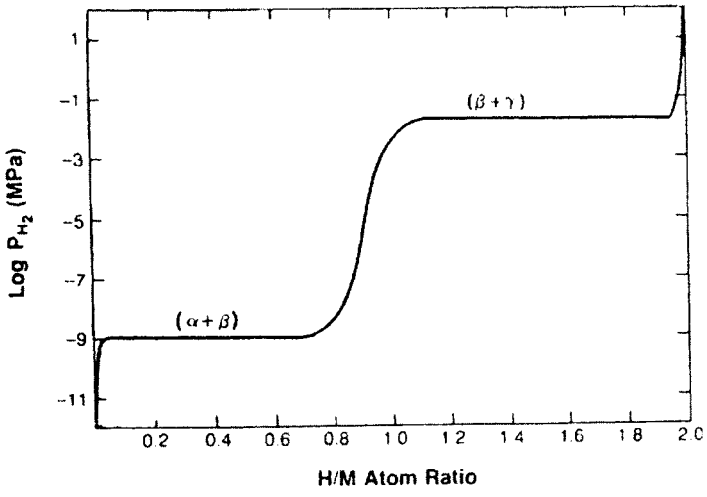

Figure 3. Pressure/Composition Isotherm for the V/H System.[17]

Multiple plateaus are possible as illustrated in Figure 3 for the V/H_2 system which exhibits two such plateaus. The first corresponds to the formation of a non-stoichiometric monohydride, the β-phase, while the second plateau represents conversion of the dihydrogen saturated monohydride phase to the non-stoichiometric dihydride γ-phase.

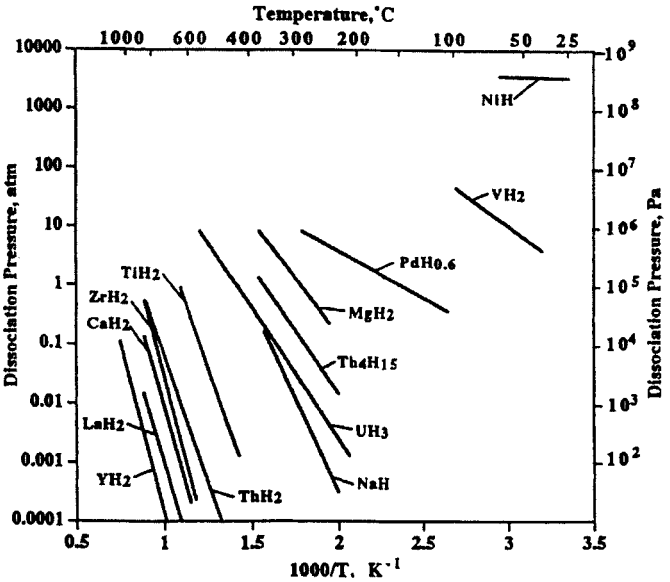

Figure 4. Dissociation Pressures vs Temperature [8, 10]. With kind permission from Kluwer Academic Publishers.

The equilibrium dissociation pressure, which is one of the most important properties of a hydride storage material, is temperature dependent. If the log of the dissociation pressure is plotted *vs* 1/T, a straight line is obtained (van't Hoff plot) as seen in Figure 4 for a representative number of binary hydrides.[8, 10] The line can be described by the well known van't Hoff equation, $\ln P = \Delta H/RT - \Delta S/R$, where ΔH and ΔS represent the enthalpy and the entropy change, respectively, for reaction (3), R is the gas constant and T the absolute temperature. The enthalpy change is determined from the slope of the line and the entropy change from the intercept (at $1/T = 0$). ΔH is a measure of the strength of the H-metal bond and varies from metal to metal while ΔS, basically reflecting the configurational entropy loss of dihydrogen on going from the gaseous to the solid state, does not vary greatly. It is clear from the figure that most binary metal hydrides require moderate to high temperature to liberate hydrogen at usable pressures. MgH_2 and TiH_2, for example, require heating to about 575 K and more than 875 K, respectively, to recover dihydrogen

at 0.1 MPa. Only VH_2 is capable of releasing dihydrogen reversibly at room temperature; however, only about one half of the dihydrogen is liberated, [$VH_2 \rightarrow VH_{0.95}$], corresponding to a 1.9 % by weight. High temperature is needed to recover the remainder. The situation is much improved when we consider the intermetallic hydrides, as shown in Figure 5.[8, 10] Several intermetallic hydrides have equilibrium dissociation pressures above 0.1 MPa at room temperature, e. g. $LaNi_5H_6$, $CaNi_5H_4$ and $FeTiH_2$.

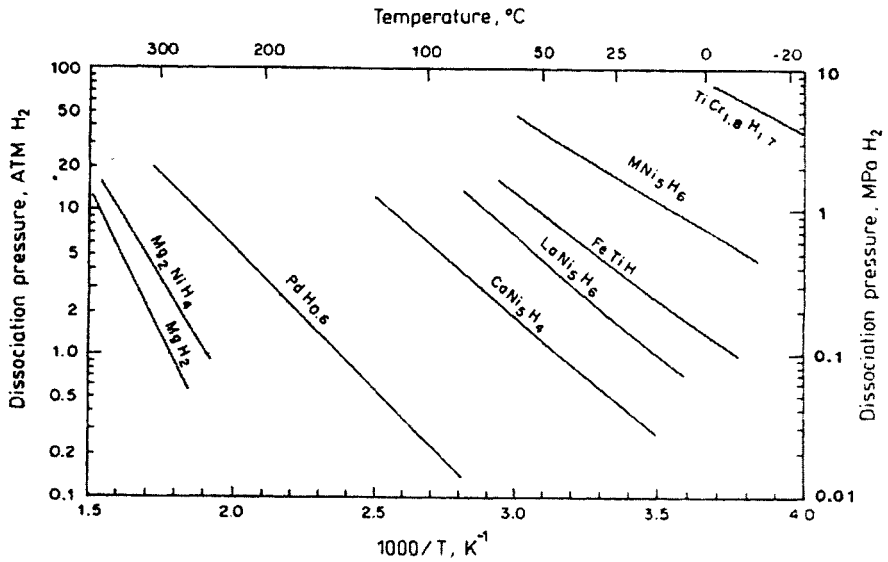

Figure 5. Dissociation Pressures vs. Temperature [8, 10]. With kind permission from Kluwer Academic Publishers.

The metallic hydrides are frequently referred to as interstitial hydrides due to the fact that hydrogen occupies interstitial sites in the metal host lattice. In the binary hydrides, however, the metal sub-lattice of the hydride is frequently different from that of the metal from which it is formed (e.g. the metal sub-lattice of TiH_2 and VH_2 is face-centred-cubic, while Ti is hexagonal-close-packed and V is body-centred-cubic) and the term interstitials hydrides seems inappropriate at least in such cases. There are in any case many types of interstitial sites which will depend on the host lattice. Tetrahedral sites, where hydrogen is located inside a tetrahedron formed by metal atoms and octahedral sites where hydrogen is surrounded by 6 atoms forming an octahedron are the most common, but square pyramidal, triangular or triangular bi-pyramidal sites are known to be occupied in some intermetallic hydrides. Not all available sites in a particular structure are necessarily occupied or completely filled.

There are, in addition to the high density and easy dihydrogen recovery, a number of other factors to consider when evaluating metal hydrides as hydrogen storage materials; we mention briefly a few of the more important ones, namely gravimetric hydrogen density, activation, rates of hydriding and dehydriding, hysteresis, disproportionation and deactivation due to poisoning.

It is an unfortunate circumstance that most metal hydrides are heavy in comparison to the amount of hydrogen they contain, i. e. they have a relatively low gravimetric hydrogen density. $FeTiH_2$ and $LaNi_5H_7$, for example, only contain 1.9 and 1.6 % of hydrogen by weight, respectively, and the light hydrides, e. g. MgH_2 and LiH, which do have high hydrogen contents of 7.6 and 12.6 %, respectively, are quite stable and require high temperatures to release dihydrogen. Much of the hydride research effort in the past 25 - 30 years has been concentrated on designing and modifying intermetallic hydrides with high gravimetric hydrogen density and capable of delivering dihydrogen at useful pressures (> 0.1 MPa) and acceptable temperatures (< 425 K). High gravimetric densities are particularly important in most mobile applications where hydrogen would be used as fuel in a combustion engine or a fuel cell. It has proven difficult, however, to exceed the 2 % by weight value and it remains a challenge to increase this figure if metal hydrides are to become viable hydrogen storage materials for the transportation industry. National as well as international research programs are ongoing to meet the challenge. In Japan, for example, the research goal for the WE-NET (World Energy Network) is a material with more than 3 wt % hydrogen storage capacity, desorption temperature below 393 K, operating pressure below 1 MPa and retention of more than 90 % of the initial capacity after 5000 cycles.[18] The goals of the IEA (International Energy Agency) are more ambitious calling for identification of a metal hydride (or carbon material) that is capable of 5 wt % hydrogen capacity with a decomposition temperature of less than 373 K.[19] In the USA the goal of DOE (Department of Energy) for vehicular hydrogen storage systems is 6.5 wt %.[20]

The problem of increasing the gravimetric density is of course rooted in the chemistry of the metal hydrides. The gravimetric density depends on the H/M molar ratio. For the binary metallic hydrides this ratio has a maximum value of 1 for the Groups 6-9 elements, 2 for the Groups 4 and 5 elements and 3 for the Group 3 elements. Thorium is an exception in that a hydride for which H/M is 3.75, the highest value known for metallic hydrides, exists. The maximum H/M ratio for hydrides of intermetallic compounds is generally less, but never more than expected from the constituent elements. A few examples will illustrate the point. The maximum observed H/M for iron titanium hydride is 1 ($FeTiH_2$) and not 1.5, which is the maximum possible from the constituting elements (H/M = 2 for TiH_2 and H/M = 1 for FeH). The maximum H/M for lanthanum nickel hydride is 7/6 ($LaNi_5H_7$) not 8/6 which is the maximum possible from the

constituting elements (H/M = 3 for LaH_3 and H/M = 1 for NiH), for magnesium nickel hydride the maximum H/M is 4/3 (Mg_2NiH_4) not 5/3 (H/M = 2 for MgH_2 and H/M = 1 for NiH). Zirconium nickel hydride represents the case where the maximum H/M ratio is equal to that expected from the constituting elements; the observed maximum is 1.5 ($ZrNiH_3$), maximum expected 1.5 (H/M = 2 for ZrH_2 and H/M = 1 for NiH). Since the H/M ratio is fixed by the intrinsic chemical properties of the systems, it is natural to look for hydrides of the light elements for high gravimetric density. Magnesium-based alloys rank high on the list to increase the gravimetric hydrogen density, but efforts so far have had limited success. Lithium-beryllium hydrides have recently been reported. They are made by reacting ultrafine mixtures of Li and Be (or LiH and Be) and ball-milling the components at an elevated temperature.[21] The hydride formation reaction was reported to be completely reversible making absorption-desorption cycling possible. A 3:2 Li-Be alloy exhibited a dissociation pressure near 0.2 MPa at 523 K and storage capacity of more than 8 wt % H, an impressive figure indeed. The toxic nature of ultrafine beryllium and beryllium alloys is of course a matter of concern in considering practical applications. Vanadium and titanium based solid solution alloys (with hydrogen contents of 3.8 and 4.0 wt % in the binary hydrides, respectively) are also of interest.[22, 23, 24] In the compressed hydrogen gas storage issue, the technology provides the highest available value. Recent breakthrough in cylinder construction have resulted in 11.3 wt % hydrogen.[25] The light weight cylinders are made of carbon fibre composites wrapped around a thin metalised plastic liner which acts as a diffusion barrier to hydrogen; the operating pressure is 35 MPa. This is considerably higher than liquid hydrogen systems which have been optimised to about 8 wt % H. The volumetric density is of course low even at these pressures for gas storage compared to hydride or liquid hydrogen storage.

Metals and alloys exposed to air are generally covered with a natural oxide film. The film acts as a barrier to hydrogen absorption and activation must take place before absorption can occur. In the initial stage of activation hydrogen dissociate into hydrogen atoms which penetrate the oxide layer to form the first nuclei of hydride. The activation occur in some cases at room temperature after an induction time, e.g. in $LaNi_5$, while in other cases heating to dissolve the oxide is necessary, e.g. with titanium alloys. The final stage in the activation is brought about by the stresses generated by the expanding hydride phase which causes the breaking up of large particles into highly cracked smaller particles with clean surfaces which readily allow for hydrogen absorption.

Rapid absorption and desorption is clearly desirable from an application's point of view. Intrinsic isothermal rates of hydriding and dehydriding are not easy to determine experimentally. In the case of rapid reactions, heat transfer becomes a difficult variable to control and the surface structure is always a problem. It is a fortunate circumstance that the reaction kinetics of most

intermetallic alloys of interest as storage materials are very fast and the cycling rates in practical storage systems are controlled by the rate of heat transfer to the material.

An hysteresis phenomenon is observed when the plateau pressure determined for an absorption isotherm is higher than the plateau pressure measured at the same temperature for the desorption process. Hysteresis is caused by the large stresses associated with the metal to hydride transformation which give rise to internal defects such as dislocations and stacking faults. Hysteresis decreases with increasing temperature as thermally activated stress relaxation processes set in. It is in general important to eliminate or at least minimize hysteresis for most applications.

As an intermetallic hydride undergoes repeated hydrogen absorption-desorption cycles, disproportionation, i.e. decomposition of the intermetallic compound, and loss of capacity may occur. This is illustrated in the following examples of eqs. (5) and (6).

$$LaNi_5 + 3\,H_2 \rightarrow LaNi_5H_6 \quad (5)$$

$$LaNi_5 + H_2 \rightarrow LaH_2 + 5\,Ni \quad (6)$$

While equation (5) represents the desired reversible reaction, the thermodynamically driven process is represented by (6). Formation of LaH_2 according to (6) will result in loss of hydrogen capacity since LaH_2 is quite stable and reversible only at high temperature. Disproportionation requires relative large movements of metal atoms as opposed to minor movements occurring in hydride formation and is therefore more likely to occur at higher temperatures. It can also be reversed by vacuum annealing at a few hundred degrees.

It should be mentioned that the hydride-forming reaction is sensitive to certain poisons. Deactivation and rapid loss of capacity can occur with only monolayer exposure. Typical poisons include CO and sulphur containing gases. The poisoning is probably due to interference and prevention of the dissociation of the hydrogen molecule.

18.4 APPROACH TO INCREASING HYDROGEN CONTENTS

It should be clear from the discussion above that new and creative approaches to increasing the gravimetric densities of metal hydrides are needed if they are to become viable hydrogen storage materials. A number of research programs address this issue. In this section two conceptually different recent approaches will be discussed; in one the focus is on ordinarily 'nonreversible' metal hydrides

with low M values, made reversible with the aid of catalysis, and in the other the focus is on increasing the hydrogen packing efficiency in metal hydrides (increased H/M molar ratio).

18.5 COMPLEX METAL HYDRIDES

The complex metal hydrides are distinctly different from the metallic binary and intermetallic hydrides both in structure and properties. They are in general not formed with the same ease of reversibility as implied in equation (1) and are not interstitial, but consist of metal ions and complex anions containing hydrogen. Many of them have very high gravimetric hydrogen storage capacities, but are much less reversible than metallic hydrides. The complex hydrides are conveniently classified as transition metal complex hydrides and non-transition metal complex hydrides. Examples of transition metal complex hydrides include Mg_2NiH_4, Mg_2CoH_5, Mg_2FeH_6, Mg_3MnH_7, K_2ZnH_4 and $BaReH_9$ which has the highest H/M value known (H/M = 4.5).[26] $BaReH_9$ has a good volume efficiency, low dissociation temperature (< 373 K at atmospheric pressure), but the weight efficiency is low (2.7 wt %), and the material cost is prohibitive for large-scale storage. These transition metal complexes are formed and stabilized in the presence of hydrogen by donation of electrons from the less electronegative elements of Group 1 or 2. Thus, in Mg_2NiH_4, for example, 4 hydrogen atoms bind to a single Ni atom and the two Mg atoms donate two electrons each to stabilize the $[(NiH)_4]^{4-}$ moiety. Transition metal complex hydrides are formed by solid-state reactions of the appropriate elements and/or binary hydrides (MH or MH_2); the reactions are typically carried out between 573 and 773 K under dihydrogen pressures up to 10 MPa. Special techniques are in some cases required such as solution methods, mechanical alloying, etc.

Mg_2NiH_4 is distinctly different from the other transition metal complex hydrides in that the hydrogen-free intermetallic species Mg_2Ni exists. None of the other transition metal complex hydrides have the corresponding hydrogen-free intemetallic precursors In addition Mg_2NiH_4 forms reversibly according to reaction (1). The formation and decomposition of transition metal complex hydrides require metal atom diffusion. The kinetics are therefore sluggish compared to the conventional metal hydrides and high temperatures are required to release dihydrogen. It is possible that catalysts could improve the viability of these materials as storage media.

The non-transition metal complex hydrides have long been used as reducing agents in the pharmaceutical, chemical and metallurgical industries. They can be described by the general formula $M(M'H_4)_n$ where M is a metal (typically Group 1 or 2) of the oxidation number n and M' is a metal of Group 13 of oxidation

number III.[27] Structurally the non-transition complex hydrides consist of M^+ cations and $M'H_4^-$ anions. The hydrogen atoms are tetrahedrally coordinated to M^+ or M^{2+}; examples include $LiBH_4$, $NaBH_4$, $Ca(BH_4)_2$, $LiAlH_4$, $NaAlH_4$ and $Mg(AlH_4)_2$. Among the non-transition metal complex hydrides, $NaAlH_4$ and Na_3AlH_6, an intermediate in the two-step decomposition of $NaAlH_4$ are of particular interest. The non-transition metal hydrides had not until recently been considered to be likely candidates for hydrogen storage; this despite the fact that many of them have gravimetric hydrogen densities substantially higher than any of the intermetallic hydrides known. The volumetric densities are of course also high (see Table I). $NaAlH_4$ and Na_3AlH_6, for example contain 7.5 and 5.9 wt % hydrogen, respectively, and $LiAlH_4$ (Table I) a 10.6 wt %. The reasons for the neglect are twofold, slow kinetics and lack of reversibility. While hydrogen liberation is thermodynamically favourable at moderate temperatures, the processes are hampered by slow kinetics and are reversible only under severe conditions. Bogdanovic and Schwickardi,[28] however, showed that doping with small amounts of transition metals (especially titanium compounds, e.g. β-$TiCl_3$) or rare earth metal compounds could effectively catalyse the reactions and suggested that alkali metal hydrides should be considered potential novel reversible hydrogen storage materials. The reversible reactions for $NaAlH_4$ are:

$$NaAlH_4 \rightleftharpoons 1/3\ Na_3AlH_6 + 2/3\ Al + H_2 \qquad (7)$$

5.6 wt % hydrogen is theoretically available in this two-stage reaction, 3.7 % in the first step and 1.9 % in the second one. For Na_3AlH_6 a total of 3.0 wt % is available:

$$Na_3AlH_6 \rightleftharpoons 3\ NaH + Al + 3/2\ H_2 \qquad (8)$$

The decomposition of NaH occurs at much higher temperature and brings the total, if included, to 7.5 wt %. Bogdanovic and Scwickardi reported reversible hydrogen capacities in cycling tests of 4.2 - 3.1 wt % for $NaAlH_4$ and 2.7 - 2.1 wt % for Na_3AlH_6. Zidan et al. [29] found zirconium to be inferior to titanium as a catalyst for dehydriding $NaAlH_4$ according to (7), but a superior catalyst for dehydriding Na_3AlH_6 according to (8). By combining both catalysts, $NaAlH_4$ with greater than 4 wt % recyclable hydrogen capacity and onset of rapid hydrogen liberation at temperatures below 373 K were obtained. Synergistic catalytic effects have also been reported for Ti and Fe in enhancing both the dehydriding and rehydriding of $NaAlH_4$; a constant 4 wt % hydrogen storage capacity was reached in cycling tests.[30] Zaluska et al [31] investigated the effects of mechanical grinding and chemical modification (addition of carbon) of both alloys and reported remarkable absorption-desorption kinetics of the alloys. In the case of $NaAlH_4$ reversible hydrogen storage between 2.5 and 3.0

wt % were observed in the relatively low temperature range 353 - 413 K. An even higher reversible capacity was observed when the operating temperature increased to 433 - 453 K.[30] Sandrock [32] has made an engineering study of this system and concluded that the desorption kinetics are indeed fairly good. He reported that 3 - 4.5 wt % hydrogen can be stored and recovered in reasonable times at 373 - 398 K. These results are encouraging, but many questions relating to the practical operation of an "engineering-scale" catalysed alanate bed (cycling effects, volume effects, effects of the heat of reaction, etc.) remain unanswered according to Sandrock. He did suggest, however, that Na_3AlH_6 decomposition might ultimately provide 3 wt % hydrogen at room temperature for low-rate applications.[32] The hydrogen storage properties of catalysed alanates are treated in some detail in two recent reviews.[33, 34]

Hydrogen stored in complex hydrides, e. g. $NaBH_4$, can also be recovered [35] by hydrolysis in the presence of a catalyst according to the following reaction (9):

$$NaBH_4 + 2\,H_2O \rightarrow 4\,H_2 + NaBO_2 + \text{Heat} \qquad (9)$$

The reaction occurs to some extent in the absence of a catalyst if the pH of the solution is less than 9, but it does not occur under more basic conditions, and $NaBH_4$ solutions are typically stabilized and maintained strongly alkaline by adding NaOH. A high purity hydrogen generator based on reaction (9) using a highly alkaline borohydride solution and ruthenium as catalyst has recently been described.[36] The generator is reported to be safe, responds quickly from ambient temperatures to 273 K and in a controllable way to H_2 demand (H_2 generation is directly proportional to the exposed catalyst surface area which can be regulated), and stores up to 7 wt % hydrogen. Reaction (9) is environmentally clean, but it is not reversible. Recharging is accomplished by adding fresh $NaBH_4$ solution and the catalysts are reusable. The process is currently too expensive for practical use. Based on an estimated price of about \$45/kg of $NaBH_4$ the cost to generate hydrogen is \$45/kg, but it has been claimed that new large volume process technology could bring the price to as low as \$2.34/kg.[37]

18.6 INCREASING PACKING EFFICIENCIES IN METAL HYDRIDES

Switendick made the observation from compilation of experimental structures that the minimum hydrogen - hydrogen separation in ordered binary metal hydrides is 0.21 nm.[12] The empirical observation was supported by band structure calculations which ascribe the effect to the repulsive interaction generated by the partially charged hydrogen atoms. The same empirical

observation has been made for the intermetallic compound hydrides and found to be quite general and is frequently referred to as the Switendick criterion.[38]

A practical consequence of the repulsive H-H interaction in metal hydrides leading to the rule of minimum H-H distances is to establish a limit on the amount of hydrogen which can be accommodated within the structure by limiting site occupancies. It is, therefore, of interest to ask if materials exist or can be made in which shorter H-H distances occur and explore the possibility of increasing the hydrogen density.

The bond length of dihydrogen is 0.074 nm and the binding energy is 4.5 eV. H-H distances considerably shorter than observed in the hydrides would clearly result if hydrogen were present in molecular form, but is it possible for two hydrogen atoms immersed in a metallic environment to pair off in the molecular form? Weber and co-workers addressed the question and calculated self-consistent energies and electronic structures of hydrogen pairs as a function of their interatomic distances in the metals Li, Al, Y and Pd.[39] They concluded that while molecular bonds between hydrogen atoms in metals are possible, hydrogen prefers to optimise its bond with the metal atoms through charge transfer from metal atoms to hydrogen; hydrogen atoms involved in a molecular bond in the metal would by contrast be neutral. They made the interesting observation, however, that in some cases, such as in the rare earth metals, pairing across the metal atom might be energetically preferable.[39] This kind of pairing has in fact been observed experimentally in diffuse neutron scattering studies of, for example, $YD_{0.19}$,[40] $ScD_{0.19}$ and $ScD_{0.33}$.[41] Hydrogen preferentially occupies the tetrahedral sites separated by the rare earth atoms and forms a periodic arrangement along the c axis. The rare earth mediated H-H distance is 3/4 c which is larger than the Switendick minimum distance and the pairing energy is estimated to be 0.10 eV per pair.

18.7 CHEMICAL BONDING OF HYDROGEN TO METAL CENTERS

Chemical bonding of hydrogen molecules to metal centres were first reported by Kubas et al.[42] Neutral dihydrogen (H_2) was shown to form nonclassical, stable bonds with molybdenum and tungsten complexes. The results were unexpected because hydrogen in metal systems had up to that time been assumed to involve hydrogen in its atomic state. Since Kubas' discovery, stable bonding of neutral hydrogen molecules to metal centres have been reported in a large number of organometallic complexes. $W(CO)_3(PR_3)_2(H_2)$, for example, is such a complex (PR_3 stands for a bulky organophosphine ligand). This complex is a stable crystalline solid under ambient conditions. Hydrogen can be

removed reversibly under vacuum at room temperature to give the hydrogen-free precursor, $W(CO)_3(PR_3)_2$. The hydrogen dissociation pressure is 1.3×10^4 to 1.3×10^3 MPa depending on the tertiary phosphine; the binding energy of the dihydrogen ligand to the complex is around 15 kcal/mol.[43] The H-H distances observed in the "dihydrogen" complexes are longer than in free molecular hydrogen, ranging from 0.078 nm to 0.16 nm in the complexes compared to 0.074 nm in free hydrogen. More than 40 complexes with H-H distances less than 0.16 nm, determined by X-ray and neutron diffraction and NMR techniques, have been reported [44] (as of 1997).

Theoretical investigations of the metal-dihydrogen bond [45-47] have led to the following picture: The main interaction is a result of the donation of electron density from the H_2 bonding electron pair (i.e. the σ orbital) to a vacant metal d orbital. In addition, backdonation from a filled metal d orbital into the σ^* antibonding orbital of the H_2 molecule is regarded to occur to a lower extent. Both interactions, however, effectively contribute to the weakening of the H-H bond as evidenced by the elongation. Upon sufficient weakening the bond breaks and a dihydride in the classical sense results. This can occur, for example, by increasing the electron density on the metal to the point where back donation to the antibonding orbital on H_2 causes bond rupture due to overpopulation of the antibonding orbital. It has been shown [43] that the interactions of H_2 with metal complexes can be fine tuned to bind either as a dihydrogen ligand or as a dihydride. The fine tuning is done by adjusting the electron donating properties of the ligands.

Jensen and co-workers at the University of Hawaii have explored the potential of nonclassical metal complex hydrides for hydrogen storage, focusing on materials based on Group 9 metals such as $IrH_aX_b(H_2)(PR_3)_2$, where X = Cl, Br or I, R = C_6H_{11}, $C(CH_3)_3$ or $CH(CH_3)_2$, and a and b are stoichiometric coefficients ranging from 1 to 2. By adjusting the strength of the dihydrogen ligand with the transition metal atom, the heat of H_2 absorption and desorption can be adjusted to values which make the process viable around room temperature. The Hawaiian group reported an unimpressive 0.5 wt % reversible hydrogen in these systems.[48] It is interesting to note, however, that in the course of this investigation these materials were found to be useful as catalysts for the reversible hydrogenation/dehydrogenation of unsaturated hydrocarbons.[49, 50, 51] An impressive 7 wt % hydrogen storage is theoretically possible.

It is also of interest to note that hydrogen has been determined to bind as molecules to metal surfaces, e.g. the 510 plane of Ni [52, 53] and to small atom clusters, e.g. $Cu_2(H_2)_2$ and $Cu_2(H_2)_3$.[54]

18.8 HYDROGEN - HYDROGEN INTERACTION IN METAL HYDRIDES

The local hydrogen densities of the dihydrogen complexes are very high, but the bulk densities are low, lower in fact than the typical metal hydride storage materials. It is clear, however, that molecularly bound hydrogen to metal centres is a common phenomenon and fuels the speculation that hydrogen pairing in metal hydride systems with the possibility of H-H distances considerably shorter than 0.21 nm might occur under appropriate conditions. Halet et al. suggested this might occur in the following manner.[55] The two H atoms in the metal hydride would come very close to each other in a manner in which the H-H antibonding states, being strongly destabilized, would rise above the Fermi level and leave behind their electrons to bonding or nonbonding metallic levels. The resulting structure containing H_2 'dimers' located inside a metallic matrix might appear to be highly unusual, but Halet points out that the idea that H_2, dihydrogen, could act as a simple two-electron ligand as discussed above was no less strange when first proposed. Halet et al further suggested that one way of enhancing the chances of forming the H_2 bond was to destabilize the hydride structure by removing electrons from the metallic d-band,[55] for example, by alloying the hydride with a third element, more electronegative than the parent metal and that Th_2AlD_4 might be a case in point. The electronegativity of Th is 1.1 and that of Al 1.5 in the Allred and Rockow scale.[4] In a neutron diffraction study of Th_2Al deuteride (this was in fact the first neutron diffraction study made of an intermetallic hydride structure) it was reported that among the four crystallographically different tretrahedrally coordinated interstitial sites, two (16*l* and 4b) coordinated by Th_4, one (32m) by Th_3Al and one (16k) by Th, deuterium occupied only the 16*l* sites in the Al_2Cu-type structure of Th_2Al.[56, 57] The 16*l* site occupancy is complete for Th_2AlD_4 resulting in an ordered structure where each Th_4 tetrahedron shares a common face with another Th_4 tetrahedron. The reported D-D separation of 0.179 nm [56, 57] is clearly in violation of the Switendick criterion and is only one of two such cases mentioned in an extensive review by Yvon and Fischer.[58] They pointed out that the instrumental resolution at the time the data were obtained (1961) was rather poor and questioned the accuracy of the structure determination. Due to the uncertainty in the structure determination, the question of D-D pairing through space as suggested above was therefore impossible to answer.[55] A recent high resolution powder neutron diffraction reinvestigation of $Th_2AlD_{3.9}$ has shown the structure to be essentially as earlier reported with deuterium in the 16*l* sites, but compared to the earlier study the deuterium atoms have been shifted away from the face shared by the neighbouring Th_4 tetrahedra resulting in an elongation of the D-D distance.[59] The refined D-D distance is 0.197 nm in much better agreement with the Switendick criterion. On the basis of these observations we

conclude hydrogen-hydrogen pairing does not occur in Th_2AlH_4.

Evidence of through-space pairing in metallic hydrides, however, may have come from a recent study where unusually short H-H distances were reported in a group of intermetallic compound hydrides (deuterides) by Yartys et al.[60] who prepared and studied intermetallic compound deuterides of the composition $RENiInD_{4/3}$, where RE is La, Ce or Nd. Crystal structures were determined from high resolution powder - X ray and neutron diffraction data. The structures of the deuterium-free materials are of the hexagonal ZrNiAl type and are retained on deuterium absorption. The saturated deuterides have the composition $RENiInD_{4/3}$ and deuterium is located in RE_3Ni tetrahedra sharing a common face and forming a trigonal bipyramid. This site filling produces an anisotropic expansion along [001]. The structure leads to extraordinary short D-D distances around 0.16 nm [60] which is believed to be the shortest observed in a metallic hydride and is substantially shorter than expected from what the Switendick criterion would predict. NMR data supporting hydrogen pairing in these materials have been published.[61-63] Estimation of H-H distances from NMR data is 0.148 nm in $CeNiInH_x$ [61] and 0.15-0.18 in $PrNiInH_x$.[62] Preliminary results from ongoing electronic structure calculations indicate no H-H bonding interaction in another member of the group, $LaNiInD_{4/3}$.[64] The local hydrogen density in these hydrides is very high, but it is an open question whether or not the results can be extrapolated and applied to increasing the bulk hydrogen density of metal hydrides. The nature of the H-H interactions in these compounds is intriguing and further work is in progress and will hopefully provide answers. It should be noted, however, that the electronegativities of the rare earth metals referred to above are 1.1 and that both Ni and In are both more electronegative, 1.8 and 1.5, respectively. The $RENiInD_x$ materials fit the picture suggested by Halet et al. [55] of destabilizing the hydride structure, by removing electrons from the RE metallic d-band by alloying with another element more electronegative than the RE, and thus favouring the formation of hydrogen pairs.

18.9 ELECTROCHEMICAL STORAGE OF HYDROGEN

Many metals and alloys will not only absorb hydrogen from the gas phase according to (1), but will also absorb hydrogen electrolytically in aqueous solutions, see eq. (10)

$$M + s/2\ H_2O + s/2\ e^- \rightarrow MH_s + s/2\ OH^- \qquad (10)$$

The reaction is the basis for the rechargeable nickel metal hydride (NiMH) battery, first commercialised in Japan in 1991 [65] and now a strong competitor to the nickel cadmium (NiCad) battery. The NiMH battery uses an AB_5 type alloy for the metal hydride electrode. In the early stages of development it was established that $LaNi_5$ electrodes in alkaline solutions corroded rapidly resulting in poor cycle-lives. A breakthrough came in the mid-eighties when Willems and van Beek [66, 67] succeeded in stabilizing the $LaNi_5$ electrode. They identified the main cause of the degradation of the electrode during electrochemical cycling as being due to volume expansion during hydride formation and the associated particle size reduction and increase in surface area. By reducing the volume expansion the electrode was stabilized; the reduction in volume expansion was accomplished by partially substituting other elements for the La and Ni atoms in the lattice.

In the NiMH battery as in the NiCad battery the reversible electrochemical reaction at the positive Ni electrode is:

$$Ni(OH)_2 + OH^- \rightarrow Ni(O)(OH) + H_2O + e^- \quad (11)$$

The simultaneous reaction at the negative electrode is for the MH electrode:

$$M + s\,H_2O + s\,e^- \rightarrow MHs + s\,OH^- \quad (12)$$

and for the corresponding negative cadmium electrode:

$$Cd(OH)_2 + 2\,e^- \rightarrow Cd + 2\,OH^- \quad (13)$$

The net reaction for the NiMH battery:

$$M + s\,Ni(OH)_2 \rightarrow MH_s + s\,Ni(O)OH \quad (14)$$

and the net reaction for the NiCad battery is:

$$2\,Ni(OH)_2 + Cd(OH)_2 \rightarrow 2\,Ni(O)(OH) + Cd + 2\,H_2O \quad (15)$$

The reactions typically take place in a 30 % aqueous KOH solution. Charging occurs from left to right, discharging from right to left. The negative electrode in the NiMH batteries is typically a multicomponent alloy, e. g. $MmNi_{3.5}Co_{0.8}Mn_{0.4}Al_{0.3}$ where Mm stands for Mischmetal, but other alloy types are under investigation. The NiMH battery has certain advantages over the NiCad battery. These include freedom from the "memory effect", higher gravimetric energy density, higher charging and discharging rate capabilities and no change

in electrolyte concentration. Also important is the freedom from the problem of dendrite formation, which is a destructive process in the NiCad battery, since there is no metal dissolution/deposition occurring in the NiMH battery. The NiMH battery is environmentally more friendly than the NiCad battery because it does not contain toxic Cd and appropriate methods for recycling the relatively valuable metals in the battery have been developed.[68, 69]

18.10 SUMMARY

The concept of hydrogen as energy carrier is especially attractive from an environmental point of view, but since hydrogen is a gas of very low density at STP, the storage of large quantities required for most applications is not a trivial matter. High pressure compressed gas storage is energy intensive if high volume efficiency is desired, and liquid and solid hydrogen storage even more so. Storing hydrogen in the form of solid metal hydrides from which it can readily be recovered by heating is a alternative and safe, highly volume efficient storage method. For typical mobile applications, however, both volume and weight efficiencies are important. Conventional metal hydrides suffer from low weight efficiencies (< 2 wt % hydrogen) and the challenge is to improve the weight efficiencies substantially. To this end some of the recent work has concentrated on new and creative approaches. The results on complex metal hydrides, e. g. $NaAlH_4$, appears to be particularly promising with hydrogen weight efficiencies approaching 5 wt %. The hydrogen absorption/desorption reactions in these systems suffer from slow kinetics and poor reversibility, but the addition of catalysts makes these processes feasible under moderate and acceptable conditions. The search for hydrides with reduced H-H distances is another interesting approach. The Switendick criterion of minimum H-H distances in metal hydrides (0.21 nm) effectively limits the amount of hydrogen that can fit in the structure. However, hydride structures with H-H distances as low as 0.16 nm have recently been reported. Such hydrides have increased local hydrogen density. It remains to be seen if the results can point the way to increase the bulk hydrogen density.

Hydrogen storage can also be accomplished electrochemically. The NiMH hydride battery, based on electrochemical hydrogen storage was commercialised ten years ago and is now a strong competitor to the NiCad battery.

REFERENCES

[1] T. N. Veziroglu, Int. J. Hydrogen Energy, 25 (2000) 1143.
[2] A. J. Appleby, The Electrochemical Engine for Vehicles, Scientific American, (1999) 58-63.
[3] J. H. Ausubel, Where is Energy Going?, The Industrial Physicist, February (2000) 16-19.
[4] J. Elmsley, The Elements, 3rd Edition, Oxford University Press, Oxford, UK, 1968.
[5] G. Alefeld and J. Volkl, eds., Hydrogen in Metals I and II, Topics in Appl. Phys., vol. 28 and 29, Springer-Verlag, Berlin Heidelberg, Germany, 1978.
[6] L. Schlapbach, ed., Hydrogen in Intermetallic Compounds I & II, Topics in Appl. Phys., vol. 63 and 67, Springer-Verlag, Berlin Heidelberg, Germany, 1988 and 1992.
[7] K. H. J. Buschow, P. C. P. Bouten, and A. R. Miedema, Rep. Prog. Phys., 45 (1982) 937-1039.
[8] G. Sandrock, Hydrogen Metal Systems and Applications of Hydrides, in Hydrogen Energy Systems, Production and Utilization of Hydrogen and Future Aspects, Y. Yurum, ed., NATO ASI Series, 295 (1995), 135-166 and 253-280, Kluwer Publishing, The Netherlands.
[9] G. Sandrock, State-of-the-art Review of Hydrogen Storage in Reversible Metal Hydrides for Military Fuel Cell Applications, Final Report, Contract N00014-97-M-0001, July 1997, Office of Naval Research, Arlington, VA, USA.
[10] G. Sandrock, J. Alloys Comp., 293-295 (1999) 877.
[11] J. W. Hanneken, Int. J. Hydrogen Energy, 24 (1999) 1005.
[12] A. C. Switendick, Z. Phys. Chem., 117 (1979) 89.
[13] G. G. Libowitz, H. F. Hayes and T. R. P. Gibb, Jr., J. Phys. Chem., 62 (1958) 76.
[14] J. J. Reilly and R. H. Wiswall, Inorg. Chem., 7 (1968) 2254.
[15] J. H. N. van Vucht, F. A. Kuijpers and H. C. A. M. Bruning, Philips Res. Repts., 25 (1970) 133.
[16] K. C. Hoffman, W. E. Winsche, R. H. Wiswall, J. J. Reilly, T. V. Sheehan and C. H. Waide, Paper 690232, Metal Hydrides as a Source of Vehicular Propulsion, Society of Automotive Engineers, New York 1969.
[17] G. G. Libowitz and A. J. Maeland, Hydride Formation in BCC Solid Solution Alloys, in Materials Science Forum, R. G. Barns, ed., Trans Tech Publications Ltd., Aedermannsdorf, Switzerland, 1988.
[18] I. Uehara, T. Sakai and H. Ishikawa, J. Alloys Comp., 253-245 (1997) 635.
[19] G. Sandrock, IEA H2 Task 12:Hydrogen Storage in Metal Hydrides and Carbon, Sandia National Laboratories, CA, http://hydpark.ca.gov./iea.html
[20] A. C. Dillon and M. J. Heben, Appl. Phys. A 72, (2001) 133.
[21] A. Zaluska, L. Zaluski and J. O. Strom Olsen, J. Alloys Comp., 307 (2000) 157.
[22] J. F. Lynch, A. J. Maeland and G. G. Libowitz, Z. Phys. Chem. NF 145 (1985) 51.
[23] K. Kuriiwa, T. Tamura, T. Amemiya, T. Fuda, H. Takamura and M. Okada, J. Alloys Comp., 293-295 (1999) 431.
[24] J. Shi, M. Tsukahara, H. T. Takeshita, N. Kuriyama and T. Sakai, J. Alloys Comp., 293-295 (1999), 716.

[25] Hydrogen and Fuel Cell Letter, Vol. XV/No. 10, October 2000, p. 1.
[26] K. Yvon, Chimia, 52 (1998) 613.
[27] E. A. Sullivan and R. C. Wade, Kirk-Othmer Encyclopedia of Chemical Technology, 12 (1980) 772.
[28] B. Bogdanovic and M. Schwickardi, J. Alloys Comp., 253 (1997) 1.
[29] R. A. Zidan, S. Takara, A. G. Hee and C. M. Jensen, J. Alloys Comp., 285 (1999) 119.
[30] B. Bogdanovic, R.A. Brand, A. Marjanovic, M. Schwickardi and J. Tolle, J. Alloys Comp.,302 (2000) 36.
[31] A. Zaluska, L. Zaluski, J. O. Strom-Olsen, J. Alloys Comp., 298 (2000), 125.
[32] G. Sandrock, K. Gross, G. Thomas, C. Jensen, D. Meeker and S. Takara, J. Alloys Comp., accepted for publication.
[33] C. M. Jensen and K. J. Gross, Appl. Phys. A72 (2001) 213.
[34] K. J. Gross, G. J. Thomas and C. M. Jensen, J. Alloys Comp., accepted for publication.
[35] H. I. Schlesinger, H. C. Brown, A. E. Finholt, J. R. Gilbreath, H. R. Hoekstra and E. K. Hyde, J. Am. Chem. Soc., 75 (1953) 215.
[36] S. C. Amendola, S. L. Sharp-Goldman, M. S. Janjua, N. C. Spencer, M. T. Kelly, P. J. Petillo and M. Binder, Int. J. Hydrogen Energy, 25 (2000) 969.
[37] Hydrogen & Fuel Cell Letter, Vol XVI/No. 3, March 2001, p. 4.
[38] B. K. Rao and P. Jena, Phys. Rev. B 31 (1985) 6726.
[39] S. E. Weber, Feng Liu, S. N. Khanna, B. K. Rao, and P. Jena, J. Alloys Comp., 172-174 (1991) 485.
[40] M. W. McKergow, D. K. Ross, J. E. Bonnet, I. S. Anderson and O. Schaerph, J. Phys. C: Solid State Phys., 20 (1987) 1909.
[41] O. Blaschko, J. Pleschiutschnig, G. Ernst, L. Pintaschovius, J. P. Burger, J. N. Daou and P. Vajda, Phys. Rev. B, 40 (1989) 907.
[42] G. J.Kubas, R. R. Ryan, B. I. Swanson, P. J. Vergamini and H. J. Wasserman, J. Am. Chem. Soc., 106 (1984) 451.
[43] G. J. Kubas, J. Alloys Comp., 172 (1991) 1.
[44]. B. R. Bender, G. J. Kubas, L. H. Jones, B. I. Swanson, J. Eckert, K. B. Capps and C. D. Hoff, J. Am. Chem. Soc., 119 (1997) 9179.
[45] G. J. Kubas, Acc. Chem. Res., 21 (1988) 120.
[46] R. H. Crabtree, Acc. Chem. Res., 23 (1990) 95.
[47] P. J. Hay, J. Am. Chem. Soc., 109 (1987) 705.
[48] R. A. Zidan, R. E. Rocheleau and C. M. Jensen, Proc. 1996 U. S. DOE Program Review, Rept. NREL/CP-430-21968, II (1996), National Renewable Energy Lab., 795.
[49] C. M. Jensen, Proc. 1996 U. S. DOE Program Review, Rept. NREL/CP-430-21968, II (1996) National Renewable Energy Lab., 787.
[50] M. Gupta, W. C. Kaska, R. E. Cramer and C. M. Jensen, J. Am. Chem. Soc., 119 (1997) 840.
[51] C. M. Jensen, US Patent Number 6,074,447, June 13, 2000.
[52] A. S. Martensson, C. Nyberg and S. Andersson, Phys. Rev. Lett., 57 (1986) 2045.
[53] A. S. Martensson, C. Nyberg and S. Andersson, Surf. Sci., 205 (1988) 12.
[54] R. H. Hauge, J. L. Margrave and Z. H. Kafafi, NATO ASI Ser. B, 158 (1986) 787.

[55] J-F. Halet, J-Y. Saillard, C. Koudou, C. Minot, Z. Nomikou, R. Hoffman and C. Demangeat, Chem. Mater, 4 (1992) 153.
[56] J. Bergsma, J. A. Goedkoop and J. H. N. van Vucht, Acta. Cryst., 14 (1961), 223.
[57] J. H. N. van Vucht, Philips Res. Repts. 18 (1963), 35.
[58] K. Yvon and P. Fischer, Topics Appl. Phys. 63 (Ref. 6 above, p. 87.
[59] M. H. Sørby, H. Fjellvåg, B. C. Hauback, A. J. Maeland and V. A. Yartys, J. Alloys Comp., 309 (2000) 154-164..
[60] V. A. Yartys, R. V. Denys, B. C. Hauback, H. Fjellvåg, I. I. Bulyuk, A. B. Ryabov and Ya. M. Kalychak, Accepted for publication J. Alloys Comp.
[61] K. Ghoshray, B. Bandyopadhyay, M. Sen, A. Ghoshray and N. Chatterjee, Phys. Rev. B., 47 (1993) 8277.
[62] M. Sen, S. Giri, K. Ghoshray, G. Bandyopadhyay, G. Ghoshray, and N. Chatterjee, Sol. State Commun., 89 (1994) 327.
[63] M. Sen, A. Ghoshray, K. Ghoshray, S. Sil and N. Chatterjee, Phys. Rev. B, 53 (1996) 14345.
[64] P. Vajeeston et al., private communication July 9, 2001.
[65] I. Uehara, T. Sakai and H. Ishikawa, J. Alloys and Comp., 253-254 (1997) 635.
[66] J. J. Willems, Philips J. Res. Suppl., 39 (1984) 1.
[67] J. R. G. K. van Beek, J. J. Willems and H. C. Dunkersloot, Proc. 14 th Int. Power Sources Symp., Brighton, UK, 1984; L. C. Pearce, Ed., Power Sources 10 (1985) 317.
[68] P. Zang, T. Yokohama, O. Itabashi, Y. Wakui, T. M. Suzuki and K. Inoue, J. Power Sources, 77(1999) 116.
[69] J. W. Lyman and G. R. Palmer in, P. D. Bennett and T. Sakai, Eds., Hydrogen and metal hydride batteries, The Electrochemical Society, Inc., vol. 94-97 (1994) 415.

Index